AD-753 974

PROPAGATION OF VISIBLE AND INFRARED WAVES IN THE ATMOSPHERE

V. E. Zuev

Army Foreign Science and Technology Center
Charlottesville, Virginia

4 November 1972

DISTRIBUTED BY:

NTIS

National Technical Information Service
U. S. DEPARTMENT OF COMMERCE
5285 Port Royal Road, Springfield Va. 22151

AD753974

FSTC-HT-23-2475-72
13 November 1972

ARMY MATERIEL COMMAND

U.S. ARMY
FOREIGN SCIENCE AND TECHNOLOGY CENTER

PROPAGATION OF VISIBLE AND INFRARED WAVES IN THE ATMOSPHERE

by

V. E. Zuyev

USSR

DDC
RECEIVED
JAN 22 1973
C

Reproduced by
NATIONAL TECHNICAL
INFORMATION SERVICE
U S Department of Commerce
Springfield VA 22151

This document is a rendition of the original foreign text without any analytical or editorial comment.

Approved for public release; distribution unlimited.

SI-72-60-430

551

UNCLASSIFIED
Security Classification

DOCUMENT CONTROL DATA - R & D

(Security classification of title, body of abstract and indexing annotation must be entered when the overall report is classified)

1. ORIGINATING ACTIVITY (Corporate author)
Foreign Science and Technology Center
US Army Materiel Command
Department of the Army

2a. REPORT SECURITY CLASSIFICATION
Unclassified

2b. GROUP

3. REPORT TITLE

PROPAGATION OF VISIBLE AND INFRARED WAVES IN THE ATMOSPHERE

4. DESCRIPTIVE NOTES (Type of report and inclusive dates)
Translation

5. AUTHOR(S) (First name, middle initial, last name)

V. E. Zuyev

6. REPORT DATE	7a. TOTAL NO. OF PAGES	7b. NO. OF REFS
4 November 1972	~~547~~ 551	N/A

8a. CONTRACT OR GRANT NO.	9a. ORIGINATOR'S REPORT NUMBER(S)
b. PROJECT NO. T702301 2301	FSTC-HT-23- 2475-72
c. Requester AMSEL	9b. OTHER REPORT NO(S) (Any other numbers that may be assigned this report)

10. DISTRIBUTION STATEMENT
Approved for public release; distribution unlimited.

11. SUPPLEMENTARY NOTES	12. SPONSORING MILITARY ACTIVITY
	US Army Foreign Science and Technology Center

13. ABSTRACT

The monograph generalizes the main results of theoretical and experimental studies which examine various aspects of the problem of the propagation of visible and infrared waves in the atmosphere. The generalization is based on the studies made by the author and his collaborators and other studies which were made both in the USSR and abroad.

The first two parts of the book examine problems dealing with the absorption and dissipation of both monochromatic and non-monochromatic radiation under various meteorological conditions, distances and directions in which the radiation is propagated. The third part of the book describes the laws which govern the spatial propagation of bounded radiation beams from heat sources and lasers in the atmosphere: the structure of the beam in various scattering media, the effect of atmospheric turbulence on the beam parameters and nonlinear effects which accompany the propagations of powerful radiation in the atmosphere.

DD FORM 1 NOV 68 1473 REPLACES DD FORM 1473, 1 JAN 64, WHICH IS OBSOLETE FOR ARMY USE.

UNCLASSIFIED
Security Classification

14. KEY WORDS	LINK A		LINK B		LINK C	
	ROLE	WT	ROLE	WT	ROLE	WT
WAVE PROPAGATION MONOCHROMATIC RADIATION OPTICS ATMOSPHERIC RADIATION SPECTOSCOPY METEOROLOGY GEOPHYSICS GEODESY ASTROPHYSICS ELECTRONICS LASER OPTICS COSATI Subject Code: 20, 09, 04, 03 Country Code: UR						

TECHNICAL TRANSLATION

FSTC-HT-23-2475-72

ENGLISH TITLE: PROPAGATION OF VISIBLE AND INFRARED WAVES IN THE ATMOSPHERE

FOREIGN TITLE: RASPROSTRANENIYE VIDIMYKH I INFRAKRASNYKH VOLN V ATMOSFERE

AUTHOR: V. E. Zuyev

SOURCE: Sovetskoye Radio (Soviet Radio)
Moscow, 1970

Translated for FSTC by LEO KANNER ASSOCIATES

NOTICE

The contents of this publication have been translated as presented in the original text. No attempt has been made to verify the accuracy of any statement contained herein. This translation is published with a minimum of copy editing and graphics preparation in order to expedite the dissemination of information.

Approved for public release. Distribution unlimited.

The monograph generalizes the main results of theoretical and experimental studies which examine various aspects of the problem of the propagation of visible and infrared waves in the atmosphere. The generalization is based on the studies made by the author and his collaborators and other studies which were made both in the USSR and abroad.

The first two parts of the book examine problems dealing with the absorption and dissipation of both monochromatic and nonmonochromatic radiation under various meteorological conditions, distances and directions in which the radiation is propagated. The third part of the book describes the laws which govern the spatial propagation of bounded radiation beams from heat sources and lasers in the atmosphere: the structure of the beam in various scattering media, the effect of atmospheric turbulence on the beam parameters and nonlinear effects which accompany the propagations of powerful radiation in the atmosphere.

The book was written for a wide class of readers working in the fields of optics and atmospheric spectroscopy, meteorology, geophysics, geodesy and astrophysics, optic-electronic and laser technology, and also for advanced students in the corresponding specialties.

Foreword

The last few years have been characterized by a substantial increse in interest on behalf of engineers and scientists in the study of laws which govern the propagation of electromagnetic waves in the optical range in the earth's atmosphere. This interest is primarily due to the possibility of using optical quantum generators in communication systems,

information transmission systems, range and location finders and other devices designed for work in the atmosphere. In addition to this a wide class of meteorological, geophysical and astrophysical problems requires more and more precise quantitative data about the characteristics of the propagation of visible and infrared radiation in the atmosphere. Such data include, above all: the interpretation of radiation data obtained from artificial earth satellite observations and the solution of the related reverse problemsof satellite meteorology, the calculation of radiation heat transfer in the atmosphere and the determination of the heat balance of the earth as a planet; finding the radiation term in equations which forecast the weather; obtaining astrophysical observation data which are unaffected by the earth's atmosphere, etc.

The solution of the above problem requires the knowledge of a large collection of quantitative data which characterize the propagation of optical radiation in the atmosphere, when both the characteristic radiation as well as the conditions under which it propagates vary within wide limits. Some of the radiation characteristics are: the width of the spectral interval or the degree of monochromacity; the power and its variation in time (continuous and pulse radiation); coherence; the direction and geometric dimensions (from an infinite wave to beams bounded in space characterized by the initial diameter and the divergence angle); spatial homogeneity of the field. The propagation conditions depend on instantaneous and mean temperature values of the total and partial pressures of gas components in the atmosphere, the chemical composition, concentration, the spectral dimensions and forms of aerosol particles in the atmosphere, i.e., quantities which have an effect on the parameters of the radiation propagating in the atmosphere.

In the first monograph of the author [1] and in the recently published monographs of K. Ya. Kondrat'ev [2] and R. Gudi [3] certain aspects of the interaction between the optical radiation and the atmosphere were considered. In [1], data on the absorption, dissipation and attenuation of thermal radiation in the visible and infrared regions in the atmosphere were generalized under various meteorological conditions. In [2] problems associated with heat transfer calculations are discussed systematically. The monograph of R. Gudi [3] is mainly dedicated to the theory of heat radiation absorption by atmospheric gases.

This monograph discusses the results of theoretical and experimental studies of various aspects of the problem of the propagation of visible and infrared waves in the atmosphere,

obtained both in the USSR and abroad.

The book consists of three parts. The first part considers absorption problems of visible and infrared radiation from heat sources and optical quantum generators by atmospheric gases under various propagation conditions. The possible variations in these conditions, the mean temperature, pressure and humidity profiles, and the absorbing gas concentrations in the atmosphere are described in Chapter 1. Chapter 2 is devoted to the origin of the absorption spectra of atmospheric gases (water vapor, carbon dioxide, ozone, nitrogen oxide, carbon monoxide, oxygen). In Chaps. 3 & 4 the results of theoretical and experimental studies of optical radiation absorption propagating along horizontal and slanted directions under various conditions in the atmosphere are analyzed.

In the second part of the monograph problems of aerosol and molecular scattering of visible and infrared radiation from heat sources and optical quantum generators under various atmospheric conditions are discussed. These conditions are characterized in Chapter 5. The laws which describe the optical radiation scattering by one particle are discussed in Chapter 6. The results of theoretical and experimental scattering studies of visible and infrared waves under various conditions in the earth's atmosphere are presented in Chapter 7.

The third part of the book discusses systematically various aspects of the problem of the propagation of spatially bounded radiation beams from optical quantum generators and heat sources in the atmosphere. The main radiation parameters of optical quantum generators of various types are considered in Chapter 8. Chapter 9 analyzes the results of investigations which study the structure of the light field in a cross section of the beam, which is propagated through various scattering media. The nonlinear effects which accompany the propagation of powerful light radiation in the atmosphere are discussed in Chapter 10. In the last chapter, Chapter 11, the fluctuations in the parameters of spatially bounded radiation beams caused by turbulent movements in the atmosphere are discussed.

The author considers it his pleasant duty to express his deep gratitude to the workers of the Infrared Radiation Laboratory of the Siberian Physics-Technological Institute at Tomsk University, B. A. Antipov, P. A. Bokhan, A. G. Borov, E. A. Vedernikovaya, O. K. Voytsekhovskaya, V. M. Genin, L. I. Gerasimova, I. I. Ippolitov, M. V. Kabanov, G. M. Krekov, P. N. Kokhanenko, M. Ya. Krylova, V. P. Lopasov, E. V. Lugin, Yu. S. Makushkin, A. A. Nalivayko, L. I. Nesmelova, B. A. Savel'ev,

I. V. Samokhvalov, V. A. Sapozhnikova, V. K. Sonchik, V. V. Fomin, S. S. Khmelevtsov, N. A. Chernyavskaya, for the many-sided help which he received during his work on the manuscript of the book. The author would like to express particularly his gratitude to Stanislav Dmitrievich Tvorogov, together with whom he wrote Chapters 4, 6, 10 and paragraph 2 in Chapter 7. The author expresses his gratitude to G. P. Puchkov, S. I. Sokolov for their great help in shaping the technical form of the monograph.

The author is very grateful to Professors K. Ya. Kondrat'ev and A. A. Semenov for the valuable critical remarks and advice which were made and given when the manuscript of the monograph was reviewed.

Part 1: ABSORPTION OF VISIBLE AND INFRARED WAVES IN THE EARTH'S ATMOSPHERE

1. The Earth's Atmosphere As An Absorbing Medium

The earth's atmosphere is an absorbing medium which varies exceptionally in time and space. The absorption of visible and infrared waves in the atmosphere depends substantially on the pressure, temperature and concentration of the absorbing gases. Each of these quantities varies with the altitude, in time, and in accordance with the geographical region within rather wide limits. Without knowing the laws which govern the changes of these elements, it is not possible to solve any problem which requires quantitative data about the absorption of visible and infrared waves in the earth's atmosphere.

In this chapter we will discuss the laws which determine the variation in pressure, temperature and the concentration of the absorbing gases in the atmosphere. The main attention is given to the problem of water vapor distribution in the atmosphere, since it is the main absorbing component. In addition to this, this component varies more than the other components.

We will discuss in great detail the variations of all elements which interest us in the lower 30-km layer of the atmosphere, where the main mass of all gases which absorb the radiation in the visible and infrared region of the spectrum is concentrated.

1. Composition of the Atmosphere. Variations in Pressure and Temperature.

Among the elements which have an effect on the absorption

of the visible and infrared radiation in the atmosphere, pressure is the only element the variation of which in time can be always ignored at all altitudes below 30-km in the lower layer of the atmosphere. The vertical pressure profiles for various regions of the globe can also be considered to be equal for all practical purposes.

The atmosphere consists mainly of nitrogen, oxygen and argon the percentage contents of which is given in Table 1.1. The table gives, in addition, data about other components of the atmosphere with the exception of water vapor.

TABLE 1.1

DRY AIR COMPOSITION [3]

a Составляющие атмосферы	b Средняя объемная концентрация в тропосфере, %	c Примечание
N_2	78,084	В верхней ионосфере диссоциирует; на более низких уровнях перемешан.
O_2	20,946	Диссоциирует выше 95 *км*; на более низких уровнях перемешан.
Ar	$9{,}34 \cdot 10^{-1}$	Перемешан до 110 *км*; выше — диффузионное разделение.
CO_2	$3{,}3 \cdot 10^{-2}$	Испытывает незначительные изменения; перемешан до 100 *км*; выше диссоциирует.
Ne	$1{,}818 \cdot 10^{-3}$	Перемешан до 100 *км*; выше — диффузионное разделение.
He	$5{,}24 \cdot 10^{-4}$	Перемешан до 110 *км*; выше — диффузионное разделение.
CH_4	$1{,}6 \cdot 10^{-4}$	В тропосфере перемешан; в стратосфере окисляется; в мезосфере диссоциирует.
Kr	$1{,}14 \cdot 10^{-4}$	Перемешан до 110 *км*; выше — диффузионное разделение.
H_2	$5 \cdot 10^{-5}$	В тропосфере и стратосфере перемешан, выше диссоциирует.
N_2O	$3{,}5 \cdot 10^{-5}$	У поверхности земли испытывает незначительные изменения; постепенно диссоциирует в стратосфере и мезосфере.
CO	$7 \cdot 10^{-6}$	Продукт окисления, содержание изменчиво.
O_3	10^{-6}	Испытывает сильные изменения, имеет фотохимическое происхождение.
NO_2, NO	от 0 до $2 \cdot 10^{-6}$	В тропосфере имеет промышленное происхождение; в мезосфере и ионосфере — фотохимической природы.

Key: a. Atmospheric components; b. Mean volume concentration in troposphere, %; c. Remarks. (cont. next page)

Key, Table 1.1 (cont'd):

c. Remarks

In the upper ionosphere dissociated; at lower levels, mixed.

Dissociated above 95 km; at lower levels, mixed.

Mixed up to 110 km; above, separated by diffusion.

Mixed in troposphere; [illegible] in stratosphere; dissociated in mesosphere.

Mixed up to 110 km; above, separated by diffusion.

Mixed in troposphere and stratosphere; above dissociated.

Undergoes minute changes near the surface of the earth; gradually dissociates in stratosphere and mesosphere.

Oxidation product, variable content.

Undergoes drastic changes, has photochemical origin.

Of industrial origin in the troposphere; in the mesosphere and ionosphere of a photochemical nature.

The atmosphere contains also traces of many other gases, which, however, do not have an important effect on the absorption of visible and infrared waves. In some local regions gases may be encountered which absorb the visible and infrared radiation, which are not given in Table 1.1.

The average pressure value on the scale of the globe at sea level is equal to 1013 mb. This quantity varies between the limits 980-1040 mb [4]. Thus, the deviation from the mean pressure value lies approximately between the limits $\pm$ 3%.

The drop in the pressure as a function of altitude (vertical profile) is sufficiently well described by the exponential law, which is obtained by solving the barometric equation.

The numerical values of the pressure at various altitudes in the lower 30-km layer in accordance with standard models of the atmosphere are given in supplement 1. The same supplement contains data about the pressure at altitudes up to 100 km.

The mean vertical temperature profile points to the presence of a number of layers in the atmosphere. The lowest layer, in which the mean temperature decreases as a function of height is usually called the troposphere. The vertical thickness

of this layer depends on the width of the region and the time of the year. In tropical regions it is equal to 16-18 km, in polar regions to 7-10 km. The next layer of the atmosphere, the stratosphere, extends approximately up to 50 km. This layer is characterized first by a slow (approximately up to 20 km) and then a quick rise in temperature. The boundary layer between the troposphere and stratosphere in which the vertical temperature gradient changes sign is called the tropopause.

The temperature reaches its maximum value on the upper boundary of the stratosphere. This is followed by the stratopause, in which the vertical temperature gradient again changes sign. Above 50 km is the atmospheric layer called mesosphere which extends up to a height of 80-90 km. Here the temperature drops with the altitude and reaches a mean value which is approximately equal to 200° K. This is followed by the mesopause, with a new change of sign in the temperature gradient, and the thermosphere in which the temperature rises continuously.

Among all layers of the atmosphere which were considered, the least stable vertical temperature behavior occurs in the troposphere, especially in its lowest level which is 2-3 km thick. In this layer inversions are often observed in the vertical temperature movement.

Figure 1.1 [3] shows the mean vertical cross section of the temperature field in the lower 30-km layer of the atmosphere for the 80° meridian longitude west in the northern hemisphere. The isotherms in the diagram are given in °C. The thick lines show the boundaries of the layers in which temperature inversion is observed and the levels with sharp vertical temperature gradient changes.

The mean vertical temperature profile adopted in standard models of the atmosphere for various altitudes from 0 to 30 km are given in supplement 1. The same supplement contains data about the mean temperature for altitudes from 25 to 100 km.

2. Distribution of Water Vapor In The Atmosphere

To characterize air humidity, the following concepts are usually introduced: 1) the absolute humidity a, measured in grams per cubic meter; 2) the water vapor elasticity e or its partial pressure, expressed in millimeters mercury or in millibars; 3) the relative humidity r, the ratio of water vapor elasticity contained in the air to the saturated vapor pressure E at a given temperature, measured as a percentage; 4) specific humidity q, the amount of the water vapor per unit mass

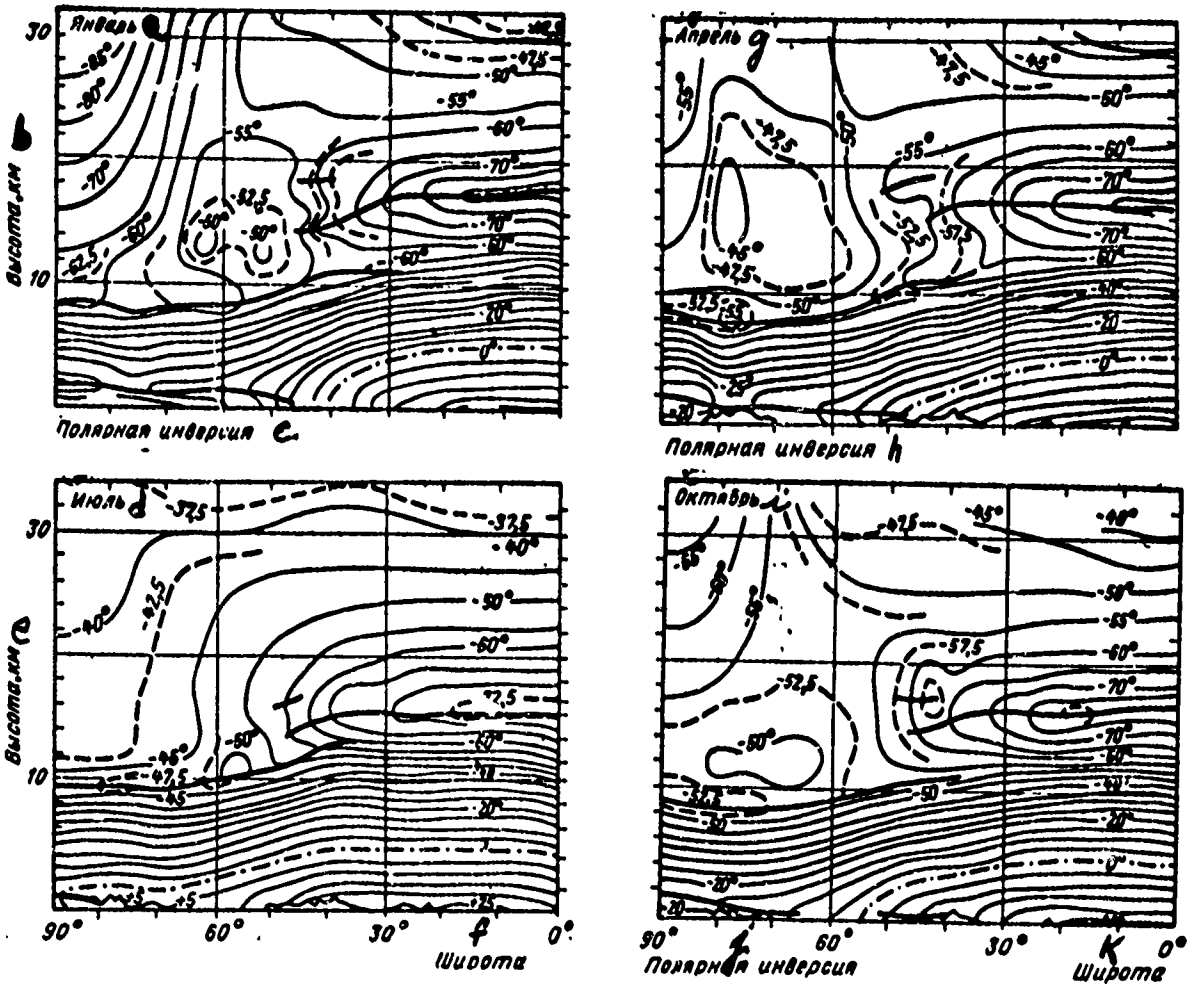

Fig. 1.1. Yearly course of mean isotherms in the atmosphere along the 80° meridian, longitude west at altitudes from 0 to 30 km

Key:
a. January
b. Height, km
c. Polar inversion
d. July
e. Height, km
f. Width
g. April
h. Polar inversion
i. October
j. Polar inversion
k Width

of moist air; 5) the mixture ratio δ, the amount of water vapor per unit mass of dry air; 6) the settled layer of water ω characterizes the thickness of the water layer obtained when the water vapor is completely condensed in a given layer of the atmosphere; 7) the humidity shortage d, the difference between the maximum and actual elasticity of the water vapor at a given temperature and pressure; 8) the dew point τ, the air temperature cooled to the state when the water vapor in it is saturated.

The humidity characteristics are related to one another by the relations [4, 5]:

$$a = 217\frac{e}{T}\ [мб] = 289{,}4\frac{e}{T}\ [мм\ рт.\ ст.]; \tag{1.1}$$

$$q = \frac{\delta}{1+\delta} = 0{,}622\frac{e}{P-0{,}378e}; \qquad \delta = \frac{q}{1-q} = 0{,}622\frac{e}{P-e}; \tag{1.2}$$

$$r = \frac{e}{E}\cdot 100\%;\quad d = E - e; \qquad e = E_0 \cdot 10^{b\tau/c+\tau}, \tag{1.3}$$

Key: a. mb
b. mm Hg.

where T is the absolute temperature, P is air pressure measured in the same units as e, E_0 = 4.58 mm Hg/cm = 6.11 mb; τ is measured in °C; b and c are equal to 7.5 and 237.3 for air, and 9.5 and 265.5 for ice.

Since in the atmosphere $e \ll P$; $q \ll 1$, and $\delta \ll 1$, we obtain from (1.2)

$$q \cong \delta \cong 622\frac{e}{P}.$$

The amount of the settled water layer ω' per 1 km is related to the absolute humidity expressed in grams per cubic meter, by the simple relation

$$\omega' = 10e. \qquad (1.4)$$

The concept of a settled water layer is widely used in the study of radiation absorption by water vapors.

Table 1.2 gives the values of E, a, q and δ for P= 1000 mb (the atmospheric layer near the surface of the earth) and various temperatures.

TABLE 1.2

THE ELASTICITY VALUES OF SATURATED WATER VAPOR E ABOVE A PLANE SURFACE OF CLEAN WATER, THE ABSOLUTE HUMIDITY VALUES a, SPECIFIC HUMIDITY VALUES q, THE MIXTURE RATIO δ AT A PRESSURE OF P = 1000 mb AND VARIOUS TEMPERATURES

t, °C	E, мб (a)	a, г/м³ (b)	q, г/кг (c)	δ, г/кг (d)
—20	1,254	1,073	0,780	0,781
—10	2,863	2,357	1,782	1,786
0	6,108	4,845	3,808	3,822
10	12,270	9,39	7,67	7,73
20	23,37	17,27	14,67	14,89
30	42,43	30,33	26,82	27,56
40	73,78	65,30	47,20	49,54
50	123,40	82,76	80,51	87,56

Key: a. mb
b. g/m^3
c. g/kg
d. g/kg

The water vapor concentration varies very much in time and space. It can be said that each concrete measurement of the vertical humidity profile is not reproducible. This can be said in spite of the fact that the mean statistical horizontal and vertical profile picture is known with sufficient detail in the troposphere region at the present time.

The mean distribution of the water vapor concentration along the altitude in the troposphere is described by a simple

exponential law [5]:

$$e(z) = e(0)e^{-\alpha z}, \qquad (1.5)$$

where e(z) and e(0) are the elasticities of the water vapor at altitude z and on the surface of the earth respectively, and α is an empirical constant.

The water vapor concentration in the layer of the atmosphere near the surface of the earth can vary, depending on the time and the location, approximately from 0 to 7%.

Humidity measurements in the stratosphere are connected with great difficulties. Therefore, more or less essential results have only been obtained in the last few years. These results have been generalized by Gutnik [6], who constructed the mean vertical specific humidity profile (Fig. 1.2), and in the surveys of M. S. Malkevich, Yu. B. Samsonov, L. I. Koprova [7], Houton [8] and V. S. Komarov's article [13].

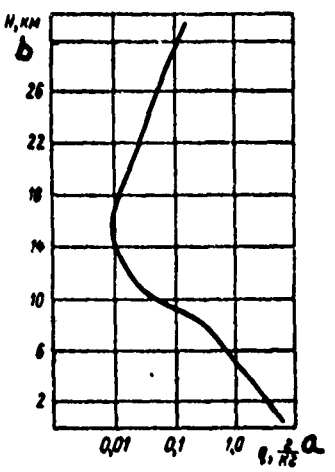

Fig. 1.2. Mean vertical specific humidity profile according to the data of Gutnik [6].

Key: a. g/kg
b. H,. km

An analysis of the available data led the authors to conclude that there are two types of vertical water vapor distributions in the stratosphere. The first type is characterized by a sharp drop in the water vapor concentration to very small specific humidity values on the order of 10^{-3}-10^{-2} g/kg in the lower layers of the stratosphere (to 16 km). Above this layer the concentration rises and reaches a maximum (for which data is available) value at an altitude of 31 km, which is 1-2 orders larger than at the 16 km level. The second type of water vapor distribution which varies with height is characterized by the constant value of the specific humidity from a certain altitude onward in the stratosphere. The relation between the specific humidity and the altitude can be written in both cases as follows:

$$q(z) = \begin{cases} q_0 e^{-\alpha_0 z}, & 0 \leqslant z \leqslant z_1, \\ q_1 e^{\alpha_1 (z - z_1)}, & z_1 < z \leqslant z_{\text{макс}}. \end{cases} \quad \text{(a)} \qquad (1.6)$$

Key: a. max

From (1.6) it is seen that when the second type of humidity distribution is described by the altitude, the parameter α_1 must be set equal to zero.

Table 1.3 gives the values of the parameters in (1.6) which were obtained by analyzing the measurement results of various authors.

TABLE 1.3

VALUES OF THE SPECIFIC HUMIDITY q_0 AND q_1 AND THE PARAMETERS α_0 AND α_1 IN FORMULAS (1.6) ACCORDING TO THE DATA FROM ARTICLE [7]

a q_0, г/кг	b α_0, км$^{-1}$	c q_1, г/кг	b α_1, км$^{-1}$	d z_1, км
12,2	0,52	0,012	0,08	12
11,5	0,49	0,006	0,23	14
1,6	0,43	0,05	0	8
5,1	0,42	0,01	0,27	15
17,5	0,56	0,04	0	10
3,6	0,51	0,002	0,18	14
5,7	0,48	0,002	0,24	16
2,6	0,55	0,002	0,31	16

Key: a. g/kg b. km^{-1} c. g/kg d. km

The two types of specific humidity distributions in the atmosphere which were described are called in the Foreign Literature the "humid" and "dry" models of the stratosphere [10]. Both Models presuppose an equal distribution of water vapors with altitudes up to the tropopause level. Because of this the differences in these models are not important in infrared radiation calculations over layers of the atmosphere which include its lower layers. These differences may become important when radiation absorption is calculated in the upper atmosphere.

The controversy between the proponents of the dry and humid stratosphere models has continued until now, since more recent publications keep appearing in which reports are made about measurements confirming in some cases one hypothesis and in other cases the other hypothesis.

From our point of view the aforementioned controversy cannot be solved only by analyzing the results of individual measurements. What is needed is a statistical treatment of systematic measurements of the vertical distribution of the water vapor concentration. This approach has been used in the studies [9, 11-13], the main results of which are discussed below.

1. Mean Vertical Specific Humidity Profile

When the mean vertical specific humidity profile is obtained in the winter and summer periods for the measured latitudes, the mean temperature and relative humidity values on the main isobar surfaces obtained by 95 aerological stations in the Soviet Union with the aid of an A-22 radiosonde are used. The mean values of the aforementioned meteoelements were calculated from 280-307 two-period observations in the 400-100 mb layer, and from 20-100 observations at the levels 50, 30, 20 and 10 mb. In the last case data was used which was obtained in the MGSS (Internation Year of the Quiet Sun). Corrections were added to the mean specific humidity value to compensate for the systematic measurement error due to the inertia of the radiosonde pickup.

Figure 1.3 gives the mean vertical specific humidity profiles for January and June, and also the Gutnik profile. It can be seen from the figure that in the upper troposphere the specific humidity drops sharply with the altitude in all cases. Qualitatively the profile trace in Fig. 1.3 is approximately analogous to the Gutnik profile trace. However, the absolute specific humidity values at various altitudes differ considerably. The mid-January and mid-June specific humidity

profiles for the measured latitudes above the territories of the USSR extend further to the right than the Gutnik profile. Also the profiles for individual regions lie both to the right and to the left of the Gutnik profile.

Table 1.4 gives the mid-month specific humidity values near the surface of the earth and on various isobar surfaces for January and June in the Baltic region, Central Asia and Eastern Siberia, which were determined from various observations at the Riga, Tashkent and Irkutsk stations.

TABLE 1.4

MEAN SPECIFIC HUMIDITY IN JANUARY AND JUNE FOR THE RIGA, TASHKENT AND IRKUTSK STATION FROM THE DATA [9], g/kg

a Изобарическая поверхность, мб	b Ст. Рига		c Ст. Ташкент		d Ст. Иркутск	
	e январь	f июль	e январь	f июль	e январь	f июль
Земля	2,30	8,70	2,78	7,80	1,62	9,40
900	2,00	6,50	2,30	5,50	1,10	8,40
850	1,75	5,50	2,10	4,70	0,90	6,90
700	0,88	3,20	1,42	3,60	0,60	4,50
600	0,53	2,00	0,86	2,50	0,35	3,00
500	0,33	1,15	0,53	1,60	0,25	1,90
400	0,10	0,28	0,16	0,60	0,07	0,68
300	0,03	0,11	0,04	0,17	0,031	0,20
200	0,020	0,07	0,03	0,06	0,024	0,048
150	0,029	0,08	0,04	0,024	0,041	0,061
100	0,036	0,09	0,05	0,011	0,068	0,088
50	0,048	0,16	0,06	0,037	0,130	0,14
30	0,053	0,31	0,12	0,12	0,245	0,30
20	0,070	0,59	0,20	0,25	0,36	0,49
10	0,180	1,50	0,65	1,20	0,85	1,50

Key: a. Isobar surface, mb
b. Riga station
c. Tashkent station
d. Irkutsk station
e. January
f. July

The statistical treatment is based on data obtained as a result of probing the atmosphere four times daily at the aforementioned stations near the surface of the earth and on the isobar surfaces from 900 to 100 mb in January and June over the period from 1961 to 1966. For the levels from 50 to 10 mb data was used obtained in the MGSS (International Year of the Quiet Sun), (1964-1965). At the levels from the surface of the earth to 100 mb, each station in January and June had 560 to 740 observations and, on the levels from 50 to 10 mb, 30-150 observations in January and 50-18 observations in June.

The minimum mean specific humidity values are underlined in each column of Table 1.4. We note that the data in Table 1.4 do not contain corrections for the systematic measurement error which is due to the inertia of the radiosonde.

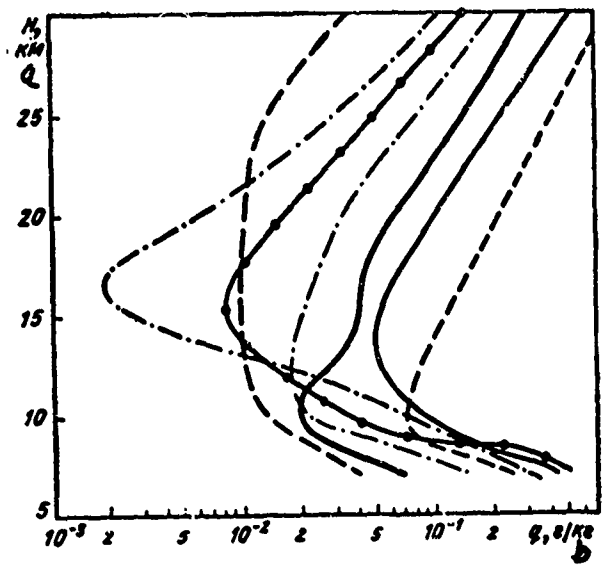

Fig. 1.3. Mean vertical specific humidity profile for the measured latitudes USSR (————); for the stations Barentsburg (– – –), Ashkhabad (– . –), – . – –, Gutnik profile.
Thick lines denote January profiles, thin lines June profiles.

Key: a. km
b. g/kg

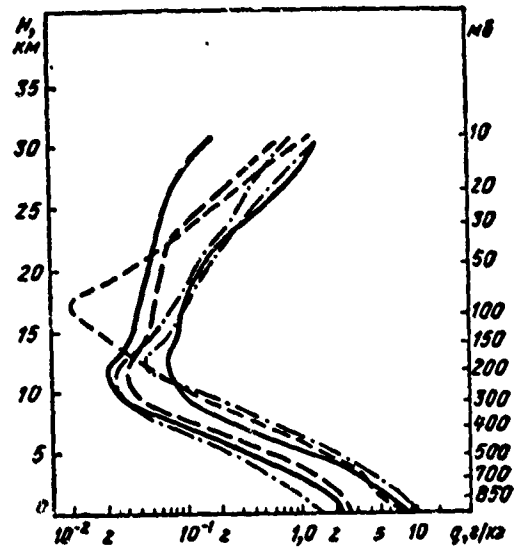

Fig. 1.4. Mid-month vertical specific humidity profiles for the stations Riga (——), Tashkent (– – –), Irkutsk (– . –) according to V. S. Komarov's data [9].

Thick lines denote January profiles, thin lines July profiles.

Table 1.5 gives the mean vertical specific humidity gradients calculated from the data in Table 1.4.

The mean vertical specific humidity profiles for the three stations considered are plotted in Fig. 1.4. The specific features of the behavior of individual profiles can be clearly seen from Table 1.4 and Fig. 1.4.

The fastest drop in specific humidity with altitude occurs, as is seen from Table 1.4, in the lower part of the troposphere up to the 600 mb level (the altitude interval 0-4 km).

The minimum mid-month specific humidity value is observed, for all three stations near the tropopause, approximately 0.5-1 km above the minimum temperature level.

An analysis of the individual observations for any station shows the presence of pronounced scatter in the vertical specific humidity profiles. All profiles can be classified

TABLE 1.5

MEAN VERTICAL SPECIFIC HUMIDITY GRADIENTS FOR THE RIGA, TASHKENT AND IRKUTSK STATIONS, g/kg/100 m

a Слой, мб	Ст. Рига b		Ст. Ташкент c		Ст. Иркутск d	
	январь e	июль f	январь e	июль f	январь e	июль f
0—900	0,03	0,22	0,05	0,23	0,05	0,10
900—850	0,05	0,20	0,04	0,16	0,04	0,30
850—700	0,07	0,15	0,05	0,07	0,02	0,25
700—600	0,04	0,12	0,06	0,11	0,03	0,15
600—500	0,02	0,09	0,03	0,09	0,01	0,11
500—400	0,02	0,04	0,02	0,05	0,01	0,06
400—300	0,004	0,009	0,006	0,021	0,002	0,024
300—200	0,0003	0,0013	0,0003	0,0036	0,0002	0,005
200—150	—0,0005	—0,0005	0,0005	0,0018	—0,0008	—0,0006
150—100	—0,0002	—0,0003	—0,0003	0,0004	—0,0009	—0,0009
100—50	—0,0003	—0,0018	—0,0002	—0,0006	—0,0013	—0,0010
50—30	—0,0002	—0,0050	—0,0020	—0,0028	—0,0038	—0,0053
30—20	—0,0008	—0,0140	—0,0040	—0,0065	—0,0058	—0,0095
20—10	—0,0027	—0,0180	—0,0110	—0,0190	—0,0120	—0,0202

Key:
a. Layer, mb
b. Riga station
c. Tashkent station
d. Irkutsk station
e. January
f. July

into three types. In the first type we include profiles with a considerable rise in the specific humidity from an altitude above the tropopause level with a sufficiently large humidity content in the mid-stratosphere (on the order of 0.1-0.5 g/kg). The second type is characterized by a constant specific humidity value at various altitudes in the stratosphere when the humidity content in the entire stratosphere layer is small (on the order of 0.01-0.02 g/kg). Finally, the third type includes profiles in which the specific humidity drops slowly with altitude in the stratosphere, when the humidity content in the mid-stratosphere is low (on the order of 0.01-0.02 g/kg). Figure 1.5

gives examples of all three types of profiles.

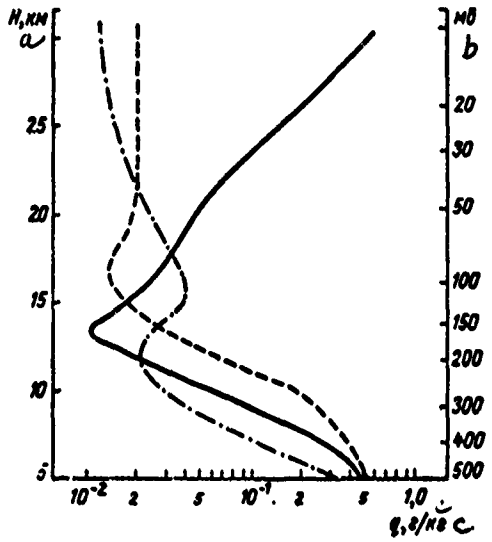

Key:
a. km
b. mb
c. g/kg

Fig. 1.5. Examples of various types of vertical specific humidity profiles obtained in Irkutsk 28.7.64 (—), Tashkent 7.7.63 (– – –) and Riga 5.1.66 (–•–).

Thus in each concrete observation the stratosphere can be either "humid" or "dry." However, the mean statistical vertical specific humidity profile shows that this quantity increases considerably with altitude in the stratosphere for all stations, both in January and in July. To explain this fact we must answer the question: Where does the considerable amount of moisture come from in the upper layers of the stratosphere?

2. Transfer of Water Vapors from the Troposphere into the Stratosphere

One answer to the question posed was given by V. S. Komarov [13] who studied the vertical water vapor transfer from the troposphere into the stratosphere. The study was based on a statistical analysis of radiosonde observations data obtained at twelve stations in the Soviet Union which cover more or less uniformly the entire territory of the country. Only those radiosonde levels were considered in which the data about the humidity,

velocity and direction of the wind were obtained for all isobar surfaces. The analysis used the corresponding data for 9 standard levels: 400, 300, 200, 150, 100, 50, 30, 20 and 10 mb for the MGSS (International Year of the Quiet Sun), (1964-1965). As a result of the study data was obtained about the reproducibility of vertical movement directions, which characterize the frequency with which ascending air currents pierce the tropopause.

An analysis of the results obtained shows that the repeatability of vertical air movements in the tropopause region for 9 stations out of 12 is in January 52-67%, and in July for 10 stations out of 12 is 52-64%. For three stations in the winter and for two stations in the summer, descending air movements are dominant in the tropopause region with a repeatability from 52 to 60%.

Table 1.6 gives the mean repeatability of upward and downward vertical air movements for medium latitudes on the territory of the USSR for January and July for various layers of the atmosphere on clear and cloudy days. The table is compiled for a number of cases $n \geqslant 30$.

It can be seen from Table 1.6, that the repeatability of ascending and descending flows depends to a very large extent on the cloudiness in the atmosphere. When there are clouds, the repeatability of ascending air movements is dominant both in winter and in summer in the entire troposphere and up to the 100 mb level in the stratosphere. In the summer when the weather is cloudy, the ascending air flows dominate the descending air flows both in the troposphere and in the stratosphere up to the maximum radio probing height. These flows humidify the stratosphere. Thus, on clear days the stratosphere should be drier, and conversely, on cloudy days it should more humid. This conclusion agrees with the mean vertical specific humidity profiles of the stratosphere which are obtained on clear and cloudy days.

3. Variability of the Humidity Field at Various Altitudes in the Atmosphere

The humidity field changes considerably both in the troposphere and atmosphere, depending on the time and physical-geographical region. Therefore, together with the mean statistical vertical humidity profiles it is also important that we have information about the corresponding confidence intervals. The necessary calculations were made for four stations situated in various climatic regions of the USSR. The calculations were based on the treatment of data obtained from radio

probes over a protracted period at the levels from 100 mb, and for the MGSS (International Year of the Quiet Sun) at the levels from 50 to 10 mb.

TABLE 1.6

MEAN REPEATABILITY OF ASCENDING AND DESCENDING VERTICAL AIR MOVEMENTS IN VARIOUS LAYERS OF THE ATMOSPHERE FOR MEDIUM LATITUDES ON THE TERRITORY OF THE USSR [13]

a Слой, мб	Январь · b						Июль c							
	ясно d		облака e Ci, Cs, Ce		средняя f		ясно d		облака e Ci, Cs, Ce		облака f Cb		средняя f	
	восх.	нисх. g	восх.	нисх. g	восх.	нисх. g	восх.	нисх. g	восх.	нисх. g	восх.	нисх. g	восх.	нисх. g
400—300	49	51	63	37	56	44	51	49	57	43	56	44	55	45
300—200	51	49	58	42	56	44	44	56	52	48	54	46	52	48
200—150	43	57	58	42	58	48	48	52	52	48	53	47	52	48
150—100	40	60	51	49	51	49	46	54	62	38	56	44	53	47
100—50	32	68	50	50	40	60	57	43	60	40	56	44	55	45
50—30	31	69	37	63	40	60	60	40	60	40	50	50	54	46
30—20	32	68	—	—	44	56	51	49	58	42	42	58	55	45

Key:
a. layer, mb
b. January
c. July
d. clear
e. clouds
f. mean
g. ascending. descending

Figures 1.6-1.13 give the mid-month vertical specific humidity profiles for January and July and the confidence intervals. The latter characterize the number of cases in which the profiles which were obtained will fall within the given intervals. The specific humidity can vary in very short time intervals. These variations are due to the fluctuations in the water vapor content which can cause corresponding fluctuations in the light beam which is propagated through the atmosphere [14]. At the present time the problem of humidity fluctuations is only in the initial stages of study.

4. The Total Contents of Water Vapors in Various Layers of the Atmosphere

From the data about the mean vertical specific humidity profile one can easily obtain the total water vapor content in various layers of the atmosphere both in the vertical and the horizontal directions, (Table 1.7, 1.8).

It is very important that we know the settled water layer between two points in the atmosphere in order to be able to solve problems connected with calculating the visible and infrared radiation in the atmosphere. For this purpose we will note a method for finding this quantity between any two points in the atmosphere which takes into account the earth's curvature and refraction when the vertical distribution of the gas concentration is assumed to be known. This method was proposed in article [15]. The mass of the absorbing gas in [15] is determined from the formula

$$\omega = \omega_{z_1} f(z_1) - \omega_{z_2} f(z_2), \tag{1.7}$$

where ω_{z_1} and ω_{z_2} are the mass of the absorbing gas in the vertical column of the atmosphere from the altitudes z_1 and z_2 to ∞. For the function f(z) the approximate expression

$$f(z) = (\cos z + ke^{-m\cos z})^{-1}, \tag{1.8}$$

proposed by G. V. Rosenberg [16] is used, where m and k are constant coefficients.

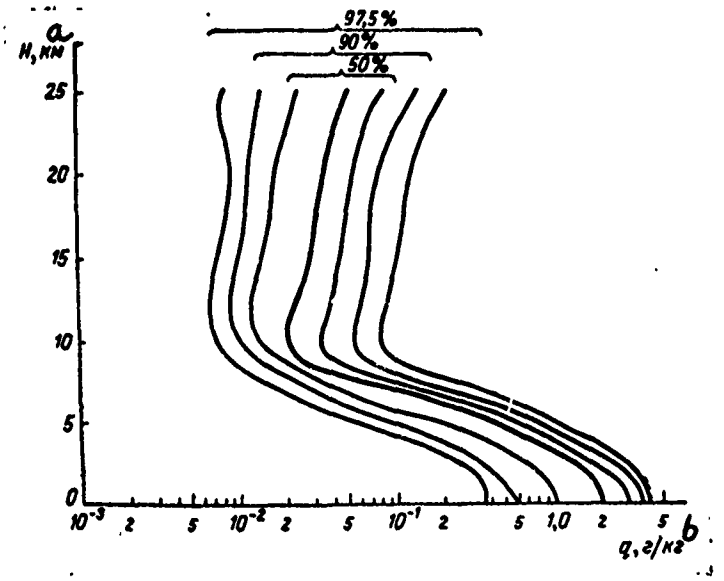

Fig. 1.6. Mean vertical specific humidity profile in January for the Station Voeykovo and confidence intervals (50, 90 and 97.5%)

Key: a. km
b. g/kg

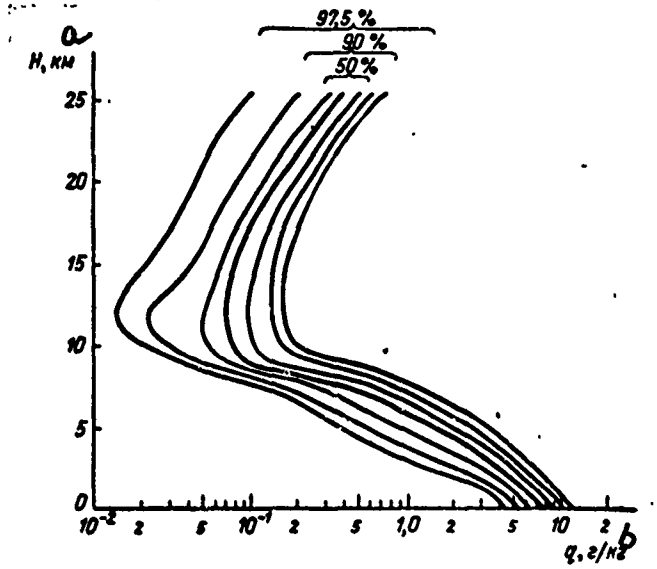

Fig. 1.7. Mean vertical specific humidity profile in July for the Station Voeykovo and confidence intervals (50, 90 and 97.5%)

Key: a. km
b. g/kg

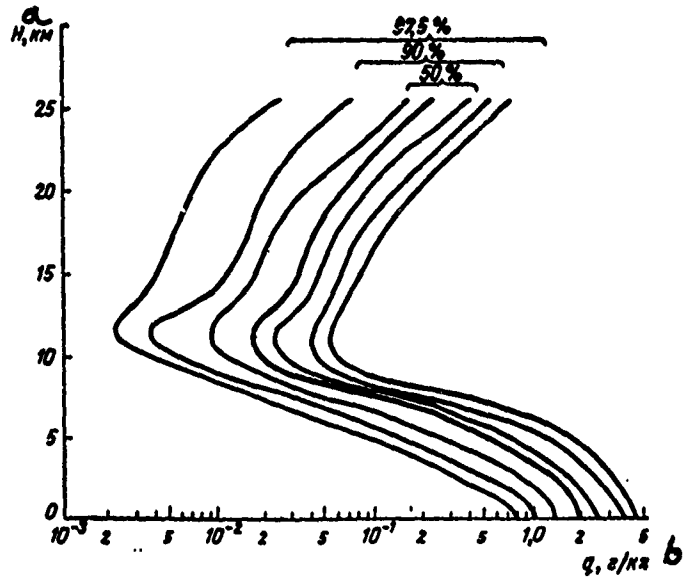

Fig. 1.8. Mean vertical specific humidity profile in January for the Alma-Ata Station and confidence intervals (50, 90 and 97.5%)

Key: a. km
b. g/kg

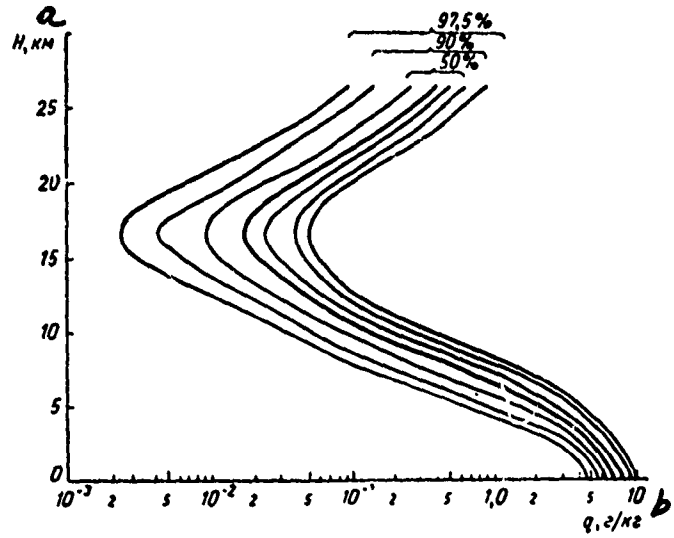

Fig. 1.9. Mean vertical specific humidity profile in July for the Alma-Ata Station and confidence intervals (50, 90 and 97.5%)

Key: a. km; b. g/kg

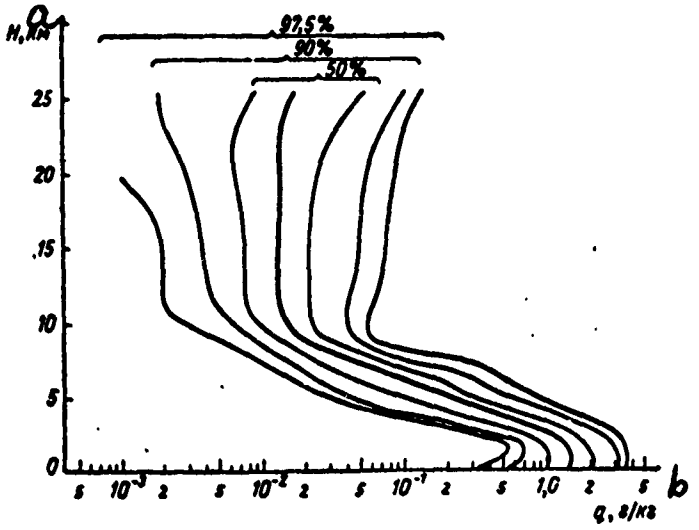

Fig. 1.10. Mean vertical specific humidity profile in January for the Murmansk Station and confidence intervals (50, 90 and 97.5%)

Key: a. km; b. g/kg

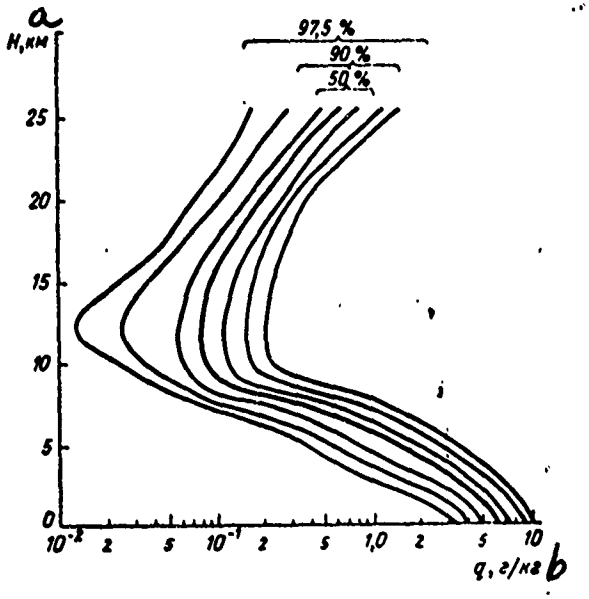

Fig. 1.11. Mean vertical specific humidity profile in July for the Murmansk Station and confidence intervals (50, 90 and 97.5%)

Key: a. km; b. g/kg

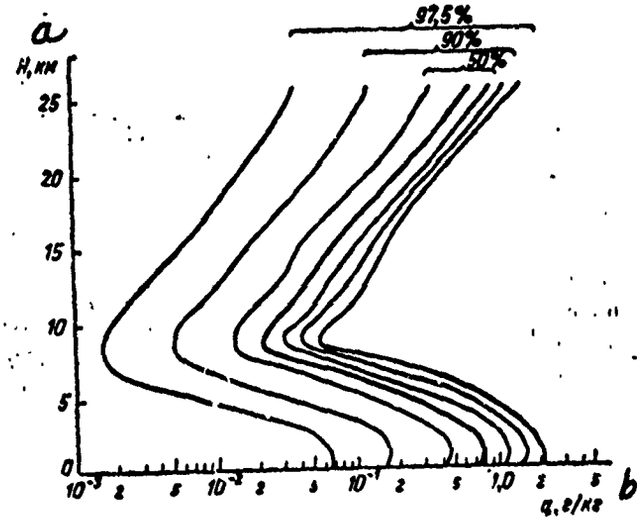

Fig. 1.12. Mean vertical specific humidity profile in January for the Nagaevo Station and confidence intervals (50, 90 and 97.5%).

Key: a. km; b. g/kg

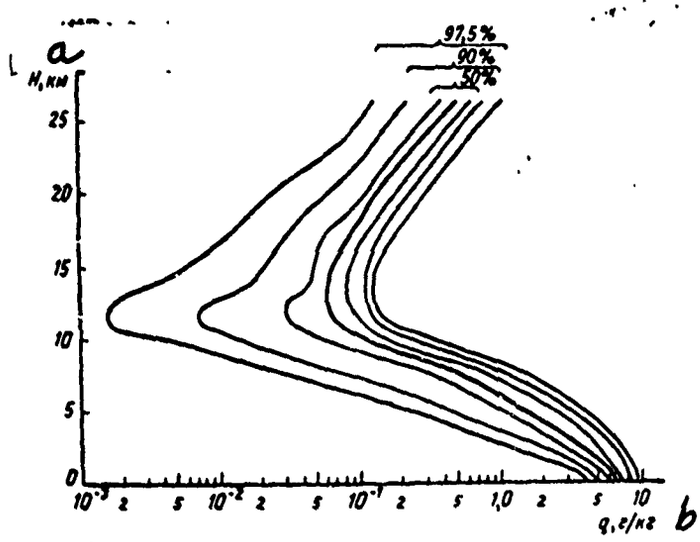

Fig. 1.13. Mean vertical specific humidity profile in July for the Nagaevo Station and confidence intervals (50, 90 and 97.5%).

Key: a. km; b. g/kg

TABLE 1.7

MID-MONTH SETTLED WATER VALUES IN CM·KM^{-1} IN LAYERS AT VARIOUS HEIGHTS FOR THREE STATIONS IN JANUARY AND JUNE [13]

a Слой, мб	Ст. Рига b		Ст. Ташкент c		Ст. Иркутск d	
	январь e	июль f	январь e	июль f	январь e	июль f
g Земля—850	0,2070	0,7240	0,2490	0,6380	0,1290	0,8340
850—700	0,1340	0,4440	0,1790	0,4230	0,0770	0,5800
700—500	0,0620	0,2230	0,1000	0,1300	0,0430	0,3270
500—400	0,0110	0,0370	0,0180	0,0560	0,0560	0,0660
400—300	0,0030	0,0102	0,0051	0,0200	0,0024	0,0250
300—200	0,0013	0,0046	0,0018	0,0060	0,0017	0,0063
200—150	0,0007	0,0020	0,0009	0,0010	0,0010	0,0014
150—100	0,0006	0,0014	0,0008	0,0003	0,0013	0,0013
100—50	0,0001	0,0012	0,0001	0,0003	0,0019	0,0013
50—30	0,0004	0,0016	0,0006	0,0005	0,0017	0,0015
30—20	0,0001	0,0015	0,0005	0,0006	0,0011	0,0014
20—10	0,0003	0,0027	0,0011	0,0010	0,0016	0,0026

Key:
a. Layer, mb
b. Riga Station
c. Tashkent Station
d. Irkutsk Station
e. January
f. July
g. Earth

5. A Comparison of the Available Data About Specific Humidity in the Stratosphere

An analysis of the available data about the specific humidity in the stratosphere points to the considerable scatter in the quantitative values of this magnitude which were obtained by various authors. Thus, the mid-year Gutnik profile [6] and the mid-month profiles, which were constructed by V. S. Komarov [12], differ to a considerable extent from the profiles obtained by many investigators in individual measurements, including those made in the last few years. Thus, in Houton's survey [8], many concrete humidity measurements in the stratosphere

are studied, on the basis of which the author concludes that the mixture ratio is constant within the limits $1\text{-}4\cdot10^{-3}$ g/kg, which would favor a dry stratosphere. The minimum specific humidity value on the basis of Gutnik's model at the tropopause level is equal to $9\cdot10^{-3}$ g/kg; according to the mid-January and mid-June V. S. Komarov profile it is even greater. Above the tropopause level, the specific humidity increases with altitude rather substantially both in the Gutnik and V. S. Komarov profiles. We note that the humidity measurements which were made recently in the mesosphere at an altitude of 70-80 km, show a considerabl moisture content at these altitudes [17]. The value which the authors [17] obtained for the specific humidity was 1.7 g/kg. The presence of nacreous and noctilucent clouds also point in favor of a humid stratosphere.

TABLE 1.8

MIDMONTH VALUES OF SETTLED WATER IN VARIOUS LAYERS OF THE ATMOSPHERE IN THE VERTICAL DIRECTION [13] FOR THREE STATIONS

a Слои, мб	Ст. Рига · b				Ст. Ташкент c				Ст. Иркутск d			
	январь e		июль f		январь e		июль f		январь e		июль f	
	g см	%	g см	%	g см	%	g см	%	g см	%	g см	%
h Земля — 10 *	0,673		2,334		0,903		2,026		0,442		3,022	
h Земля — 200 *	0,666	99,0	2,300	98,5	0,893	98,8	2,014	99,5	0,414	93,5	2,962	98,0
h Земля — 500 *	0,635	94,0	2,197	94,0	0,842	94,3	1,851	91,4	0,394	89,3	2,772	91,8
200 — 10	0,008	1,0	0,034	0,034	0,010	1,2	0,012	0,5	0,028	6,5	0,061	2,0

*These values were calculated relative to the settled water layer earth 1 - 10 mb

Key: a. layers, mb
b. Riga station
c. Tashkent station
d. Irkutsk station
e. January
f. July
g. cm
h. earth

Nevertheless, at the present time it is still not possible to give an unequivocal answer to the question why there are such considerable discrepancies in the specific humidity data obtained by various authors. It seems to us that to answer the question first of all the measurement errors which occur when various instruments and methods are used must be determined with high reliability. Above all, it is necessary to solve the problem of errors which occur when the humidity is determined with the aid of the mass radiosonding measurement method, since for the time being only this method gives a sufficient amount of data which is necessary for a statistically reliable analysis.

3. Distribution of Ozone in the Atmosphere

Because of the considerable effects of ozone on the radiation processes which take place in the atmosphere, many papers have been devoted to its study, a survey and bibliographies of which can be found in monographs and collected articles [18-21, 557, 560, 562, 865].

We can obtain an idea about the vertical ozone concentration profile from Fig. 1.14, from which we can see that the mid-month ozone concentration at maximum altitudes can change approximately six times as much. Below and above the maximum, the range within which the mid-month ozone changes occur is smaller the farther the given altitude from the maximum layer. The law which was mentioned is valid in various geographical regions, although absolute values of the concentration undergo considerable changes within 24 hours and within one year and do depend on the latitude and longitude of the location.

The fluctuations in the mid-month values of the total ozone content in the atmosphere can be estimated from Table 1.9.

As we see from Table 1.9, the mid-month value of the total ozone content from location to location and from month to month varies between the limits 0.172-0.536 cm, i.e., 3 times as much. The mean yearly values of the total O_3 content fluctuates on a smaller scale (from 0.394 cm to 0.204 cm, or approximately twice as much).

In spite of the large number of ozone concentration measurements in the atmosphere, until now a mean vertical O_3 profile has not been constructed. Various sources give average data for a series of measurements (see, for example, Table 1.10).

TABLE 1.9

MEAN MONTHLY VALUES OF TOTAL OZONE CONTENTS (IN CM) IN SEVERAL STATIONS WHICH PARTICIPATED IN THE INTERNATIONAL GEOPHYSICAL YEAR IN 1958 [21]

№ п/п	Название станции	Координаты: широта	долгота	I	II	III	IV	V	VI	VII	VIII	IX	X	XI	XII	За год
1	Алерт	82°30′ С	62°20′ В	0,259	0,480	0,536	0,470	0,429	0,355	0,331	0,292	0,299	0,320	0,366	0,370	0,376
2	Резольют	74°43′	94°59′ З	0,376	0,502	0,499	0,491	0,419	0,373	0,344	0,306	0,323	0,339	0,427	0,321	0,394
3	Лервик	60°08′	01°11′ З	0,335	0,397	0,408	0,385	0,415	0,358	0,346	0,321	0,289	0,290	0,258	0,266	0,339
4	Оксфорд	51°46′	01°16′ З	0,342	0,353	0,396	0,392	0,398	0,381	0,360	0,337	0,300	0,292	0,284	0,317	0,346
5	Ароза	46°47′	09°41′ В	0,347	0,340	0,394	0,401	0,358	0,352	0,338	0,314	0,292	0,292	0,288	0,308	0,335
6	Эльбрус	43°17′	42°25′ В	0,299	0,320	0,362	0,402	0,345	0,304	0,256	0,228	0,222	0,250	0,241	0,274	0,295
7	Вашингтон	38°51′	77°02′ З	0,330	0,373	0,359	0,367	0,364	0,333	0,313	0,315	0,289	0,295	0,285	0,315	0,328
8	Терисима	30°29′	140°18′ В	0,279	0,292	0,337	0,339	0,329	0,329	0,321	0,300	0,285	0,269	0,246	0,256	0,298
9	Таманрассет	22°48′	05°31′ В	0,172	0,196	0,227	0,258	0,214	0,185	0,173	0,212	0,212	0,213	0,199	0,192	0,204
10	Мауна-Лоа	19°29′	155°36′ З	0,256	0,251	0,270	0,290	0,289	0,284	0,271	0,271	0,268	0,264	0,257	0,253	0,269
11	Кодайканал	10°14′	77°28′ З	0,227	0,224	0,233	0,247	0,240	0,249	0,246	0,244	0,241	0,239	0,237	0,217	0,237
12	Леопольдвиль	4°30′ Ю	15°00′ З	0,257	0,253	0,252	0,245	0,239	0,244	0,245	0,249	0,254	0,245	0,251	0,244	0,248
13	Брисбен	27°28′	153°02′ З	0,285	0,276	0,282	0,289	0,292	0,303	0,314	0,318	0,348	0,329	0,320	0,337	0,308
14	Веллингтон	41°17′	174°46′ З	0,294	0,271	0,261	0,269	0,281	0,319	0,340	0,339	0,370	0,364	0,331	0,289	0,311
15	О. Аргентина	65°15′	64°16′ З	0,295	0,259	0,234	0,251	0,289	0,301	0,278	0,298	0,324	0,300	0,350	0,309	0,291
16	Литл-Америка	78°12′	162°15′ З	0,314	0,310	0,334	0,266	0,380	0,480	0,368	0,536	0,334	0,373	0,420	0,316	0,360

Key: a. Serial number
b. Name of Station
c. Coordinates
d. Latitude
e. Longitude
f. In one year

b. Name of Station

1. Alert
2. Resolute
3. Lerwick
4. Oxford
5. Arosa
6. El'brus
7. Washington
8. Terisima
9. Tamanrasset
10. Maunaloa
11. Kodaikanal
12. Leopoldville
13. Brisbane
14. Wellington
15. O. Argentina
16. Little-America

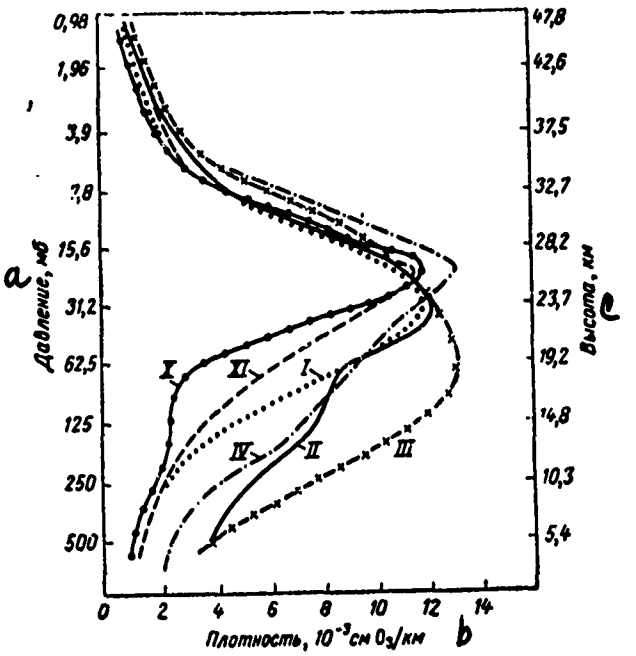

Fig. 1.14. Mid-month vertical ozone profiles for the Arosa Station obtained by Deutsch [22] in 1956-57. The numbers at the curves indicate the serial numbers of the month.

Key: a. pressure, mb
b. density, 10^{-3} cm O_3/km
c. Altitude, km

TABLE 1.10

OZONE CONCENTRATION C IN VARIOUS LAYERS OF THE ATMOSPHERE ACCORDING TO THE DATA OF ARTICLE [23], $C = C_i \cdot 10^{-3}$

H, км a b	0–5	5–10	10–13	13–16	16–18	18–20	20–21	21–23
C_1, см/км b	1,9	4,1	5,8	7,6	11,1	15,6	16,8	17,5
C_2, см/км b	1,6	2,8	3,9	6,1	10,3	14,1	14,3	15,2

H, км a	23–24	26–28	28–40,5	40,5–45,5	45,5–50,5	50,5–55,5
C_1, см/км b	10,8	6,5	1,6	0,3	0,1	0,1
C_2, см/км b	11,3	5,4	1,4	0,3	0,09	0,04

Key: a. km; b. cm/km;

When the visible and infrared radiation in the atmosphere is calculated exactly, both the variations in the total ozone content as well as the distribution of its concentration along the altitude must be taken into account. In particular, this applies to those cases when the calculation is made for spectral intervals in which the radiation is mainly absorbed by O_3. Here, in the first place, we must mention the range of wavelengths 9.0-1.3 mcrm, which is occupied by the ozone absorption band with maximum intensity near the same center of the long-wave atmospheric transmittance window.

4. Distribution of CO_2, O_2, CH_4, N_2O and CO In the Atmosphere

A common feature of all these gases is that the specific concentration is approximately constant at all altitudes, at least in the lower 30-km atmosphere layer. The absolute oxygen concentration does practically not depend on time or location approximately up to an altitude of 90 km.

Many studies were devoted to the study of the CO_2 concentration. At the present time measurements were made above all most characteristic locations on the globe, above oceans, continents, in the Arctic region, in Antarctica, in rural regions and in industrial cities, in mountains and in the open atmosphere. A sufficiently complete summary of the available data which also gives the points where the measurements were made and the mean minimum and maximum values of the CO_2 subconcentration in the atmosphere is given in articles [24-38], which enables us to analyze the problem and draw certain conclusions. This analysis shows that among the measurements of the mean CO_2 concentration values which were made at 64 points in various parts of the world in terms of millionths of the air volume, these values were, in 60 cases, between the limits 280-340. In the remaining 4 cases, the values were equal: 253 (England, at an altitude of 4-10 km), 256 (near Cape Horn, 56° L.N.), 354 (Pacific Ocean) and 650 (London). It is of interest to note that near London the mean concentration is approximately equal to 300.

The maximum deviation of the absolute concentration from its mean value was 46% only in one case (London, maximum concentration 900, minimum concentration 425). It should also be noted that the CO_2 concentration measurements in London were made as early as 1936 [24] and possibly need to be corrected. In Articles [39, 40], as noted in [41], the minimum and

maximum CO_2 concentration values which were obtained were equal respectively to 0.015 and 0.078% of the volume. Taking into account this data, the absolute minimum and maximum CO_2 concentrations in the atmosphere should be considered equal to 0.015 and 0.09% of the volume.

From the analysis of the data available in the literature about the CO_2 concentration in the atmosphere, it follows that the difference between the absolute minimum and maximum concentration attains a large value. However, when infrared radiation absorption by carbon dioxide in the earth's atmosphere is calculated, its concentration can be considered to be constant and equal to 0.03% of the volume, since a large deviation from this value occurs very rarely. Data about the concentrations of small mixtures in the atmosphere, such as methane, nitrogen monoxide (N_2O), and carbon monoxide (CO), were obtained in very few articles. Seeley and Houghton [42] found values for the CH_4, CO and N_2O mixture ratios which were equal to $1.05 \cdot 10^{-6}$, $0.12 \cdot 10^{-6}$ and $0.12 \cdot 10^{-6}$ g/g, respectively. For such values of the mixture ratios, the total content of these gases over the entire thickness of the atmosphere in the vertical direction is equal to 0.84, 0.10 and 0.10 atm/cm.

As noted in [42], these data agree well with the measurement results of the Migeotte Group [43]. Bauman and Shaw [44] obtained two concentrations of these gases in the atmosphere layer near the earth's surface in terms of millionths of the volume: 1.7 ± 0.03 (CH_4), 1.3 (CO); 0.28 ± 0.04 (N_2O). At the same time it must be noted that the CO content fluctuates considerably. The same conclusion is reached in Shaw's article [45], in which the CO content in the entire cover of the atmosphere was found to vary between the limits 0.04-0.13 atm/cm. In article [46] the CH_4 content is determined most precisely in the entire cover of the atmosphere. It turned out to be equal to 1.11 ± 16 apm/cm.

K. P. Vasilevskiy, V. A. Kazbanov and V. A. Boldyrev [866] investigated, with the aid of an automatic balloon high resolution spectrometer, the transmission spectra in the atmosphere in two narrow bands near the wavelengths 3.31 and 3.39 mcrm at altitudes from 0 to 30 km. A treatment of the measurement results made it possible to obtain data about the vertical methane content profiles in the atmosphere (Fig. 1.15).

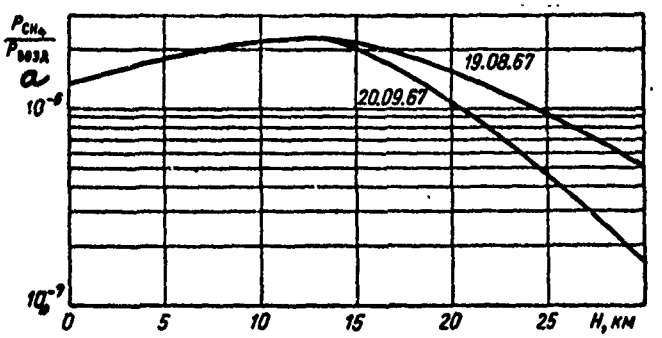

Fig. 1.15. Vertical profile of the ratio of methan pressure to air pressure obtained from two measurements with the aid of an automatic balloon spectrometer [866].

Key: a. P_{air}

The ratio of the mixture for N_2O given in articles [47, 48, 49] turned out to be equal to $0.27 \cdot 10^{-6}$, $0.27 \cdot 10^{-6}$ and $0.05 \cdot 10^{-6}$ g/g, respectively. The differences are explained by the difficulty of interpreting spectroscopic data [42].

Thus, the available data shows that the CH_4, CO and N_2O concentrations in millionths lie between the limits 1.05-1.7, 0.04-1.3, 0.12-0.5, respectively. The improvement of the accuracy of these limits as well as the statistical determination of the mean CH_4, N_2O and CO concentration value in the atmosphere requires corresponding systematic measurements, which, for the time being, are not carried out.

2. Origin and General Characterization of Absorption Spectra of Atmospheric Gases

1. Energy and Spectra of Molecules

In first approximation the energy of an isolated molecule can be represented in the form

$$E = E_{pr} + E_{el} + E_{osc} + E_{rot}, \qquad (2.1)$$

where E_{pr} is the energy of progressive motion which can take on any value, E_{el} is the electron energy, E_{osc} and E_{rot} are the oscillatory and rotary energy. E_{el}, E_{osc} and E_{rot} can take on only discrete values. Thus, they can change only discontinuously, which is accompanied either by absorption or radiation of a light quantum at a definite frequency.

Formula (2.1) holds only for the case when the interactions in the motion of various types of molecules can be ignored. In the general case the energy of the molecule is written as

$$E = E_{pr} + E_{el} + E_{osc} + E_{rot} + E_{el\ osc} + E_{el\ rot} + \\ + E_{osc\ rot}, \qquad (2.2)$$

where the last three terms take into account the interactions between various types of molecular motion.

The magnitudes of the electronic, oscillatory and rotary energy of the molecule have various orders. Thus, the electronic transition energy is on the order of several electrovolts, the oscillation energy is measured in terms of tenths and hundreths of electrovolts and the rotary energy in thousandths and tenths of thousandths of electron volts. According to the energy values, the electronic molecular spectra occupy the ultraviolet and visible part of the spectrum, the oscillation values the near infrared spectrum and the rotation values the distant infrared and microwave spectrum. Since the molecule has both electronic, oscillatory and rotary energy, which, generally during emission or absorption vary simultaneously, the electronic and oscillation spectra do not occur in pure form. Thus, depending on the wavelength band, we are dealing either with electron-oscillation-rotation or oscillation-rotation or with pure rotation molecular spectra. For the sake of brevity, these spectra are often called electronic, oscillation and rotation spectra, respectively.

To each electronic state there corresponds a grid of oscillatory energy levels, which is characterized by a certain value of the oscillatory quantum number v (Fig. 2.1). To each oscillatory level, in turn, there corresponds a series of rotary levels, which is characterized by a certain value of the rotation quantum number j.

Using Fig. 2.1, we can easily see why the electronic and oscillatory transitions in the molecule do not occur in pure form. In fact, in the collection of molecules, we are only dealing with their statistical distribution in terms of the electronic, oscillatory and rotary energy. For each electronic transition in the molecule, the oscillation and rotation energy changes at the same time. The entire set of electronic transitions forms the electron-oscillation-rotation spectrum, in which the line intensities are determined by the molecular distribution over the energy levels and by the probabilities of the corresponding transitions.

The electron-oscillation-rotation spectrum is a set of bands. To each set of molecular transitions between two electronic states, there corresponds an electron band consisting of a set of oscillation-rotation bands.

The number of different oscillation transitions which accompany a change in electronic energy and the number of different rotation transitions which are related to changes in the oscillation energy of the molecule can be very large. This fact is responsible for the very complex structure of molecular spectra. The character of this structure depends on the rules selected for the transition between the energy levels with certain values for the set of quantum numbers. We will discuss the selection rules in greater detail below.

The highest oscillation levels of the lower electronic molecular state can overlap with the lower levels of the adjacent higher electronic state. Analogously the rotation levels of adjacent oscillation states may overlap (this can be clearly seen in Fig. 2.1). Such overlapping of levels lead to the overlapping of corresponding neighboring electronic and oscillation bands, which further complicates the band picture of the molecular spectrum.

In order to understand the spectral structure of molecules of various types. it is useful to consider separately the rotation, oscillation, electronic energy of molecules and their interaction.

2. Rotation Energy and Rotation Spectra of Molecules

A rotating molecule can be considered approximately as a rigid body (rigid gyroscope). The properties of rotating molecules and their rotation spectra depend on the relation between the three principal moments of inertia $\mathcal{J}_a, \mathcal{J}_b$, and $\mathcal{J}_c$, with respect to the three main axes of inertia of the molecule.

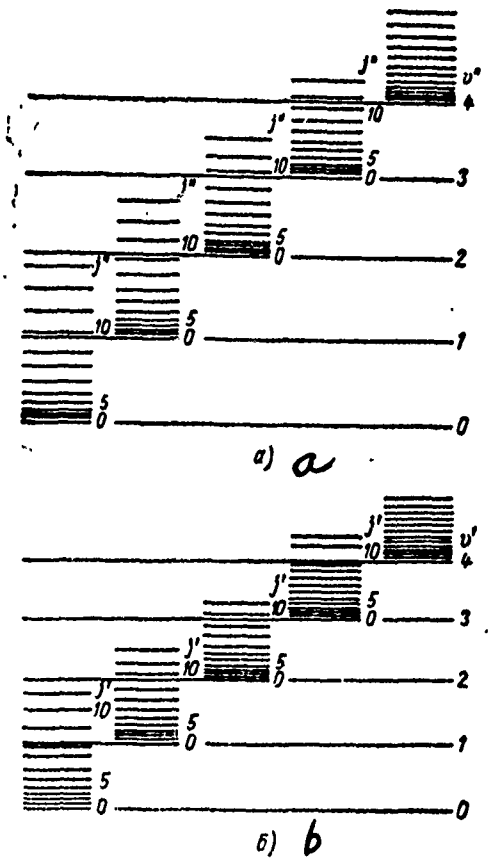

Fig. 2.1. Diagram of oscillation and rotation levels of two electron states (a and b) for the molecule (the time and double time in v and j indicate that the corresponding levels belong to the upper and lower electronic molecular states.

Key: a. a; b. b

According to their rotation properties, all molecules are classified into four groups (Table 2.1).

1. Linear Molecules. The rotation energy of a linear molecule is equal to [51]:

$$E = \frac{\vec{M}_p^2}{2J}, \qquad (2.3)$$

TABLE 2.1

CLASSIFICATION OF MOLECULES BY THEIR ROTARY PROPERTIES

a № п/п	b Моменты инерции	c Типы молекул	d Атмосферные газы, принадлежащие к соответствующим типам молекул
1	$J_a=0\ J_b=J_c\neq\neq 0$	Линейные молекулы	CO_2, N_2O, NO, CO, O_2, N_2
2	$J_a\neq 0\ J_b=J_c\neq\neq 0$	Молекулы типа симметричного волчка	Нет среди распространенных в «планетарном масштабе атмосферных газов
3	$J_a=J_b=J_c$	Молекулы типа сферического волчка	CH_4
4	$J_a\neq J_b\neq J_c$	Молекулы типа асимметричного волчка	H_2O, O_3, HDO

Key: a. Serial number
b. Moment of inertia
c. Types of molecules
d. Atmospheric gases which belong to the corresponding types of molecules

c. Types of molecules

Linear molecules

Molecules of the symmetric gyroscope type

Molecules of the spherical gyroscope type

Molecules of the asymmetric gyroscope type

d. Atmospheric gases which . . .

CO_2, N_2O, NO, CO, O_2, N_2

There are no atmospheric gases among those propagated on the planetary scale

CH_4

H_2O, O_3, HDO

where $\vec{M}_p^2$ is the square of the moment of momentum, $\mathcal{J}$ is the moment of inertia with respect to the axis of rotation which is perpendicular to the axis of the molecule and which passes through the center of gravity of the latter. The quantization $\vec{M}_p^2$ is determined from the formula

$$\vec{M}_p^2 = \hbar^2 j(j+1), \tag{2.4}$$

where $\hbar = \frac{h}{2\pi}$, h is the Planck constant, j is the rotary quantum number which takes on the integer values

$$j = 0, 1, 2, 3, \ldots \tag{2.5}$$

From (2.4) and (2.3) we obtain expression for the quantized rotation energy of the molecule

$$E_j = \frac{\hbar^2}{2\mathcal{J}} j(j+1) = Bj(j+1), \tag{2.6}$$

where the quantity

$$B = \frac{\hbar^2}{2\mathcal{J}} = \frac{2{,}80 \cdot 10^{-39}}{\mathcal{J}} \overset{a}{[см^{-1}]} = \frac{0{,}83 \cdot 10^{-28}}{\mathcal{J}} \overset{b}{[сек^{-1}]} = \frac{0{,}83 \cdot 10^{-34}}{\mathcal{J}} \overset{c}{[Мгц]} \tag{2.7}$$

Key: a. cm^{-1}
b. sec^{-1}
c. MHz

is called the rotation constant.

Table 2.2 gives the values of E_j for various j.

The distance between successive energy levels

$$E_{j+1} - E_j = 2B(j+1) \tag{2.8}$$

TABLE 2.2

VALUE OF THE ROTATION ENERGY E_j FOR VARIOUS VALUES OF THE ROTATION QUANTUM NUMBER j

j	0	1	2	3	4	5	6	7	8	9	10
E_j	0	$2B$	$6B$	$12B$	$20B$	$30B$	$42B$	$56B$	$72B$	$90B$	$110B$

is proportional to the quantity j.

It can be seen from (2.8) and (2.7) that the absolute value of the distance between the rotation energy levels is inversely proportional to the moment of inertia of the molecule. The heavier the molecule and the larger its dimensions, the farther out on the long wave band its rotation center will lie. At the same time with quantizing the square of the moment of momentum $\vec{M}_p^2$, the projection $\vec{M}_p^2$ in the given direction z is quantized

$$M_{pz} = \hbar m_j, \tag{2.9}$$

where m_j is the magnetic quantum number which takes on the $2j + 1$ value:

$$m_j = j, j-1, \ldots, -j. \tag{2.10}$$

The energy of any free molecule is determined by the moment of momentum and does not depend on the projection of this moment, and, consequently, the quantum number m_j. However the set of values of the quantum numbers j and m_j determines completely the rotary movement of the linear molecule with two degrees of freedom for the rotary motion.

As we already have mentioned, for a given j, m_j takes on $2j + 1$ values. Thus, a linear molecule has $2j + 1$ degenerate states for a given j. The statistical weight of the rotation level with a given j is equal to $g_j = 2j + 1$ ($j = 0, 1, 2, \ldots$).

The number of molecules with a given value j during heat balance is determined from the formula

$$n_j = (2j+1)\, n_0 e^{-\frac{\varepsilon_j}{kT}} = (2j+1)\, n_0 e^{-\frac{Bj(j+1)}{kT}}, \qquad (2.11)$$

where n_0 denotes the number of molecules in the state with $j = 0$.

Pure rotation spectra can only have molecules which have a constant dipole moment which is different from zero. Linear molecules may have a constant dipole moment, when the centers of gravity of the positive and negative charges do not coincide. The selection rules solve the pure rotation transitions when

$$\Delta j = \pm 1. \qquad (2.12)$$

(2.12) and (2.8) imply that the frequencies of the possible successive rotation transitions differ by the amount 2B. Thus, a pure rotation spectrum of a linear molecule which is approximated by a rigid gyroscope consists of equidistant lines.

The rigid gyroscope approximation assumes that the states between the molecular cores do not change during the rotation. However, in fact, these distances increase because of the centrifugal expansion, which increases in proportion to the rotation energy and consequently in proportion to the magnitude of the rotation quantum number j. As the distance between the cores increases, the rotation constant B decreases [see (2.7)]. This leads to a decrease in the distance between the lines in the spectrum on the frequency scale.

The quantum mechanics perturbation theory for the case of small centrifugal molecular expansions enables us to obtain the following approximate formula for the rotation energy of the molecule:

$$E_j = Bj(j+1) - D[j(j+1)]^2. \qquad (2.13)$$

The constant D does not exceed the value 10^{-4} B. It need only be taken into account when the values of j are large.

2. Molecules of the Spherical Gyroscope Type. Molecules of the spherical gyroscope type ($\mathcal{J}_a = \mathcal{J}_b = \mathcal{J}_c \neq 0$) are the simplest type of non-linear molecules. The rotation energy levels of these molecules are determined by the same formula as the energy levels of linear molecules [see (2.6)]. But the properties of the rotation levels of these two types of molecules are substantially different. Molecules of the spherical gyroscope type have three degrees of freedom for the rotary movement; hence, to fully describe the rotation levels, three quantum numbers are needed. In addition to the quantum numbers, j and m_j, which characterize the rotary movement, the quantum number k is introduced, which determines the projection value of the moment of momentum onto any axis, which is rigidly connected to the molecule.

The projection of the moment of momentum on the axis which is connected to the molecule, is quantized in the same way as the projection of this moment on a fixed axis. Therefore, the quantum number k, just as the quantum number m_j, takes on $2j + 1$ values for a given j.

The energy of the molecule depends only on the quantum number j. Therefore, the total degree of degeneracy for the rotation levels of a molecule of the spherical gyroscope type which depends on m_j and k turns out to be equal to

$$g_j = (2j+1)^2. \tag{2.14}$$

For each value j the molecule can have $2j + 1$ orientations with respect to the fixed axis which is not connected to the molecule and $2j + 1$ orientations with respect to the axis which moves together with the molecule.

The distribution of molecules with respect to the rotation states has now the form

$$n_j = (2j+1)^2 n_0 e^{-\frac{E_j}{kT}} = (2j+1)^2 n_0 e^{-\frac{Bj(j+1)}{kT}}. \tag{2.15}$$

By comparing (2.15) and (2.11) it follows that the number of molecules of the spherical gyroscope type at high rotation levels (larger than j) will be greater than the number of linear

molecules for the same B and T.

The effect of centrifugal expansion when molecules of the spherical gyroscope type are rotated is taken into account in the same manner as in the case of linear molecules and is determined by the same formula (2.13).

3. Molecules of the Symmetric Gyroscope Type. Among the atmospheric gases which are propagated on the planetary scale there are no gases the molecules of which would belong to this type. Nevertheless this problem must be studied. We will denote by a, b and c the axes with respect to which the principal moments of inertia obey the relation

$$\mathcal{J}_a \leqslant \mathcal{J}_b \leqslant \mathcal{J}_c. \qquad (2.16)$$

The symmetric gyroscope can either be elongated or flattened. For an elongated gyroscope

$$\mathcal{J}_a < \mathcal{J}_b = \mathcal{J}_c. \qquad (2.17)$$

For a flattened gyroscope

$$\mathcal{J}_a = \mathcal{J}_b < \mathcal{J}_c.$$

To each moment of inertia corresponds its own rotational constant (A, B and C):

$$A = \frac{h^2}{8\pi^2 \mathcal{J}_a}; \quad B = \frac{h^2}{8\pi^2 \mathcal{J}_b}; \quad C = \frac{h^2}{8\pi^2 \mathcal{J}_c}. \qquad (2.18)$$

The expression for the rotation energy of a rigid elongated gyroscope has the form

$$E_{jk} = Bj(j+1) + (A-B)k^2; \quad (A > B), \qquad (2.19)$$
$$j = 0, 1, 2, \ldots; \quad k = 0; \pm 1; \pm 2; \ldots; \pm j.$$

In the case of a flattened gyroscope

$$E_{jk}=Bj(j+1)+(C-B)k^2;\ \ (C<B);$$
$$j=0, 1, 2, \ldots;\ \ k=0;\ \pm 1;\ \pm 2;\ \ldots;\ \pm j. \qquad (2.20)$$

The first term in (2.19) and (2.20) coincides in form with the expression for the rotation energy of a linear molecule and a molecule of the spherical gyroscope type [see (2.7)]. The second term depends on the absolute value of the quantum number k, which determines the value of the projection of the moment of momentum on the axis of symmetry of the molecule. If, in the case of a spherical gyroscope, every level with a given j has a degree of degeneracy 2j + 1 relative to the quantum number k, for a molecule of the symmetric gyroscope type it is broken up into j + 1 levels which correspond to the values $|k| = 0, 1, 2, \ldots, j$. Thus, for k it is not necessary to indicate the sign.

The levels of the molecule with given j and k have a degree of degeneracy which is 2(2j + 1), except the level with the value k = 0. In the last case the degree of degeneracy is (2j + 1).

The selection rules for pure rotation transition in molecules of the symmetric gyroscope type allow for transitions which satisfy the conditions

$$\Delta j=\pm 1;\ \ \Delta k=0. \qquad (2.21)$$

From (2.18), (2.19) and (2.20) we obtain for the transition energy of the molecule between the levels with quantum number values j'k and j"k

$$\Delta E=E_{j'k}-E_{j''k}=B[j'(j'+1)-j''(j''+1)]. \qquad (2.22)$$

From (2.22) we have for the transition energy between neighboring levels ($\Delta j = 1$)

$$\Delta E=E_{j+1,k}-E_{jk}=2B(j+1). \qquad (2.23)$$

Thus, as in the case of linear molecules, a pure rotation spectrum of molecules of the symmetrical gyroscope type consists of equidistant lines, while the rotation absorption and emission spectra can have only molecules of the symmetric gyroscope type with a dipole moment which is different from zero.

The effect of centrifugal molecular expansion is taken into account by the following formula for the rotation energy of a molecule of the symmetric gyroscope type:

$$E_{jk} = E_{jk}^{(0)} - D_j j^2 (j+1)^2 - D_{jk} j (j+1) k^2 - D_k k^4, \qquad (2.24)$$

where $E_{jk}^{(0)}$ is the rotation energy of the rigid symmetric gyroscope determined from formulas (2.19) and (2.20), D_j, D_{jk} and D_k are constants which are small relative to B, A and C.

For the possible rotation transitions in the molecule we now obtain from (2.21) and (2.24)

$$\Delta E = E_{j+1,k} - E_{jk} = 2B(j+1) - 4D_j (j+1)^3 - 2D_{jk} (j+1) k^2. \qquad (2.25)$$

It is seen from the last formulas that the rotation spectrum of a real molecule consists of converging lines, where to each value j correspond j + 1 levels determined by the values K = 0, 1, ..., j.

4. Molecules of the Asymmetric Gyroscope Type. For molecules of the asymmetric gyroscope type

$$\mathcal{J}_a < \mathcal{J}_b < \mathcal{J}_c; \quad A > B > C. \qquad (2.26)$$

In contrast to the cases considered, the case of an asymmetric gyroscope cannot be described by simple analytic expressions. To determine the rotation energy with j = 2 and j = 3 we must solve quadratic equations. To determine the energy of the levels with j> 3, we must solve third and fourth degree equations. The corresponding calculations until now have been made up to the value j = 40 [52].

The qualitative picture of the rotation energy levels of a molecule of the asymmetric gyroscope type can be obtained by considering this molecule as an intermediate case between a completely flattened and completely elongated gyroscope.

It is easily seen that the less J_b differs from the J_a or J_c the closer the asymmetric gyroscope will be to the corresponding symmetric gyroscope. To characterize the asymmetry of the gyroscope we introduce the parameter

$$\varkappa = \frac{2B - A - C}{A - C}. \qquad (2.27)$$

For an elongated gyroscope $\varkappa = -1$, for a flattened gyroscope $\varkappa = 1$. For $B = \frac{A+C}{2}$ (most asymmetric gyroscope) $\varkappa = 0$. For example for water molecules, $\varkappa = -0.430$.

For a molecule of the asymmetric gyroscope type, the level with a given j is broken up into 2j + 1 levels, which are denoted by the index τ, which takes on the values

$$\tau = -j, -j+1, \ldots, j-1, j. \qquad (2.28).$$

The levels are situated in the order of increasing energy from j_{-j} to j_{+j} (see, for example, Table 2.3).

The centrifugal expansion of a molecule of the asymmetric gyroscope type causes only the displacement of the energy levels, which can be considerable when the molecules are light and the values of j are large. Taking into account the effect of the centrifugal expansion of molecules on the rotation levels is a rather difficult problem. This problem is solved for various special cases in [53].

The spectra of molecules of the asymmetric gyroscope type are extremely complex. The selection rules allow for transitions with changes in the rotation quantum number

$$\Delta j = 0, \pm 1. \qquad (2.29)$$

Here the Q, R and P branches correspond to the transitions with $\Delta j = 0$, +1 and -1.

TABLE 2.3

ROTATION LEVEL ENERGY OF A WATER MOLECULE (cm^{-1}) [51]

$j=0$	$j=1$	$j=2$	$j=3$	$j=4$
0,0	1_{-1} 23,78	2_{-2} 70,09	3_{-3} 136,76	4_{-4} 222,07
	1_0 37,09	2_{-1} 79,43	3_{-2} 142,23	4_{-3} 224,81
	1_1 42,31	2_0 95,15	3_{-1} 173,31	4_{-2} 275,50
		2_1 134,98	3_0 206,35	4_{-1} 300,44
		2_2 136,24	3_1 212,24	4_0 315,83
			3_2 286,18	4_1 384,03
			3_3 286,93	4_2 385,44
				4_3 490,64
				4_4 490,79

In addition to the selection rules (2.29) for molecules of the asymmetric gyroscope types there are bounds in the transitions which are related to the symmetric properties of the inertial ellipsoid. When the inertial ellipsoid rotates about the rotation axis, the wave function may not change or change sign. In the first case we speak about an even function (we will denote it by e), in the second case about an odd function (we will denote it by o). A rotation of the ellipsoid relative to one of the two axes through a 180° angle is equivalent to a rotation through the same angle relative to the third axis. Thus, it is sufficient if we consider the rotation of the ellipsoid with respect to two axes. The following types of symmetry of the molecule can occur: ee, eo, oe and oo or ++, +-, -+ and --.

Depending on the principal axis along which the dipole moment of the molecule is oriented, we distinguish three types of selection rules: A, B and C. In the first case the dipole moment is oriented along the a-axis, in the second case along the b-axis and in the third case along the c-axis. The dipole moment of a water molecule is directed along the b-axis. In this case the selection rules have the form of type B

$$++\leftrightarrow--\ ^{a}\ +-\leftrightarrow-+. \qquad (2.30)$$

Key: a. and

For the types A and C we have respectively

$$++\leftrightarrow-+\overset{a}{\underset{H}{}}+-\leftrightarrow-- \qquad (2.31)$$

and

$$++\leftrightarrow+-\overset{a}{\underset{H}{}}-+\leftrightarrow--. \qquad (2.32)$$

Key: a. and

If the orientation of the dipole moment does not coincide with the orientation of a principal axis of rotation, then in this case all three selection rules hold.

As in the cases which were considered earlier, pure rotation spectra can only have molecules of the asymmetric gyroscope type which have a constant dipole moment which is different from zero. Among the atmospheric gases such molecules are the molecules of the principal absorption components in the atmosphere (water vapor and ozone). The pure rotation H_2O and O_3 spectra are very complex and have a large number of strong absorption lines which lie in a wide long wave band.

3. Vibration Energy And Vibration-Rotation Spectra of Molecules

1. Molecular Vibration Energy. A molecule consisting of N atoms has 3N degrees of freedom among which it has 3 for the progressive motion of the center of gravity of the molecule as a whole, 3 or 2 for rotary motion. Linear molecules have 2 degrees of freedom for the rotary motion, nonlinear 3 degrees of freedom. Thus, a nonlinear molecule has 3N - 6 degrees of freedom for the oscillatory movement, and in the general case, 3N - 6 different vibration frequencies. A linear molecule has 3N - 5 degrees for the vibration movement and 3N - 5 vibration frequencies. In symmetric molecules certain frequencies coincide because of degeneracy.

The simplest model of the vibration movement of a molecule is the model of a harmonic oscillator. For this model quantum mechanics provides the well-known expression for the vibration energy

$$E_v = h\nu\left(v+\frac{1}{2}\right), \qquad (2.33)$$

where

$$\nu = \frac{1}{2\pi}\sqrt{\frac{k}{M}} \qquad (2.34)$$

is the classical vibration frequency, v is the vibration quantum number which takes on the integer values v = 0, 1, 2, ..., k is the constant of the quasielastic, M is the vibrator mass.

As seen from (2.33), the energy levels of a harmonic oscillator are equidistant. The energy difference between neighboring levels is equal to

$$E_{v+1} - E_v = h\nu. \qquad (2.35).$$

For a harmonic oscillator, the quantum transition frequency between neighboring vibration levels coincides with the classical vibration frequency.

If the vibrations of the molecule are considered as a set of harmonic oscillator vibrations with the frequencies ν_1, ν_2, ν_3, ..., then according to quantum mechanics the vibration energy of the molecule has the form

$$E_v = \left(v_1+\frac{1}{2}\right)h\nu_1 + \left(v_2+\frac{1}{2}\right)h\nu_2 + \left(v_3+\frac{1}{2}\right)h\nu_3 + \ldots, \qquad (2.36)$$

where ν_1, ν_2, ν_3, ..., are the vibration quantum numbers.

The vibration states of molecules are denoted by a set of values of these numbers. For example, the state (001) corresponds to the values $v_1 = 0$, $v_2 = 0$, $V_3 = 1$. The frequencies ν_1, ν_2, ν_3, etc., are usually called the principal or fundamental vibration frequencies.

The selection rules resolve the transitions between the energy levels of a harmonic oscillator, which satisfy the condition

$$\Delta v = \pm 1. \tag{2.37}$$

Further, if the molecule is represented by a set of harmonic oscillators, only one quantum number of a single vibration need be changed.

Thus, the selection rules resolve the transitions between neighboring levels with the same frequency ν [see (2.35)].

The model of a harmonic oscillator oversimplifies the descritpion of real vibrations. Taking into account the anharmonicity of the molecule vibrations leads to second and third order terms in the expression for the energy (2.36). Thus, in the case of a two-atom molecule, we can obtain the following approximate expression for E_v:

$$E_v = \left(v + \tfrac{1}{2}\right) h\nu - \left(v + \tfrac{1}{2}\right)^2 xh\nu, \tag{2.38}$$

where x is the anharmonicity constant.

For an N-atom molecule the expression for the vibration energy, taking into account anharmonicity has the form [54]

$$E(v_1, v_2, \ldots) = \sum_i h\nu_i \left(v_i + \tfrac{1}{2}\right) + \sum_i \sum_k x_{ik} \left(v_i + \tfrac{1}{2}\right)\left(v_k + \tfrac{1}{2}\right) + \ldots, \tag{2.39}$$

where x_{ik} are the anharmonicity and intercoupling constants of individual vibrations.

The anharmonicity of the vibrations reduces the distances of neighboring vibration energy levels of the molecule as the vibration quantum number increases. Instead of a single vibration frequency there is a series of frequencies which decrease in series $v = 0 \rightarrow v = 1$, $v = 1 \rightarrow v = 2$, etc.

The distance between the levels decreases successively as the vibration quantum numbers v_1, v_2, and v_3 increase (Fig. 2.2).

When the anharmonicity vibrations are taken into account the selection rules change considerably. Now transitions are resolved which satisfy the condition

$$\Delta v = 2, 3, 4 \text{ etc.} \qquad (2.40)$$

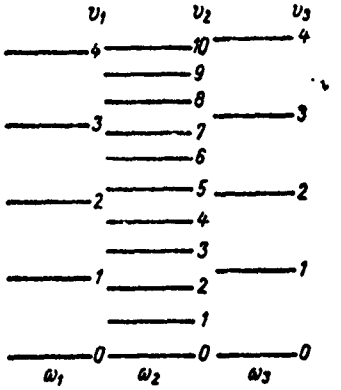

Fig. 2.2. Vibration energy levels of the H_2O molecule

Moreover, transitions are resolved for which two quantum numbers change simultaneously.

Transitions which are characterized by a change in Δv by 2, 3, etc., cause the occurrence of corresponding overtones in the fundamental vibration frequencies. When two or more vibration quantum numbers change at the same time, so-called composite vibration frequencies occur (sums and differences of frequencies). Thus, in a real molecule, the number of vibration frequencies exceeds considerably the number of its fundamental frequencies.

The anharmonicity of the vibrations can cause considerable interaction between the vibrations in the presence of random resonance. Thus, for example, the CO_2 molecule has energy levels which almost coincide $\nu_1 = 1337\ cm^{-1}$ ($v_1 = 1$, $v_2 = 0$, $v_3 = 0$) and $2\nu_2$ ($v_1 = 0$, $v_2 = 2$, $v_3 = 0$). Such random coincidence of the energy levels which belong to the same symmetry class called the Fermi resonance, causes the mutual perturbation of the vibration energy levels which manifest itself in the displacement in opposite directions.

2. Vibration-Rotation Spectra of Molecules. The energy of vibration and rotation molecular quanta have the orders 100-100 cm^{-1} and 1-10 cm^{-1}, respectively. Therefore, if the rotation spectra are observed in pure form, pure vibration spectra can be observed only in special, extremely rare cases. In practice a change in the vibration state of a molecule is always connected with the emission or absorption of energy, and the rotation state also changes. The small energy of rotation quanta in comparison with the vibration energy of the quanta is explained by the fact that the rotation does not disturb the vibration structure of the molecular spectrum. Since to each vibration level corresponds a series of rotation levels, each vibration transition in the collection of molecules is converted into a series of lines or a spectral band. Every line corresponds to the same change in vibration energy and to a definite change in rotation energy.

Thus the spectrum of pure vibration transitions of the molecule must be considered as a skeleton, around the elements of which are grouped the vibration-rotation bands. If we ignore the vibration and rotation interactions of the molecule, then its vibration-rotation spectrum is easily represented as an additive superposition of vibration and rotation transitions, which are resolved by the appropriate selection rules.

We will first consider the character of the vibration structure of the spectra which is the basis for the vibration-rotation bands. The simplest structure occurs in the case of 2-atom molecules. The condition for the occurrence of vibration bands in the spectrum is that the variation in the dipole moment of the molecule be different from zero during the corresponding quantum transition. Two-atom molecules consisting of the same atoms, which consequently have a dipole moment which does not vary during the vibrations and which is equal to zero, cannot have vibration-rotation spectra. The frequencies of such vibrations are said to be optically inactive.

The vibration transition spectrum of a two-atom molecule consisting of different atoms can easily be obtained from fromula (2.38), from which we have from the vibration frequencies ν_k

$$\nu_k = \nu(1-x)(v''-v') - \nu x(v''^2 - v'^2), \qquad (2.41)$$

where v'' and v' are the vibration quantum numbers of the upper and lower molecular states.

It is seen from the last formula that the vibrations spectrum of a two-atom molecule consists of a set of band series. Each band corresponds to a set of molecular transitions from a given vibration level to the neighboring level. We recall that the selection rules for the anharmonic oscillator for which we obtained formula (2.38), resolves the transitions with arbitrary variations in the vibration quantum number. For example, for the series which starts with the zero vibration level (v' = 0), we obtain from (2.41)

$$\nu_k(0, v'') = \nu(1-x)v'' - \nu x v''^2, \tag{2.42}$$

from which we further obtain the following set of vibration transition frequencies and hence vibration-rotation bands:

$$\begin{gathered}\nu_1 = \nu(1-2x); \quad \nu_2 = 2\nu(1-3x); \\ \nu_3 = 3\nu(1-4x); \ \ldots\end{gathered} \tag{2.43}$$

It can be seen from (2.43) that the distance between adjacent lines decreases as v" increases and as the frequency increases. The lines of the series converge to some boundary, which corresponds to the molecular dissociation. All other series have an analogous structure.

Such a picture of vibration-rotation bands (in the form of a set of band series) exists also in the case of multiatom molecules. However, because of the complex configuration of the vibration levels, and the possibility that a large number of vibrations may be induced simultaneously (the fundamental frequencies, overtones, composite frequencies) the structures of individual vibrations overlap and the spectrum obtained is very complex. We will now consider the fine structure of the individual vibration-rotation bands. We can conveniently start with two-atom molecules. The vibration-rotation energy for two levels characterized by the vibration and rotation quantum numbers v", j" and v', j', can be written in the form

$$E'' = E_{v''} + B_{v''} j''(j''+1), \tag{2.44}$$

$$E' = E_{v'} + B_{v'} j'(j'+1), \tag{2.45}$$

where $E_{v''}$ and $E_{v'}$ are determined by formulas of the type (2.38), and the rotation energy is written for simplicity in the form $Bj(j + 1)$.

The interaction between the vibrations and rotation of the molecule is taken into consideration in (2.44) and (2.45) by the rotation constant, which is a function of the vibration quantum number v:

$$B_v = B_e - \alpha\left(v + \frac{1}{2}\right), \tag{2.46}$$

where B_e is the rotation constant of a molecule which does not vibrate, α is a constant which does not exceed several hundredths relative to B_e.

It can be seen from (2.46) that B_v decreases linearly as v increases. This is due to the fact that the distance between the atoms in a vibrating molecule increases, and consequently the moment of inertia also increases, and the constant B_v decreases [see formula (2.7)]. From (2.44) and (2.45) we obtain

$$E'' - E' = E_{v''} - E_{v'} + B_{v''}j''(j''+1) - B_{v'}j'(j'+1). \tag{2.47}$$

The quantity $E_{v''} - E_{v'} = \nu_{00}$ determines the frequency of a pure vibration transition, or the frequency of the so-called zero line which would be obtained if $j'' = j' = 0$. The transition which corresponds to the zero line is not allowed by the selection rules. The position of this line is determined computationally.

Since the first difference in (2.47) is much larger than the second difference, the position of the vibration-rotation band in the spectrum is determined by the zero line.

In contrast to the pure rotation spectra for the transitions determined from formula (2.47), we must consider not only the values $\Delta j = j'' - j' > 0$, but also the values $\Delta j < 0$, and in individual cases also $\Delta j = 0$. Then

when $\Delta j = j'' - j' = +1$ the transitions form an R branch,
when $\Delta j = j'' - j' = 0$ the transitions form a Q branch (2.48)
when $\Delta j = j'' - j' = -1$ the transitions form a P branch

The transitions with $\Delta j = +1$ correspond to frequencies which exceed ν_{00}, the transitions with $\Delta j = -1$ correspond to frequencies less than ν_{00} (Fig. 2.3). Therefore, the branches R and P are called the positive and negative branch, respectively.

The transitions with $\Delta j = 0$ (Q branch) in two-atom molecules are resolved only when the electronic moment of momentum is different from zero (for example in an NO molecule). For the Q branch, we obtain from (2.47) for the transition frequency ν_j

$$\nu_j = \nu_{00} + (B_{v''} - B_{v'}) j(j+1). \qquad (2.49)$$

Since the difference $B_{v''} - B_{v'}$ is very small, the lines of the Q branch lie very close to one another.

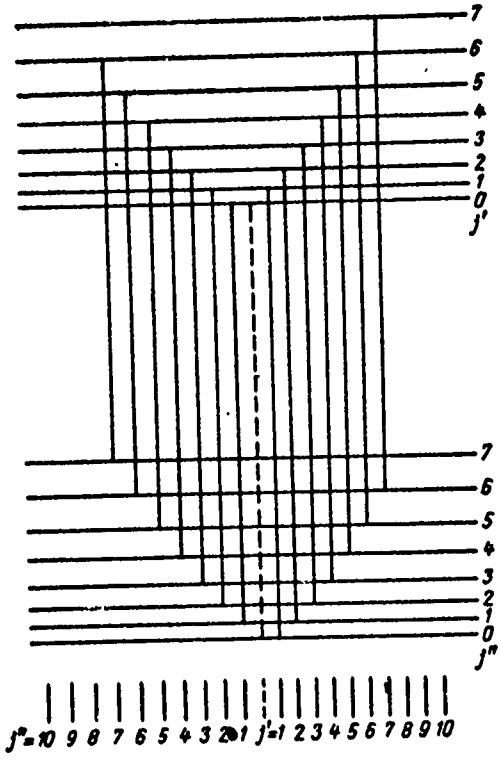

Fig. 2.3. Configuration of energy jumps in the vibration-rotation band

It is customary to divide the infrared absorption bands into parallel (denoted by the symbol $\parallel$) and perpendicular (denoted by the symbol $\perp$) bands. Parallel bands are bands which occur when the direction of the transition dipole moment coincides with the selected molecular axis of symmetry. Perpendicular bands are defined analogously.

We pass on to characterize the fine structure of vibration-rotation molecular bands, which differ in rotation properties (linear, of the spherical, symmetric and asymmetric gyroscope types).

1. Linear Multi-Atom Molecules. The position of the rotary lines in the case of a linear multi-molecule is determined by a formula which is analogous to (2.47), but now the rotation constants depend on all rotation quantum numbers of the molecule:

$$B_{v_1, v_2, \ldots, v_k} = B_e - \sum_i \alpha_i \left(v_i + \frac{1}{2} g_i \right), \qquad (2.50)$$

where g_i is the degeneration multiplicity of the i-th vibration.

For perpendicular bands the selection rules in the case considered resolve the transitions in all three branches (R, Q and P branches). In the case of parallel bands there is no Q branch, and the bands themselves are analogous in structure to the bands of a two-atom molecule, without an electronic moment of momentum. Among the main vibration-rotation bands of linear molecules, both parallel and perpendicular bands are encountered. For bands which correspond to the vibrations in the direction of valent connections between the atoms, the dipole moment is oriented along the molecular axis (parallel bands). The deformation vibrations induce the perpendicular bands. For example, in the case of CO_2, the main bands, (001) with frequency $\nu_3 = 2349.3\ cm^{-1}$ and (010) with frequency $\nu_2 = 667.3\ cm^{-1}$ are the parallel and the perpendicular bands respectively. Among overtones and composite frequencies also both parallel and perpendicular bands occur. We note that the character of the band (parallel or perpendicular) can be determined from the outer form of the band spectrum. In the case of a parallel band, the minimum occurs around the zero line, which is due to the absence of the Q branch. For a perpendicular band the maximum occurs in the neighborhood of the zero line, which is due to the Q branch.

2. Molecules of the Spherical Gyroscope Type. In the case of molecules of the spherical gyroscope type, the position of the rotary lines in the vibration-rotation band are determined by the same type of formula as in the case of linear molecules. The absorption band consists of R, Q and P branches. The interaction of the molecular vibration and rotation movements causes the breakup of vibrations which degenerated three times.

3. Molecules of the Symmetric Gyroscope Type. Molecules of the symmetric gyroscope type as well as linear molecules have both parallel and perpendicular bands, for which different selection rules are available. The character of the vibration-rotation spectrum is more complex than in linear molecules and molecules of the spherical gyroscope type, in particular, if the direction of the dipole moment does not coincide with the molecular axis. Among atmospheric gases there are no molecules of the symmetric gyroscope type; hence, we will not discuss in greater detail the characteristic of the fine structure of these molecules.

4. Molecules of the Asymmetric Gyroscope Type. Molecules of this type have the most complex rotation and, consequently, vibration-rotation spectra. The dependence of the rotation constants A, B and C on the vibration quantum numbers has a character which is analogous to (2.50). In the special case of a three-atom molecule

$$\begin{aligned} A &= A_e - \alpha_{A_1}\left(v_1+\tfrac{1}{2}\right) - \alpha_{A_2}\left(v_2+\tfrac{1}{2}\right) - \alpha_{A_3}\left(v_3+\tfrac{1}{2}\right), \\ B &= B_e - \alpha_{B_1}\left(v_1+\tfrac{1}{2}\right) - \alpha_{B_2}\left(v_2+\tfrac{1}{2}\right) - \alpha_{B_3}\left(v_3+\tfrac{1}{2}\right), \\ C &= C_e - \alpha_{C_1}\left(v_1+\tfrac{1}{2}\right) - \alpha_{C_2}\left(v_2+\tfrac{1}{2}\right) - \alpha_{C_3}\left(v_3+\tfrac{1}{2}\right). \end{aligned} \qquad (2.51)$$

The constants α can be expressed in terms of the anharmonicity constants.

The selection rules for transitions in the molecules under consideration depend on the axes along which the dipole transition moment is oriented. In the general case we obtain three types of bands: type A, type B and type C (the dipole moment is oriented respectively along the a-axis, b-axis, and c-axis). In the case of a symmetric three-atom molecule XY_2, the dipole moment is oriented either along the molecular axis of symmetry

or along the axis which is perpendicular to it and which lies in the plane of the molecule. In the process, perpendicular and parallel bands may arise. For the special case of a water molecule, the molecular axis coincides with the axis of the central moment of inertia, parallel bands belong to type B, and perpendicular bands to type A. Most H_2O bands are perpendicular.

The interaction between the vibration and rotation movements of the molecules have an important effect on the nature of the vibration-rotation structure of molecular bands of all types and on the position of individual lines, their form and intensity. To solve exactly the problem of the position of the lines of the fine structure the anharmonicity of the vibrations, the centifugal molecular expansion, the resonance perturbation of energy levels and the effects of Coriolis forces must be taken into account. Taking into account correctly all these effects is a very difficult and complex problem.

4. Electronic Energy And Electronic Spectra of Molecules

The systematics of molecular electronic energy levels and the selection rules for electronic transition are rather complex. Keeping this in mind, and also taking into account that in the visible and infrared electromagnetic wave region which interests us, all atmospheric gases except oxygen do not have electronic spectra; we do not consider it useful to study in detail the problem of electronic energy and electronic molecular spectra. With regard to the oxygen absorption spectrum in the visible regions, a description will be given later.

We note that in spite of the great complexity of calculating quantitatively the electronic-vibration-rotation spectrum, it must be considered as the most promising way of investigating correctly the vibration-rotation spectra. This problem will be discussed in greater detail in the next chapter.

5. Form of a Spectral Line

When we considered the transitions between the discrete molecular energy levels, we assumed that the absorption or emission processes associated with these transitions are fully characterized by certain frequencies. The spectra which were obtained as a result of these transitions were assumed to consist of individual monochromatic lines. However, in fact, for a number of reasons we are never dealing with strictly

monochromatic lines. Real lines have a shape which is completely determined, the form of which depends on conditions under which the light is absorbed or emitted by the molecules.

Under the earth's atmospheric conditions the form of the spectral line contour is mainly determined by the action of the following three effects: 1) radiation damping, 2) Doppler effects and 3) molecular collision effects.

1. Natural broadening of the spectral line. The transition of a molecule from a particular quantum energy state into another occurs in a finite time interval. This results in the vibration process which accompanies this transition in being an infinite set of frequencies in a particular spectral interval, which follows from classical emission theory. The width of this interval depends on the time at which the molecule is in an excited state. If, during the absorption or emission by molecules with a definite frequency, they are not subjected to any external effects, the emission (absorption) intensity distributions obtained by frequencies will be the natural contour of the spectral line. Quantum mechanics gives the following expression for this contour (Fig. 2.4, curve 2):

$$k(\nu)=\frac{1}{\pi}\frac{\gamma_N}{(\nu-\nu_0)^2+\gamma_N^2}, \qquad (2.52)$$

where

$$\gamma_N=\frac{1}{2\pi\tau} \qquad (2.53)$$

is the so-called natural width of the line, ν_0 is the frequency at the center of the line, or the transition frequency for the hypothetical case which corresponds to the time when the molecule is in an excited state, $\tau = \infty$.

By the width of a line we will mean the spectral interval between the points of the contour ν_1, ν_2 which satisfies the condition

$$k(\nu_1)=k(\nu_2)=\frac{1}{2}k(\nu_0). \qquad (2.54)$$

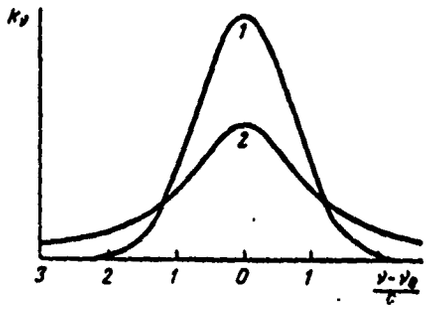

Fig. 2.4. The form of line contours induced by broadening due to the Doppler effect (1) and the collision effect, or the radiation damping effect (2), when the intensities and width of the lines are equal

Expression (2.52) is often called the dispersion or Lorentz contour. We note that usually when we talk about the dispersion contour, we have in mind the contour of the line which is obtained when the collision effect is studied.

The quantity γ_N is very small for atmospheric gases. In fact, the most probable value of τ for vibration and rotation molecular transitions in atmospheric gases is on the order of 0.1 sec. For such a value of τ the quantity $\gamma_N = 3 \cdot 10^{-11} \text{cm}^{-1}$ [3]. This value is negligibly small in comparison to the width of the line induced both by the Doppler effect and the collision effects. Therefore, in visible and infrared wave propagation problems in the atmosphere the natural broadening of the spectral lines is not taken into account.

2. Broadening of the spectral line due to the Doppler Effect

Assuming the validity of thermodynamic equilibrium for successive degrees of freedom of the molecule when the Maxwell molecular velocity distribution holds for the contour of the spectral line (Fig. 2.4, curve 1) in which widening is induced only by the Doppler effect, we obtain the following expression:

$$k(\nu) = \frac{S}{\sqrt{\pi}\alpha_D} \exp\left[-\left(\frac{\nu-\nu_0}{\alpha_D}\right)^2\right], \qquad (2.55)$$

where S is the intensity of the line, which will be determined in the next paragraph,

$$\alpha_D = \frac{\nu_0}{c}\sqrt{\frac{2kT\ln 2}{m}} \qquad (2.56)$$

is the Doppler half-width of the line; T is the absolute temperature, m is the molecular mass; c is the velocity of light; k is the Boltzman constant.

It can be seen from (2.56) that α_D is a function of ν_0, m and T. The temperature in the lower part of the atmosphere (troposphere and stratosphere) varies on the average by not more than a factor of 1.5. Thus, for a given spectral line (ν_0 = const, m = const) α_D can vary, as the temperature varies, approximately within the limits $\pm$ 15% of the mean value, which corresponds to the mean temperature.

Two extreme values of B are given in [3] for the atmospheric conditions when T = 300° K:

1) For the forbidden atomic oxygen line with wavelengths about 5577 Å

$$\alpha_D = 3{,}3\cdot 10^{-2}\ c_M^{-1},$$ Key: a. cm^{-1}

2) For the H_2O line of the rotation band, about 200 cm^{-1}

$$\alpha_D = 3{,}5\cdot 10^{-4}\ c_M^{-1}.$$ Key: a. cm^{-1}

3. Broadening of Spectral Lines Due to Molecular Collisions.

The interaction of a light absorbing or emitting molecule with the neighboring molecules leads to the deformation of the energy levels and the related broadening of the spectral lines. It is clear that this interaction must depend on pressure. Therefore, the effect considered is often called the broadening effect due to pressure or the collision effect. If these absorption or emission processes take place in a pure gas, we sometimes speak of the self-broadening effect of the lines.

An exact solution of the problem dealing with the effect of molecular collisions on the broadening of spectral lines, taking into account all characteristics of the collisions has, so far, not been obtained. In all cases only double molecular collisions are considered and those where the interacting molecular forces have a complex character are described by the interaction models dipole-dipole, dipole-quadrupole, dipole-induced-dipole.

Depending on the value of the phase shift in the molecular absorption or emission process caused by the collision with another molecule, we distinguish weak and strong collisions. The collisions studied in kinetic theory belong to the strong type. The first theories of broadening spectral lines during molecular collisions took only into account strong collisions. Among these theories we first mention the Lorentz theory [55] which he developed as early as 1906. The results of this theory are still widely used.

According to the theory of strong collisions, the center of a spectral line is not displaced when the colliding molecules interact. In contrast during weak collisions, the center of the line is displaced. Under real conditions only strong and weak collisions occur. Applied to atmospheric conditions (the pressure $P < 1$ atm) in the visible and infrared regions of the spectrum the contours of the lines which are obtained from the theory of strong collisions describe satisfactorily the central part of the spectral lines, the centers of which are not displaced when the pressure changes.

From the standpoint of quantum mechanics, when the colliding molecules interact, the energy jump can occur in both molecules. It is customary to call the collisions which are accompanied by energy jumps nonadiabatic collisions. By adiabatic collisions are meant those collisions for which only the energy of the levels changes. Given this collision classification, the weak collision can be considered as adiabatic collisions.

From qualitative considerations it follows that the theory of nonadiabatic collisions describes best the cases where the probabilities of the jumps are large. On the other hand, the theory of adiabatic collisions is more suitable for describing transitions with small probabilities. For atmospheric conditions in the infrared region, the transition probabilities of the molecules are large; hence, here the theory of nonadiabatic collisions is preferable. An example of a widely used theory for calculations from this class is the Anderson theory.

In addition to the classifications of the theories of spectral line broadening due to pressure, we should also note that all theories are divided into shock theories and statistical theories. In shock theories it is assumed that the duration of the collisions between the molecules is negligibly small compared to the time between collisions. In statistical theories we study the distribution of the energy levels of the molecule at rest, which was caused by its interaction with all other molecules.

Since the most widely used theory which describes the broadening effect of spectral lines due to molecular collisions in atmospheric gases in the visible and infrared regions are the Lorentz and Anderson theories, we will only give the results of these theories.

The Lorentz theory for the contour of the spectral absorption line gives the well-known expression:

$$k(\nu)=\frac{S}{\pi}\frac{\gamma_L}{(\nu-\nu_0)^2+\gamma_L^2}, \tag{2.57}$$

which is often called in the literature the dispersion contour, or the Lorentz contour. In (2.57), S is the line intensity, ν_0 is the position of the line center and

$$\gamma_L=\frac{1}{4\pi\tau(v)} \tag{2.58}$$

is the halfwidth of the line.

Here $\tau(v)$ is the excited state lifetime of the absorbing or emitting molecule, which depends on its velocity v.

To find γ_L, we must take into account the relation $\tau(v)$. Usually γ_L is found as the width of the line which corresponds to the mean value $\tau(v) = \bar{\tau}$. In this case we obtain from the kinetic theory of gases the expression

$$\gamma_L=\frac{1}{2\pi\tau}=\sum_i n_i\sigma_i^2\left[\frac{2kT}{\pi}\left(\frac{1}{m}+\frac{1}{m_i}\right)\right]^{1/2}, \tag{2.59}$$

where n_i is the molecular concentration of the i-th type, σ_i is the effective distance between the emitting or absorbing molecule and the molecule of the i-th type, m and m_i are the masses of the aforementioned molecules. By an effective distance we mean such distance for which the molecular interaction effect leads to a widening of the spectral line.

In any gas mixture the molecular concentration n_i is proportional to the pressure. Thus, it follows from (2.59), that the width of the line is proportional to the pressure. Since the pressure under atmospheric conditions varies within wide limits, the relation between γ_L and P is very important. The relation between γ_L and σ is also very important since the quantity σ depends not only on the type of the colliding molecular pair, but also on the molecular energy level, or the rotation quantum number j. With regard to the dependence of α_L on the temperature, it is rather weak. In the study of many visible and infrared wave propagation problems in the atmosphere, it can be ignored. In the subsequent discussion we will often refer to the question of the dependence of γ_L on various quantities.

For the case of a two-component mixture for γ_L we obtain the simpler expression

$$\gamma_L = \frac{1}{4}\left\{2\pi kT\left[N_a D_{aa}^2\left(\frac{2}{m_a}\right)^{1/2} + N_b D_{ab}^2\left(\frac{1}{m_a}+\frac{1}{m_b}\right)^{1/2}\right]\right\}^{1/2}, \qquad (2.60)$$

where the subscripts a and b refer to the absorbing and non-absorbing molecules, N_a and N_b are the number of molecules a and b per unit volume, D_{aa} and D_{ab} are the sums of the optical collision diameters between the molecules a ↔ a and a ↔ b, m_a and m_b are the masses of the molecules.

Often, for a two-component mixture, γ_L is written in an even simpler form:

$$\gamma_L = \gamma_L^0 \frac{P}{P_0}\sqrt{\frac{T_0}{T}}, \qquad (2.61)$$

where γ_L^0 is the halfwidth of the line under standard conditions (P_0 = 1 apm, T_0 = 273°K).

The theory of broadening spectral lines due to pressure, which was developed in 1949 by Anderson [56], is a quantum mechanics nonadiabatic theory of molecular spectra. According to this theory, it is assumed that the transitions can take place in both colliding molecules. The initial formula taken for γ_L is the formula for shock theory (2.59); however, the effective distances or optical collision diameters are determined taking into account possible energy jumps in the colliding molecules. For γ_L we obtain the following expression:

$$\gamma_L^{ij} = \sum_{j_2} \left[\frac{2kT}{\pi}\left(\frac{1}{m}+\frac{1}{m_0}\right)\right]^{1/2} n(j_2)\,\sigma^2(i, j, j_2), \qquad (2.62)$$

where $n(j_2)$ is the perturbed molecular concentration

$$\sigma(i, j, j_2) = \sum_{j_2', i'} \sigma(i, i'; j_2, j_2'; j) + \sum_{j_2', j'} \sigma(i; j_2, j_2'; j, j'); \qquad (2.63)$$

i, i', j, j', are indices, which characterize the state of the absorbing molecule for which the transition i → j takes place without interaction with the perturbing molecule, j_2 and j_2' are indices which characterize the state of the perturbing molecule. The colliding molecules cause the transitions i → i' and j → j' in the absorbing molecule and $j_2 \rightarrow j_2'$ in the perturbing molecule.

Using Anderson's theory, Benedict and Kaplan [57, 58] carried out a detailed calculation of the halfwidth of the lines in a pure water vapor rotation spectrum, when its molecules coincided with nitrogen and oxygen molecules. The results of the calculations have shown that the value of γ_L for the colliding H_2O - N_2 molecules varied from line to line between the limits 0.03 to 0.1 cm^{-1} at a pressure of P = 1 atm. The more detailed data obtained in [57] and [58] will be considered in the next chapter.

4. The Joint Action of the Doppler and Molecular Collision Effect. Under real conditions the Doppler effect and the effects of colliding molecules act simultaneously. However, their role differs considerably at different altitudes, since the widening of the lines due to the Doppler effect is independent of pressure. Maximum widening due to molecular collisions occurs in the layer near the earth's surface and decreases with the altitude proportionally with the decrease in pressure. In the layer near the earth the Doppler width of the line is negligibly small compared to the halfwidth induced by the effects of colliding molecules. The width of each spectral line induced by collision effects at a definite altitude in the atmosphere becomes equal to the Doppler width. As the altitude further increases, the Doppler width becomes increasingly larger in comparison with the dispersion width.

If we take for γ_L the most probable value 0.08 cm^{-1} for atmospheric gases under standard conditions, the altitudes at which $\gamma_L = \gamma_D$ for the extreme values $\gamma_D = 3.3 \cdot 10^{-2}$ cm^{-1} and $3.5 \cdot 10^{-3}$ cm^{-1} (see para. 2 in this section) turn out to be equal to 7 and 37 km. For narrower dispersion lines these altitudes will be correspondingly lower and vice versa. As we have seen from the estimates which were given, taking into account the joint effect in the broadening of spectral lines, may become necessary, in individual cases, already starting with the upper troposphere layers.

The joint study of the two effects on the broadening of spectral lines leads to the following expression for the absorption coefficient:

$$k(\nu) = \frac{k_0 y}{\pi} \int_{-\infty}^{\infty} \frac{e^{-t^2}}{y^2 + (x-t)^2} dt, \qquad (2.64)$$

where

$$k_0 = \frac{S}{\gamma_D} \left(\frac{\ln 2}{\pi} \right)^{1/2};$$
$$y = \frac{\gamma_L}{\gamma_D} (\ln 2)^{1/2}; \quad x = \frac{\nu - \nu_0}{\gamma_D} (\ln 2)^{1/2}, \qquad (2.65)$$

S is the line intensity, and ν_0 is the center of the line.

5. The Form of the Tails of the Lines. It can be seen from Fig. 2.4 that at the tails the Doppler contour of the line drops considerably faster than the dispersion contour. This means that the far tails of the lines in the case of the joint Doppler and molecular collision effect must be dispersion contours. However, the problem whether the dispersion contour describes correctly the far tails of the lines cannot be considered to be solved. If we start out with the qualitative concepts which underlie the assumptions made in various theories for the broadening of spectral lines due to pressure, we should expect that the form of the far tails of the lines can be better described by statistical rather than shock theories. At the present time not enough experimental data is available to make definite conclusions in favor of either theory for the tails of the lines. The available results indicate that the form of the far tails can be different for different molecules.

6. Intensity of a Spectral Line

The spectral line intensity S is written in terms of the absorption coefficient $k(\nu)$:

$$S = \int_0^\infty k(\nu)\, d\nu. \tag{2.66}$$

Quantum mechanics gives for the intensity of a single molecular transition from the state with index j into the state characterized by the index i the following expression [3]:

$$S_{i,j} = \frac{n_j}{g_i n} \frac{8\pi^3 \nu_{i,j} |R_{i,j}|^2}{3hc} (1 - e^{-h\nu_{i,j}/kT}), \tag{2.67}$$

where n_j is the molecular concentration in the lower state, n is the concentration of all molecules, g_i is a statistical weight, $\nu_{i,j}$ is the transition frequency, $|R_{i,j}|^2$ is the square of the dipole moment matrix element, T is absolute temperature, h, k and c are the Planck, Boltzman constants and the velocity of light.

The matrix element of the dipole moment $\vec{M}$ is expressed in terms of the wavestate functions of the molecule ψ_i and ψ_j:

$$R_{i,j} = \int \psi_i^* \vec{M} \psi_j \, dv. \tag{2.68}$$

In (2.68) the integration is carried out over the entire configuration space, and dv is an element of this space. The wave functions are obtained from the solution of the Schrödinger equation.

The wave functions satisfy the orthogonality condition

$$\int \psi_i^* \psi_j \, dv = 0 \, (i \neq j). \tag{2.69}$$

From (2.69) and (2.68) when $\vec{M}$ = const, we obtain

$$\vec{M} \int \psi_i^* \psi_j \, dv = 0. \tag{2.70}$$

The last relation is the basis for the proposition which we used earlier, namely that the transition of a molecule from one energy state into another during dipole emission occurs only when the dipole moment changes. We note that light emission or absorption may occur not only during the dipole interaction of the electromagnetic field with the particle. When the magnetic dipole or electrical quadrupole of the molecule changes, which accompanies the energy jump, spectral lines also appear. However, the intensity of these lines is very small. The transitions which are related to the changes in the electrical dipole moment of the molecule yield a line intensity which is greater on the order of 10^5 and 10^8 than in cases when the magnetic dipole and electric quadrupole moments change.

The matrix elements $R_{i,j}$ are related to the well-known Einstein coefficients $A_{i,j}$, which characterize the probability of a forced emission and absorption between the molecular levels with the subscript i and j:

$$A_{i,j} = \frac{64\pi^4 \nu_{i,j}^3}{3hg_i c^3} |R_{i,j}|^2. \tag{2.71}$$

We note that for electrical dipole emission the quantity $A_{i,j}$ is on the order of 10^8, 10 and 1 sec^{-1} for electronic, vibration and rotation emissions, respectively.

The most difficult problem in determining the line intensities is finding the squares $|R_{i,j}|^2$ of the matrix elements.

7. General Characterization of Absorption Spectra of Atmospheric Gases

We first note that we are interested in atmospheric gas absorption spectra in the visible and infrared regions. We will consider both the spectra of the principal absorbing gases (water vapor, carbonic acid, ozone) as well as the spectra of gases, the contribution of which to the total absorption in the visible and infrared emission in the atmosphere is less important, in some cases due to the relative smallness of the absorption coefficient (oxygen), and in other cases due to the low concentration (methane, carbon monoxide, nitrous oxide).

The main component of the atmosphere, nitrogen, has absorption bands only in the far ultraviolet region.

The general picture of the absorption spectrum of the earth's atmosphere is represented in Fig. 2.5 which is taken from [3].

We will now consider the absorption spectra of the individual components in the atmosphere.

1. Water Vapor. A water molecule is an isosceles triangle with the oxygen atom at its vertex (Fig. 2.6). The angle ϑ between the bonds O–H is equal to 104°30'. The distance between the oxygen and hydrogen atoms is 0.958 Å. The electronic jumps in the H_2O molecule occur in the region with wavelengths less than 1860 Å (the distant ultraviolet region).

The vibration-rotation water vapor absorption spectrum is exceptionally complex. This is primarily explained by the fact that the moments of inertia of the molecule relative to the three principal axes of the inertial ellipsoid differ considerably (they are equal to $\mathcal{J}_a = 1{,}004 \cdot 10^{-40}$; $\mathcal{J}_b = 1{,}929 \cdot 10^{-40}$; $\mathcal{J}_c = 3{,}014 \cdot 10^{-40}$ g·cm²). In this case the rotation structure of these spectra of molecules of the asymmetric gyroscope type turns out to be chaotic and complex. Fig. 2.6 shows the axes a, b and c, with respect to which the moment of inertia $\mathcal{J}_a$, $\mathcal{J}_b$, $\mathcal{J}_c$ of the H_2O molecule

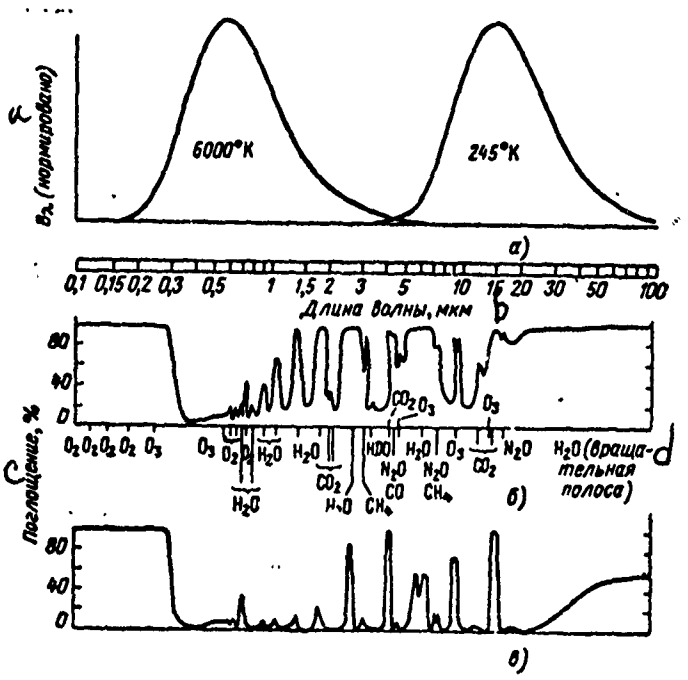

Fig. 2.5. General picture of atmospheric gas absorption spectrum

a. emission curves of absolute black body at temperatures 6000 and 245°K; b. absorption spectrum of solar radiation reaching the surface of the earth; c. spectrum of solar radiation reaching a height of 11 km (the spectra b and c were obtained for medium widths for a zenith distance of the sum of 40° under the most probable conditions.

Key: a. normalized
b. wavelength, μ
c. absorption
d. H_2O (rotation band)

are defined. The absolute values of the moments of inertia are not large, since the molecule contains two hydrogen atoms. Therefore, the distance between the rotary lines is large.

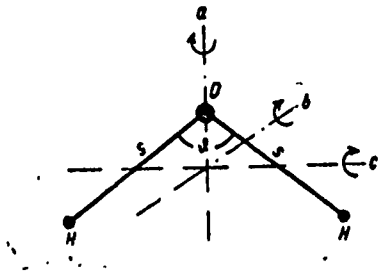

Fig. 2.6. Structural diagram of H_2O molecule

The large values of dipole moments in the H_2O molecule and its isotopes is the reason for the intense rotation spectrum. The dipole moment M of the H_2O molecule and its isotopes are equal to : M_b = 1.94D for H_2O, M_b = 1.87D for D_2O, M_a = 0.64D and M_b = 1.70D for HDO.

In the solar spectrum the lines of the following four water isotopes have been discovered: H_2O^{16}, H_2O^{18}, H_2O^{17} and HDO^{16}, which are present in the atmosphere in the proportions 99.73, 0.2039, 0.0373 and 0.0298. The rotation and vibration constants of the first three isotopes differ slightly. The lines of the H_2O^{18} molecule are shifted relative to the corresponding H_2O^{16} lines by 1 to 11 cm^{-1}. For the H_2O^{17} molecule this shift is twice as large [3]. The rotation constants for the H_2O^{16} and HDO^{16} molecule are given in Table 2.4.

TABLE 2.4

ROTATION CONSTANTS OF THE HHO^{16} AND HDO^{16} MOLECULES IN THE FUNDAMENTAL STATE (cm^{-1}) [3]

Ось a	HHO16	HDO16
a	27,79	23,38
b	14,51	9,06
c	9,29	6,38

Key: a. axis

The pure rotation absorption spectrum of water vapor occupies a very wide region approximately from 8 μ up to several centimeters of the wavelength.

Beside the three fundamental vibration-rotation bands, the origin of which is induced by the fundamental vibrations with frequencies ν_1, ν_2 and ν_3 (Table 2.5), a large number of overtone bands and combined frequencies in the visible and infrared regions are found in the vibration-rotation H_2O spectrum (Table 2.6, 2.7).

TABLE 2.5

FUNDAMENTAL BAND FREQUENCIES OF THE H_2O MOLECULE [3]

a Полоса	b Переход	c Центр полосы, см⁻¹	
		HHO^{18}	HDO^{18}
ν_1	000—100	3657,05	2723,66
ν_2	000—010	1594,78	1403,3
ν_3	000—001	3755,92	3707,47

Key: a. band
b. transition
c. band center, cm^{-1}

Fig. 2.7 gives the configuration of the fundamental molecular vibrations which induce the frequencies ν_1, ν_2 and ν_3.

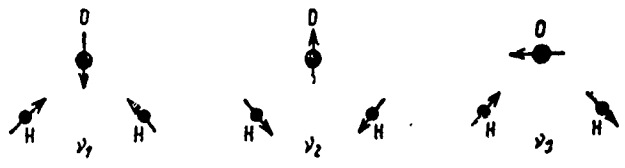

Fig. 2.7. Diagram of fundamental vibrations for the H_2O molecule

TABLE 2.6

H_2O BANDS IN THE VISIBLE REGION OF THE SPECTRUM [3]

a Переход	Центр полосы b		c Тип	d Интенсивность, см
	см$^{-1}$ e	мкм f		
000—411	18 394	0,54	*A*	$2 \cdot 10^{-23}$
000—203	17 495	0,57	*A*	$1 \cdot 10^{-22}$
000—401	16 899	0,59	*A*	$3 \cdot 10^{-23}$
000—302	16 898	0,59	*B*	$3 \cdot 10^{-23}$
000—321	16 822	0,59	*A*	$2 \cdot 10^{-23}$
000—113	15 832	0,63	*A*	$2 \cdot 10^{-23}$
000—311	15 348	0,66	*A*	$2 \cdot 10^{-23}$
000—103	14 319	0,69	*A*	$1 \cdot 10^{-21}$
000—400	14 221	0,70	*B*	$1 \cdot 10^{-23}$
000—301	13 831	0,72	*A*	$3 \cdot 10^{-21}$
000—202	13 828	0,72	*B*	$2 \cdot 10^{-23}$
000—221	13 653	0,73	*A*	$6 \cdot 10^{-21}$
000—013	12 565	0,79	*A*	$1 \cdot 10^{-23}$
000—112	12 408	0,81	*B*	$6 \cdot 10^{-21}$
000—211	12 151	0,82	*A*	$6 \cdot 10^{-23}$
000—210	12 140	0,82	*B*	$1 \cdot 10^{-23}$
000—131	11 813	0,85	*A*	$2 \cdot 10^{-21}$

Key: a. transition
b. band center
c. type
d. intensity, cm
e. cm^{-1}
f. μ

The deformation vibration ν_2 has the lowest frequency. The molecular transitions associated with the fundamental frequencies ν_1 and ν_3 for overlapping bands, in the region of which lies the first overtone of band ν_2. The overlap of the bands ν_1, ν_3 and $2\nu_2$ causes a complex interaction between the corresponding energy levels.

TABLE 2.7

H_2O BANDS IN THE NEAR INFRARED REGION OF THE SPECTRUM [3]

a Полоса	b Переход	Центр полосы c		d Тип	e Интенсивность, см
		$см^{-1}$ f	мкм g		
ρ	000—003	11 032	0,91	*A*	$2 \cdot 10^{-21}$
	000—102	10 869	0,92	*B*	$4 \cdot 10^{-22}$
σ	000—201	10 613	0,94	*A*	$1 \cdot 10^{-20}$
	000—300	10 600	0,94	*B*	$6 \cdot 10^{-22}$
τ	000—121	10 329	0,97	*A*	$2 \cdot 10^{-21}$
	000—220	10 284	0,97	*B*	$< 4 \cdot 10^{-23}$
	000—041	9 834	1,01	*A*	$6 \cdot 10^{-23}$
φ	000—012	9 000	1,11	*B*	$3 \cdot 10^{-29}$
	000—121	8 807	1,13	*A*	$8 \cdot 10^{-21}$
	000—210	8 762	1,14	*B*	$1 \cdot 10^{-23}$
	000—130	8 274	1,20	*B*	$7 \cdot 10^{-24}$
	000—031	8 374	1,19	*A*	$3 \cdot 10^{-23}$
ψ	000—002	7 445	1,34	*B*	$1 \cdot 10^{-21}$
	000—101	7 250	1,37	*A*	$1{,}5 \cdot 10^{-19}$
	000—200	7 201	1,38	*B*	$1{,}5 \cdot 10^{-20}$
	000—021	6 871	1,45	*A*	$1 \cdot 10^{-20}$
	000—120	6 775	1,47	*B*	$2 \cdot 10^{-22}$
Ω	000—011	5 331	1,87	*A*	$2{,}2 \cdot 10^{-19}$
	000—110	5 235	1,91	*B*	$7 \cdot 10^{-21}$
	000—030	4 667	2,14	*B*	$3 \cdot 10^{-22}$

Key: a. band
b. transition
c. band center
d. type
e. intensity, cm
f. cm^{-1}
g. μ

In addition to the fundamental bands, overtones and composite frequencies in the solar spectrum there are upper state bands in which the vibration transition does not occur from the fundamental state (Table 2.8).

The upper state band intensity depends considerably on the temperature, since the density of the corresponding vibration levels of the H_2O molecule depend on it to a very large extent.

The density of the fundamental vibration state can be assumed not to depend, for all practical purposes, on the temperature.

TABLE 2.8

H_2O UPPER STATE BANDS [3]

a Переход	Частота b		c Тип	Интенсивность d (при 259° K), см
	$см^{-1}$ e	мкм f		
010—001	2161,14	4,62	*A*	$2 \cdot 10^{-22}$
010—100	2062,27	4,84	*B*	$8 \cdot 10^{-23}$
010—020	1556,82	6,42	*B*	$9 \cdot 10^{-23}$
010—010	0—500	∞ — 20	*B*	$4{,}6 \cdot 10^{-20}$

Key: a. transition
b. frequency
c. type
d. intensity (at 259°K), cm
e. cm^{-1}
f. μ

As we already have noted the vibration-rotation spectra of HHO^{18} and HHO^{17} water isotopes are similar to the HHO^{16} spectrum, only these are slightly shifted. The intensity ratios of the lines of these isotopes and the HHO^{16} lines correspond to their concentration ratios. The HDO^{16} bands (Table 2.9) differ noticeably from the HHO^{16} bands.

An analysis of the vibration-rotation spectrum of water vapor shows that the most intense and widest absorption band is the fundamental band ν_2, which corresponds to the deformation vibration of the molecule. The center of this band lies near the wavelength 6.25 μ. In the literature this band is often called the 6.3 μ band. In the vertical column of the atmosphere, this band completely absorbs the radiation from the sun in thewavelength range approximately from 5.5 to 7.5 μ [59]. The center of the band ν_3 with the next intensity is around 2.66 μ. The centers of the bands ν_1 and $2\nu_2$ are near the wavelengths 2.74 and 3.17 μ. The bands ν_1, ν_3 and $2\nu_2$ cause complete solar radiation absorption in the vertical

TABLE 2.9

HDO[16] BANDS [3]

a Переход	Частота b		Интенсивность, см c	
	см$^{-1}$ d	мкм e	компонента типа A f	компонента типа B g
000—010	1403,3	7,12	$5\cdot10^{-23}$	$2,3\cdot10^{-22}$
000—100	2723,66	3,67	$5\cdot10^{-22}$	$<5\cdot10^{-24}$
000—020	2782,16	3,59	$1,4\cdot10^{-23}$	$9\cdot10^{-24}$
000—001	3707,47	2,69	$3\cdot10^{-23}$	$1,4\cdot10^{-22}$
000—110	4100,05	2,43	$2\cdot10^{-23}$	$<1\cdot10^{-24}$
000—030	4145,59	2,41	$2\cdot10^{-23}$	$<1\cdot10^{-24}$
000—011	5089,59	1,96	$3\cdot10^{-23}$	$1,6\cdot10^{-23}$
000—200	5363,59	1,86	$3\cdot10^{-23}$	$<2\cdot10^{-24}$
000—101	6415,64	1,55	$1\cdot10^{-24}$	$9\cdot10^{-24}$
000—021	6452,05	1,54	$2\cdot10^{-24}$	$<5\cdot10^{-25}$
000—012	8611,22	1,16	$5\cdot10^{-24}$	$<5\cdot10^{-25}$

Key: a. transition
b. frequency
c. intensity, cm
d. cm^{-1}
e. μ
f. type A component
g. type B component

column of the atmosphere under typical conditions in the spectral region approximately from 2.6 to 3.3 μ. Other vibration-rotation water vapor bands are grouped and form in the spectrum obtained with small resolution, absorption bands with centers around the wavelenths 1.87, 1.38, 1.1, 0.94, 0.81, 0.72 μ. There are a few weak bands in the visible region of the spectrum.

The fine structure of the vibration-rotation spectrum of water vapor is exceptionally complex and entangled. Each band in this spectrum consists of hundreds or thousands of individual lines, the identification of which is a very complex problem. The use of spectral instruments even with the highest resolution does not always make it possible to fully resolve all the lines in the fine structure of the spectrum. As an illustration, Fig. 2.8 shows the part of the spectrum of the vibration-rotation H_2O band, the width of which is only 0.07 μ in the region

of the 1.38 μ band, which was recorded by a high resolution instrument [60]. The theoretical calculation of the center positions, the intensity and halfwidths of individual lines requires that the complex interaction between the vibration and rotation levels of the molecule be correctly taken into account.

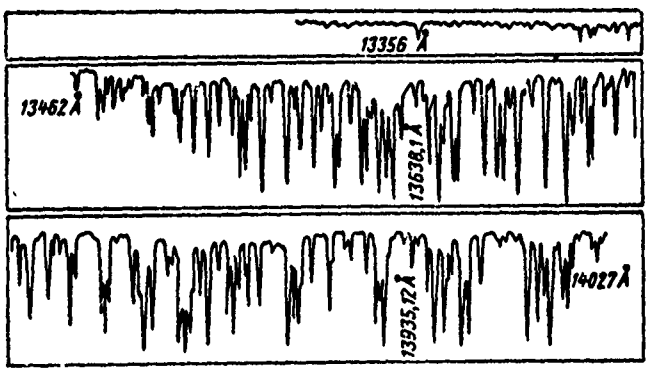

Fig. 2.8. Absorption spectrum of a part of the vibration-rotation water vapor band around 1.38 μ [60]

2. Carbon Dioxide. A linear symmetric CO_2 molecule with bond length C–O equal in the fundamental frequency state to 1.1632 Å has three fundamental vibration frequencies: ν_1, ν_2 and ν_3, which are represented in Fig. 2.9. The rotation constant of the molecule in the fundamental vibration state is equal to 0.3895 cm^{-1}. The deformation vibration ν_2 is twice degenerate. In the latter case, in addition to the selection rules which were considered in paragraph 3 in this chapter, the selection rules for the vibration quantum numbers of the vibration moment of momentum must also be taken into account

$$\Delta l = 0, \pm 1. \qquad (2.72)$$

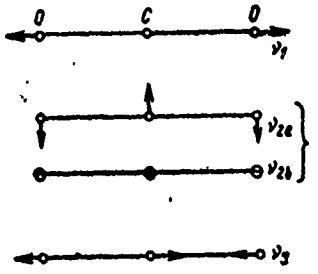

Fig. 2.9. Fundamental vibrations diagram of CO_2 molecule

Because of the symmetry of the molecule, the dipole moment does not change in the fundamental vibration ν_1, so that this vibration does not occur in the infrared spectrum. The magnitude of the frequency ν_1 is approximately twice as large as that of the frequency ν_2.

The fundamental vibration-rotation bands $\nu_2(00^00\text{-}01^10)$ and $\nu_3(00^00\text{-}00^01)$ are respectively perpendicular and parallel. Thus, the band ν_3 does not have a Q branch.

The statistical weights of the CO_2 molecule levels with even values j are equal to zero. Therefore, the fine structure of the vibration-rotation bands has only lines with odd j.

The CO_2 molecule has the following isotopes: $C^{12}O_2^{16}$, $C^{13}O_2^{16}$, $C^{12}O^{16}O^{17}$, $C^{12}O^{16}O^{18}$, the content of which in percent relative to the total carbon dioxide content in the atmosphere is equal to 98.420, 1.108, 0.0646 and 0.4078%, respectively. In addition there are two more rare CO_2 isotopes.

Table 2.10 gives the positions of the band centers ν_2 and ν_3 of three CO_2 isotopes, which are found most frequently in the atmosphere [3].

TABLE 2.10

FUNDAMENTAL ν_2 AND ν_3 BANDS OF THE CO_2 MOLECULE [3]

a Разновидности изотопов	b Процентное содержание	Центр полосы, $см^{-1}$ c	
		ν_2	ν_3
$C^{12}O^{16}O^{16}$	98,420	667,40	2349,16
$C^{13}O^{16}O^{16}$	1,108	648,52	2283,48
$C^{12}O^{16}O^{18}$	0,408	662,39	2333

Key: a. Various types of isotopes
b. Percentage content
c. Band center, cm^{-1}

The fundamental vibration-rotation band ν_2 with center near the wavelength 15 μ together with 14 upper state bands occupies a rather wide range of the spectrum, approximately from 12 to 20 μ. In the region of the central part of this band (~13.5 - 16.5 μ) the vertical atmosphere column absorbs completely the radiation from the sun. This entire set of bands is often called in the literature the 15.0 μ (Table 2.11) band. Figure 2.10 gives the part of the CO_2 spectrum for the 15 μ band. It can be seen from this figure that not all lines in the part of the spectrum shown are resolved by an instrument. We note that the 15 μ band region is very rich in fine structure lines. Thus, for example, Drayson [62] in his paper when he calculated the CO_2 absorption coefficient in this band region (more precisely the set of bands) took into account about 2000 lines.

The fundamental vibration-rotation absorption band of the $C^{12}O_2^{16}$ molecule $\nu_3 = 2349.16\ cm^{-1}$ causes very strong radiation absorption in the atmosphere in the 4.3 μ region. Two other bands overlap with this band: the fundamental band of the $C^{13}O_2^{16}$ molecule $\nu_3 = 2283.48\ cm^{-1}$ and the combination band $\nu_1 + \nu_3 - 2\nu_2$ ($02^00 - 10^01$) with center around wavelength $2429.37\ cm^{-1}$. Together these bands form the region of the

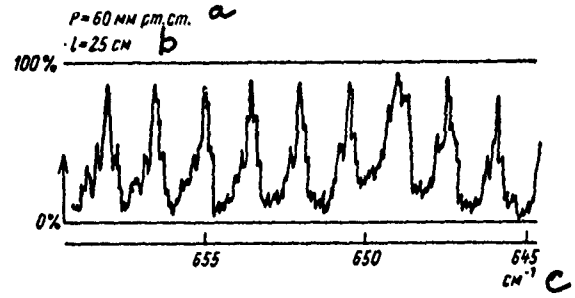

Fig. 2.10. Part of the CO_2 absorption spectrum 15.0 μ band, recorded with high resolution in [61]

Key: a. P = 60 mm Hg
b. L = 25 cm
c. cm^{-1}

absorption spectrum which is usually called the CO_2 4.3 μ band in the literature. All these bands are parallel and, hence, do not have Q branches. The 4.3 μ is sufficiently narrow, its intensity is so large that up to a height on the order of 20 km the radiation from the sun in the region from approximately 4.2 to 4.4 μ in the vertical column of the atmosphere is completely absorbed.

In addition to the 15.0 and 4.3 μ bands which were considered, in which the absorption is caused mainly by the fundamental vibration-rotation band ν_2 and ν_3 of the $C^{12}O_2^{16}$ molecule, carbon dioxide has bands, the centers of which lie near the wavelengths 10.4, 9.4, 5.2, 4.8, 2.7, 2.0, 1.6, 1.4 μ, and a number of weak bands in the range from 1.24 to 0.78 μ. All these bands are relatively narrow (their width is on the order of 0.1 μ).

Two parallel bands in the 10 μ range have vibration frequencies 1063.8 cm^{-1} (transition $02^{0}0$-001) and 961.0 cm^{-1} (transition 100-001). Absorption in the region 1.4, 1.6, 2.0, 2.7, 5.2 and 4.8 μ is caused by bands for which the data are presented in Tables 2.12, 2.13, 2.14

TABLE 2.11

CO_2 BAND IN THE 15 μ REGION [3]

a Разновидности изотопов	b Переход	Центр полосы c		d Молекулярная интенсивность полосы *, см	e E'', см$^{-1}$
		см$^{-1}$ f	мкм g		
$C^{12}O^{16}O^{16}$	00^00-01^10	667,40	15,0	$7,89\cdot10^{-18}$	0,0
$C^{13}O^{16}O^{16}$	00^00-01^10	648,52	15,4	$7,9\cdot10^{-20}$	0,0
$C^{12}O^{18}O^{16}$	00^00-01^10	662,39	15,1	$3,7\cdot10^{-20}$	0,0
$C^{12}O^{16}O^{16}$	01^10-02^00	618,03	16,2	$1,75\cdot10^{-19}$	667,4
—	01^10-10^00	720,83	13,9	$2,3\cdot10^{-19}$	667,4
—	01^10-02^20	667,76	15,0	$6,2\cdot10^{-19}$	667,4
—	10^00-03^10	647,02	15,5	$4,2\cdot10^{-20}$	1285,43
—	10^00-11^10	791,48	12,6	$8,2\cdot10^{-22}$	1285,43
—	02^20-03^10	597,29	16,7	$5,83\cdot10^{-21}$	1335,16
—	02^20-11^10	741,75	13,5	$5,2\cdot10^{-21}$	1335,16
—	02^20-03^30	668,3	15,0	$3,2\cdot10^{-20}$	1335,16
—	02^00-03^10	544,26	18,4	$1,64\cdot10^{-22}$	1388,19
—	03^30-04^20	581,2	17,2	$1,56\cdot10^{-22}$	2003,28
—	03^30-12^20	756,75	13,2	$2,2\cdot10^{-22}$	2003,28
—	03^10-12^20	828,18	12,1	$1,8\cdot10^{-23}$	1932,45
—	03^10-12^00	740,5	13,5	$5,2\cdot10^{-22}$	1932,45
—	04^40-13^30	769,5	13,0	$1,5\cdot10^{-23}$	2674,76

1. * Эти данные получены по отношению к общему числу молекул всех разновидностей изотопов. Каждое значение интенсивности содержит больцмановский множитель основного состояния.

Key:
a. Various types of isotopes
b. Transition
c. Band center
d. Molecular intensity of band,[1] cm
e. E'', cm^{-1}
f. cm^{-1}
g. μ

1. This data was obtained from the total number of molecules for all types of isotopes. Each intensity value contains the Boltzman multiplier for the fundamental state.

TABLE 2.12

CO_2 5.2 and 4.8 μ ABSORPTION BANDS [3]

a Полоса, мкм	b Разновидности изотопов	c Переход	d Центр полосы: см⁻¹ g	d Центр полосы: мкм h	e E'', см⁻¹	f Молекулярная интенсивность полосы при 259° K, см
5,2	$C^{12}O_2^{16}$	000—03¹0	1932,45	5,17	0	$2,4 \cdot 10^{-21}$
4,8	$C^{13}O_2^{16}$	000—11¹0	2037,08	4,90	0	$4,0 \cdot 10^{-22}$
	$C^{12}O_2^{16}$	000—11¹0	2076,86	4,81	0	$3,2 \cdot 10^{-20}$
	$C^{12}O_2^{16}$	01¹0—12²0	2093,35	4,77	667,40	$2,0 \cdot 10^{-21}$
	$C^{12}O_2^{16}$	01¹0—200	2129,79	4,69	667,40	$8,0 \cdot 10^{-22}$

Key:
a. Band, μ
b. Various types of isotopes
c. Transition
d. Band center
e. E', cm^{-1}
f. Molecular intensity of band at 259°K, cm
g. cm^{-1}
h. μ

TABLE 2.13

CO_2 ABSORPTION BANDS NEAR 2.7 μ [3]

a Разновидности изотопов	b Переход	c Центр полосы: см⁻¹ f	c Центр полосы: мкм g	d E'', см⁻¹	e Молекулярная интенсивность полосы при 259° K, см
$C^{12}O_2^{16}$	000—02⁰1	3613,03	2,76	0	$1,0 \cdot 10^{-18}$ ($1,4 \times 10^{-18}$)
—	000—101	3714,56	2,69	0	$1,3 \cdot 10^{-18}$ ($2 \cdot 10^{-18}$)
—	01¹0—03¹0	3580,81	2,79	667,40	—
—	01¹0—11¹1	3723,05	2,68	667,40	—
$C^{13}O_2^{16}$	000—02⁰1	3527,70	2,83	0	$1,1 \cdot 10^{-20}$
—	000—101	3632,92	2,75	0	$1,4 \cdot 10^{-20}$
—	01¹0—03¹1	3498,72	2,85	667,40	—

Key:
a. Various types of isotopes
b. Transition
c. Band center
d. E'', cm^{-1}
e. Molecular band intensity at 259°K, cm
f. cm^{-1}
g. μ

TABLE 2.14

CO_2 ABSORPTION BANDS NEAR 2.0, 1.6 AND 1.4 μ [3]

a Полоса, мкм	b Разновидности изотопов	c Переход	d Центр полосы: g $см^{-1}$	d Центр полосы: h мкм	e E'', $см^{-1}$	f Молекулярная интенсивность полосы при 259° K, см
2,0	$C^{12}O_2^{16}$	00^00-04^01	5100	1,96	0	$1,6\cdot10^{-20}$
	$C^{12}O_2^{16}$	00^00-12^01	4978	2,00	0	$3,7\cdot10^{-20}$
	$C^{12}O_2^{16}$	00^00-20^01	4853	2,06	0	$1,0\cdot10^{-20}$
	$C^{12}O_2^{16}$	01^10-05^10	5132	1,94	667,40	—
	$C^{12}O_2^{16}$	01^10-13^11	4965	2,01	667,40	—
	$C^{12}O_2^{16}$	00^10-21^11	4808	2,07	667,40	—
	$C^{13}O_2^{16}$	00^00-04^01	5016	1,98	0	$1,8\cdot10^{-22}$
	$C^{13}O_2^{16}$	00^00-12^01	4887	2,04	0	$4,1\cdot10^{-22}$
	$C^{13}O_2^{16}$	00^00-20^01	4748	2,10	0	$1,1\cdot10^{-22}$
	$C^{12}O^{16}O^{18}$	00^00-04^01	5042	1,98	0	$7\cdot10^{-23}$
	$C^{12}O^{16}O^{18}$	00^00-12^01	4905	2,03	0	$1,5\cdot10^{-23}$
	$C^{12}O^{16}O^{18}$	00^00-20^01	4791	2,08	0	$4\cdot10^{-23}$
1,6	$C^{12}O_2^{16}$	00^00-06^01	6503	1,53	0	—
	$C^{12}O_2^{16}$	00^00-14^01	6350	1,57	0	—
	$C^{12}O_2^{16}$	00^00-22^01	6228	1,60	0	$2,9\cdot10^{-22}$
	$C^{12}O_2^{16}$	00^00-20^01	6076	1,64	0	—
1,4	$C^{12}O_2^{16}$	00^00-00^03	6973	1,43	0	$8,6\cdot10^{-22}$

Key:
a. Band, μ
b. Various types of isotopes
c. Transition
d. Band center
e. E'', cm^{-1}
f. Molecular band intensity at 259°K, cm
g. cm^{-1}
h. μ

In Tables 2.12, 2.13 and 2.14 the band intensity is determined relative to a single CO_2 molecule, taking into account all different types of isotopes in the molecule.

3. Ozone. The magnitude of the dipole moment of the O_3 molecules (Fig. 2.11) is equal to 0.58 D. The electronic transitions in the molecule form the Hartley and Huygens bands which lie in the ultraviolet region of the spectrum (wavelength shorter than 3400 Å) and the Chappuy 4500 - 7400 Å (visible region). The maximum value of the absorption coefficient in the Chappuy bands is equal to $5 \cdot 10^{-21} cm^2$, which causes a total solar radiation of 7% when the magnitude of the atmospheric mass is equal to two.

All three fundamental vibration frequencies of the O_3 molecule are active during absorption in the infrared region. They form vibration-rotation bands with centers ν_1 = 1110 cm^{-1} (9.1 μ), ν_2 = 710 cm^{-1} (14.1 μ) and ν_3 = 1043 cm^{-1} (9.6 μ). The band ν_1 is very weak and overlaps with the band ν_3. The overlap causes considerable interaction between the corresponding molecular energy levels.

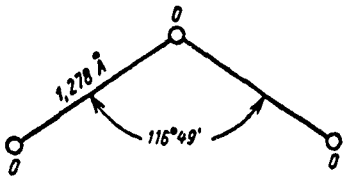

Fig. 2.11. Structure of ozone molecule

The following three isotope modifications of the ozone molecule are found in the atmosphere: O_3^{16}, $O^{16}O^{18}O^{16}$ and $O^{16}O^{16}O^{18}$ (Table 2.15).

The overtones and combination O_3 vibration frequencies form the vibration-rotation bands of this molecule in the regions 2.7, 3.27, 3.59, 4.75, 5.75 μ, of which the most intense is the 4.75 μ region. The widths of all these bands are on the order of 0.1 cm^{-1}.

When solar radiation absorption by the earth's atmosphere is studied it is customary to take into account only the 9.6 μ O_3 absorption band, which is in the center of the longwave transparent atmosphere 8 - 13 μ window. Its central part with

TABLE 2.15

POSITION OF FUNDAMENTAL BANDS OF THE O_3 MOLECULE [3]

Полосы a	O_3^{16}, $см^{-1}$ b	$O^{16}O^{18}O^{16}$, $см^{-1}$ b	$O^{16}O^{16}O^{18}$, $см^{-1}$ b
ν_1	1110 (?)	1080	1095
ν_2	701,42	697	688
ν_3 c	1045,16	1008	1029
Процентное содержание	99,4	0,21	0,41

Key: a. Bands
b. cm^{-1}
c. Percentage contents

width about 1.0 μ in the vertical column of the atmosphere absorbs approximately half the solar radiation. Other bands either overlap with stronger H_2O and CO_2 absorption bands or have low intensity. The 9.6 μ band is very rich in fine structure lines, which so far have not yet been resolved in the experiment. It was only possible to obtain from the experiment constants for the disturbed vibration state. These constants together with fundamental state constants determined from the pure rotation O_3 spectrum in the microwave region enable us to calculate the fine band structure.

The O_3 molecule has an intense pure rotation spectrum in the microwave region.

4. Oxygen. Oxygen is present in the atmosphere in molecular and atomic states. Atomic oxygen arises as a result of molecular oxygen dissociation under the action of ultraviolet solar radiation. During this dissociation atoms are formed from which ozone is formed.

Atom oxygen in the visible and infrared regions does not have resolved dipole radiation electronic transitions. A series of forbidden transitions yields the single line with wavelengths 5571 Å and a multiplet in the 6300 - 6364 Å region. The intensities of these lines are small and they must be taken into account only when the luminescence of the upper

layers of the atmosphere is studied.

Molecular oxygen has strong electronic bands in the ultraviolet region and relatively weak bands in the red and near infrared regions (Table 2.16).

In the near infrared region the O_2^{16} molecule has two noticeable bands, the centers of which lie near wavelengths 1.2683 μ (transition 0 - 0) (Fig. 2.12) and 1.0674 μ (transition 0 - 1).

Because of the symmetry of the O_2^{16} molecule only lines with alternating values of the rotation quantum number j appear in the spectra of its bands.

TABLE 2.16

RED BANDS OF THE O_2^{16} MOLECULE [3]

a Переходы	b Центр полосы, мкм	c Интенсивность полосы *, см	d Характеристика интенсивности полосы в солнечном спектре **
0,0	0,7621	$4{,}3 \cdot 10^{-22}$	и e
0,1	0,6884	$2{,}0 \cdot 10^{-23}$	и
0,2	0,6288	$5{,}1 \cdot 10^{-25}$	си f
0,3	0,5796	$2{,}0 \cdot 10^{-26}$	си
0,4	0,5384	$8{,}1 \cdot 10^{-28}$	—
1,1	0,7710	$2{,}7 \cdot 10^{-27}$	ми g
1,2	0,6970	$2{,}3 \cdot 10^{-23}$	ми
1,3	0,6379	—	си f

/1 * Интенсивности полос отнесены к числу молекул в исходном состоянии.
/2 ** и — полоса интенсивная; си — полоса средней интенсивности; ми — полоса малой интенсивности.

Key: a. Transitions
b. Band Center, μ
c. Band intensity,[1] cm
d. Band intensity characteristic in solar spectrum[2]
e. i
f. si
g. mi

1. The band intensities refer to the number of molecules in the initial state.
2. i--intense band, si--band of medium intensity, mi--low intensity band

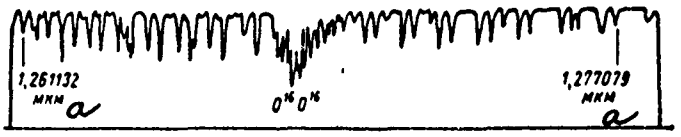

Fig. 2.12. Solar spectrum in the $O_2{}^{16}$ band region 1.2683 μ [63]

Key: a. μ

The molecule of the isotope hydrogen modification $O^{16}O^{18}$ has bands which lie in the red range in the region near the waves 0.7620 μ (transition 0 - 0), 0.6901 μ (transition 0 - 1) and 0.6317 μ (transition 0 - 2). These bands contain lines with all values j, which is due to the reduced symmetry of $O^{16}O^{18}$ molecule compared to the $O_2{}^{16}$ molecule.

Beside the molecular electronic bands considered, oxygen has in the ultraviolet, visible and near infrared regions diffusion bands, induced by systems of $[O_2]_2$ molecules. The spectra of these systems have been studied in the work of Dufay [64] and V. I. Dianov'klokov [65]. The band intensity of these systems is not high. Moreover, they overlap with more intense ozone and water vapor absorption bands. Taking into account the absorption in the $[O_2]_2$ band is apparently only necessary in a number of special cases (for example, for inclined paths which are close to the horizontal radiation propagation path).

5. Nitrogen monoxide. The N_2O nitrogen monoxide molecule is a linear asymmetric molecule, the dipole moment and rotation constant of which are equal to 0.166 D and 0.4182 cm^{-1}, respectively, for the fundamental isotope modification $N_2{}^{14}O^{16}$.

The strong electronic N_2O bands lie in the far ultraviolet region.

All three fundamental vibration frequencies ν_1 = 1285.6 cm^{-1} (7.8 μ), ν_2 = 588.8 cm^{-1} (17.0 μ) and ν_3 = 2223.5 cm^{-1} (4.6 μ) (Fig. 2.13) are active in the infrared spectra.

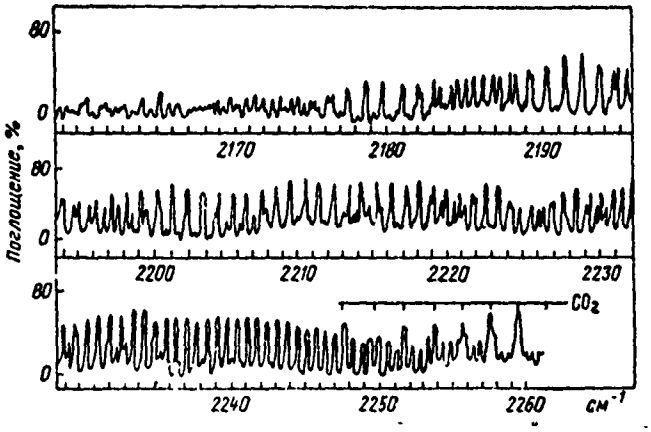

Fig. 2.13. Spectrum of the N_2O molecule ν_3 band, recorded with the aid of a 15 cm long vessel at a partial N_2O pressure of 10 mm Hg [3].

Lines from the combination band $\nu_3 + \nu_2 + \nu_2$ also lie in the ν_3 band region as well as several CO_2 absorption lines.

The N_2O molecule has many overtone bands, combination frequencies and upper state bands. Thus, in the region with frequencies above 8000 cm^{-1} there are 23 bands, between the frequency 4417 and 1880 cm^{-1} 18 bands, between the frequencies 4062 and 7431 cm^{-1} 14 bands and between 2209.53 and 2798.30 cm^{-1} 7 bands, not counting the upper state bands [3]. Most of these bands are very weak. In the solar spectrum there are 9 bands, about which some data are given in Table 2.17.

The N_2O molecule has 12 stable isotopes, formed from the atom combinations N^{14}, N^{15}, O^{16}, O^{17} and O^{18}. The vibration-rotation spectrum of the fundamental $N_2{}^{14}O^{16}$ isotope modification and certain of the isotopes have been studied in greater or lesser detail.

6. Methane. The CH_4 methane molecule is a tetrahedron. The electronic CH_4 bands are in the far ultraviolet region (wavelength less than 1450 Å). The high degree of symmetry of the molecule causes the high degeneracy of the vibration energy levels. Among the 9 fundamental vibration frequencies

TABLE 2.17

N_2O BANDS IN SOLAR SPECTRUM [3]

Центр полосы [a]		Переход [b]	Тип [c]	Молекулярная интенсивность полосы при нормальных условиях, см [d]
$см^{-1}$ [e]	мкм [f]			
4730,86	2,11	$00^00—20^01$	Парал. [g]	—
4630,31	2,16	$00^00—12^01$	»	—
4417,51	2,27	$00^00—00^02$	»	—
4389,06	2,28	$01^10—01^12$	»	—
3481,2	2,87	$00^00—10^01$	»	$1,29 \cdot 10^{-18}$
3365,6	2,97	$00^00—02^01$	»	—
2798,6	3,57	$00^00—01^11$	Перпен. [h]	$9 \cdot 10^{-20}$
2577	3,88	$01^10—21^10$	Парал. [g]	—
2563,5	3,90	$00^00—20^00$	»	$1,6 \cdot 10^{-18}$
2461,5	4,06	$00^00—12^00$	»	$4,3 \cdot 10^{-19}$
2223,5	4,50	$00^00—00^01$	»	$6,88 \cdot 10^{-17}$
2210	4,52	$01^10—01^11$	»	—
1285,0	7,78	$00^00—10^00$	»	$9,78 \cdot 10^{-18}$
1167,0	9,56	$00^00—02^00$	»	$4,08 \cdot 10^{-19}$
588,8	17,0	$00^00—01^10$	Перпен. [h]	$7,75 \cdot 10^{-19}$

Key:
a. Band center
b. Transition
c. Type
d. Molecular intensity of band under normal conditions, cm
e. cm^{-1}
f. μ
g. Parallel
h. Perpendicular

one is degenerate twice, two thrice. Thus, the molecule has altogether four fundamental vibrations which differ in frequency. The band ν_1 is completely symmetric, ν_2 is degenerate twice, ν_3 and ν_4 are degenerate thrice. In the infrared region only the bands ν_3 = 3220.3 cm^{-1} (3.3 μ) and ν_4 = 1306.2 cm (7.7 mm) occur. The vibration frequencies of the optically inactive bands ν_1 and ν_2 are equal to 2914.2 and 1526 cm^{-1}, respectively. The vibration frequencies of the first overtone of

the band ν_2 and the bands ν_1 and ν_3 are close. The overlap of these three bands leads to strong interaction between the vibration-rotation transitions. This interaction causes the removal of the degeneracies in the main bands ν_3 and ν_4 and the substantially greater complexity of the fine structure of the spectrum.

TABLE 2.18

METHANE BANDS IN SOLAR SPECTRUM [3]

Центр полосы [a]		[b] Переход	[c] Молекулярная интенсивность полосы при нормальных условиях, *см*
см$^{-1}$ [d]	*мкм* [e]		
6005	1,67	0000—0020	$3{,}6\cdot10^{-20}$
5861	1,71	0000—1101	—
5775	1,73	0000—0111	—
4420	2,20	0000—0110	—
4313	2,32	0000—0011	—
4216	2,37	0000—1001	—
4123	2,43	0000—0102	—
3019	3,31	0000—0010	$1{,}26\cdot10^{-17}$
3823	3,55	0000—0101	—
2600	3,85	0000—0002	$1{\cdot}04\cdot10^{-17}$
1306	7,66	0000—0001	$6{,}9\cdot10^{-18}$

Key: a. Band spectrum
b. Transition
c. Molecular band intensity under normal conditions, cm
d. cm^{-1}
e. μ

TABLE 2.19

POSITION OF THE CO BAND CENTERS [66]

Полосы [a]	1—0	2—0	3—1	4—2	5—3	6—4	7—5	3—0	4—0
чет, *см*$^{-1}$ [b]	2143, 2740	4260, 0646	4207, 1664	4154, 4056	4101, 7820	4049, 2958	3996, 9466	6350, 4404	8414, 4702
ілюдения, [c] *м*$^{-1}$	2143, 2740	4260, 0646	4207, 1680	4154, 4040	—	—	—	6350, 436	8414, 458

(key on next page)

Key to Table 2.18: a. Bands
b. Calculated, cm^{-1}
c. Observed, cm^{-1}

Beside the two principal vibration-rotation bands, methane has a large number of overtone and combination frequency bands (Table 2.18), 9 of which were detected in the solar spectrum.

Methane does not have a pure rotation spectrum.

7. Carbon Monoxide. The carbon monoxide spectrum, because of its simplicity, has been studied in sufficient detail. The dipole moment of this molecule is equal to 0.1 D. The pure rotation spectrum lies in the far infrared and microwave regions.

The fundamental vibration-rotation band of the $C^{12}O^{16}$ molecule lies near 2143.2 cm^{-1} (4.67 μ). The first overtone of the band has the center near 4260 cm^{-1}.

Table 2.19 shows the center positions of various CO bands which were discussed in article [66].

The carbon monoxide molecule has two isotope modifications $C^{12}O^{16}$ and $C^{13}O^{16}$.

The fine structure of many vibration-rotation CO bands has been studied sufficiently well. The results of these studies will be discussed in the next chapter.

3. Absorption Of Visible And Infrared Waves In A Homogeneous Atmosphere

1. Fundamental Definitions

1. Absorption Coefficient. Optical Layer. Spectral Transmission (Absorption). By the absorption coefficient $k(\nu)$ of the medium for emitting the frequency ν, we shall understand the proportionality coefficient in the Buger law, which is written in differential form as

$$dI(\nu) = -k(\nu) I(\nu) dl, \tag{3.1}$$

where $dI(\nu)$ is the attenuation of the emitted intensity $I(\nu)$

which passed through a medium layer of thickness dl.

Integrating (3.1) along the thickness of the layer l yields, for the case of a homogeneous medium, the well-known expression for the Buger law

$$I(\nu) = I_0(\nu)\, e^{-k(\nu)l}, \tag{3.2}$$

where $I_0(\nu)$ and $I(\nu)$ are the emission intensities before and after passage through the medium layer of thickness l.

By the optical layer τ of the medium layer l we mean the exponent in expression (3.2):

$$\tau = k(\nu)\, l. \tag{3.3}$$

The limits within which relations (3.1) and (3.2) can be applied will be considered in paragraph 4.

The quantities

$$f(\nu) = \frac{I(\nu)}{I_0(\nu)}; \quad A(\nu) = \frac{I_0(\nu) - I(\nu)}{I_0(\nu)} \tag{3.4}$$

will be called the spectral transmission and spectral absorption respectively.

2. The Absorption and Transmission Functions. Integral Absorption. The absorption function A of the radiation in the spectral interval $\Delta\nu = \nu_2 - \nu_1$ is the ratio of the radiation absorbed by the medium layer to the radiation incident on this layer. The transmission function T is definied analogously.

In accordance with the definition above, we can write

$$A = \frac{\int_{\nu_1}^{\nu_2} [I_0(\nu) - I(\nu)]\, d\nu}{\int_{\nu_1}^{\nu_2} I_0(\nu)\, d\nu}; \quad T = \frac{\int_{\nu_1}^{\nu_2} I(\nu)\, d\nu}{\int_{\nu_1}^{\nu_2} I_0(\nu)\, d\nu}. \tag{3.5}$$

For a homogeneous layer from (3.5), using (3.4), we obtain

$$A=\frac{\int_{\nu_1}^{\nu_2} I_0(\nu)\,A(\nu)\,d\nu}{\int_{\nu_1}^{\nu_2} I_0(\nu)\,d\nu},\quad T=\frac{\int_{\nu_1}^{\nu_2} I_0(\nu)\,f(\nu)\,d\nu}{\int_{\nu_1}^{\nu_2} I_0(\nu)\,d\nu}. \tag{3.6}$$

As can be seen from (3.6), the absorption and transmission functions in the spectral interval $[\nu_1, \nu_2]$ characterize the mean spectral absorption and spectral transmission in this interval.

In the special case, when $I(\nu)=\text{const}\in[\nu_1, \nu_2]$

$$A=\frac{\int_{\nu_1}^{\nu_2} A(\nu)\,d\nu}{\nu_2-\nu_1},\quad T=\frac{\int_{\nu_1}^{\nu_2} f(\nu)\,d\nu}{\nu_2-\nu_1}, \tag{3.7}$$

or taking into account (3.4) and (3.2)

$$A=\frac{1}{\nu_2-\nu_1}\int_{\nu_1}^{\nu_2}(1-e^{-k(\nu)l})\,d\nu;$$
$$T=\frac{1}{\nu_2-\nu_1}\int_{\nu_1}^{\nu_2} e^{-k(\nu)l}\,d\nu. \tag{3.7a}$$

In another special case, when $k(\nu)=\text{const}\in[\nu_1, \nu_2]$,

$$A=A(\nu);\quad T=f(\nu). \tag{3.8}$$

The functions A and T depend [see (3.5) and (3.6)] not only on the absorption properties of the medium expressed in terms of $A(\nu)$ or $f(\nu)$ but also on the spectral intensity of the source radiation density $I_0(\nu)$. Therefore, to characterize the absorption properties of the medium in a given central

interval $[\nu_2, \nu_1]$ which do not depend on the function $I_0(\nu)$, we introduce the integral absorption concept B, by which we mean the value of the integral

$$B = \int_{\nu_1}^{\nu_2} A(\nu)\, d\nu. \tag{3.9}$$

It is easily seen that the maximum value of the abosrption integral is reached when $A(\nu) = 1$ in the entire spectral interval, which is equal to $\Delta\nu = \nu_2 - \nu_1$. The integral absorption is expressed in frequency units and can be considered as the width of some spectral interval for which, when $A(\nu) = 1$, the integral absorption is equal to the given value. In this sense the integral absorption is often called the equivalent width of the given interval (line band, etc.).

Expressions (3.1) - (3.9) are obtained for the case when the frequency ν is taken as the spectral coordinate. Formally identical formulas are obtained if the wavelength λ is taken as the spectral coordinate. Keeping in mind the relation between ν and λ

$$\nu\,[\text{a}] = \frac{10^4}{\lambda\,[\text{b}]}, \tag{3.10}$$

Key: a. cm^{-1}
b. μ

it can be shown that formulas (3.5) and (3.6) written in terms of ν and λ, taking into account (3.10) yield the same numerical values of A and T. At the same time formulas (3.7), expressed in terms of ν and λ, are not equivalent, i.e.,

$$\frac{\int_{\nu_1}^{\nu_2} A(\nu)\, d\nu}{\nu_2 - \nu_1} \neq \frac{\int_{\lambda_1}^{\lambda_2} A(\lambda)\, d\lambda}{\lambda_2 - \lambda_1}; \quad \frac{\int_{\nu_1}^{\nu_2} f(\nu)\, d\nu}{\nu_2 - \nu_1} \neq \frac{\int_{\lambda_1}^{\lambda_2} f(\lambda)\, d\lambda}{\lambda_2 - \lambda_1}. \tag{3.11}$$

The smaller the spectral interval $[\nu_1, \nu_2]$ or the equivalent interval $[\lambda_1, \lambda_2]$, the weaker the inequality (3.11). In the limit $\nu_2 - \nu_1 \to 0$ or $\lambda_2 - \lambda_1 \to 0$, $A(\nu) = A(\lambda)$ and $T(\nu) = f(\lambda)$.

We note that formula (3.10) holds strictly for a vacuum. When the radiation propagates in a medium with the refraction index $n \neq 1$, we must take into account the relation $\lambda = \lambda_0 n^{-1}$, where λ and λ_0 are respectively, the wavelengths in the medium and in the vacuum.

We emphasize that the expressions for the absorption and transmission functions (3.7), (3.7a) are often used in the literature without the stipulation that they are only valid in the case when within the limits of the spectral interval $\Delta\nu = \nu_2 - \nu_1$ the relation between the intensity of the incident radiation and the frequency can be ignored. In practice these expressions can be used to calculate the absorption functions from heat sources within narrow regions of the spectrum (with widths on the order of 0.1 nm).

2. Absorption of Individual Lines

The absorption spectrum of an arbitrary isolated molecule is a set of individual spectral lines, the position, intensity, and form of which are uniquely determined by the corresponding quantum changes in the electronic, oscillation and rotation energy of the molecule. The spectral line is, thus, the basic element of the molecular spectrum. For this reason many papers were devoted to the study of laws which govern the radiation absorption by a single spectral line, the results of which have been generalized in a number of monographs and surveys [67-71]. Partially we considered the absorption by a single line in the second chapter. Here we will touch only on certain problems, the knowledge of which is necessary for discussing and understanding the subsequent material.

1. The Form of the Line Contour. As we already have mentioned, the form of the absorption line contour under the conditions of the earth's atmosphere is determined by the finite life of molecules in the excited state, the Doppler effect, and the molecular collision effect of the absorbing gas with one another and with molecules of the gases which are not absorbed, i.e., the extraneous gases. The formulas which describe the contour of a line, induced by the corresponding effects or their joint action, are given above [see formulas (2.55), (2.57)

and (2.64).

Strictly speaking none of the above formulas can be used to describe exactly the contour of the line under real atmospheric conditions. For this reason it is important to know in which cases and with what accuracy one can use this or that expression to describe the real contour of the line.

The accuracy requirements for describing the real contour of a line depend, to a considerable extent, on the nature of the corresponding problem. Let us assume, for example, that we must determine the integral absorption function in a very wide spectral interval for a black or gray emitter. In this case the accuracy requirements on the forms of individual lines are less strict, since the central part of the lines and its tails will contribute to the total absorption. If we must know the absorption function in a relatively narrow interval which contains only the central parts of several lines, or, conversely, which includes the tails of the far lines, the energy distribution absorbed by the line in the central part and the tails becomes now very important. Finally, to determine monochromatic radiation absorption in the atmosphere, the accuracy requirements for describing the contour of the line are most rigorous.

In the overwhelming majority of studies dealing with the absorption of visible and infrared waves in the atmosphere, the dispersion or Lorentz contour of the line is used. This is due to the fact that the dispersion contour is very simple and describes sufficiently well the central part of the line at altitudes, on the average up to 30 km, where the main mass of the gases which are absorbed in the visible and infrared regions of the spectrum is concentrated [1].

In recent years new problems appeared, for the solution of which the dispersion contour either does not provide the required accuracy or cannot be used. This applies primarily to problems connected with the use of OKG (lasers) in various systems which are designed to operate in the atmosphere, reverse artificial satellite meteorology problems and the problem of calculating more precisely the radiation flows in the atmosphere. To solve these problems we must have data about the contour of the central part of the line at those altitudes where the Doppler effect can no longer be ignored in comparison with the broadening of lines due to molecular collisions. The dispersion contour will deliberately not be used to describe the real absorption by the far tails of the lines. We will briefly consider the results of Lorentz-Doppler contour studies and the forms of the far tails of a line.

In the theoretical study made by S. G. Rautian and I. I. Sobel'man [72] various cases are discussed of a line contour caused by the joint action of the Doppler and Lorentz effects. The action of these effects is considered both as statistically independent and statistically dependent. It has been shown in [72] that the real contour of a line must have less intense tails than is the case in the Lorentz contour. The intensity in the tails decreases proportionally with the fourth power of the frequency, not its square as the dispersion contour implies.

For the statistically dependent broadening of lines due to the Doppler and Lorentz effects, the authors obtained line contours which were asymmetric and displaced relative to the center.

Drayson [62] calculated the total line absorption for the Lorentz and Lorentz-Doppler contours. The calculations used various values of the product $S\omega$, where S is the intensity of the line and ω is the absorbing gas layer. It turned out that for medium values of $S\omega$ the total absorption of the line with a mixed contour at low pressures (high altitudes in the atmosphere) can exceed the total absorption of the line with the Lorentz contour by more than a factor of 2. Thus, when the pressure varies from 100 to 0.5 mb (altitudes from 16 to 55 km) the error in calculating the total absorption of the line due to ignoring the Doppler effect varies from 0.05 to 60%. At a pressure of 10 mb (altitude 30 km) this error is approximately 5%. It has been shown in the work of Plass and Fivel [73] that for the limiting cases of small and large values of $S\omega$ the Doppler effect can be ignored up to an altitude of 50 km, when the total absorption of the line is calculated.

Thus, it follows from article [62], that when the total absorption of individual lines is calculated and, hence, also of groups of lines up to an altitude of 30 km with an accuracy not less than 5%, the Doppler effect need not be taken into account. We emphasize that this conclusion applies to the total line absorption and cannot be applied to the calculation of monochromatic radiation absorption in the atmosphere. The methods for calculating the absorption coefficients for a fourth line contour are studied in articles [74 - 77].

Winters, Silverman, and Benedict published the results of experimental absorption studies for CO_2 in the 4.3 μ band. The analysis of the results has shown that beyond the limit 5 cm^{-1} from the center of the line, the absorption coefficient $k(\nu)$ decreases faster than the dispersion contour implies. The authors of [78] propose the following empirical expression for

$k(\nu)$, which satisfies the described results of their experiment:

$$k(\nu)=\left(\frac{\gamma}{\pi}\right)[(\nu-\nu_i)^2+\gamma^2]e^{-a(|\nu-\nu_i|-\Delta\nu_0)^b}; \quad |\nu-\nu_i|>\Delta\nu_0, \tag{3.12}$$

where γ is the halfwidth of the line, a and b are empirical constants depending on the type of expanding gas and the quantity $\Delta\nu_0$, according to Benedict's estimate, does not exceed 3 cm^{-1}.

In the work of Murcray and his collaborators [71], the spectral solar absorption radiation was varied in the band 4.3 μ at altitudes from 10 to 30 km with 0.5 cm^{-1} resolution. This resolution turned out to be sufficient for interpreting the spectrum from line to line using the calculations. When the calculated results were compared with the experimental data, it was found that the theory agreed sufficiently well with the experiment when at high altitude a Lorentz contour was used and at lower altitudes the contour (3.12) proposed by Benedict. The latter was used when the high frequency tails of the band were calculated.

In the work of Burch and his collaborators [80, 81] experimental studies of water vapor and carbon monoxide spectral absorption were made in the wavelength range from 0.6 to 5.5 μ. The analysis of the results obtained led the authors to conclude that none of the existing expressions for the form of the far tails of the contour of the line is suitable for the exact description of the experimental data. The experiment has shown that the form of the far tails of the line is different for H_2O and CO_2 and that for the same absorbing gas it depends on the absorption band, the extraneous gas, and temperature.

Thus, even though the central part of the line is described more or less satisfactorily by the available formulas for the line contour, the same cannot be said at all about the far tails of the line. Here new endeavors are required from the theoreticians. Also, as the analysis of the available experimental data implies, formulas must be obtained for the far tails of the line which will take into account the absorbing and extraneous gases, the properties of the absorption band, and the temperature relation.

2. Total Absorption and the Absorption Function for A Single Line. The expression for the total absorption of a single nonoverlapping line with a dispersion contour has been obtained in the well-known work of Ladenburg and Reiche [82]:

$$B=\int_{-\infty}^{+\infty} A(\nu)\,d\nu = 2\pi\gamma f(x);$$
$$f(x)=xe^{-x}[J(x)+J_1(x)], \tag{3.13}$$

where

$$x=\frac{S\omega}{2\pi\gamma},$$

$J_0(x)$ and $J_1(x)$ are Bessel functions of zero and first orders of a pure imaginary argument, ω is the mass of the absorbing gas, which is sometimes called the settled gas layer. The values of the function f(x) have been tabulated for various x by Elsasser and for the values of x from 0.01 to 10 they are given in K. Ya. Kondrat'ev's monograph [84].

In the limiting cases we obtain from (3.13)

$$B=S\omega \quad \text{при}^{a} \quad x\ll 1, \tag{3.14}$$

$$B=2\sqrt{S\gamma\omega} \quad \text{при}^{a} \quad x\gg 1. \tag{3.15}$$

Key: a. for

The absorption function for a single line with the dispersion form under the condition that the incident radiation intensity is constant, $I(\nu)$ = const, within the limits of the spectral interval $\nu_2 - \nu_1$ occupied by the line has the form

$$A=\frac{\int_{\nu_1}^{\nu_2}(1-e^{-k(\nu)\omega})\,d\nu}{\nu_2-\nu_1}, \tag{3.7a}$$

where k(ν) is determined from formula (2.57).

In paper [85] a general expression was obtained for the function A:

$$A = 1 - e^{-x(1+\cos 2\delta)} - \frac{e^{-x}}{2b} \sum_{n=0}^{\infty} \delta_n (-1)^n J_n(x) B_n(\delta), \tag{3.16}$$

$$B_n(\delta) = -4n \left[\sum_{k=0}^{n} \delta_k (-1)^{n-k} \frac{\sin 2k\delta}{2k} - \frac{\sin 2(n-1)\delta}{2(n-1)} \right], \tag{3.17}$$

where $x = \frac{S\omega}{2\pi\gamma}$; S and γ are the intensity and halfwidth of the line, ω is the absorbing gas mass, δ = arc tg b, 2bγ is the width of the spectral interval in which the function A is defined and $J_n(x)$ is a Bessel function of order n of an imaginary argument.

The following asymptotic formulas for A can be obtained from (3.16)

$$1)\ x \ll 1,\ A = 2x\delta/b; \tag{3.18}$$

$$2)\ x \gg 1,\ A = 1 - e^{-z^2} + \sqrt{\pi z}[1 - \Phi(z)]; \tag{3.19}$$

$$3)\ b \gg 1,\ A = A_1 + A_2,$$

$$A_1 = \frac{\pi}{b} x e^{-x} [J_0(x) + J_1(x)], \tag{3.20}$$

$$A_2 = 1 - e^{-z^2} - \sqrt{\pi z}\,\Phi(z); \tag{3.21}$$

$$4)\ b \gg 1,\ x \ll 1,\ A = \frac{S\omega}{2\gamma b}. \tag{3.22}$$

In formulas (3.19) and (3.21) Φ(z) is the error probability integral, with the argument $z = \frac{1}{b}\sqrt{2x}$.

We will compare the asymptotic formulas which were given for the absorption functions with the corresponding formulas for the total absorption of a single line B [formulas (3.14) and (3.15)].

As can be seen by comparing formulas (3.22) and (3.14), the expressions for A and B coincide with an accuracy up to a constant multiplier. This means that the physical results which follow from the analysis of one formula can be applied to the other formula. Thus, both A and B do not depend, in this case, on the pressure.

A comparison of the limiting formulas (3.19) and (3.15) for $x \gg 1$ shows that in this case the physical results which follow from an analysis of the expression for the total absorption of a line cannot be used when the absorption function is studied in a fixed spectral interval. In particular, B is expressed in terms of the square root of the absorbing mass (the so-called square root law for a single line), whereas the expression for A is entirely different, and the square root law cannot be applied to describe the absorption function for a single line for large values of x (large w or small pressures).

In conclusion we note that neither the absorption function A, nor the total absorption B in a single line when $x \ll 1$ for sufficiently large b when arc tg b can be replaced by $\frac{\pi}{2}$, does not depend on the pressure [see (3.18), (3.22) and (3.14)]. For $x \gg 1$ the mass of the absorbing gas w and the pressure P are included, according to the law, in the corresponding expression for A and B [see (3.19) and (3.15), which include the halfwidth $\gamma = \gamma^0 P$].

3. Absorption By Groups Of Overlapping Lines

The spectra of all atmospheric gases consist of groups of overlapping lines. Depending on the radiation source, the absorption of which in the atmosphere must be known, the overlap of the individual lines must be taken into account for individual wavelengths (for example, in the case of gas OKG (lasers)) or in certain spectral intervals.

One of the following three ways is used to find the absorption functions: 1) calculations based on taking into account the radiation absorption at a given frequency for each line of the spectrum, 2) calculations based on formulas for the spectral models, 3) experimental determination of the corresponding quantities under natural or laboratory conditions. We will study each of these approaches.

1. Direct Calculation of Absorption Functions. The absorption function for a group of overlapping lines (bands), which occupy the spectral interval $[\nu_1, \nu_2]$ for the case when

the pressure along the trace of the beam and the intensity of the incident radiation in the interval $[\nu_1, \nu_2]$ are constant has the form

$$A = \frac{1}{\nu_2 - \nu_1} \int_{\nu_1}^{\nu_2} (1 - e^{-k(\nu)\omega})\, d\nu, \tag{3.23}$$

where

$$k(\nu) = \sum_i S_i b_i(\nu); \tag{3.24}$$

$b_i(\nu)$ is the contour of the i-th line normalized to unity. In the last formula the summation is carried out over all lines which contributes to the radiation absorption with the frequency ν.

If we assume that all lines contributing to the radiation absorption with frequency ν have a dispersion contour, then we obtain from (3.24)

$$k(\nu) = \sum_i S_i \frac{\gamma_i}{\pi} \frac{1}{(\nu - \nu_{0i})^2 + \gamma_i^2}. \tag{3.25}$$

Thus, the direct calculation of the absorption function requires that the position of the centers, the intensity and the halfwidth of all lines which can contribute to radiation absorption in the spectral interval under consideration be known. The calculation and experimental determination of the line parameters for the atmospheric gases is a very complex problem. Only in the last few years has progress been made in this problem. A number of publications appeared in which the absorption functions were calculated in a number of atmospheric gas bands and a series of articles which dealt with the experimental determination of the line parameters. We will consider this work in subsequent paragraphs when we will consider the concrete results of studies dealing with particular atmospheric gases. Here we will only emphasize, that in spite of the considerable mathematical and computational difficulties the direct calculation of absorption functions has undoubtedly great promise, since, with the aid of it, we obtain the most general data without any constraints on the spectral interval width for which the absorption

function must be known.

In conclusion we note the approximate method for calculating the absorption function which we proposed in our article [86].

The formula which was obtained for the absorption function has a general character and can be used to calculate radiation absorption in various narrow spectral bands, where the absorption lines can be described by a dispersion contour with constant halfwidths. An essential fact is that this formula takes into account radiation absorption in a given interval by lines, the centers of which lie within this interval.

2. Models of Absorption Spectra. The direct calculation of absorption functions is very laborious and cannot always be used because of the paucity of data about the parameters of individual lines in the absorption spectra of atmospheric gases. Because of this when absorption functions are calculated, models are widely used to model the spectra. According to this method, the spectra of the atmospheric gases are modeled by a certain set of assumptions made about the character of the positions and intensities of the lines. In all models the dispersion contour is assumed for the lines and the halfwidths of all lines are assumed to be equal. We will consider briefly the main models which are used in the calculation of atmospheric gas absorption functions (this problem is discussed in greater detail in R. Gudi's monograph [3] and in our article [88]):

1. The absorption function in the Elsasser Model.

This model assumes equal intensities of the lines A, equal halfwidths γ and equal distances d between the lines within the limits of the spectral region under consideration. If this region is sufficiently wide, so that the number of lines in it can be considered to be large, then we obtain the following expression for the absorption coefficient:

$$k(\nu)=\frac{S\,\mathrm{sh}\,\beta}{d}\,\frac{1}{\mathrm{ch}\,\beta-\cos t}, \qquad t=\frac{2\pi\nu}{d}; \quad \beta=\frac{2\pi\gamma}{d}. \tag{3.26}$$

Substituting (3.26) in (3.23), after several changes of variable we can obtain

$$A=\mathrm{sh}\,\beta\int_0^{x'} e^{-\xi\,\mathrm{ch}\,\beta}J_0(\xi)\,d\xi, \tag{3.27}$$

$$x' = \frac{S\omega}{d \operatorname{sh} \beta}, \tag{3.28}$$

where $J_0(\xi)$ is a Bessel function of order zero of a pure imaginary argument.

Integration within the limits stated means that A is calculated in the spectral interval occupied by a single line. However, keeping in mind that in the given model $k(\nu)$ is a periodic function with period d, the value A for any spectral interval containing n lines will also be determined from (3.27).

We can obtain from (3.27) the following expression for the absorption function [88]:

$$A = \operatorname{sh} \beta x' e^{-x' \operatorname{ch} \beta} J_0(x') + \operatorname{th} \beta x' e^{-x' \operatorname{ch} \beta} J_1(x') + \\ + \frac{\operatorname{sh}^2 \beta}{\operatorname{ch} \beta} \int_0^{x'} \xi e^{-\xi \operatorname{ch} \beta} J_0(\xi)\, d\xi. \tag{3.29}$$

For the atmosphere $\beta \ll 1$ (the distance between the lines is much larger than their halfwidths). For this case, we obtain from (3.29)

$$A = \beta x e^{-x(1+\beta^2/2)} [J_0(x) + J_1(x)] + \\ + \beta^3 \int_0^x \xi e^{-\xi(1+\beta^2/2)} J_0(\xi)\, d\xi, \tag{3.30}$$

$$x = \frac{\omega S}{2\pi\gamma}. \tag{3.31}$$

We will consider the asymptotic expression for A, which is derived from (3.30):

1) $x \ll 1$. Expanding (3.30) in a series gives

$$A = \beta x = \frac{S}{d} \omega. \tag{3.32}$$

In this case the absorption function does not depend on the pressure. It should be noted that (3.32) is also directly obtained from (3.29), and, hence, the result obtained here does not depend on the quantity β.

2) $x \gg 1$. Using the asymptotic expressions for the Bessel function for large values of the argument leads in this case to the relation

$$A = \Phi\left(\sqrt{\tfrac{1}{2}\beta^2 x}\right) = \Phi\left(\tfrac{1}{2}\sqrt{\pi S \gamma \omega}\right). \qquad (3.33)$$

The formula which was obtained implies that the absorption function does not depend, in the given case, on the product ωP and on ω and P taken separately. We emphasize that this conclusion also applies to the case $\beta \ll 1$.

3) $x \gg 1$ and $\beta^2 x \ll 1$ (the lines do not overlap for all practical purposes). (3.33) implies directly

$$A = \beta\sqrt{\frac{2x}{\pi}} = \frac{2}{d}\sqrt{\pi \gamma S \omega}. \qquad (3.34)$$

4) $x \approx 1$. For this assumption $\beta^2 x \ll 1$, and expanding the integral in (3.30) in powers of x gives

$$A = \beta x e^{-x}[J_0(x) + J_1(x)]. \qquad (3.35)$$

We note that in [89] and [90] the expression for the square root law (3.34) was obtained from the Elsasser model in the limiting case $\omega \ll 1$ and $\beta \ll 1$. We have shown in our article [88] that this result is erroneous.

2. The Absorption Function in a Statistical Model

The fundamental assumption in the statistical model which was proposed for the first time by Gudi [91] is that the distribution of the positions and the line intensities in the spectrum when their halflengths are equal are random and obey probability theory laws. The idea of a stochastic model was further developed in the work of Plass [92], Godson [93], Kaplan [94].

We note that the analytic expressions which were obtained in [91] - [94] give, in fact, the spectral absorption for a particular frequency but not the value of the absorption function. A correct mathematical analysis of the statistical model which is based on introducing the "mean measured absorption coefficient" is given in the work of V. N. Soshnikov [95]. Below we give formulas for the function A, from which the defect which occurred in [91 - 94] has been removed.

The absorption function in the case of the statistical models for a sufficiently wide interval $\nu_2 - \nu_1$, given an equiprobable distribution of the lines, has the form:

$$A = 1 - \frac{1}{\nu_2 - \nu_1} \int_{\nu_1}^{\nu_2} d\nu \exp\left\{ -\frac{1}{\bar{d}} \int_{\nu_a}^{\nu_b} d\nu' \times \right.$$
$$\left. \times \int_0^\infty Q(S)\left[1 - e^{-\frac{\omega S \gamma}{\pi} \frac{1}{(\nu-\nu')^2+\gamma^2}}\right] dS \right\}, \tag{3.36}$$

where Q(S) is the normalized probability density function for the distribution of line intensities, $\bar{d}$ is the mean distance between the lines, $\nu_a - \nu_b = D$ is the interval, the lines in which contribute to the absorption in the region $\nu_2 - \nu_1$ under consideration.

If we further assume $|\nu_b - \nu_a| \gg |\nu_2 - \nu_1|$, then

$$A = 1 - \exp\left\{ -\frac{1}{\bar{d}} \int_{-\infty}^{\infty} d\nu' \int_0^\infty Q(S)\left[1 - e^{-\frac{S\gamma\omega}{\pi} \frac{1}{\nu'^2+\gamma^2}}\right] dS \right\}. \tag{3.37}$$

Gudi [91] considered the case when

$$Q(S) = \frac{1}{\bar{S}} e^{-S/\bar{S}}, \tag{3.38}$$

where $\bar{S}$ is the mean intensity of the line and obtained

$$A = 1 - \exp\left[-\frac{\bar{\beta}\bar{x}}{(1+2\bar{x})^{1/2}} \right], \tag{3.39}$$

where

$$\bar{x}=\frac{\bar{S}\omega}{2\pi\gamma};\quad \beta=\frac{2\pi\gamma}{\bar{d}}. \tag{3.40}$$

Plass [92] and Godson [93] considered the case when all lines have equal intensity, i.e.,

$$Q(S)=\delta(S-\bar{S}_0), \tag{3.41}$$

and obtained

$$A=1-\exp\{\bar{\beta}\bar{x}_0e^{-\bar{x}_0}[J_0(\bar{x}_0)+J_1(\bar{x}_0)]\}, \tag{3.42}$$

where

$$\bar{x}_0=\frac{\bar{S}_0\omega}{2\pi\gamma}. \tag{3.43}$$

Formula (3.39) has the following asymptotic expressions

1) $\bar{x}\ll 1$,

$$A=\bar{\beta}\bar{x}=\frac{\bar{S}}{\bar{d}}\omega; \tag{3.44}$$

2) $\bar{x}\gg 1$,

$$A=1-\exp\left(-\sqrt{\frac{1}{2}\bar{\beta}^2\bar{x}}\right). \tag{3.45}$$

The asymptotic representation for formula (3.42) is analogous, only in (3.44) $\bar{x}$ must be replaced by $\bar{x}_0$ and in (3.45) by $4\bar{x}_0/\pi$.

As in the case of the Elsasser model, the absorption function for small $\bar{x}$ does not depend on the pressure, and for

$\tilde{x}$ it depends on the product ωP.

Relations (3.38) and (3.41), which define the distribution of line intensities are very arbitrary. However, the calculations made by V. N. Soshnikov [95] for the Boltzman line distribution by intensities have shown that the values of the function A do coincide, in this case, for all practical purposes with the values obtained using formulas (3.39) and (3.42).

3. The Absorption Function in a Combined Model

According to this model, proposed by Kaplan [94] and Plass [92], it is assumed that all lines in the corresponding region of the spectrum can be broken up into several groups, within each of which these lines lie at an equal distance from one another and have the same intensity and halfwidth, i.e., they can be described by the Elsasser model. The groups themselves are situated randomly, as the lines in the statistical model. The expression for A, in this case, is written in the form

$$A = 1 - \prod_{j=1}^{N} \operatorname{sh}\beta_j \int_{x_j}^{\infty} e^{-\xi \operatorname{ch}\beta_j} J_0(\xi)\, d\xi, \tag{3.46}$$

where

$$\beta_j = \frac{2\pi\gamma}{d_j}; \quad x_j = \frac{S_j\omega}{d_j \operatorname{sh}\beta_j}; \tag{3.47}$$

d_j is the distance between the lines in the j-th group, described by the Elsasser model with line S_j, N is the number of groups.

The limiting relations for $\beta_j \ll 1$ are obtained analogously as in the Elsasser model:

1) All $x_j \gg 1$,

$$A = \sum_{j=1}^{N} x_j\beta_j = \omega \sum_{j=1}^{N} S_j/d_j; \tag{3.48}$$

2) All $x_j \gg 1$,

$$A = 1 - \prod_{j=1}^{N} \left(1 - \Phi \sqrt{\tfrac{1}{2}\beta_j x_j}\right); \qquad (3.49)$$

3) All x_j on the order of unity,

$$A = \prod_{j=1}^{N} \{1 - \beta_j x_j e^{-x_j} [J_0(x_j) + J_1(x_j)]\}. \qquad (3.50)$$

As in the case of preceding models, for small x_j A does not depend on the pressure, and for large x_j the absorption function does depend on the product ωP.

4. Quasistatistical Model. This model was proposed by Wyatt, Stull and Plass [96] and is based on using the fundamental idea in the statistical model. The spectral interval $\Delta\nu$ in which the absorption function must be determined is broken up into smaller intervals δ for each of which a statistical model is used. In this manner the main disadvantage of the statistical model is eliminated, namely the assumption that the position and line intensities in a given interval are random. In fact, the smaller the spectral interval, the more valid this assumption of the statistical model must be.

The lines which lie within each interval δ are classified by intensity into five groups, for each of which the spectral transmission $f_i(\nu)$ is determined in the center of the interval. Then a simple multiplication of the values of $f_i(\nu)$ which were obtained gives the spectral transmission in the center of the interval δ, which is considered to be the mean spectral transmission of the interval. When we know the mean spectral transmissions in the intervals δ, we can easily find the transmission function in a wider interval Δ. The procedure which has been described makes it possible to take into account with sufficient accuracy the contribution to the radiation absorption in a given spectral interval from the lines, the centers of which lie beyond the limits of this interval.

We note that the method of breaking up the spectral intervals under consideration into small intervals and using the statistical model has also been applied in the work of V. N. Soshnikov [95, 97].

5. Some General Conclusions. A comparison of the main formulas for the absorption function in the models which have been considered shows that in all cases the argument is the quantity

$$x = \frac{S\omega}{2\pi\gamma^0 P}, \qquad (3.51)$$

where S is the total line intensity in the Elsasser model, $S = \bar{S}$ or $S = \bar{S}_0$ in the statistical model and $S = S_j$ in the combined model.

Depending on the quantity x, in each model one or another simple asymptotic formula will hold for the absorption function. It is essential that the parameter x depends on the ratio ω/P, but not on the pressure P and the mass of the absorbing gas ω, which are taken into account separately.

In the case $x \ll 1$ the absorption function in all models of the spectrum does not depend on the pressure. It can be shown that the inequality $x \ll 1$ is equivalent to the condition $\omega k(\nu) \ll 1$ for all ν in a given interval $\Delta\nu = \nu_2 - \nu_1$ [88]. By equivalence we mean here that both conditions yield the same results.

For $x \gg 1$ the absorption function in all models depends on $\sqrt{\omega P}$. It can be shown that the corresponding asymptotic formulas are obtained from the general expression (3.23) for the absorption function when $(\nu - \nu_i)^2 \gg \gamma^2$. The physical meaning of this condition is that the value of the integral (3.23) is determined by integration over the regions occupied by the tails of the lines.

The limits of the applicability of various formulas for the absorption functions in the case of the Elsasser, the statistical and the combined models have been studied by Plass [98]. The numerical calculations which we carried out have shown that the transition region between the asymptotic cases $x \ll 1$ and $x \gg 1$ is comparatively small. It can be assumed approximately that a relation of the first type becomes directly a relation of the second type.

The expressions for the absorption functions in all models contain also the characteristics of the spectral lines in the interval under consideration, i.e., the distance between them,

their intensity and halfwidth. For the time being not enough theoretical or experimental data is available for these line characteristics. Therefore, the coefficients in the formulas for the absorption functions which contain the line parameters are usually considered when the models are used in practice as fitted parameters which are determined from the experimental data. The methods used to determine these parameters in the case of the statistical models have been worked out in detail by Godson [99, 100].

The second factor which restricts the possible use of the method of modeling the spectrum is the assumption that the linewidth is constant, i.e., ignoring the relation between the halfwidth of the lines and the rotary quantum number.

In spite of the shortcomings which have been pointed out, calculating the absorption functions using the concept of a model yields satisfactory accuracy for all practical purposes.

The important advantage of the model method besides the simplicity of the calculations is the fact that it is possible to estimate quantitatively with their aid the infrared radiation absorption in the atmosphere in those cases when this cannot be done experimentally or when doing this would be so costly and laborious that the expenses entailed in the process would be incommensurate with the results obtained (for example, when radiation propagation is studied at high altitudes both along the horizontal and slanted directions, etc.). The model method has also the important property that it is possible to obtain for the absorption function A formulas, which can be expressed in terms of elementary functions, which in turn makes it possible to analyze the dependence of this function on its arguments in general form.

It should also be noted that in experimental absorption studies due to the limited resolution capacity of spectral instruments we measure not the spectral absorption $A(\nu)$ or the transmission $f(\nu)$ but the absorption (transmission) function in a certain spectral interval, which depends on the spectrometer parameters.

Finally, the formulas from model theory can be very useful when absorption function calculations are made using the direct method. They can reduce considerably the amount of computational work after the positions of the centers, the intensity and the halfwidth of the lines in the corresponding regions of the spectrum are calculated using the direct method.

3. Experimental Determination of Absorption Functions. A great amount of work has been devoted to determining experimentally the absorption functions for various atmospheric gases under natural and laboratory conditions, the main results of which will be considered below. Here we will only touch on the advantages and disadvantages of determining experimentally absorption functions in comparison with the computational methods considered above.

The experimental determination of absorption functions is free of the requirement that the overlap in the lines be taken into account, since the latter takes place atomatically. The methods used to measure the absorption functions are relatively simple, which, however, does not apply to the corresponding apparatus.

Besides the complexity of the apparatus, the experimental methods used to find the absorption functions has also some other disadvantages. The most important disadvantage is related to the limited resolution capacity of spectral apparatus, which distorts the real picture of the spectrum and causes errors in the determination of the absorption functions in relatively narrow spectral intervals (of widths less than the entire absorption band). In several cases the experimental determination of absorption functions is a very difficult problem (for example, absorption function measurements along the horizontal traces at various altitudes or in slanted directions when the terminal points of the measurement trace lie in the atmosphere).

Concluding the paragraph about the methods used to determine the absorption functions, we should note that each of the methods considered has its own advantages and disadvantages and an equal claim to existence. The development of all methods considered can ensure a quick solution to the problem of obtaining sufficiently accurate quantitative data about atmospheric gas absorption functions in various sections of the visible and infrared region of the spectrum.

4. Limits of Applicability of the Buger-Beer Law

When the absorption coefficient $k(\nu)$ [see (3.1)] and the absorption function A [see (3.7a)] were defined, we assumed that the Buger-Beer Law holds. This assumption is also used when the analytical expressions for the absorption functions are derived in all spectral models. Finally, when the experimental data are processed it is also usually assumed that the Buger-Beer law holds. With regard to what has just been said

it is necessary to study the limits of applicability of this law. In the process we must distinguish real and apparent deviations from the law. We will consider both types of deviations.

The Buger-Beer law is derived from two fundamental assumptions, which were later analyzed theoretically by A. A. Gershun [101] and Strong [102]. To characterize these assumptions we will write the expression for the law in the following form:

$$I(\nu) = I_0(\nu)\, e^{-k(\nu)cl}. \tag{3.52}$$

When (3.52) is derived, the assumption is made that the absorption coefficient $k(\nu)$ depends neither on the intensity of the incident radiation $I_0(\nu)$ nor in the concentration c. The first assumption was verified experimentally by S. I. Vavilov [103], who has shown that it is valid, when $I_0(\nu)$ changes almost by 20 orders, for electronic transitions in which the lives of the atom are of short duration in the excited state τ. When S. I. Vavilov studied electronic transitions with large τ, he found that the absorption coefficient does depend on $I_0(\nu)$.

To the best of our knowledge, the dependence of the coefficient $k(\nu)$ on $I_0(\nu)$ has not been verified for vibration-rotation transitions in atmospheric gas absorption spectra. However, in this respect certain conclusions can be made, starting out with the fact that the total solar radiation absorption in the earth's atmosphere which was calculated for individual lines and groups of lines did agree well with the experimental data, for example, in the work of Houghton [104]. Analogous results were obtained in a number of other papers, for wide spectral intervals which contained entire absorption bands. This shows that for the lines and bands which were studied for values of $I_0(\nu)$ which are characteristic of the solar radiation spectrum, the dependence of $k(\nu)$ or $I_0(\nu)$ is negligible. It is not possible to draw any other conclusions without additional studies. Apparently, we should expect a dependence of $k(\nu)$ on $I_0(\nu)$ when powerful lasers are used for the radiation sources. Here the dependence of $k(\nu)$ on $I_0(\nu)$ will be different for different lines.

The independence of $k(\nu)$ of the concentration c, means that every molecule absorbs the radiation independently of the other molecules. As many experimental studies have shown, this assumption is valid when the absorbing particle concentrations are small. If the absorbing gas concentrations are increased and extraneous gases are added, the intermolecular interaction effects are magnified, which, in turn, change the values of the absorption coefficient and lead to real deviations from the Buger-Beer law. In the infrared region this effect was observed experimentally for the first time by Angstrom [105] in his studies of total carbon monoxide absorption. Schaefer [106] studied CO_2 spectral absorption in the bands 2.7 and 4.3 μ and also discovered a relation between $k(\nu)$ and the partial pressure. Eva Bahr [107] studied the infrared radiation absorption by mixtures consisting of various absorbing and extraneous gases and reached the conclusion that the observed deviations from the Buger-Beer law are caused by intermolecular collisions. The intermolecular interactions lead to a broadening of the spectral absorption lines which depends on the partial pressures of the absorbing and extraneous gases and temperature. The broadening in the spectral lines leads, in turn, to a change in $k(\nu)$. When applied to the infrared radiation absorption conditions in the atmosphere where the total pressure does not vary much in time at a given altitude and the partial pressures of the absorbing gases are small compared to the total pressure, in the majority of cases, when great accuracy of the solution of the corresponding problem is not required, the Buger-Beer law can be considered to be valid. It must be kept in mind that the absorption coeffient $k(\nu)$ when the radiation is propagated along the horizontal traces at various altitudes will be different for the same frequency ν, since the total and partial pressure of the absorbing components do depend on the altitude. In the case when certain infrared radiation absorption characteristics must be determined with great accuracy when the radiation is propagated along the horizontal traces, it must be kept in mind that for a concentration of the fundamental absorbing component of the atmosphere (water vapor), equal to 1% of the volume, the contribution to the broadening of the absorption lines due to molecular collisions in the water will be equal approximately to 5% of that obtained from the collision of water and air molecules.

We will now consider the apparent deviation from the Buger-Beer law caused by the limited resolution capacity of instruments used in experiment absorption studies. It is known that a light beam emanating from any spectrometer contains the frequency interval which is determined by the resolving power of

the instrument. The highest resolution obtained in spectrometers with the fraction lattices in the nearest infrared region is equal to 0.025 cm^{-1} [108] - [110]. The halfwidth of the individual lines of the rotation-vibration absorption bands (see para. 5) in the lower layers of the atmosphere fluctuates from several hundredths to several tenths of an inverse centimeter. This means that even if instruments with a high resolution capacity are used, the spectral width of the instrument slit has the same order of magnitude as the width of the absorption line. The output slit of standard spectrometers receives several lines or several groups of lines. The spectral transmissions $T(\nu)$ recorded by the instrument will not be equal to its real value $f(\nu)$. In fact, $T(\nu)$ will characterize the transmission function which is distorted by the action of the spectrometer apparatus function for the interval $\Delta\nu$, which is equal to the spectral width of the output slit of the instrument (Fig. 3.1, 3.2).

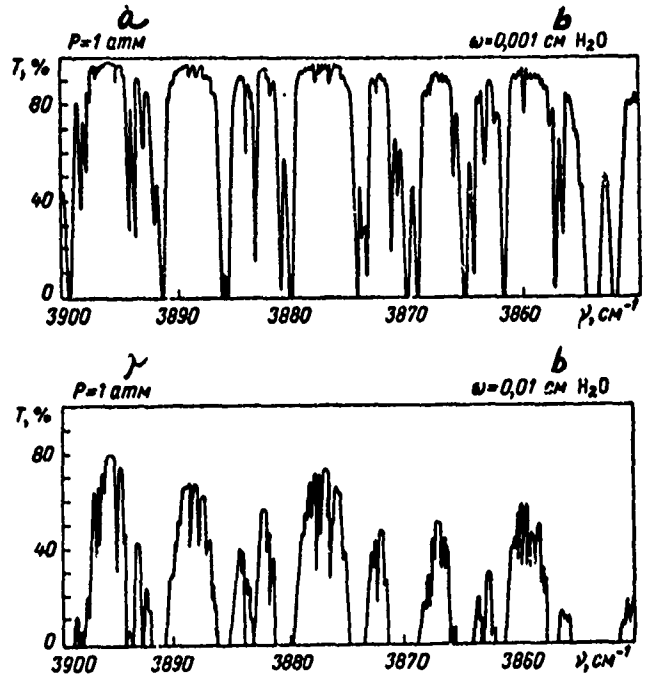

Fig. 3.1. Completely resolved absorption spectrum of water vapor in the region 3850 - 3900 cm^{-1} (2.56 - 2.6 μ) at a pressure P = 1.0 apm and a settled water layer w = 0.001 cm (top curve) and w = 0.01 cm (bottom curve) [189].

Key: a. atm
b. cm

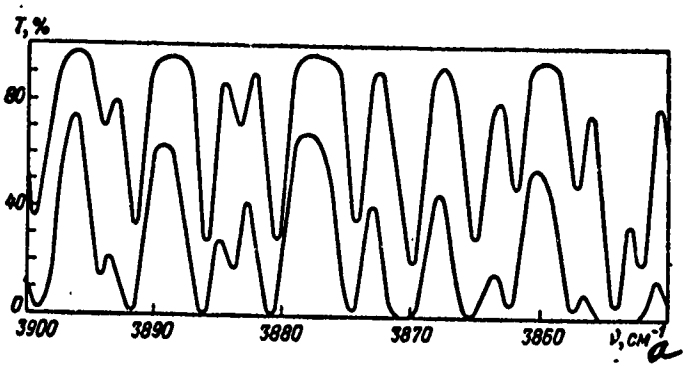

Fig. 3.2. Water vapor absorption spectrum obtained by multiplying T(ν) (Fig. 3.1) by the apparatus function with widths 2a = 2.0 cm^{-1} [189]

Key: a. cm^{-1}

The distorting effect of the spectrometer on the actual spectral picture and the related deviation from the Buger-Beer law is greater the smaller the resolution power of the instrument and the more the absorption coefficient depends on the frequency. Only in the case when k(ν) = const in the spectral interval under consideration the spectral transmission will be equal to the actual value.

The spectral absorption A'(ν) is related to the actual absorption A(ν) and the apparatus function S by the relation

$$A'(\nu)=\int_{-\infty}^{\infty} S(\nu-\nu')A(\nu')d\nu'.$$

If the apparatus function given is a Gaussian distribution, then A'(ν) takes on the form

$$A'(\nu)=\frac{\sqrt{\ln 2}}{a^2\sqrt{\pi}}\int_{-\infty}^{\infty}\exp\left\{-\frac{\ln 2}{a^2}(\nu-\nu')^2\right\}A(\nu')d\nu',$$

where a is the halfwidth of the apparatus function. Using the Fourier transform, we can write

$$A(\nu)=\frac{1}{2\pi}\int_{-\infty}^{\infty}\frac{A'(\omega)}{S(\omega)}\exp(-i\omega\nu)\,d\omega,$$

where $A'(\omega)$ and $S(\omega)$ are the transforms of $A(\nu)$ and $S(\nu)$.

Kostkowski and Bass [784] calculated $A(\nu)$ exhaustively for the cases when the absorption line has the dispersion form and the apparatus function is described by the Gaussian distribution. A detailed theoretical study of the effect of the spectrometer on the spectral and total transmission measurement result has been carried out in the work of Nielsen, Thronton and Dolle [111], where it was shown for the first time that the total band absorption does not depend on the width of the instrument slit. This was subsequently confirmed experimentally in the work of Howard [112] and in our work [113, 114]. V. P. Kozlov and E. O. Fedorova [115] derived a formula, which can be used to estimate the maximum error made on the interval $\Delta\nu$ when the total transmission is determined by the spectrometer from its known apparatus function.

The effect of the spectrometer on the spectral absorption measurement results due to the apparatus function, the spectral width of the slit and the scanning speed and the selection of optimum measurement conditions have been studied in many papers (see, for example, the surveys [116, 117, 785] and articles [118 - 123]).

5. Fine Structure of the Vibration-Rotation and Pure Rotation Spectrum of Water Vapor

We will consider the state of theoretical and experimental studies of the position of line centers, their intensities and halfwidths in the vibration-rotation and pure water vapor spectrum.

1. Position of Line Centers

1. Theoretical Study

The position of the absorption line centers ν_{0i} can be calculated on the basis of quantum absorption theory. To find ν_{0i}, we must have the molecular energy levels and the transition combinations from which we can obtain according to the known selection rules the quantities sought. The vibration-rotation molecular levels can be obtained approximately by

simply summing the vibration and rotation energy, which were determined separately.

The vibration energy problem of a molecule has been studied in detail by Dennison [124], Bonner [125], Escart [126] and others, who have shown that the solution of the quantum mechanics anharmonicity oscillator problem requires that the anharmonicity constants be known. To find these constants, the corresponding experimental data must be used. G. A. Khachkuruzov [127] calculated in this manner the energy for the first 100 water molecule vibration levels.

The problem of determining the rotation energy for a molecule of the asymmetric gyroscope type, which includes the water molecule, was solved by Wang [128] and Ray [129]. Ray introduced the concept of an asymmetric parameter and has shown that the problem can be reduced to finding a certain quantity which depends only on this parameter. The Ray method was further developed and reduced to numerical calculations by King, Hainer and Cross, who published tables which can be used to calculate the rotation energy up to $j = 12$ [130]. These authors have shown in article [131] the method for calculating the rotation energy for $j > 12$ which Erlandsson used to calculate the rotation energy up to $j = 40$ [52].

Thus, the apparatus for calculating approximately the vibration-rotation energy of an H_2O molecule has been worked out. The accuracy with which ν_{0i} is determined is fully adequate for the solution of many problems which require that the transmission function be known in intervals which are not very narrow. In those cases when the problem requires spectral transmission data $T(\nu)$, for example, when a laser is used as the light source, the approximation considered is inadequate, especially for lines caused by transitions with high j. To determine exactly the vibration-rotation energy levels of the molecule, and consequently the ν_{0i} values, we must take into account the interactions between the vibrations and oscillations. The first attempt to do this with the aid of the perturbation method was made by Wilson and Howard [132]. These men have shown that when the interactions are taken into account new terms appear in the operator for the rotation energy, the coefficients of which were called the "centrifugal distortion constants." Wilson [133] was able to find an analytic relation between these constants and the parameters of the molecule. The study of M. A. El'ychevich [134] is also devoted to this problem, who derived general formulas for the centrifugal distortion constants.

Schaefer and Nielsen [135] found the vibration-rotation energy values, the centrifugal distortion constants for a molecule of the XY_2 type and derived an equation which can be used to determine most anharmonicity constants. The solution of Schrödinger's differential equation for an asymmetric gyroscope is also treated in the work of Majumdar [136, 137], who, in particular, carried out the numerical calculations of the vibration-rotation energy for j = 10. A comparison of the calculations with Benedict's data [138] has shown that their difference does not exceed 3.48 cm^{-1} for energy values from 1114.6 cm^{-1} ($j_\tau = 10_{-10}$) to 2698.6 cm^{-1} ($j_\tau = 10_{10}$), which shows good agreement between the corresponding calculated and experimental data.

However, the accuracy for calculating the positions of the lines which was mentioned is completely inadequate in the solution of problems related to the quantitative estimation of OKG (laser) radiation absorption in the atmosphere and for problems in which the absorption functions must be found in narrow spectral intervals. Thus, the results which have been obtained in the theory until the most recent time have not given the required accuracy for determining the position of the line centers. For this reason the appropriate studies were made in the laboratory of the author, the results of which were described in detail and published in articles [139-147, 343, 779].

To find the system of vibration-rotation levels, the complete Schrödinger equation for the vibration-rotation movement of molecular nuclei,

$$H\psi = E\psi, \tag{3.53}$$

must be solved where H and ψ are the vibration-rotation Hamiltonian and the wave function of the molecule, E are the eigenvalues of the energy operator.

The vibration-rotation Hamiltonian for molecules of the XY_2 is written in the form

$$H = H_0 + \frac{1}{2}\sum_{\alpha\beta}\mu_{\alpha\beta}P_\alpha P_\beta - \frac{1}{2}g_z P_z, \tag{3.54}$$

where H_v is the Hamiltonian of the anharmonicity vibrations of the system of nuclei, which is written either in exact form [132, 135, 148, 149] or in approximate form [145], P_α is an operator of the projection of the complete angular moment on the α axis of the coordinate system rigidly connected to the molecule (α = x, y, z), $\mu_{\alpha\beta}$ is a known [132] function of the normal coordinates q_k(k = 1, 2, 3), $g_z = \mu_{zz}P_z + P_z\mu_{zz}$; $P_z = \sum_{ik} G^z_{ik} q_i P_k$ is the projection of the angular vibration moments on the z axis and G^z_{ik} is the Coriolis constant.

Since it is not possible to obtain a solution of the Schrödinger equation with a Hamiltonian of the form (3.54) in closed form, various approximate methods are used. The usual approach is as follows: using a unitary transformation [134] or a sequence of contact transformations [150-153], the matrix of the operator H is reduced to diagonal form in terms of the vibration quantum numbers. Next from the diagonal elements the rotation energy operator is isolated and the eigenvalue problem for a non-rigid asymmetric gyroscope is solved.

We will follow this general procedure, but we will diagonalize the matrix of the operator H with the aid of perturbation theory. In (3.54) we take for the zero approximation $H^0 = H_v$, so that the perturbation operator is

$$\omega = \frac{1}{2}\sum_{\alpha\beta}\mu_{\alpha\beta}P_\alpha P_\beta - \frac{1}{2}g_z P_z, \qquad (3.55)$$

and the matrix elements $\langle v|\omega|v'\rangle$ are noncommutative relative to the rotation variables. If we use the available formulas from ordinary perturbation theory, then we run into difficulties already in the third approximation, which are due to the indeterminacy of the order of the matrix elements. However, in the process of writing the formulas from perturbation theory, we can determine uniquely the order in which the matrix elements follow one another.

We will consider the limits of the applicability of perturbation theory in this case.

It is known that the condition for the applicability of perturbation theory is written in the form [154]

$$\left|\frac{\langle v|w|v'\rangle}{E_v - E_{v'}}\right| \ll 1. \tag{3.56}$$

We note that as El'yashevich has shown [134] in the expansion for the vibration energy operator the ratio of the last term to the preceding term is approximately equal to λ. For light molecules, such as the water molecule, $\lambda \approx 10^{-1}$. Simple estimates further enable us to write

$$\left|\frac{\langle v|w|v'\rangle}{E_v - E_{v'}}\right| \approx \lambda^3 j^2, \tag{3.57}$$

where j is the rotation quantum number, E_v are the eigenvalues and $\langle v|$ are the eigenfunctions of the operator $H^0 = H_v$.

Thus, for rotation levels with the quantum number $j<31$, the condition for the applicability of perturbation theory is satisfied in the given case. We must note that for those vibration levels, for which the energy is approximately equal (random degeneracy), the estimates which were given need not hold, so that if the method which was described is used in such cases, caution must be exercised.

Equality (3.57) enables us to estimate the orders of the contributions of various approximations in the rotation energy operator $H_R^{[r]}$ in relation to the zero approximation. For the zero approximation we take the Hamiltonian of an effective rigid asymmetric gyroscope:

$$(H_R^{[r]})^{(0)} = \frac{1}{2}\sum_{\alpha} a_{\alpha\alpha} P_\alpha^2, \tag{3.58}$$

where $a_{\alpha\alpha} = \langle v_1 v_2 v_3 | \mu^0_{\alpha\alpha} | v_1 v_2 v_3\rangle_0$ are the effective rotation constants.

Because of the properties of the perturbation operator, the corrections from each approximation are nonhomogeneous. For approximation number n there are n + 1 terms for n even and n terms for n odd. The orders of these terms for each j are generally different. For example eighth degree terms of the angular moment projections from the fourth approximation become larger as j increases (for $j \geqslant 10$) than sixth order angular moment projection terms from the third approximation,

i.e., a redistribution of the contribution of individual terms occurs. Within each approximation a redistribution of the contributions also occurs. For example, in the second approximation, for $j<10$, the greatest contribution to the nonrigid gyroscope Hamiltonian should occur from terms with P_a^2 while for $j \approx 30$ the maximum contribution comes from the terms with P_a^1.

A detailed analysis of the problem made it possible to obtain an estimate of the absolute admissible error when the matrix elements of the $H_{it}^{[v]}$ operator are calculated for any $1 \leqslant j \leqslant 30$ and the maximum error when the rotation level energy is determined. Thus, in order that the errors for $j = 10$ do not exceed 0.1 cm^{-1}, we must take into account all terms which contain P^2, P^3, P^4, P^5, P^6, P^8 up to the fourth approximation. At the same time we need not take into account terms with P^7. After transformation with the aid of the commutative relations, the nonrigid gyroscope Hamiltonian $H_{it}^{[v]}$ can be written in the fourth approximation in the following form:

$$H_R^{[v]} = \sum_{\alpha} b_{\alpha\alpha} P_\alpha^2 + \sum_{\alpha\beta\gamma\delta}' \tau_{\alpha\beta\gamma\delta} P_\alpha P_\beta P_\gamma P_\delta + \\ + \sum_{\alpha\beta\gamma\delta\varepsilon\eta} [\alpha\beta\gamma\delta\varepsilon\eta] P_\alpha P_\beta P_\gamma P_\delta P_\varepsilon P_\eta + \\ + \sum_{\alpha\beta\gamma\delta\varepsilon\eta\nu\xi} [\alpha\beta\gamma\delta\varepsilon\eta\nu\xi] P_\alpha P_\beta P_\gamma P_\delta P_\varepsilon P_\eta P_\nu P_\xi. \tag{3.59}$$

Simple but laborious calculations enable us to find an analytic expression for the effective rotation constants $b_{\alpha\alpha}$ and the centrifugal distortion constants $\tau_{\alpha\beta\gamma\delta}$, $[\alpha\beta\gamma\delta\varepsilon\eta]$ and $[\alpha\beta\gamma\delta\varepsilon\eta\nu\xi]$. For example

$$[\alpha\beta\gamma\delta\varepsilon\eta\nu\xi] = \sum_k \mu_{\alpha\beta}^k \mu_{\nu\xi}^k \frac{\tau_{\gamma\delta\varepsilon\eta}^k}{2\hbar\omega_k^2} + \\ + \sum_{ik} \mu_{\alpha\beta}^k \mu_{\gamma\delta}^i \mu_{\varepsilon\eta}^k \mu_{\nu\xi}^i \frac{1}{\omega_i^2 - \omega_k^2} \left(v_k + \frac{1}{2}\right). \tag{3.60}$$

Here ω_i is the fundamental frequency, $\tau_{\gamma\delta\varepsilon\eta}^k$ is the linear coefficient in the expansion for the centrifugal distortion constants of order two in terms of the rotation quantum numbers, $\mu_{\alpha\beta}^k = \left(\frac{\partial \mu_{\alpha\beta}}{\partial q_k}\right)_{q=0}$. We will now write the complete vibration-rotation

Schrödinger equation in the following form:

$$[H_v + H_R^{[v]} + H_{Rv} - H_R^{[v]}]\,\psi = E\psi, \tag{3.61}$$

where we introduced H_{Rv} to denote the second and third terms in (3.54).

Perturbation theory is used to solve equation (3.61). The operator $H_v + H_R^{[v]}$ is taken for the zero approximation. Then from the method used to obtain the operator $H_R^{[v]}$ it follows that the total vibration-rotation energy is

$$E = E_v + E_R^{[v]} \tag{3.62}$$

with an accuracy up to the terms which were ignored in $H_R^{[v]}$.

The complete normalized vibration-rotation functions in the second approximation in perturbation theory are written in the form

$$\begin{aligned}\psi_{vj\tau} = (1 + C^{(2)}_{vj\tau,\,vj\tau})\,\psi_v\psi_{j\tau}^{[v]} + \sum_{v'j'\tau'}{}' (C^{(1)}_{vj\tau,\,v'j'\tau'} + \\ + C^{(2)}_{vj\tau,\,v'j'\tau'})\,\psi_v\psi_{j'\tau'}^{[v']},\end{aligned} \tag{3.63}$$

where

$$C^{(1)}_{vj\tau,\,v'j'\tau'} = \langle v'j'\tau' \,|\, RH_{Rv} \,|\, vj\tau\rangle; \tag{3.64}$$

$R = \frac{1}{E_v - H_v}$ is the resolvent operator in the vibration problem

$$\begin{aligned}C^{(2)}_{vj\tau,\,v'j'\tau'} = [\langle v'j'\tau' \,|\, R_{Rv} \,|\, v'j'\tau'\rangle - \\ - \langle vj\tau \,|\, H_{Rv} \,|\, vj\tau\rangle]\,\langle v'j'\tau' \,|\, R^2H_{Rv} \,|\, vj\tau\rangle + \\ + \tfrac{1}{4} b_{zz}(vv')\,\langle j\tau' \,|\, P_z^2 \,|\, j\tau\rangle + \\ + \tfrac{1}{4}\sum_{\alpha\beta}[b_{\alpha\beta z}(vv')\,\langle j\tau' \,|\, P_\alpha P_\beta P_z \,|\, j\tau\rangle + \\ + b_{z\alpha\beta}(vv')\,\langle j\tau' \,|\, P_z P_\alpha P_\beta \,|\, j\tau\rangle + \\ + \tfrac{1}{4}\sum_{\alpha\beta\gamma\delta} t_{\alpha\beta\gamma\delta}(vv')\,\langle j\tau' \,|\, P_\alpha P_\beta P_\gamma P_\delta \,|\, j\tau\rangle;\end{aligned} \tag{3.65}$$

$$C^{(2)}_{vj\tau,\,vj\tau} = \frac{1}{2}\sum_{\alpha} b_{\alpha\alpha}(vv)\langle j\tau|P_\alpha^2|j\tau\rangle + \\ + \frac{1}{4}\sum_{\alpha\beta\gamma\delta} t_{\alpha\beta\gamma\delta}(vv)\langle j\tau|P_\alpha P_\beta P_\gamma P_\delta|j\tau\rangle. \qquad (3.66)$$

The constants $b_{\alpha\alpha}(vv)$ are analogous to the corrections for the effective rotation constants and the constants $t_{\alpha\beta\gamma\delta}$ - to the corrections for the centrifugal distortion constants:

$$b_{zz}(vv) = -\frac{1}{2}\langle v|g_z R^2 g_z|v\rangle;$$
$$b_{\alpha\alpha}(vv) = \pm i\hbar\langle v|g_z R^2|\mu_{xy}|v\rangle, \quad \alpha = x, y; \qquad (3.67)$$
$$t_{\alpha\beta\gamma\delta}(vv) = \langle v|\mu_{\alpha\beta}R^2\mu_{\gamma\delta}|v\rangle.$$

With regard to the constants $b_{\alpha\beta z}(vv')$, $b_{z\alpha\beta}$, b_{zz} and $t_{\alpha\beta\gamma\delta}$, these have the following form:

$$A(vv') = (-1)^n\langle v'|R_a R_b|v\rangle, \qquad (3.68)$$

where a, b are various combinations of the g_z and $\mu_{\alpha\beta}$ operators, n is the number of g_z operators among a and b.

On the basis of the expressions obtained estimates were calculated for the contribution of various terms in the 2-nd, 3-rd and 4-th approximation to the Hamiltonian of the nonrigid gyroscope for j = 1 (1) 30. The data obtained enable us to determine the maximum order of the approximation for the operator $H_R^{[v]}$, which must be used to find for a known j the position of the center of the corresponding line with the required accuracy. The subsequent procedure for solving the problem reduces to the following. All coefficients in the expression for $H_R^{[v]}$ are found, the operator matrix is constructed, and is diagonalized numerically. Then the eigenvalues of the operator $H_R^{[v]}$ are found, and from formula (3.67) the values of the total vibration-oscillation energy are found, from which, using the selection rules the centers of the corresponding lines are easily found.

2. Experimental Studies

A great deal of work has been devoted to the study of the fine structure of the pure rotation and vibration-rotation

spectra [206]. The first studies of the vibration-rotation bands were carried out by Sleator [155] and Sleator and Phelps [156]; however, the resolution obtained did not make it possible to carry out an analysis of the rotational structure. In this connection Plyler and Sleator [157] and then Plyler [158] investigated new bands with improved resolution. Using the data in [157 and 158] and also the results of natural measurements in the photographic region of the spectrum, Mecke and his collaborators [159 - 161] carried out for the first time an analysis of the rotation structure of individual bands and determined the moments of inertia and the geometric parameters of a water molecule.

Nielsen [162] studied the water vapor spectrum with high resolution in the region of fundamental vibration frequencies and the combination frequency bands $(\nu_1 + \nu_3)$ and $(\nu_2 + \nu_3)$. Nielsen and Benedict [163] with a somewhat better resolution than in [162] studied the spectral region from 1.34 to 1.97 μ. In [164] Benedict and Plyler made a second study of the 2.7 μ band, with high resolution. The authors of [164] gave a new identification for lines in the band ν_1, extended the structural analysis of the band ν_3 and gave the values of the rotation terms (100) and (001) states up to j = 13. Additional data for the analysis for the fine structure of the water vapor spectrum is given in the work of Benedict [165]. Plyler, Gailar and Wiggins [60] studied with high resolution the vibration-rotation water vapor spectrum and determined with great difficulty certain wavelengths which are needed to calibrate spectrometers.

The water vapor spectrum in the regions 4.5 - 5.7 and 6.6 - 13 μ have been studied in detail by Benedict, Claassen and Shaw [166]. As a result of the work a more detailed analysis of the rotation structure of the ν_2 band was carried out, the rotation terms of the fundamental state were determined up to j = 18, and the terms for the (010) and (020) states were calculated, and the values for several rotation constants of the H_2O molecule were obtained. The 5.26 - 7.14 μ spectral region has been studied in detail with high resolution by Dalby and Nielsen [167]. The studies of the section of the water vapor sector in the 1.9 μ region with high resolution [168] made it possible to obtain data about high vibration state levels and absorption bands between the high vibration levels: (021) → (010) and (031) → (020).

The pure rotation water vapor absorption spectrum with high resolution was studied by Barnes and Benedict [169] who

improved the accuracy of the Mecke data. The most detailed study in the 18 - 135 μ region was carried out by Randall, Dennison, Ginsberg and Weber [170] and Dennison [171], who recorded more than 200 absorption bands. N. G. Yaroslavskiy and A. E. Stanevich [172] extended considerably the high resolution rotation absorption spectrum studied. Their measurements were made in the range 20 - 2500 μ. New data about the pure water vapor rotation spectrum in the wavelength range 55 - 1000 μ was obtained by N. I. Furashov [173].

We will briefly consider studies of the fine structure of the water vapor absorption spectrum under natural conditions. In the majority of cases, the radiation source used was the sun. Together with the water vapor absorption spectrum measurements which were made under natural conditions, the spectra of other gases in the atmosphere were also recorded. For this reason it is not always possible to fully identify the lines because of the corresponding overlap of the spectra. Nevertheless, most lines were identified.

The first atlas of the solar radiation absorption spectrum in the earth's atmosphere was published by Minnaret, Mulders and Houtgast in 1940 [174]. This atlas contains the spectral region 3612 - 8771 Å which is easily accessible to photograph recording of the spectrum. In 1947 Babcock and Moore [175] published the data which they obtained for the solar spectrum in the wavelength region 6600 - 13495 Å. Mohler and his collaborators carried out measurements and compiled the atlas of the solar spectrum in the region from 0.8 to 2.6 μ [176]. In articles [177] and [178] Mohler and Benedict identified the lines of this atlas. A group of researchers from the Ohio University published atlases of the solar spectrum for the regions 3.0 - 5.2 μ [179] and 7 - 13 μ]180]. In the 1 - 13 μ region of total complexity above 1600 lines were found, out of which more than 70% belonged to water vapor.

Migeotte, Neven and Swenson at the Jungfrau High Altitude Station in the Swiss mountains (altitude 3580 m) recorded the solar spectrum in the wavelength range 2.8 - 23.7 μ [181]. In this atlas, the authors of [181] together with Benedict identified over 3600 individual lines [182]. Using perfected apparatus, Delbouille and Roland [183] obtained at the same Jungfrau station a new atlas of the solar spectrum. About 10 500 lines were discovered in the relatively narrow region from 0.75 - 1.2 μ.

Farmer and Key [184] recorded the solar radiation spectrum at an altitude of 5200 m in the Bolivian Andes for the wavelength range 7 - 400 μ. In the 7 - 30 μ region the spectrum

was obtained with 0.3 cm^{-1} resolution, and new telluric H_2O absorption lines were recorded. In the region from 40 - 400 μ, the solar radiation in the atmosphere column above 5.2 μ is absorbed almost completely for all practical purposes with the exception of a relatively narrow transparent atmosphere window which was discovered by the authors [184] near the wavelength 345 μ.

The absorption spectrum near the earth's atmosphere layer at a distance of 16.3 km which was obtained with high resolution in the range from 5400 to 8520 Å was published by Curcio [185] in 1963. Due to the sufficiently high resolution and the thick atmosphere many weak absorption lines were detected in [185] in the visible spectral region.

In 1966, Moore, Minnaret and Houtgast published tables of the absorption spectrum of the earth's atmosphere which contained in the region 2935 - 8770 Å about 24 000 lines.

Oppenheim and Goldman [187] compiled an atlas of the water vapor absorption spectrum in the band regions 1.9 and 2.7 μ at a temperature of 1200°K. The atlas reflected lines caused by the transitions between the high energy vibration-rotation levels of the H_2O molecule.

We will summarize the main experimental studies of the water vapor absorption spectrum under laboratory and natural conditions. At the present time the position of many lines in both the vibration-rotation as well as the pure rotation H_2O spectrum have been determined. However, it should be noted that in many cases even in the spectra which were recorded with the highest resolution, many lines which lie closely to one another have not been resolved. Often groups of lines are taken for the individual lines. In particular, this applies to the regions of the spectrum which contain both strong and weak lines. The accuracy with which the line centers are determined in the ultraviolet, visible and near infrared regions fluctuates between the limits from several hundredths to 0.1 - 0.2 Å.

2. Line Intensities

1. Theoretical Studies

The calculation of the spectral line intensities of molecules of the rigid asymmetric gyroscope type presents no theoretical difficulties. At the present time sufficiently detailed data is available [188, 878], which gives the approximate

picture of the line intensities for the water vapor rotation spectrum. The real picture of the spectrum can be obtained by solving the rotation problem for the nonrigid gyroscope.

When the line intensities are calculated exactly in the vibration-rotation water vapor spectrum, the nonrigidity of the molecule and the interaction of all types of its motion must be taken into account. Usually the line intensities in the vibration-rotation H_2O bands are found using this approach [879, 880]. It is assumed that the intensity of the line is

$$S = S_{rot}S_{vib}, \qquad (3.69)$$

where S_{rot} is the rotation intensity of the corresponding line from the pure rotation spectrum, the value of which is assumed to be known, and S_{vib} is a factor which takes into account the vibration and rotation interaction. The quantity S_{vib} is determined from the experiment. It is assumed that S_{vib} is the same for all lines in a given vibration-rotation band. It is assumed that S_{vib} is the same for all lines in a given vibration-rotation band. Under such assumption integration of (3.69) along the light band gives the total intensity of the band which is determined from the experiment, and on the right the product of S_{vib} with the sum of the line intensities caused by the corresponding pure rotary transitions.

On the basis of the procedure described, the line intensities of the vibration-rotation absorption bands ν_1, $2\nu_2$ and ν_3 in the 2.7 μ region (2857 - 4444 cm^{-1}) were calculated in articles [879, 880].

In a series of calculations carried out by Benedict and Calfee [881], data were obtained for the intensity of lines in the absorption band region 1.9 and 6.3 μ. In these calculations, the interactions between the vibration and rotation movement of the H_2O molecule were partially taken into account. The tables published by the authors of [881] contain data about the position of the centers, the intensity and halfwidth of the lines in the bands $\nu_2\nu_3$, $\nu_1\nu_2$ and $3\nu_2$ in the 1.9 μ region, and the band ν_2 in the 6.3 μ region. The tabulation was carried

out for lines with $j \leqslant 20$. In [881] data were also obtained for all three parameters of the fine structure of the four "hot" bands (021 - 010, 100 - 010, 020 - 010, 001 - 010), the H_2O^{17}, H_2O^{18} isotope bands and the HDO ν_2 band. [881] contains 4110 absorption lines for bands in the 1.9 μ region (4212 - 6254.3 cm^{-1}) and 5054 lines in the 6.3 μ region (640 - 2885 cm^{-1}).

The tables contain lines the intensity of which exceeds the value 0.0001 $cm^{-1}/g \cdot cm^{-2}$. An exception to this is the central region in the band ν_2 (1400 - 1850 cm^{-1}), which included lines with intensity above 0.001 $cm^{-1}/g \cdot cm^{-2}$. The parameters of the lines of the pure rotation H_2O spectrum were calculated in the region 640 - 1000 cm^{-1}. This was done in order to obtain more complete data in the entire wave band. We note that the maximum intensity value of the lines in the band regions 1.9 and 6.3 μ were equal, respectively, to 1042.7 (the line 5413.90cm^{-1}) and 10976.2 $cm^{-1}/g \cdot cm^{-2}$ (the line 1684.84 cm^{-1}).

The assumption that S_{vib} is constant for all lines in the band on which the procedure considered is based is, strictly speaking, invalid. It does not take into account the specifics of the interaction between the molecular vibration and rotation movement for individual lines. The latter can lead to considerable errors when the intensity of the lines is calculated, which are caused by the transitions between molecular levels with high energy.

In our laboratory we attempted to develop a new procedure for calculating the intensity of lines in the vibration-rotation water vapor spectrum and take subsequently into account the interaction between the molecular vibration and rotation movements [139 - 141, 147, 190, 220, 779, 907]. We will describe the results which were obtained.

The expression for the intensity of the line is written in the form [191].

$$S_{vR}^{v'R'} = \frac{8\pi^3 N}{hcz} \Delta\omega [2-(-1)^{|\tau|}] e^{-\frac{hc}{kT}\omega_{\tau R}} \times \\ \times [1-e^{-\frac{hc}{kT}\Delta\omega}] |\langle v'R'|M_z|vR\rangle|^2. \qquad (3.70)$$

Here $\Delta\omega = \omega_{v'R'} - \omega_{vR}$, $\omega_{v'R'}$ and ω_{vR} - are the upper and lower state levels, M_z is the component of the electrical dipole moment vector in a fixed coordinate system, N is the number of particles in the absorbing gas per unit volume, z is a statistical sum, τ is the rotation quantum number, h is the Planck constant, c is the velocity of light, k is the Boltzman constant, T is the complete vibration-rotation wavefunction. The component M_z can be written in the form

$$M_z = \Phi(zx)\mu_x + \Phi(zy)\mu_y, \tag{3.71}$$

where μ_x and μ_y are the projections of the dipole moment vector on the coordinate axes, which are rigidly connected to the molecule, and Φ(z x) and Φ(zy) are direction cosines.

It follows from the symmetry of the H_2O molecule [134] that when the interaction between the vibrations and the rotation is not taken into account, for parallel bands only the second term contributes to M_z. The quantities μ_x and μ_y are expanded in a series in the normal coordinates.

For the quantity $\langle vR|M_z|v'R'\rangle$ in formula (3.70) we can obtain with the aid of function (3.63)

$$\begin{aligned}\langle vR|M_z|v'R'\rangle = \langle vR|M_z|v'R'\rangle_0 + C^{(1)}_{v'R',\,vR}[\langle vR|M_z|vR\rangle_0 - \\ - \langle v'R'|M_z|v'R'\rangle_0] + \sum_{v''R''}[C^{(1)}_{vR,\,v''R''}\langle v''R''|M_z|v'R'\rangle_0 + \\ + \langle vR|M_z|v''R''\rangle_0 C^{(1)}_{v'R',\,v''R''}].\end{aligned} \tag{3.72}$$

The terms with the coefficient $C^{(2)}$ have been omitted, since their contribution to the matrix element is of a very small order of magnitude. The second term in formula (3.72) is identically equal to zero, since $\langle R|\Phi|R\rangle \equiv 0$. because of the symmetry of the molecule. The matrix elements in the right member of (3.72) are calculated with the aid of the zero approximation function $\psi^0_{vR} = \psi_v\psi^{[v]}_R$. The rotation wavefunction $\psi^{[v]}_R$

is written in the form of an expansion in terms of the functions of a rigid symmetric gyroscope:

$$\psi_R^{[v]} = \sum_{k=-j}^{j} g_{k\tau}^{[v]} |jkm\rangle. \tag{3.73}$$

In the third term in formula (3.72), we found it necessary to sum over the rotation structure of intermediate vibration states. We will consider in greater detail this term in (3.72). Taking into consideration (3.64) and (3.61) it can be represented in the form

$$\begin{aligned}
&\frac{1}{2}\sum_{R''v''}\sum_{g}\Big\{\sum_{\alpha\beta}\Big[\frac{\langle v'|\mu_g|v''\rangle\langle v''|\mu_{\alpha\beta}|v'\rangle}{E_{v'}-E_{v''}}\times\\
&\times\langle R'|\Phi(z_g)|R''\rangle\langle R''|P_\alpha P_\beta|R\rangle+\frac{\langle v'|\mu_{\alpha\beta}|v''\rangle\langle v''|\mu_g|v\rangle}{E_{v'}-E_{v''}}\times\\
&\times\langle R'|P_\alpha P_\beta|R''\rangle\langle R''|\Phi|(zg)|R\rangle\Big]-\frac{\langle v'|\mu_g|v''\rangle\langle v''|g_z|v\rangle}{E_v-E_{v''}}\times\\
&\times\langle R'|\Phi(zg)|R''\rangle\langle R''|P_z|R\rangle-\\
&-\frac{\langle v'|g_z|v''\rangle\langle v''|\mu_g|v\rangle}{E_{v'}-E_{v''}}\langle R'|P_z|R''\rangle\langle R''|\Phi(zg)|R\rangle\Big\}.
\end{aligned} \tag{3.74}$$

The sums over the rotation states when (3.73) is taken into account have the forms

$$\begin{aligned}
&\sum_{\substack{k''\tau''\\ kk'}} g_{k\tau}^{[v]}(g_{k\tau''}^{[v'']})^2 g_{k'\tau}^{[v']}\langle jkm|P_\alpha P_\beta|jk''m\rangle\times\\
&\times\langle jk''m|\Phi|j'k'm'\rangle,
\end{aligned} \tag{3.75}$$

$$\begin{aligned}
&\sum_{\substack{\tau''k\\ k'}} g_{k\tau}^{[v]}(g_{k\tau''}^{[v'']})^2 g_{k'\tau}^{[v']}\langle jkm|P_z|jkm\rangle\times\\
&\times\langle jkm|\Phi|j'k'm'\rangle.
\end{aligned} \tag{3.76}$$

The summation over k'' in (3.75) is carried out in an elementary manner since the $\langle jkm|P_\alpha P_\beta|jk''m\rangle$ are different from zero only for k'' = k, k $\pm$ 2. Further, since the matrix $g_{k\tau}^{[v]}$

is normalized [130], $\sum_{\tau'} (g_{k\tau'}^{[v']})^2 = 1$.

The matrix elements for the direction cosines are expressed as a product of the Klebsh-Gordon coefficients, it should be noted that the approximation considered does not violate the selection rules for the rotation quantum numbers j and τ.

We will now pass on to calculating the sums over the intermediate vibration quantum states. The matrix elements which appear in these sums are calculated with the aid of the functions of a three-dimensional anharmonicity oscillator. The functions of the normal coordinate μ, $\mu_{\alpha\beta}$, g_z, v are represented in the form of series in normal coordinates, for example,

$$v = \sum_i \omega_i^2 q_i^2 + \sum_{ik} a_{iik} q_i^2 q_k + \\ + \sum_{ikl} a_{iikl} q_i^2 q_k q_l + \cdots \qquad (3.77)$$

In (3.77) the ratio of the next term to the preceding term is equal to λ. According to El'yashevich's estimates [134] $\lambda \sim 10^{-1}$. Further, the fact that the orders of the coefficients in the expansions for v, g_z, μ, $\mu_{\alpha\beta}$ increase in the same manner, we can assume the validity of the above estimate for all these quantities. This is confirmed by direct calculations using the data from papers [190, 193, 194]. To estimate the order of the contribution to the matrix element of the dipole moment from expression (3.74), we must calculate the order

$$\mu_{\alpha\beta}^0 P_\alpha P_\beta \frac{1}{E_v - E_{v'}} = \varepsilon j^2.$$

Direct calculations in accordance with El'yashevich's estimates [134] give $\varepsilon \sim \lambda^2$ for small j. We note that the quantity $\frac{g_z \mu_z}{E_v - E_{v'}}$ has also order λ^2.

In calculating the contribution from (3.74), we will restrict ourselves only to terms of order not greater than λ^3. The contribution from (3.74) can be evaluated with the aid of the formulas for the matrix elements μ and the operator g_z from the functions of the anharmonic three-dimensional oscillator [142, 144]. Because of the unwieldiness of the final

results, as an illustration, we will give only the contribution from (3.74) for the vibration transition 000 - 010:

$$\langle 000j\tau|M_z|010j'\tau'\rangle = \langle 000j\tau|M_z|010j'\tau'\rangle_0 \times$$
$$\times\left[1+\alpha+\beta\frac{S'}{S}+\gamma\frac{S(k)}{S}\right];\quad \beta=\frac{\mu_0\mu_{\lambda\tau}^{(2)}\hbar}{\sqrt{2}\,\mu_2\omega_2};$$
$$\alpha=\frac{\hbar\mu_0}{2\mu_2\omega_2}(\mu_{xx}^2+\mu_{zz}^2)+\frac{\mu_3\mu_{zz}^{(0)}\zeta_{23}^z\hbar}{2\omega_3\mu_2}\frac{\omega_2+\omega_3}{\omega_3-\omega_2};$$
$$\gamma=-\frac{\mu_0\mu_{zz}^{(2)}\hbar}{\mu_2\omega_2}-\frac{\mu_3\mu_{zz}^{(0)}\zeta_{23}^z\hbar}{\omega_3\mu_2}\frac{\omega_3^2+\omega_2^2}{\omega_3^2-\omega_2^2}; \qquad (3.78)$$
$$S=\sum_{kk'}g_{k\tau}^{[v]}(j)\,g_{k'\tau}^{[v']}(j')\,[(1j-1k|j'k')+(1j1k|j'k')];$$
$$S(k)=\sum_{kk'}kg_{k\tau}^{[v]}(j)\,g_{k'\tau}^{[v']}(j')\,[(1j-1k|j'k')-(1j1k|j'k')];$$
$$S'=\sum_{kk'}g_{k\tau}^{[v]}(j)\,g_{k'\tau}^{[v']}(j')[\sqrt{(j-k)(j+1+k)}\,(1j0k+1|j'k')+$$
$$+\sqrt{(j+k)(j-k+1)}\,(1j0k-1|j'k')].$$

The approximation considered takes into account the anharmonicity of the vibrations, the nonrigidity of the molecule and the Coriolis interaction.

We note that unlike in the zero approximation, the vibration-rotation interaction leads to the occurrence of the dipole moment in the matrix elements and its components along the x and y axes. For parallel bands the component is directed along the x axis and for perpendicular bands along the y axis. The selection rules in the rotation spectrum which are determined by the symmetry of the molecule are not violated.

2. Experimental Studies

The experimental determination of line intensities is a very complex problem. The main difficulty is that the overlap in the lines must be taken into account. At the present time the intensities of a very limited number of lines in the water vapor absorption spectrum have been determined experimentally.

Benedict, Claassen and Shaw [166] found under laboratory conditions the intensities of several rotation lines and lines from the vibration-rotation ν_2 band at a relatively high temperature and H_2O concentration. In the work of K. P. Vasilevskiy the intensity of a number of lines in the vibration-rotation H_2O spectrum was found in the band region centered

2.7 μ [195 - 197]. Sanderson and Ginsberg [198] measured the intensities of three lines in the pure water vapor rotation spectrum which lie near 92, 170 and 188 cm^{-1}. Saidy [199] determined the intensity of three rotation and two vibration-rotation H_2O lines. In a short summary of the Bole report [200], it is mentioned that the intensities of a number of weak H_2O lines were determined in the 8 - 20 μ region from the emission spectra in the atmosphere by comparing the measurement results with monochromatic absorption calculations. This comparison has shown in the case of the weakest lines a discrepancy between the data of approximately 30%, where the calculated data were smaller than the experimental data. The discrepancy is due apparently to not having taken into account the interaction between molecular vibration and rotation movement when the line intensities were calculated.

Goldman and Oppenheim [187, 201] measured the intensity of a single line in the 6.3 μ band. Using the result obtained, they then determined the total intensity of the band in an analogous way as in [202] and [203] for the 2.7 μ band.

In their paper, Burch and Gryvnak [81] report measurement results for water vapor and CO_2 absorption in the regions from 0.6 to 5.5 μ, from which, in particular, information can be derived about the intensities and halfwidths of several hundreds of most important H_2O lines. However, no data are given in the article about the line parameters.

The intensities and halfwidths of a number of lines in the tails and in the central part of the ν_2 band were determined in articles [885 - 887]. In article [888] the intensities of several lines in the visible part of the spectrum were measured in the 0.69 μ region.

3. Line Halfwidths

1. Theoretical Studies

Benedict and Kaplan [7], using Anderson's theory [56], calculated the halfwidths of γ lines in the water vapor rotation spectrum up to j = 13 and several lines from the ν_2 band of the vibration-rotation spectrum during water and nitrogen molecular collisions. The authors of [57] also investigated the dependence between the temperature and the halfwidths of the lines in the range 220 - 2400°K and the effect of the interaction between the vibrations and oscillations.

The main results of the calculations reduce to the following: at a temperature of 300°K the halfwidth of the lines varies from 0.11115 $cm^{-1} \cdot atm^{-1}$ for the lines $1_1 - 1_{-1}$ to 0.032 $cm^{-1} \cdot atm^{-1}$ for the line $14_{-13} - 13_{-13}$. An analysis of the results obtained showed that the halfwidth of the lines decreases as j increases and for a given j γ decreases as the secondary rotation quantum number τ increases.

For the temperature range which is characteristic of the stratosphere, the following formula was obtained which describes the relation between γ and T: $\gamma(T)/\gamma(300) = (T/300)^n$.

Here the quantity n varies from line to line and its mean value is 0.62 at T = 260°K. For temperatures in the range 300 - 2400°K the relation between γ and T varies considerably from line to line.

Using the methodology which was developed, Benedict and Kaplan give in article [58] the results of halfwidth calculations of pure rotation water vapor lines during H_2O - H_2O and H_2O - O_2 molecular collisions. It turned out that at a temperature of 300°K the halfwidths of the lines lie between the limits 0.5663 to 0.6607 $cm^{-1} \cdot atm^{-1}$.

The halfwidth ratios of the lines which were calculated during the H_2O - H_2O and H_2O - N_2 molecular collisions vary from line to line between the limits 1.90 to 6.85. For the widest and strongest lines, which correspond to small j, this ratio lies between the limits 4.5 - 6.0. The mean value of this ratio for the entire rotation band turned out to be equal to 5.49.

In the work of Benedict and Kaplan and the work of Gates, Calfee, Hansen and Benedict [879, 880, 189, 881] the halfwidth of the lines in the water vapor vibration-rotation spectrum has been calculated without taking subsequently into account the interaction in the vibration and rotation movements of the molecule.

In articles [139 - 141] an attempt is made to take into account this interaction. The essence of the argument is the following: if we take for the complete vibration-rotation eigenfunction the expression

$$\psi_{vj\tau} = \psi_v \psi_{j\tau}^{[v]}, \qquad (3.79)$$

where ψ_v is the vibration wavefunction obtained by taking into account the vibration anharmonicities, and $\psi_{j\tau}^{[v]}$ is the wavefunction of the nonrigid gyroscope, then to obtain the halfwidth of the line we can use the method of contributions from the well-known Anderson theory [56].

Adopting the Dirac notation for the wavefunctions, we have for the halfwidth of a spectral line

$$\gamma(vj\tau m \to v'j'\tau'm') = \frac{Nv}{2c}\sum_{j_2} B_{j_2}\sigma_{j_2}; \tag{3.80}$$

$$\sigma_{j_2} = \int_0^\infty 2n\rho S_{j_2}(\rho)\,d\rho; \tag{3.81}$$

$$S_{j_2}(\rho) = \frac{1}{2}\sum_{M_2}\frac{\langle vj\tau m;\ j_2M_2 \mid P^2 \mid vj\tau m;\ j_2M_2\rangle}{(2j+1)(2j_2+1)} + \\ + \frac{1}{2}\sum_{M_2}\frac{\langle v'j'\tau'm';\ j_2M_2 \mid P^2 \mid v'j'\tau'm';\ j_2M_2\rangle}{(2j'+1)(2j_2+1)}; \tag{3.82}$$

$$P = \frac{1}{\hbar}\int_{-\infty}^{+\infty} e^{\frac{-H_0t}{ih}} C(t)\, e^{\frac{H_0t}{ih}}\,dt, \tag{3.83}$$

where N is the particle concentration per unit volume, v is their average velocity, ρ is the sight distance, vjm are quantum numbers which denote the level from which the transition takes place, v'j'm' are the quantum numbers of the terminal level, j_2M_2 are the quantum numbers for the disturbed molecular states, Bj_2 is the density of state j_2, determined from the Boltzman distribution, C(t) is the potential interaction energy of the absorbing and perturbing molecules, H_0 is the Hamiltonian of the isolated absorbing molecule. On the basis of article [204] for the dipole-quadrupole interaction of two charge systems we can obtain:

$$C(t) = \sum_{\alpha\beta}\left[\frac{5}{2}\frac{D_{\alpha\beta}R_\alpha R_\beta(\vec{M}\vec{R})}{R^7} - \frac{D_{\alpha\beta}R_\alpha M_\beta}{R^5}\right], \tag{3.84}$$

where α and β take on the values x, y, z, D are the components of the quadrupole moment of the perturbing molecule tensor, M_β, R_α are the components of the dipole moment and the distance R between the interacting molecules on the axes of the fixed coordinate system, the center of which is the H_2O molecule.

Using the transition matrices of the dipole vector components and the quadrupole moment tensor from the fixed system to the system which is connected to the molecule, we obtain easily an expression for C(t), based on (3.84):

$$C(t)=\sum_{\substack{m_1k_1\\m_2k_2}} C^{j_1j_2}_{m_1k_1m_2k_2}D^{j_1}_{m_1k_1}D^{j_2}_{m_2k_2}, \tag{3.85}$$

where $m_1 = 1.0 - 1$: $m_2 = 2, 1, 0, -1, -2$; $k_1 = 1, -1$; $k_2 = 0$; $j_1 = 1$; $j_2 = 2$; D^j_{mk} are generalized spherical functions.

Substituting (3.83) in (3.84) and taking into account (3.84), we obtain after several transformations

$$S_{j_2}(\rho)=\frac{1}{2}\sum|a^{12}_{m_1k_1m_2k_2}|^2\langle j_2M_2|D^2_{m_2k_2}|j_2'M_2'\rangle\times$$
$$\times\langle j_2'M_2'|D^2_{m_2'k_2'}|j_2M_2\rangle\langle j\tau m|D^1_{m_1k_1}|j''\tau''m''\rangle\times$$
$$\times\langle j''\tau''m''|D^1_{m_1'k_1'}|j\tau m\rangle\frac{1}{(2j+1)(2j_2+1)}+$$

$$+\text{ a similar term for the final state} \tag{3.86}$$

where

$$a^{12}_{m_1k_1m_2k_2}=$$
$$=\left\langle v\left|\frac{1}{\hbar}\int_{-\infty}^{\infty}e^{-i\omega_{\alpha\beta}t}C^{12}_{m_1k_1m_2k_2}(t)\right|v\right\rangle, \tag{3.87}$$

$$\omega_{\alpha\beta}=\frac{E_{v''j''\tau''}-E_{vj\tau}+E_{j_2}-E_{j_2'}}{\hbar}. \tag{3.88}$$

In expression (3.86) the summation extends over all indices except v, j, m, j_2 for the original state and v', j', m', j_2 for the final state.

Using the representation (3.73), the relation between the rotor wavefunction and the D-functions, the expression for the integral of the product of the three D-functions in terms of the Klebsh-Gordon coefficients [205] and summing over m, m'', M_2, M_2', in (3.86), we obtain

$$S_{j_2}(\rho) = \sum |a^{12}_{m_1k_1m_2k_2}|^2 \frac{(g_k^{[vjr]})^2 (g_{k''}^{[v''j''r'']})^2}{15} \times$$
$$\times (jj_1k-k_1|j''k'')^2 (2j_200|j_2''k_2') +$$

$$+ \text{ a similar term for the final state} \qquad (3.89)$$

where (abcd|ef) are the Klebsh-Gordon coefficients.

In (3.89) the summation over m_1, m_2, k_1 can be carried out using supplement C in article [71]. In the end we obtain

$$\sum_{m_1k_1m_2} |a^{12}_{m_1k_1m_2k_2}|^2 = \frac{D^2\mu^2_{vv''}}{\hbar^2v^2\rho^6} f(x). \qquad (3.90)$$

where

$$f(x) = \frac{1}{288}\{x^0[18k_3^2 + 12k_2^2 + 78k_1^2 + 84k_0^2] +$$
$$+ x^4[-32k_2^2 - 96k_1^2]\};$$
$$x = \frac{\rho}{v}\omega_{\alpha\beta};$$
$$\mu^2_{vv''} = |\langle v|\mu_{x'} + i\mu_{y'}|v''\rangle|^2,$$

where $k_n(x)$ are Hankel functions for which we use the representation (8, 432, 5) in article [207], μ_x and μ_y are the components of the dipole moment of the H_2O molecule in the moving

coordinate system. The integral (3.81), after (3.89) is substituted in it and (3.90) is taken into account, diverges for small ρ. This is a consequence of assuming when (3.84) is derived that the distance between the systems of charges is larger than the dimensions of the systems themselves.

Following article [71], we let

$$S(\rho)=1 \text{ при } 0\leqslant\rho\leqslant\rho_0.$$

Key: a. when

Taking this into account, we obtain from (3.82)

$$\sigma_{j_2}=\pi\rho_0^2+2\pi\int_{\rho_0}^{\infty}S_{j_2}(\rho)\,d\rho. \tag{3.91}$$

From (3.80), (3.89), (3.90), (3.91), after a number of computations we obtain the following formulas for the half-width of the spectral line:

$$\gamma(vj\tau m\to v'j'\tau'm')=$$
$$=\frac{Nv}{2c}\sum_{j_2}B_{j_2}\rho_{j_2}^2(vj\tau m\to v'j'\tau'm')\times$$
$$\times\rho_{j_2}^2(vj\tau m\to v'j'\tau'm')=$$
$$=\rho_0\left\{1+\frac{1}{45\hbar^2v^2\rho_0^6}\sum D^2\mu_{vv''}^2(g_k^{[vj\tau]})^2\times\right.$$
$$\times(g_{k''}^{[v''j''\tau'']})^2(j\,|\,k-k_1\,|\,j''k'')^2(j_2j_200\,|\,j_2'0)^2f(x_0)+$$

$$\left.+\text{ a similar term for the final state}\right\},$$

$$f(x_0)=\frac{1}{32}x_0^6[3k_2(x_0)k_4(x_0)+2k_1(x_0)k_3(x_0)+$$
$$+13k_0(x_0)k_2(x_0)-3k_3^2(x_0)-2k_2^2(x_0)+k_1^2(x_0)-14k_0^2(x_0)-$$
$$-\frac{x_0^4}{3}\int_{x_0}^{\infty}\frac{1}{x}[k_2^2(x)+3k_1^2(x)]\,dx,$$

where

$$x_0 = \left| \frac{\rho_0}{v} \omega_{\alpha\beta} \right| > 0,$$

since its sign has no effect on the results, which was seen when the calculations were made.

In the last expressions D is the quadrupole moment of the perturbing molecule, $\mu^2_{v'v''}$ is the square of the matrix elements of the dipole moment transition $v \rightarrow v''$, for which it is possible to obtain analytic expressions [142].

2. Experimental Studies

Experimental studies of the halfwidths of lines are usually carried out at the same time as the intensities of the lines are determined and represent a sufficiently complex problem. This is due to the fact that until now a very limited amount of data has been available about the halfwidths of H_2O absorption lines.

Becker and Autler [208] determined the halfwidths of H_2O lines in the microwave region of the H_2O rotation spectrum ($\nu_0 = 0.744$ cm^{-1}). The authors of [208] found out that the collisions among the molecules broaden the line 4.7 times as much as the collisions between water and air molecules.

In the work of K. P. Vasilevsky [195 - 197] the halfwidths of a series of lines were measured in the region of the 2.7 μ band. A detailed study of the widening effect of various gases was carried out for the line with the center $\nu_0 = 4025,38$ cm^{-1}. The experimental data obtained are well described by the formula

$$\gamma = \gamma^0 (P_a + \sigma_{a,b} P_b), \qquad (3.92)$$

where γ^0 is the halfwidth of the lines at an effective pressure $P = P_a + \sigma_{a,b} P_b = 1$ atm and the temperature $T = 293^\circ$K, P_a and P_b are the partial pressure of the absorbing and extraneous gases, $\sigma_{a,b}$ is the relative optical collision efficiency of the

a molecules with the b molecules.

The values $\sigma_{a,b}$ for the collisions between the H_2O and CO_2, air, N_2, A_r molecules turned out to be equal, respectively, to 0.239, 0.170, -.165, 0.123,. which points to the pronounced dependence of γ on the nature of the broadening gas. The broadening of the lines due to the collision of water molecules turned out to be 6 times as large than during the collision of water and air molecules.

In the work of Saidy [199] the halfwidths of the line with the center $\nu_0 = 914.03$ cm^{-1} was measured. Sanderson and Ginsberg [198] determined the halfwidths of three lines, which turned out to be approximately 1.5 times as large as those obtained from calculations based on Anderson's theory. The halfwidth of the line $1_1 - 1_{-1}$($\nu_0 = 18.6$ cm^{-1}) for water molecule collisions and collisions with air, oxygen and nitrogen molecules has been determined in article [786]. The values turned out, respectively, to be equal to 0.5 + 0.2, 0.05 + 0.01, 0.03 + 0.02 and 0.06 + 0.02 cm^{-1}·atm^{-1}. The halfwidth of the lines $4_0 - 5_{-4}$ ($\nu_0 = 10.86$ cm^{-1}), $2_2 - 3_{-2}$ ($\nu_0 = 6.1$ cm^{-1}) and $3_1 - 4_{-3}$($\nu_0 = 12.67$ cm^{-1}) for water and air molecular collisions were measured in articles [787 - 789], and the halfwidth values for these lines turned out to be equal to 0.101, 0.107 $\pm$ 0.005 and 0.105 $\pm$ 0.004 cm^{-1} in the earth's layer of the atmosphere.

6. Absorption Function In Narrow Regions Of The Vibration-Rotation And Pure Rotation Spectrum of Water Vapor

1. Direct Calculation of Absorption Functions

The absorption functions were calculated for sectors with widths 25 cm^{-1}, in the region of the pure water vapor rotation spectrum from 100 to 350 cm^{-1} by Cowling [209]. The data about the position of the lines and their intensities were taken from article [170]. The halfwidth of the lines was assumed to be constant and was taken from 0.05 to 0.4 cm^{-1} Benedict [210], using data obtained theoretically for the parameters of the lines of the pure H_2O rotation spectrum, calculated the absorption function for various frequency intervals. It turned out that for sufficiently wide intervals the values of these functions which were obtained did not differ much from those which were calculated using the model method for the spectra.

In the work of Calfee [189], the absorption functions were calculated in sectors of the water vapor vibration-rotation spectrum in the infrared region. The calculations were based on experimental data about the positions of line centers. The intensities and halfwidths of the lines were determined using the method described in the preceding paragraph. The vibration and rotation movement of the H_2O molecules were not taken subsequently into account. The relation between the spectral absorption and the wavelength which was obtained was multiplied by the apparatus function of the spectrometer in order to be able to compare on one hand the results of the calculations with the experiment and on the other hand to study the effect of the spectrometer parameters on the nature of the spectrum recorded with the aid of the spectrometer.

A. G. Pokrovskiy [882] developed the algorithms and calculated the spectral absorption and absorption functions in a narrow sector of the spectrum (3795 - 3836 cm^{-1}) and for the single line (ν_0 = 1677.95 cm^{-1}). The essential advantage of the algorithms developed in this work is that they take into account both the Doppler and dispersion contours of the lines. From the radiation absorption data obtained for a single line at various altitudes it is clearly evident that the broadening of the lines due to the Doppler effect in the central part of the line must be taken into account already from the altitude of 10 km.

In the work of K. Ya. Kondrat'ev and Yu. N. Timoseev [211] the absorption functions were calculated for 8 narrow sectors of the spectrum with widths from 5.3 to 8.5 cm^{-1} in the 20 - 50 μ region at pressures of 1000, 500, 100 and 10 mb and temperatures 300, 260 and 220°K. An analysis of the relation between the temperature and the absorption functions has shown that it depends mainly on the temperature effect on the line intensities peculiar to each concrete sector of the spectrum. Thus, the quantity m in the temperature correction for the transmission function

$$f(T) = (T/T_0)^m$$

varies from 0.86 to 4.0 for the regions studied.

Yu. M. Timoseev [883] used a direct calculation of the absorption functions A to estimate the errors which occur when the quantity A is calculated using approximate methods. It has been shown in [883] that the maximum error in these methods

occur only when the ratio of the absorbing gas mixture increases as the altitude increases.

K. Ya. Kondrat'ev and Yu. M. Timofeev [884] analyzed the possibility of using the direct method to calculate the transmission functions in narrow regions of atmospheric gas absorption spectra for various atmospheric stratifications. In [884] the promise of this method has been shown for overlapping bands and for the solution of reverse problems.

The absorption functions were calculated for individual sectors of the water vapor vibration-rotation spectrum in the visible and infrared regions of the spectrum in our paper [780] on the basis of data about the position of the line centers, their intensities and halfwidths which were derived theoretically.

2. Calculation of Absorption Functions Using The Spectral Model Method. The calculation of the infrared radiation absorption functions by H_2O and CO_2 vapors for relatively narrow sectors of the spectrum with widths 10 - 20 cm^{-1}, using a statistical, combined and Elsasser model was carried out by Plass and Stull [212]. To determine the fitted parameters the data from the experimental studies made by Howard, Burch and Williams were used [213].

In the work of Wyatt, Stull and Plass a new series of absorption function calculations was made for the narrow sectors of the main vibration-oscillation bands of the water vapor [214] and CO_2 [215] spectrum, using the quasistatistical model proposed by the authors (see para. 3). The water vapor absorption functions were calculated in the wave band from 1 to 10 μ for spectral intervals with widths 2.5 cm^{-1} in the 997.5 - 3400 cm^{-1} region and widths 20, 50 and 100 cm^{-1} in the 1000 - 10 000 cm^{-1} region. In the last three cases, the data were obtained, respectively, every 10, 25 and 50 cm^{-1}. The absorption functions for the 2.5 cm^{-1} intervals were calculated using the results of article [166]. The remaining data were obtained on the basis of relative line intensity calculations for the vibration-rotation water vapor spectrum carried out in [214] and reduced to absolute scale with the aid of the experimental results of article [216].

The absorption functions for the above spectral intervals were calculated for 15 values of the settled water vapor layer w between the limits 0.001 to 50 cm for 7 values of the pressure P: 1.0, 0.5, 0.2, 0.1, 0.05, 0.02 and 0.01 atm.

and for three temperature values T: 200, 250 and 300°K.

A part of the data obtained together with computational methods were published in [217], where a table of the transmission function values is given for sectors with widths 100 cm^{-1} at the temperature T - 300°K and the pressure P = 1 apm for 15 values of ω.

In Fig. 3.3 the calculated [214] and experimental [216] results are compared for the most intense and widest vibration-rotation 6.3 μ water vapor bands. The satisfactory agreement of the data seen in the figure point to the possibility of calculating sufficiently accurately the absorption functions in narrow sectors of the spectrum with the aid of band models, if their fitted parameters are correctly determined from the experimental data [216, 218].

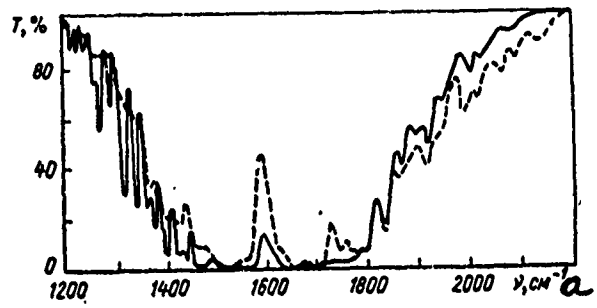

Fig. 3.3. Transmission functions in narrow sectors of the H_2O spectral band 6.3 μ according to the experimental data [216] and the calculated data [214]:

— — experiment, P = 805 mm Hg, w = 0.0707 cm,
– – – –calculated, P = 760 mm Hg, w = 0.1 cm

Key: a. cm^{-1}

In an attempt to obtain values of the absorption function for spectral intervals with widths 0.1 μ which are convenient for practical use, we carried out the corresponding calculations [219] based on the fitted parameters obtained in article [212], with the exception of the absorption bands 3.2, 1.87, 1.38 and 1.1 μ for which the statistical model formula with the fitted parameter obtained in article [213] was used:

$$T=\exp\left[\frac{-\frac{\omega}{\omega_0}k\gamma}{\overline{d}\left(\gamma^2+\frac{\omega}{\omega_0}\frac{k\gamma}{\pi}\right)^{1/2}}\right]=\exp\left[\frac{-\frac{\omega}{\omega_0}\alpha}{\left(1+\frac{\omega}{\omega_0}\delta\right)^{1/2}}\right] \qquad (3.93)$$

where $\alpha = k/\overline{d} = 1{,}97; \delta = k/\pi\gamma = 6{,}67$ - are the fitted parameters determined from the experimental data, ω_0 is the settled water vapor layer which corresponds to the value T = 0.5. The calculations were made for the total pressure values 1.0, 0.9, 0.7, 0.5, 0.3, 0.1, 0.05 and 0.01 apm, which corresponds in the atmosphere to the altitudes 1, 3, 5, 10, 16, 21 and 31 km. The values for the settled water vapor layer were selected for each altitude in such a way that for the humidity occurring in the atmosphere distances from 0.1 to 100 km were covered.

All calculated data were plotted on graphs from which it is possible to find directly the value of the transmission function for a particular interval with widths 0.1 μ for any values of the pressure P and the settled layer ω which are encountered in the horizontal layers of the atmosphere at distances from 0.1 to 100 km and altitudes from 0 to 30 km [790].

3. Experimental Determination of the Absorption Functions. Many papers were devoted to the experimental determination of the absorption functions. The most extensive studies were carried out by the teams of Howard [112, 213], Burch [216, 221] and B. M. Golubitskiy [791 - 793].

Howard's team studied the spectral absorption of the fundamental vibration-rotation H_2O bands in the infrared spectral region 6.3, 3.2, 2.7, 1.87, 1.38, 1.1, 0.94 μ and the 3.7 HDO band. Treatment of the experimental data made it possible to obtain the following empirical relations for the total band absorption:

$$\int_{\nu_1}^{\nu_2} A(\nu)\,d\nu = c\omega^{1/2}(P+P_a)^k, \qquad (3.94)$$

$$\int_{\nu_1}^{\nu_2} A(\nu)\,d\nu = C + D\lg\omega + K\lg(P+P_a), \qquad (3.95)$$

where ω, P_a are the settled layers in cm and the partial water vapor pressure in mm Hg, $P = P_{N_2} + P_a$ is the total pressure,

c, k, C, D, K are empirical constants.

Formulas (3.94) and (3.95) describe the total band absorption for small and large values of w, respectively, which were given in [112] for each band. For intermediate values of w, the total band absorption is determined by extrapolating the data obtained according to (3.94) and (3.95).

The results which were obtained by the Howard team were quickly and widely applied in various calculations. Larmor and Passman [222] constructed on the basis of these results a series of tables for radiation transmission through the atmosphere at sea level and at various altitudes in the spectral intervals up to and through 0.1 μ. Langer [223] determined the transmission in the main "windows" of the transparent atmosphere. Roach [224] calculated solar radiation absorption in the cloudless atmosphere. This data has been widely used in our work to calculate the complete absorption function and the absorption functions in the spectral intervals occupied by individual bands [225].

Higher resolution spectral apparatus was used in the work of the Burch team than in [213], which made it possible to obtain more reliable data about radiation absorption in narrow sectors of the spectrum and investigate the broadening effect of absorption bands when the total and partial pressures of the absorbing and nonabsorbing gases were varied. The absorbing gases studied were H_2O, CO_2, N_2O, CO and CH_4. The problem was to determine the quantity $B = C_{a,a}/C_{a,b}$, which characterizes the ratio of gas capacity to the broadening of the lines due to molecular collisions of the gas (self-broadening) and collisions with the extraneous gas molecules for which N_2 was used.

As the results of the experiments have shown, the quantity B varies with the spectrum (Table 3.1). This is understandable, if we consider that the optical collision diameters vary from line to line. For example, for the N_2O 2224 cm^{-1} band between the limits 2250 to 2175 cm^{-1} B varies from 0.9 to 1.3, i.e., it increases one and one-half times as much.

On the basis of the treatment of measurement results formulas were selected in [216] which approximate well the experimental data for the total band absorption

$$\int_{\nu_1}^{\nu_2} A(\nu)\,d\nu = c\,[\omega P_e^a]^b, \qquad (3.96)$$

$$\int_{\nu_1}^{\nu_2} A(\nu)\,d\nu = C + D \lg[\omega P_e^a], \qquad (3.97)$$

where a, b, c, C and D are experimental constants, $P_e = P + (B - 1)P_a$ is the effective pressure which includes the total pressure P, the partial pressure P_a and the self-broadening coefficient B of the lines.

A valuable result of this series of papers is that not only water vapor and CO_2 were investigated but also small mixtures. This makes it possible now to evaluate quantitatively their role in infrared radiation absorption under natural atmospheric conditions.

Table 3.2 gives the ranges used in the Howard and Burch teams in the experiments for the settled water vapor layer in cm for various absorption bands.

TABLE 3.2

RANGE OF VALUES FOR THE SETTLED WATER VAPOR LAYER DURING TOTAL ABSORPTION MEASUREMENTS FOR VARIOUS H_2O BANDS GIVEN IN [213, 216]

a Полоса, мкм	Осажденный слой ω, см b	
	Говард [213] c	Бёрч [216] d
0,94	0,01—3,85	
1,1	0,01—3,85	
1,38	0,01—3,85	
1,87	0,01—3,85	0,003—0,11
2,7	0,002—2,4	0,003—0,11
3,2	0,002—2,4	0,003—0,11
6,3	0,02—1,2	0,002—0,07

Key: a. band, μ
b. settled layer ω, cm
c. Howard [213]
d. Burch [216]

TABLE 3.1

VALUES OF SELF-BROADENING COEFFICIENTS B OF ABSORPTION LINES AND BANDS FOR H_2O, N_2O, CO_2, CO, AND CH_4 ACCORDING TO THE DATA OF VARIOUS AUTHORS

a Газ	b Полосы, $см^{-1}$	c Авторы	B
d Пары H_2O	5332, 3756, 1595	Бёрч и др. [226]	5±1,5
	Район 500 e	Пальмер [227]	11−67 *
	Линия 4025,4 f	Василевский и Непорент [195]	6
	4 линии в районе 500—600 g	Изэтт [228]	3,6−5,5
N_2O	2224, 1285, 1167	Бёрч и др. [226]	1,12±0,07
	1285	Гуди и Вормелл [229]	1,27±0,04
	1167	То же	1,35±0,07
	2224	Кросс и Даниелс [230]	1,29
CO_2	3716, 3609, 2350, 961, 875—495	[226]	1,30±0,08
	3716, 3609, 2350, 961, 875—495	Эдвардс [231]	$2+0,5P_a$ **
CO	2143	[226]	1,02±0,06
	4260	[226]	1,08±0,06
CH_4	3020	[226]	1,30±0,08
	1306	[226]	1,38±0,08

* T — спектральное пропускание $T(\nu)$.
** P_a — парциальное давление CO_2 в атмосфере.

Key:
a. gas
b. bands, in cm^{-1}
c. authors
d. vapors
e. region
f. line
g. 4 lines in region

(continued next page)

Key, Table 3.1 (cont'd.)

Column c (authors):

Burch, et al. [226]
Palmer [227]
Vasilevskiy & Neporent [195]
Izatt [228]
Burch, et al. [226]
Goody & Wormell [229]
Same authors
Cross & Daniels [230]
[226]
Edwards [231]

1. T--spectral T(ν) transmission
2. P_a--partial CO_2 pressure in atmosphere

The new series of water vapor spectral absorptions measurements which was carried out by Burch and his collaborators [81] in the region 0.6 - 5.5 μ makes it possible to determine the absorption function in very narrow sectors of the spectrum in the visible and near infrared regions. In this series the measurements were made at various air pressures up to and including 1800°K.

In the work of B. M. Golubitskiy and his collaborators [791 - 793] the water vapor absorption functions were studied experimentally for regions of the spectrum with widths 3 to 20 cm^{-1} in the wave band 1 - 14 μ. The measurements were carried out for various water vapor temperatures and values of the settled water layer, which were equivalent to its values in the earth's layer of the atmosphere, which reacned 12 cm. An empirical relation was obtained on the basis of a treatment of the measurement results which described satisfactorily the dependence of the transmission function on the settled water layer ω and the pressure P:

$$T_\lambda = \exp\{-\beta_\lambda \omega^{m_\lambda} P^{n_\lambda}\}, \qquad (3.98)$$

where β_λ, m_λ, n_λ are empirical parameters which are determined for spectral intervals of various widths.

The authors of [785 - 787] maintain that formula (3.98) describes the measurement data for the absorption function with

a sufficiently high accuracy (the relative error does not exceed 6 - 8% for the values $w \leqslant 12$ cm, $P \leqslant 1$ atm). The comparison made by the authors showed satisfactory agreement between the available experimental data for the absorption functions with the data calculated according to formula (3.98).

In the work of M. S. Kiseleva [794] empirical formulas are proposed which describe approximately the absorption function in a given spectral interval, when its values lie in the interval $0.05 \leqslant A \leqslant 0.9$.

Stauffer and Walsh [232] measured the transmission of a mixture of water vapor and nitrogen in the 14-20 μ region. A set of curves was constructed for various values of the total and partial pressure. The settled layer of water varied from 0.0037 to 1.163 cm, the nitrogen pressure from 0.00286 to 0.805 atm, the water vapor pressure from $0.264 \cdot 10^{-1}$ to $11.5 \cdot 10^{-3}$ atm. The measurement results agreed well with Benedict's calculations [210].

The transmission functions in the region of the pure rotation H_2O spectrum were measured by Palmer [233] for various partial H_2O pressure values and nitrogen which was used as an extraneous gas. The transmission functions for intervals with widths 10 cm^{-1} were found in the 500 - 320 cm^{-1} region, for intervals with widths 5 cm^{-1} in the 340 - 200 cm^{-1} region, and for seven overlapping intervals with widths 50 cm^{-1} in the 200 - 500 cm^{-1} region. For wide intervals the data obtained agreed well with Benedict's calculations [210]. As the spectral interval becomes smaller, the experimental data differ from the calculated values, the smaller the width of the interval.

Burch and Reissman [234] measured the absorption of steam vapor and its mixture with nitrogen in the region of the long wave transparent window near the wavelength 340 μ.

4. Total Intensities of Absorption Bands. The knowledge of the total intensities of absorption bands is important for the study of the fine structure of spectra and for determining the absorption functions both of entire bands and their parts. This explains the considerable amount of work in which the total intensities of the bands of various atmospheric gases are measured, including water vapor. In the last few years new intensity measurements were made for a number of bands when the spectra were recorded at high temperatures.

The total intensities of the bands 1.38, 1.87, 2.7 and 6.3 μ were measured at temperatures 200, 400, 600 and 727°C by Goldstein [235]. In a series of articles by Ferriso, Ludwig and collaborators [236 - 239] the emission spectra of water vapor at various temperatures were studied. The 6.3 μ band was recorded at temperatures 540, 1030, 1535, 1850, 2200°K. At the temperature above 1800°K, the fine structure of the spectrum practically erodes, making measurements of the total intensity easier. The spectral transmission in the 10 - 22 μ region was recorded at the temperatures 50°, ..., 2200°K.

At the temperature 2750°K measurements of the H_2O transmission spectra were carried out in the wide wavelength band 1 to 25 μ. From the measurements of the emission spectra the authors of [236-239] found the total intensities for various bands.

Goldman and Oppenheim [240] determined the total intensities of the bands 1.87 and 2.7 μ on the basis of H_2O emission spectra at a temperature of 1200°K.

In article [241] the results of water vapor absorption measurements are given when the temperature varies from 300 to 1100°K, from which the total intensities of the vibration-rotation bands 1.38, 1.87 and 6.3 μ and the short wave tail of the rotation band up to the wavelength 20 μ were obtained.

The total intensity values of H_2O bands obtained by various authors are given in Table 3.3.

5. Absorption by the Far Tails of Strong Lines. The role of the far tail of strong lines in radiation absorption in transparent windows of the atmosphere is very important. When the absorption functions are determined in the transparent windows the continuous absorption due to the far tails of strong lines can be the dominant factor. For this reason it is very important that sufficiently accurate data for the absorption coefficients and functions of the so-called continuum be available. It should also be added that it is precisely through the spectral intervals of the transparent windows that the radiation is mainly transferred in the atmosphere.

The idea of the possible role of continuous absorption played by the far tails of strong lines in weakening the radiation in the "windows" was stated by Elsasser as early as 1938. Moller [244] arbitrarily set the continuous absorption coefficient in the 8 - 13 μ region equal to 0.1 per

unit of air mass and estimated this absorption value for meteorological purposes. In the measurements of Gebbie, et al., [245], Taylor and Yattes [246] in the earth's layer, and Adel [247] and Anthony [248] when the sun was used as the source, the existence of continuous absorption was confirmed in the 8 - 13 μ window. V. G. Kastrov expressed the absorption coefficient in the interval 8 - 13 μ as the sum of continuous absorption coefficients using Adel's data and the absorption by weak lines using the Weber and Randall data [249].

TABLE 3.3

TOTAL INTENSITIES OF H_2O ABSORPTION BANDS ACCORDING TO THE DATA OF VARIOUS AUTHORS

a Полосы, мкм	b Интегральная интенсивность $см^{-2} \cdot атм^{-1}$	c Температура при измерениях, °К	d Авторы
6,3	300±20%	273	[236]
	350±15%	2750	[239]
	220±22 *		[201]
	247±10%	273	[235]
2,7	230±15%	2750	[239]
	206±21 **	1000	[235]
	177±18 ***	1000	[235]
	182±36 **	530—2200	[242]
	165±33 ***	530—2200	[242]
	198±20 **	1200	[240]
	180±18 ***	1200	[240]
	192±28	300	[202]
	172±7	300	[203]
1,87	22,3±2,2 **	873	[235]
	23,7±1,7 **	1000—2200	[243]
	18,0±2,7 **	1200	[240]

1 * — приведенная к нормальным условиям.
2 ** — приведенная к температуре 300° К.
3 *** — приведенная к температуре 300° К и откорректированная авторами [203].

Key:
a. bands, μ
b. total intensity $cm^{-2} \cdot atm^{-1}$
c. temperature during measurements, °K
d. authors
1. reduced to normal conditions
2. reduced to the temperature 300°K
3. reduced to the temperature 300°K and corrected by the authors [203]

A quantitative experimental study of continuous absorption in the 8 - 13 μ window was carried out by Roach and Goody [250] in 1958. The measurements which were made in London and Essex of the attenutation of solar infrared radiation in individual narrow sectors of the spectrum with a resolution of approximately 7 cm^{-1} made it possible to single out from the total attenuation the selective absorption by weak lines in the given sector. The measurements were made on clear days. For the continuous attenuation coefficients in Essex values were obtained which were approximately 50 times as large as the values caused by aerosol attenuation under the same weather conditions obtained according to Volz's data [251]. The attenuation in London exceeded several times the attenuation in Essex which is due to the considerable pollution in the London atmosphere. An important shortcoming in the work of Roach and Goody was that they did not carry out the attenuation measurements in the visible region with data from which aerosol attenuation could be singled out.

A second study dealing with the quantitative investigation of continuous absorption in the same 8 - 13 μ window was made by Bignell, Saiedy and Sheppard [252], who eliminated the methodological shortcomings in the first study which included, in addition to the absence of measurements in the visible region, the low resolution capacity value of the spectrometer. The studies were made using two methods for 19 frequencies in the range 1202 - 479 cm^{-1}(8.32 - 20.9 μ): 1) using the sun as the source (the band 1202 - 790 cm^{-1}); 2) on horizontal paths 200 and 400 m long using the Nernst rod (range 716 - 479 cm^{-1}). The results of the measurements have shown that the continuous absorption coefficient in the wavelength range considered varies from 0.06 to 4.1 $g^{-1} \cdot cm^2$. More detailed data are given in Table 3.4.

A special study of CO_2 absorption under laboratory conditions has shown that beyond the limits of the spectral interval 790 - 560 cm^{-1} (12.7 - 18 μ) the effect of CO_2 absorption on the measurement results can be ignored.

Table 3.5 gives the values of the continuous absorption coefficient obtained during solar spectra measurements at the high-mountain station of the Atmospheric Physics Department of the Leningrad University at Mt. El'brus [253].

Data for the continuous absorption coefficients in the wavelength range 8 - 25 μ were also obtained in article [874 - 875] and in the range 8 - 14 μ in article [876].

TABLE 3.4

VALUES OF THE CONTINUOUS ABSORPTION COEFFICIENT k_a FOR STRONG WATER VAPOR LINE TAILS FOR VARIOUS WAVELENGTHS ACCORDING TO THE DATA IN ARTICLE [252] (PRESSURE P = 1 atm, ABSOLUTE HUMIDITY 12 mb)

a) λ, мкм	8,32	8,66	8,86	9,13	10,14	10,40	11,10
b) $k_п$, c) $г^{-1} \cdot см^2$	0,074	0,0601	0,0595	0,0625	0,0666	0,0685	0,0925
a) λ, мкм	11,44	11,82	12,02	12,20	12,66	13,96	
b) $k_п$, c) $г^{-1} \cdot см^2$	0,105	0,114	0,119	0,119	0,158	0,6±0,2	
a) λ, мкм	16,38	17,02	17,88	18,83	20,12	20,88	
b) $k_п$, c) $г^{-1} \cdot см^2$	0,8±0,1	1,4±0,1	1,7±0,1	2,0±0,1	3,0±0,1	4,1±0,1	

Key: a. μ
b. a
c. $g^{-1} \cdot cm^2$

TABLE 3.5

VALUES OF CONTINUOUS ABSORPTION COEFFICIENTS k_a IN THE FAR TAILS OF STRONG WATER VAPOR LINES IN VARIOUS NARROW SECTORS OF THE SPECTRUM ACCORDING TO THE DATA IN ARTICLE [253]

a) λ, мкм	3,58	3,70	8,15	8,30	8,53	8,76	8,86
c) $k_п$, b) $см^{-1}$	0,07	0,062	0,15	0,12	0,10	0,10	0,095
a) λ, мкм	9,10	10,18	10,40	10,62	10,92	11,11	
c) $k_п$, b) $см^{-1}$	0,090	0,085	0,085	0,090	0,11	0,12	
a) λ, мкм	11,51	11,98	12,18	12,72	12,95	13,95	
c) $k_п$, b) $см^{-1}$	0,15	0,15	0,16	0,21	0,22	0,225	

Key: a. μ
b. cm^{-1}
c. a

In conclusion we emphasize the need for continuing the experimental study of the phenomenon considered. Such studies are important primarily because it is difficult to solve theoretically this problem since analytic expressions which describe with sufficient accuracy the far tails of spectral absorption lines are not available.

7. Fine Structure Of Absorption Spectrum of Carbon Dioxide

The fine structure of the vibration-rotation CO_2 spectrum has been investigated in many experimental and theoretical studies. In the first studies the bands in the 15 and 4.3 μ regions were subjected to the most detailed analysis. The bands in the 15 μ region play an important role in long wave radiation absorption in the atmosphere. The bands 4.3 μ are so strong that their absorption can be detected even in the thermosphere. Investigators try to use this fact to reconstruct the vertical temperature profiles up to high altitudes with the aid of the corresponding emitted radiation measurements [254].

The possibility of using CO_2 absorption bands in the regions 4.3, 15.0 μ and other regions to solve problems of artifical satellite meteorology has brought on in the last few years a considerable number of publications in which the fine structure of all fundamental bands has been studied. Below we present the results of studies obtained by various authors for individual absorption bands.

1. Bands in the 15.0 μ Region. The detailed structure of the spectral band in the region considered has been studied for the first time theoretically by Kaplan [255], Yamamoto and Sasamory [256]. In [255] and [256] data were obtained about the positions and intensities of the lines. The calculations were made for the fundamental isotope, without subsequently taking into account the interaction between the vibration and oscillation movements of the molecules and the Coriolis interaction. The relative intensities of the band lines in the region considered were calculated by Wyatt, Plass and Stull [212, 215].

The most accurate experimental data about the position of the line centers in the band region 15.0 μ were obtained by Gordon and McCubbin [257]. The authors of this article were able to obtain very high spectral resolution, which corresponded, for all practical purposes, to the limit for

Echelette interferometer technology. This made it possible to determine the positions of the line centers with an accuracy of several thousandths cm^{-1}. A comparison of the experimental data obtained with the calculated values has shown that for most lines the data agreed with an accuracy up to 0.01 cm^{-1}, and the maximum deviation did not exceed 0.027 cm^{-1}.

The halfwidth of the γ line in the band considered was determined experimentally in the work of Kaplan and Eggers [258] and Madden [61]. In the first study, only strong lines were investigated for which the value of γ obtained was equal to 0.064 cm^{-1}. However, later Kaplan revised the results of this study and under normal conditions found for γ the value 0.075 cm^{-1}. Madden [61] found a relationship between the halfwidths of the lines and the rotation quantum number for each band in the region studied.

In papers [795 - 797] the halfwidths and intensities of a series of P lines and R branches of the band $10^00 - 00^01$ were found when a laser based on a CO_2 mixture with nitrogen was used as the radiation source. In this case the centers of the radiation and absorption lines coincide, and the expressions for the Doppler and Lorentz contours of the line simplify and can be used to determine with sufficient accuracy the parameters of the corresponding lines.

2. Bands in the 4.3 μ region. The positions of the line centers and their intensities in the bands considered have been studied several times by a number of authors. The most important results were obtained in the work of Nielsen and Yao [259], Benedict, Herman, Silverman [260], Winters, Silverman and Benedict [78], Wyatt, Plass and Stull [212, 215], Courtoy [261], Gray and Selvidge [262], Kyle, D. Murcray, F. Murcray and Williams [79], Migeotte, Neven, Swenson and Benedict [182]. In article [259] the band ν_3 was analyzed for the $C^{12}O_2^{16}$ and $C^{13}O_2^{16}$ isotopes, and in [260] R branches of bands were studied, and in [261] the spectrum in the 4.3 μ region was recorded in greatest detail.

In articles [212, 215] the intensities of lines were calculated in eight isotope CO_2 modifications. The relative intensities of the lines for the transitions from the molecular states 00^00 and 01^10 were obtained in [262]. In [79] the positions and intensities of approximately 300 lines have been calculated. The calculations have shown that the contribution of the 80 strongest lines to the total band intensity

was equal to 97.1%. Table 3.6 gives data for the bands which were studied in article [79].

The halfwidths of the γ lines in the 4.3 μ band region have not been studied adequately. Usually when the absorption coefficients and functions are calculated, the quantity γ is assumed to be the same and taken equal to 0.066 cm^{-1} under standard conditions.

TABLE 3.6

DATA FOR THE CO_2 BANDS IN THE 4.3 μ REGION INVESTIGATED IN ARTICLE [79]

a Изотоп	b Состояние	c Разрешенные значения j	d Центр полосы, $см^{-1}$	e Наибольшее значение j
$C^{12}O_2^{16}$	0 0^0 0	Четные f	2349,5	70
$C^{13}O_2^{16}$	0 $1^{\pm1}$ 0	Четные и нечетные g	2339,2	54
$C^{13}O_2^{16}$	0 0^0 0	Четные f	2283,7	70
$C^{13}O_2^{16}$	0 $1^{\pm1}$ 0	Четные и нечетные g	2273,4	54
$C^{12}O^{18}O^{16}$	0 0^0 0	Четные и нечетные g	2331,8	48
$C^{13}O^{18}O^{16}$	0 0^0 0	Четные и нечетные g	2266,0	48

Key:
a. isotope
b. state
c. resolved values of j
d. center of bands, cm^{-1}
e. maximum value of j
f. even
g. even and odd

3. Bands in the 2.7 and 2.05 μ Regions. The positions of the line centers and their intensities in the band regions 2.7 and 2.05 μ have been studied in greatest detail in comparison to all other bands, due to the work of Calfee and Benedict [263].

The authors of [263] calculated the positions of the centers and intensities of 2826 lines in the band region 2.05 μ and 4790 lines in the band region 2.7 μ. In the article all molecular parameters which were used when each band was calculated has been tabulated in detail. When the positions of the lines were calculated, the interaction between the

vibration and rotation molecular movements caused by centrifugal distortions and Coriolis forces have been taken into account. The intensities of the lines were calculated without subsequently taking into account the interactions between the vibration and rotational molecular movements. The computational procedure described in paragraph 5 has been used to calculate the line intensities, using the data for band intensities obtained in the work of the Burch team.

The table of the frequencies of the line centers and their intensities in [263] contains all rotation levels of the molecule with values of the rotation quantum number $j \leqslant 100$. This means that the table includes practically all lines which can occur during measurements in the earth's atmosphere. Reviewing paper [263], Williams [264] states that he is ready to consider himself as one of those who propose a reward for the discovery of lines which have not been tabulated in [263].

The relative intensities of the lines in the bands considered have been calculated in articles [212, 215].

The fine structure of the spectrum and its individual elements in the absorption band regions 2.7 and 2.05 μ has been studied by various authors in many papers. A bibliography of these papers can be found in the well-known Herzberg monographs [798] and Goody monographs [3] and in Gordon's and McCubbin's articles [265].

The positions of lines in the 2.7 μ region have been studied experimentally in greatest detail in article [265]. The authors of [265] measured the positions of the centers in 10 $C^{12}O_2^{16}$ bands, one $C^{13}O_2^{16}$ isotope band and two $C^{16}O^{16}O^{18}$ isotope bands. All measurements were made with an accuracy of $\pm$ 0.005 cm^{-1}.

K. B. Vasilevskiy and his collaborators [266] measured the halfwidths of several tens of absorption lines in the band $4\nu_2 + \nu_3$ (2.05 μ). The measurements were carried out both with pure CO_2 and with $CO_2 + N_2$ mixtures. The intensities and halfwidths of almost all P lines and R branches in the band have been determined. In pure CO_2 the halfwidths of the γ lines varies between the limits 0.126 - 0.06 $cm^{-1} \cdot atm^{-1}$ when the rotation quantum number varies from 4 to 50 - 56. In the gas mixture the quantity γ varies from 0.122 to 0.09 $cm^{-1} \cdot atm^{-1}$.

4. Weak Absorption Bands. In addition to the most intense CO_2 bands which have been considered, there is a series of very weak bands, the fine structure of which cannot be obtained either theoretically or experimentally under laboratory conditions with a large mass of the absorbing carbon dioxide. These bands lie in the spectral regions near 10.4, 9.4, 5.2, 4.8, 1.6, 1.4 μ and also in the intervals between these and between the strong absorption bands or in the transparent windows of the atmosphere which include the visible region of the spectrum.

The fine structure of the weak CO_2 bands has not been studied sufficiently, since their role in atmospheric processes is not important and their study presents a rather difficult problem. A bibliography of the work which has been carried out is contained in monograph [1, 3] and in article [267].

We will state a number of results. From an analysis of the result of theoretical and experimental studies of the fine structure of the CO_2 absorption spectrum, the following conclusions can be made. The most complete data about the positions of the line centers were obtained in experimental studies. For most lines the positions of their centers in all fundamental bands were found with an accuracy of 0.005 - 0.1 cm^{-1}. The positions of the line centers were also calculated for the vast majority of lines. The calculations did not take subsequently into account the interaction between the vibration and rotation molecular movements for individual lines. The errors which were generated in the process must still be estimated.

The greatest amount of data about the line intensities has been obtained by calculation. The number of lines, the intensities of which have been determined from the experiment, is very limited. The calculation of the line intensities and their positions have been carried out without taking into account subsequently the interaction between the vibration and rotation levels of the molecule.

A very limited number of both theoretical and experimental data are available about the halfwidths of the lines in all vibration-rotation CO_2 bands. In all calculations the halfwidth of a line is considered to be constant within the limits of the given band, which strictly speaking is invalid.

The inaccuracies when all three line parameters are determined are most pronounced in the value of the absorption

coefficient in the central regions of the lines.

8. Absorption Functions in Various Regions of the CO_2 Spectrum

The absorption functions in various regions of the CO_2 spectrum are determined as in the case of water vapor, using three methods, the application of which will be discussed below.

1. Direct Calculation of Absorption Functions. The absorption functions were calculated in detail in the interval from 12 to 18 μ by Drayson [62]. Altogether about 2000 lines were used in the calculations, the halfwidth of which was assumed to be constant and equal to 0.064 cm^{-1} at a pressure of 1 apm and a temperature of 298°K. The relation between the halfwidths of the lines and the rotation quantum number was not taken into account. The absorption coefficient which is then used to calculate the absorption functions is determined on the basis of the data for the intensity, positions of the centers and the halfwidths of lines.

When the absorption coefficient is calculated in the expression for the line contour

$$k(\nu) = \frac{S}{\pi} \frac{\gamma}{(\nu - \nu_0)^2 + \gamma^2}$$

the term γ^2 is ignored for frequencies which satisfy the conditions $(\nu - \nu_0) > 7.0$ cm^{-1}. The error due to this operation did not exceed 10^{-4} times the value of $k(\nu)$ for all pressures.

The absorption band was broken up into small intervals with a minimum width of 0.001 cm^{-1} in the central regions of the lines and 0.1 cm^{-1} in the tails of the lines. The absorption functions were obtained for regions with widths 0.1 cm^{-1} and were then averaged for intervals with widths 5 cm^{-1}.

The computational results were compared with the experimental data obtained by the Burch team and with Yamamoto's calculations. Satisfactory agreement between the data compared was obtained for a pressure of 0.2 and 1.0 atm. For low pressure in the central part of the band the differences were

considerable which, in the opinion of the author [62], may be related to the accuracy with which the total intensity of the band has been determined (in article [62] it was taken to be equal to 194 cm^{-1}) or to not taking into account the relation between the halfwidth of the lines and the rotary quantum number. We note, however, that for very small pressures the data of Drayson and Yamamoto differ so much that it is doubtful that this can be explained by the reasons which were stated. Thus, for example, for the sector of the spectrum with center near 15.1 μ for a pressure of P = 1 mb this difference exceeds by 2 orders of magnitude the value of the absorption function [268]. It is difficult to make any statement for the time being about the real causes for such pronounced difference.

2. Calculation of Absorption Functions Using Formulas for Models of the Spectra. The most detailed data about the absorption functions in the region of the fundamental vibration-rotation CO_2 bands were obtained in the studies of the Plass, Stull and Wyatt [212, 215 and 270]. In the first article data was obtained for the absorption function in sectors 10 - 20 cm^{-1} wide in the region of the bands 15, 4.3, 2.7 and 2.0 μ. In [215] using a quasistatistical model, the absorption functions were calculated in regions 2.5 cm^{-1} wide in the interval 500 - 100- cm^{-1} (1 - 20 μ) for three values of the temperature T: 200, 250 and 300°K for the same 7 values of the pressure used in the water vapor calculations: 1.0, 0.5, 0.2, 0.1, 0.05, 0.02 and 0.01 atm and 15 values of the CO_2 mass from 0.2 to 10 000 atm·cm. We note that the kilometer layer of the atmosphere near the earth's surface is characterized by a CO_2 mass which is approximately equal to 30 atm·cm. For the above values of the calculated parameters, in [215] the absorption functions were also obtained in the intervals 20, 50 and 100 cm^{-1} with centers, respectively, at every 10, 25 and 50 cm^{-1}. A part of the data obtained in [215] was published in [269]. A comparison of the data calculated in [215] with the experimental values [216] has shown good agreement.

To obtain results which are convenient for practical use, we used the numerical values of the fitted parameters which were obtained in [212] and calculated the CO_2 absorption functions for spectral intervals of width 0.1 μ. The absorption functions were calculated in regions of the spectrum 0.1 μ with within the bands 15, 4.3, 2.7 and 2.0 μ for the pressures 1.0, 0.9, 0.7, 0.5, 0.3, 0.1, 0.05 and 0.01 atm and a CO_2 mass corresponding to the distances over which the radiation was propagated along horizontal paths from 0.1 to 100 km at

each altitude. The computational results which were obtained are represented in the form of detailed graphs in monograph [1] and in article [790].

A reference is made in article [271] to the absorption functions which were calculated in the regions of the 9.4 and 10.4 μ CO_2 bands. The value $\gamma = 0.07$ cm^{-1} was used for the halfwidths of the lines, and for the total intensity of bands the values 0.036 and 0.030 $cm^{-2} \cdot atm^{-1}$ were taken at a temperature of 300°K. A comparison of the calculated results with the experimental values for the temperature range from 296 to 555°K has shown satisfactory agreement of the data.

Gray and McClatchey [272] calculated the absorption functions for CO_2, N_2O and CO mixtures in the spectral region 4.2 - 4.8 μ. The calculated results were represented for various altitudes of the homogeneous atmosphere. Originally the calculations included 99 vibration levels. However, later it became evident that the results do not change, for all practical purposes, if only 27 of these are used.

3. Experimental Determination of the Absorption Functions. The most detailed data for the absorption functions in the fundamental vibration-rotation CO_2 band regions were obtained in studies of the Howard team [213, 220], Burch [216, 273] and B. I. Golubitskiy [792-868].

In the first group of studies a series of recordings of the absorption spectra of CO_2 and N_2 mixtures were obtained in the absorption band region near 1.4, 1.6, 2.0, 2.7, 4.3, 4.8, 5.2 and 15.0 μ for various partial pressures of the components. The measurements were made when the absorbing CO_2 mass varied greatly. In the second group of studies, the absorbing masses when the spectra of the bands 2.7, 4.3 and 15.0 μ were recorded were considerably smaller than in [213, 220]; however, the weak bands 9.4 and 10.4 μ were studied using very large masses, from 48 to 11 200 atm·cm. We recall that the CO_2 mass in a 1 km horizontal layer of the earth's atmosphere is equal to 30 atm·cm.

Just as in water vapor studies, a treatment of the measurement data for the CO_2 absorption spectra made it possible to find empirical formulas for the total absorption of entire bands in both groups. These relations turned out to

be the same as in the case of water vapor [see formulas (3.94), (3.95) and (3.96), (3.97)]. The empirical constants were found separately for each band.

The experimental study of the absorptions functions in the regions of the CO_2 spectrum with widths from 5 to 15 cm^{-1} which was carried out by B. M. Golubitskiy's team [792, 867, 868] made it possible to find an empirical formula to determine the absorption function for different CO_2 absorbing masses and pressures.

Burch and Gryvnak [81] studied in detail CO_2 absorption in the spectral region 0.6 - 5.5 μ, when the pressure varied within very wide limits (from several thousandths mm Hg to 15 atm). The authors [81] identified 30 new absorption bands. The total intensities were determined for the most important bands.

In the work of Edwards [231, 274, 275] experimental data was obtained about the total absorption of various CO_2 bands at higher temperatures. The total intensity of the CO_2 15 μ band was determined most accurately in article [276], which turned out to be equal to 200 ± 10 $cm^{-2}.atm^{-1}$. In [276] the data was compared with the data of other investigators. In five other studies values were obtained for this quantity between the limits 170 ± 18 - 218 ± 5 $cm^{-2}.atm^{-1}$. However, in two other studies, the total intensity of the band turned out to be equal to 330 ± 90 and 146 ± 18 $cm^{-2}.atm^{-1}$.

9. Structure and Absorption Functions in the Ozone Spectrum

The fine structure of the vibration-rotation and pure ozone rotation spectrum has been studied theoretically and experimentally in a number of articles, for which a bibliography is given in [1, 3, 277].

The most detailed analysis of the fine structure of the fundamental overlapping O_3 bands 9.1 and 9.6 μ was made by Clough and Kneizis [277, 278].

The authors calculated the positions of the centers and the intensities of over 1200 and 1800 absorption lines in the spectral regions 995-1070 cm^{-1} and 1065 - 1155 cm^{-1}, respectively. The Coriolis interaction between the lines in the ν_1 and ν_3 was taken into account in the calculations.

The computational results were used to find the O_3 spectral absorption contour, which was subsequently compared with the corresponding experimental curves of White, Alper, Debell and Chapman [279], which were recorded with 0.08 - 0.06 cm^{-1} resolution. When the line intensities were calculated the total intensity value of the band ν_3 obtained by Walshaw [280] was used which is equal to 455 $cm^{-2}.atm^{-1}$ under standard conditions.

The structure of the ν_2 ozone band near 14 μ was measured by Nexen [281] and the same author made the first attempt to analyze this band.

In article [282] the structure of the complex band $\nu_1 + \nu_3$ with center near 4.7 μ was studied experimentally under natural and laboratory conditions. Using the results obtained in [282], Trajmar [283, 284] analyzed the fine structure of the band.

An analysis of the fine structure of the pure O_3 rotation spectrum was made by Gora [285]. New data for the high resolution O_3 spectrum in the region 80 - 92 cm^{-1} was obtained in article [286].

A. P. Gal'tsev and V. M. Osipov [889] calculated the intensities and positions of line centers in the 4.7 μ band and also the absorption functions in sections of the spectrum 10 cm^{-1} wide in the bands 9.6 and 4.7 μ.

The most complete experimental data for the absorption functions of the O_3 9.6 μ band were obtained by Walshaw [287]. The measurements were made under laboratory conditions, the settled O_3 layer was varied from 0 to 1.5 cm and the pressure was varied from 0.5 to 760 mm Hg. In [890] the settled O_3 layer reached 4.7 cm, and the pressure took on 8 values from 10 to 400 mb and above. A rather complex empirical formula for the absorption function of the entire band was proposed in [287] on the basis of a treatment of the measurement results, a simpler formula for the absorption function in three spectral intervals was selected in [890] into which the band was broken up: 990 - 1110 cm^{-1} (center of the band), 960 - 990 and 1080 - 1110 cm^{-1} (tails of the band).

Quantitative data for absorption in the 4.7 μ ozone band was also obtained in article [287]. Using the Walshaw data about infrared radiation absorption in the 9.6 and 4.7 μ band,

Altshuller [288] constructed graphs, which made it possible to estimate the radiation absorption by these bands in atmospheric conditions. Elsasser [289] constructed very useful curves which were based on the Walshaw data, which characterize the spectral transmission of this band with low resolutions for various values of the settled ozone layer (Fig. 3.4).

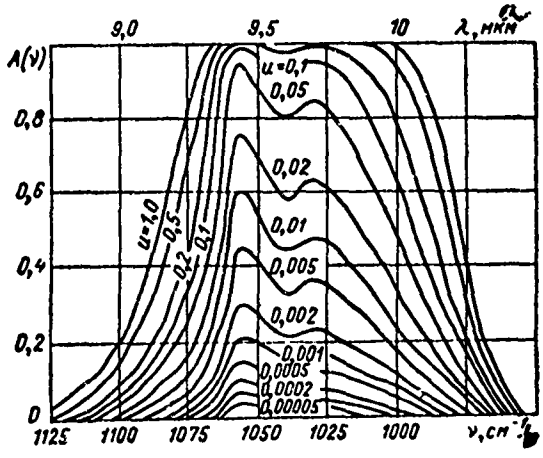

Fig. 3.4. Spectral absorption curves in the 9.65 μ ozone band for various values of the settled layer u, constructed in [289]

Key: a. μ
b. cm^{-1}

10. Fine Structure and Absorption Functions of the Oxygen Spectrum

The position of the lines in the fine structure of the red system of the bands of the atmospheric oxygen absorption spectrum has been studied by Babcock and Herzberg [799]. The distribution of line intensities in the 0.76 μ band (transition 0 - 0) and the halfwidth of the lines were measured by T. G. Adiks and V. I. Dianov-Klyukov [800], who also determined the power of the band oscillator. The mean halfwidth values of the line during $O_2 - O_2$ molecular collisions and collisions with oxygen and air molecules turned out to be equal to 0.085 and 0.077 $cm^{-1}.atm^{-1}$, respectively. No important dependence of the halfwidth of the line on the value of the rotation quantum number was found in [800].

Using the data obtained for the power of the band oscillator, the mean line intensities, and also the data about the position of the lines from [799], and the distribution of their intensities in the band from [801], the authors of [800] calculated the absorption functions for the band in the earth's layer of the atmosphere.

The transmission function for the 0.76 μ band was also calculated by Wark and Mercer [802] on the basis of the data which they obtained for the total absorption of the band. It is noted in [800] that in order to obtain agreement between the calculated and experimental data, the authors of [802] had to change the value of the total intensity of the band. Because of the possibility of using the 0.76 μ oxygen absorption band to determine the altitude of the upper boundary of clouds from artificial earth satellities, a great deal of attention has lately been given to the study of this band [802 - 804].

The relation between equivalent widths S of telluric O_2 lines in the 0.69 μ band and the temperature in the atmosphere has been studied in article [891]. The studies have shown that when the temperature rises, the values S vary in different ways, which depend on the rotation levels where they begin.

11. Fine Structure and Absorption Functions of Spectra of Small Admixtures in the Atmosphere

1. Methane. More than 20 papers were devoted to a study of the vibration-rotation methane absorption spectrum, the bibliography of which up to the year 1964 is given in [237]. The ν_3 band was investigated by Allen and Plyler [290]. The high resolution spectrum of the ν_2 band was obtained in article [292]. The occurrence of the forbidden band ν_2 in the spectrum is due to the vibration-rotation interaction. In addition to an analysis of the positions of lines, their relative intensities are calculated in [292] using the formulas obtained earlier in [291].

The data for the absorption functions CH_4 bands are: 3.33, 6.45, 7.65 μ, the N_2O bands: 3.9, 4.05, 4.5, 7.78, 8.55, 14.5, 17.0 μ and the CO bands: 2.32, 467 μ were obtained by the Burch team [216, 293, 294]. The measurements were made both with pure gases and also with nitrogen mixtures and other extraneous gases. The N_2O, CH_4 and CO concentrations were varied within limits which were known to overlap

with their values under natural conditions.

As a result of the studies which were made, not only data for the total absorption but also for the coefficients B which characterize the relative efficiency of molecular collisions of the absorbing gas and collisions with molecules of the extraneous gas N_2 were obtained (see Table 3.1). In addition to this the values of the relative optical collision diameters $d_{a,a}/d_{a,b}$ were obtained in [216] (the subscripts a and b refer, respectively, to the absorbing and extraneous gases), and the values of the relative expansion coefficients p where P_b is the gas pressure required for the same broadening line effect as the effect due to N_2 (Table 3.7).

TABLE 3.7

VALUES OF THE RELATIVE EXPANSION COEFFICIENTS F^b, AND THE RELATIVE OPTICAL COLLISION DIAMETERS $\frac{d_{a,a}}{d_{a,b}}$ FOR VARIOUS GASES ACCORDING TO THE DATA IN ARTICLE [216]

a Поглощающий газ	Полоса b $см^{-1}$	P_a, c мм pm. cm.	P_b, d мм pm. cm.	Газ расширитель e	F^b	$\frac{d_{a,a}}{d_{a,b}}$
N_2O	2224	10	15—990	O_2	0,83	0,93
				CH_4	1,08	0,94
	1285	100	80—900	O_2	0,72	0,87
				CO_2	1,17	1,14
				CO	0,97	0,99
CO	2143	100	100—2900	CH_4	1,12	0,96
CO_2	2350	50	30—650	O_2	0,81	0,92
CH_4	3020	50	50—2450	CO_2	1,25	1,15

Key: a. absorbing gas
b. band, cm^{-1}
c. P_a, mm Hg.
d. P_b, mm Hg
e. expanding gas

The data obtained by the Burch team for the total band absorption of the gases studied make it possible to determine the absorption functions for these bands and to evaluate quantitatively the role played by each band in infrared radiation attentuation from sources with a continuous spectrum at different temperatures.

The absorption functions were studied experimentally in narrow regions of the methane spectrum by the B. M. Golubitskiy team [793 - 869]. A treatment of the measurement results made it possible to find the parameters in the empirical formula for the absorption functions.

Edwards and Menard [274] obtained a relation for the total absorption in the 7.6 and 3.3 μ bands for CH_4 on the basis of models. The parameters in the relations were determined for the temperatures 300, 555 and 833°K.

2. Nitrogen Monoxide. The positions of line centers in the fine structure of the vibration-rotation and pure rotation N_2O spectra have been studied in great detail at the present time. The corresponding bibliography for the papers can be found in Goody's monograph [3] and in the surveys of Howard and Garing [296].

The intensities and halfwidths of the N_2O absorption lines have not been studied adequately. Gray [297], using the approximations for a harmonic oscillator, calculated the relative intensities for the lines of the band (4.6 μ) for the temperature range 200 - 300°K. To determine the absolute values of the line intensities, the value of the total band intensity was used, which was equal to 1850 $cm^{-2}.atm^{-1}$ at 300°K. Given the data for the line intensities and assuming that they had the same halfwidth equal to 0.05 cm^{-1} under normal conditions, using a statistical model, the author of [297] calculated the absorption functions for narrow regions of the spectral band.

Abels and Ford [298] measured the intensities and halfwidths of more than 70 lines in the N_2O 5.3 μ band. The authors of [298] detected a relationship between the halfwidths of the lines and the rotation quantum number.

Oppenheim and Goldman [299] used an approximate method to determine the halfwidths of the lines, which was based on the use of the formulas for the absorptions functions in the Elsasser model and the experimental data for the absorption

functions with low resolution. The authors of [299] found for the 4.5 μ part of the band the halfwidth $\gamma^0 = 0.08$ $cm^{-1}.atm^{-1}$ at the temperature 300°K, when the expanding gas used was nitrogen.

Rank and his collaborators [300], found the intensities of individual lines in the region of the 3.9 μ N_2O band.

Various molecular and molecular force constants were found in articles [301, 302].

The total intensities of the N_2O bands were investigated in the studies of the Burch team [216], by Abels and Shaw [303] and by Yamada and Person [304]. The absorption functions in narrow regions of the fundamental N_2O bands were measured by the B. M. Golubitskyi team [869 - 870]. The absorption functions were measured for overlapping N_2O and CO absorption bands in the 2200 cm^{-1} region in article [305].

3. Carbon Monoxide. Because of their relative simplicity the vibration-rotation and pure rotation CO spectra have been studied in sufficient detail. A bibliography of the papers can be found in Goody's monograph [3] and in the article by Rank, Pierre and Wiggins [66]. The last article gives detailed data for the molecular and molecular force constants.

The intensities and halfwidths of lines in the vibration-rotation CO bands have been studied experimentally in the work of Benedict and his collaborators [307]. Shaw and France found the halfwidths and intensities of individual lines in the fundamental 4.6 μ band. The halfwidths of the lines in the pure rotation CO spectrum in the interval 100 - 3 cm^{-1} were measured by Dowling and Hall [309]. In [307] and [308] an important relation between the halfwidths of the γ line and the rotation quantum number j was found (when j varies from 1 to 25, γ decreases from 0.1 to 0.05 cm^{-1} under normal conditions).

An analysis of the fine structure of the spectrum for "hot" CO bands consisting of lines with large values of the rotation quantum number was made in article [310].

The total absorption of CO bands for various CO partial pressures and extraneous gases was measured by the Burch team [216] and by Gryvnak and Shaw [311]. In article [312] the total absorption by the fundamental vibration-rotation CO

4.6 μ band was studied at the temperatures 300, 273 and 198°K when the pressure and absorbing mass varied over a wide range. The total absorption of the fundamental band (the interval 1900 - 2450 cm^{-1}) was measured in [313] at the temperatures 300, 600, 900, 1200 and 1500°K when the pressure varied from 0.25 to 3 atm for a path length in the gas vessel of 1, 5, 10 and 20 cm. The total absorption of the fundamental band and its first overtone were also calculated in [313] (the 4050 - 4450 cm^{-1} region) for various temperatures and pressures.

The absorption functions in narrow regions of the CO spectrum were measured in article [793].

Shaw and Houghton [314] calculated the total absorption in the 4.6 μ band from the data for the intensities, halfwidths and forms of the lines which were obtained in article [307]. The total absorption in this band was calculated by Edwards [306].

TABLE 3.8

ATMOSPHERIC GAS ABSORPTION BANDS FOR WHICH EMPIRICAL COEFFICIENTS WERE OBTAINED IN FORMULA (3.98) USED IN CALCULATING THE ABSORPTION FUNCTIONS IN ARTICLES [791 - 793, 867 - 870]

Газ a Полоса, мкм	H_2O										b Континуум
	0,94	1,1	1,38	1,87	2,7	6,3	8—14	14—40 •			1—14
Газ a Полоса, мкм	CO_2										
	1,4 •	1,6 •	2,0	2,7	4,3	4,8	5,2	9,6	10,4	15,0	
Газ a Полоса, мкм	N_2O										
	2,12	2,3	2,94	3,04	3,57	3,86	4,0	4,5	7,8	8,6	15 •

Газ a Полоса, мкм	CH_4		CO		O_3		O_2	N_2
	2,3	3,3	7,6	4,7	9,6 •	4,75 •	1,26 •	4,3 •

b • Эмпирические коэффициенты получены на основании обработки данных других исследователей.

Key: a. gas
band, μ
b. continuum
1. The empirical coefficients were obtained on the basis of a treatment of the data from two investigators

Concluding the study of the atmospheric gas absorption function problems, we give a summary of the basic result (Table 3.8) obtained by the B. M. Golubitskiy team [791 - 793, 867 - 870]. A specific feature of this series of studies is that in it results were obtained which are convenient for practical use and which make it possible to determine quickly the absorption functions in relatively narrow regions of the spectrum at various pressures and for various masses of the absorbing gases. In particular, the great value of this work is that wide ranges of the absorbing gas masses are covered during the measurements. We note that N_2 absorption in the 4.3 μ region is caused by groups [871, 872]. V. L. Filippov and S. O. Mirumyants [873] constructed nomograms for calculating the spectral transparency of the atmosphere in the region 2.8 - 5.6 μ on the basis of calculated data for the absorption functions in the narrow regions of the spectrum given in Table 3.8.

12. Absorption In Overlapping Lines And Bands

In the real atmosphere we often deal with the absorption of overlapping lines and bands of the same gas and different gases. Therefore, when the absorption coefficients and absorption functions are determined, the overlap in the lines must be taken into account. With regard to the absorption coefficient, this problem is solved rather simply theoretically in those cases when all line parameters are known which contribute to the radiation absorption with a given frequency ν. In this case the resulting absorption coefficient is calculated as the sum of the absorption coefficients of all lines.

Since, at the present time, not enough data is available for the intensities and halfwidths of the absorption lines of atmospheric gases, it is not possible to determine in most cases the monochromatic radiation absorption coefficients. So far only when lasers are used, these quantities can be determined experimentally. The absorption functions for the vector $\Delta\nu=\nu_2-\nu_1$ of a complex band consisting of overlapping bands of n gases has the form

$$T=\frac{1}{\Delta\nu}\int_{\nu_1}^{\nu_2}T(\nu)\,d\nu=\frac{1}{\Delta\nu}\int_{\nu_1}^{\nu_2}\prod_{i=n}T_i(\nu)\,d\nu, \qquad (3.99)$$

where $T(\nu)$ is the spectral transmission of the gas mixtures for radiation with frequency ν, and $T_i(\nu)$ is the same for the i-th gas.

For the case which occurs most frequently, when the bands of two gases overlap in the atmosphere, we can obtain from (3.99) the following expression for the absorption function in the region $\Delta\nu$:

$$A=\frac{1}{\Delta\nu}\int_{\nu_1}^{\nu_2}A(\nu)\,d\nu=\frac{1}{\Delta\nu}\int_{\nu_1}^{\nu_2}A_1(\nu)\,d\nu+$$
$$+\frac{1}{\Delta\nu}\int_{\nu_1}^{\nu_2}A_2(\nu)\,d\nu-\frac{1}{\Delta\nu}\int_{\nu_1}^{\nu_2}A_1(\nu)\,A_2(\nu)\,d\nu, \qquad (3.100)$$

where $A_1(\nu)$, $A_2(\nu)$, $A(\nu)$ is the spectral radiation absorption with frequency ν for the first and second gas and their mixture, respectively.

Thus, in the case considered, the absorption function for the complex band is smaller than the sum of the absorption functions of the individual gases by the amount $A'=\frac{1}{\Delta\nu}\int_{\nu_1}^{\nu_2}A_1(\nu)\,A_2(\nu)\,d\nu$, formed by the overlapping bands of two gases.

Only in the last few years data began to appear which could be used to determine the spectral absorption of atmospheric gases needed to calculate the quantity A'. The first studies devoted to determining the absorption function for overlapping bands were experimental studies. Before we pass on to a discussion of the results obtained in individual studies, we write down an approximate expression for the transmission of a mixture consisting of two gases, which follows from formula (3.99):

$$T=T_1\cdot T_2, \qquad (3.101)$$

where T_1 and T_2 are the transmission functions for the first and second gas in the interval $\Delta\nu$, for which the quantity T must be found.

Already in the first series of studies Howard made an attempt to find the total absorption functions for a mixture of water vapor and CO_2 in the 2.7 μ band region, using known data for these functions for H_2O and CO_2 separately. As the

treatments of the corresponding measurements has shown the transmission function on the interval $\Delta\nu$ of a complex band consisting of H_2O and CO_2 lines can be represented with sufficient accuracy for all practical purposes in the form of a product of the transmission functions for the H_2O and CO_2 bands taken separately.

Hoover, Hathaway and Williams [305, 315] studied experimentally the spectral transmission of CO, N_2O, CH_4 bands and their mixtures. For the CO and N_2O bands in the region 2200 cm^{-1} and for the CH_4 and N_2O bands in the region 1300 cm^{-1} the limits for the applicability of formula (3.101) for describing the absorption functions of the corresponding gas mixtures were found. The experimental data obtained was compared with the data calculated by Gray and McClatchey [316]. The absorption functions were also calculated in the last paper in the narrow regions of the spectrum of the gas mixtures: CO_2, N_2O and CO in the region 4.2 to 4.8 μ. The calculations were made using the formulas for the Elsasser model [272].

Penner and Varanasi [317] calculated the absorption in overlapping water vapor and CO_2 bands in the regions 2.7 and 15 μ at a temperature above 800°K.

Expressions for the equivalent width of two overlapping lines were obtained in the work of Sakai [318, 319] and Plass [320]. The method proposed in [318] was extended by Sakai to the case of overlapping bands [321].

13. Radiation Absorptions by Selective Sources

The exact calculations of radiation heat transfer in the atmosphere requires that the absorption functions be known both for sources with a continuous and selective radiation spectrum. In accordance with the well-known Kirchhoff law all gases which absorb the radiation in the visible and infrared regions of the spectrum have corresponding electronic, vibration-rotation and pure rotation radiation spectra. When the radiation heat transfer is calculated, both the radiation flows from the sun and the earth must be taken into account, which penetrate through the corresponding layers in the atmosphere and also the radiation emitted from the atmosphere itself. The last problem requires that the selective radiation absorption laws in a selectively absorbing medium be known.

The second group of problems which requires that the absorption of nonselective sources in the atmosphere be known is related to the development of rocket technology and nuclear aviation. The high temperature of the propellant sprays causes high energy transitions in the molecules and the emission of so-called "hot" bands of atmospheric gases. A study of the spectra of the propellant rays at various distances from these requires the knowledge of the radiation absorption from these sources.

Depending on the type of emitting and absorbing gas and the temperature at which a particular gas finds itself, we are dealing with one of the following possible cases or a combination of these: 1) the centers of the emission and absorption lines coincide, 2) the centers of the emission and absorption lines are displaced relative to one another and 3) the emission and absorption lines do not coincide at all.

The first case occurs when both emission and absorption are caused by the same gas at the same temperature. In the second case, the same gas emits and absorbs; however, the emission conditions are different from the absorption conditions. Finally the third case can occur when one gas emits and another gas absorbs or when a given gas emits such bands which, under atmospheric conditions, do not manifest themselves practically in the absorption. The latter applies primarily to the "hottest" absorption bands. The absorption function for the radiation from a selective source can be written, in the spectral interval $\Delta\nu = \nu_2 - \nu_1$, in the following form [322]:

$$A = \frac{\int_{\nu_1}^{\nu_2} \left[1 - \exp\left(-\sum_i k^{b}_{n_i} \omega^{b}_{n}\right)\right] \left[1 - \exp\left(-\sum_i k^{a}_{n_i} \omega^{a}_{n}\right)\right] d\nu}{\int_{\nu_1}^{\nu_2} \left[1 - \exp\left(-\sum_i k^{b}_{n_i} \omega^{b}_{n}\right)\right] d\nu}, \qquad (3.102)$$

Key: a. a
b. e

where k_{e_i} and k_{a_i} are the i-th absorption coefficients in the spectral line in the emitting and absorbing gases, ω_e and ω_a are the settled layers of the emitting and absorbing gases.

To calculate directly the exact quantitative data for the absorption coefficients and functions of selective radiation sources, all elements of the fine structure as well as the

radiation spectra and the absorption spectra must be known. At the present time the available information is very inadequate. Therefore, to find the absorption functions we resort either to spectral models or to an experiment.

Plass [322, 323] derived a series of expressions for the absorption functions for the radiation from selective sources for various cases of overlapping lines, both in the radiation source and in the absorbing medium (overlapping lines, overlapping lines described by the Elsasser model, overlapping lines described by a statistical model). Cases were also studied in [322] when the pressure, temperature and concentration of the absorbing gas varied along the trace of the beam.

The numerical calculation given in [322] has shown that, in the case when the same lines participate both in the radiation and absorption, the flare absorption function is considerably larger than that for a source with a continuous radiation spectrum. The absorption by carbon dioxide from a selective source was calculated in the work of M. V. Podkladenko and his collaborators [324, 325].

Burch and Gryvnak [81] made an experimental study of heated H_2O and CO_2 radiation absorption by the same gases at a normal temperature. The CO_2 absorption functions were studied experimentally for flares at a temperature of 2800°K for different pressures and emission path lengths in the vessel. The temperature of the vessel was equal to 24°C. In the spectral regions 2.5 - 3.5 and 4.0 - 5.5 μ the authors of [326] detected relatively high transmission. Thus, in the CO_2 layer which was equivalent in magnitude to a 50 km absorbing mass layer of the earth's atmosphere, the transmission function turned out to be equal to 0.2 in the region 4.0 - 5.5 μ

14. Laser Radiation Absorption in the Atmosphere

The high monochromatism, acute direction, coherence, the possibility of obtaining supershort periodic impulses and giant radiation powers from lasers creates a number of specific propagation features for this radiation in the atmosphere in comparison with the radiation emitted from other sources. The halfwidth of laser emission lines is considerably smaller than the halfwidths of lines in the absorption spectra of atmospheric gases. In this respect to estimate quantatively the radiation absorption from lasers in the atmosphere, we must know with very high accuracy the positions, intensities and forms of the lines in the spectra of the atmospheric gases.

All quantitative data for the absorption spectra of atmospheric gases which were available prior to the appearance of lasers were unsuitable for evaluating the radiation absorption from lasers in the atmosphere [1].

The interaction between a light beam bounded in space with an aerosol leads to a change of the light intensity in the propagation direction, due to the direct radiation attenuation according to the Buger law and due to single and repeated dissipation. The contribution of directly attenuated and dissipated light varies with the depth that the radiation penetrated into the dissipating medium. It turns out that the light field in the medium depends not only on its optical properties but also on the geometric parameters of the source.

The small diameter of laser beams and their weak divergence together with the radiation coherence are responsible for the spotty three-dimensional time structure of the beam propagated in the turbulent atmosphere.

The giant radiation power of lasers is the reason for the formation of a series of nonlinear effects which accompany laser rad ation in the atmosphere. Among these effects we have primarily: 1) the spectroscopic saturation effect (the dependence of the absorption coefficient on the power of the incident and absorbing radiation layer), 2) multiphoton effects (excitation, ionization, atomic and molecular dissociation of atmospheric gases which do not absorb radiation with a given frequency at relatively small radiation powers), 3) the radiation interaction effect on aerosol particles in the atmosphere (light pressure, vaporization, explosions, etc.), 4) forced combined dissipation, 5) self-focusing of the beam.

The wide use of lasers in various devices designed to operate in the atmosphere has great promise (communication, information transmission, radar, rangefinders, etc.) and requires that all features of laser radiation propagation in the atmosphere be studied intensely.

1. The General Picture of the Fine Structure of the Absorption Spectrum In The Earth's Atmosphere In Regions Of Laser Radiation. A general idea about the fine structure of the absorption spectrum in the earth's atmosphere in the spectral radiation regions of the most widely used lasers can be obtained on the basis of available data in the literature. Figures 3.5 - 3.15 show the absorption spectra of the earth's atmosphere recorded by various authors with high resolution in the radiation regions of the most widely used lasers: the first ruby harmonic (λ = 0.345 μ), the gas laser based on

argon (λ = 0.5 μ), the first laser harmonic on glass with neodymium, (λ = 0.53 μ), the gas laser based on a mixture of helium and neon (λ = 0.63 μ), the ruby laser (λ = 0.69 μ), the semiconductor laser based on gallium arsenide (λ = 0.84 μ), the glass laser with neodynium (λ = 1.06 μ), the gas laser based on a mixture of helium and neon (λ = 1.15 μ), the gas laser based on a mixture of helium and neon (λ = 3.39 μ), the gas laser based on a mixture of xenon and helium (λ = 3.51 μ), the gas laser based on a mixture of carbon dioxide and nitrogen (λ = 1.6 μ).

From Figs. 3.5 - 3.15 one can clearly see the exceptionally sharply pronounced absorption selectivity of the earth's atmosphere in any laser radiation region.

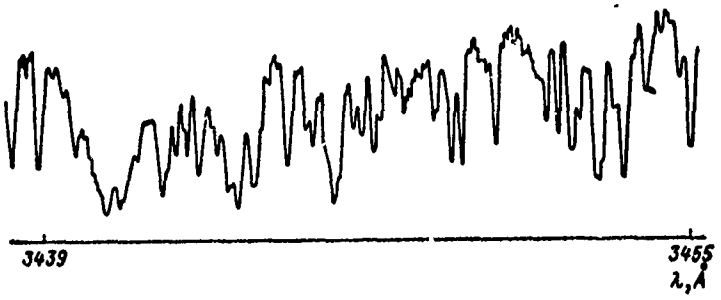

Fig. 3.5. Recording of the fine structure of the absorption spectrum of the earth's atmosphere in the region λ = 0.345 μ [174].

Fig. 3.6. Recording of the fine structure of the absorption spectrum of the earth's atmosphere in the region 0.5 μ [174].

It should be noted that all diagrams represent a recording of the absorption spectrum of the earth's atmosphere with high but finite resolution, which smoothes the true but even more pronounced absorption selectivity. In all diagrams, for example, by far not all absorption lines are resolved as individual lines. It is easily seen that if the laser radiation wavelength changes for any reasons, the absorption of this radiation in the atmosphere can also change correspondingly.

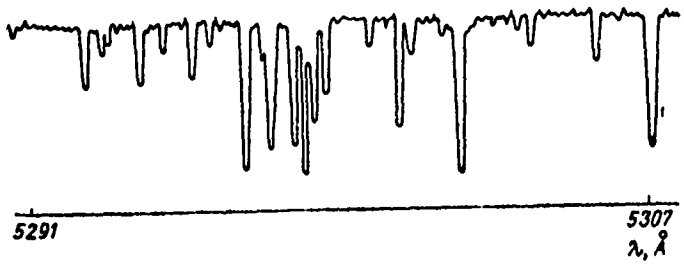

Fig. 3.7. Recording of the fine structure of the absorption spectrum of the earth's atmosphere in the region $\lambda = 0.63$ μ [174]

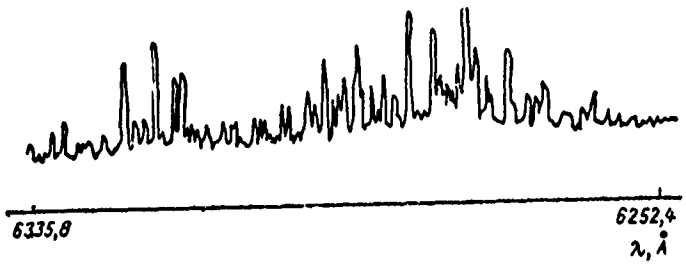

Fig. 3.8. Recording of the fine structure of the absorption spectrum of the earth's atmosphere in the region $\lambda = 0.63$ μ [185]

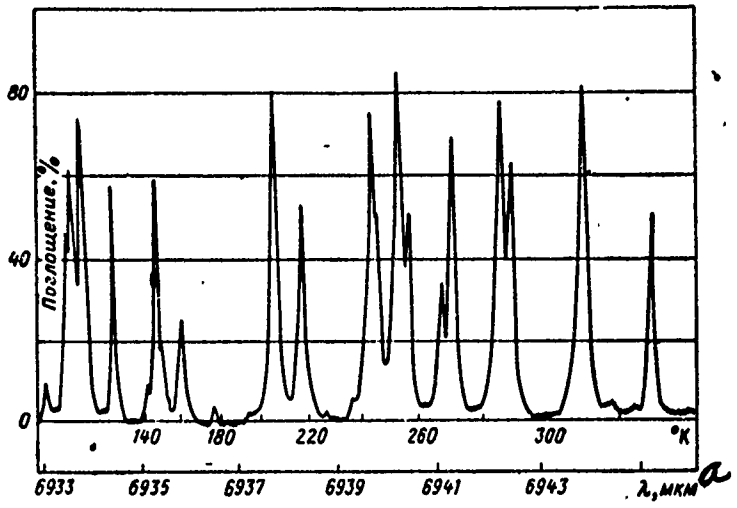

Fig. 3.9. Recording of the fine structure of the absorption spectrum of the earth's atmosphere in the region $\lambda = 0.69$ μ [295]

Key: a. μ

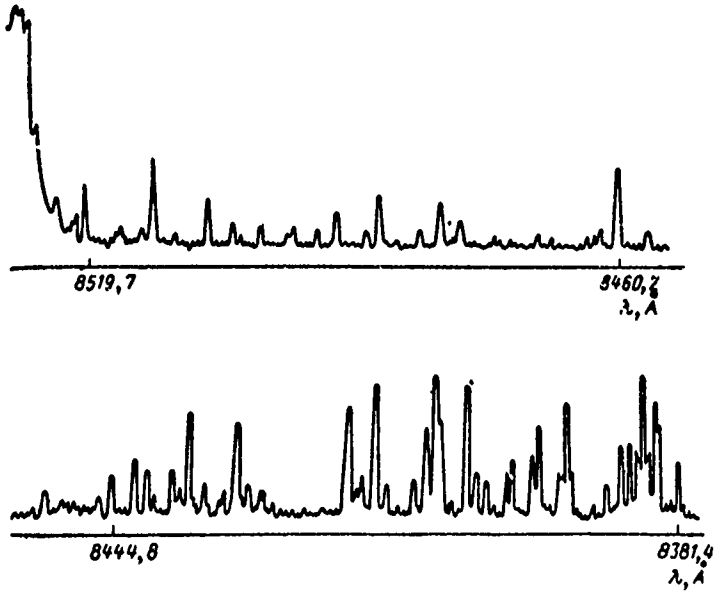

Fig. 3.10. Recording of the fine structure of the absorption spectrum of the earth's atmosphere in the region $\lambda = 0.84$ μ [185]

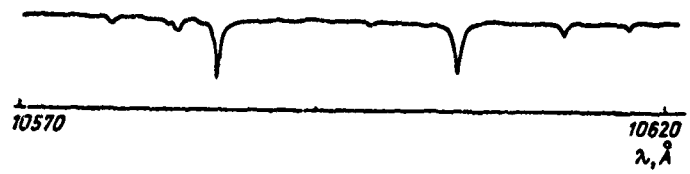

Fig. 3.11. Recording of the fine structure of the absorption spectrum of the earth's atmosphere in the region λ = 1.06 μ [183]

Fig. 3.12. Recording of the fine structure of the absorption spectrum of the earth's atmosphere in the region λ = 1.15 μ [183]

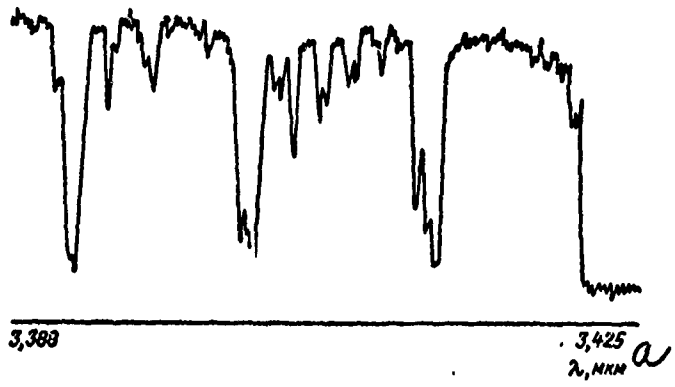

Fig. 3.13. Recording of the fine structure of the absorption spectrum of the earth's atmosphere in the region λ = 3.39 μ [181]

Key: a. μ

Fig. 3.14. Recording of the fine structure of the absorption spectrum of the earth's atmosphere in the region $\lambda \approx 3.51$ μ [181]

Key: a. cm^{-1}
b. μ

Fig. 3.15. Recording of fine structure of the absorption spectrum of the earth's atmosphere in the region $\lambda \approx 10.6$ μ [181]

Key: a. cm^{-1}
b. μ

This fact can be illustrated on the radiation example of the most widely used ruby laser. In Fig. 3.9, the spectral absorption of the entire layer of the atmosphere recorded with high resolution using the sun as the radiation source is entered along the ordinate. The scale for the wavelengths in Angstrom and the temperature scale T for which the corresponding radiation wavelengths of the ruby laser are generated are entered on the abscissa. It is clearly seen from the figure that the ruby laser radiation absorption in the atmosphere can vary considerably in accordance with the temperature of the

operating body of the generator. It should be noted that there are no strong absorption lines in the radiation region of the ruby laser.

The diagrams which were presented also make it easy to understand that an important role in laser absorption radiation may be played by very weak lines in those cases when the centers of these lines coincide with the centers of the corresponding emission lines of the laser. Therefore, ignoring the absorption by weak lines which is justified when the absorption functions are calculated in wide regions of the spectrum can never be applied to the calculation of laser radiation absorption. Usually when the absorption functions were calculated in relatively wide regions of the spectrum until very recently water vapor, carbon dioxide and ozone absorption have been taken into account. The radiation absorption in the entire vibration-rotation bands of small mixtures, such as methane, nitrous monoxide, carbon monoxide, are ignored. This ignoring is more and more valid the wider the regions of the spectrum for which the absorption functions are determined, since the absorption bands of small mixtures occupy sufficiently narrow regions.

When laser radiation absorption is calculated, neither bands nor lines can be ignored and the calculations cannot be based only on the knowledge of their intensities. Above all the positions of the absorption line centers and the laser radiation lines must be known with high accuracy.

Table 3.9, which was taken from the paper by Lond [295], contained data about the positions of radiation lines for 67 gas lasers and the atmospheric gas absorption lines situated near these, which were detected by various investigators in the absorption spectra which were recorded with high resolution.

2. Accuracy Requirements for Determining the Centers of Absorption Lines. We will assume that the centers of the laser radiation lines are known with very high accuracy and that the halfwidths of the radiation lines are considerably smaller than the halfwidths of the absorption lines. The last assumption is fully justified for gas lasers.

We will estimate the accuracy with which the lines of the absorption spectra of the atmospheric gases must be determined in order to estimate quantiatively the laser radiation absorption in the atmosphere, and we will follow paper [327]. This accuracy depends on: 1) the value of the total and partial pressures and the temperature, or the altitude at which the

TABLE 3.9

POSITIONS OF RADIATION LINES OF VARIOUS GAS LASERS, AND NEIGHBORING ABSORPTION LINES OF ATMOSPHERIC GASES [295]

a Газы	b Длина волны излучения ОКГ в воздухе, Å	c Ближайшие линии поглощения атмосферных газов, Å	d Примечания
He—Ne	6328,172	1 Нет	
O_2	8446,2	2 Нет в земной атмосфере	1
He—Ne	10798	1 Нет	
He—Ne	10845	1 Нет	
He—Ne	11143	11143,32—H_2O	
He—Ne	11177	11175,59—H_2O 11177,45—? 11177,49—H_2O	
He—Ne	11390	3 Неидентифицированная линия	
He—Ne	11409	1 Нет	2
He—Ne	11522,76	11522,77—H_2O 11523,19—H_2O 11523,73—H_2O 11524,20—H_2O 11521,23—H_2O	
He—Ne	11601	11600,21—H_2O 11601,05—H_2O	
He—Ne	11614	11613,84—H_2O	
He—Ne	11767	11768,37—H_2O	
He—Ne	11985	11984,8 —?	
He—Ne	12066	12067,24—H_2O	
Ne	15231	15230,59—H_2O	
Ar	16180	1 Нет	
Kr	16900	16900,97—H_2O 16901,41—CH_4 16901,3 —H_2O	
Kr	16935,81	16935,1 —CH_4 16936,25—CH_4 16937,22—H_2O	
Ar	16940,59	16940,13—H_2O	
Kr	17843	17843,37—H_2O	3
Ar	17930	17934,71—H_2O	4
Kr	18185	18180 —H_2O	5
Kr	19211	— —H_2O	3
Xe	20262,28	20260,75—CO_2 20263,21—CO_2	
He	20603	20604,57—CO_2 20615,75—H_2O 20618,04—CO_2	
Ne	21019	21018,45—CO_2	6
Kr	21165	21165,76—$OC^{13}O$	4

Key: a. gases
b. laser radiation wavelength in air, Å
c. nearest absorption lines for atmospheric gases, Å
d. remarks

(continued on next page)

Key, Table 3.9 (Cont'd):

Column c:

1. none
2. none in earth's atmosphere
3. unidentified line

TABLE 3.9 (Cont'd)

a Газы	Длина волны излучения ОКГ в воздухе Å b	Ближайшие линии поглощения атмосферных газов, Å c	Примечания d
Kr	21902,53	21899,5 —H_2O	4
Xe	23193,28	23192,89—H_2O	
		23194,44—CH_4	
Kr	25234	25234,39—H_2O	3
	25414	— —H_2O	3
Xe	26268,95	—H_2O	3
Xe	26510,96	—H_2O	3
Xe	26600,6	—H_2O	3
	31069,14	31053,8 —H_2O	2
		31081,5 —H_2O	
Ne	33333	33336,3 —CH_4	
Xe	33666,5	33658,6 —CH_4	
		33666,6 —CH_4, H_2O	
		33676,8 —CH_4	
Ne	33913,17	33913,0 —CH_4	
Xe	34341	34344,1 —CH_4	
		34348,7 —CH_4	
		34352,1 —CH_4	
		34357,2 —CH_4	
Xe	35070,4	35069,5 —?	4
Xe	36209	36205,5 —CH_4	
Xe	36503	36501,0 —HDO, CH_4	6
Xe	36788,36	36790,1 —CH_4	6
Xe	36848,56	—	6
Ne	37734	37732,9 —CH_4, HDO	4
Xe	38686	38686,7 —N_2O	
Xe	38939,74	38937,5 —N_2O	
Xe	41516		4
Xe	41516		4
Xe	46096	46096,8 —N_2O, CO	
Ne	54072	54077,1 —CO, H_2O	7
Xe	55738	— —H_2O	3
Cs	71821	71600,9 —H_2O	
		71801,4 —H_2O^{17}	
Xe	73147	73042,3 —H_2O, CH_4	
		73143,8 —CH_4	
		73181,3 —CH_4, H_2O	
Xe	90040	90057,6 —O_3	
Xe	97003,36	96979,1 —O_3	
Xe	122990		4
Xe	122630	122564 —CO_2	4
		122731 —H_2O	
Xe	129130	129134 —CO_2	6
Ne	182760	182505 —H_2O	5

Key: a. gases
b. laser radiation wavelength in air, Å
c. nearest absorption lines of atmospheric gases, Å
d. remarks

(continued next page)

TABLE 3.9 (Cont'd)

a Газы	b Длина волны излучения ОКГ в воздухе Å	c Ближайшие линии поглощения атмосферных газов, Å	d Примечания
Ne	182820	182989—H_2O	
Ne	183040	182989—H_2O	3
Ne	183970		4
Xe	185010	184771—H_2O	5
Ne	185910	185805—CO_2, H_2O	4
Ne	185970		
Ne	203510	203215—H_2O	5

e Примечание: 1 — поглощение атомарным кислородом; 2 — между двумя сильными линиями H_2O; 3 — полное поглощение; 4 — поглощения практически нет; 5 — крыло линий H_2O; 6 — слабые линии; 7 — солнечный CO.

Key: a. gases
b. laser radiation wavelength in air, Å
c. nearest absorption lines of atmospheric gases, Å
d. remarks
e. Remarks: 1--atomic oxygen absorption, 2--between two strong H_2O lines, 3--total absorption, 4--practically no absorption, 5--tail of H_2O lines, 6--weak lines, 7--solar CO

laser radiation is propagated, 2) on the distance from the center of the absorption line of the laser radiation line.

As was shown in chapter 2, in the lower 20 - 30 km layer of the atmosphere the center of the absorption line of atmospheric gases is described satisfactorily by a dispersion contour:

$$k(\nu)=\frac{S}{\pi}\frac{\gamma}{(\nu-\nu_0)^2+\gamma^2},$$

where $k(\nu)$ is the monochromatic absorption coefficient for the frequency ν, S, $\gamma \doteq \gamma^0(P_a+\sigma_{ab}P_b)$, ν_0 are the intensity, halfwidths, and position of the center of the absorption line, γ^0 is the halfwidth of the line under standard conditions, P_a is the pressure of the nonabsorbing gas, P_b is the pressure of the absorbing gas, σ_{ab} is the molecular collision efficiency

of the absorbing and nonabsorbing gas. In the lower 30-km layer of the atmosphere, for all gases absorbed in the infrared region of the spectrum, the product $\sigma_{nb}P_b$ can be ignored in comparison with the quantity P_a. Consequently, we can assume that $\gamma = \gamma^0 P$, where P is the total pressure.

Further, taking into account the weak dependence of γ^0 on the temperature, $\left(\gamma^0 \sim \frac{1}{\sqrt{T}}\right)$, and the relatively small changes in the temperature with the altitude, we can assume with sufficient accuracy for all practical purposes that γ^0 does not depend on the altitude.

Taking into account the assumptions which were made, we calculated the values of k(ν) for S = 1, γ^0 = 0.03 and 0.1 $cm^{-1}.atm^{-1}$, P = 1 and 0.1 atm. The values of γ^0 which were used in the calculations correspond to the minimum and maximum halfwidth of the absorption lines of the fundamental absorption component of water vapor in the atmosphere. The pressures 1.0 and 0.1 atm correspond to the altitudes 1 and 16 km above sea level.

TABLE 3.10

VALUES OF k(ν) AT VARIOUS DISTANCES FROM THE CENTER OF THE LINE WITH INTENSITY S = 1 FOR VARIOUS HALFWIDTHS OF THE LINES

Δν, cm^{-1} a	b c $\gamma^0 = 0{,}1\ cm^{-1}.atm^{-1}$, $P = 1\ atm$	b c $\gamma^0 = 0{,}03\ cm^{-1}.atm^{-1}$, $P = 1\ atm$	b c $\gamma^0 = 0{,}1\ cm^{-1}.atm^{-1}$, $P = 0{,}1\ atm$	b c $\gamma^0 = 0{,}03\ cm^{-1}.atm^{-1}$, $P = 0{,}1\ atm$	Δν, cm^{-1} a	b c $\gamma^0 = 0{,}1\ cm^{-1}.atm^{-1}$, $P = 1\ atm$	b c $\gamma^0 = 0{,}03\ cm^{-1}.atm^{-1}$, $P = 1\ atm$	b c $\gamma^0 = 0{,}01\ cm^{-1}.atm^{-1}$, $P = 0{,}1\ atm$	b c $\gamma^0 = 0{,}03\ cm^{-1}.atm^{-1}$, $P = 0{,}1\ atm$
0	3,18	10,6	31,8	106,1	0,1	1,59	0,9	0,3	0,1
0,005	3,17	10,3	25,4	28,1	0,2	0,6	0,2	0,1	0,02
0,01	3,15	9,5	15,9	8,8	0,3	0,3	0,1	0,04	0,01
0,02	3,06	7,3	6,4	2,4	0,4	0,2	0,06	0,02	0,01
0,03	2,92	5,3	3,2	1,1	0,5	0,1	0,04	0,01	
0,04	2,74	3,8	1,9	0,6	1,0	0,03	0,01		
0,05	2,54	2,8	1,2	0,4	2,0	0,01			

Key: a. cm^{-1}
b. $cm^{-1}.atm^{-1}$
c. atm

The results of the calculations of $k(\nu)$ which were made for the four cases mentioned above are represented in table 3.10.

Table 3.11 gives the values of the coefficient $k(\nu)$ for the four cases considered but not for unit line intensities. For the convenience of interpreting the results of the calculations, the values of $k(\nu)$ were taken in all four cases in the center of the line ($\Delta\nu = 0$) equal to 100.

It can be seen from the tables that in the earth's layer of the atmosphere ($P = 1$ atm) for the widest lines (as a rule, these are also the most intense lines) the value of $k(\nu)$ decreases 10 times as much at the distance $\Delta\nu = 0.3$ cm^{-1} from the center of the line, and for narrow lines this decrease occurs already for $\Delta\nu = 0.1$ cm^{-1}. At an altitude of 16 km $k(\nu)$ decreases by one order at a distance of 0.03 cm^{-1} and 0.01 cm^{-1} for wide and narrow lines, respectively, and for the values $\Delta\nu = 0.1$ cm^{-1} and 0.03 cm^{-1} for wide and narrow lines at the same altitude $k(\nu)$ decreases 100 times as much.

Thus, if the monochromatic laser radiation falls into the central part of the water vapor absorption lines, to estimate the quantity $k(\nu)$, one must know beside the exact value of the laser radiation frequency the position of the absorption line center with very high accuracy. This accuracy is characterized in the earth's layer of the atmosphere by a magnitude which is several hundredths of a cm^{-1}, which increases considerably with the altitude. All recorded absorption spectra of the earth's atmosphere obtained until now (Elsasse's spectra) do not determine the positions of the line centers with such high accuracy. In this regard, when these atlases are used even for a gross quantitative estimate of $k(\nu)$ values in the central regions of the lines, great caution must be exercised.

The accuracy requirements for determining the position of the center of the absorption line of the atmospheric gas are less stringent the farther the frequency of the laser radiation absorption lies from the center of this line. A quantitative measure for these requirements can be obtained from the tables which were presented.

The conclusions which were made hold not only for the water vapor absorption spectrum. They can also be applied to the absorption spectra of other atmospheric gases, as long as the halfwidth of the lines in the latter is of the same order of magnitude.

TABLE 3.11

VALUES OF K(ν) AT VARIOUS DISTANCES FROM THE LINE CENTERS, FOR VARIOUS HALFWIDTHS REDUCED TO A SINGLE SCALE WITH $\Delta\nu = 0$

Δν, cm⁻¹ a	γ = 0,1 cm⁻¹·atm⁻¹, P = 1 atm b c	γ = 0,03 cm⁻¹·atm⁻¹, P = 1 atm b c	γ = 0,1 cm⁻¹·atm⁻¹ P = 0,1 atm b c	γ = 0,03 cm⁻¹·atm⁻¹ P = 0,1 atm b c
0	100	100	100	100
0,005	99,8	97,3	80,0	26,5
0,01	99,1	89,5	50,0	8,3
0,02	96,2	69,2	20,1	2,3
0,03	91,7	50,0	10,1	1,0
0,04	86,2	36,0	6,0	0,6
0,05	80,0	26,5	3,8	0,4
0,1	50,0	8,3	1,0	0,1
0,2	20,1	2,2	0,3	0,02
0,3	10,1	1,0	0,1	0,01
0,4	6,0	0,6	0,06	0,01
0,5	3,8	0,4	0,03	—
1,0	1,0	0,1	—	—
2,0	0,3	—	—	—

Key: a. cm^{-1}
b. cm^{-1} atm^{-1}
c. atm

3. Results of Laser Radiation Absorption Studies in the Atmosphere

1. Theoretical Studies

Keeping in mind the rigorous accuracy requirements for determining the position of the lines and also their intensities and halfwidths, when the problem of calculating the absorption spectra of atmospheric gases is solved theoretically, we must take into account all factors which have an effect on the characteristics of these spectra.

The most important effects on all these characteristics is the interaction between the vibration and rotation molecular movements, which becomes more important the larger the value of

the rotation quantum number used when we calculate the absorption lines. In fact, it can be said that lines with a large rotation quantum number, as a rule, fall into practically all important spectral intervals between the absorption bands (the transparent "windows" of the atmosphere).

The most complex vibration-rotation spectrum among all atmospheric gases is the spectrum of the fundamental absorption component of the atmosphere, water vapor. Because of this, the author first attempted to calculate correctly quantitatively the positions, intensities and halfwidths of lines and the absorption coefficients for water vapor in his laboratory and then take into account the interaction between the vibration and rotation molecular movements.

The method used to calculate the positions of the line centers, their intensities and halfwidths has been discussed in detail in paragraph 5. The data obtained for all three H_2O absorption line parameters were then used to find the monochromatic absorption coefficient in individual narrow bands of the water vapor vibration-rotation spectrum in the radiation regions of most widely used lasers. The calculations were made for several pairs of values of the temperature and pressure, which were characteristic for certain altitudes in the atmosphere. It was assumed that the lines had a dispersion contour. Thus, for the monochromatic absorption coefficient the expression

$$k(\nu)=\sum_i \frac{S_i(T)}{\pi}\frac{\gamma_i(T,\ P)}{(\nu-\nu_{0i})^2+\gamma_i^2(T,\ P)}$$

was used.

The analysis of the spectral behavior of the H_2O absorption coefficient within the spectral intervals studied has shown an exceptional selectivity of the magnitude $k(\nu)$ even in regions in which there were no strong absorption lines. Thus, in laser radiation regions with wavelengths 0.84 μ (semiconductor laser based on gallium arsenide) and 1.06 μ (laser based on glass with neodymium), the value of the absorption coefficient varies by several orders when the wavelength varies only by several inverse cm. The unavailability of the corresponding experimental data for the monochromatic absorptions coefficients, unfortunately, does not make it possible to estimate the accuracy of the calculations made.

The greater part of laser radiation is absorbed by water vapor. However, in a number of cases, laser radiation is also found in part of the spectra of other atmospheric gases. For example, the radiation absorption from lasers based on $CO_2 + N_2$ (spectral region 10.6 μ) and He + Ne (wavelength 3.39 μ) is caused in the first case simultaneously by carbon dioxide and water vapor and in the second case practically only by methane.

It is not difficult to calculate the monochromatic absorption coefficients for a laser based on a mixture of CO_2 and nitrogen in the region of the 10.6 μ wavelength. We obtained the components of this coefficient due to carbon dioxide and water vapor absorption. In the centers of the lines, the P branches of the CO_2 band with values of the rotation quantum number j from 14 to 28, the component of the carbon dioxide absorption coefficient varies in the earth's layer of the atmosphere from 0.12 to 0.19 km^{-1}. The component of the water vapor absorption coefficient in the narrow region of the spectrum occupied by these lines caused by the continuous absorption by distant tails of strong lines does not depend practically on the wavelengths. Its value is equal to 0.08 km^{-1} at a humidity of the earth's atmosphere layer equal to $10g/m^3$ [192].

To calculate theoretically the monochromatic absorption coefficients in the methane band region in most sectors in the spectra of other atmospheric gases, not enough data is available at the present time about the parameters of individual lines.

We note in conclusion that in spite of the well-known successful theoretical solution of the problem of the monochromatic absorption coefficients in the atmosphere we are still very far, at the present time, from forecasting sufficiently accurately the monochromatic or quasimonochromatic radiation absorption in the atmosphere, even if we know in advance with high accuracy the spectral composition of this radiation. Therefore, the absorption characteristic of the radiation from various lasers in the atmosphere will for the time being be determined on the basis of the corresponding experimental studies.

2. Experimental Studies

A series of studies was carried out in the author's laboratory, the purpose of which was to determine experimentally the absorption of the radiation from lasers of various types.

The results which were obtained were published in articles [328 - 331, 782, 806, 893, 908 - 910].

The absorption coefficients of atmospheric gases in laser radiation regions cannot be determined experimentally directly in practice because of the insufficient resolution capacity of the best spectrometer models. However, when lasers themselves are used as radiation sources during the measurements, it is possible to obtain directly from the experiment the coefficients or the absorption functions for particular generators. In the case of gas lasers it is possible to obtain in practice the absorption coefficients. For other types of generators, the absorption function or the average absorption coefficient is obtained directly from the experiment.

Experimental studies of radiation absorption from various lasers are beingstudied in the author's laboratory in two ways: 1) of a multipath vacuum cell, 2) under natural conditions on proving grounds. In the first case it is possible to study pure absorption, in the second case the absorption is singled out from the total attentuation. However, during measurements in the cell large layers cannot be obtained. Thus, the measurements in the cell and on the proving grounds compliment one another.

When the measurements were made with the cell, absorption coefficients were obtained for helium-neon laser radiation with wavelengths 1.15 and 3.39 μ. The absorption coefficient for radiation with wavelengths 1.15 μ in the earth's layer turned out to be equal to 0.3 mm^{-1}, where mm^{-1} is an inverse millimeter of settled water. Since this radiation is absorbed by water vapor, the value of the absorption coefficients in inverse units of the distance or in db/km depends on the humidity. At a humidity of 12 g/m^3 in the earth's layer, the attenuation coefficient is equal to 16 db/km.

Table 3.12 gives the transmission values for the earth's transparent layer of the atmosphere for laser radiation with wavelengths 1.15 μ with various humidities.

The absorption coefficient for laser radiation with wavelengths 3.39 μ for the earth's layer turned out to be equal to 1.4 km^{-1} for 6 db/km. This radiation is absorbed by methane. It should be emphasized that when the radiation absorption of heat sources is calculated, it is customary to ignore the methane absorption because of its very small concentration (a millionth of the volume). The considerable laser radiation with wavelength 3.39 μ which was detected during measurements

shows that in this case it is not possible to ignore methane absorption. The relatively strong absorption is caused in this case by the fact that the centers of the methane absorption and laser radiation lines practically coincide. This fact is confirmed by the phenomenon of the brightness of the atmosphere detected in our measurements in the laser radiation region with wavelengths 3.39 μ when the total pressure of the gas mixture rises and the methane content remains constant (Fig. 3.16).

TABLE 3.12

TRANSMISSION T OF THE TRANSPARENT ATMOSPHERE FOR LASER RADIATION WITH WAVELENGTH 1.15 μ AT VARIOUS VALUES OF THE ABSOLUTE HUMIDITY a FOR THE DISTANCES 0.1, 0.5 AND 1.0 KM IN THE EARTH'S LAYER OF THE ATMOSPHERE

a D, km	T a = 1 mm/km	a = 5 mm/km	a = 10 mm/km	a = 15 mm/km
0,1	0,97	0,86	0,74	0,64
0,5	0,86	0,47	0,22	0,11
1,0	0,74	0,22	0,05	0,01

Key: a. km
b. mm/km

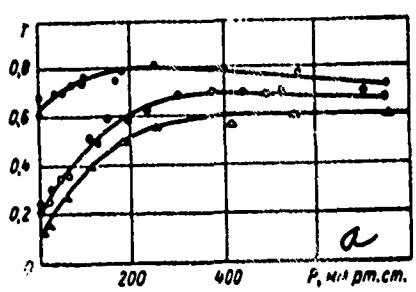

Fig. 3.16. Laser radiation transmission with wavelenth λ = 3.39 μ vs. the total pressure with various constant partial methane pressures and geometrical thickness of the layer L = 64 m

Key: a. mm Hg

The laser radiation absorption measurements with various wavelengths on the proving grounds were carried out for considerably thicker layers than in the cell. The distances at which the measurements were made varied from several hundredths of meters to 3.5 km (the maximum length of the beam path in the cell was 96 m).

In the proving ground measurements, the radiation sources used were lasers, the parameters of which are given in Table 3.13.

TABLE 3.13

LASER RADIATION PARAMETERS USED DURING PROVING GROUND MEASUREMENTS

a Тип ОКГ	b Длина волны излучения, км	c Мощность излучения	d Режим излучения	e Расходимость луча
Газовый на смеси гелий—неон	0,63	10 мвт	Непрерывный многомодовый	1′
Твердотельный на рубине	0,69	1 квт	Импульсный	1,5′
Полупроводниковый на арсениде галлия	0,84	1 мвт	Импульсный	20′
Твердотельный на стекле с неодимом	1,06	0,1 квт	Импульсный	3′
Газовый на смеси гелий—неон	1,15	10 мвт	Непрерывный многомодовый	1′
Газовый на смеси гелий—неон	3,39	20 мвт	Непрерывный многомодовый	1′
Газовый на смеси гелий—ксенон	3,51	20 мвт	Непрерывный многомодовый	2′
Газовый на смеси углекислого газа с азотом	10,6	1 вт	Непрерывный многомодовый	2′

Key: a. type of laser
b. radiation wavelength, km
c. radiation power
d. radiation regime
e. beam divergence

(continued next page)

Key, Table 3.13 (cont'd)

Column a.

Gas based on a helium-neon mixture
Solid body, ruby
Semiconductor on gallium arsenide
Solid body based on glass with neodyme
Gas based on helium-neon mixture
Gas based on helium-neon mixture
Gas based on helium xenon mixture
Gas based on carbon dioxide and nitrogen mixture

Column c.

1. milliwatt
2. kilowatt
3. watt

Column d.

Continuous multimodal
Impulse
Impulse
Impulse
Continuous multimodal
Continuous multimodal
Continuous multimodal
Continuous multimodal

The absorption coefficient for laser radiation with wavelengths 1.15 μ during measurements on the proving grounds turned out to be the same as during the measurements in the cell. For laser radiation with wavelength 3.39 μ under natural conditions, the absorption coefficient varied from one series of measurements to another between the limits 1.4 to 5.0 km^{-1}. Thus, the minimum value of the absorption coefficient coincides with the values measured under laboratory conditions. Further studies are needed to explain the reasons for the changes in the absorption coefficient. It is possible that the reason is related to the changes in the methane concentration at the locality where the measurements were made.

During measurements with lasers based on a $CO_2 + N_2$ mixture (wavelength 10.6 μ) the measured attenuation was not broken up into components caused by molecular absorption and aerosol scattering. The values of the attentuation coefficients which were obtained lie between the limits 0.12 - 4 db/km. This range within which the attenutation coefficient varies is determined by the various meteorological conditions under which the measurements were made (mist with visibility range $S_M \geqslant 2$ km, snowfall, light clouds).

The radiation absorption from a ruby laser varied in accordance with the temperature of the operating body. The limits within which the absorption coefficient varies at a humidity of $10 g/m^3$ were 1.1 to 4.7 db/km.

Laser radiation absorption with wavelengths 0.63, 0.84, 1.06 and 3.51 μ during the proving ground measurements was completely masked by the measurements errors which attained values in the 10 - 30% range, depending on the meteorological conditions and the distance.

Edwards and Burch [332] measured the radiation absorption from a gas laser based on a helium and neon mixture with wavelength $\lambda = 3.39$ μ, using a small cell. As a result of the measurements they determined the distance between the laser radiation line centers and the methane absorption lines and the halfwidth of the CH_4 line, which turned out to be equal to 0.003 ± 0.002 cm^{-1} and 0.13 ± 0.04 cm^{-1} under normal conditions, which shows that the centers of the radiation and absorption lines coincide for all practical purposes.

Chu and Hogg [333] measured the radiation absorption from a gas laser with wavelengths 3.39 μ at a distance of 2.9 km under natural conditions. For the attenuation coefficient they found the value 5.5 ± 0.5 db/km, which agrees well with the data of Edwards and Burch [332] and our measurement data in the cell, but differs from our measurement results on the proving grounds. In fact, we note that in a new series of measurements which we made we again obtained absorption coefficients which were 1.5 - 3 times as large as in article [332, 333] and our measurements in the cell. The reasons for the discrepancies have so far not been explained.

Absorption from a gas helium-neon laser with wavelength 1.15 μ was measured by Long and Lewis [334]. The values of the absorption coefficient obtained in article [334] and in our measurements are in satisfactory agreement.

McCubbin and Darone [335], using a laser based on a CO_2 and nitrogen mixture, measured the absorption in the gas mixture at various pressures of the absorbing and extraneous gases in several lines in the CO_2 10.4 μ band. Using the measurement results the intensities of halfwidths of the lines were determined. Analogous measurements were made in articles [795 - 797].

Long and McCoy [336] measured the absorption from a laser based on a CO_2 mixture with nitrogen in a long cell. The radiation was generated on the line of the P branch with the rotation quantum number j = 20. At a CO_2 pressure of 0.25 mm Hg and a nitrogen pressure of 760 mm Hg, which corresponds to the conditions in the earth's layer of atmosphere, the authors of [336] found for the center of the radiation line an absorption coefficient equal to 0.125 db/km. It should be noted that the radiation generated from a CO_2 and N_2 mixture can appear in various lines. For example, in article [337] the positions of 17 lines in the band $(01^11) \rightarrow (11^10)$ were measured in the interval from 897.00 to 911.33 cm^{-1}, which gave laser radiation. In the interval 9 - 11 μ more than 100 lines generated by CO_2 and N_2O molecules were detected [805]. Taking into consideration that the line intensities in the CO_2 absorption spectrum vary as the rotation quantum number varies, we should expect various values of the absorption coefficients for generators in which the radiation takes place in different lines.

Thus, when we speak about the laser radiation absorption coefficient, we must know with high accuracy not only the positions of the atmospheric gas absorption lines but also the positions of the laser radiation lines. We emphasize once more that we can only speak meaningfully about laser radiation absorption when the halfwidth of the radiation lines is much smaller than the halfwidths of the absorption lines. We can assume that this condition is satisfied with sufficient accuracy for all practical purposes in the case of gas lasers. If the aforementioned condition is not satisfied, the Buger law cannot be applied to describing the laser radiation absorption. In this case we must determine the absorption function for selective radiation sources.

4. Absorption of Visible and Infrared Waves in the Nonhomogeneous Atmosphere

1. Spectral Transmission (Absorption). Transmission (Absorption Function)

The relation for the change in radiation intensity in the absorbing medium written in differential form is (see Chap. 3):

$$dI_\nu = -I_\nu k(\nu)\rho(l)dl, \tag{4.1}$$

where I_ν is the radiation intensity at frequency ν, $k(\nu)$ is the absorption coefficient, ρ is the density of the absorbing gas, and dl is an element of the beam path in the absorbing medium.

If the absorption coefficient is a function of the points of the beam trace, we say that the radiation is propagated in a nonhomogeneous medium. The reason why the atmosphere is nonhomogeneous in the sense mentioned above is rather obvious: the halfwidths and intensity of lines which determine the quantity $k(\nu)$ depend on the pressure and the temperature, the latter (see Chap. 1) vary considerably with the altitude and depend on the geographical coordinates of the point under consideration. Therefore, the absorption coefficient is a function of the point of the trace of the beam when it is propagated in slanted directions in the atmosphere or in the case of horizontal propagation when it is propagated over a distance for which the curvature of the earth is considerable.

Integrating equation (4.1) we obtain an expression for the spectral transmission

$$F(\nu) = \frac{I_\nu}{I_{0\nu}} = \exp\left(-\int_{(l)} \rho(l)\, k(\nu, l)\, dl\right), \tag{4.2}$$

where $I_{0\nu}$ is the radiation intensity at frequency ν at the beginning of the path. The exponent contains a curvilinear integral of the first kind, calculated over the points of the beam path. Strictly speaking, the integration can be carried out over the actual trajectory of the beam, taking into account refraction. However, usually the refractive phenomenon is not taken into account when spectral transmission is determined.

The spectral absorption $A(\nu)$ as in the case of the homogeneous atmosphere is determined from the simple relation

$$A(\nu) = 1 - T(\nu), \tag{4.3}$$

The transmission function F and the absorption H for a nonhomogeneous path in the spectral interval i are written, by definition, as follows:

$$F = \frac{1}{\nu_2 - \nu_1} \int_{\nu_1}^{\nu_2} \exp\left[- \int_{(l)} \rho(l)\, k(\nu, l)\, dl \right] d\nu, \tag{4.4}$$

$$H = 1 - F. \tag{4.5}$$

We recall that expressions (4.4) and (4.5) hold for the case when the spectral radiation density of the source is constant in the interval $\Delta\nu$. The function F is the ratio of the radiation which passes through a given nonhomogeneous layer of the atmosphere to the radiation incident on the layer in a given spectral interval $\Delta\nu$. The function H is defined analogously.

2. Direct Calculation Of Spectral Transmission And Transmission Functions

As can be seen from (4.2), to calculate directly $F(\nu)$ we must know the functions $\rho(l)$ and $k(\nu, l)$. The distribution of the concentration of the absorbing gases in the atmosphere is more or less known at the present time (see Chap. 1). At any rate, the function ν can be specified at least as the mean vertical statistical profile for the concentration of a particular gas.

The absorption coefficient for radiation with frequency ν is the sum of the coefficients of the individual spectral lines $k(\nu, l) = \sum_i S_i(l) b_i(\nu, l)$, where S_i and b_i are the total intensity and the contour of the line. The sum in the last expression can only be summed numerically. The exponent in (4.2) is now equal to $\sum_i \int_{(l)} \rho(l)\, S_i(l)\, b_i(\nu, l)\, dl$, i.e., the terms of

the series are different functions of the frequency than in the case of a homogeneous atmosphere and depend on the form of the distribution of meteorological elements. This means that in every concrete case the sum under consideration must be recalculated. Moreover, the integrals in the last relation, as a rule, are not expressed in terms of elementary functions.

If we assume the validity of the dispersion contour for the spectral lines, then

$$k(\nu, l) = \sum_i \frac{S_i[T(l)]}{\pi} \frac{\gamma_i[T(l), P(l)]}{(\nu-\nu_{0i})^2 + \gamma_i^2[T(l), P(l)]}, \qquad (4.6)$$

where T(1) and P(1) are the temperature and effective pressure at the point 1.

Thus, to calculate directly the spectral transmission (absorption) in the nonhomogeneous atmosphere according to formulas (4.2) and (4.6), we must have the following data: 1) the distribution of the concentration of the absorbing gases and the temperature and the distribution of the effective pressure along the path of the beam, 2) the position of the ν_{0i} lines which contribute to the radiation absorption at frequency ν, 3) the intensities and halfwidths of these lines for the corresponding values of the temperature and effective pressure. It should be emphasized that to calculate $F(\nu)$ exactly we must have data about the line parameters which must be determined with exceptionally high accuracy (see para. 13, Chap. 3). This applies, in particular, to spectral transmission calculations in the central region of the lines.

Only recently is there some hope that the spectral transmission data can be obtained by calculating directly this quantity. This kind of calculation has been carried on in our laboratory for a limited number of wavelengths, on the basis of the data for the line parameters of water vapor, obtained using the method described in paragraph 5, Chapter 3. The problem of calculating directly the absorption functions for the nonhomogeneous atmosphere is even more complex.

To the difficulties described in Chapter 3 of calculating the absorption functions which are related to evaluating the integral over a certain frequency interval, we must now add the requirement that the integral in the exponent must be evaluated. It is easily seen that this complicates the

problem considerably, since integration with respect to ν and l cannot be interchanged. With the exception of some special cases for the distribution of meteorological elements and the absorption spectra which are not of particular interest, (4.4) can only be evaluated numerically. However, the large number of computations and the need to take into account every special case and the abundance of parameters make this approach very unwieldy. At the present time a number of papers have been published in which the absorption functions were obtained for slanted directions in the atmosphere on the basis of a direct calculation which takes into account the absorption in each line.

Kyle, D. Murcray, F. Murcray and Williams [79] calculated the absorption functions in the bands 4.3 μ (the interval 2235 - 2415 cm^{-1}). In the beginning the absorption spectrum was calculated with a very small step. In the spectral region described, the calculation was made for 1800 points. Then the relation between the spectral transmission and the wavelengths which was obtained was multiplied by the spectrometer apparatus function, which was used in the measurement [79]. The positions and the intensities of the CO_2 lines were calculated without subsequently taking into account the interaction between the vibration and rotation movements of the molecule. The half-width was assumed the same for all lines and equal to 0.066 cm^{-1} under standard conditions. The CO_2 concentration was taken to be equal to 0.033% of the volume at all altitudes. In spite of the approximate character of the calculation, the results agreed sufficiently well with the experiment. This fact shows, as we already have pointed out, that the accuracy requirements for determining the line parameters when the absorption functions are calculated are not as high as those when the spectral absorption is calculated.

An analogous calculation for the CO_2 15.0 μ band was made by Drayson [62] who took into account more than 2000 lines in the wavelength range 12 - 18 μ. As we have already mentioned in Chapter 3, the author of [62] used a mixed Lorentz-Doppler line contour for pressures below 100 mb. For pressures above 100 mb the dispersion contour was used. The atmosphere was broken up into 34 layers, so that within each layer the temperature varied only by several degrees. The calculation was made for 6 zenith angles. The average data for the spectral intervals with widths 5 cm^{-1} were given for various layers of the atmosphere.

Calfee and Gates [338] calculated the completely resolved water vapor absorption spectrum in the region 3848 - 3860 cm^{-1}.

Other gases do not have absorption lines in this region. The calculation procedure, as in [62], presupposes that the atmosphere is broken up into layers. For altitudes above 13.7 km (tropopause) 10 layers were selected. The data obtained were compared with the corresponding measurement results after transformation using the apparatus function of the spectrometer. The comparison of the calculated and experimental data enabled the authors to determine the vertical humidity profiles for a large number of cases. The initial data for the halfwidths and intensities of the absorption lines were obtained without subsequently taking into account the interaction between the vibration and rotation movements of the H_2O molecule. The position of the line centers were taken from the experiment.

In all articles considered [79, 62, 338], generally speaking, the absorption functions were determined on the basis of spectral transmission data obtained for many wavelengths. The calculations which included data about the line parameters, did not give sufficiently accurate values for the actual spectral transmission for the corresponding concrete wavelengths. Nevertheless, the values of the absorption functions obtained in this manner can satisfactorily describe the true absorption picture in finite spectral intervals. This is due to the fact that when the absorption functions are calculated, it is not important whether the exact position of the lines is known. However, it is important that the given lines lie in the interval $\Delta\nu$ under consideration. In addition to this not taking into account the interaction between the vibration and rotation movements of the molecule is reflected mostly in the parameters of weak lines, which cannot contribute much to the value of the absorption function.

3. Approximate Calculation Of The Absorption Function H

The basic idea of the approximate methods used to calculate the absorption function H boils down to reducing this problem to the problem of finding the absorption function for the case when the concentrations of the absorbing gas, the pressure, and the temperature are constant along the path of the beam. In the process, usually either the effective absorbing mass method or the Curtis-Godson approximation is used.

In the first case the effective absorbing mass is selected in such a way that the relation

$$H = A(P_0, \omega^*), \qquad (4.7)$$

is satisfied, where P_0 is the pressure at the earth's surface, ω^* is the effective absorbing mass.

Usually the expression

$$\omega^* = \int_{l_1}^{l_2} \rho(l) \left[\frac{P(l)}{P_0}\right]^{(n)} dl. \tag{4.8}$$

is used for ω^*. The magnitude of the parameter n is selected.

Sometimes the formula

$$\omega^* = \int_{l_1}^{l_2} \rho(l) \frac{P(l)}{P_0} \left(\frac{T_0}{T(l)}\right)^{1/2} dl. \tag{4.9}$$

is used for ω^*.

In formulas (4.8), (4.9) $\rho(1)$ is the density of the absorbing gas, P(1) and T(1) are the pressure and temperature at the point 1, P_0, T_0 are the pressure and temperature near the surface of the earth.

According to the Curtis-Godson approximation or the mean-weighted pressure method, the absorption function H is written as

$$H = A(\overline{P}, \omega), \tag{4.10}$$

$$\overline{P} = \frac{\int_{l_1}^{l_2} \rho(l) P(l)\, dl}{\int_{l_1}^{l_2} \rho(l)\, dl}, \tag{4.11}$$

$$\omega = \int_{l_1}^{l_2} \rho(l)\, dl. \tag{4.12}$$

The meanweighted pressure method was proposed independently by Curtis in 1952 and by Godson in 1953 [3]. Since then a rather large number of absorption functions of atmospheric gases have been calculated for slanted directions in the atmosphere. For water vapor and carbon dioxide absorption bands, the method gives fairly good approximate results not only for weak and strong lines, for which formulas (4.10) - (4.12) were obtained, but also for intermediate values of the parameter x [see formula (3.52)]. A discussion of the applicability of the mean-weighted pressure method for various values of the parameter x has been given in our paper [339]. In the case of the ozone 9.6 μ absorption band the Curtis-Godson approximation does not give the mean values of x with sufficient accuracy.

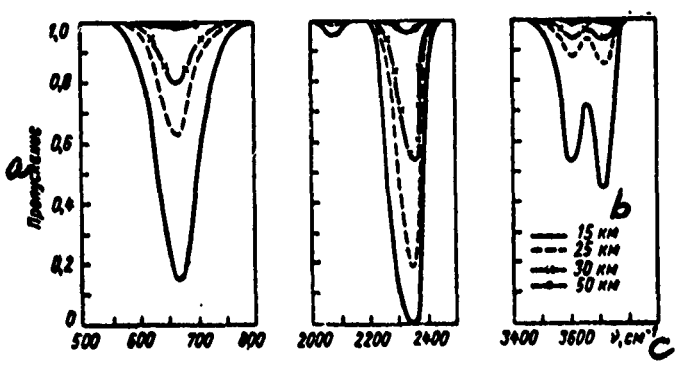

Fig. 4.1. Transmission in the CO_2 bands 15.0, 4.3 and 2.7 μ for a vertical layer of the atmosphere above 15, 25, 30 and 50 km according to the data of Plass [342] (the calculation was carried out averaging over the spectrum in intervals with widths 50 cm^{-1}).

Key: a. transmission
b. km
c. cm^{-1}

Plass [340] obtained a series of formulas for calculating the absorption functions H from the well-known data for the absorption function for the homogeneous atmosphere. The author of [340] obtained exact expressions for the function H for the case when the weak and strong lines were closed, when the concentration of the absorbing gas and the temperature did not vary over the path of the beam. Analogous expressions were

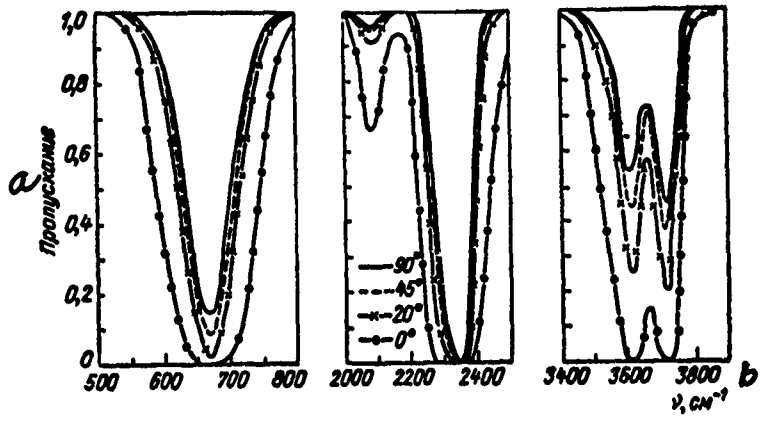

Fig. 4.2. Transmission in the CO_2 bands 15.0, 4.3 and 2.7 μ for layers of the atmosphere pierced by a beam at an altitude of 15 km at an angle to the local horizon $\theta = 0^o$, 20^o, 45^o, 90^o according to the data of Plass [342] (the calculations were carried out averaging over the spectrum in the intervals with widths 50 cm^{-1})

Key: a. transmission
b. cm^{-1}

obtained for the case when the pressure, concentration and temperatures varied along the path of the beam. In addition to this a procedure was developed in [340] for calculating approximately the function H. The initial data for the absorption functions for the homogeneous atmosphere which are needed to determine the function H can be represented in the form of theoretical or empirical relations or in tabular form.

In articles [341, 342] Plass carried out, on the basis of the formulas and tabular data for the absorption functions for the homogeneous atmosphere obtained in [340], extensive calculations of the absorption function H in the narrow regions of the spectrum for the fundamental vibration-rotation water vapor and carbon dioxide bands, taking into account variations in the pressure, the concentration of the absorbing gas and the temperature with the altitude.

Some of the results of calculating the H functions obtained by Plass are given in Figs. 4.1 - 4.5.

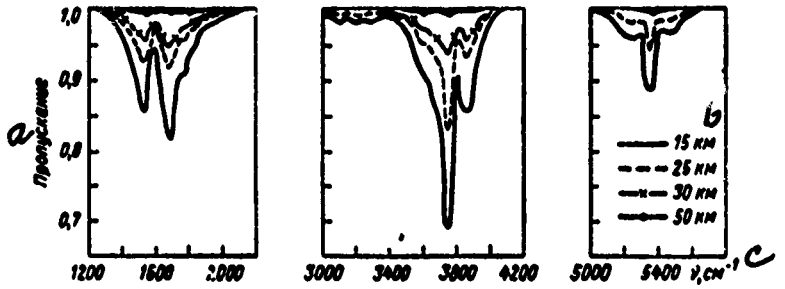

Fig. 4.3. Transmission in the H_2O band 6.3, 2.7 and 1.87 μ for a vertical layer of the atmosphere above 15, 25, 30 and 50 km according to the data of Plass [342] (the calculations were made averaging over the spectrum in intervals with widths 50 cm^{-1} for the humid stratosphere model.

Key: a. transmission
b. km
c. cm^{-1}

The calculation of the absorption function H in the spectral region with width 0.1 μ for water vapor and carbon dioxide were carried out in our laboratory for a model of the atmosphere which takes into account the variation in the pressure, temperature and H_2O and CO_2 concentration with the altitude. The calculations included all fundamental H_2O and CO_2 vibration-rotation bands. The values of H were obtained with a 1 km step for the lower 30-km layer of the atmosphere. The corresponding results are discussed in detail in the author's monograph [1]. The absorption function of entire vibration-rotation water vapor bands were calculated for: 6.3, 3.2, 2.7, 1.87, 1.38, 1.1, 0.94 μ, and for carbon dioxide: 15.0, 5.2, 4.8, 4.3, 2.7, 2.0, 1.6, 1.4 μ for various directions in the lower 8-km layer of the atmosphere in our article [59]. References to other work can be found in [1] and [342].

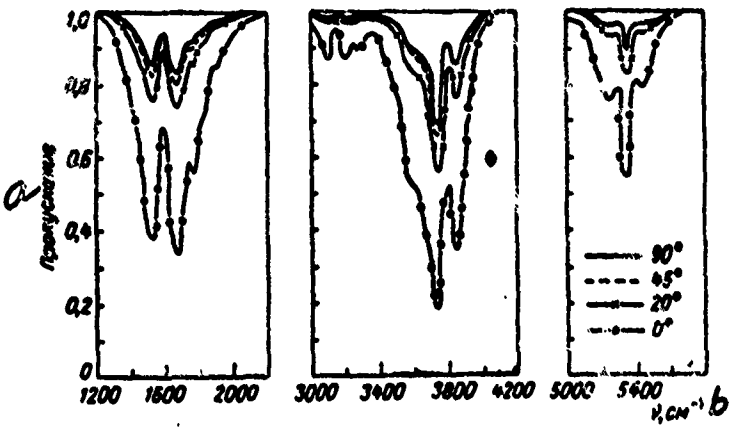

Fig. 4.4. Transmission in the H_2O bands 6.3, 2.7 and 1.87 μ for layers of the atmosphere pierced by a beam at an altitude of 15 km at an angle to the local horizon $\theta = 0^\circ$, 20°, 45°, 19° according to the data of Plass [343] for the humid stratosphere with averaging over the spectrum through 50 cm^{-1}

Key: a. transmission
b. cm^{-1}

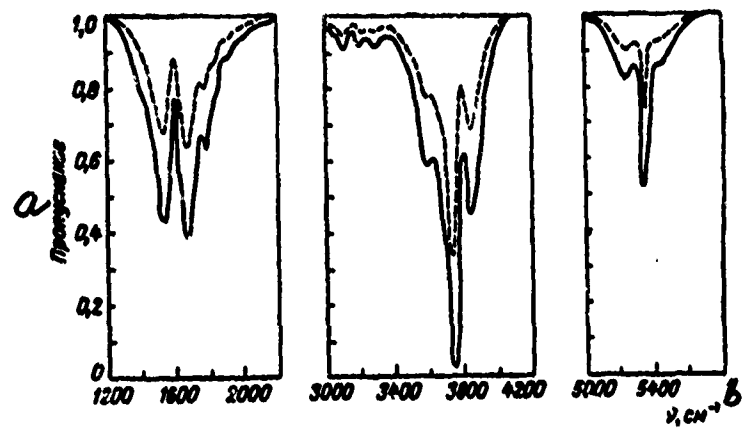

Fig. 4.5. Transmission in the H_2O bands 6.3, 2.7 and 1.87 μ calculated by Plass [343] for a dry and humid model of the stratosphere, for a layer of the atmosphere pierced by the beam propagated in the horizontal direction from a point at an altitude of 30 km: ——— humid stratosphere; – – – – dry stratosphere

Key: a. transmission
b. cm^{-1}

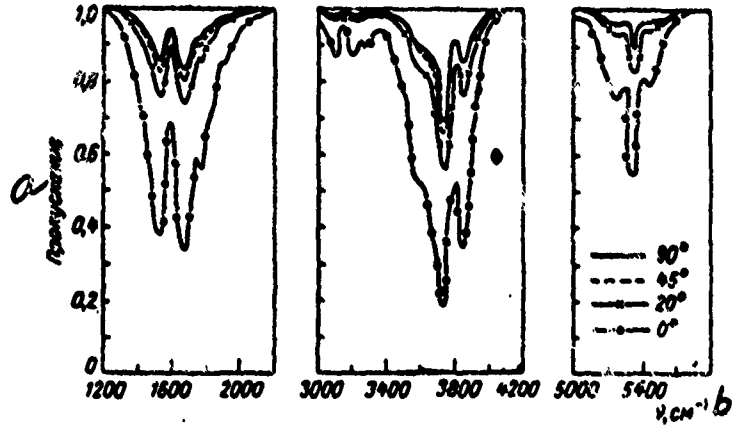

Fig. 4.4. Transmission in the H_2O bands 6.3, 2.7 and 1.87 μ for layers of the atmosphere pierced by a beam at an altitude of 15 km at an angle to the local horizon $\theta = 0^\circ$, 20°, 45°, 19° according to the data of Plass [343] for the humid stratosphere with averaging over the spectrum through 50 cm^{-1}

Key: a. transmission
b. cm^{-1}

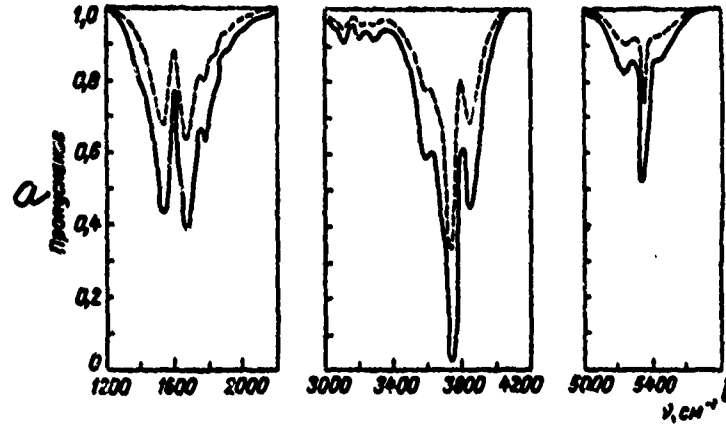

Fig. 4.5. Transmission in the H_2O bands 6.3, 2.7 and 1.87 μ calculated by Plass [343] for a dry and humid model of the stratosphere, for a layer of the atmosphere pierced by the beam propagated in the horizontal direction from a point at an altitude of 30 km: ——— humid stratosphere; – – – – dry stratosphere

Key: a. transmission
b. cm^{-1}

4. Approximate Methods for Taking Into Account the Temperature when the Function H is Calculated

Often when the function H is calculated its dependence on the temperature is ignored, because the temperature varies with altitude within limits which are not very wide. Nevertheless, in many cases the dependence of the function H on the temperature must be taken into account. Below we give an approximate method for taking into account this relationship, which can be conveniently applied to the vibration-rotation spectra of steam vapor and carbon dioxide.

The dependence of the function H on the temperature is defined in terms of the relation between the halfwidths and intensities of the absorptions lines and the temperature. The latter is expressed approximately by the following formulas:

$$\gamma_l(T) = \gamma_{0l}\frac{P(l)}{P_0}\left(\frac{T_0}{T(l)}\right)^{1/2} = \gamma_{0l}\frac{T_0^{1/2}}{P_0}\beta(l), \tag{4.13}$$

$$S_l(T) = S_l(T_0)\left[\frac{T_0}{T(l)}\right]^{3/2}\times$$
$$\times\exp\left[-E_l(T(l)-T_0)(kT(l)T_0)^{-1}\right], \tag{4.14}$$

where γ_{0i} is the halfwidth i of the line under standard conditions, $P = P_0$, $T = T_0$, $S_i(T_0)$ are the intensities i of the line at standard temperature, E_i is the energy of the lower level with which the transition begins, which determines the line $\beta(l) = \frac{P(l)}{[T(l)]^{1/2}}$.

Henceforth we will consider the quantity γ_{0i} to be independent of the temperature.

The quantity E_i for the lines of the vibration-rotation spectra can be written approximately as

$$E_l = E_{l0} + E_{lR}, \tag{4.15}$$

where E_{iv} and E_{iR} are the vibration and rotation energy of the lower state i of the line. Taking into account that $E_{iv} \gg E_{iR}$ (see Chap. 2) we may set

$$E_i = E_{iv}. \tag{4.16}$$

Within the limits of a single vibration-rotation band, the quantity E_{iv} is independent of the rotation quantum number. Moreover, for the fundamental vibration-rotation band of water vapor and carbon dioxide, we can take for the quantity E_{iv} the energy of the fundamental vibration state. The analysis of the fundamental vibration-rotation bands of these gases shows that each of these consists of lines which refer to different vibration transitions. However, the majority of such overlapping transitions have the lower state as the fundamental state, and most importantly, their intensity exceeds considerably the intensity of transitions from a nonfundamental state. Therefore, when the absorption functions are calculated the rotation lines of these transitions can be ignored. Also, E_v could be replaced by the mean $\overline{E_v} = \Sigma E_{vk}\tau_k$, where E_{vk} is the vibration energy of the lower state k of the transitions (which forms a given band) and τ_k is its relative intensity ($\Sigma\tau_k = 1$). However, estimates have shown that $\overline{E}_v$ has a value which is close to the energy value of the fundamental state. Consequently, we can write

$$\left.\begin{aligned} S_i(T) &= S_i(T_0)\varphi, \\ \varphi &= (T_0/T)^{3/2}\exp\left(-C(T-T_0)(TT_0)^{-1}\right), \end{aligned}\right\} \tag{4.17}$$

where φ is independent of i, C is a certain quantity which corresponds to the H_2O and CO_2 spectral lines. We emphasize that the approximation considered (the independence of φ of i) does not hold for the lines of the rotation spectrum, since it is based on the inequality $E_{iv} \gg E_{iR}$. In the approximation which was described

$$k_\nu = \sum S_i(T_0)\, b_i(\nu, \beta), \tag{4.18}$$

$$A = A(\omega', \beta), \quad \omega' = \omega\varphi, \tag{4.19}$$

where

$$\beta = P\sqrt{\frac{T_1}{T_2}}.$$

Therefore, the procedure developed in [1, 339] for calculating H proceeds without any changes after P has been replaced by β and ρ' by ρφ. The final result can now be written as follows:

$$\left.\begin{aligned} H &= A(m', \bar{\beta}), \\ m' &= \int \varphi(l)\rho(l)\,dl, \\ \bar{\beta} &= \frac{\int \beta(l)\varphi(l)\rho(l)\,dl}{m'}. \end{aligned}\right\} \qquad (4.20)$$

5. Approximate Determination of the Spectral Transmission of The Nonhomogeneous Atmosphere

Formula (4.2) makes it possible to calculate in the general case the spectral transparence of a nonhomogeneous path. However, the difficulties which were described above force us to seek approximate methods.

The meanweighted pressure method can be extended to the case considered, and we can find the final formula for F(ν) in the following form:

$$F(\nu) = I_\nu / I_{0\nu} = \exp[-\omega k(\nu, \bar{P})], \qquad (4.21)$$

where ω and P are determined from the relations (4.11) and (4.12).

If we take into account the temperature variation along the path of the beam, then we have for the vibration-rotation spectrum

$$F(\nu) = \exp(-m' k(\nu, \bar{\beta})) \qquad (4.22)$$

and when m' and $\bar{\beta}$ are calculated we can use relations (4.20).

It should be noted that now formulas (4.21) and (4.22) are evidently grosser approximations than the analogous results for the absorption functions.

It can be easily shown that the relations considered are asymptotically valid for spectral regions in which the absorption is caused by the tails of the lines. The results (4.10) - (4.12) and (4.20) follow automatically from (4.21) and (4.22), but this, of course, does not mean that the converse proposition is valid.

However, one can easily give cases which are not covered by the procedure developed, for example: 1) absorption in the center of the line, 2) absorption at frequency ν caused by various lines with different low vibration energy levels.

At the present time no numerical material is available which can be used to determine the accuracy of the approximate expressions obtained in paragraphs 4, 5.

6. Calculation Of the Absorption Function Taking Into Account The Curvature Of The Earth

In many cases it is necessary to have the absorption functions for the nonhomogeneous atmosphere, which take into account the curvature of the earth. We will consider the corresponding exact formulas and also an approximate method for solving this problem. We will first write down several geometric relations which will be used later.

Suppose that we are given the geographic coordinates of the radiation and receiving source and their altitudes above the surface of the earth. All quantities which refer to this source will have the index "1" (point 1) and those which refer to the receiver the index "2' (point 2).

We introduce a Cartesian coordinate system, the origin of which coincides with the center of the earth, the z axis is oriented through the North Pole, the x axis through Greenwich, and the x,y,z axes form a right-handed system. In this system we define in the usual manner the polar coordinates r, θ, φ. The Cartesian and polar coordinates are related, as usual,

$$\begin{gathered} x = r\sin\theta\cos\varphi;\ y = r\sin\theta\sin\varphi;\ z = r\cos\theta; \\ r = \sqrt{x^2+y^2+z^2};\ \cos\theta = z/r;\ 0 < \theta < \pi; \\ \sin\varphi = (y/r)\sin\theta;\ \cos\varphi = (x/r)\sin\theta. \end{gathered} \tag{4.23}$$

The altitude of the point above the earth's surface will be denoted by h. It can be easily shown that

$$\left.\begin{array}{l}\text{if } \xi \text{ is the longitude east of the point } \varphi = \xi,\\ \text{if } \xi \text{ is a given longitude of the point } \varphi = 2\pi - \xi,\\ \text{if } \eta \text{ is the northern latitude of the point } \theta = \frac{\pi}{2} - \eta,\\ \text{if } \eta \text{ is the southern latitude of the point } \theta = \frac{\pi}{2} + \eta,\end{array}\right\} \qquad (4.24)$$

$$r = R + h$$

where R is the radius of the earth.

(4.10) - (4.12) imply that to determine the function H we must evaluate integrals of the type

$$B = \int F(l)\,dl, \qquad (4.25)$$

where F(l) is a function of the points on the path of the beam and where the integration takes place over the path of the beam.

When the ω quantity is calculated, the function F coincides with the distribution for the concentration of the absorbing gas, and when $\bar{P}$ is calculated

$$F = \rho(l)\,P(l).$$

In general F depends on the geographical coordinates of the point and its altitude. Now we can easily construct the function $F(r, \theta, \varphi)$ from formula (4.24). We will assume that this procedure was carried out. Then r, θ, and φ will be functions of the points of the path l. Using the usual rules for curvilinear integrals of the first kind, we can obtain the following exact formulas which enable us to calculate the function H:

$$B = \int_0^s F[r(l), \theta(l), \varphi(l)]\,dl, \qquad (4.26)$$

$$s = \sqrt{r_1^2 + r_2^2 - 2r_1 r_2 \cos\delta}, \qquad (4.27)$$

$$\cos\delta = \cos\theta_1\cos\theta_2 + \sin\theta_1\sin\theta_2\cos(\varphi_2 - \varphi_1), \tag{4.28}$$

$$r(l) = \left(r_1^2 + l^2 + 2l\frac{r_1 r_2\cos\delta - r_1^2}{s}\right)^{1/2}, \tag{4.29}$$

$$\cos\theta(l) = \frac{r_1\cos\theta_1 + l\cos\gamma}{r(l)}, \quad 0 < \theta < \pi, \tag{4.30}$$

$$\cos\varphi(l) = \frac{r_1\sin\theta_1\sin\varphi + l\cos\beta}{r(l)\sin\theta(l)}, \tag{4.31}$$

$$\sin\varphi(l) = \frac{r_1\sin\theta_1\sin\varphi_1 + l\cos\alpha}{r(l)\sin\theta(l)}, \tag{4.32}$$

$$\cos\alpha = \frac{r_2\sin\theta_2\cos\varphi_2 - r_1\sin\theta_1\cos\varphi_1}{s}, \tag{4.33}$$

$$\cos\beta = \frac{r_2\sin\theta_2\sin\varphi_2 - r_1\sin\theta_1\sin\varphi_1}{s}, \tag{4.34}$$

$$\cos\gamma = \frac{r_2\cos\theta_2 - r_1\cos\theta_1}{s}. \tag{4.35}$$

The evaluation of the integrals B using the exact formulas (4.26) - (4.35) presupposes a great amount of information about the meteorological situation in various geographic regions.

We will now consider an approximate method which can be used to evaluate the integrals over the path of the beam which is adequate for most practical applications.

For definiteness we will assume that the radiation detector lies above the source, which, of course, has no effect on the generality of the result, since the integrals under consideration are invariant with respect to interchanged limits of integration.

We denote by x_3, y_3, z_3 the coordinates of the point (point 3) which lies on the line passing through the points at which the detector and source lie, and which is at a minimum distance from the origin of the coordinate system. Then

$$\begin{aligned} x_3 &= x_2 + t^*(x_1 - x_2), \\ y_3 &= y_2 + t^*(y_1 - y_2), \\ z_3 &= z_2 + t^*(z_1 - z_2), \\ t^* &= \frac{x_2(x_2 - x_1) + y_2(y_2 - y_1) + z_2(z_2 - z_1)}{(x_2 - x_1)^2 + (y_2 - y_1)^2 + (z_2 - z_1)^2}. \end{aligned} \tag{4.36}$$

The formula for t* can be also written in the form

$$t^* = \frac{r_2(r_2 - r_1\cos\delta)}{r_1^2 + r_2^2 - 2r_1r_2\cos\delta}. \tag{4.37}$$

The last formula implies that $t^* > 0$.

Depending on the value of t* there are two possible cases for the position of the points 1, 2 and 3.

$$\left.\begin{array}{ll} 1) & 0 \leqslant t^* \leqslant 1 \text{ point 3 lies between 1 and 2,} \\ 2) & t^* > 1 \quad \text{point 1 lies between 2 and 3.} \end{array}\right\} \tag{4.38}$$

We will now use two facts: 1) the vertical profile of the meteorological characteristics is much more variable than the horizontal profile, 2) for infrared radiation absorption the most important part of the atmosphere is the part where the concentration of the absorption component is a maximum. Keeping in mind these points, we can replace in the exact formulas (4.26) - (4.35) $\theta(1)$ and $\varphi(1)$ by the coordinates of the points of the path, which is closest to the surface of the earth. These will be the coordinates of point 3, if the first variant in (4.38) holds, and the coordinate of point 1 if the second variant in (4.38) holds. Further, as (4.10) - (4.12) and the formulas which describe the H_2O and CO_2 pressure and concentration distributions in the troposphere imply the function F has the form $\exp(-\alpha h)$, where α is a constant. (4.26) is integrated from the

point which lies at the distance r' from the coordinate origin described above to the point which lies at a distance r'' from this origin with the angle σ subtended by these two directions. The integral defined in this manner will be denoted by $B(\alpha, \sigma, h', h'')$, where h' and h'' are the altitudes of the points r' and r'' above the surface of the earth. Assuming r' and r'' sufficiently small compared to R, we can obtain for $B(\alpha, \sigma, h', h'')$

$$B(\alpha, \sigma, h', h'') = \\ = e^{-\alpha h'} \sqrt{\frac{\pi R}{2\alpha}} \frac{1}{\sin \psi} e^{\xi_0^2} [\Phi(\xi^0) - \Phi(\xi_0)]. \tag{4.39}$$

Here Φ is the probability integral defined by equation

$$\Phi(z) = \frac{2}{\sqrt{\pi}} \int_0^z e^{-z'^2} dz', \tag{4.40}$$

$$\xi^0 = \xi + \xi_0, \quad \xi = l \sqrt{\frac{\alpha}{2R}} \sin \psi, \\ \xi_0 = \left(\frac{\alpha R}{2}\right)^{1/2} \operatorname{ctg} \psi, \\ \cos \psi = \frac{r'' \cos \sigma - r'}{l}, \quad \sin \psi = \sqrt{1 - \cos^2 \psi}. \tag{4.41}$$

The angle σ is easily determined from the relation

$$\sigma = \sigma'' - \sigma', \quad \cos \sigma' = \frac{r_3}{R + h'}, \quad \cos \sigma'' = \frac{r_3}{R + h''}.$$

The geometric meaning of ψ is as follows: it is the angle between the direction r' and the straight line which connects the points r' and r''. Special cases of equation (4.39) can be found in monograph [1].

As the material in chapter 1 implies, the quantity α which was introduced there, is different, generally speaking, for various altitudes, when we consider the distribution of the concentration of any absorbing gas with the altitude in the troposphere and stratosphere. In such a case the integration path must be broken up into sections in which α has a fixed value.

7. Experimental Study of Absorption Functions H

It is practically impossible to have under laboratory conditions a nonhomogeneous atmosphere with continuous variation in pressure, temperature and absorbing gas concentrations. Therefore, the absorption functions H are measured under natural conditions using the sun as the radiation source.

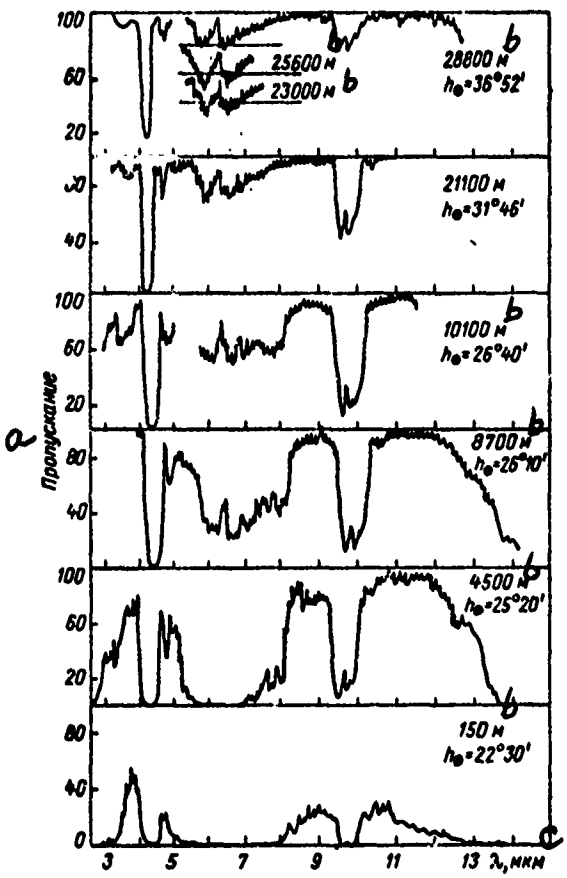

Fig. 4.6. Transmission in various layers of the atmosphere from various levels according to the data of K. Ya. Kondrat'ev, et al., [344] in the 3 - 13 μ region (absorption in the band 6.3 μ above 20 km the authors [344] attribute to the humidity contained in the spectrometer)

Key: a. transmission
b. m
c. μ

At the present time a considerable number of measurements of the quantity H have been made from the earth and from various altitudes with various spectral resolutions in all fundamental vibration-rotation atmospheric gas rotation bands (Fig. 4.6 - 4.12). The H_2O absorption bands which were studied in greatest detail are: 6.3, 3.2, 2.7, 1.87, 1.38, 1.1 μ; the CO_2 bands are 4.3, 2.7 μ and the O_3 band is 9.6 μ. The measurements from various altitudes are carried out using apparatus mounted on airplanes or balloons. In the first case altitudes approximately up to 20 km are covered, in the second case altitudes up to 30 km are covered.

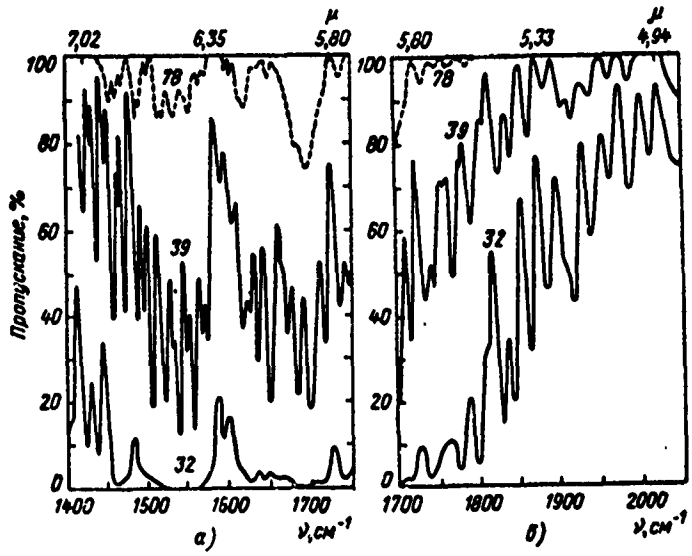

Fig. 4.7. Transmission in various layers of the atmosphere from various levels in the spectral region 1400 - 2050 cm^{-1} according to the data in article [345]

Curve 32: pressure P = 453 mb, altitude z = 6.3 km, sec θ = 2.75, airmass w = 1.23, settled CO_2 layer u = 2.95 atm.cm, curve 39: P = 270 mb, z = 9.9 km, sec θ - 2.42, w = 0.646, u = 155 atm.cm, curve 78: P = 23.8 mb, z = 25.5 km, sec θ = 1.517, w = 0.0356, u = 8.54 atm.cm)

In studies made under natural conditions pure solar radiation absorption in the atmosphere is not measured, but its attenuation due to scattering aerosol and molecular absorption.. To reduce the minimum effect of aerosol scattering, the measurements are made only on the clearest cloudless days.

With regard to molecular scattering, its effect can be taken into account whenever necessary, since the corresponding coefficients have been determined with sufficient accuracy for a wide range of wavelengths (see Chap. 6).

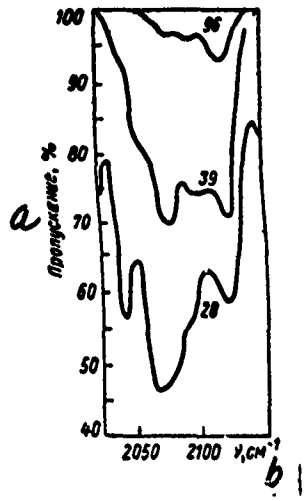

Fig. 4.8. Transmission in various layers of the atmosphere from various levels in the spectral region 2000 - 2150 cm^{-1} according to the data in article [345]

(Curve 28: pressure P = 557 mb, altitude z = 4.8 km, sec θ = 2.97, air mass w = 1.63, settled CO_2 layer u - 395 atm.cm, Curve 39: P = 370 mb, z = 9.9 km, sec θ = 2.42, w = 0.646, u = 155 atm.cm, Curve 96: P = 10.3 mb, z = 30.9 km sec θ = 1.321, w = 0.0135, u = 3.24 atm.cm).

Key: a. transmission
b. cm^{-1}

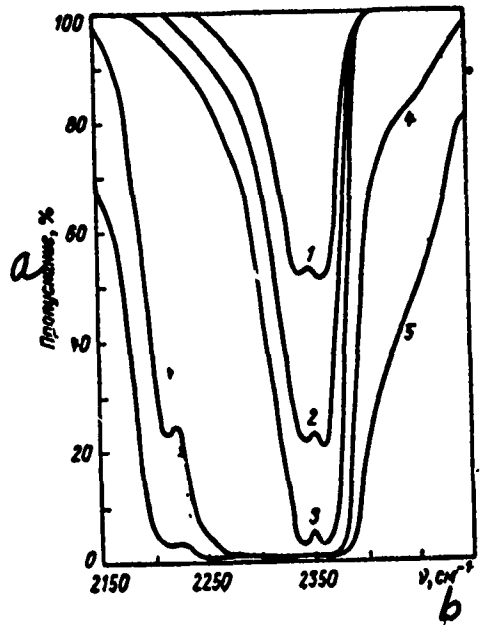

Fig. 4.9. Transmission in various layers of the atmosphere from various levels in the spectral region 2150 - 2500 cm^{-1} according to the data of article [345]

(Curve 1: pressure P = 10.3 mb, altitude z = 30.9 km, sec θ = 1.273, air mass w = 0.0130, settled CO_2 layer u = 3.12 atm.cm, Curve 2: P = 18.6 mb, z = 27.1 km, sec θ = 1.476, w = 0.0272, u = 6.53 atm.cm, Curve 3: P = 41.5 mb, z = 21.9 km, sec θ = 1.63, w = 0.0668, u = 16.0 atm.cm, Curve 4: P = 453 mb, z = 6.3 km, sec θ = 2.75, w = 1.23, u = 295 atm.cm, Curve 5: P = 764 mb, z = 2.3 km, sec θ = 3.45, w = 2.60, u = 624 atm.cm)

Key: a. transmission
b. cm^{-1}

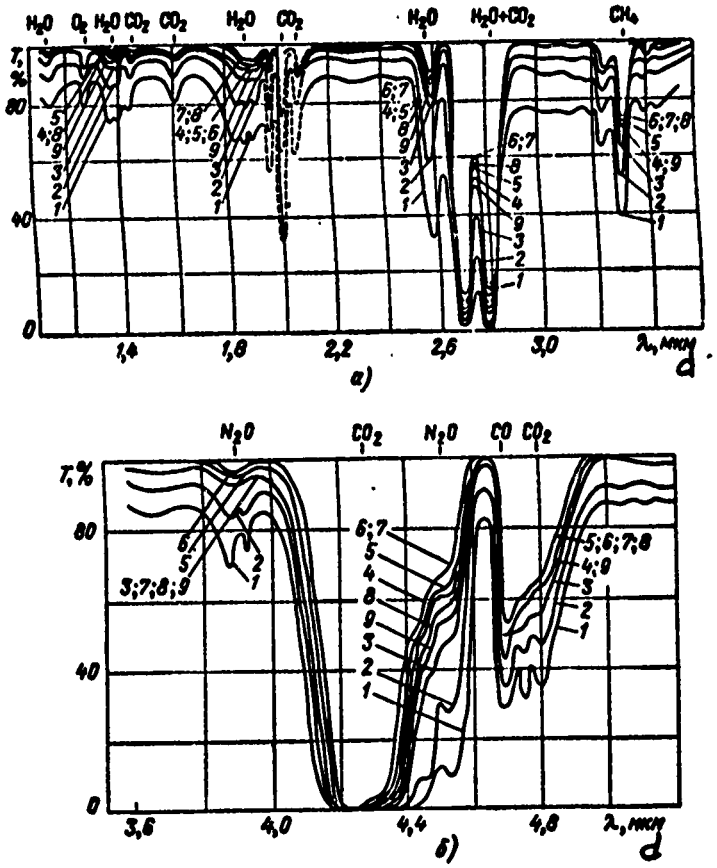

Fig. 4.10 Atmospheric transmission at various altitudes in the region 1 - 3, 5(a) and 3.5 - 5.5 (b) μ, when the position of the sun is low in the summer period according to the data of article [804]:

a — № кривой	b — Высота, км	c — Высота Солнца
1	12	1°57'
2	13	2°39'
3	14	3°24'
4	15	4°24'
5	15,6	4°54'
6	15	5°54'
7	14,6	7°06'
8	13,8	8°15'
9	12,8	91°8'

Key: a. Number of curve
b. Altitude, km
c. Altitude of sun
d. μ

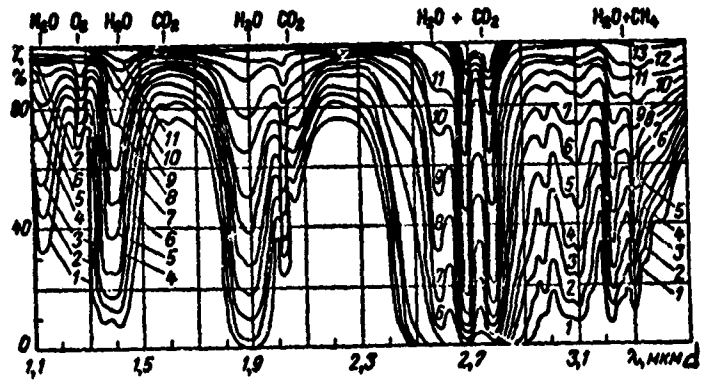

Fig. 4.11. Atmospheric transmission at various altitudes in the region 1 - 3.5 μ according to the data in article [804]

a. № кривой	b. Высота, км	c. Высота Солнца
1	0	20°10'
2	1,0	20°50'
3	2,3	21°20'
4	3,4	22°00'
5	4,4	22°40'
6	5,6	23°20'
7	6,8	24°00'
8	8,5	24°30'
9	9,8	25°10'
10	11,5	25°50'
11	12,5	26°30'
12	15,4	27°40'
13	17,6	28°20'
14	19,6	29°30'
15	22,1	30°40'
16	24,0	32°40'

Key: a. Number of curves
b. Altitude, km
c. Altitude of sun
d. μ

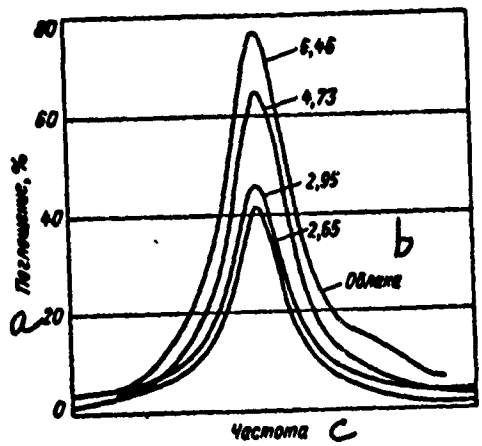

Fig. 4.12. Transmission in the entire layer of the atmosphere in the water vapor absorption line region with center near 6943.8 Å for various air masses according to the measurement data of Long [295], carried out on Dec. 26, 1965

Key: a. absoprtion, %
b. clouds
c. frequency

The most complete data for the functions H were obtained by the team of K. Ya. Kondrat'ev [253, 344, 807], B. S. Neporent and E. O. Fedorova [348, 808, 809, 877], Murcray [79, 345 - 347], Yates [349, 350], Houghton [351 - 353] and Cumming [354]. A series of results was also obtained in articles [355 - 357].

8. Laser Radiation Absorption in the Nonhomogeneous Atmosphere

The halfwidth of radiation lines of many lasers is smaller than the halfwidth of the atmospheric gas absorption lines. Therefore, to evaluate quantitatively the radiation absorption from lasers, we must have data about the spectral absorption for fixed frequencies in certain very narrow regions of the spectrum. Such data, generally speaking, can be calculated in those cases, when the positions of the centers, the intensities and the form of the line contours which contribute to the radiation absorption at the given frequencies are known with very high accuracy. In addition to this such calculation requires that data be available about the distribution of pressure, temperature and the concentration of the absorbing gases with the altitude.

In principle, a quantitative estimate of the laser radiation absorption can be obtained from measurements of the solar radiation spectrum in the earth's atmosphere. However, the spectral resolution of the instruments must be exceptionally high in order to ignore the distortions in the spectrum caused by the apparatus function of spectrometers. Moreover, the positions of the laser absorption and radiation lines must be known with an accuracy not less than 10^{-2} - 10^{-4}cm^{-1}, depending on the distance between the centers of the absorption and radiation lines (see para. 14, Chap. 3). Laser radiation absorption in a nonhomogeneous atmosphere can also be measured using a laser as the radiation source.

In paragraph 5, we considered the approximate methods which we proposed for calculating spectral absorption in the nonhomogeneous atmosphere, which reduces to the problem of finding the spectral absorption in the homogeneous atmosphere. It is assumed that the solution to the latter problem is known.

A number of useful formulas which can be used to evaluate the laser radiation absorption propagated in slanted directions in the atmosphere has been obtained by Plass [409]. In the case when the volume concentration of the absorbing gas can be considered to be constant at all altitudes and when the relation

between the line intensities, their halfwidths and temperature can be ignored, Plass obtained the following expression for the spectral transmission of monochromatic radiation at frequency ν in the slanted direction:

$$F(\nu)=\prod_i[(1+\xi_{0i}^2)/(1+\xi_{1i}^2)]^{\theta_i}, \tag{4.42}$$

where

$$\xi_{0i}=\gamma_{0i}(\nu-\nu_{0i})^{-1}, \tag{4.43}$$

$$\xi_{1i}=\gamma_{1i}(\nu-\nu_{0i})^{-1}, \tag{4.44}$$

$$\theta_i=\frac{S_i c P_{s_i}\sec\theta}{2\pi\gamma_{s_i}g}. \tag{4.45}$$

Here γ_{0i} and γ_{1i} are the halfwidths i of the line at the beginning and end of the slanted path, c is the volume concentration of the absorbing gas, P_{s_i} and γ_{ji} are the effective pressure and halfwidth of the line under standard conditions, θ is the angle between the radiation propagation direction and the vertical line, g is acceleration due to gravity, ν_{0i}, S_i are the center and intensity of the line i.

The case when the temperature and the concentration of the absorbing gas vary along the path of the beam has also been considered in article [409]. The product of the intensity of the line with the gas concentration c is written in the form

$$Sc=S_0c_0\gamma_0^{-m}\gamma^m. \tag{4.46}$$

Then for $F(\nu)$ the expression

$$F(\nu)=\exp\left\{-2\theta_0\gamma_0^{-m}\int_{\gamma_0}^{\gamma_1}\gamma^{m+1}[(\nu-\nu_0)^2+\gamma^2]^{-1}d\gamma\right\}, \tag{4.47}$$

is obtained, where

$$\vartheta_s = S_s c_s P_s \sec\theta / 2\pi\gamma_s g. \qquad (4.48)$$

S_s, c_s, γ_s, P_s are the values of S, c, γ and P under standard conditions, and m is a number which, generally speaking, is different for each line, depending on the altitude. For the water vapor line in the troposphere the value of m turned out to be approximately equal to 4. In this case we obtain from (4.48)

$$F(\nu) = \exp\left(\vartheta_s \xi_{s0}^{-4}\left\{\frac{1}{2}(\xi_{s1}^4 - \xi_{s0}^4) - (\xi_{s1}^2 - \xi_{s0}^2) + \right.\right.$$
$$\left.\left. + \ln[(1+\xi_{s1}^2)(1+\xi_{s0}^2)^{-1}]\right\}\right), \qquad (4.49)$$

where

$$\xi_{s0} = \gamma_s (\nu - \nu_0)^{-1}. \qquad (4.50)$$

Finally, Plass studied the case, when the center of the absorption line with a dispersion contour can be displaced by the pressure. In this case the absorption coefficient has the form:

$$k(\nu) = \frac{S}{\pi} \frac{\gamma}{(\nu - \nu_0 + A\gamma)^2 + \gamma^2}, \qquad (4.51)$$

where $A\gamma$ determines the shift of the line center and depends on the pressure, since the quantity γ depends on the pressure.

Using expression (4.51), we easily obtain the following formula for $F(\nu)$:

$$F(\nu) = \{[(1 + A\xi_{s0}^2) + \xi_s^2]/[(1 + A\xi_{s1}^2) + \xi_{s1}^2]\}^{\vartheta (1+A^2)^{-1}} \times$$
$$\times \exp[(1 + A^2)^{-1} \cdot 2\vartheta A\{\mathrm{tg}^{-1}[(1 + A^2)\xi_{s1} + A] - \qquad (4.52)$$
$$- \mathrm{tg}^{-1}[(1 + A^2)\xi_{s0} + A]\}],$$

where ν_0 is the position of the line center at a pressure equal to zero.

Formulas (4.51) and (4.52) are valid for atomic lines, the shift in which in the visible region of the spectrum has been detected experimentally. For the quantity A the value 0.725 was found. In the vibration-rotation atmospheric gas absorption spectra, shifts in the line centers caused by the effect of the pressure has so far not been observed by anyone. The applications of lasers for this purpose will undoubtedly help to solve this important problem. If a shift exists, then it must be taken into account when the quantity $F(\nu)$ is found.

An experimental atmospheric transmission study with high resolution in the radiation region of a ruby laser using the sun as the radiation source was carried out by Long [295]. The spectral absorption curve which was obtained at an altitude of the sun which varied from 17.4° to 19.3° is given in Fig. 3.9. The spectrum was recorded in the region 6933 - 6946 Å into which the radiation from a ruby laser which operates at various temperatures of the crystal falls. It can be seen from the figure that the spectral absorption can vary from 0 to 80% when the radiation wavelength varies by less than 1 Å.

Figure 4.12 gives the results of more detailed studies of atmospheric transmission carried out by Long [295] in the region of the water vapor absorption line with wavelengths 6943.8 Å into which the radiation from a ruby laser at a temperature of the crystal 305 - 310°K falls. The figure gives the transmission curves which were obtained with four values of the air mass: 6.46, 4.73, 2.95, 2.65, on December 26, 1965. It can be seen from the figure that the absorption in the central part of the line when the air mass varies from 2.65 to 6.46 increases approximately from 40% to 80%. We note that this result characterizes atmospheric absorption in the winter period. The absorption in all water vapor lines increases substantially if the corresponding measurements are carried out in the summer period.

Part 2: SCATTERING OF VISIBLE AND INFRARED WAVES IN THE EARTH'S ATMOSPHERE

5. The Earth's Atmosphere As a Scattering Medium

The electromagnetic waves of the visible and infrared ranges are attenuated during propagation in the earth's

atmosphere due to absorption by the gas components and due to scattering: 1) on fluctuations in molecular density (molecular scattering), 2) on aerosol particles (aerosol scattering), 3) on nonhomogeneities, caused by turbulent movement in the atmosphere.

The attenuation coefficients caused by radiation scattering on micro- and macroturbulent nonhomogeneities are negligibly small compared to the molecular and aerosol scattering coefficients. The attentuation of the visible and infrared radiation due to molecular scattering in the atmosphere has been studied in sufficient detail. At the present time extensive tables are available for the molecular or Rayleigh scattering in a wide range of wavelengths in the ultraviolet, visible and infrared spectral regions. The Rayleight scattering coefficients do practically not depend on the time and the locality. On the other hand the aerosol scattering coefficients do depend considerably on the dimensions, the chemical composition and aerosol particle concentration, which are subject to great variability in time and space. Thus, a quantitative estimate of the attenuation of visible and infrared waves in the atmosphere due to aerosol scattering requires reliable data about all fundamental characteristics of atmospheric aerosols.

Notwithstanding the fact that the dimensions, concentration and chemical composition of atmospheric aerosol particles vary within very wide limits, it is possible to single out certain characteristic types of aerosols (clouds, nebula, smoke, precipitation, dust).

This chapter studies the spectral dimensions, the chemical composition and concentration of the most characteristic aerosol particles found in the atmosphere.

1. Clouds and Nebulae

1. The Dimension Spectra of Particles. The processes which are responsible for the formation of clouds and nebula are related to a variety of factors which vary within wide limits and which determine the rate with which the drops increase (the dependence between the rate of growth and the concentration, the distribution over the dimensions and the nature of the condensation nuclei, the temperature and rate at which the air cools, the turbulence scale and its intensity). All this, for the time being, did not enable us to solve theoretically the problem of the particle distribution functions over the dimensions.

The existing analytical expressions were derived as approximate expressions from the corresponding experimental histograms. The overwhelming majority of experimental data obtained by various investigators both in the USSR [358 - 360 and others] and abroad [361, 362 and others] show that the distribution function for cloud and nebula particles by the dimensions are a unimodal asymmetric curve similar to the curve depicted in Fig. 5.1.

We will give the most widely used approximating expression for the distribution function of the particles by the dimensions in liquid drop clouds and nebula.

Best [363] when he treated the experimental data obtained by the foreign investigators Dim, Mazur, Frish and Hageman [361] used the formula

$$1 - F = \exp\left[\left(\frac{d}{b}\right)^c\right], \tag{5.1}$$

where F is the fraction of liquid water in the cloud where a drop of water with a diameter less than d, and b and c are parameters.

It turned out that the parameter c fluctuates between the limits 12 to 29, the parameter b between the limits 1.92 to 4.90. Rittberger [362], who studied the distribution of the dimensions of 300 000 drops found that the parameter b fluctuates in fact within much wider limits, from 0.4 to 12.5. Because of this he concludes that Best's formula should not be applied to the physics of clouds.

In 1952, A. Kh. Khrgian and I. E. Mazin [364] used the following formula for the treatment of a large number of systematized data about the dimensions of drops in the atmosphere collected by A. M. Borovikov [365]:

$$f(a) = Aa^2 e^{-ba}, \tag{5.2}$$

where A is a normalized factor, and b is a parameter.

In 1954 L. M. Levin [366] proposed that the lognormal law be used which describes the dimension spectrum of gold dust in the scatter which occurs during multiple grinding [367] to describe the distribution of cloud drops by dimensions:

$$f(a)=\frac{1}{\sqrt{\pi t}}\frac{1}{r}e^{-\frac{1}{4}-\frac{1}{t}(\ln\tau)^2} \qquad (5.3)$$

where $\tau = a/r$, r is the most probable radius, and t is the parameter.

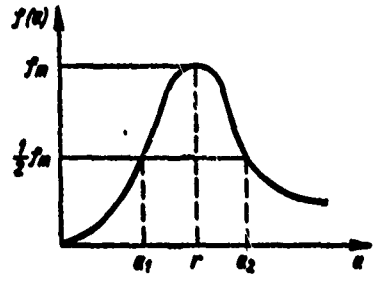

Fig. 5.1. Typical distribution curve for the water particles in clouds and nebula by dimensions

Noting the complexity of the analytical expression for the lognormal law and a certain inconvenience in its use in theoretical calculation, L. M. Levin in 1958 [368] proposed that the cloud drop spectrum be described by the gamma distribution which in the notation adopted by us is written as:

$$f(a)=\frac{1}{\Gamma(\mu+1)}\mu^{\mu+1}\frac{a^{\mu}}{r^{\mu+1}}e^{-\mu\frac{a}{r}}, \qquad (5.4)$$

where $\Gamma(\mu + 1)$ is the gamma function which is equal to $\mu!$ when μ is an integer and r and μ are parameters.

We note that the formula of A. Kh. Khrgian and I. P. Mazin is a special case of the gamma distribution when $\mu = 2$. The gamma distribution, in turn, is a special case of the four-parameter distribution [369]:

$$f(a) = Aa^{\mu}e^{-\beta a^{\nu}}. \qquad (5.5)$$

The expressions for f(a) which were discussed are most widely used, other formulas can be found in [358, 370, 371].

The formula of A. Kh. Khrgian and I. P. Mazin was used by the authors to describe the spectrum of the drops when large quantities of statistical data were treated (660 000 drops were measured in cloud formations with layer forms). The simplicity is the main advantage of this formula over the other formulas. A. Kh. Khrgian and I. P. Mazin have shown in [372] that in the case of stratus clouds in which no precipitation is found, their formula, Best's formula, and the expression for the lognormal law approximate the experimental curves of the particle spectrum with an error of the same order of magnitude.

Studying the applicability of various expressions for f(a) which are used to approximate the experimental data obtained for the dimensions of cloud and nebula drops, L. M. Levin [358] showed on the basis of a large amount of statistical material collected by the Elbrus expedition, that the formula of A. Kh. Khrgian and I. P. Mazin gives good results in the region in which the drops have dimensions with radius $a > 5$ μ, and the lognormal law and the gamma distribution described satisfactorily practially the entire picture of the drop spectrum in the entire range of dimensions studied in clouds and nebula by the author. Khuan-Mey-Yuan' who studied the microstructure of powerful cumulus clouds [360] concluded that the gamma distribution can be applied to describe the dimension spectrum of the particles in these clouds.

2. Quantitative Data For The Microstructure Parameters. The methods used to determine the microstructure parameters have been discussed in detail in special monographs [359, 361, 370]. Depending on the problems which the investigator must solve, he may be interested in a particular combination of the following characteristics of the distribution curve for the particles by dimension [358, 361]:

1) the mean arithmetic radius a_1,
2) the mean square radius a_2,
3) the mean cubed radius a_3,

4) the most probable or modal radius r,

5) the radius of drops with maximum contribution to the geometric section, a_Q,

6) the radius of drops with a maximum contribution to the water volume, a_q,

7) the median radius, a_m,

8) the minimum and maximum radii r_{min} and r_{max},

9) the particle concentration N per 1 cm^3

The first seven characteristics are related in a definite manner and analytical expressions for these were obtained for all distribution functions considered [358, 359, 364]. To apply the A. Kh. Khrgian and I. P. Mazin formula only one of the characteristics must be known. When the gamma distribution or the lognormal law are used all characteristics must be known. In the experiment the values of a_1 and r are determined most often.

The most important studies of the microstructure of clouds which were mainly carried out by foreign authors until 1957 are generalized in B. G. Meyson's monograph [361]. The results of domestic and foreign studies which were made until 1960 have been analyzed in the monograph of A. M. Borovikov, et al. [359]. An analysis of the data for the numerical values of the microstructure parameters of clouds and nebula given in this monograph and also in monograph [358] and in articles [360, 371, 373 - 384] makes it possible to draw a number of definite conclusions about the applicability of a particular approximation formula to the description of the dimension spectra of the particles and about the ranges within which the mean values of individual parameters vary.

1. To stratus clouds the simple single-parameter formula of A. Kh. Khrgian and I. M. Mazin can be fully applied which is easy to handle. To determine the spectrum of the particles using this formula, it suffices to know only the mean arithmetic value of the radius of the drops in the cloud. The experimental statistical material given in [359] recommends the value a_1 = 5 μ for St, Sc, Ns and Ac clouds. The results of other studies of the same type of clouds gave mean values for A_1 between the limits 5 to 10 μ. On one hand this discrepancy can be explained by the fact that in the first experiments the capture coefficients for small drops were not taken into account, which can cause the values of a_1 to shift by 1 - 2.5 μ [359], and on the other hand by the peculiarities of the region with the characteristic values of

a_1 and values of μ which are different from 2 which have an effect [385].

2. The formula of A. Kh. Khrgian and I. P. Mazin is not suitable for approximating narrow spectra of particles. Generally speaking, in this case we can also use a single parameter function by letting the parameter μ in the gamma distribution be equal to the value which is most often encountered in such clouds. However, if the value of the parameter μ is not fixed, then with the aid of the gamma distribution we can describe with an accuracy which is adequate for all practical purposes the spectra of the drops in any clouds, at any stage of their development and in various parts of the volume. A larger value of μ will correspond to a narrower dimension spectrum. Thus, for the clouds and nebula in high mountains L. M. Levin [358] obtained a value of μ in the range 4 to 8, where in more than 70% of the cases $\mu = 8$. V. I. Kazas [378] during his study of warm cumulus clouds obtained in 72% of the cases a value of μ in the range $\mu = 8 - 10$. Khuan-Mey-Yuan' [360] obtained a value of μ for powerful cumulus clouds which varied from 0.5 to 5.5, depending on the level above the cloud base. The studies of G. T. Nikandrova [386] also indicate that the values of the parameters μ and r of the gamma distribution vary in accordance with the altitude above the cloud base.

If we use the relation between the mean a_1 and the most probable radii of the particle r, to determine the values of μ for the data about the microstructure of various clouds given in [361], it turns out that it is equal to 2 for stratus, nimbostratus and cumulus clouds in good weather, 7 for stratocumulus clouds, 9 for high cumulus clouds and 0.33 for powerful cumulus and cumulonimbus clouds. Thus, if we take into account all the information considered we may conclude that the parameter μ varies within very wide limits from 0.33 to 10. If we add together all the data about the most probable radius, its value varies approximately from 3 to 10 μ for all clouds. We note that here we talk about the variation of mean characteristics. For individual clouds and, in particular, for individual local sectors and in different development phases of the same cloud, these variations are considerably wider because of the inevitable fluctuations in the microstructure characteristics of clouds [358, 360].

3. As in the case of clouds the overwhelming majority of the results of nebula microstructure studies show that their dimension spectra are approximated by the gamma distribution. The value of the mean most probable radius may vary

approximately in the range from 2 to 10 μ. With regard to the value of μ, so far not enough data is available for its estimate with any confidence.

All the data about the microstructure of the clouds which we considered are characterized by unimodal distribution curves. It should be noted that sometimes bimodal distribution curves are observed (see, for example [382, 387, 388]).

3. Water Content of Clouds and Nebula. To fully characterize the microstructure of a cloud or nebula, in addition to the distribution function of particles by dimension we must also know the particle concentration N per unit volume. The latter may be obtained if the function f(a) and water content q, are known where by q is meant the amount of liquid water contained in the drops per unit volume, which is usually expressed in grams per cubic meter. Because of the great importance of this characteristic and the relatively simple method by which it is determined, the measurements of this quantity are carried out in the USSR not only by individual investigators but also by a network of aerological probing stations. The methods used to measure the water content are studied in detail in [359, 361, 370].

Table 5.1 gives a summary of the water content for various clouds and nebula obtained by different authors. The same table gives the mean water content characteristics for various clouds and nebula, which can differ substantially from the water content values at various levels and at various stages of development for the same cloud. In addition to this a relation between the mean water content of clouds and the temperature holds. It is precisely this relationship which is responsible for the scatter of the mean water content values given in Table 5.1/ according to the data in [359]. On the other hand when clouds of the same type are formed and develop under different conditions, their water content can differ considerably at the same temperature [376].

It can be seen from Table 5.1 that the mean water content values for clouds of various forms with the exception of powerful cumulus clouds fluctuate within limits which are not very wide: 0.1 - 0.3 g/m^3. The maximum water content values can reach 3 - 4 g/m^3 and even 43 g/m^3. However, in St, Sc, Ac, Ns, As clouds such water contents occur very rearly. In this connection we will discuss the water content repeatability in clouds of various forms at different temperatures.

V. E. Minervin who processed about 5000 airplane measurements constructed the repeatability curve for the average

TABLE 5.1

HUMIDITY OF VARIOUS CLOUDS AND NEBULA
ACCORDING TO THE DATA OF DIFFERENT INVESTIGATORS

a Облако	b Число измерений	Водность г/м³ c: d минимальная	e средняя	f максимальная	g Автор	h Район измерений
Sc, St, Ac	752	—	0,17 * (0,08—0,23)	1,15	А. М. Боровиков [359]	Рига
Sc, St, Ac	571	—	0,27 * (0,08—0,38)	1,79	То же	Минск
Sc, St, Ac	493	—	0,23 * (0,11—0,28)	1,89	» »	Внуково
St, Sc, Ac	4897		0,21 * (0,09—0,33)	3,14	» »	Все пункты ЦАО
Ns, As	184		0,22 * (0,07—0,23)	1,56	» »	Рига
Ns, As	123		0,31 * (0,14—0,35)	1,11	» »	Минск
Ns, As	156		0,23 * (0,09—0,28)	0,87	» »	Внуково
Ns As	1654		0,22 * (0,145—0,356)	1,56	» »	Все пункты ЦАО
Различные формы	493		0,11 * (0,005—0,161)		Л. Т. Матвеев и В. С. Кожарин [359]	Ленинград
Cu, Cb, Ac	} 2157			1,5	Петтит [359]	Канада
Sc, St, Ac				1,4	То же	»
Ac—As						
St, Sc	327 **			0,9	Льюис [359]	США
Ac, Ac—As	246 **			0,5	То же	»
Cu, Cb	324 **			1,8	» »	»
Cu cong	102		1,7 ***	4,1 ***	В. А. Зайцев [359]	СССР
Sc	174 полета	0,06	0,30	1,30	Клайн Уолкер [361]	США
Cu	> 1000		1,2 (0,47—1,91)		Хуан-Мей-Юань [360]	СССР
Sc	Сетевые данные	0,08	0,17—0,32	0,6	В. Е. Минервин [389]	»

Key:
a. Cloud
b. Number of Measurements
c. Water content g/m^3
d. Minimum
e. Mean
f. Maximum
g. Author
h. Region where measurements were made

Column a.

1. Different forms

Column b.

1. 74 flights > 1000
   Network data

Column g.

A. M. Borovikov [359]

(continued next page)

Key, Table 5.1 (Cont'd)

Column g. (cont'd)

Same author
" "
" "
" "
" "
" "
" "
L. T. Matveev and V. S. Kozharin [359]
Peptit [359]
Same author
Lewis [359]
Same author
" "
V. A. Zaytsev [359]
Klein Yolker [361]
Khuan-Mey-Yuan' [360]
V. E. Minervin [389]

Column h.

Riga
Minsk
Vnukovo
All points of the Central Aerological Observatory
Leningrad
Canada
"
USA
"
"
USSR
USA
USSR
"

TABLE 5.1 continued on next page

TABLE 5.1 (Cont'd)

Облако (a)	Число измерений (b)	Водность г/м³ (c) мини-мальная (d)	средняя (e)	макси-мальная (f)	Автор (g)	Район измерений (h)
Ns	1 Сетевые данные	0,03	0,18—0,35	0,6	В. Е. Минервин [389]	СССР
As—Ns	2137		0,154	0,77	А. И. Воскресенский [376]	Арктика
St			0,10	0,58		»
Sc			0,12	0,67	И. М. Долгин [375]	»
Cu	21	0,05	0,14	0,20	В. И. Казас [378]	СССР
	2 22 полета		7—12	43	Шумахер [390]	Западная Европа
1 Туман	21 полет	0,1		0,22	Радфорд [361]	
Туман				0,4	Куроива и Киносита [361]	Япония
2 Туман зимний		10^{-4}		10^{-2}	Окита [383]	
3 Туман океанский			$4{,}2 \cdot 10^{-3}$		Винер и др. [380]	
1 Туман			0,10—0,30	0,60	А. Л. Дергач [313]	Арктика

1 * Данные рассчитаны на основании приведенных в [359] результатов измерений средних водностей облаков при различных температурах. В скобках указаны пределы изменений средних величин.

2 ** Результаты измерений в переохлажденных облаках.

3 *** Данные относятся к наиболее плотным частям мощных кучевых облаков.

Key:
a. Cloud
b. Number of Measurements
c. Water content g/m^3
d. Minimum
e. Mean
f. Maximum
g. Author
h. Region where measurements were made

Column a.

1. Nebula
2. Winter nebula
3. Ocean nebula

Column b.

1. Network data
2. 22 flights
   21 flights

(continued next page)

Key, Table 5.1 (Cont'd)

Column g.

V. E. Minervin [389]
A. I. Voskresenskiy [376]
I. M. Dolgin [375]
V. I. Kazas [378]
Schumacher [390]
Radford [361]
Kuroiva and Kinosita [361]
Okita [383]
Wiener, et al. [380]
A. L. Dergach [313]

Column h.

USSR
Arctic
"
"
USSR
Western Europe
Japan
"
Arctic

Footnotes

1. The data was calculated on the basis of the measurement results given in [359] for the mean water content of clouds at various temperatures. The parentheses indicate the ranges within which the mean values vary.
2. Measurement results in uncooled clouds.
3. The data referred to the densest parts of powerful cumulus clouds.

water content in internal masses and front clouds at various temperatures. As an analysis of the curves shows the repeatability maxima for the average water content of clouds considered at temperatures from -25 to +15°C lie between the limits 0.1 - 0.3 g/m^3. The repeatability of clouds with an average water content of 1.0 g/m^3 is practically equal to zero. Analogous data were obtained by Pettite in Canada and Lewis in the USA [359].

In the greater part of the work devoted to the experimental study of the dimension spectra of cloud and nebula particles not much attention was given to obtaining data about the

concentration of large particles in spite of the fact that their contribution to the humidity of the clouds can be very large.

Certain data about the concentration of large particles in the clouds were obtained in the work of A. M. Borovikov, I. P. Mazin, A. N. Nevzorov [392, 393] and Okito [394]. It turned out that the concentration of large particles (during the measurement, particles with radius larger than 75, 85, 130, 200, 300, 400, 500, 650, 800 μ were selected) depends to a considerable degree on the form of the cloud and varies substantially within a single cloud. The distribution of large particles by dimensions is described in some cases by the exponential law and in other cases by an inverse power law. Often for many kilometers not a single large particle is encountered.

4. Mean Values of the Microstructure Parameters and the Water Content in Clouds and Nebula. As we mentioned the mean dimension spectra of clouds of various forms and nebula are approximated satisfactorily by the gamma distribution where the values of the parameter μ lie in the range 1 to 10 μ and the values of the parameter r in the range 3 to 10 μ. The water content values q vary approximately from 10^{-2} to 43 g/m^3. When the attenuation coefficients are calculated for real clouds and nebula of various forms and development stages, these ranges in which the parameters μ, r and q vary much eventually overlap. When the data obtained from such calculations are used in practice, it is very important that the mean, or most probable, values of these parameters be known (Table 5.2).

5. Chemical Composition of Particles in Clouds and Nebula. When the aersol attenuation coefficients are calculated for clouds and nebula, it is usually assumed that the particles consist only of clear water. This approximation is justified in the vast majority of cases since the concentration of admixtures in cloud and nebula drops is very low. To illustrate this quantitatively, we can use the study of O. P. Petranchuk and B. M. Drozdova [395], which give the measurement results for the concentration of admixtures found in drops of clouds and in precipitation in certain ETS (European Territory of the Soviet Union) regions. It turned out that the total ion content of $SO_4^{\cdot\cdot}$, $Cl^{\cdot}$, $HCO_3^{\cdot}$, $NO_3^{\cdot}$, $NH_4^{\cdot}$, $Na^{\cdot}$, $K^{\cdot}$, $Mg^{\cdot\cdot}$, $Ca^{\cdot\cdot}$ in the water in the clouds in the Leningrad region, the Northern European Territory of the Soviet Union, the Southwestern European Territory of the Soviet Union (the Kiev neighborhood) is on the average

TABLE 5.2

THE MOST PROBABLE VALUES OF THE PARAMETERS r AND μ IN THE GAMMA DISTRIBUTION, AND THE WATER CONTENT IN VARIOUS CONDENSED CLOUDS AND NEBULA

Вид облака a	r, мкм b	μ c	q, г/м³ d
Мощные кучевые *Cu cong*	6	3	1,2
Кучевые *Cu*	6	3	0,2
Кучево-дождевые *Cb*	6	1	
Слоисто-кучевые *Sc*	5	2	0,1
Слоистые *St*	5	2	0,1
Слоисто-дождевые *Ns*	5	2	0,2
Высокослоистые *As*	5	2	0,2
Высококучевые *Ac*	5	2	0,1
Туманы радиационные	5	6	0,1
Туманы адвективные	5	3	0,1

Key: a. Type of cloud
b. r, μ
c. μ
d. q, g/m^3

Column a.

Powerful cumulus Cu cong
Cumulus Cu
Cumulo-nimbus Cb
Strato-cumulus Sc
Stratus St
Nimbo-stratus Ns
Alto-stratus As
Alto-cumulus Ac
Radiational nebula
Advective nebula

11.0, 13.0 and 15.1 mg/l, respectively. In precipitation this content in the same regions is equal to 13.7, 14.6 and 37.1 mg/l. The authors of [395] detected the strong effect of cities on the content of the mixtures in water in clouds and precipitation. Thus, for example, during one flight which was made above Dneproptrovsk, the total concentration of admixtures in the water in the clouds was equal to 300 mg/l, above Odessa about

120 mg/l, and between these cities it was approximately 10 mg/l. In polluted precipitation copper, iron, berrylium, vanadium, chromium, molybdium, manganese, aluminum, zinc, nickle, silicon in concentration higher than 2.10^{-3} mg/l were detected.

However, even in the most polluted regions and precipitation the concentration of the admixtures does not exceed 1%. Taking into consideration the fact that the complex refractive indices of the water solution in which the admixtures were discovered with this concentration does practically not differ from the values of the complex refractive index of clear water, we can assume that the admixtures in the water in the clouds have hardly any effect on their attenuation coefficients.

2. Mists

By a mist usually is meant the most often encountered state when the atmosphere is clouded by particles with relatively small dimensions when $S_M > 1$ or 2 km. The particles can be solid, liquid, soaked or not soaked. Solid particles can have various forms, liquid particles have the form of a sphere. The particles which occur most frequently are particles with a solid nucleus and a watery shell. The form of such two-layer particles depends on the relation between the dimensions of the nuclei and shells.

The available methods used in experimental investigations so far cannot provide an exact answer to the question of the form of mist particles. The available data about the dimensions of the particles can also not claim great accuracy. The dimensions of aerosol particles depend considerably on condensation processes, on sublimation and evaporation of the moisture in the atmosphere. We will give the available experimental data about the microstructure characteristics of mist, for which the remarks which were made above must be kept in mind when these are used.

1. Dimension Spectra of Mist Particles. C. Jung [396, 894] classifies aerosol particles by dimension into three parts: 1) the "Aitken nucleus" (the radius of the particle $r = 10^{-7} - 10^{-5}$ cm), 2) large particles ($r = 10^{-5} - 10^{-4}$ cm), 3) giant particles ($r > 10^{-4}$ cm). From the standpoint of the attenuation of visible and infrared waves in the atmosphere, atmospheric aerosol particles can be divided into optically active and inactive particles. The first group includes particles which have a considerable effect on radiation attenuation. By optically inactive particles we will mean particles

for which the attenuation due to radiation can be ignored. The maximum dimension of particles which can be considered optically inactive depends on the radiation wavelength λ. The larger λ, the greater the corresponding critical dimension of the particle. An analysis of the attenuation coefficients shows that for any wavelength of the visible and infrared radiation, particles with linear dimensions less than 0.1 μ can be considered as optically inactive.

Depending on the dimension spectrum of mist particles, on the basis of most available data, two characteristic cases can be singled out: 1) a multimodal distribution for particles with dimensions approximately less than 0.1 μ which was found in articles [397 and 398], 2) a unimodal distribution obtained by many authors for particles with dimensions $\alpha > 10^{-2}$ μ. As in the case of clouds, various authors proposed different analytical expressions for the distribution of particles by dimension. Thus, the experimental results of the measurement of urban aerosols obtained by M. M. Fedorov [399], K. P. Makhon'ko [400], Spurni and Picha [401] are approximated satisfactorily by the lognormal distribution [see (5.3)]. As mentioned in [400], this distribution law was discovered experimentally for stone [402] and uranium [403] ore dust. The distribution of the gigantic chloride and sulfate condensation nuclei which were measured by Podzimek [404, 405] are described satisfactorily by the formula of A. Kh. Khrgian and I. P. Mazin [see (5.2)].

Junge [406] has shown that a part of the distribution curves which characterize the large particles is approximated satisfactorily by an expression which is called in the literature the Junge distribution

$$N = Ca^{-\beta}. \qquad (5.6)$$

Here a is the radius of the particle, C is a constant which is determined from the experiment and which depends on the particle concentration, and β is a constant which takes on the value 3 for continental aerosols near the surface of the earth.

The Junge formula has been used rather widely. The value of the exponent β characterizes the curvature of the large-drop tail of the distribution curve. Various investigators obtained different values of β. Thus, during measurements over various regions in the USSR, A. G. Laktionov [407, 408] obtained at

the altitude 100 m, 1 km, 2 - 3 km values of β which were equal, respectively, to 3, 4 and 5 for large particles ($a > 4\ \mu$). For nonhydroscopic giant nuclei, Okita [410] obtained values of β in the range 1.7 - 3.2.

During measurements in the stratosphere at altitudes from 12 - 21 km at various latitudes (40° L. So. - 70° L. No.) Junge [411, 412] obtained for particles with dimensions from 0.1 to 2 μ the value $\beta = 2$.

Friedlander [413], assuming dynamic equilibrium between the aerosol formation, coagulation and settlement processes, obtained theoretically by introducing several sensible assumptions the following expressions for the distribution functions (Table 5.3).

TABLE 5.3

DISTRIBUTION FUNCTION FOR AEROSOL PARTICLES ACCORDING TO THE DATA IN ARTICLE [413]

Диаметр частиц, мкм (a)	Тропосферные аэрозоли (b)	Стратосферные аэрозоли (c)
0,5—0,1	$n \approx a^{-3/2}$	$n \approx a^{-2}$
(d) Больше 0,5	$n \approx a^{-19/4}$	$n \approx a^{-4}$

Key: a. Diameter of particles, μ
b. Aerosols in the troposphere
c. Aerosols in the stratosphere
d. Greater than 0.5

Thus, the theoretical values of β obtained by Friedlander for the troposphere and stratosphere lie between the limits 2 - 4.75. G. M. Idlis [414] obtained for the distribution function of dust particles in space a formula which is similar to (5.6) when $\beta = 4$.

L. S. Ivlev [810] as a result of measurements which were made in the earth's layer of the atmosphere in the summer of 1965 in the Ryl'ska area (Kursk region) discovered that two main types of particle distributions by dimensions exist.

Approximately every third case out of 100 spectra for the distribution of particles by dimension in the range 0.0 - 1.5 μ which were treated represent a distribution of the Junge type with the exponent β = 4 (first type of distribution). In the second type of distribution the count concentration has a minimum in the region where the particles have dimensions 0.25 - 0.6 μ and a small maximum for particles with dimensions from 2 to 3 μ.

In the work of Fenn [811] deviations were detected from the Junge distribution for particles by dimensions. The author of [811] found maxima in the distribution of particles in the region where the dimensions of the particles were 0.4 μ and in the region of large particles and minima in the region where the dimensions were 0.2 - 0.25 μ and 0.4 - 0.5 μ.

The results of observations of sky brightness carried out by the Bullrich team [812] shows that the spectrum for dimensions of particles greater than 1 μ obeys the Junge distribution with the parameter value β = 4 and the upper bound a_2 = 10 μ.

In summary, we can conclude apparently that on the basis of the results of most studies the active (in the optical sense) part of the distribution curve for atmospheric aerosol particles by dimensions can be approximated by formula (5.6) where β can vary from 2 to 5. However, it should be emphasized that individual realizations of the dimension spectra of particles can differ considerably from the smoothed distribution (5.6) which, as G. B. Rosenberg [895] pointed out correctly, reflects the properties of the real distributions only in the most general form. The real distributions are often curves with one or several maxima [811, 812, 896].

For the time being very little information about the variation of the maximum in the distribution is available.

K. P. Makhon'ko [400] found during measurements of urban dust that the dimensions of the particles which occur with the greatest frequency fluctuates from 0.6 to 0.34 μ. Goetz, Priening and Kallai [415] who studied various aerosols over the territory of the USA did not detect particles with dimensions less than 0.1 μ even though the spectrometer used could measure particles with dimensions up to 0.08 μ. The most probable dimension of particles in [415] varies from 0.2 to 0.5 μ. Junge [411] obtained the value 0.03 μ for this dimension. Keeping in mind what has been said above about the role of small particles in radiation attenuation on the

basis of this data, we can assume in the corresponding calculations when formula (5.6) is used that the minimum dimensions of the particles have the value 0.1 μ.

In conclusion we note that the Junge formula is only an approximate expression which describes more or less accurately the real distributions of the largest smoke particles. It does not cover all possible concrete distributions. However, for the time being not enough experimental data is available to carry out the corresponding statistical analysis in order to determine how often one type of distribution or another occurs by dimension for the particles.

2. Particle Concentration. Depending on the distribution function used, we are either interested in the total particle concentration taking into account the proportion of small drops or the particle concentration in the range of dimensions under consideration. In both cases we must know how the quantity varies as a function of the location, time and altitude. It is well known that these variations are horrendous. In the atmosphere of industrial cities the aerosol concentration reaches tens of thousands of particles per 1 cm^3 and more, while the cleanest air samples in a rural area may contain tens and in isolated cases several particles per 1 cm^3 [416].

When he studied the distribution for the particle concentration by altitude in the atmosphere, A. Kh. Khrgian [416] has shown theoretically that the concentration decreases according to the exponential law. An analogous result was obtained by A. G. Laktionov [417]. I. I. Gayvoronskiy [418] confirmed this experimentally for condensation nucelii up to an altitude of 4 km. Penndorf [419], who generalized the data of various investigators, concluded that the concentration of particles with dimensions 0.06 - 1 μ decreases according to the exponential law up to an altitude of 5 km. A theoretical and experimental justification for the exponentially decreasing law for the concentration of condensation nuclei with dimensions 10^{-2} - 1 μ up to an altitude of 4 - 6 km

$$N(z)=N(0)e^{-z/h} \qquad (5.7)$$

is given in the work of E. S. Selezneva [420, 421, 900]. In formula (5.7) N(z) and N(0) are the concentration at the altitudes z and 0, h is an empirical constant which is different for different points. The numerical values for N(0) and h which were obtained when condensation nuclei were studied over various regions of the USSR are also given in the work

of A. L. Dergach [422] and A. I. Voskresenskiy [376].

Extensive studies of atmospheric aerosol particles for the altitudes from 6 to 27 km were carried out by Junge and his collaborators [411, 412, 423 - 426]. The important advantage of this work is the separate study of particles with various dimensions (0.01 - 0.1 μ, 0.1 - 1.0 μ are larger). The main results of this work reduce to the following. The concentration of condensation nuclei in the upper troposphere does not depend for all practical purposes on the altitude, while in the lower troposphere and in the stratosphere it drops sharply with the altitude. For particles with dimensions 0.08 - 1 μ an aerosol layer was detected with maximum concentration at altitudes from 15 to 23 km. It turned out that the particle concentration in this layer varies with time by not more than a factor of 3. The measurements which were made at various latitudes led the authors to the conclusion that this layer had a planatary character. In the upper layers of the troposphere, as in the case of condensation nuclei, the concentration of large particles does not depend much on the altitude, conversely, at the altitudes 10 - 15 and 23 - 27 km the concentration rises and drops sharply.

Very few giant particles ($a>1$ μ) were detected in the stratosphere; this agrees with the data of the Durbin study [427 - 429] who has shown that these particles contribute considerably to the concentration only near the surface of the earth. There concentration drops very quickly with the altitude. Its largest measured value at an altitude of 0.8 km was equal to 2.5 cm^{-3}. For the particle concentration greater than 3 μ, in article [430] at the altitudes 13 - 16, 20 and 17 - 29 km the values obtained were, respectively, 4000, 2800, and 1000 m^{-3}.

In the work of A. G. Laktionov [431] a large amount of data about the concentration of particles with dimensions $r>4$ μ was obtained above various regions in the USSR at altitudes from 0.1 to 3.0 km. It turned out that the concentration of such particles depends on the underlying surface. Thus, above various lakes (Aral', Okhotsk, Barents) at an altitude of 0.2 km the particle concentration was approximately equal, with 1.5 - 5 particles per liter. At the same altitudes above dry regions near the coastline, the particle concentration varied considerably and had the values: 1.5 l^{-1} above tundra, 30 l^{-1} above forest covered steppes and 65 l^{-1} above sand. In the steppes the concentration varied sharply during the transition from winter to summer. Thus, at an altitude of 0.1 km in the winter the concentration of

particles with $r>4$ μ was equal to 3 l^{-1}, and in the summer to 60 l^{-1}.

At altitudes above 30 km, direct measurements of aerosol particle concentrations have so far not been made. However, from the analysis of the results of optical investigations made during intermediate probes [432] and also when rockets were launched, aerosols were detected up to an altitude of 100 km and above. Thus, Rossler and Vassy [433] found that at altitudes up to 50 km the aerosol scattering exceeds the Rayleigh scattering. At an altitude of 25 km the maximum of the aerosol layer was detected and at the tropopause level the minimum. A. E. Mikirov [434] obtained data for the aerosol attenuation component at altitudes from 48 to 102 km. At all altitudes the aerosol attenuation was larger than the Rayleigh attenuation and at altitudes of 80 km and above a new aerosol layer was discovered. In the studies of G. P. Gushchin [435] and Yu. I. Rabinovich [436] it has been shown that the aerosol attenuation of visible light by the atmospheric layer above 6 km is 20 - 30% of the attenuation of the layer below. These results show that considerable aerosol particle concentrations are present in the upper layers of the atmosphere. At the same time in the work of Newkirk and Eddy [446], a value equal approximately to $2 \cdot 10^{-4}$ was obtained for the magnitude of the optical layer of the atmosphere above 25 km, which shows the negligible role played by aerosol attenuation at high altitudes.

In the last few years a great deal of data about the behavior of atmospheric aerosol particle concentrations were obtained at different altitudes [illegible].

The most complete data was obtained by Elterman [441 - 444]. The atmosphere was probed in the New Mexico region up to altitudes of 70 km for the period of one year from December 1963 to December 1964 and the distance between the source and the receiver was 30.2 km. The measurements were made on the wavelength 0.55 μ. Aerosols were present at all altitudes. However, the aerosol density above 35 km is very low. 105 vertical profiles for the aerosol attenuation coefficients are given in [444]. All profiles are classified into three types: 1) profiles with a weakly pronounced structure (Fig. 5.2), 2) with a medium pronounced structure (Fig. 5.3), 3) with pronounced structure (Fig. 5.4). The vertical profile of the aerosol attenuation coefficients obtained by averaging the 105 individual profiles is given in Fig. 5.5.

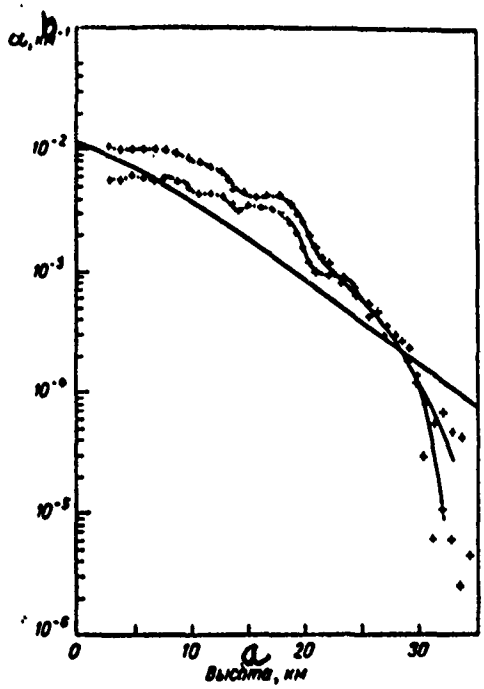

Fig. 5.2. Examples of vertical profiles of the aerosol attenuation coefficient with a weakly pronounced structure obtained by Elterman [444] on April 9, 1964, and December 10, 1964; solid line--the Rayleigh scattering coefficient vs. the altitude

Key: a. altitude, km
b. km^{-1}

An analysis of the individual aerosol attenuation profiles shows that aerosols are present [illegible] The aerosol layer discovered by Junge at altitudes from 15 to 23 km did not manifest itself sufficiently clearly in all probes. In many cases in the layer from approximately 5 to 18 km, the aerosol attenuation coefficient does not vary much with the altitude. This fact was also reflected in the behavior of the average profile.

The comparison of the mean values of the aerosol attenuation coefficient with the values of the molecular scattering coefficient shows the following picture. At altitudes approximately from 0 to 10 km and above 25 km, the molecular scattering coefficient is larger than the aerosol attenuation coefficient. The maximum difference between these coefficients

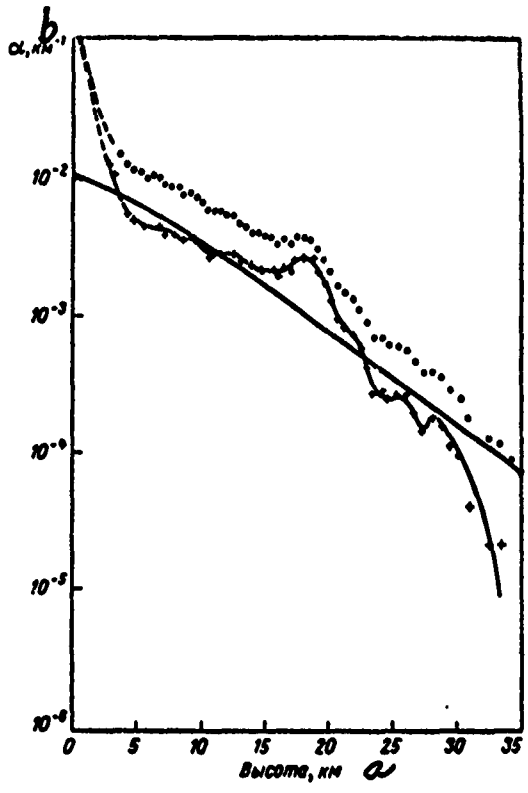

Fig. 5.3. Example of the vertical profile of the aerosol attenuation coefficient with medium pronounced structure obtained by Elterman [444] on May 8, 1964 (curve with crosses); solid line--Rayleigh scattering coefficient vs. altitude; the points denote values of the attenuation coefficient

Key: a. altitude, km
b. km^{-1}

occurs at altitudes approximately from 18 to 22 km, and at an altitude of 35 km. In the first case the aerosol attenuation coefficient is approximately 2 - 2.5 as large as the molecular scattering coefficient and in the second case the relation is reversed.

The team of K. Ya. Kondrat'ev carried out in the last few years many experimental studies in atmospheric optics, using a variety of apparatus raised with the aid of balloons to altitudes between 25 to 30 km. One of the main branches in

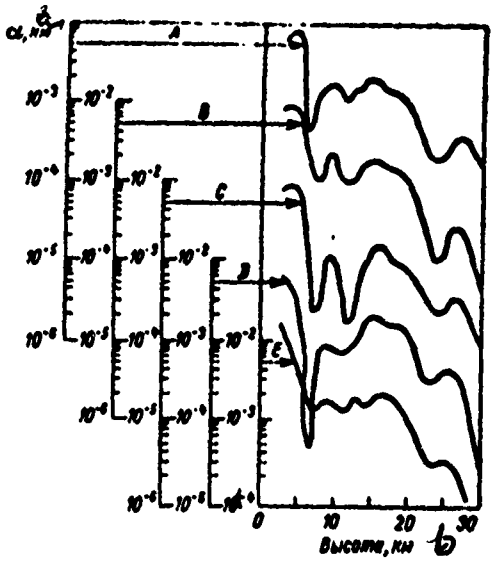

Key:
a. km^{-1}
b. altitude, km

Fig. 5.4. Examples of vertical profiles of an aerosol attenuation coefficient with pronounced structure obtained by Elterman [444] in the period between 8:00 pm, April 12, 1964, and 2:19 am, April 13, 1964

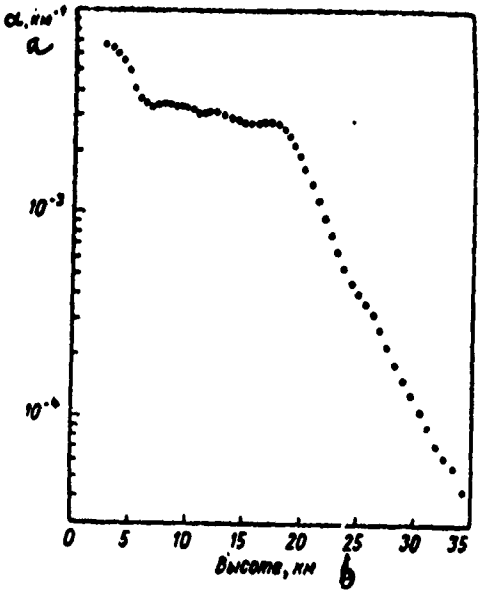

Key:
a. km^{-1}
b. altitude, km

Fig. 5.5. Mean vertical profile of the aerosol attenuation coefficient obtained by Elterman [444] by averaging 105 individual profiles.

this series of studies is related to the study of the optical properties of aerosols and its stratification. Measurements have shown the presence of aerosol layers at different altitudes. The vertical profile of the particle concentration varies between wide limits (Fig. 5.6). Both the altitude of aerosol layers and also the absolute concentration of particles at various altitudes are subject to variation [344, 445, 813].

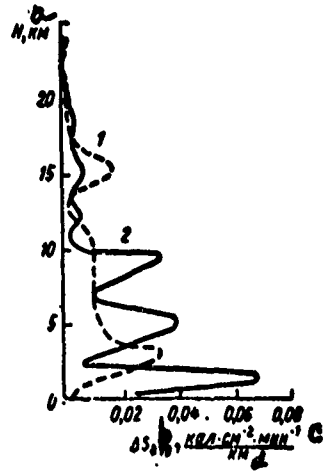

Fig. 5.6. Vertical attenuation profile of direct solar radiation due to aerosol according to the data of K. Ya. Kondrat'es, et al. [445]:

1 -- fall 2 -- summer

Key: a. H, km
b. aer
c. cal.cm^{-2} min^{-1}
d. km

From the material considered one can see the presence of a great variety of data about vertical atmospheric aerosol concentration profiles. Notwithstanding the fact that at the present time a great amount of data about particle concentrations at various altitudes and in different geographic regions has been obtained, this information is still inadequate for solving the problem of the mean statistical concentration profiles of the particles. However, many practical problems do require that certain mean values of this quantity which characterize the aerosol model of the atmosphere be known.

By approximating the experimental data of Junge about the concentration for particles with dimensions 0.08 - 1.0 μ at various altitudes, we constructed the following aerosol model of the atmosphere [1]:

$$
\begin{aligned}
&N(z)=N(0)e^{-bz}, \quad z<5 \text{ км},^{a}\\
&N(z)=0{,}03, \quad 5 \text{ км}^{a}<z<15 \text{ км},^{a}\\
&N(z)=0{,}03e^{0{,}06z}, \quad 15 \text{ км}^{a}<z<20 \text{ км},^{a}\\
&N(z)=0{,}1\,e^{-0{,}09z}, \quad z>20 \text{ км}^{a},
\end{aligned}
\qquad (5.8)
$$

Key: a. km

where N(z) and N(0) is the particle concentration at the altitudes z and 0.

Elterman [447, 448] generalized the available data for the aerosol attenuation coefficients and constructed an aerosol model of the atmosphere.

According to this model, the distribution function by dimension for the particles does not vary with the altitude and the particle concentration at the meteorological range visibility S_M = 25 km near the surface of the earth was taken to be equal to 200 cm^{-3}. The concentration values at other altitudes are given in Table 5.4.

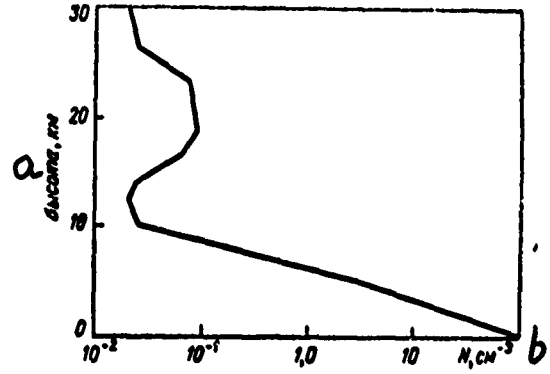

Fig. 5.7. Vertical concentration profile for aerosol particles in the atmosphere adopted in the Elterman model [447]

Key: a. Altitude, km
b. N, cm^{-3}

Figure 5.7 shows the vertical profile for the concentration of aerosol particles constructed from the data in Table 5.3. We note that the Elterman model does not take into account possible variations in the parameters of the distribution function by dimension for the particles. These variations can, as the material under consideration shows, be very large. Hence, we must conclude that the particle concentration may vary between wide limits for the same value of the meteorological visibility range.

TABLE 5.4

CONCENTRATION OF AEROSOL PARTICLES AT VARIOUS ALTITUDES IN THE ELTERMAN MODEL

a								
Высота, км	0	1	2	3	4	5	6	7
Концентрация, $см^{-3}$	200	87	38	16	7,2	3,1	1,1	0,4
Высота, км	8	9	10	11	12	13	14	15
Концентрация, $см^{-3}$	0,14	0,05	0,026	0,023	0,021	0,023	0,025	0,041
Высота, км	16	17	18	19	20	21	22	23
Концентрация, $см^{-3}$	0,067	0,073	0,080	0,090	0,086	0,082	0,080	0,076
Высота, км	24	25	26	27	28	29	30	31—50
Концентрация, $см^{-3}$	0,052	0,036	0,025	0,024	0,022	0,020	0,019	0

Key: a. Altitude, km
Concentration, cm^{-3}

In conclusion we note that the models of the atmosphere which were considered are very approximate statistical averages of the true aerosol stratification picture in the atmosphere. In each concrete case more or less pronounced deviations from the real aerosol particle concentration profile can be observed than those which were adopted in the models.

In addition to the variations of the dimension spectra and the atmospheric aerosol particle concentration, the question of the chemical composition of the particles which determines the components of their complex refractive index is important. A change in these components can have a substantial effect on the corresponding optical aerosol characteristics (the scattering coefficients, the scattering indicatrix, etc.). We should expect differences in these characteristics not only in sea and continental aerosols but also in different types in each group, depending on their origin. At the present time at least several tens of papers have been published. In some of these continental and sea aerosols were studied (for example, [814 - 819]). Nevertheless, the data obtained is completely inadequate to make any definite conclusions about the chemical composition of both the sea and continental particles. The assumption which is made most often when atmospheric aerosol scattering coefficients are calculated is that their particles consist of water. In this case the refractive index is taken to be equal to 1.33. In a number of cases the calculations are carried out for transparent particles, for which the refractive index takes on various discrete values between 1.2 to 1.5 [820].

Atmospheric aerosol models which must be developed in the future must without any doubt take into account the dimension spectra, the concentration and the chemical composition of the particles as well as the variations in these characteristics under real conditions.

3. Precipitation

All precipitation is characterized by the presence of large particles for which the values of the parameter $\rho = \frac{2\pi a}{\lambda}$. ($\lambda$ is the wavelength, a is the radius of the particle) are such that the attenuation coefficients can be considered proportional to the area of the particle cross-section (see Chap. 6 and 7). Therefore, to find the aerosol attenuation coefficients in precipitation, it is more important that we know their intensity or water content than the microstructure parameters. The latter have been studied in greater or lesser detail during rains.

The microstructure studies of rain [449 - 453] have shown that with rare exceptions the distribution of drops by dimension are characterized by unimodal asymmetric curves as in the case of clouds and nebula.

The parameters of the microstructure vary with the rain intensity and the distance from the cloud in which the rain originated. Kelkar [449] has shown that the farther the base of the cloud from the earth, the relative number of small drops due to evaporation during the rainfall incrases in accordance with a certain law. Mason and Andrews [450] detected large oscillations in the microstructure parameters for various types of rain. The most complete data about the microstructure of rainfall was obtained by E. A. Polyakova [451-453] (Table 5.5).

TABLE 5.5

MAXIMUM AND MINIMUM VALUES OF RAINFALL CHARACTERISTICS [451 - 453]

Количество дождя a	$I, \frac{мм}{час}$ b	$\omega, \frac{г}{м^3}$ c	$n, м^{-3}$ d	$a_{наиб}$ мм e	$a_{макс}$ мм f	$a, км^{-1}$ g
1 Минимальное	0,3	0,02	80	0,7	0,025	0,10
2 Максимальное	57	1,98	19 750	3,2	0,3	3,34

Key: a. Amount of rainfall

b. $I, \frac{mm}{hr}$

c. $\omega, \frac{g}{m^{-3}}$

d. n, m^{-3}

e. $a_{largest}$ mm

f. a_{max} mm

g. a, km^{-1}

Column a.

1. Minimum
2. Maximum

The data in Table 5.4 characterize the scatter in the microstructure parameters which are encountered in the most frequent rainfalls. We note that in very rare cases the intensity I and the rain humidity ω can be considerably larger than the values given in Table 5.4. Thus, in the USSR the absolute maximum intensity recorded in Sochi in 1913 was equal to 3.74 mm/min (224 mm/hr), an intense downpour in Panama in 1911 yielded 12.6 mm/min, which corresponded to a humidity of 38 g/m^3 and on the Hawaiian Islands an intensity up to 21.5 mm/min was recorded (1290 mm/hr) [416].

The distribution function for drops by dimension in rainfall was approximated in article [451] by the gamma distribution with the parameter value $\mu = 2$. Marshall and Palmer [454] used the same distribution with $\mu = 0$. L. M. Levin [368] assumes that μ must vary between 0 to 2.

The microstructure of snowfall was studied by I. L. Zel'manovich [455]. The dimensions of the particles were identified from the radii of the spots which remained on the filtering paper after the snowflakes thawed. Using the formula $dn/dr = Ar^{\beta}e^{-\beta r}$, for the distribution function by dimension for the particles, where r is the radius of the particle, the author of [455] found on the basis of the experimental data obtained for the attenuation coefficient and the number of snowflakes, the values of the parameters A and β. Using the values which were obtained for A and β the unimodal distribution curves which were constructed agreed well with the experimental curves.

6. Scattering of Visible and Infrared Waves by a Single Particle

1. Representation Of Polarized Light

We will consider a plane monochromatic wave, the intensity of the electrical field $\vec{E}$ which in complex form has the form

$$\vec{E} = \vec{E}_0 e^{-i\omega t + i\vec{k}\vec{r}}. \qquad (6.1)$$

Here ω is the frequency of the field, the direction $\vec{k}$ coincides with the direction in which the wave is propagated, n is the refractive index of the medium, c is the velocity of light, $\vec{E}_0$ is a vector of constants which is perpendicular to $\vec{k}$. The intensity of the magnetic field $\vec{H}$ is related to $\vec{E}$ as usual by

$$\vec{H} = m_a [\vec{n}, \vec{E}], \tag{6.2}$$

where $\vec{n} = \vec{k}/k$.

The energy flow in the electromagnetic field calculated per unit area, is defined by the Umov-Poynting vector

$$\vec{P} = \frac{c}{4\pi} [\mathrm{Re}\,\vec{E}, \mathrm{Re}\,\vec{H}]. \tag{6.3}$$

Since the radiation receivers react to the energy characteristics of fields, the components (6.3) which are averaged over time represent in optics measurable magnitudes. Averaging over time is related to the fact that the time needed to analyze experimentally the properties of the field exceeds considerably the oscillation period of the light wave. We will now consider a complete set of measured quantities. The first quantity represents the total intensity of the wave, which is defined as the mean value of P over time. Further, we can also measure the oscillation intensity along a certain line which is averaged over time. The oscillations described above can be singled out by placing on the path of the wave an oriented analyzer in a certain way. The characteristics which were enumerated represent the complete information about the light beam determined from the experiment. We can describe quantitatively this information as follows. We substitute (6.1) and (6.2) in (6.3) and take into consideration that when we average over time all terms with the factor $\exp(\pm i2\omega t)$ vanish. Then for the total intensity I we have

$$I = \frac{c}{8\pi} m_a (\vec{E}_0, \vec{E}_0^*). \tag{6.4}$$

We now introduce a Cartesian coordinate system x, y, z, in which the wave under consideration is propagated in the negative direction along the third axis. Then the vector $\vec{E}_0$ lies in the plane formed by the orths of the first two axes. The direction of the lines along which the oscillation intensity must be measured can be given in terms of the angle η relative to the first axis. If $I(\eta)$ is the intensity of the corresponding oscillations, we can obtain easily from (6.4)

$$I(\eta) = \frac{c}{16\pi} m_a (S_1 + S_2 \cos 2\eta + S_3 \sin 2\eta). \tag{6.5}$$

If an additional device is placed on the path of the light beam which introduces the constant phase difference δ into the mutually perpendicular components of the field (for example, a plate at one-quarter of the wave), then

$$I(\eta) = \frac{c}{16\pi} m_a [S_1 + S_2 \cos 2\eta + (S_3 \cos\delta - S_4 \sin\delta) \sin\eta]. \qquad (6.6)$$

In (6.5) and (6.6) S_j are the Stokes parameters which are defined as follows:

$$\begin{aligned} S_1 &= E_{01}E_{01}^* + E_{02}^*E_{02}, \\ S_2 &= E_{02}E_{02}^* - E_{01}E_{01}^*, \\ S_3 &= E_{02}E_{01}^* + E_{02}^*E_{01}, \\ S_4 &= i(E_{02}E_{01}^* - E_{02}^*E_{01}). \end{aligned} \qquad (6.7)$$

Here E_{oj} are the first and second components of the vector $\vec{E}_0$.

By comparing (6.4) and (6.7) we can write the formula for the total intensity

$$I = \frac{c}{8\pi} m_a S_1. \qquad (6.8)$$

It can be shown easily that S_1 and S_4 are invariant with respect to rotations about the third axis, and S_2 and S_3 are transformed according to

$$S_2' = S_2 \cos 2\psi + S_3 \sin 2\psi, \quad S_3' = -S_2 \sin 2\psi + S_3 \cos 2\psi,$$

where S_2' and S_3' are the values of the Stokes parameters in the system which was obtained by rotating the old coordinate system through the angle ψ about the third axis.

Further it can be shown that the end point of the vector $\vec{E}$ of the wave (6.1) describes a particular ellipse. Therefore, a wave of this type is called an elliptically polarized wave. The polarization ellipse can be described in terms of the angle

φ between the major semi-axis of the ellipse and the first orth of the selected coordinate system, and the eccentricity β defined by the relation $tg\beta = a_2/a_1$, where a_1 and a_2, respectively, are the minor and major semi-axis of the ellipse, and β has positive sign for clockwise rotation (relative to k_0) and negative sign for counterclockwise rotation. After some computations we find the following relations:

$$\begin{aligned} S_2 &= S_1 \cos 2\beta \cos 2\varphi, \\ S_3 &= S_1 \cos 2\beta \sin 2\varphi, \\ S_4 &= S_1 \sin 2\beta. \end{aligned} \tag{6.9}$$

Formulas (6.6), (6.8) and (6.9) enable us to calculate the characteristics of the polarization ellipse from the measurements.

2. Scattering Of A Plane Monochromatic Wave

We will now identify the field which was considered in paragraph 1 with the wave which falls on on a certain object. Suppose that the origin of the coordinate system is situated at the center of the object and the first axis of the system coincides with the major semi-axis of the polarization ellipse of the wave. The orths of this system will be denoted by $\vec{l}_1$, $\vec{l}_2$, $\vec{l}_3$.

The material from which the object under consideration is made has a complex refractive index $j_b \neq m_a$ and consequently represents a certain optical nonhomogeneity. Therefore, a scattered field must be present in the object. Further, all quantities which characterize the incident wave have the superscript (0) which corresponds to the scatter with superscript (a).

We will now consider a point $\vec{r}$ where the scattered field is studied. We denote by Q the plane in which the selected point lies and the propagation direction of the incident wave (i.e., the third axis in the selected coordinate system).

We introduce a right handed coordinate system g with the orth triplet $\vec{g}_1$, $\vec{g}_2$, $\vec{g}_3$, where $\vec{g}_3 = -\vec{l}_3$, $\vec{g}_1$ is perpendicular to the plane Q and $\vec{g}_2$ is parallel to it. In the system g the

Stokes' parameters of the scattered wave $S_j^{(0)}$ have the form (6.9), and φ is the azimuth angle of the point $\vec{r}$. The scattered wave is more conveniently analyzed in the system j, the right orth triplet of which is determined as follows: $\vec{j}_3 = \vec{r}/r$; $r = |\vec{r}|$, $\vec{j}_1$ is perpendicular to Q and $\vec{j}_2$ is parallel to this plane. From the linearity of the Maxwell equations and the emission principle it follows that in the wave zone the scattered wave can be represented in the form

$$E_1^{(a)} = \frac{e^{-i\omega t + ikr}}{ikr}(a_{11}(\theta, \varphi) E_1^{(0)} + a_{12}(\theta, \varphi) E_2^{(0)}),$$
$$E_2^{(a)} = \frac{e^{-i\omega t + ikr}}{ikr}(a_{21}(\theta, \varphi) E_1^{(0)} + a_{22}(\theta, \varphi) E_2^{(0)}). \qquad (6.10)$$

In (6.10) r, θ, φ are the polar coordinates of the points $\vec{r}$, $E_i^{(0)}$ are the components of $\vec{E}_0^{(0)}$ in the system g, $E_j^{(a)}$ are the components of the scattered field in the system j. The intensity of the magnetic field of the scattered wave $\vec{H}$ is again calculated from (6.2). The function $a_{ij}(\theta, \varphi)$, is determined by the form, the dimensions of the particle and the properties of the material.

The wave (6.10) has the form which was discussed in paragraph 1, since its characteristics are constant at all points of a sphere with fixed radius, $E_3^{(a)} = 0$ in the wave zone, and the factors $\exp(-i\omega t + i\vec{kr})$. and $\exp(-i\omega t + ikr)$ are essentially equal. Therefore, in the system j we can introduce the Stokes' parameters $S_j^{(a)}$ of the scattered light, and again determine the relations (6.7). If the Stokes parameters are written in the form of a matrix with a single column $\{S\}$ we obtain easily

$$\{S^{(a)}\} = \frac{1}{k^2 r^2}\{M\}\{S^{(i)}\}. \qquad (6.11)$$

Relation (6.11) defines the scattering matrix $\{M\}$ which as the meaning of the Stokes parameters implies contains essentially all the information about the scattered light. We will write out in explicit form the components of the scattering matrix

$$M_{ij}=\frac{1}{2}\sum_{\alpha,\beta=1}^{2}|a_{\alpha\beta}|^2 e_{\alpha\beta ij},\quad i,j=1,2,$$

$$e_{\alpha\beta ij}=\begin{pmatrix}1 & 1 & 1 & 1\\ -1 & 1 & -1 & 1\\ -1 & -1 & 1 & 1\\ 1 & -1 & -1 & 1\end{pmatrix};$$

$$M_{13}=\mathrm{Re}\,(a_{12}a_{11}^{*}+a_{21}a_{22}^{*}),\quad M_{41}=-\mathrm{Im}\,(a_{12}a_{22}^{*}+a_{21}a_{11}^{*}),$$
$$M_{23}=\mathrm{Re}\,(a_{21}a_{22}^{*}-a_{12}a_{11}^{*}),\quad M_{43}=-\mathrm{Im}\,(a_{11}a_{22}^{*}+a_{12}a_{21}^{*}),$$
$$M_{31}=\mathrm{Re}\,(a_{12}a_{22}^{*}+a_{21}a_{11}^{*}),\quad M_{44}=\mathrm{Re}\,(a_{11}a_{22}^{*}-a_{12}a_{21}^{*}),$$
$$M_{32}=\mathrm{Re}\,(a_{12}a_{22}^{*}-a_{21}a_{11}^{*}),\quad M_{24}=\mathrm{Im}\,(a_{21}a_{22}^{*}-a_{12}a_{11}^{*}),$$
$$M_{33}=\mathrm{Re}\,(a_{11}a_{22}^{*}+a_{12}a_{21}^{*}),\quad M_{42}=-\mathrm{Im}\,(a_{12}a_{22}^{*}-a_{21}a_{11}^{*}).$$
$$M_{14}=\mathrm{Im}\,(a_{12}a_{11}^{*}+a_{21}a_{22}^{*}),\quad M_{34}=-\mathrm{Im}\,(a_{11}a_{22}^{*}-a_{12}a_{21}^{*}).$$

The explicit form of the coefficients a_{ij} is determined after the corresponding electrodynamic boundary value problem which reduces to the solution of the Maxwell equations with the condition that the tangential component of the field on the surface which separates the media with different electromagnetic characteristics is continuous is solved. This problem is very complex, and, therefore, solutions to it have been found only in a few special cases. In the case of spherical particles $a_{12} = a_{21} = 0$, the a_{11} and a_{22} depend only on θ and when $\theta = \pi$, i.e., when the direction in which the scattered wave is propagated coincides with the direction of the incident wave, $a_{11} = a_{22}$. We also note that M_{11} by definition coincides with the scattering indicatrix.

3. Scattering, Absorption And Attenuation Coefficients

Relations (6.8) and (6.11) imply that the scattering light intensity $I^{(a)}$ is determined as follows:

$$I^{(a)} = \frac{m_a c^2}{16\pi k^2 r^2}(S_1^{(0)}M_{11} + S_2^{(0)}M_{12} + S_3^{(0)}2M_{13} + S_4^{(0)}M_{14}). \qquad (6.12)$$

Further, the direction of the Umov-Poynting vector, as formulas (6.2), (6.3) and (6.10) imply coincides with the direction of the orth $\vec{j}_3$. Therefore, the energy flow of the scattering field $P^{(a)}$ through a medium with a sufficiently large radius is equal to $\int I^{(a)} r^2 \sin\theta d\theta d\varphi$. The ratio of the last quantity to the intensity of the incident light defines the scattering coefficient σ_s.

Substituting (6.12) into the formula which defines the flow and using formula (6.8) to calculate the intensity of the incident light and relations (6.9), we find

$$\sigma_p^{a\nu} = \frac{1}{2k^2}\int (M_{11} + M_{12}\cos 2\beta \cos 2\varphi + \\ + 2M_{13}\cos 2\beta \sin 2\varphi + 2M_{14}\sin 2\beta)\sin\theta\, d\theta\, d\varphi. \qquad (6.13)$$

Key: a. s

From (6.13) we easily obtain formulas for σ_s in the case of linear polarized light scattering ($\beta = 0$) and polarized light along a circle ($\beta = \pm \pi/4$ depending on the polarization direction). If the particle is spherical, we obtain using the properties a_{ij}

$$\sigma_p^{a\nu} = \frac{\pi}{k^2}\int_0^{\pi} M_{11}\sin\theta\, d\theta \qquad (6.14)$$

Key: a. s

regardless of the polarization state of the incident radiation.

The absorption coefficient σ_a is defined as the ratio with opposite sign of the Umov-Poynting flow vector for the complete field through the sphere with radius r to the intensity of the incident radiation. It is easily seen that the flow which was defined above is equal in absolute value to the amount of energy in the field absorbed in the volume

considered. The minus sign denotes outgoing energy.

The Umov-Poynting vector $\vec{P}$ for the complete field according to the superposition principle for fields and formula (6.3) can be written in the form

$$\text{e } \vec{P} = \vec{P}^{(0)} + \vec{P}^{(a)} + \vec{P}', \text{ где e} \qquad (6.15)$$
$$\vec{P}' = \frac{c}{8\pi} \operatorname{Re}\{[\vec{E}^{(a)}, \vec{H}^{(0)*}] + [\vec{E}^{(0)}, \vec{H}^{(a)*}]\}.$$

Key: a. where

The vector $\vec{P}'$ in (6.15) is averaged over time.

In accordance with the definition for the absorption coefficient

$$\sigma_n^{a} = -\frac{1}{I^{(0)}} \int (\vec{P}, \vec{j}_s)\, ds, \qquad (6.16)$$

Key: a. a

here, as usual, $ds = r^2 \sin\theta\, d\theta\, d\varphi$.

The sum of the scattering and absorption coefficients defines the attenuation coefficient σ:

$$\sigma = \sigma_{a} + \sigma_p. \qquad (6.17)$$

Key: a. a

If the expression for $\vec{P}$ is substituted in (6.16) and if we take into consideration the fact that the integral in the first term vanishes but in the second term gives the value of the scattering coefficient, we obtain from (6.17)

$$\sigma = -\frac{1}{I_0} \int (\vec{P}', \vec{j}_s)\, ds. \qquad (6.18)$$

After substitution of (6.15) in (6.18), we can write the integrand in explicit form, using (6.1) and (6.10) for the components of the electrical field and formula (6.2) for the components of the magnetic field. We then obtain integrals of the form $\int F(\theta, \varphi) \exp[ikr(1+\cos\beta)] \sin\theta d\theta$. Since in the wave zone $kr \gg 1$ the above integrals can be calculated using the stationary phase method, after several computations we obtain the following expression for σ [456]:

$$\sigma = -\frac{1}{k^2} \operatorname{Re} \int_0^{2\pi} [(a_{11}+a_{22}) + \cos^2\beta \cos 2\varphi (a_{22}-a_{11}) + (a_{12}+a_{21}) \cos 2\beta \sin 2\varphi + i(a_{21}-a_{12}) \sin 2\beta] d\varphi. \quad (6.19)$$

All functions a_{ij} in (6.19) have the argument $\theta = \pi$.

The results (6.19) essentially represent a well-known theorem in optics, which is generalized to the case of elliptically polarized light and a scattering particle of arbitrary form.

For spherical particles, we can write on the basis of the corresponding properties of a_{ij} and (6.19)

$$\sigma = -\frac{4\pi}{k^2} \operatorname{Re} a(\pi) \quad (6.20)$$

regardless of the polarization state of the incident wave. Here $a(\pi) = a_{11}(\pi) = a_{22}(\pi)$ represents the amplitude of the wave which is scattered forward.

It can be seen from (6.19) that to calculate the attenuation coefficient one must know the amplitude of the wave scattered at a small angle to the propagation direction of the following wave. The reasons for this are rather simple if we keep in mind that any experimental procedure which is used to determine σ is related essentially to the study of the interference of an incident wave and a scattered wave at small angles. Since the integrals of the type given above which are evaluated using the stationary phase method are independent of the upper limit, it can be shown that the σ defined according to (6.17) coincides with the screening coefficient η.

The latter is determined from the experimental diagram: $\eta = I_0^{-1}(\Pi_0 - \Pi)$, where Π and Π_0 are the amounts of energy held in the radiation receiver in cases when the particle is in the radiation flux and far from it. From a purely computational point of view formula (6.19) is useful in the sense that it can be used to define for σ approximately any information about the amplitudes of the light scattered at small angles.

4. The Scalar Approximation in the Scattering Light Problem

When the solutions of Maxwell's vector equations are replaced by the solution of the scalar Helmholz equation for some function ψ, we say that this is a scalar approximation. The latter has the form

$$\Delta\psi + k^2 V(\vec{r})\psi = 0. \qquad (6.21)$$

The advantage of the scalar approximation is that in a number of cases the approximate solution (6.21) is found much more easily than certain asymptotic solutions of the Maxwell equations. Moreover, it turns out that such solutions include the region of small scattering angles, which enables us to find approximate representations of the attenuation coefficients. We also mention that the replacement of Maxwell's equations by the Helmholz equation was discussed in articles [457 - 459] in order to elucidate the meaning of the term "scalar perturbation" which is used in optical defraction theory.

We will first discuss the scalar approximation for particles of a spherical form. The solution of equation (6.21) is sought usually with the following boundary conditions on the surface of a sphere of radius a:

$$\psi_1 + \psi_2 = \psi_3, \quad P_0(\partial(a\psi_1 + a\psi_2)/\partial a) = P_1 \frac{\partial}{\partial a}(a\psi_3),$$

where ψ_1, ψ_2 and ψ_3 are functions which describe the incident external and internal waves (where ψ represents a plane wave), and P_1 and P_0 are constants.

The following proposition can be proved [460]. In the range of small scattering angles the solution of Maxwell's equations for the potential of the field of a sphere can be written as the sum of the solutions of equations (6.21)

multiplied by 1/2 when $P = P_0 = 1$ and $P_0 = 1/P = m$, where m is the relative complex refraction index for the sphere substance. The first solution corresponds to oscillations of the electric type and the second to oscillations of the magnetic type. The proposition which was stated can be established by simply comparing the corresponding solutions when $\theta \simeq \pi$.

Using the proposition which was formulated and certain methods from quantum collision theory we can obtain, for example, all the results in Chapter II in the well-known Van-de-Heust monograph [461]. As an example we will give the expression for the light attenuation coefficient in a two-layer transparent sphere, the dimensions of which exceed considerably the wavelength

$$\sigma = \pi r_2^2 (2 - x_1 - x_2), \quad x_i = [2 - k(\rho_2, \beta)]\,[1 - a_1/a_2],$$

$$x_2 = 4 \int_0^{a_1/a_2} \cos\{\rho_2 \sqrt{1-\xi_2^2} + \rho_2 [(n_1-1)/(n_2-1) - 1] \sqrt{(r_1/r_2)^2 - \xi^2}\}\, \xi\, d\xi.$$

Quantities which refer to the "nucleus" have the subscript "1" and those which refer to the "shell" have the subscript "2," $k = \sigma'/\pi a_2^2$, σ' is the attenuation coefficient for a sphere with radius a_2, $m = n_2$, $\rho_2 = 2\pi a_2 (n_1 - 1)/\lambda$, λ is the wavelength of the scattering light.

We also write the formula for the refractive index α of the medium which contains N particles with radii $a \gg \lambda$:

$$\alpha = 1 + Na^2 \frac{2\pi}{k} \left\{ e^{-\rho \operatorname{tg}\beta} \frac{\cos\beta}{\rho} \cos(\rho - \beta) + e^{-\rho \operatorname{tg}\beta} \frac{\cos^2\beta}{\rho^2} \sin(\rho - 2\beta) + \frac{\sin 2\beta \cos^2\beta}{\rho^2} \right\},$$

$$k = 2\pi/\lambda, \quad \rho = 2(n-1)ka, \quad \operatorname{tg}\beta = \varkappa/(n-1), \quad m = n + i\varkappa.$$

We will now analyze light scattering under small angles by particles of arbitrary form with dimensions which exceed considerably the wavelength of the scattering light. It turns

out that in this case the field can be written in terms of a scalar function. This magnitude under certain assumptions coincides with the results of Kirchhoff's diffraction theory applied to Fraunhofer's diffraction.

We introduce the vector and scalar potentials $\vec{A}$ and φ of the electromagnetic field and the relations $\vec{H} = m_a \operatorname{rot} \vec{A}$, $\vec{E} = -(m_a/c)(i\omega \vec{A})$ and we write the Lorentz condition in the form $\operatorname{div} \vec{A} + (m_a/c)(i\omega\varphi) = 0$. The usefulness of this notation for $\vec{A}$ and φ for scattering problems will become evident later.

Using the relations given above, we can obtain from Maxwell's equations the following equation for $\vec{E}$:

$$\vec{E}(\vec{r}) = \vec{E}_0 e^{-i\vec{k}\vec{r}} + B(\vec{r}) \int U(\vec{r}') \vec{E}(\vec{r}') G(\vec{r}/\vec{r}')\, d\vec{r}'. \tag{6.22}$$

Here $B(\vec{r}) = (4\pi)^{-1}(k^2 + \operatorname{grad} \operatorname{div})$, $G(\vec{r}/\vec{r}') = e^{-ikR}/R$, $R = |\vec{r} - \vec{r}'|$, $U = m^2 - 1$ inside the particle and $U = 0$ outside the particle, $m = m_j/m_a$.

The subsequent solution procedure is as follows. Using equation (6.22) we find the field $\vec{E}_j$ inside the particle, and then from the formulas

$$\left.\begin{aligned} \vec{E}_a &= \frac{e^{-ikr}}{r}(C_0 i_0 + C_\varphi i_\varphi), \\ C &= \frac{k^2}{4\pi} \int U(\vec{r}') \vec{E}_j(\vec{r}')\, e^{-ik\vec{r}_a\vec{r}'}\, d\vec{r}' \end{aligned}\right\} \tag{6.23}$$

which follow from (6.22) we determine the scattering fields $\vec{E}_a$ in the wave zone. Here i_θ and i_φ are the orths of a spherical coordinate system with origin at the center of the particle.

The derivation of equation (6.22) and of relation (6.23) show that the free term in (6.22) can be represented in the form of an incident wave and that the integration region can be reduced to the volume of the particle only when the potentials of the field and the Lorentz conditions are written in the above form. The solution of (6.22) by successive approximations gives $\vec{E}_j = \sum_{n=0}^{\infty} \vec{D}_n$, where $\vec{D}_0 = \vec{E}_0 e^{-i\vec{k}\vec{r}}$ and for $n \neq 0$

$$\begin{aligned} \vec{D}_n(\vec{r}) = B(\vec{r}) \int d\vec{r}_1 U(\vec{r}_1) G(\vec{r}/\vec{r}_1) \times \\ \times B(\vec{r}_1) \int d\vec{r}_2 U(\vec{r}_2) G(\vec{r}_1/\vec{r}_2) B(\vec{r}_2) \dots B(\vec{r}_{n-2}) \times \\ \times \int d\vec{r}_{n-1} U(\vec{r}_{n-1}) G(\vec{r}_{n-2}/\vec{r}_{n-1}) \times \\ \times B(\vec{r}_{n-1}) \int d\vec{r}_n U(\vec{r}_n) G(\vec{r}_{n-1}/\vec{r}_n) \vec{E}_0 e^{-i\vec{k}\vec{r}_n}. \end{aligned} \tag{6.24}$$

Further, we assume that the complex refractive index for the particle substance varies little at distances on the order of magnitude of the wavelength. Then, when we evaluate the integral in (6.24) using the stationary phase method, and then operating with the operator B we can see that by virtue of the assumption which was made, the second term which is related to the operator grad div can be ignored. Since in this approximation $B(\vec{r}_{n-1})\int d\vec{r}_n U(\vec{r}_n) G(\vec{r}_{n-1}/\vec{r}_n) \vec{E}_0 e^{-i\vec{k}\vec{r}_n}$ differs only by a scalar multiple from the vector $\vec{E}_0 e^{-i\vec{k}\vec{r}_{n-1}}$, the procedure described above can be continued. This is equivalent to setting the operator B equal to $k^2(4\pi)^{-1}$. Then the transformation (6.24) given our assumptions is analogous to the calculations made in the corresponding section in Schiff's work [462]. For this reason we give here only the final result for the vector $\vec{C}$:

$$\vec{C} = -\vec{E}_0 \frac{ik}{2\pi} \int e^{-i(q_1 x_1 + q_2 x_2)} dx_1 dx_2 \times \times \left(1 - e^{-\frac{ik}{2}\int U(\vec{r})\, dx_3}\right), \tag{6.25}$$

where $\vec{q} = \vec{k} - \vec{k}_0$, and the integration is over the volume of the particle and the x_3 axis is oriented along $\vec{k}$.

If $|m| \gg 1$, then in (6.25) we can ignore the second term. Then the formula for the components of the diffracted field will represent the well-known result of Kirchhoff for Fraunhofer's diffraction.

It is obvious that relations (6.23) and (6.25) in essence extend the scalar approximation to large particles of arbitrary form. If the exponent in the parentheses in (6.25) is small, then the relation $\vec{C} = (k^2/4\pi) \times \int U(\vec{r})\, e^{-i(q_1 x_1 + q_2 x_2)} d\vec{r}$ follows immediately from (6.25). In the case of small scattering angles this expression together with (6.25) is the original expression when the propagation of the wave is analyzed in a turbulent atmosphere (see, for example, [463]) and when the Hans-Rayleigh scattering is considered (in the terminology of [461]).

The following expression for the light attenuation coefficient σ follows from formulas (6.23), (6.21) and (6.19):

$$\sigma = 2\mathrm{Re} \int \left(1 - e^{-\frac{ik}{2}\int U(\vec{r})\, dx_3}\right) dx_1 dx_2.$$

To illustrate the last relation, we will give the expression for the attenuation coefficient of a non-absorbing ellipsoid with a relative refractive index which is close to one.

$$\frac{\sigma}{S}=2-\frac{4}{\pi}\left(\frac{\cos b}{b^2}+\frac{\sin b}{b}\right)+\frac{4}{b^2}\sum_{n=0}^{\infty}(-1)^n(1-P^2)\times$$

$$\times\frac{\partial^{2n}}{\partial z^{2n}}J_0(z)+\frac{4\sqrt{1-P^2}}{b}\sum_{n=0}^{\infty}(-1)^n(1-P^2)\frac{\partial^{2n}}{\partial z^{2n}}J_1(z).$$

Here

$$z=b\sqrt{1-P^2};$$
$$P=4S/(SV\sqrt{a});$$
$$b=2k(m-1)/\sqrt{a};$$
$$a=a_1^{-2}\cos^2\alpha_1+a_2^{-2}\cos^2\alpha_2+a_3^{-2}\cos^2\alpha_3,$$

S is the area of the projection of the ellipsoid onto the perpendicular plane, v is the volume of the ellipsoid, α_j is the angle between k and j of the principal ellipsoid semi-axis with value a_j, J_0 and J_1 are Bessel functions.

If $\vec{k}$ is parallel to one of the principal axes of the ellipsoid, then σ/S is equal to the corresponding expression for a sphere with a radius equal to the length of the semi-axis along which the wave incident on the ellipsoid is propagated.

Evidently, the last formula plays the same role as the formula for the attenuation coefficient by "soft" spheres, i.e., it describes qualitatively accurately the behavior of the attenuation coefficient by ellipsoids with arbitrary dimensions.

5. Scattering Of The Nonhomogeneous Field

We will call a wave the form of which is different from that described in paragraph 1 a nonhomogeneous wave. This can either be a nonmonochromatic wave or a non-planar wave or a wave with vector $\mathbf{E}_0$ which is not constant. Any combination of these reasons is also possible.

In the case under consideration, all measured quantities can be constructed from the components of the matrix $D(\vec{r}_1, \vec{r}_2, t_1, t_2)$, where $\vec{r}_1$ and $\vec{r}_2$ are some arbitrary points in the field, and t_1, t_2 are arbitrary instants of time. Formally the matrix D can be written as follows. We represent the vectors $\vec{E}$ and $\vec{H}$ by single column matrices, the elements of which are the components of the vector in some coordinate systems. Such matrices will be denoted by E and H. Then

$$D(\vec{r}_1, \vec{r}_2, t_1, t_2) = \langle E(\vec{r}_1, t_1) \overline{H}(\vec{r}_2, t_2) \rangle, \qquad (6.26)$$

where the bar above H denotes transpose matrices and the symbol $\langle\ \rangle$ indicate that every component of the tensor $E\overline{H}$ is averaged over time in accordance with the rule

$$\langle f_1 f_2 \rangle = \lim_{T \to \infty} \frac{1}{2T} \int_{-T}^{T} f_1(\vec{r}_1, t_1 + \xi) f_2(\vec{r}_2, t_2 + \xi) d\xi,$$

where f_1 and f_2 are certain components of $\vec{E}$ and $\vec{H}$.

Next, we will consider stationary fields, for which D depends only on the difference $t_2 - t_1$ which can be decomposed as follows

$$D(\vec{r}_1, \vec{r}_2, t_1, t_2) = \int \Gamma(\vec{r}_1, \vec{r}_2, \omega) e^{-i\omega(t_1 - t_2)} d\omega, \qquad (6.27)$$

where the components of the matrix Γ are the Fourier coefficients of the corresponding elements in the matrix D. The Stokes parameters at a point r are constructed from the components of D when $\vec{r} = \vec{r}_1 = \vec{r}_2$ and $\tau = t_1 - t_2 = 0$. The total intensity for example, according to (6.26) and (6.4) is equal to $SpD(\vec{r}, \vec{r}, t_1, t_1)$. Experimental procedures for determining $D(\vec{r}_1, \vec{r}_2, t_1, t_2)$ have been discussed in [464]. For example, the components $D(\vec{r}, \vec{r}, t_1 - t_2)$ occur when interference is studied in Junge's experiment, and $D(\vec{r}_1, \vec{r}_2, 0)$ are needed to analyze diffraction at sufficiently large aperatures. In the scalar variant D is called usually the coherence function.

We will now consider an arbitrary electromagnetic field scattered by some object [465]. We assume that the external medium relative to the object is nonmagnetic and homogeneous in space.

The basic idea of the computations made below is sufficiently well known. We denote by $\vec{F}(\vec{r}, t)$ and $\vec{F}_b(\vec{r}, t)$ the electrical $\vec{E}(\vec{r}, t)$ or magnetic $\vec{H}(\vec{r}, t)$ vectors of the incident and complete fields in the object (t is time, r are the coordinates of some point). The relation $\vec{F}_b(\vec{r}, t) = \hat{T}\vec{F}(\vec{r}, t)$ determines the reciprocity operator $\hat{T}$ which within the framework of linear electrodynamic theory is a linear operator. We must find the operator on the assumption that the solution to the scattering problem of a plane monochromatic wave on the object considered is known. The operator $\hat{T}$ can be found by decomposing the incident field into plane waves and by using the linearity property of $\hat{T}$.

From Maxwell's equations and the relation between $\vec{E}$ and the electrical induction vector it follows that

$$\Delta\vec{F} - \frac{1}{c^2}\frac{\partial^2\vec{F}}{\partial t^2} - \frac{1}{c}\int \vec{F}(\vec{r}, \tau)\frac{\partial^2 f}{\partial\tau^2}d\tau = 0, \qquad (6.28)$$

where $f(\tau)$ is the relaxation function (see for example [466]).

Using the apparatus of δ-functions, it can be shown that for real F which satisfy the equation (6.28) the decomposition

$$\vec{F}(\vec{r}, t) = 2\mathrm{Re}\int \frac{\omega\sqrt{\varepsilon(\omega)}}{2c}\vec{G}\left(\frac{\omega\sqrt{\varepsilon}}{c}\vec{k}_0\omega\right)e^{\frac{-i\omega\sqrt{\varepsilon}\vec{k}_0\vec{r}}{c}+i\omega t}d\vec{k}_0\,d\omega,$$
$$\frac{\omega\sqrt{\varepsilon}}{2c}\vec{G}\left(\frac{\omega\sqrt{\varepsilon}}{c}\vec{k}_0, \omega\right) = \frac{1}{(2\pi)^4}\int \vec{F}(\vec{r}', t')e^{-i\omega t'+i\vec{k}\vec{r}'}k^2\,dk\,d\vec{r}'\,dt'. \qquad (6.29)$$

holds where $\omega \in [0, \infty]$; $d\vec{k}_0 = \sin\beta d\beta d\psi$; β and ψ are the coordinates of the unit vector k_0 on the unit sphere, $\varepsilon(\omega) = 1 + \int f(\tau)\exp[-i\omega\tau]\,d\tau$ is the dielectric permeability at frequency ω and c is the velocity of light.

The relation $\vec{G}\left(\frac{\omega\sqrt{\varepsilon}}{c}\vec{k}_0, \omega\right)\vec{k}_0 = 0$, follows from the condition

$\operatorname{div}\vec{F} = 0$ and the Maxwell equations give $\vec{G}_H = \left(\frac{c}{\omega}\right)^2 [\vec{k}_0\vec{G}]$.

The last relations show that (6.2) represents a decomposition of the incident field into plane waves.

The decomposition (6.2) presupposes that $\vec{F}(\vec{r}, t)$ can be integrated by quadratures with respect to time. However, in experiments we are often dealing with the converse case, since the measured values are constructed from the components of the tensor D.

Following [464] we can introduce the function

$$\vec{F}^{(T)}(\vec{r}, t) = \begin{cases} \vec{F}(\vec{r}, t), & |t| \leqslant T, \\ 0, & |t| > T, \end{cases} \qquad (6.30)$$

which can be integrated by quadratures for which the tensor F_{pq} coincides with the corresponding tensor for the function $\vec{F}$. We will assume that the procedure which was described has always been carried out.

After commutation of $\hat{T}$ with the integral symbol in (6.29) it will, in fact, act on the plane monochromatic wave. During scattering of such waves the field inside the object consists of the incident and scattering fields, i.e., $\hat{T} = \hat{P} + \hat{T}_a$, where $\hat{P}$ is an operator which does not change the plane wave and $\hat{T}_a$ is the scattering operator. The latter is defined usually as follows (see [461] and para. 2). The following field is represented in a coordinate system with the orths g_1, g_2, g_3, where g_1 is perpendicular to the plane containing the vector $\vec{k}_0$ and the vector $\vec{r}$ which connects the origin of the coordinate system and the point at which the scattering field is observed, g_2 is parallel to this plane, and $g_3 = k_0$. The components of the scattering field are then obtained in the coordinate system with orths m_1, m_2, m_3, where $m_3 = \vec{r}_0 = \vec{r}/|r|$, and the vector $\vec{m}_1$ is perpendicular to and $\vec{m}_2$ is parallel to the plane described above.

In relations (6.26) - (6.30) all vectors are defined in an arbitrary coordinate system with orths $\vec{l}_1$, $\vec{l}_2$, $\vec{l}_3$ with origin at the center of the scattering object. Therefore, in this system the scattering operator is $\hat{T}_a = N^{-1}\hat{T}_g M$, where $\hat{T}_g$ is the scattering operator for the plane wave in the system $\vec{g}_1$, $\vec{g}_2$, $\vec{g}_3$ and M is a transformation which transforms a given vector in $\vec{k}$-space from the system $(\vec{l}_1, \vec{l}_2, \vec{l}_3)$ into the system $(\vec{g}_1, \vec{g}_2, \vec{g}_3)$ and N is the transformation which transforms this vector from the system $(\vec{l}_1, \vec{l}_2, \vec{l}_3)$ into the system $(\vec{m}_1, \vec{m}_2, \vec{m}_3)$. It can be shown that the energy of the field is invariant with respect to these transformations, i.e., after the appropriate transformation the field is equivalent to the original field.

To be able to introduce in the usual manner the operator matrices, we will represent the vectors by single-column matrices, the elements of which are the components of the vectors in the system $(\vec{l}_1, \vec{l}_2, \vec{l}_3)$. Then, from the relations (6.29) and (6.30) and the expression for the scattering operator in $(\vec{l}_1, \vec{l}_2, \vec{l}_3)$ it follows that

$$F_b(\vec{r}, t) = F(\vec{r}, t) + \frac{2\mathrm{Re}}{(2\pi)^4} \int U^{(\vec{E}, \vec{H})}(\omega, \vec{k}_0, \vec{r}) F(\vec{r}', t') \times \\ \times e^{i\vec{k}\vec{r}' - i\omega(t-t')} d\vec{k}\, d\omega\, d\vec{r}'\, dt' \equiv F + F_a, \tag{6.31}$$

where F, F_b are matrices which correspond to $\vec{F}$ and $\vec{F}_b$, U = $= N^{-1}T_g^{(\vec{E}, \vec{H})}$, $\hat{N}$ and $\hat{M}$ are invariant matrices of the operator $\hat{N}$ and $\hat{M}$, written in explicit form below n is the matrix of the operator $\hat{T}_g$ in the system $(\vec{g}_1, \vec{g}_2, \vec{g}_3)$. The last matrix is equal to $T_g^{(\vec{E})}$, if by $\vec{F}$ we mean $\vec{E}$, and $\vec{E}$, и $T_g^{(\vec{H})}$, when $\vec{F}$ denotes the vector $\vec{H}$. The matrices $T_g^{(\vec{E})}$ and $T_g^{(\vec{H})}$ are determined when the Maxwell equations are solved, which are obtained after the time multiplier has been eliminated.

In the derivation of (6.31) we must take into account the fact that the action of the scattering operator on the complex conjugate terms in (6.29) leads to complex conjugate expressions for the scattering field. This can be shown by using the integral equation for the scattering amplitude

described in paragraph 4.

We will denote by D_b and D_0 the matrices D for the complete and incident fields.

Substituting (6.31) into the definition for D and ignoring terms which contain in the integrand the factor $\exp[i(\omega' + \omega'')t]$, we obtain the relation:

$$D_b = \frac{2}{(2\pi)^6} \operatorname{Re} \lim_{T\to\infty} \frac{1}{2T} \int U^{(\vec{E})}(\omega', \vec{k}_0', \vec{r}_1) E(\vec{r}', t') \times$$
$$\times \overline{H(\vec{r}'', t'')}\, U^{(\vec{H})+}(\omega'', \vec{k}_0'', \vec{r}_2)\, e^{i\vec{k}'\vec{r}' - i\omega'(t'-t_1-\xi) - i\vec{k}''\vec{r}'' + i\omega''(t''-t_2-\xi)} \times$$
$$\times d\vec{k}'\, d\vec{k}''\, d\vec{r}'\, d\vec{r}''\, d\omega'\, d\omega''\, dt'\, dt''\, d\xi +$$
$$+ \frac{2}{(2\pi)^4} \operatorname{Re} \lim_{T\to\infty} \frac{1}{2T} \int_{-T}^{T} E(\vec{r}_1, t_1+\xi)\, \overline{H(\vec{r}'', t'')} \times$$
$$\times U^{(\vec{H})+}(\omega'', \vec{k}_0'', \vec{r}_2)\, e^{-i\vec{k}''\vec{r}'' + i\omega''(t''-t_2-\xi)}\, d\vec{k}''\, d\vec{r}''\, d\omega''\, d\xi +$$
$$+ \frac{2}{(2\pi)^4} \operatorname{Re} \lim_{T\to\infty} \frac{1}{2T} \int_{-T}^{T} U^{(\vec{E})}(\omega', \vec{k}_0', \vec{r}_1) E(\vec{r}', t)\, \overline{H(\vec{r}_2, t_2+\xi)} \times$$
$$\times e^{i\vec{k}'\vec{r}' - i\omega'(t'-t_1-\xi)}\, d\vec{k}'\, d\vec{r}'\, d\omega'\, dt'\, d\xi + D_0.$$

Here and below the symbol "+" in the matric $U^{(H)+}$ denotes Hermitian conjugation.

After the change of variables $t' = \tau' + \xi$, $t'' = \tau'' + \xi$, $\xi = \eta$, using the spectral decomposition of D_0 and integrating with respect to τ', τ'', ω' and ω'', we obtain

$$D_b = \frac{2}{(2\pi)^6} \operatorname{Re} \int U^{(\vec{E})}(\omega, \vec{k}_0', \vec{r}_1)\, \Gamma(\vec{r}', \vec{r}'', \omega) \times$$
$$\times U^{(\vec{H})+}(\omega, \vec{k}_0'', \vec{r}_2)\, e^{i\vec{k}'\vec{r}' - i\vec{k}''\vec{r}'' + i\omega(t_1-t_2)}\, d\vec{k}'\, d\vec{k}''\, d\vec{r}'\, d\vec{r}''\, d\omega +$$
$$+ \frac{2}{(2\pi)^5} \operatorname{Re} \int \Gamma(\vec{r}_1, \vec{r}'', \omega)\, U^{(\vec{H})+}(\omega, \vec{k}_0'', \vec{r}_2)\, e^{-i\vec{k}''\vec{r}'' + i\omega(t_1-t_2)} \times \qquad (6.32)$$
$$\times d\vec{k}''\, d\vec{r}''\, d\omega + \frac{2}{(2\pi)^5} \operatorname{Re} \int U^{(\vec{E})}(\omega, \vec{k}_0', \vec{r}_1) \times$$
$$\times \Gamma(\vec{r}', \vec{r}_2, \omega)\, e^{i\vec{k}'\vec{r}' - i\omega(t_1-t_2)}\, d\vec{k}'\, d\vec{r}'\, d\omega + D_0.$$

In the case of functions which can be integrated by quadratures

$$\Gamma_{pq}(\vec{r}', \vec{r}'', \omega) = E_p(\vec{r}', \omega) H_q^*(\vec{r}'', \omega).$$

In the contrary case

$$\Gamma_{pq}(\vec{r}', \vec{r}'', \omega) = \lim \frac{1}{2T} E_p^{(T)}(\vec{r}', \omega) H_q^{(T)*}(\vec{r}'', \omega).$$

Here E_p, $E_p^{(T)}$, H_q, $H_q^{(T)}$ are the Fourier coefficients of the components $\mathbf{E}$, $\mathbf{E}^{(T)}$ and $\mathbf{H}$, $\mathbf{H}^{(T)}$, and the symbol * denotes complex conjugation.

The explicit form of the matrices of the operators $\hat{M}$ and $\hat{N}$ can be obtained from the relations

$$\begin{aligned}
&\vec{g}_1 = (\sin\alpha)^{-1}[\vec{k}_0 \times \vec{r}_0], \\
&\vec{g}_2 = (\sin\alpha)^{-1}[\vec{k}_0 \times [\vec{k}_0 \times \vec{r}_0]], \quad \vec{g}_3 = \vec{k}_0, \\
&\vec{m}_1 = (\sin\alpha)^{-1}[\vec{k}_0 \times \vec{r}_0], \\
&\vec{m}_2 = (\sin\alpha)^{-1}[[\vec{k}_0 \times \vec{r}_0] \times \vec{r}_0], \quad \vec{m}_3 = \vec{r}_0.
\end{aligned}$$

More detailed expressions are given in [465].

6. Laws Which Govern The Scattering Of Visible And Infrared Waves By A Single Spherical Particle

1. Attenuation, Scattering and Absorption Efficiency Factors. When the scattering of electromagnetic waves by a spherical particle is studied, the concepts of attenuation efficiency K, scattering efficiency K_s and absorption efficiency K_a are introduced:

$$K = \frac{\sigma}{\pi a^2}, \quad K_p = \frac{\sigma_p}{\pi a^2}, \quad K_a = \frac{\sigma_a}{\pi a^2}. \tag{6.33}$$

Key: a. s
b. a

The functions K, K_s and K_a as can be seen from (6.33) and the definitions for the coefficients σ, σ_s and σ_a given in paragraph 3 are numerically equal, respectively, to the ratio of the attenuated, scattered and absorbed energy of the particles to the energy on its geometrical cross section πa^2.

1. Analytical expressions for the functions K, K_s, K_a

General formulas for K, K_s and K_a are obtained from the Mi theory which is discussed systematically and in detail in the monographs of K. S. Shifrin [467] and G. Van-de-Huest [461]. The expressions for the functions K, K_s, K_a are infinite series, and K, K_s and K_a are functions of two variables which characterize the relative dimension ρ and the relative refractive index m of the particle:

$$\rho = \frac{2\pi a}{\lambda}, \tag{6.34}$$

$$m = \frac{m_1}{m_2}, \tag{6.35}$$

where λ is the wavelength of the scattering radiation, m_1 and m_2 are the complex refractive indices of the particle and the medium.

Applied to radiation scattering conditions in the atmosphere, the relative complex refractive index can be considered to be equal to the refractive index of the particle, i.e., we can set $m = m_1 = n - i\varkappa$, where n is the usual refractive index, $\varkappa$ is the absorption index of the particle substance.

In a number of asymptotic cases expressions in finite form are used for the functions K, K_s and K_a. Some of the asymptotic formulas which we will use later are given below.

1. Small Particles. By small particles we mean particles for which $\rho \ll 1$. In this case when the asymptotic formulas for K and K_s are derived, a Bessel and Hankel

expansion is used in powers of ρ in the expressions for K and K_s. For various $|m|$ various formulas are obtained. We are interested in the case when $|m|$ is small for which the following formulas were derived in [467] and [468]:

$$K(\rho, m)=\sum_{n=1}^{5} P_n\rho^n, \quad P_1=4\,\mathrm{Im}\left(\frac{1-m^2}{m^2+2}\right), \quad P_2=0,$$

$$P_3=2\,\mathrm{Im}\left[\frac{-2(m^2-1)(m^2-2)}{(m^2+2)^2}+\frac{m^2-1}{15}-\frac{m^2-1}{3(2m^2+3)}\right],$$

$$P_4=\frac{8}{3}\,\mathrm{Re}\left(\frac{m^2-1}{m^2+2}\right)^2, \tag{6.36}$$

$$P_5=2\,\mathrm{Im}\left(\frac{3}{175}\frac{m^2-1}{m^2+2}\frac{m^6+20m^4-200m^2+200}{m^3-2}-\right.$$

$$\left.-\frac{1}{56}\frac{m^2-1}{3m^2+4}-\frac{(m^2-1)(2m^2-3)}{315}\right).$$

Letting, in (6.37), $\varkappa=0$, we obtain

$$K(\rho, m)=K_{\text{б}}^{\text{а}}(\rho,m)=\frac{8}{3}\rho^4\left(\frac{m^2-1}{m^2+2}\right)^2. \tag{6.37}$$

Key: a. s

It can be seen from (6.37) that in this special case the scattering coefficient for one particle, if its real refractory index is considered to be constant, is inversely proportional to the fourth power of the wavelength as in the case of molecular (Rayleigh) scattering. In other cases the relation is very complex, and does not resemble the following relation based on the well-known Rayleigh law.

The expressions for $K(\rho,m)$ and $K_s(\rho, m)$ for large m and $m=\infty$ are given in [461] and [467].

2. Large Particles. Particles for which $\rho \gg 1$. are called large particles. The analysis of the problem when the Mi formulas are used directly is extremely difficult in this case, since in the sums we must preserve as Debye has shown all terms with n equal from 1 to ρ. For example, in the case of raindrops we must preserve several thousands of

terms. K. S. Shiffin [469] analyzed this case for a transparent particle when he considered a scattering field consisting of geometric optical and ray beams which were difracted on the surface of the drop. Using arguments for the case of an absorbing particle which are analogous to those given in [469] we can obtain for K(ρ, m)

$$K(\rho, m)=2-\frac{8\sqrt{n^2-\varkappa^2}}{(n+1)^2+\varkappa^2}\frac{n}{n-1}\times$$
$$\times\frac{e^{-2\rho\varkappa}}{\rho}\sin\left[2\rho(n-1)-2\operatorname{arctg}\frac{\sqrt{n^2+\varkappa^2}}{\sqrt{n^2+\varkappa^2}+1}\frac{\varkappa}{\sqrt{n^2+\varkappa^2}+n}\right]. \qquad (6.38)$$

For transparent particles we have from (6.38)

$$K_p^{\mathcal{A}}(\rho, m)=2-\frac{8n^2}{\rho(n+1)^2(n-1)}\sin[2\rho(n-1)]. \qquad (6.39)$$

Key: a. s

It follows from (6.38) and (6.39) that in the case when $\rho \to \infty$ the functions K and K_s tend to 2. This means that in the limit large particles scatter twice as much radiation as the amount of radiation incident on their geometrical cross section.

3. Particles with $|m - 1| \to 0$ ("soft" particles). This case is studied in detail in [461]. We note that water particles and watery aerosol particles can be considered with sufficient accuracy for all practical purposes as "soft" particles.

In [461] a sufficiently simple and convenient formula was derived for large "soft" particles ($\rho \gg 1$):

$$K(\rho, m)=2-4e^{-\rho' tg\beta}\frac{\cos\beta}{\rho'}\sin(\rho'-\beta)-$$
$$-4e^{-\rho' tg\beta}\left(\frac{\cos\beta}{\rho'}\right)^2\cos(\rho'-2\beta)+4\left(\frac{\cos\beta}{\rho'}\right)^2\cos^2\beta, \qquad (6.40)$$

where

$$\rho' = 2\rho(n-1); \quad \operatorname{tg}\beta = \frac{\varkappa}{n-1}, \tag{6.41}$$

and for a transparent particle:

$$K_p^a(\rho, m) = 2 - \frac{4}{\rho'}\sin\rho' + \frac{4}{\rho'^2}(1-\cos\rho'). \tag{6.42}$$

Key: a. s

Expressions (6.40) - (6.42) reproduce sufficiently well the behavior of the curve K and K_s (including also small values of ρ) obtained from the tabular values of the exact Mi formulas.

2. Results of the Tabulation of the Functions K, K_s, and K_a

In the case when neither of the two conditions considered above are satisfied, the functions K, K_s and K_a can be obtained only on a basis of a calculation of the exact Mi formulas. When this is done, to ensure that the calculations are carried out with sufficient accuracy, terms of order ρ must be preserved in the series. The calculations are very unwieldy; therefore, until the appearance of high speed electronic computers, the calculations were carried out only for selected values of the parameters m and ρ.

Because of the great interest in the data about the functions K, K_s and K_a, on behalf of specialists in various branches of science, primarily chemists, geophysicists, meteorologists, comparatively many calculations have been carried out at the present time for various values of m and ρ. The vast majority of calculations were carried for real refractive indices: $1{,}0 \leqslant m \leqslant 2{,}0$ and $m = \infty$.

For us, of greatest interest are the results of the calculations when the functions K, K_s and K_a were calculated for atmospheric aerosol particles, primarily for water particles, the refractive index of which in the visible region is so small in comparison with the refractive index that it can be ignored. It is usually assumed that water in the visible region of the

spectrum has a real refractive index and in the infrared region a complex index (see Chapt. 7).

The most complete data about the functions K, K_s and K_a when applied to atmospheric aerosol particles were obtained in articles [470 - 483]. References to other studies can be found in the sources indicated in monograph [1].

Figures 6.1 - 6.20 give the most characteristic results for the calculation of the functions K, K_s and K_a which were obtained by various authors.

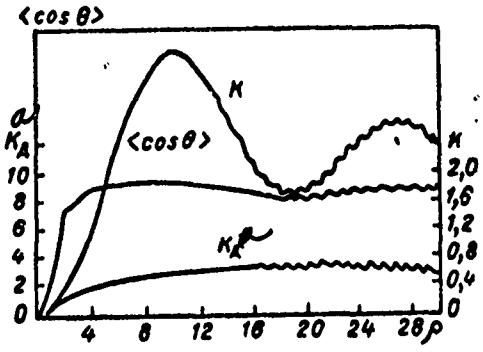

Fig. 6.1. The function K, the asymmetry factor of the scattering indicatrix ⟨cos θ⟩ and light pressure cross section K_d for dielectric spheres with m = 1.20 according to the data in [477]

The calculations were carried out for ρ = 0.5 (0.1) 10 (0.05) 20 (0.025) 30

Key: a. ρ

It can be seen from Fig. 6.1 - 6.3 that the dependence of K on the parameter ρ for transparent dielectric media with values of m from 1.20 to 1.50 is characterized by the presence of a series of large scale and a large number of small scale maxima. These maxima owe their origin to the interference nature of the electromagnetic wave scattering phenomenon on the particles.

Calculations of the factor with step size k which were carried out by Irwine [477] have shown that the

small scale maxima were detected throughout up to the values $\rho = 50$ and $\rho = 100$ (Figs. 6.4 and 6.5).

The functions K, K_s and K_a were calculated for spheres with refractive index $n = 1.01$, 1.33, 1.5, 2 and absorption index $\varkappa = 10^{-4}$, 10^{-2}, 10^{-1} and 10 for values of ρ from 0 to 30 by Plass [479] (see, for example, Figs. 6.6 - 6.11).

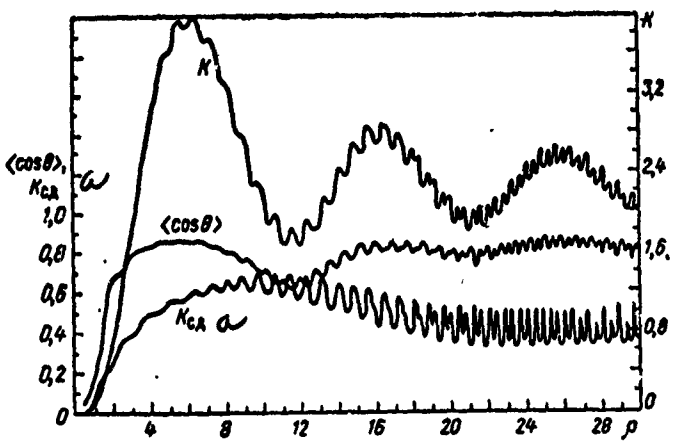

Fig. 6.2. The function K, the asymmetry factor $\langle \cos\theta \rangle$ of the scattering indicatrix and the light pressure cross section K_{lp} for dielectric spheres with m = 1.33 according to the data in [477].

The calculations were carried for $\rho = 0.5$ (0.1) 10 (0.05) 20 (0.025) 30

Key: a. lp

In Figs. 6.6 and 6.7 together with the exact values of the function K_a the approximate values are plotted which were obtained from the Van-de-Huest formula [467]:

$$K_a \approx 2Q(4\rho\varkappa), \tag{6.43}$$

Key: a. a

where

$$Q(\omega) = \frac{1}{2} + \omega^{-1}e^{-\omega} + \omega^{-2}(e^{-\omega} - 1). \tag{6.44}$$

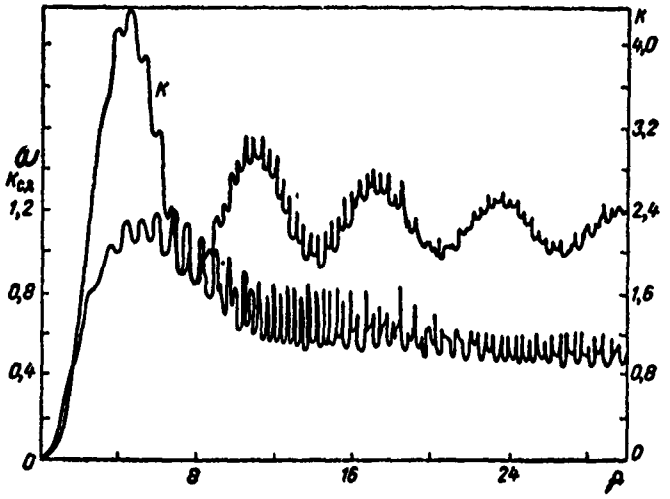

Fig. 6.3. The function K and the light pressure cross section K_{lp} for dielectric spheres with m = 1.5 according to the data in [477]

The calculations were carried out for ρ = 0.5 (0.0) 10 (0.05) 20 (0.025) 30

Key: a. lp

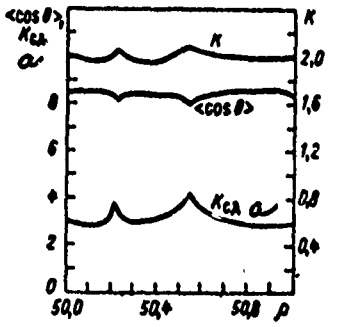

Fig. 6.4. The function K, the asymmetry factor of the scattering indicatrix $\langle\cos\theta\rangle$ and the light pressure cross section K_{lp} for dielectric spheres with m = 1.33 for ρ = 50(0.01) 51 according to the data in [477].

Key: a. lp

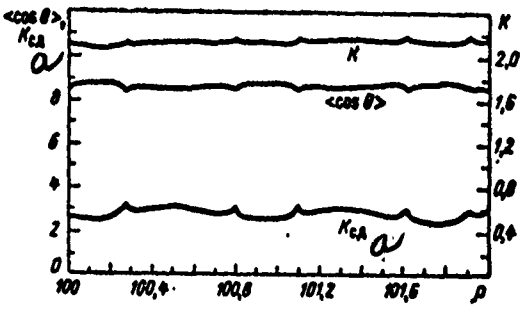

Fig. 6.5. The function K, the asymmetry factor of the scattering indicatrix $\langle\cos\theta\rangle$ and the light pressure cross section K_{lp} for dielectric spheres with m = 1.33 for ρ = 100 (0.01) 102 according to the data in [477]

Key: a. lp

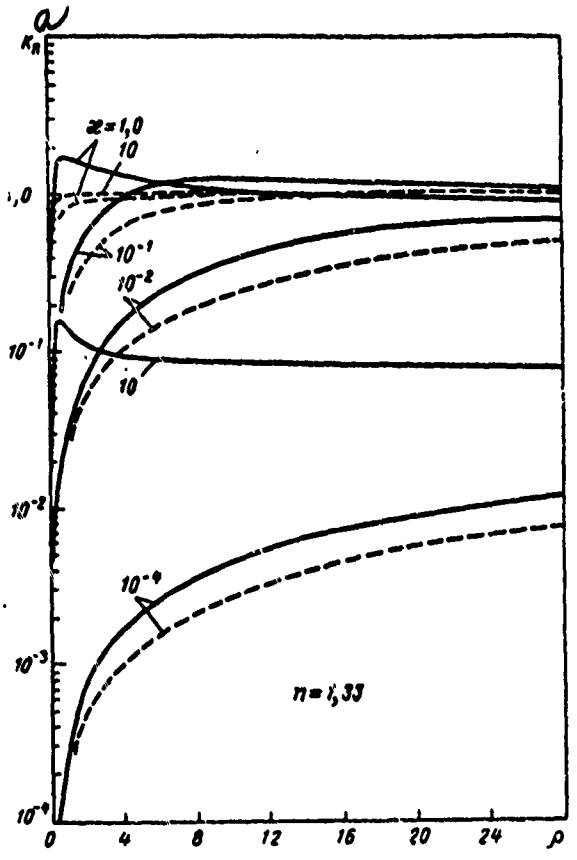

Fig. 6.6. The function K_a for spheres with n = 1.33 and $\varkappa = 10^{-4}$, 10^{-2}, 10^{-1}, 1, 10 and various ρ calculated by Plass [479] using the exact formulas from Mi theory (solid lines) and the approximate formula (6.43)

Key: a. a

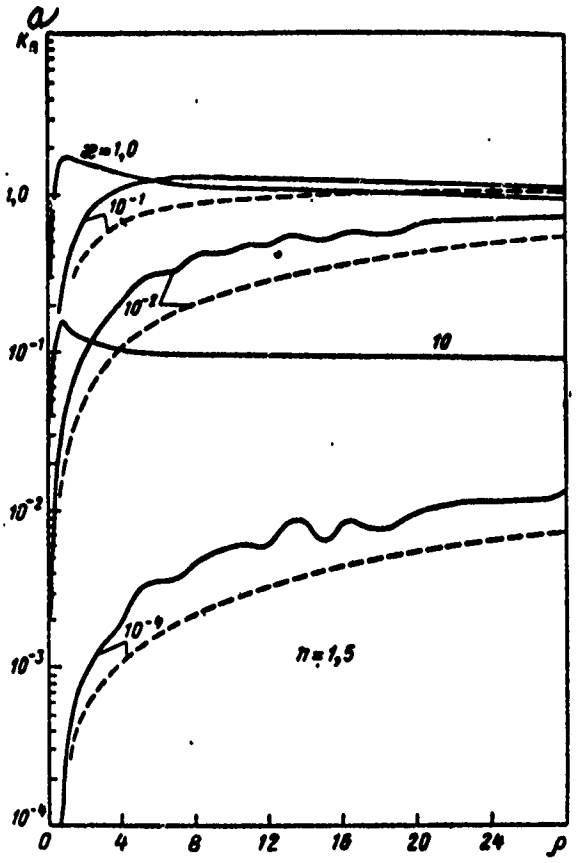

Fig. 6.7. The functions K_a for spheres with n = 1.5 and $\varkappa = 10^{-4}, 10^{-2}, 10^{-1}, 1, 10$ and various ρ calculated by Plass [479] using the exact Mi formulas (solid lines) and the approximate formula (6.43)

Key: a. a

In Figs. 6.10 and 6.11 the exact and approximate values of the function K are plotted as in Figs. 6.6 and 6.7. These were calculated using the approximate Van-de-Huest formula (6.40).

The effect of the quantity $\varkappa$ on the value of the functions K_a and K_s for various n is illustrated in Figs. 6.12 - 6.17.

Figures 6.18 - 6.20 show the functions K, K_a and K_s for water spheres with values of ρ from 0 to 30 and three wavelengths λ = 4, 6, 10 μ according to the data in article [474].

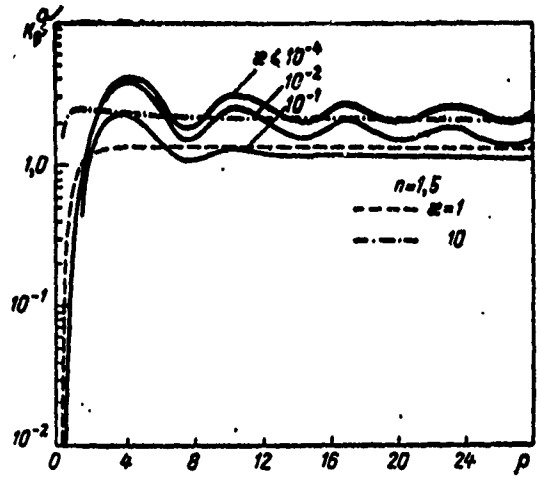

Fig. 6.8. The function K_s vs ρ according to the data in [479] for spheres with n = 1.33 and $\varkappa \leqslant 10^{-4}$, 10^{-2}, 10^{-1}, 1, 10

Key: a. s

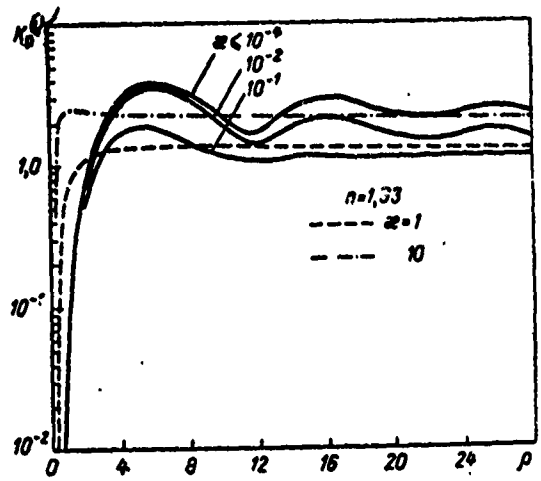

Fig. 6.9. The function K_s vs ρ according to the data in [479] for spheres with n = 1.5 and $\varkappa \leqslant 10^{-4}$, 10^{-2}, 10^{-1}, 1 and 10.

Key: a. s

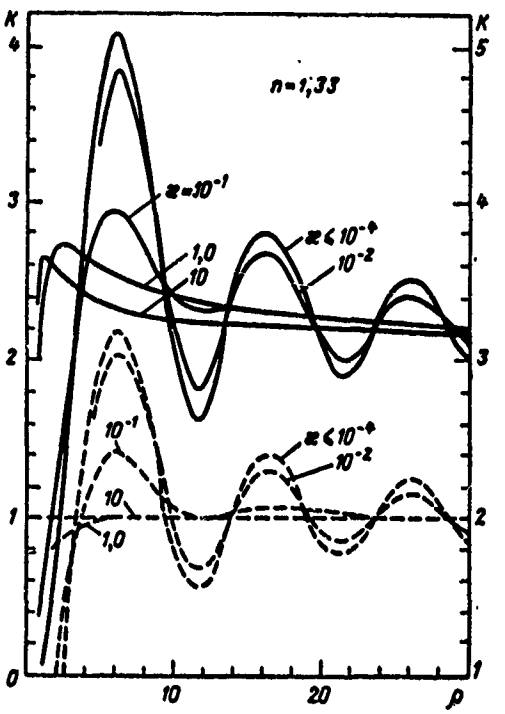

Fig. 6.10. The function K vs ρ according to the data in [479] for spheres with n = 1.33, $x \leqslant 10^{-4}$, 10^{-2}, 10^{-1}, 1, 10, calculated using the exact Mi formulas (solid lines, left ordinate axis) and the approximate formula (6.40).

A knowledge of the values of the functions K, K_s and K_a is of interest in those cases when the atmospheric aerosol particles (for example, in the case of smoke) can be considered as two-layer or multi-layer spheres. The corresponding calculations were carried out in articles [484 - 487]. In [486] K, K_s and K_a were calculated for two-layer spheres with a black soot nucleus and a water shell. The data obtained from the calculations are given in the form of graphs of the functions K for values of ρ from 0.1 to 250 and various values of the ratio of the radii of the particle and nucleus. An analysis of the results obtained has shown that if the radius of the nucleus is smaller than 0.1 of the radius of the entire sphere, the particle can be considered to be a one-layer particle. In [487] a homogeneous spherical nucleus was studied which was surrounded by concentric shells with various values

of the refractive index. It has been shown that the concentric spheres mentioned can be replaced by a homogeneous shell with the value of the refractive index equal to the mean value.

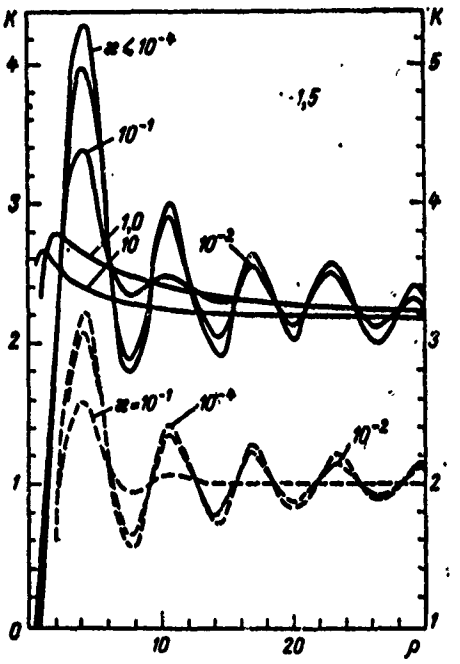

Fig. 6.11. The function K vs ρ according to the data in [479] for spheres with n = 1.5, $\varkappa \leqslant 10^{-4}$, 10^{-2}, 10^{-1}, 1, 10 calculated using the exact formulas (solid lines, left ordinate axis) and the approximate formula (6.40)

The results of the calculations of the functions K, K_s, and K_a which were considered above were obtained for a normal temperature. The exact calculation of the attenuation of visible and infrared waves on atmospheric aerosol particles, generally speaking, requires that these functions be known at various temperatures. However, the corresponding calculations have so far not been carried out because no data is available in the literature about the relation between the complex refractive indices of atmospheric aerosols and the temperature. There is only one study made by Plass [488] in which the functions K_s and K_a were calculated for spherical

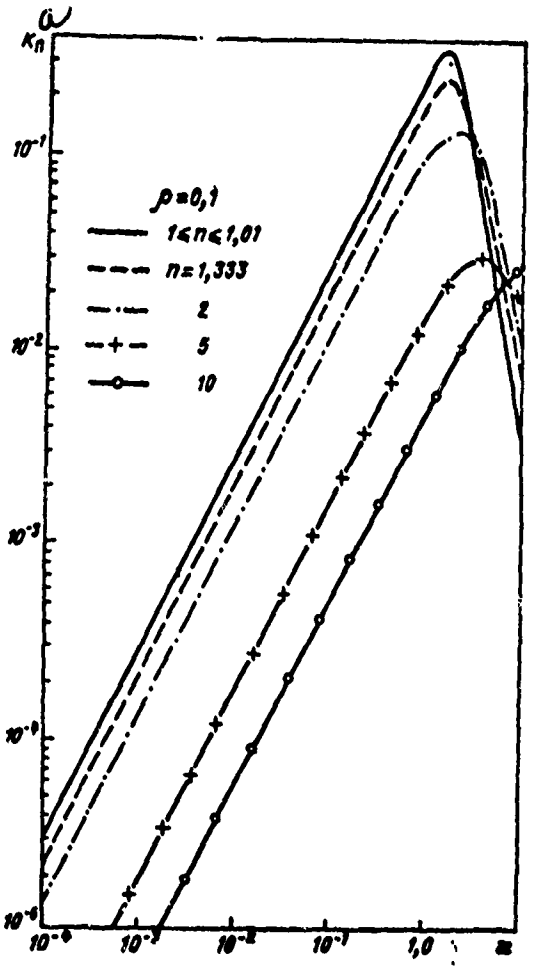

Fig. 6.12. The function K_a vs x for spheres with $\rho = 0.1$ for various values of n according to the data in article [480]

Key: a. a

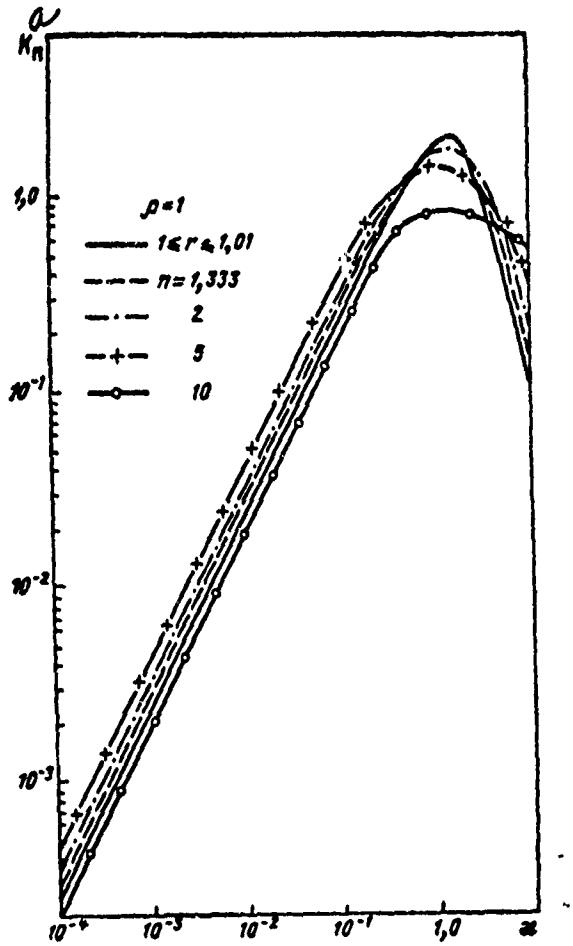

Fig. 6.13. The function K_a vs $\varkappa$ for spheres with $\rho = 1.0$ for various values of n according to the data in article [480]

Key: a. a

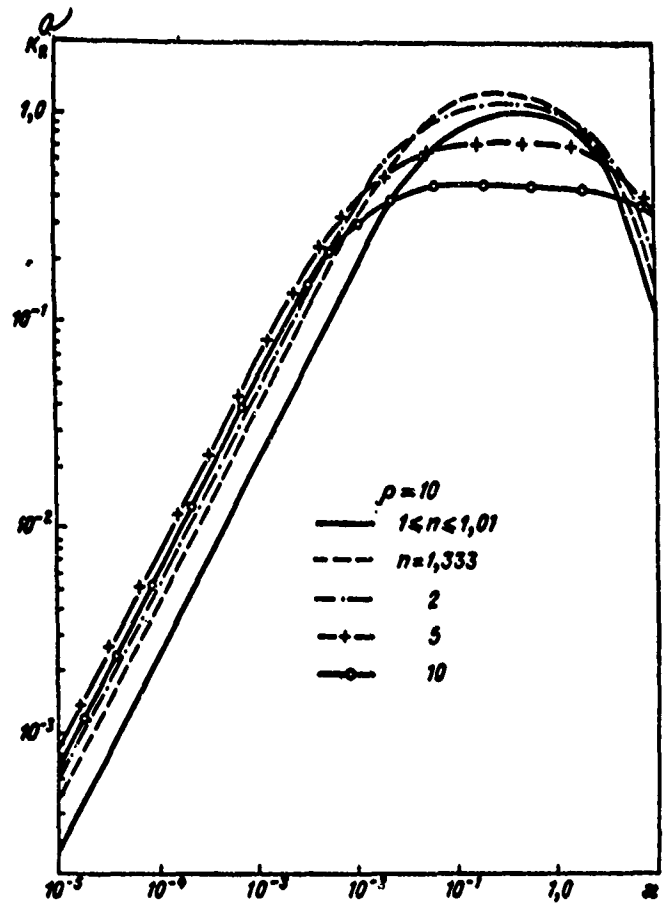

Fig. 6.14. The function K_a vs $\varkappa$ for spheres with $\rho = 10$ for various values of n in accordance with the data in article [480]

Key: a. a

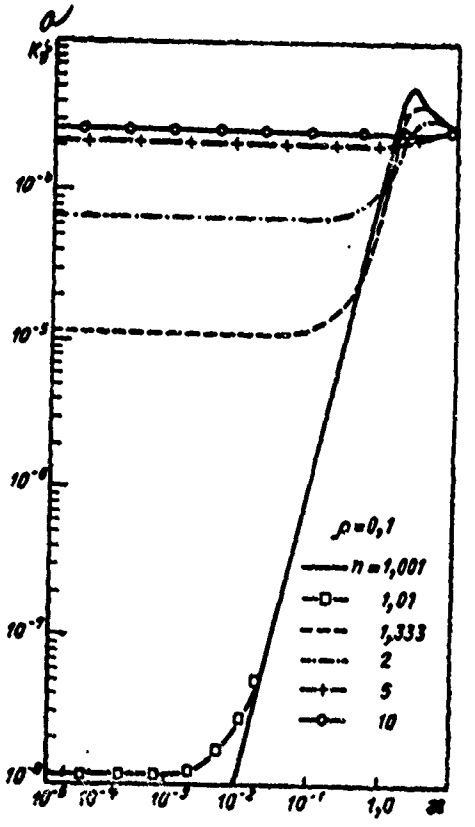

Fig. 6.15. The function K_s vs $\varkappa$ for spheres with $\rho = 0.1$ for various values of n in accordance with the data in article [480].

Key: a. s

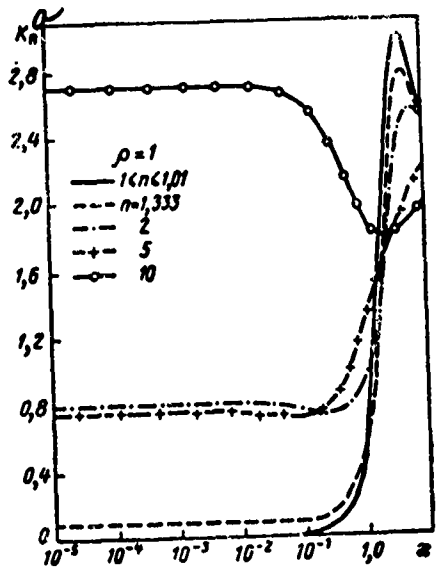

Fig. 6.16. The function K_s vs x for spheres with $\rho = 1.0$ for various values of n in accordance with the data in article [480]

Key: a. s

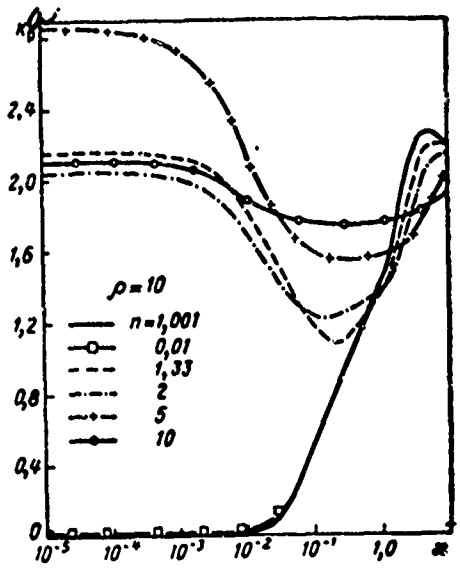

Fig. 6.17. The function K_s vs x for spheres with $\rho = 10.0$ for various values of n in accordance with the data in article [480]

Key: a. s

aluminum oxide particles in the temperature range 1200 - 2020°C. The radius of the particles and the wavelengths varied from 0.1 to 10 μ and from 0.5 to 6.0 μ, respectively. It turned out that K_a varies for the wavelength λ = 2 μ 40 times as much when the temperature changes from 1200 to 2020°C.

For the wavelength 0.5 and 6.0 μ K_a in the same temperature range increases 7 and 2 times as much. The function K_s varies under these same conditions only from 5 to 15% for various wavelengths.

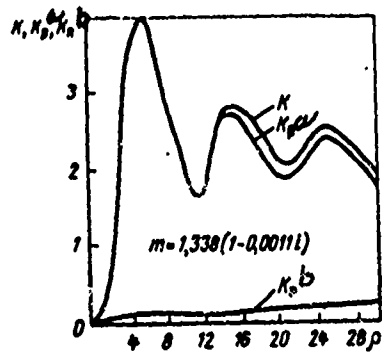

Fig. 6.18. The functions K, K_s and K_a for water spheres with values of ρ from 0 to 30 and wavelengths λ = 4 μ in accordance with the data of Herman [474]

Key: a. s
b. a

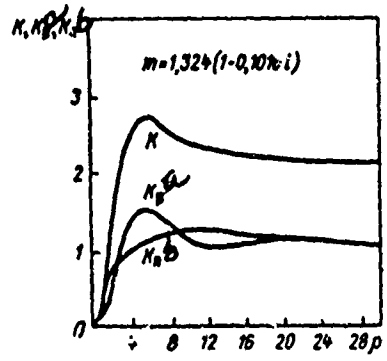

Fig. 6.19. The functions K, K_s and K_a for water spheres with values of ρ from 0 to 30 and wavelengths λ = 6 μ according to the data of Herman [474]

Key: a. s b. a

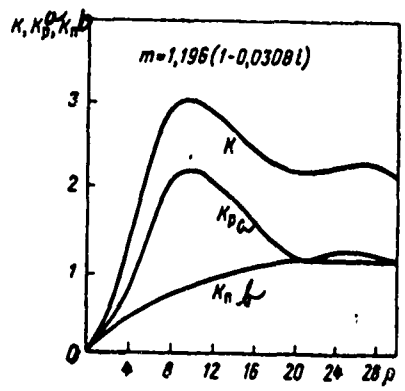

Fig. 6.20 The functions K, K_s and K_a for water spheres with values of ρ from 0 to 30 and wavelengths λ = 10 μ according to the data of Herman [474]

Key: a. s
b. a

Approximating Expressions for the Function K. A number of authors found approximating expressions for the relation between the function K and m for various values of m. L. M. Levin [358] obtained the corresponding formula for K(ρ), when ρ were arbitrary and m = 1.33 (water spheres in the visible region of the spectrum).

Deirmenjian [489] selected an approximating expression for the function K(ρ, m) which holds for any ρ and complex m, which satisfy the condition $|m|<2$. In [489] K is written in the form

$$K=(1+D)K_1, \qquad (6.45)$$

where K_1 is a function determined from formulas (6.40), (6.42) and $(1 + D)^1$ is the approximating multiplier.

The function D(ρ, m) is expressed as follows:

$$D_1=\frac{n-1}{2n}\frac{5(n-1)}{4{,}08}[d(\beta)+1]-\frac{5(n-1)-\rho'}{5(n-1)d(\beta)},$$
$$\rho'\leqslant 5(n-1)\leqslant\frac{4{,}08}{1+3\operatorname{tg}\beta};$$
$$D_2=\frac{n-1}{2n}[d(\beta)+1]\frac{\rho'}{4{,}08},\quad 5(n-1)\leqslant\rho'<\frac{4{,}08}{1+3\operatorname{tg}\beta}; \qquad (6.46)$$
$$D_3=\frac{n-1}{2n}\frac{d(\beta)+1}{1+3\operatorname{tg}\beta},\quad \frac{4{,}08}{1+3\operatorname{tg}\beta}\leqslant\rho'\leqslant\frac{4{,}08}{1+\operatorname{tg}\beta};$$
$$D_4=\frac{n-1}{2n}\frac{d(\beta)+1}{d(\beta)}\frac{40{,}8}{\rho'},\quad \rho'>\frac{4{,}08}{1+\operatorname{tg}\beta};$$
$$d(\beta)=(1+\operatorname{tg}\beta)(1+3\operatorname{tg}\beta).$$

The values of ρ' and β are determined from formulas (6.42).

It is shown in [489] that the functions $K(\rho, m)$ which were obtained with the aid of (6.45) and (6.46) approximate the data calculated by Johnson and Terrell [470] using the exact Mi formulas with an error not exceeding 4%. We note that in [470] $K(\rho, m)$ was calculated up to $\rho = 17.5$. The comparison of the computational results using formuas (6.45) and (6.46) and the asymptotic formula (6.38) which we made has shown that the accuracy of the approximation mentioned above is preserved for $\rho > 17{,}5$.

2. Scattering Indicatrices. To characterize the properties of a particle which scatters the ray under various angles from the direction of the incident wave, we can introduce the concept of the scattering coefficient of the particle in a given direction. However, in practice, to characterize the three-dimensional radiation by a particle, the concept most often used is the scattering indicatrix $f(\theta)$ or the angular scattering function given by the ratio of the radiation intensity scattered by the particle in a given direction to the energy flux scattered in all directions:

$$f(\theta)=\frac{I(\theta)}{\int\limits_{4\pi} I(\theta)\,d\omega}, \qquad (6.47)$$

where $I(\theta)$ is the intensity of the light scattered by the particle in the direction of the angle θ, and $d\omega$ is an element of the solid angle.

Many studies dealing with the calculation of the scattering indicatrices of spherical particles with various dimensions and various wavelengths in the visible and infrared spectrum are available for which a bibliography can be found in monographs [461, 467 and 1].

At the present time the scattering indicatrices of particles have been calculated for various real values of the refractive index. Calculations for particles with a complex refractive index in which both the refractive index and the absorption index vary in a wide range have only been carried out very recently. The most complete and sufficiently accurate data were obtained by K. S. Shifrian and I. L. Zel'manovich [481, 482].

In [481] the angular scattering functions were tabulated for values of the angles equal to 0° (0.1°) 5° (1°) 90° and in the region of the first water drop rainbow 135 - 140° with the step 0.2°. In [482] the values of all components of the scattering matrix and the components of the field of the scattering wave are given for water drops in the visible and infrared regions of the spectrum. Using tables [482], we can find all characteristics of the scattering field including the scattering indicatrix, the degree of polarization and the polarization eccentricity. Tables [482] contain the data mentioned above for 12 spectral sectors in the 0.4 - 12 μ wavelength range. The wavelengths were selected so that all values of the complex water refractive index in the entire range are covered with known approximations.

All characteristics of the scattering fields were calculated for 51 values of the parameter ρ = 0.5 (0.5) 6 (1) 20 (2) 50 (5) 100 and 43 values of the scattering angle θ = 0, 0.05, 0.1, 0.2, 0.5, 1, 2, 5, 10 (10) 130, 135 (0.5) 140 (10) 170, 175, 178, 179, 179.5, 179.8, 179.9, 179.95, 180°. Thus, for small forward and back scattering angles very detailed data were obtained.

We note that the values of $\Delta\lambda$ given by the authors of [482] must be corrected considerably in accordance with the new data for the components n and $\varkappa$ for the complex refractive index of water which we obtained in our study (see Chap. 7) and which are given in supplement 2.

Penndorf [490] analyzed the behavior of the function $i_1 + i_2$, in the expression for the attenuation coefficient and the scattering indicatrix of the particle for the angles θ = 0, 90 and 180° when m = 1.33. As a result of the analysis he

discovered that this function oscillates considerably, depending on the value of ρ. The frequency and amplitudes of these oscillations increases as the angle θ increases. Thus, if for $\theta = 0$ the amplitude of the oscillation is taken to be equal to 0.1, then for the angles 90 and 180° it increases to 5 and 500, respectively. We note that the discovery of the oscillations which were mentioned was possible because the calculations were carried out with a very small step $\Delta\rho = 0{,}1$.

We will consider the analytical representation of the scattering indicatrix of spherical particles. Clark [491] expressed the scattering indicatrix in terms of Legendre polynomials $P_n(\cos\theta)$:

$$f(\theta) = 1 + \sum_{n=1}^{\infty} a_n(\rho) P_n(\cos\theta) \qquad (6.48)$$

and calculated the coefficients $a_n(\rho)$ for values of ρ from 1 to 30 and m = 1.33.

For the scattering indicatrix of large particles K. S. Shifrin obtained the approximate formula [467]:

$$f(\theta) = \frac{1}{2}\left[\frac{\tau(\theta)}{2} + \rho^2(1+\cos\theta)^2 \frac{J_1^2(\rho\sin\theta)}{(\rho\sin\theta)^2}\right], \qquad (6.49)$$

where $\tau(\theta)$ is the part of the indicatrix induced by geometric optical beams which was calculated in [467] with the step size $\Delta\theta = 5°$ for spheres with m = 1.33, and J_1 is a Bessel function.

In conclusion we will describe qualitatively the variation in the character of the indicatrix of a spherical particle which depends on its dimensions and the values of the components of the complex refractive index. Small particles with $m \sim 1$ and $\rho \to 0$ have a symmetric Rayleigh indicatrix, small particles with $m = \infty$ indicate that back radiation is considerably larger than forward radiation. We note that for atmospheric aerosols in the visible region of the spectrum various authors assume a value of m which lies in the interval 1.33 - 1.5 [423, 492, 820].

As the quantity ρ increases from 0 to ∞, the scattering indicatrix of atmospheric aerosol particles continuously changes

its form, and becomes more and more asymmetric and skewed forward (the Mi effect). The following numerical example is given in [492] which illustrates this fact. For particles with m = 1.5 and radius a = 0.5, 1.5, 5.0 and 12.5 μ, the ratio of the radiation fluxes with wavelengths 0.5 μ (ρ = 6.28, 18.84, 62.8 and 157) scattered forward and backward is equal to 17, 74, 823 and 16 000. This ratio is often called the asymmetry coefficient of the indicatrix.

A considerable effect is exerted on the picture in which the scattering indicatrix changes with the change in the dimensions of atmospheric aerosol particles by the complex value of the refractive index of the particles and the oscillations in the intensity of the radiation scattered at various angles which were discovered by Pendorf and which depend on ρ, θ and m.

7. Light Scattering By Non-Spherical Particles.

Although many investigators note that the form of most atmospheric aerosols can be approximated by spheres, this problem, nevertheless, deserves special attention, since dust particles, ice crystals and crystalline cloud particles have, in fact, an arbitrary form. The knowledge of the effect of the form of the particles on their optical properties is important. Many results dealing with this question were obtained and collected in G. Van-de-Huest's monograph [461] ellipsoids, circular cylinders, circular discs and also particles with other forms with different ρ and m and orientations relative to the incident radiation. K. S. Shifrin [467] studied the optical characteristics of rod and disc-like particles which were approximated by ellipsoids.

An analysis of the available results shows that the optical characteristics of particles of various forms depend to a considerable extent on the ratio of the maximum and minimum dimensions of the particles, and their orientation relative to the incident radiation, the polarization degree of the latter, and also the values of the complex refractive index. For example, for a strongly elongated transparent bar all linear dimensions of which are much smaller than the wavelengths, the ratio of the scattering coefficients with the orientation against the field and along the field is equal to 6.25, when m = 2 and 1.64 when m = 1.64 [461]. Naturally for such an absorbing bar the ratios will be different. A change in the dimensions of the bar will entail also corresponding changes in the ratio under consideration.

The optical characteristics of particles with various forms can differ considerably from the optical characteristics of a spherical particle with the same volume. Therefore, the results of the Mi theory must be applied with extreme caution to non-spherical particles. On the other hand, if the form of the particle does not differ very much from the spherical form (for example, ellipsoids with the ratio of the semi-axes up to 1.5 - 2, cubes, cylinders in which the ratio of the height to the diameter is close to one, etc.), such characteristics as the scattering indicatrix, the attenuation, scattering and absorption coefficients will not differ very much from the corresponding characteristics of a spherical particle with the same volume.

We will indicate an important practical way in which the results of the Mi theory can be used for non-spherical particles. If we average some optical characteristic of the particle over all its possible orientations in the space, we can then express analytically its volume in terms of the volume of a spherical particle with the same optical characteristic. K. S. Shifrin [467] obtained such a relation for the scattering indicatrix of ellipsoidal particles:

$$v^* = \sqrt{\varphi(t)}\, v,$$

where v^* and v are, respectively, the volumes of the sphere and the ellipsoid of the scattering indicatrix which coincide, $t = \frac{a}{b}$ is the ratio of the semi-axes of the ellipsoid, and $\varphi(t)$ is the function which was tabulated in [464] which takes on values from 1 to 0.23 when t varies from 1 to 10. In particular, when t = 2 and 3, $\varphi(t)$ = 0.93 and 0.71.

Such relations can be obtained for various scattering characteristics and for particles of other forms.

7. Scattering Of Visible and Infrared Waves In The Atmosphere

The scattering of visible and infrared waves in the earth's atmosphere is caused mainly by fluctuations in the density of the air and by aerosol particles. In the first case, we are dealing with molecular or Rayleigh scattering and in the second case with aerosol scattering. In addition to this at least two other types of scattering can occur in the atmosphere: scattering on small and large scale nonhomogeneities caused by turbulent air fluxes and combined scattering. However,

both these types of scattering do not contribute substantially to the attenuation of the visible and infrared radiation in the atmosphere in comparison with the first two types. Therefore, in this chapter which mainly describes the energy losses which are transferred by electromagnetic waves in the atmosphere, we will not discuss scattering phenomena on turbulent non-homogeneities and combined scattering.

Molecular scattering has been studied in sufficient detail. At the present time extensive tables of the scattering coefficients in the visible and infrared regions have been compiled, which make it possible to determine with sufficient accuracy quantitatively the energy losses in waves propagated in any direction in the atmosphere. Therefore, when we describe molecular scattering we will restrict ourselves mainly to several tabular data about the scattering coefficients and the optical layers of the Rayleigh atmosphere.

When we speak about aerosol scattering, in the general case we have in mind not only the scattering but also the energy absorption from waves by particles. Therefore, it would be more correct if we talked about aerosol attenuation caused both by the scattering phenomenon and the phenomenon where the radiation flux is absorbed by aerosol particles.

In spite of the great variety of dimension spectra and the wide ranges within which the concentration and chemical composition of atmospheric aerosol particle changes, it is possible to single out certain characteristic types of aerosols which differ considerably by properties and their capacity to scatter electromagnetic waves in the optical range. These types include, primarily, clouds, nebula, and mists. Therefore, it is not accidental that the bulk of the material in this chapter is devoted to the study of the scattering of visible and infrared waves by these aerosols. Moreover, even though precipitation cannot be called aerosols, the damping of the radiation when it passes through these is also included in this chapter, since the nature of the scattering of waves on precipitation particles and mist particles, clouds and nebula is the same.

1. Molecular Scattering of Visible and Infrared Waves

The Cabann-Rayleigh molecular light scattering theory gives the following expression for the scattering coefficient in gases:

$$\sigma_{\text{рэл}}(\lambda)=\frac{8\pi^3(n^2-1)^2}{3N\lambda^4}\frac{6+3\delta}{6-7\delta}, \qquad (7.1)$$

Key: a. Ray

where N is the number of molecules per unit volume, n is the refractive index of the medium, λ is the radiation wavelength, δ is the depolarization factor of the scattered radiation, which according to the latest measurements is equal to 0.035 [447].

TABLE 7.1

MOLECULAR SCATTERING COEFFICIENTS δ_{Ray} AT TEMPERATURE VALUES $t = 15^{\circ}C$ AND AT A PRESSURE P = 1013 mb AND OPTICAL LAYERS τ_{Ray} IN THE VERTICAL LAYER IN THE ENTIRE ATMOSPHERE ACCORDING TO THE DATA IN [493] AND [494]

a Длина волны λ, мкм	b $\sigma_{рел}$, км$^{-1}$	c $\tau_{рел}$	a Длина волны λ, мкм	b $\sigma_{рел}$, км$^{-1}$	c $\tau_{рел}$
0,30	$1,446 \cdot 10^{-1}$	1,2237	0,65	5,893	0,0499
0,32	1,098	0,9290	0,70	4,364	0,0369
0,34	$8,494 \cdot 10^{-2}$	0,7188	0,80	2,545	0,0215
0,36	6,680	0,5653	0,90	1,583	0,0134
0,38	5,327	0,4508	1,06	$8,458 \cdot 10^{-4}$	0,0072
0,40	4,303	0,3641	1,26	$4,076 \cdot 10^{-4}$	0,0034
0,45	2,644	0,2238	1,67	$1,327 \cdot 10^{-4}$	0,0011
0,50	1,716	0,1452	2,17	$4,586 \cdot 10^{-5}$	0,0004
0,55	1,162	0,0984	3,50	$6,830 \cdot 10^{-6}$	0,0001
0,60	$8,157 \cdot 10^{-3}$	0,0690	4,00	4,002	0,0000

Key: a. Wavelength, λ, μ
b. σ_{Ray}, km^{-1}
c. τ_{Ray}

The molecular absorption coefficient for various wavelengths was calculated in the interval from 0.2 to 20 μ using formula 7.1 by Penndorf [493]. Using the data obtained in [493], it is possible to calculate the optical molecular scattering layers τ_{Ray} for various geometric layers in the atmosphere.

TABLE 7.2

THE COEFFICIENTS σ_{Ray} FOR VARIOUS ALTITUDES z and THE OPTICAL LAYERS τ_{Ray} IN LAYERS OF THE ATMOSPHERE ($z - \infty$) FOR THE WAVES λ = 0.30, 0.55 AND 1.06 μ ACCORDING TO THE DATA IN [447]

a Высота z, км	λ = 0,30 мкм		λ=0,55 мкм		λ=1,06 мкм	
	$\sigma_{рел}$, км$^{-1}$	$\tau_{рел} \times (z-\infty)$	$\sigma_{рел}$, км$^{-1}$	$\tau_{рел} \times (z-\infty)$	$\sigma_{рел}$, км$^{-1}$	$\tau_{рел} \times (z-\infty)$
0	$1,446 \cdot 10^{-1}$	1,2237	$1,162 \cdot 10^{-2}$	0,0984	$8,458 \cdot 10^{-4}$	0,0072
5	$8,693 \cdot 10^{-2}$	0,6538	$6,988 \cdot 10^{-3}$	0,0526	5,085	0,0038
10	4,881	0,3212	3,924	0,0258	2,855	0,0019
15	2,999	0,1471	1,848	0,0118	1,345	0,0009
20	1,049	0,0672	$8,436 \cdot 10^{-4}$	0,0054	$6,138 \cdot 10^{-5}$	0,0004
30	$2,173 \cdot 10^{-2}$	0,0146	1,747	0,0012	1,271	0,0001
40	$4,716 \cdot 10^{-4}$	0,0035	$3,791 \cdot 10^{-5}$	0,0003	$2,758 \cdot 10^{-6}$	0,0000
50	1,212	0,0010	$9,743 \cdot 10^{-6}$	0,0001	$7,089 \cdot 10^{-7}$	0,0000

Key: a. Altitude z, km
b. μ
c. σ_{Ray}, km^{-1}
d. τ_{Ray}

Tables 7.1 and 7.2 give the data for the coefficients σ_{Ray} and τ_{Ray} for various wavelengths and geometric layers in the atmosphere. We note that the Rayleigh scattering coefficient calculated according to formula 7.1 has the dimensionality of the inverse length.

2. Wave Scattering By A System Of Particles

The exact electrodynamic formulation of the problem of waves scattered by a system of particles, the methods used to solve it and certain results which were already obtained have been discussed to a considerable extent in the literature (see, for example, [494 - 503]). The main idea in the method which is used to solve the aforementioned problem is the following: it is assumed that the solution of the light scattering problem by one particle is known and that all unknown physical quantities can be obtained after appropriate statistical averaging over the positions of the particles.

A certain field exists in the medium which is filled by the particles which consists of the field of the wave incident on the system of particles, and fields which are scattered by individual particles. The latter are written on the basis of the known solution and on each particle its own field is acting, which is called the effective field. Consequently, we can write:

$$\left.\begin{aligned}\psi(\vec{r}) &= \psi_0(\vec{r}) + \sum_{j=1}^{N} T(\vec{r}, \vec{r}_j)\,\tilde{\psi}(\vec{r}_j),\\ \tilde{\psi}(\vec{r}_j) &= \psi_0(\vec{r}) + \sum_{j' \neq j} T(\vec{r}_j, \vec{r}_{j'})\,\tilde{\psi}(\vec{r}_{j'}),\end{aligned}\right\} \qquad (7.2)$$

where ψ is some component of the field, $\vec{r}_j$ are the coordinates of the j-th particle, ψ_0 is the corresponding component of the incident wave, $\vec{r}$ is the radius-vector of an arbitrary point, T is the scattering operator, $\tilde{\psi}$ is the effective field. The first equation in (7.2) gives the magnitude of the field in the medium which in essence represents a system of equations used to determine the values of the effective field which act on every particle. The sum in (7.2) determines the fixed configuration of the scattering particles.

The next step consists of averaging equations (7.2) over all configurations. Formally this is carried out by multiplying both sides of the equations by the distribution function for the configurations and by integrating over the corresponding variables. The distribution function of the configurations depends generally, to a considerable extent, on the character in which the particles interact. The corresponding calculations can be carried through to the end in general form if we assume that the particles do not interact (an ideal gas type model) or if we restrict ourselves to the first terms in the expansion with variable coefficients. We must also assume that the distances between the particles are considerably larger than the length of the light wave in order to be able to use the asymptotic form of the scattering operator in the wave zone. We further note that the effective field is usually assumed to be equal to the mean field at the points where the particle is located, since both fields differ by a quantity on the order of magnitude of 1/N, where N is the number of particles. This assumption enables us to consider only one equation for the mean field. The problem of the relative light intensity is studied using the same procedure. In the scalar variant, this quantity can be determined as $|\psi|^2$. After both

sides of equations (7.2) are multiplied by the corresponding complex-conjugate terms, the expressions obtained are again averaged over the configurations using the distribution function which was determined.

If we study particles which do not interact, then for the radiation intensity in the medium we obtain the usual transfer equation, if we do take into account the particle interaction as usual, certain corrections must be made in the aforementioned equation.

When this type of analysis is used, a relation for the attenuation coefficient $\alpha(\lambda)$ is obtained automatically, which is calculated per unit length of the beam path

$$\alpha(\lambda) = N \int_0^\infty \sigma(a, \lambda) f(a)\, da, \qquad (7.3)$$

where N is the number of particles per unit volume, $\sigma(a, \lambda)$ is the radiation attenuation coefficient with wavelength λ for a particle with radius a (here and below we assume that the scattering particles are spherical), f(a) is the distribution function by dimension for the particles which is interpreted by defining the relation $N_a da = Nf(a)\,da$, where N_a is the number of particles with radius in the interval from a to a + da.

The origin of formula (7.3) can be easily analyzed with the aid of the optical theorem (see para. 2, Chapt. 6). The attenuation coefficient for some volume can be determined in accordance with the procedure described in paragraph 3, Chapter 6 used to find the screening coefficient. This leads to the relation $\alpha = 4\pi/k^2 \operatorname{Im} A$, where A is the amplitude of the field which is scattered forward by all particles. On the basis of the superposition principle $A = \sum A_j$, where A_j is the amplitude of the wave scattered forward by the particle j. By combining the last two relations together with formula (6.20) we see that $\alpha = \sum \sigma_j$, where σ_j is the attenuation coefficient due to the j-th particle. After the distribution function f(a) is introduced the last sum can be written in the form (7.3).

From the relation (7.3) and the equality $\sigma(\lambda, a) = \sigma_a (\lambda, a) + \sigma_a (\lambda, a)$, where σ_s and σ_a are the scattering and

absorption radiation coefficients with wavelengths λ obtained from a particle with radius a, we obtain automatically expressions for the semi-dispersed scattering and absorption coefficients $\alpha_s(\lambda)$ and $\alpha_a(\lambda)$:

$$\alpha_s^{a}(\lambda) = N \int_0^\infty \sigma_p^{a}(\lambda, a) f(a)\, da, \tag{7.4}$$

$$\alpha_a^{b}(\lambda) = N \int_0^\infty \sigma_a^{a}(\lambda, a) f(a)\, da. \tag{7.5}$$

Key: a. s
b. a

With the aid of the coefficient $\alpha(\lambda)$ we can write as usual the equation for the variation in the radiation intensity I propagated along a certain path

$$dI(\lambda) = -I(\lambda)\alpha(\lambda)\, dl. \tag{7.6}$$

Integrating (7.6) we obtain the well-known relation for the aerosol component of the transparent atmosphere

$$T(\lambda) = I/I_0,$$

where I_0 is the radiation intensity at the origin of the path:

$$T(\lambda) = \exp\left(-\int_{(l)} \alpha(\lambda, l)\, dl\right). \tag{7.7}$$

In (7.7) the integration is carried out over points of the path, and $\alpha(\lambda)$ generally varies over the beam path. This variation is related to the corresponding changes in the

dimension spectrum and in the particle concentration.

Relation (7.7) describes the variation in direct radiation intensity which carries one type of information or another. We note that it is not possible to record in the experiment only direct radiation since in order to do this receivers are needed with zero angular apertures. The angular aperture of the receiving system can be made, generally speaking, arbitrarily small, but not equal to zero. Therefore, the receiving systems always record together with the direct radiation attenuated in accordance with law (7.7) the light which is scattered once and several times by aerosol particles which are considered as one type of background noise. This fact is responsible for the dependence of the quantities which are measured (scattering coefficients, the quantity $T(\lambda)$ etc.) on the conditions of the experiment.

3. Studies of the Scattering Matrix

As we already noted in paragraph 2, Chapter 6, the scattering matrix M contains the total information about the light field which is scattered by the particles. If we know the components in this matrix, we can solve quantitatively any problems related to the scattering of waves by particles.

In spite of the obvious importance of the problem, the study of the matrix M for aerosols in the atmosphere does not yet have at its disposal a sufficient amount of data about the components of this matrix. This is explained, on one hand, both by the complexity of the corresponding theoretical and experimental studies and, on the other hand, by the fact that many practical problems can be solved without the components of the scattering matrix. For example, in many cases it is sufficient if the scattering or attenuation coefficients are known.

The matrix M has the simplest form in the case of molecular scattering:

$$M(\theta) = \frac{3}{4+3d}\begin{pmatrix} 1+\cos^2\theta+d & -\sin\theta & 0 & 0 \\ -\sin^2\theta & 1+\cos^2\theta & 0 & 0 \\ 0 & 0 & 2\cos\theta & 0 \\ 0 & 0 & 0 & 2\cos\theta \end{pmatrix}. \qquad (7.8)$$

During radiation scattering by atmospheric aerosol particles, the matrix M generally can have altogether 16 different components. However, the symmetry of various particles and their orientations in space reduce the number of independent components in the matrix and are responsible for the vanishing of some of these. Thus, for spherical particles, the matrix M has the form [504]:

$$M(\theta)=\begin{pmatrix} M_{11} & M_{12} & 0 & 0 \\ M_{21} & M_{22} & 0 & 0 \\ 0 & 0 & M_{33} & M_{34} \\ 0 & 0 & M_{43} & M_{44} \end{pmatrix}, \qquad (7.9)$$

where $M_{11} = M_{22}$; $M_{12} = M_{21}$; $M_{33} = M_{44}$; $M_{34} = M_{43}$.
Thus, for spherical particles there are only altogether four independent components which can be calculated using the corresponding formulas from Mi theory. An example of this type of calculation is the work of V. S. Malkova [505] in which all four components $M(\theta)$ were calculated for values of ρ from 0.1 to 1.0, $\theta = 0\ (5)\ 180^{\circ}$ and 13 values of the complex refractive index for water which are characteristic for the wavelength band from 2 to 12 μ.

The most complete experimental data about the components of the scattering matrix were obtained by the G. V. Rozenberg team [16, 506, 507, 897, 898], who started in 1959 the corresponding studies in the layer of the atmosphere near the earth's surface using specially developed apparatus. By processing many measurements carried out in various regions of the spectrum under different meteorological conditions, G. V. Rosenberg and his collaborators obtained quantitative data about all components of the matrix M. An analysis of this data made it possible to draw important conclusions about the presence of typical aerosol states in the layer of the atmosphere near the earth's surface (nebula, nebula mist, fog above the sea, and simply fog). To each of the states mentioned corresponds a set of angular relations for the components of the matrix M. We are not talking about the concrete dependence of the components on the angle θ since G. V. Rosenberg and his collaborators obtained, in fact, data for various concrete conditions, each of which can be related to a greater or lesser extent to conditions characterized by one of the aforementioned four aerosol states in the layer of the atmosphere near the earth's surface.

4. Energy Characteristics in the Scattering of Visible and Infrared Waves by Clouds and Nebulae

In the solution of many problems dealing with the propagation of visible and infrared waves in clouds and nebula, it is necessary to know which part of the incident radiation flux is deflected by this layer from its original direction due to aerosol attenuation, i.e., due to the scattering and absorption by particles in the layer. To give an answer to this question we must have the attenuation coefficients $\alpha(\lambda)$. For this reason in this paragraph we will focus the main attention on this quantity for water clouds and nebula. So far data for the coefficients $\alpha(\lambda)$ for cold and crystalline clouds and nebula have not been obtained.

1. Analytical Expressions for the Attenuation Coefficient and Averaged Attenuation Factor. Let $f(a)$ be the distribution function for the particles of a cloud or nebula by dimension. Then, assuming that we are dealing with spherical particles, we can write for the coefficient $\alpha(\lambda)$ and the geometrical cross section Q of the particle per unit volume:

$$\alpha(\lambda) = N \int_0^\infty \pi a^2 K(\rho, m) f(a)\, da, \tag{7.10}$$

$$Q = N \int_0^\infty \pi a^2 f(a)\, da. \tag{7.11}$$

The quantity

$$F = \frac{\alpha(\lambda)}{Q} = \frac{\int_0^\infty \pi a^2 K(\rho, m) f(a)\, da}{\int_0^\infty \pi a^2 f(a)\, da} \tag{7.12}$$

will be called the average attenuation efficiency factor. This nomenclature is justified in view of relation (7.12), which defines F as the usual statistical mean attenuation efficiency

factor for a single particle $K(\rho, m)$ with density function $\pi a^2 f(a)$. The function F is numerically equal to the ratio of the optical cross section of the particle per unit volume to the geometrical section.

It can be seen from (7.12) that the function F is independent of N and characterizes with an accuracy up to a constant multiplier the three-dimensional attenuation coefficient. The values of F are determined by the quantities m and λ (F is a function of λ because $\rho = \frac{2\pi a}{\lambda}$).

From (7.10) and (7.12) we obtain immediately the relation

$$\frac{F(\lambda_1, m)}{F(\lambda_2, m)} = \frac{\alpha(\lambda_1)}{\alpha(\lambda_2)}, \qquad (7.13)$$

which is valid for the given f(a) and m.

The values of the three-dimensional attenuation coefficients $\alpha(\lambda)$ and the average attenuation efficiency factors $F(\lambda, m)$ are the principal quantitative characteristics of the attenuated radiation by polydispersed aerosols. Naturally, the form of the formulas for $\alpha(\lambda)$ and $F(\lambda, m)$ depends to a considerable extent on the type of the distribution function for particles by dimension.

To explain the effect of the form of the function f(a) on the numerical values of $F(\lambda, m)$ we will calculate, using methods which will be discussed below, the values of F using for f(a) the lognormal and gamma distributions. Both these distributions, as we already have mentioned, approximate satisfactorily the experimental curves for the dimension spectra of particles in clouds and nebula. Calculations have shown that the use of the distributions is justified when the function F is calculated. The choice for f(a) of formula (5.3) or formula (5.4) depends on the concrete problem.

A formula for the function F, which is valid for any values of the parameter ρ and $m = 1.33$, was obtained by L. M. Levin [508] on the basis of the approximating expression proposed by him for the function $K(\rho)$ and the gamma distribution for the function f(a).

Using for "soft" transparent particles the approximate expression (6.42) for $K(\rho, m)$ obtained by G. Van-de-Huest [461] and the gamma distribution used for the function f(a), K. S. Shifrin and V. F. Raskin [509] obtained a formula for

the polydispersed scattering coefficient.

With the aid of the tables given in [509] the spectral transparency of water clouds and nebula in the visible region of the spectrum can be calculated also for those sectors of the infrared region where the complex refractive index of water can be ignored.

Deirmenjian [489] using the approximate expression (6.45) and (6.46) for $K(\rho, m)$ took into account when he calculated the coefficients $\alpha(\lambda)$ the complex refractive index of water in the infrared region and obtained the values of $\alpha(\lambda)$ for a model of a cloud in the visible and infrared regions up to the wavelength $\lambda = 13\ \mu$.

S. D. Tvorogov [510], using for the distribution function of aerosol particles the lognormal law, has shown that the function F is in this case the solution of an equation of the parabolic type with a certain initial condition. In [510] three parabolic equations are given with the initial conditions which are satisfied by the function F.

We emphasize that when the aforementioned statement was proved no constraints were imposed on the function $K(\rho, m)$. Therefore, the fundamental result in article [510] remains valid, if instead of the function $K(\rho, m)$ we take the scattering or absorption efficiency factor, the scattering indicatrix, or any other component of the scattering matrix. In this sense the result obtained in [510] is universal.

In articles [511] and [512] S. D. Tvorogov developed solution methods for the parabolic equations which he derived in [510]. The results from articles [510 - 512] can be used when any average components of the scattering matrix are calculated.

We obtained analytic expressions for the function F when the gamma distribution was used as the function f(a) in our articles [513 - 515]. We give the formulas for the function F:

$$F = \frac{\int_0^\infty \tau^2 f(\tau) K(x\tau, m)\, d\tau}{\int_0^\infty \tau^2 f(\tau)\, d\tau} = F(x, \mu, m), \qquad (7.14)$$

where

$$\tau=\frac{a}{r},\quad x=\frac{2\pi r}{\lambda}; \tag{7.15}$$

where r and μ are parameters of the gamma distribution.

Expression (7.14) follows immediately from (7.12) when (7.15) is taken into account.

Substituting (5.4) in (7.14), we obtain

$$F(x,\mu,m)=\frac{\mu^{\mu+3}}{\Gamma(\mu+3)}\int_0^\infty \tau^{\mu+2}e^{-\mu\tau}K(x\tau,m)\,d\tau. \tag{7.16}$$

Now, if we substitute in (7.16) the expressions (6.36) - (6.42) for the function $K(\rho, m) = K(x\tau, m)$ we obtain rather easily the explicit formulas for $F(x, \mu, m)$ for various cases. Here we will give without derivation only the expression for $F(x, m, \mu)$, which will be used further and which is obtained by substituting in (7.16) formulas (6.40) and (6.41) which describe the function $K(x\tau, m)$ for the case of "soft" large particles:

$$\begin{aligned}F(x,\mu,m)=2-\frac{4}{\mu+2}\frac{\sin[(\mu+2)\varphi-\beta]\,[\cos(\varphi+\beta)]^{\mu+3}}{\sin\varphi\,[\cos\beta]^{\mu+2}}-\\ -\frac{4}{(\mu+2)(\mu+1)}\frac{\cos[(\mu+1)\varphi-2\beta]\,[\cos(\varphi+\beta)]^{\mu+3}}{\sin^2\varphi\,[\cos\beta]^{\mu+1}}+\\ +\frac{4\cos^2\beta\cos^2(\varphi+\beta)}{(\mu+2)(\mu+1)\sin^2\varphi};\end{aligned} \tag{7.17}$$

$$\operatorname{tg}\varphi=\frac{u}{1+u\operatorname{tg}\beta};\quad \operatorname{tg}\beta=\frac{x}{n-1};\quad u=\frac{x'}{\mu};\quad x'=2x(n-1). \tag{7.18}$$

In the special case when m is real, we obtain from (7.17) and (7.18)

$$\begin{aligned}F(x,\mu,m)=2-\frac{4}{(\mu+2)}\frac{\sin[(\mu+2)\varphi]\,[\cos\varphi]^{\mu+3}}{\sin\varphi}-\\ -\frac{4}{(\mu+2)(\mu+1)}\frac{\cos[(\mu+1)\varphi]\,[\cos\varphi]^{\mu+3}}{\sin^2\varphi}+\frac{4\operatorname{ctg}^2\varphi}{(\mu+2)(\mu+1)},\end{aligned} \tag{7.19}$$

where

$$\operatorname{tg}\varphi = u = \frac{2}{\mu} x(n-1).$$

Formula (7.19) is also given in [509].

We note the following relations in the limit:

$$\lim_{x\to\infty} F(x, \mu, m) = 2, \quad \lim_{\mu\to 0} F(x, \mu, m) = 2,$$
$$\lim_{\mu\to\infty} F(x, \mu, m) = K(x, m). \tag{7.20}$$

We will now consider the approximate method for calculating the average efficiency factor for the radiation attenuated by water clouds and nebulae in the visible and infrared regions which we proposed in [513, 514]. The method presupposes that the complex refractive index for water and the real dimension spectrum of particles in clouds and nebulae described by the gamma distribution are taken into account. The method is based on the use of expression (6.45) - (6.46) for the efficiency attenuation factor of one particle K(ρ, m) which was obtained by Deirmenjian [489] by approximation.

Substituting (6.45) and (6.46) in (7.16), we obtain

$$F(x, \mu, m) = F_1(x, \mu, m) + F_2(x, \mu, m). \tag{7.21}$$

In the above the function F_1 is defined by expressions (7.17), (7.18), and

$$F_2(x, \mu, m) = \frac{\mu^{\mu+3}}{\Gamma(\mu+3)} \sum_{j=1}^{4} \int_{h_j}^{h_{j+1}} D_j(x'\tau_m) \times$$
$$\times K(x'\tau, m)\, \tau^{\mu+2} e^{-\mu\tau} d\tau, \tag{7.22}$$

where

$$h_1 = 0; \quad h_2 = 5(n-1); \quad h_3 = \frac{4{,}08}{1+3\operatorname{tg}\beta}; \quad h_4 = \frac{4{,}08}{1+\operatorname{tg}\beta}; \quad h_5 = \infty.$$

We tabulated the function F for various values of ϖ, β and μ which were selected in such a way that the range in which these were measured

m a d e it possible to obtain the three-dimensional attenuation coefficients in the visible and infrared radiation region in clouds and nebulae with various microstructure characteristics which occur under natural conditions.

Since $D(x'\tau)$ is a continuous function, the expression for F_2 can be written in terms of F_1 and B after the application of the mean value theorem to 7.22:

$$F_2(x, \mu, m) = F_1(x, \mu, m) D(x', \bar{\tau}, m), \tag{7.23}$$

where $\bar{\tau}$ is a quantity which depends, generally, on n, β, μ, and x'.

The function F_2 was calculated according to 7.22 by numerical integration for various x', μ, β and n, and then, using formula 7.23 the value of τ was found. It turned out that the results of the calculations according to 7.22 and 7.23 coincide with an error less than 5% if we set

$$\bar{\tau} = \frac{\mu+3}{\mu}. \tag{7.24}$$

Thus, substituting 7.23 in 7.21 we obtain ultimately for F

$$F(x, \mu, m) = F_1(x, \mu, m)[1 + D(x'\bar{\tau}, m)]. \tag{7.25}$$

We use expression 7.25 and 7.24 to calculate the function F (x, μ, m) and the three-dimensional attenuation coefficients $\alpha(\lambda)$ for clouds and nebulae. Our estimates have shown, that the approximate method which was described, yields an error in the values of $K(\rho, m)$ which does not exceed 5-7% when compared with the values obtained by using the tabular values of the function $K(\rho, m)$ from [470] which were calculated from the exact formulas o f Mi theory. The accuracy mentioned above is fully adequate for practical purposes and for interpreting quantitatively the experimental data.

2. Calculation of Attenuation Coefficients.

The most complete computational data about the attenuation coefficients $\alpha(\lambda)$ for water clouds and nebulae in the spectral region 0.5-14 μ which take into account the real polydispersed particles and the complex refractive index were obtained in our study [516] which is described in detail in monograph [1]. In [1] the results of calculations of $\alpha(\lambda)$ carried out by Diermejian for two concrete models of a cloud [489,517] in the spectral region 0.45-16.6 μ are also discussed, as well as data about

calculations of the efficiency factor F obtained by L. M. Levin [508] for various models of a cloud without taking into account the complex refractive index for water.

Our calculations and those of Deirmejian were based on the data about the complex refractive indices of water published by Centeno as early as 1941 [518], which are still considered as the most complete and reliable data. However the detailed comparison of all known values of the complex complex refractive index components of water in the infrared region which we carried out, showed large scatter in the data of various investigators. Keeping in mind this fact, and also the fact that the coefficients $\alpha(\lambda)$ depend, to a considerable extent, both on the real n and the imaginary κ parts of the complex complex refractive index for water, we attempted in our laboratory to redefine these quantities. On the basis of the data obtained for the quantities n and κ for various wavelengths in the region from 0.5 to 25 μ, we recalculated the coefficients $\alpha(\lambda)$.b Below we present briefly the results obtained from a study of the components of the complex refractive index for water, and the data from the corresponding calculations of the coefficients $\alpha(\lambda)$.

1. Components of the complex refractive index of water in the spectral region 0.5-25 μ. The apparatus and measurement methods for the refractive index and the absorption index for water in the spectral region from 0.5 to 25 μ are described in detail in our articles [519-521].

Figure 7.1 shows the curves obtained in [520] for the relation between the refractive index, the absorption index κ and the wavelength in the spectral region from 2.5 to 25 μ. A comparison of the values of n and κ obtained by us and other investigators in various regions of the spectrum is plotted in Figure 7.2.

The method used in [519-520] to determine the quantity κ from the refraction spectra in the region where the values of κ are small, does not yield sufficient accuracy of the results obtained. In this connection in [521] the quantity κ in this region was determined again using a method based on transmission spectra. In addition to this, the spectral region in which n and κ were measured was extended in [521]. The results obtained are plotted in Figures 7.3 and 7.4. To find the value of the absroption index $\kappa(\nu)$ from the known data for $\alpha(\lambda)$ we must use formula (7.26).

$$\kappa(\nu)=\frac{\alpha(\nu)}{4\pi\nu}. \qquad (7.26)$$

The data which are plotted in Figures 7.3 and 7.4 were determined with a relative error not exceeding 1% for n and 4% for α.

Keeping in mind the inconveniences which arise when graphs are used in practical work, we give in Supplement 2 detailed tabular data for the quantities n and κ which we obtained in the spectral region from 0.54 to 25 μ

Fig. 7.1. The refractive index n and the absorption index κ of water versus the wavelength in the spectral region 2.5-25 μ.

Key: a. μ

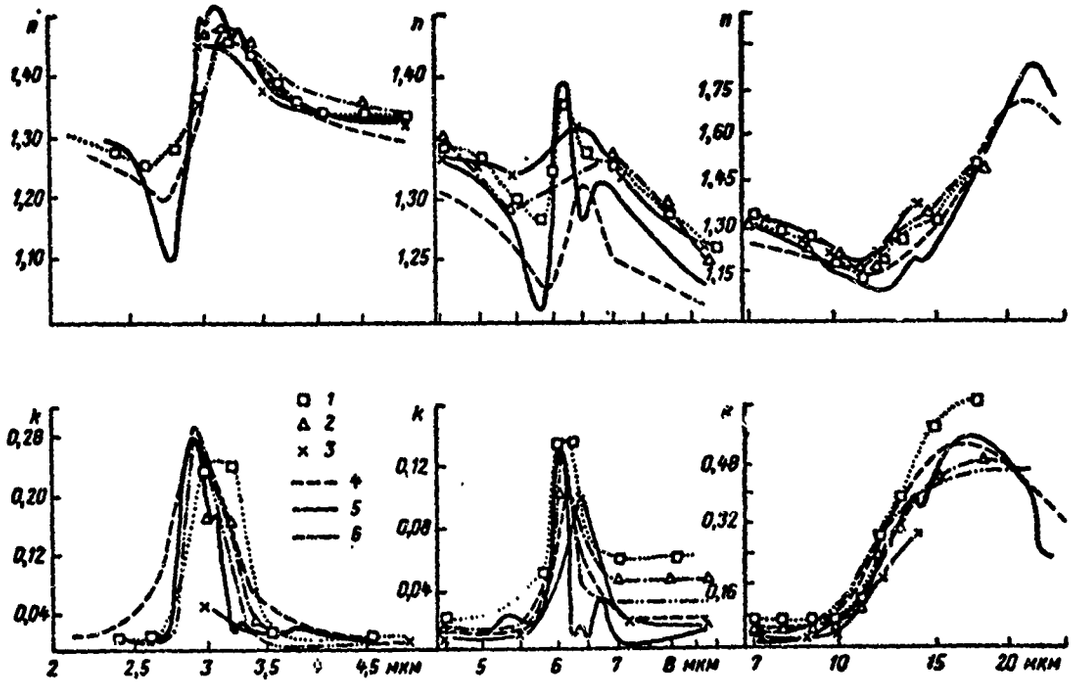

Fig. 7.2. The refractive index n and the absorption index κ of water in the region from 2.5 to 25 μ: 1. data from [522], 2. data from [467], 3. data from [558], 4. data from [523], 5. data from [520], 6. data from [524].

2. Attenuation coefficients. A new series of calculations of the attenuation coefficients $\alpha(\lambda)$ for water clouds and nebulae which take into account the real dimension spectra of particles and the data obtained by us for the components of the complex refractive index of water was made using the approximate method described in paragraph 1. The calculations were carried out for the values of the microstructure parameters r (the most probable radius of the particles) and μ (a characteristic of the distribution half-width), which were equal to respectively: 0.1,0.5, 1.0, 2.0, 6.0, 10.0 μ and 1, 2, 3, 6, and 10. The set of wavelengths for which the $\alpha(\lambda)$ was calculated was determined by the corresponding behavior of the components of the complex refractive index of water. We attempted to take into account all characteristics of this relationship. In addition to this, we selected a series of wavelengths which corresponded to the radiation frequencies of the most widely used lasers.

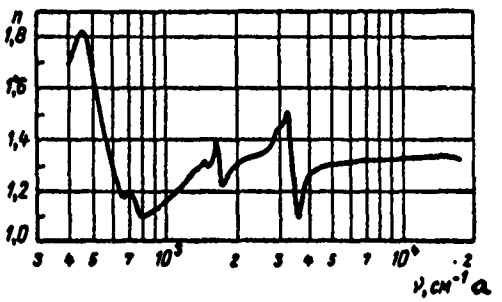

Fig. 7.3. The refractive index of water versus the wavelength in the spectral region 0.5-25 μ.

Key: a. cm^{-1}

The detailed data for our calculations are given in article [525]. Figures 7.5-7.8 and Table 7.3 give certain illustrations of these results, which show the substantial effect of the values of the microstructure parameters and the components of the complex refractive index of water on the value of the attenuation coefficient $\alpha(\lambda)$ and its spectral path.

Table 7.3 gives data about the attenuation coefficients $\alpha(\lambda)$ for clouds and nebula for the following characteristics which are encountered most frequently under natural conditions: 1) the most probable radius r = 6 μ, 2) the parameter of the distribution half-width μ , 3) the meteorological visibiltiy range S_M = 0.2 km.

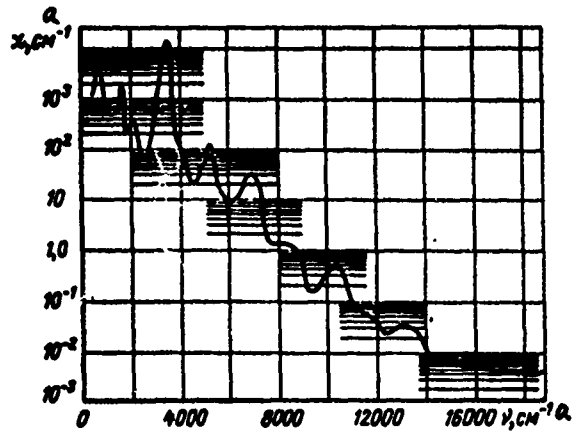

Fig. 7.4. The absorption coefficient of water versus the wavelength in the spectral region 0.5-25 μ.

Key: a. cm^{-1}

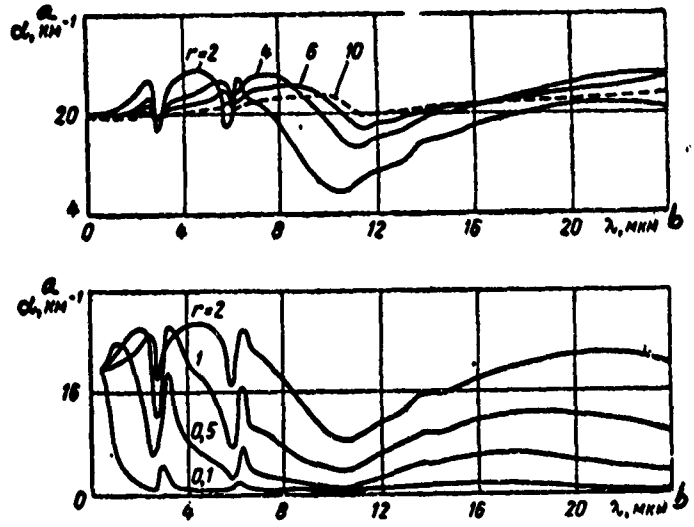

Fig. 7.5. Attenuation coefficients of water clouds and nebulae in the wavelength range 0.5-25 μ.

Key: a. km^{-1}
b. μ

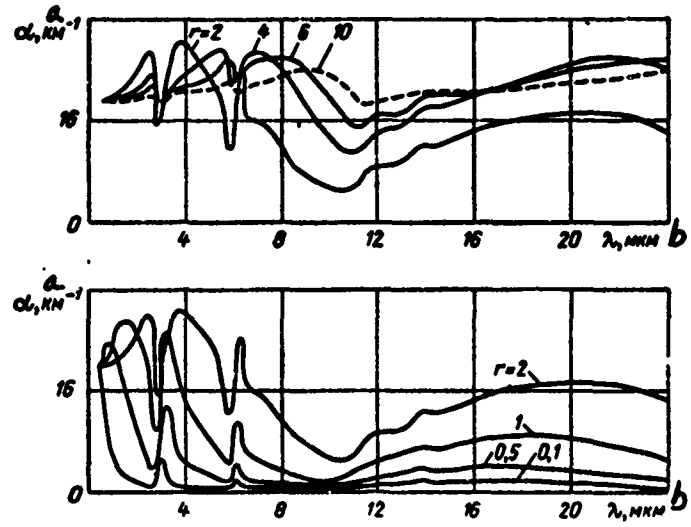

Fig. 7.6. Attenuation coefficients of water clouds and nebulae in the wavelength range 0.5-25 μ for μ = 4, r = 0.1, 0.5, 1, 2, 4, 6, 10 μ and S_M = 0.2 km.

Key: a. km-1
b. μ

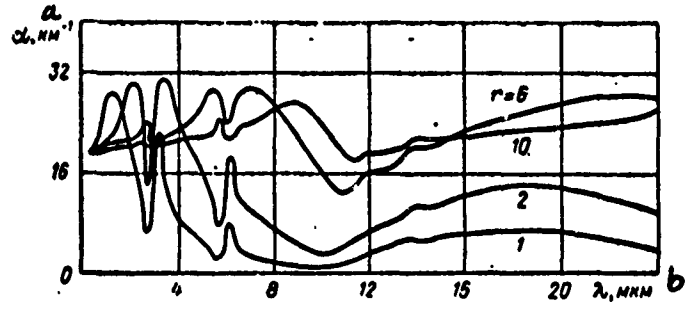

Fig. 7.7. Attenuation coefficients of water clouds and nebulae in the wavelength interval 0.5-25 μ for μ = 10, r = 1, 2, 6, 10 μ and S_M = 0.2 km.

Key: a. km-1
b. μ

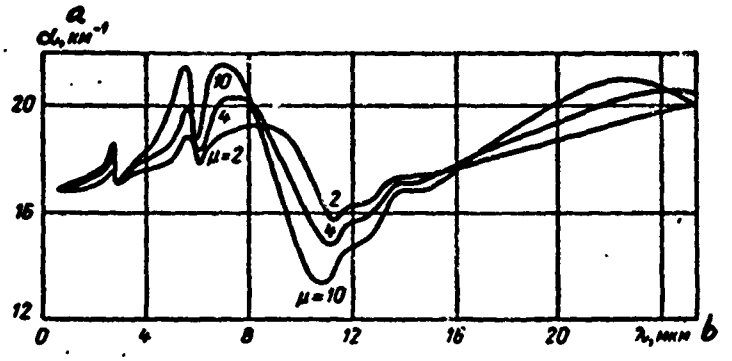

Fig. 7.8. Attenuation coefficients for water clouds and nebulae in the wavelength interval 0.5-25 μ for r = 6 μ, μ = 2, 4, 10 and S_M = 0.2 km.

Key: a. km^{-1}
b. μ

TABLE 7.3

THE COEFFICIENTS α(λ) FOR THE MOST PROBABLE VALUES OF THE MICROSTRUCTURE PARAMETERS OF CLOUDS AND NEBULAE FOR THE METEOROLOGICAL VISIBILITY RANGE S_M = 0.2 KM OR THE TRUE PARTICLE CONENTRATION N = 28 cm^{-3}

λ	α (λ)	λ	α (λ)	λ	α (λ)	λ	α (λ)
0,31	19,5	1,18	19,9	2,94	20,1	6,15	21,6
0,51	19,6	1,24	19,9	3,12	20,3	6,21	21,9
0,53	19,6	1,26	20,0	3,34	20,6	6,27	22,1
0,56	19,6	1,39	20,0	3,39	20,7	6,44	2
0,59	19,7	1,43	20,0	3,51	20,8	6,66	23,1
0,625	19,7	1,45	20,0	3,58	20,9	7,69	24,1
0,63	19,7	1,47	20,1	3,85	21,0	8,36	24,6
0,67	19,7	1,56	20,1	4,17	21,4	10,04	22,0
0,69	19,7	1,67	20,1	4,55	21,6	10,6	19,6
0,71	19,7	1,79	20,2	4,77	21,8	11,29	17,3
0,77	19,7	1,82	20,2	5,00	22,0	11,42	17,5
0,31	19,7	1,89	20,2	5,13	22,1	11,56	18,0
0,84	19,7	1,94	20,2	5,27	22,2	12,42	18,6
0,91	19,8	2,00	20,3	5,41	22,6	13,79	20,5
0,97	19,8	2,22	20,4	5,56	23,5	14,18	20,6
1,01	19,8	2,36	20,5	5,82	23,7	14,38	20,6
1,05	19,9	2,50	20,6	5,87	22,7	16,81	21,8
1,06	19,9	2,63	20,8	5,93	22,0	17,39	22,0
1,11	19,9	2,71	21,0	5,98	21,6	22,47	24,5
1,13	19,9	2,78	20,0	6,03	21,4	25,31	25,8
1,15	19,9	2,91	20,0	6,09	21,4		

The coefficients $\alpha(\lambda)$ for other values of S_M are easily obtained from the data in Table 7.3, since the quantity $\alpha(\lambda)$ is inversely proportional to the value of S_M.

Figure 7.9 gives a comparison of the results of our calculations of the coefficients $\alpha(\lambda)$ which were m a d e on the basis of the Centeno data for the complex refractive index of water and on the basis of our data. It can be seen from the figure that in a number of spectral regions the new data which we obtained for the coefficient $\alpha(\lambda)$ differ substantially from the old data.

It should be noted that the calculations in [525] cover practically all possible realizations of the parameter values of the microstructure of water clouds and nebulae with the exception of the largest drop formations for which, as we can see from Figures 7.5-7.8 and from qualitative considerations, $\alpha(\lambda)$ can be considered with sufficient accuracy to be independent of the wavelength. We also note that during the calculations the distribution function by dimension for the particles used was the gamma distribution, which describes the unimodal curves in the dimension spectra of the particles. The results of the calculations cannot be applied to other distributions of particles by dimension. However, as we have shown in Chapter 5, most data about the dimension spectra of particles in clouds and nebulae are approximated sufficiently well by the gamma distribution.

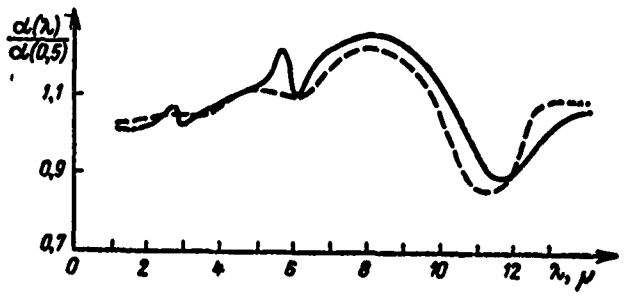

Fig. 7.9. Comparison of the results of calculations of the attenuation coefficients for water clouds and nebulae in the wavelength interval 0.5-14 μ m a d e on the basis of the Centeno data[518] (dotted curve) and the author's data[520] (solid curve), for the components of the complex refractive index of water for the microstructure parameters $\mu = 2$, $r = 6$ μ.

Finally we emphasize again that the coefficients $\alpha(\lambda)$ describe the attenuation of radiation propagated in the direction of the straight line from the source to the receiver. During experimental studies of the aerosol component of cloud and nebular transparency of visible and infrared waves, the receiving system records together with the direct attenuated radiation, the scattered radiation. The question of the limits of applicability of the data obtained for the coefficient $\alpha(\lambda)$ to determine the transparency of clouds and nebulae for various concrete sources and receivers will be considered in paragraph 9.

3. Experimental study of attenuation coefficients. The most complete experimental data for the coefficients $\alpha(\lambda)$ for various values of the microstructure parameters of artificial nebulae were obtained in our articles [513,526-529, 702], which are described in detail in monograph [1] where also the main results of other investigators [379,530-537] are discussed.

The available experimental data were analyzed and compared with the calculated values of $\alpha(\lambda)$ in [1]. The analysis has shown satisfactory qualitative agreement between the experimental data of various authors. A quantitative comparison cannot be made in most cases, because the corresponding published work does not have the necessary information about the microstructure of the clouds and nebulae in which the measurements were made.

A comparison of the experimental and calculated data for the quantity $\alpha(\lambda)$ obtained in our work has shown considerable discrepancies between the data. This discrepancy has also been noted by a number of other investigators. As a rule the measured coefficients $\alpha(\lambda)$ turn out, to be larger than the coefficients calculated from the data of simultaneous microstructure studies. In this respect, it is important that the reasons for these discrepancies be elucidated.

When the results of the first series of measurements were analyzed, the hypothesis was made that the absolute concentration of the particles which was determined using flux traps for this purpose was not correct. Assuming that the traps, for some reason, do not collect all drops from the corresponding volume, we arrive immediately at the conclusion that the coefficients calculated from the microstructure data from the traps will be smaller than the experimental data.

To confirm this hypothesis, in the second series of measurements we set up special tests in which the coefficients $\alpha(0.42$ were measured simultaneously with the aid of a photometer, and the water content, using two methods, with the aid of filters [529] and the microstructure measurement data.

From these measurements we found out that the water content which was determined with the aid of filters, exceeded in all cases the calculated water content using the data of simultaneous microstructure flux trap measurements. The coefficient $\alpha(0.42)$ which was measured with the aid of a photometer turned out to be directly proportional to the water content which was determined using the filtration method. The relation which was obtained was approximated by the expression

$$\alpha(0,42)\ [\text{см}^{-1}] = 2{,}04 \cdot 10^{-3} q\ [\text{г/м}^3]. \tag{7.27}$$

(a) (b)

Key: a. cm^{-1}
b. g/m^3

An analogous relation is easily obtained from the formulas

$$\alpha(0,42) = 2Q = 2N \frac{\pi d_2^2}{4} 10^{-6}\ [\text{см}^{-1}], \tag{7.28}$$

(a)

Key: a. cm^{-1}

$$q = N \frac{\pi d_3^3}{6} 10^{-6}\ [\text{г/м}^3]. \tag{7.29}$$

(b)

Key: b. g/m^3

Here d_2 and d_3 are the mean squared and mean cubed diameters in the distribution of the drops by dimensions (in microns).

From (7.28), (7.29) we obtain

$$\alpha(0,42) = 3 \frac{d_2^2}{d_3^3} 10^{-3} q\ [\text{см}^{-1}]. \tag{7.30}$$

(a)

Key: a. cm^{-1}

To compare the empirical (7.27) and theoretical (7.30) dependence of $\alpha(0.42)$ on q using the data of microstructure measurements, the d_2^2/d_3^3 were calculated for each water content value. The mean value of this ratio turned out to be equal to 0.0714 which, when substituted in (7.30) leads to the expression

$$\alpha(0,42) = 2{,}14 \cdot 10^{-3} q. \tag{7.31}$$

It can be seen from (7.27) and (7.31) that these expressions are very close.

A more detailed comparison of the water content measured using the filter method and calculated according to (7.30), for each measurement is given in Figure 7.10. To calculate q from (7.30), the values of $\alpha(0.42)$ were found from photometer measurements, and the ratio d_2^2/d_3^3 was determined from the data of the flux traps.

It turns out that the relation between the calculated and measured water content values q_t and q_ϕ can be approximated by the equation of a straight line

$$q_t = 0{,}983 q_\phi - 0{,}01, \tag{7.32}$$

which indicates good agreement between the calculated and measured water content values.

Thus, the complex measurements which were carried out have shown the validity of the assumption that the large discrepancie between the calculated and measured absolute values of the three-dimensional attenuation coefficients are due to the incorrect data for the absolute concentration of particles collected with the aid of flux traps.

4. Repeatability of various values of meteorological range visibility in clouds and nebulae. In the solution of many problems it is necessary that we know how often certain types of clouds or nebulae with a given value of the meteorological visibility range S_M or particle concentration N or water content Q are encountered. The quantities are related to one another by the relations:

$$N = \frac{3{,}912\mu^2}{S_M F(0{,}5)\pi r^2(\mu+2)(\mu+1)}, \tag{7.33}$$

$$Q = \frac{3{,}912 \cdot 4r(\mu+3)d}{3 \cdot S_M F(0{,}5)\mu} \tag{7.34}$$

and formula (7.11), where μ and r are parameters of the gamma distribution by dimension for the particles, F(0.5) is the effective attenuation factor for the wavelength $\lambda = 0.5\ \mu$, and d is the density of water.

We are aware of only one study made by G. M. Zabrobskiy [535] in which a repeatability table for various values of the meteorological visibility range S_M in clouds and nebulae was obtained on the basis of direct measurements made in the arctic region in the warm period of the year (203 measurements in nebulae 1457 measurements in St, 433 in Sc and 148 in Ns-As) (see table 7.4).

If we use the data about water content repeatability in clouds obtained by V. E. Minervim [391] on the basis or a treatment of 5000 water content measurements made from aircraft over various regions in the USSR on the basis of formula (7.33), then for the interval of the most probable values of the meteorological visibility range we obtain S_M = 388-130 m. To obtain this interval the most probable water content values between the limits 0.1-0.3 g/m^3. were used [391] and data for the microstructure parameters r = 6 μ and μ = 2.

In conclusion we give in Table 7.5 values of the water content Q and the particle concentration N in clouds and nebulae for certain characteristic selected values of the microstructure parameters at a meteorological visibility range of S_M = 0.2 km. The data in the table were calculated using formula (7.33), (7.34). It can be seen from the table that for the same value of S_M = 0.2 km the water content and the particle concentration in various clouds and nebulae can vary between the limits 0.015 to 0.324 g/m^3 and from 2.3 to 2.050 particles per cm^{-3}.

5. Determination of the aerosol transparency component in the infrared region from the data in the visible region of the spectrum. The possibility of determining the spectral transparency of clouds and nebulae in the infrared region from the data about the transparency in the visible wavelength range is very deceptive, since the latter problem can be solved both theoretically and experimentally much more simply. It suffices to say that the transparency in the visible region of $T_\alpha(0.5)$ can be determined from visual measurements of the meteorological visibility range S_M using the well-known relation in [539] (if we take for the contrasting eye sensitivity threshold the value 0.02).

$$T_a(0,5) = e^{-3,912\frac{l}{S_M}}, \tag{7.35}$$

where l is the distance and

$$\alpha(0,5) = \frac{3,912}{S_M}. \tag{7.36}$$

We write the expression for the spectral transparency for the wavelength λ

$$T_a(\lambda) = e^{-\alpha(\lambda)l}.$$

From the last expression and from (7.36), we obtain

$$T_a(\lambda) = e^{-\omega(\lambda)3,912\frac{l}{S_M}} = [T_a(0,5)]^{\omega(\lambda)}, \tag{7.37}$$

where

$$\omega(\lambda) = \frac{\alpha(\lambda)}{\alpha(0,5)} = \frac{F[x(\lambda), \mu]}{F[x(0,5), \mu]}. \tag{7.38}$$

We obtain the ratios of $\alpha(\lambda)/\alpha(0.5)$ for various values of the parameters of the microstructure for condensed clouds and nebulae in the wavelength range 0.5-25 μ on the basis of new data for the complex refractive index of water (see paragraph 2 in the given section).

The use of this data together with the given values of the meteorological visibility range S_M or the coefficient α (0.5) solves the probelm which has formulated.

It can be seen from Figures 7.5-7.8 that the same value of the meteorological visibility range S_M, or equivalently, the transparent atmosphere in the visible region $T_\alpha(0.5)$ correspond to various values of the transparency $T_\alpha(\lambda)$ for a given wavelength in the infrared region, which depend on the values of the parameters of the microstructure r and μ. For concrete values of these parameters between $T(\lambda)$ and $T(0.5)$ or S_M there is a unique relation.

In practice, when this method is used to solve many problems in the range in which the parameters r and μ vary, we can restrict ourselves to their most probable values given in Table 5.2 for various clouds and nebulae. The values of the meteorological visibility range S_M encountered most frequently in clouds and nebulae of various types are given in Table 7.4.

The essential advantage of the method proposed for determining the spectral transparency of clouds and nebulae in the infrared region from the data about the transparency in the visible region of the spectrum is that it does not require data about the concontration of aerosol particles which are determined only with difficulty during the experiment.

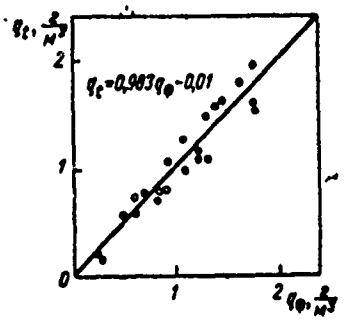

Fig. 7.10 Calculated q_t versus q_ϕ determinded in experiments from the humidities in an artificial nebula.

TABLE 7.4

REPEATABILITY IN % OF METEOROLOGICAL VISIBILITY RANGE IN IN VARIOUS CLOUDS AND NEBULAE DURING THE WARM PERIOD OF THE YEAR IN THE ARCTIC REGION ACCORDING TO THE DATA OF G. M. ZABRODSKIY [535]

a Вид облаков	$S_м$, м e					
	b меньше 26	27—50	51—100	101—200	201—300	301—400
St	0,1	2,0	21,7	36,1	21,4	5,6
Sc	0,5	2,1	18	35,6	21,1	7,1
Ns—As	8,1	5,4	10,1	33,1	20,3	12,2
c Туманы	1,0	5,4	10,3	32,9	21,7	11,3

TABLE 7.4 continued

a Вид облаков	$S_м$, м e						
	401—500	501—600	601—700	701—800	801—900	901—1000	d больше 1000
St	4,4	4,2	2,7	1,5	0,7	0,1	—
Sc	5,3	4,9	0,2	1,8	1,1	0,7	0,5
Ns—As	2,7	2,0	1,3	2,7	1,4	0,7	—
c Туманы	6,9	6,4	1,0	0,6	1,9	0,5	1,0

Key: a. Type of clouds
e. m
b. Less than
c. Nebulae
d. Above

TABLE 7.5

WATER CONTENT Q AND CONCENTRATION OF PARTICLES IN SEVERAL WATER WATER CLOUDS AND NEBULAE

a Характер облака	b Значения параметров микроструктуры		$S_м$, км	Q, г/м³	N, см⁻³
	r, мкм	μ			
c Мелкокапельное	1 1	2 10	0,2	0,031 0,015	971 2050
d Облако со средними размерами частиц	6 6	2 10	0,2	0,194 0,101	28 65
e Крупнокапельное	10 10	2 10	0,2	0,324 0,168	10 2,3

[See key on following page]

Key: a. Type of cloud
b. Values of microstructure parameters
c. Small drops
d. Cloud with mean dimension of particles
e. Large drops
f. km
g. g/m^3
h. cm^{-3}

5. Energy Characteristics of the Scattering of Visible and Infrared Waves by Mists

1. Attenuation coefficients

1. Theoretical studies

The theoretical study of the attenuation coefficients of polydispersed aerosols consisting of "soft" transparent particles with distribution functions by dimension described by the Young formula, the gamma distribution with the parameter $\mu = 2$, and the generalized gamma distribution, were carried out by K. S. Shifrin and V. F. Raskin [540-542].

L. S. Ivlev and E. L. Yanchenko [821] calculated the attenuation coefficients for polydispersed aerosols consisting of transparent particles with the refractive index m = 1.5, 1.73. For the distribution functions of the particles by dimension he used the Young formula with parameter values $\beta = 2, 2.5, 3, 3.5, 4$, and a low and upper bound on the dimensions $a_1 = 0.08\ \mu$ and $a_2 = 1.3\ \mu$ and distributions of the type obtained in articles [810] and [811]. It has been shown in [821] that in the real atmosphere, the attenuation coefficients in the visible region of the spectrum can differ substantially both in their spectral behavior as well as in their absolute values.

Deirmejian [489, 517] calculated the attenuation coefficients $\alpha(\lambda)$ for several models of mist taking into account the complex refractive index of water in the spectral region up to 13 μ.

In paper [543], the coefficients $\alpha(\lambda)$ were calculated for mist and the dimension spectrum of the particles which was described by the Young formula with parameter values of $\beta = 3, 4, 5$, taking into account the complex refractive index of water.

The minimum and maximum values of the radii of the particles which were adopted were 0.1 and 1.0 μ. The calculations were made in the wavelength range 0.5-14 μ. The values of the coefficients $\alpha(\lambda)$ which were obtained were conveniently represented in the form of the ratio $\alpha(\lambda)/\alpha(0.5) = \omega(\lambda)$.

When $\omega(\lambda)$ is known, the value of the attenuation coefficient $\alpha(\lambda)$ of the atmospheric mist is easily calculated for various values of the meteorological visibility range S_M:

$$\alpha(\lambda) = \frac{3,912}{S_M}\omega(\lambda) \ [км^{-1}]. \qquad (7.39)$$

An new series of data about the coefficients $\alpha(\lambda)$ was obtained by us on the basis of more precise values of the complex refractive index of water (see paragraph 4 and Supplement 2).

The calculuations were made for many wavelengths in the visible and infrared rgions in the range from 0.3-25 μ. Several values were taken for the minimum and the maximum dimensions of the particles, mainly a_1 = 0.01, 0.05, 0.1 μ and a_2 = 1.0, 5.0, 10 μ. This enabled us to clarify the contribution to the magnitude of the coefficients $\alpha(\lambda)$ of the proportions of particles with different dimensions. The results of the the new calculations of $\alpha(\lambda)$ are discussed in articles [544]. Some of the data obtained were plotted in Figures 7.11-7.13.

It can be seen from these figures that the most important effect on the spectral behavior of the coefficients $\alpha(\lambda)$ in mist is exerted by the parameter β, which characterizes the curvature of the distribution curve of the particles by dimension described by the Young formula. The contribution of the slow motion of particles which form small drops (dimensions a_1 from 0.1 to 0.01 μ) to the value of the attenuation coefficient is negligibly small, in spite of the fact that the concentration of these particles, in accordance with the Young formula, is very high.

Figure 7.14 compares the second series of our calculations of the coefficients $\alpha(\lambda)$, which shows a substantial discrepancy between these individual spectral regions.

Figures 7.15-7.17 show the curves for the aerosol component of the spectral mist transparency $T_a(\lambda)$, calculated using the new data for the coefficients $\alpha(\lambda)$.

Table 7.6 gives the values of the coefficients $\alpha(\lambda)$ obtained by us for the most probable values of the parameters of the mist microstructure: $\beta = 4$, $a_1 = 0.05$ μ, $a_2 = 5.0$ μ, for the meteorological visibility range in the layer of the atmosphere near the earth's surface S_M = 10 km. The coefficients $\alpha(\lambda)$ for other values of S_M are obtained directly from Table 7.6, since their values are inversely proportional to S_M.

We will now consider the limits of applicability of the data obtained for the coefficients $\alpha(\lambda)$. We will analyze two assumptions which are used during the calculations: 1) the

mist particles are assumed to be spherical water particles, 2) the dimension spectrum is described by the empirical Young formula.

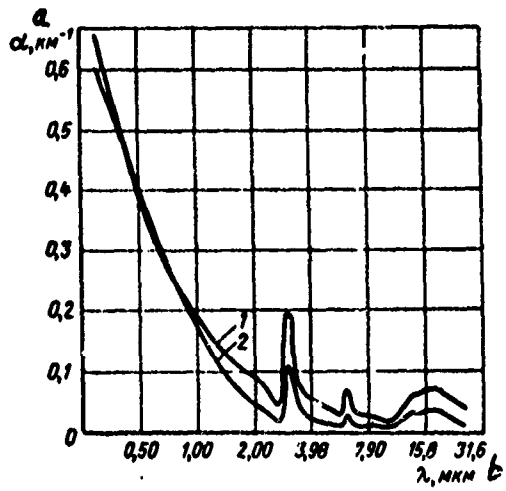

Fig. 7.11. Attenuation coefficient for mist in the wavelength range 0.3-25 μ for S_M = 10 km, β = 4, a_1 = 0.1μ, a_2 = 1.0 μ (curve 1), β = 1, a_1 = 0.01 μ, a_2 = 10 μ (curve 2).

Key: a. km^{-1}
b. μ

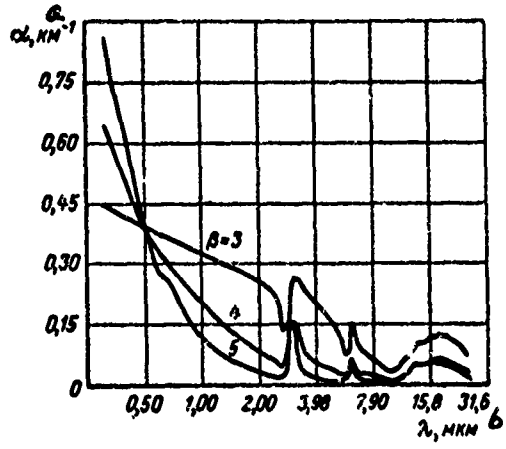

Fig. 7.12. Attenuation coefficients in mists for the wavelength range 0.3-25 μ for S_M = 10 km, a_1 = 0.05 μ, a_2 = 5.0 μ.

Key: a. km^{-1}, b. μ

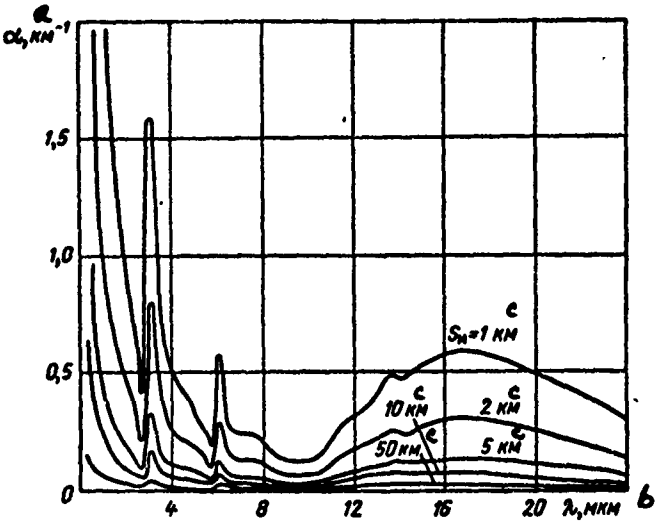

Fig. 7.13. Attenuation coefficients for mist in the wavelength range 0.3-25 μ for various values of S_M for $\beta = 4$, $a_1 = 0.05$ μ, $a_2 = 5.0$ μ.

Key: a. km^{-1}
b. μ
c. km

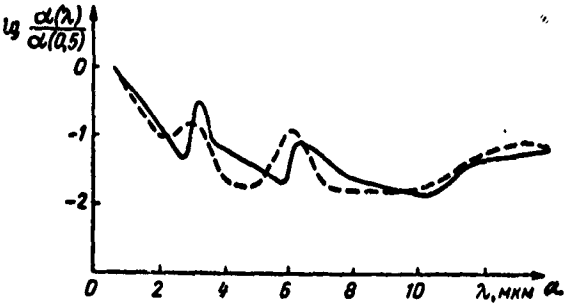

Fig. 7.14. Comparison of attenuation coefficients for mist in the wavelength range 0.5-14.0 μ calculated from the Centano data [518] for the complex refractive index of water and the author's data for the microstructure parameters $\beta = 4$, $a_1 = 0.1$ μ, $a_2 = 1$ μ.

Key: a. μ

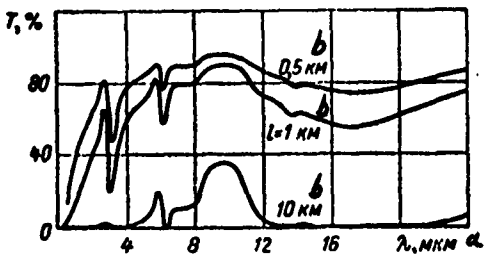

Fig. 7.15. Aerosol components of spectral transparency of mist in the wavelength range 0.3-25 μ for S_M = 1 km, $\beta = 4$, $a_1 = 0.05$ μ, $a_2 = 5.0$ μ.

Key: a. μ
b. km

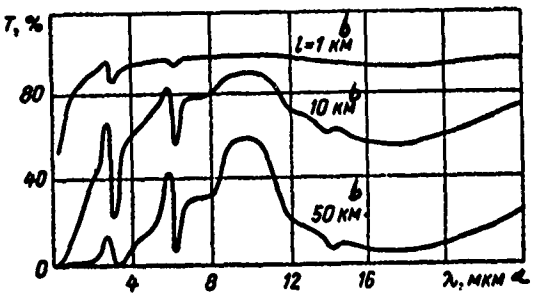

Fig. 7.16. Aerosol components of spectral transparency of mist in the wavelength range 0.3-25 μ for S_M = 1 km, $\beta = 4$, $a_1 = 0.05$ μ, $a_2 = 5.0$ μ.

Key: a. μ
b. km

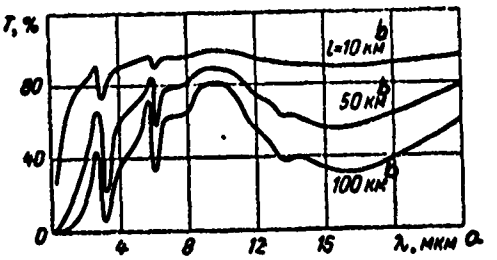

Fig. 7.17. Aerosol components of spectral transparency of mist in the wavelength range 0.3-25 μ for S_M = 50 km, $\beta = 4$, $a_1 = 0.05$ μ, $a_2 = 5.0$ μ.

Key: a. μ, b. km

TABLE 7.6

THE COEFFICIENT $\alpha(\lambda)$ FOR THE MOST PROBABLE VALUES OF THE MICROSTRUCTURE PARAMETERS AND THE METEOROLOGICAL VISIBILITY RANGE S_M = 10 km IN THE ATMOSPHERE LAYER NEAR THE SURFACE OF THE EARTH.

λ, мкм a	α (λ), км⁻¹ b	λ, мкм a	α (λ), км⁻¹ b	λ, мкм a	α (λ), км⁻¹ b	λ, мкм a	α (λ), км⁻¹ b
0,31	0,65	1,18	0,17	2,94	0,16	6,15	0,05
0,50	0,40	1,24	0,15	3,12	0,13	6,21	0,04
0,53	0,38	1,26	0,15	3,34	0,09	6,27	0,04
0,56	0,36	1,39	0,14	3,39	0,08	6,44	0,03
0,59	0,34	1,43	0,13	3,51	0,07	6,66	0,02
0,625	0,32	1,45	0,13	3,58	0,06	7,69	0,02
0,63	0,32	1,47	0,13	3,85	0,05	8,36	0,01
0,67	0,30	1,56	0,12	4,17	0,05	10,04	0,01
0,69	0,29	1,67	0,11	4,55	0,04	10,6	0,01
0,71	0,26	1,79	0,10	4,77	0,04	11,29	0,02
0,77	0,26	1,82	0,10	5,00	0,03	11,42	0,02
0,81	0,25	1,89	0,10	5,13	0,03	11,56	0,03
0,84	0,24	1,94	0,09	5,27	0,03	12,42	0,03
0,91	0,22	2,00	0,09	5,41	0,03	13,79	0,05
0,97	0,21	2,22	0,08	5,56	0,02	14,18	0,05
1,01	0,20	2,36	0,07	5,82	0,02	14,38	0,05
1,05	0,19	2,50	0,06	5,87	0,02	16,81	0,06
1,06	0,18	2,63	0,05	5,93	0,03	17,39	0,06
1,11	0,18	2,71	0,04	5,98	0,04	22,47	0,04
1,13	0,17	2,78	0,06	6,03	0,05	25,31	0,02
1,15	0,17	2,91	0,15	6,09	0,06		

Key: a. μ
b. km^{-1}

The results which were obtained strictly speaking, cannot be applied to mist which consists of other than only condensed two layer particles with hard nuclei. However, as shown in article [484, 486], the admissible error which occurs when the two-layer form of the particles is ignored is small, when the dimension of the hard nuclei are considerably smaller than the dimensions of the water shells. If the mist particles have nonspherical form, then the results obtained must be considered as a certain approximation of reality, keeping in mind that the chaotic orientation of the particles makes it possible, in principle, to find a spherical dimension spectrum for the particles which is equivalent with respect to the attenuated radiation.

As we already mentioned in Chapter 5, the Young formula gives an approximate idea about the real dimension spectrum of atmospheric aerosol particles which are obtained, as a rule, after a large number of particle distributions by dimension which occurred are averaged. In this regard, the data obtained about the polydispersed attenuation coefficients in mist must be considered as certain mean characteristics. In every concrete case, the coefficients $\alpha(\lambda)$ will differ from those calculated with the aid of the Young formula. However, to calculate the value of $\alpha(\lambda)$, using real distributions by dimension for the particles, so far the data available for these distributions are completely inadequate.

2. Experimental studies. Most experimental studies consider the visible region of the spectrum. This is explained by the fact that measurements are made comparatively easily in this region, and that the radiation is almost not absorbed at all by gases in these regions, so that the quantity which interests us is easily obtained from the measurement results corrected for molecular scattering, the exact characteristics of which are known sufficiently well.

Below we will show the main difficulty in determining experimentally the attenuation coefficients $\alpha(\lambda)$ in the infrared region of the spectrum. This difficulty is related not only to the necessity of taking into account the selective absorption by the gas component in the atmosphere, but also to the presence of continuous absorption by the tails of far, strong lines, which lie in the corresponding vibration-rotation and also pure rotation absorption bands. For the time being, not enough data is available about this continuous absorption (see paragraph 6, Chapter 3).

Thus, the most reliable experimental data about the coefficients $\alpha(\lambda)$ in the atmosphere during direct measurements can be obtained in the visible region of the spectrum, and also in most shortwave transparent "windows" in the infrared region, where the effect of continuous absorption still plays an important role.

O. I. Popov [545] measured mist transparency for the wavelengths 0.313, 0.546, 1.024 μ, during various meteorological visibility ranges S_M (1.6-58 km) in the layer of the atmosphere near the surface of the earth. Extrapolating the results obtained for other wavelengths in the interval studied, he constructed curves for the spectral behavior of the coefficient $\alpha(\lambda)$ in the mist for various S_M which are given in Fig. 7.18.

In the work of Curcio [546] and Knestricka, Cosden and Curcio [547], the coefficients $\alpha(\lambda)$ were measured in ten narrow regions of the spectrum in the range 0.4-2.27 μ. The values

of $\alpha(\lambda)$ for the wavelengths 1.65 and 2.27 μ are free of the effect of absorption by water vapor and methane. The data about absorption by water vapor and methane were taken from the work of Passman and Larmore [548]. All measurements were made in the layer of the atmosphere near the earth's surface on measurement paths 515 and 16.3 km long, at various meteorological visibility ranges.

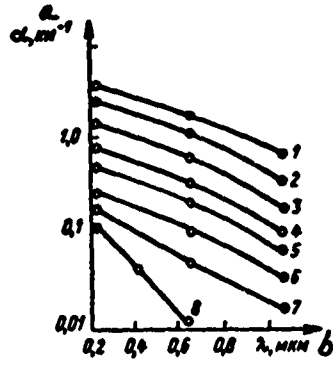

Fig. 7.18. Scattering coefficients in mist for various values of S_M according to the data in [545]:
1) S_M = 1.6 km 2) S_M = 2.5 km
3) S_M = 4.3 km 4) S_M = 8.4 km
5) S_M = 13.4 km 6) S_M = 29.6 km
7) S_M = 58.5 km 8) Rayleigh scattering coefficient

Key: a. km^{-1}
b. μ

[Note: Pages 310 and 311 missing in original]

An original investigation of the aerosol attenuation coefficients in the infrared region for the wavelengths 2, 4, 8 and 10 μ was carried out by Dennis [555]. His method completely eliminates the effect both of the selective and the continuous absorption by the gas component of the atmosphere, however the accuracy of the measurement results can hardly be considered to be satisfactory.

Summarizing the discussion of the experimental work, we note an essential shortcoming which all of this work has in common. This shortcoming is that the microstructures of the aerosols which make the atmosphere turbid are not taken into account simultaneously with the optical measurements. This fact makes

it practically impossible to carry out a one to one comparison of the experimental data with the corresponding theoretical data.

2. The Aerosol Transparency Component of Mist at Various Altitudes and in Slanted Directions in the Atmosphere

1. Theoretical studies. We write down the general formulas for the aerosol components of the spectral transparency of mist for slanted directions in the atmosphere

$$T_a(\lambda) = e^{-\tau}, \tag{7.40}$$

$$\tau = \int_0^l \alpha(\lambda, l)\, dl, \tag{7.41}$$

$$\alpha(\lambda, l) = N(l) \int_{a_1}^{a_2} \sigma(\lambda, a) f(a, \beta)\, da, \tag{7.42}$$

$$\sigma(\lambda, a) = \pi a^2 K(\rho, m), \tag{7.43}$$

where $T_a(\lambda)$ is the component of the spectral transparency of mist which originated only as a result of aerosol radiation attenuation, l is radiation path, N is the particle concentration which varies along the beam, $\sigma(\lambda, a)$ is the attenuation coefficient of a particle of radius a, and K is the attenuation efficiency factor of the particle.

The distribution of the particle concentration along the altitude can be described by formulas(5.8), which were selected by us on the basis of the approximate data of Young for the concentration of optically reactive aerolol particles at various altitudes.

Formulas (7.40)-(7.43), (5.8) together with the formulas and tabular data for the function $K(\rho,M)$ which were studied in Chapter 6, enable us to calculate the aerosol component of the spectral mist transparency along slanted directions in the atmosphere. Using the procedure described, the calculation of $T_a(\lambda)$ has shown, that for the model of the atmosphere described by formulas (5.8), aerosol attenuation need not be taken into account in atmospheric layers above 5 km when the radiation is propagated under all possible angles to a distance up to 1000 km. Consequently, only aerosol attenuation in the lower 5-km atmospheric layer in which the particle concentration decreases exponentially with the altitude is of interest [see (5.8)]. In this case, we can obtain a relatively simple formula for calculating $T_a(\lambda)$.

Introducing the notation $C' = \int_{a_1}^{a_2} \pi a^2 f(a, \beta)$, we can write

$$\alpha(\lambda) = QF = N(z) C'F, \tag{7.44}$$

where Q is the geometric section of the particle per unit volume [see (7.11)];

$$F = \frac{\int_{a_1}^{a_2} \pi a^2 K\left(\frac{2\pi a}{\lambda}, m\right) f(a, \beta)\, da}{\int_{a_1}^{a_2} \pi a^2 f(a, \beta)\, da}. \tag{7.45}$$

We write (7.40), taking into account (7.44), in differential form

$$dT_a(\lambda) = -N(z) C'F\, dl. \tag{7.46}$$

The initial condition for equation (7.46) is $T_a(\lambda) = 1$ when $l = 0$.

Suppose that the beam travels over a certain distance between the altitudes z_1 and z_2 at an angle θ formed with the vertical line. Then $dl = \sec\theta dz$. We will assume that only the particle concentration changes with the altitude, and that the parameter β in formula (5.6) for the distribution functions of particles by dimension does not depend on the altitude. Taking into account that in this case C' and F also do not depend on the altitude, integrating (7.46) over the altitude and transforming the equation obtained, we obtain the following formulas for the quantity τ in the expression for $T_a(\lambda)$ [see formula (7.40)]:

$$\tau(\lambda, z_1, z_2, \theta) = \sec\theta \frac{3{,}912}{S_M} \omega(\lambda) \frac{1}{b} (e^{-bz_1} - e^{-bz_2}), \tag{7.47}$$

or

$$\tau(\lambda, z_1, z_2, \theta) = \sec\theta [\tau(z_1) - \tau(z_2)], \tag{7.48}$$

where

$$\tau(z) = \frac{3{,}912}{S_M} \omega(\lambda) \frac{e^{-bz}}{b}, \tag{7.49}$$

$$\omega(\lambda) = \frac{\int_{a_1}^{a_2} \pi a^2 K\left(\frac{2\pi a}{\lambda}, m\right) f(a, \beta)\, da}{\int_{a_1}^{a_2} \pi a^2 K\left(\frac{2\pi a}{0{,}5}, m\right) f(a, \beta)\, da} = \frac{\alpha(\lambda)}{\alpha(0, 5)}. \tag{7.50}$$

Using the fact that $N(5) = 0.03$ (see the second formula in (5.8)], using formula (7.36), (7.42) and (7.50), we can obtain

$$b = 2{,}78 - 0{,}460 \lg S_M(0), \tag{7.51}$$

where $S_M(0)$ is the meteorological visibility range near the surface of the earth.

Formula (7.47), (7.51) and Table 7.6 make it possible to solve the question of the aerosol component of the spectral transparency of mist for various geometric arrangements of the source and receiver in the lower 5-km layer of the atmosphere. Fig. 7.21 gives the results of the calculations of the quantity $T_a(\lambda)$ in the vertical direction when $\beta = 4$, $a_1 = 0.05\ \mu$, $a_2 = 5\ \mu$. The role played by various layers in the radiation attenuated by mist in the vertical direction is demonstrated in Fig. 7.22.

It should be kept in mind, that the quantities $T_a(\lambda)$ considered were obtained for a model of the atmophere with a definite mean from the statistical distribution of the atmospheric aerosol particle concentration along the height. The dimension spectrum of the particles was considered to be independent of the height. In each concrete case, the real distribution of the concentration and dimensions of the particle differed to a greater of lesser extent from that described by the adopted model. In addition to this, it is also necessary to keep in mind the remarks made about the applicability l i m i ts of the data to the coefficients $\alpha(\lambda)$ which were made in the previous section.

The quantitative data obtained in article [544] and the quantitative data considered above, which characterize the radiation scattering on mist particles in slanted directions in the ammosphere, apply mainly to the infrared region of the spectrum. Analytical expressions for the scattering coefficients and the optical layers in the visible region of the spectrum in slanted directions in which the radiation is propagated in the atmosphere were obtained in the work of K. S. Shifrin and I. N. Minin [555], which was devoted to developing a theory of a nonhorizontal visibility range.

2. Experimental studies. In the last few years, substantial progress whas made in the experimental study of aerosol scattering at various altitudes in a wide band of waves. Only a few years ago, we mainly had data in the visible region of the spectrum which were obtained from measurements made from earth and a limited number of observations from airplanes. At the present time, however, many studies were carried out at various altitudes both in the visible and in the infrared regions. In all measurements the radiation source used is the sun, and the receiving apparatus is mounted on airplanes, aerostats, artificial earth satellites, or on the ground, when the atmosphere is probed with

the aid of projector and laser beams using the twilight and some other methods.

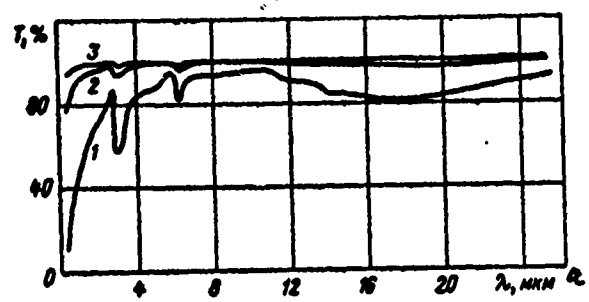

Fig. 7.21. Aerosol components of spectral mist transparency in the vertical direction in the lower 5-km layer of the atmosphere when: 1) $S_M(0)$ = 1 km, 2) $S_M(0)$ = 10 km, 3) $S_M(0)$ = 50 km.

Key: a. μ

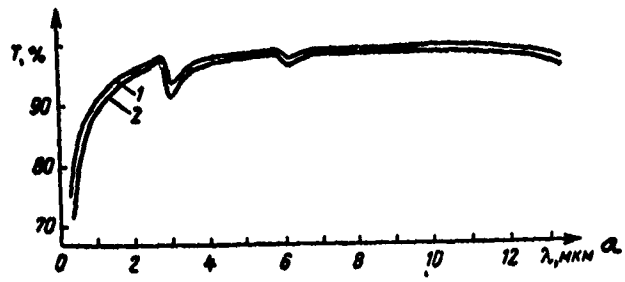

Fig. 7.22. Aerosol components of spectral mist transparency in the vertical direction for the atmosphere layer: 1) 0-0.5 km, 2) 0-5.0 km when S_M = 5 km.

Key: a. μ

The most important results of the studies of the vertical aerosol attenuation coefficients profiles which are used when the atmosphere is described as a scattering medium have been considered in Chapter 5. We will characterize briefly the work

which is not included in the survey in Chapter 5. The most detailed data from airplane investigations were obtained by G. P. Farapanova [556], Yu. I. Rabinovich [436. 558, 559] and G. P. Gushchin [435, 561, 562]. The measurements were carried out for a series of wavelengths in the visible and nearest infrared regions at various altitudes up to 6-7 km above various regions of the USSR. The results of the studies reduce to the following. The values of the aerosol attenuation coefficient at various altitudes and the aerosol optical layer of the atmosphere above the given altitudes vary on the order of 1-2 magnitudes from case to case. The relation between the aerosol attenuation coefficients and the altitude is approximated with an accuracy up to 15-20% by an exponential curve. The lower 1-km layer plays the dominant role in the general radiation attenenuation over the entire layer of the atmosphere. The same conclusion was reached in articles [563-565].

Since the aerosol attenuation coefficients decrease exponentially with the altitude, they decrease on the order of 1-2 magnitudes at the altitudes 3-5 km in comparison with the values near the surface of the earth. Nevertheless, only in the violet and blue regions of the spectrum at these altitudes the Rayleigh coefficients turn out to be equal to or even somewhat exceed the aerosol coefficients. In the red and even more so in the infrared part of the spectrum, the aerosol coefficients are larger than the Rayleigh coefficients at all altitudes which were studied in the papers discussed. At high altitudes, the aerosol coefficients were also observed to exceed the Rayleigh coefficients: in article [433], up to 50 km, and in [434], up to 100 km.

The measurements of G. P. Farapanova detected the practically neutral spectral behavior of the aerosol attenuation coefficients, which is equivalent to the exponent n being equal to 0 in the well-known empirical Angstrom formula which describes the relation between the scattering coefficient α and the wavelength λ:

$$\alpha = C\lambda^{-n}, \qquad (7.52)$$

where C is a constant determined from the experiment.

Yu. I, Rabinovich obtained an analogous result for atmospheric layers above 1 km, and for the lower kilometer layer and for the entire layer of the atmosphere, the exponent n in formula (7152) turned out to be approximately equal to 1. G. P. Gushchin determined the mean value $n \approx 1.32$ during the measurements, and the minimum and maximum values were equal respectively to 1.03 and 1.48.

The neutral spectral behavior of the attenaution coefficient is understandable if we assume that the corresponding layers of the atmosphere contain large particles. Such an assumption

agrees with the data in articles [432, 563, 566, 567].

We note that the Angstrom formula has been rather widely used in describing the experimental data about the spectral behavior of the aerosol attenuation coefficient. When this was done, various investigators obtained different values for n. Thus, Schmolinsky [568] gives n = 0.92 ± 0.25, Curcio [546] obtained n = 1.3 ± 0.6, T. P. Toropova [565], n = 1.1, 2.1 and 2.3, K.S. Shifirn and V. F. Raskin [540], using the gamma distribution for the dimensions of the particles, for $\mu = 2$, obtained with the mean radii of the particles equal to 0.05, 0.1, 0.2 and 0.5 μ values of n which were equal to respectively 3.3, 3.0, 2.5 and 2.1. Foitzik and Zskhaeec [569] found from measurements when $S_M > 7.5$ km that n = 1.2 -- 1.5, when $S_M \approx 2$ km, $n \approx 0.9$. O. P. Popov [545] for the transparency range 49-60% obtained for $\Delta\lambda = 1.2 - 1.5$ μ, $n \approx 2$, and for $\Delta\lambda = 1.014 - 0.546$ μ, $n \approx 1.2 - 1.3$. In article [820] the quantity n was measured between the limits 0.30 - 2.15, with the mean value equal to 0.81. The authors of [820] make the valid remark that formula (7.52) is by far not always justified.

The team of K. Ya. Kondrat'ev [445] obtained from balloons the vertical profiles of the solar radiation attenuation (in steps of 1.0 km) by atmospheric aerosols in layers of the atmosphere up to the altitudes 25 - 30 km. The profiles which were obtained differ somewhat from those determined by V. V. Nikolaeva-Tereshkov and G. V. Rozenberg [822] from measurements made from a spaceship. In the last study, two maxima were discovered in the vertical profile of the attenuation coefficient (Fig. 7.23). In [445], these maxima are not quite as pronounced, and are somewhat shifted laterally in the direction of lower altitudes. In addition of this, in [445] additional maxima were found in the altitude profile of the attenuation coefficient, in particular, near the 6-km level.

The existence of an aerosol layer with higher values of the attenuation coefficient at an altitude of about 19 km was detected during measurements which were made in twilight and in daytime from the spaceships Vostok and "Voskhod" (East and rise) [823].

Newkirk [440, 446] on the basis of measurements which were made using balloons, discovered very thin layers with higher values of the scattering coefficients. These layers were approximately 30 m thick. The intervals between these layers were filled by layers of relatively clean air with vertical height on the order of 300 m.

The presence of maxima in the vertical profile of the aerosol attenuation coefficients is observed up to altitudes at which the ionosphere layers are found. The upper boundary of atmospheric

aerosol according to the data of various investigators lies in the range from 100 to 150 km [824].

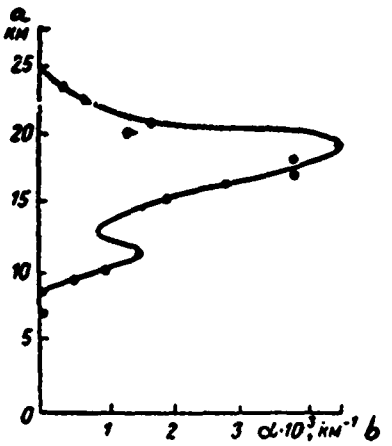

Fig. 7.23. Vertical profile of the aerosol attenuation coefficient according to the data in article [822].

Key: a. km
b. km^{-1}

G. V. Rozenberg [895] constructed a summary graph for the dependence of the aerosol attenuation coefficient on the altitude, on the basis of optical measurements which were made in studies [435, 559,822, 901-905]. The data which were obtained in these studies using various methods turned out to be close and represented the entire picture of the approximately exponentially decreasing attenuation coefficients for a series of wavelengths in the visible region of the spectrum up to the altitude of 100 km. The value of the attenuation coefficient decreased approximately by 6 orders of magnitude for all wavelengths when the altitude varied from 0 to 100 km. For all altitudes, the aerosol attenuation coefficient turned out to be at least several times larger than the molecular scattering coefficient. An exception to this were two narrow altitude intervals (approximately from 5 to 8-9 km and from 25 to 30 km) where the aerosol attenuation coefficients were very small.

Summing up the data of the experimental studies of aerosol scattering at different altitudes, primarily the great variability of the vertical scattering coefficient profile must be emphasized, and the presence of a layer structure in the entire aerosol layer of the atmosphere. The maxima in the altitude

profiles of the scattering coefficients are caused by the presence of the corresponding aerosol lyaers. Some of these layers are stable in time (for example, the layer at an altitude of approximately 20 km), others occur randomly. In spite of the considerable amount of work dedicated to the experimental study of the aerosol component of the transparent atmosphere for the visible and infrared waves, the data which was obtained so far is still inadequate to make definite conclusions about the mean statistical vertical profiles of the attenuation coefficients and their variability.

As in the case of the experimental work discussed in paragraph 1, allmeasurements of aerosol attenuation coefficients at different altitudes were not accompanied by...

[Note: Pages 320 and 321 missing in original.]

...the coefficients $\alpha(\lambda)$ are easily obtained directly from the table, since $\alpha(\lambda)$ is inversely proportional to the value $S_M(0)$.

We note that the Elterman model describes only very approximately the aerosol scattering at various altitudes. It does not take into account the jump in the vertical aerosol concentration profile which occurs at the altitude of 5 km, and the presence of aerosol layers. In addition to this, it is assumed that above 30 km the aerosol attenuation is equal to 0. However, so far, a better model has not yet been developed.

6. Energy Characteristics of the Scattering of Visible and Infrared Waves by Precipitation

Precipitation particles for the visible and infrared wave bands can be considered as large particles for which we can assume $K(\rho, m) = 2$. In this case, if the particles are assumed to be spherical, we obtain for the attenuation coefficients

$$\alpha(\lambda) = N \int_0^\infty \pi a^2 K(\rho, m) f(a)\, da = 2Q,$$

where Q is the geometric unit section of the particle cross section, determined from formula (7.11).

The assumption that raindrops are spherical is fully justified. Thus, the attenuation coefficient of rain does not depend on the wavelength and is uniquely determined by the geometric cross section Q which, for the given characterisitcs of the microstructure, is uniquely related to the water content.

The relation between the coefficient $\alpha(\lambda)$ and the parameters of the microstructure of rains, as the measurement of E. A. Polyakova [453] have shown, is negligible when compared to the correlation between the coefficient $\alpha(\lambda)$ and the rain intensity I:

$$\alpha = 0{,}21 I^{0{,}74}, \qquad (7.53)$$

where I is expressed in mm/h and α in km^{-1}. The correlation coefficient between $\lg \alpha$ and $\lg I$ turned out to be equal to 0.95 ± 0.01. $\lg \alpha$ and $\lg \omega$ are even more highly correlated. Here ω is the rain water content in g/m^3 (the correlation coefficient is equal to 0.97 ± 0.01).

An analogous correlation between the coefficient α and snowfall intensity was obtained in the work of E. A. Polyakova and V. D. Reet'yakov [570]. The correlation coefficient turned out to be equal to $.91 \pm 0.02$. The correlations between the coefficients α and the rain and snowfall intensities, which were obtained in [453] and [570], have been confirmed in the study of Jefferson [571].

Thus, the attenuation coefficients of the visible and infrared radiation by precipitation particles can be considered for all practical purposes to be independent of the wavelength. This conclusion holds, at least, for radiation wavelengths which satisfy the condition $\lambda < 15$-$20\ \mu$. Numerical values of the coefficient are easily determined if the precipitation intensity is know.

7. Scattering Indicatrices of Polydispersed Aerosols

Analytical expressions which can be used to calculate the scattering indicatrixes of polydispersed aerosols consisting of "soft" transparent particles with various distribution functions by dimension were obtained by K. S. Shifrin and V. F. Raskin [540-542]. The distributions used were the gamma distribution with the parameter $\mu = 2$, the generalized gamma distribution, the Young formula with parameter values $\beta = 4$, 5 and 6. The data for the scattering indicatrixes for the Young distribution and distributions of the Young type with parameter values $\beta = 3$, 4, 5, 6, and 8 with a minimum dimension $a_1 = 0.0175$, 0.052, 0.082 μ and refractive index $n = 1.33$, 1.44, 1.50 [2, 105] were obtained in the work of K. S. Shifrin and E. A. Chayanova [572]. Tables for calculating the scattering indicatrix in the region of small scattering angles were obtained in article [573].

Diermejian [517] calculated the scattering indicatrix for two models of mist and one model of a cloud taking into account the complex refractive index of the particles for various wavelengths in the region from 0.45 to 16.6 μ.

The polydispersed scattering indicatrixes were calculated for media in which the dimensions of the particles were distributed according to the Young distribution for values of n = 1.25 and 1.50 for five wavelengths in the visible region of the spectrum by T. P. Toropova [825, 826]. The parameters β and u p p e r bound for the particle dimensions took on various values.

A considerable number of studies were devoted to the experimental study of the scattering indicatrixes of visible radiation under various conditions in the layer of the atmosphere near the earth's surface, and during solar radiation measurements in a cloudless sky. The results of these studies were generalized in monographs [583, 820, 827, 828].

Detailed experimental studies of the scattering indicatrixes of visible radiation in the layer of the atmosphere near the earth's surface were carried out in various geographical regions by O. V. Barteneva [574]. All indicatrixes were grouped on the basis of the value of the coefficient of asymmetry K, which is equal to the ratio of the light fluxes scattered forward and back, into 10 classes. Each class included indicatrixes for which the values of K differed by a factor of 1.5. In one series of observations at El'brus, for the first time a case was discovered where the scattering indicatrix was almost Rayleigh with K = 1 for $\alpha = 0.0136$ km^{-1} or $S_M = 220$ km. The maximum value of K attained was the value 35.

The measurements have shown that no single-valued relation exists between the form of the indicatrix and the transparent atmosphere. As noted in [574], this conclusion agrees with the measurement data of V. F. Belov [575], while in the work of Foltzik and Zschaeck [569], Huelbert [576], Bullrich [577, 578], Reger and Siedentopf [579], the transparency interval determined is compared to a certain value of K. In [574], it is shown that the conclusion was based on an analysis with an insufficient number of measurements.

In article [580], on the basis of an analysis of the results of the studies [574], it was shown that it is possible to use the nonphelometric method for measuring the transparency. The theoretical justification for this method is given in the work of K. S. Shifrin and E. Ya. Chayanova [829].

The measurements of the scattering indicatrixes for visible light in the layer of the atmosphere near the surface of the earth were carried out by T. P. Toropova [565, 581. 582], who also concludes that there is no single-valued relation between the coefficient K and the transparent atmosphere. In article [581] the values of K were determined separately for the complete indicatrix and its aerosol parts. The intervals in which these

varied turned out to be respectively equal to 1.57-8.75 and 1.69-15.1, with mean values 3.29 and 6.23. In [581] it is noted that, in the measurements of Bullrich [577], Foitzik and Zskhaek [569], Reger and Siebentopf [579], the mean values obtained were equal to 6.41, 8.17, and 11.5 respectively.

In article [582], the relation between the light intensity scattered at an angle of 10 and 140° was found which characterizes the elongation of the indicatrix and which varies from 8.8 to 63.8. In the same article, the ratios of the light intensities scattered at various angles to the corresponding intensities in the case of Rayleigh scattering were also determined. In particular, for the minimum and maximum measurement angles of 10 and 160°, these ratios varied between the limits 8-314 and 1.1-9.6 respectively.

In article [565], the indicatrixes were measured for two narrow regions of the spectrum with effective wavelengths λ_{eff} = 0.428 and 0.560 μ. It turned out that the elongation of the indicatrix increases with the wavelength. The same effect for the entire layer of the atmosphere was discovered by E. V. Pyaskovskaya-Fesenkova [583]. A detailed explanation of this phenomenon, which is puzzling at first sight (as λ increases, $\rho = \frac{2\pi a}{\lambda}$ decreases, which in the case of a monodispersed ash should decrease the elongation of the indicatrix), is given in the work of V. G. Kastrov [584], when he analyzes the contributions of small and large particles to the polydispersed aerosol indicatrix.

A detailed investigation of the halo part of the scattering indicatrix in the layer of the atmosphere near the earth's surface for various spectral regions, approximately 50 Å wide with centers near 0.47, 0.585, and 0.888 μ, was carried out by Yu. S. Lyubovtsva and G. V. Rozenberg [585, 906]. An analysis of the results obtained made it possible to conclude that three qualitatively different optical states exist in the layer of the atmosphere near the earth's surface: mist, nebula mist, and nebula. Each of these states is characterized both by the angular intensity profile during scattering at small light angles, and fluctuations in the halo part of the indicatrix. For clouds, the intensity I (θ) decreases very sharply. When the scattering angle varies form 10' to 7°, I (θ) varies by 3-7 orders of magnitude. In the case of nebula mist, corona were observed, which pointed to the presence of proportions of particles of definite demensions.

In mist and in stable nebula mist, the fluctuations of the scattering indicatrix halo were small. In the process when the nebula mist is transformed into a nebula, the intensity of the light scattered at the angles 10'-3° can vary within several

seconds by 2-3 orders of magnitude! The authors of [585] note that, in a very large number of halo indicatrixes obtained by them, there are practically no cases which repeat themselves.

The large number of scattering indicatrixes in the layer of the atmosphere near the surface of the earth was obtained by G. V. Rozenberg and G. I. Gorchakov [506, 507] when the components of the scattering matrix were studied experimentally (see paragraph 3, Chapter 6) In [507] graphs are given for the dependence of the components of the scattering matrix M_{11} on the angle (the scattering indicatrix) for mist, dense mist, nebula and fine rainfall.

The scattering indicatrixes in the free atmosphere at various altitudes were measured by V. F. Belov [586], B. A. Chayanov [587], and Kompaniets [588]. The results of these measurements show that the elongation degree of the indicatrixes varies from measurement to measurement. The symmetry of the indicatrixes is preserved at all altitudes which were studied up to 20 km, and is intensified in the tropopause region.

Measurements of the atmospheric scattering indicatrix for several wavelengths for visible and ultraviolet radiation in the region of scattering angles near 0° and 180° were carried out by V. E. Pavlov [830]. In the region of small scattering angles, it was discovered that the elongation of the indicatrix increases as the wavelength and as the absolute value of the sun halo increases. In the ultraviolet region, the scattering indicatrix approaches the Rayeligh indicatrix.

We note, in conclusion, that in the studies with which we are familiar, the experimental studies of the scattering indicatrixes of polydispersed aerosols under natural and laboratory conditions, have been carried out only for several wavelengths in the visible and nearest infrared regions (not farther than the wavelength 0.9 μ). At the same time, in most cases, simultaneous measurements of the microstructure of aerosols were not made, so that the experimental data cannot be compared quantitatively with one another and with the corresponding results obtained from calculations. The latter are available in more or less adequate numbers for the visible and nearest infrared regions. The calculations of the polydispersed scattering indicatrixes for the infrared region, taking into account the refractive index of particles, have been carried out only for several concrete models of the distribution functions by dimension for water spheres. It should be noted, that to calculate the polydispersed scattering indicatrixes of aerosols other than water aerosols, the necessary data about the chemical composition of the particles and, even more important, about the components of the complex refractive indices are not available for the time being [589].

8. Laser Radiation Scattering in the Atmosphere

The coherence, the high degree of monochromaticity, the great directivity and power of laser radiation, generally speaking, may be the reason for the corresponding properties which govern the laws under which this radiation is propagated in the atmosphere. This property can occur both in the radiation absorption and in its scattering, both in the linear optical region, when the Buger law holds, and in the nonlinear optic region.

The properties of laser radiation absorption in the linear optical region were considered by us in paragraph 14, Chapter 3. The nonlinear effects, which accompany the absorption and scattering of powerful laser radiation in the atmosphere, will be described in Chapter 10. Here we will only consider the energy problem of laser radiation propagated in a scattering media when the Buger law can be assumed to hold.

Purely qualitative considerations show that the attenuation coefficients for laser radiation and noncoherent radiation from heat sources of the same spectral composition should not differ much. In fact, the coherence of the incident wave on the layer consisting of the scattering particles can cause interference of the waves scattered by the particles. This leads to a distribution of the light intensity scattered in various directions which differs from the corresponding picture which is obtaieed when the layer is irradiated by noncoherent radiation. An experimental proof for this situation was obtained in our laboratory by M. V. Kabanov [590]. The effect mentioned is responsible for various values of the effective field for particles in various sectors of a laser beam cross-section. However, if the particles are uniformly distributed in the medium, and the increases in the effective field studied still do not cause nonlinear effects, we should expect that the attenuation of the beam which is averaged over its section will not differ substantially from the attenuation when the same layer of the medium was irradiated by noncoherent radiations of the same spectral composition.

The purely qualitative cosiderations which were discussed must be verified experimentally. This check is even more necessary, since in article [591] a difference was found between the laser radiation attenuation coefficients and the noncoherent radiation of the same spectral composition.

The attenuation coefficients of water clouds for laser radiation and heat sources with the correspoding interference filters were measured by a team of workers in our laboratory [592]. The types of lasers used and some of their characteristics are given in Table 7.7.

TABLE 7.7

CERTAIN LASER TYPES AND THEIR CHARACTERISTICS

Type of laser	radiation wavelength λ, μ	Operating conditions
Gas, based on a He-Ne mixture	0.63	Continuous, multimodal
Rigid, based on a ruby	0.69	Impulse, multimodal
Rigid, based on glass, Nd activated	1.06	Impulse, multimodal
Gas, based on He-Ne mixture	1.15	Continuous, multimodal
Gas, based on He-Ne mixture	3.39	Continuous, multimodal

Fig. 7.27 gives the results obtained from comparing the radiation attenuation coefficients of lasers based on an He-Ne mixture with wavelength 0.63 μ and the ruby laser (λ = 0.69 μ), and the attenuation coefficients from a heat source with the corresponding heat filters. It can be seen from Fig. 7.27, that all three attenuation coefficients are close to one another. The equation of the line which passes through the experimental points has the form

$$\alpha(0,63)=\alpha(0,69)=1,06\alpha_{\phi}, \tag{7.54}$$

where α(0.63), α(0.69) are respectively the radiation attenuation coefficients of lasers with wavelengths 0.63, 0.69 and the radiation from the heat sources with interference filters. Analogous results about the closeness of the radiation attenuation coefficients of lasers and heat sources can also be obtained for lasers with wavelengths 1.60, 1.15 and 3.39 μ regardless of the fact that in these cases, the measurements of the radiation attenaution coefficients of the heat source were only given for the wavelengths 0.4 μ. We note that in article [593], when the radiation attenuation coefficients were measured for lasers and radiation from a heat source with various wavelengths, a difference was detected in the values of the coefficients which were obtained, for which an exact interpretation of the reasons was not made.

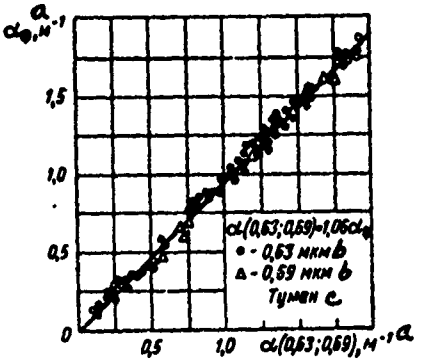

Fig. 7.27. Comparison of radiation attenuation coefficients for lasers with wavelengths 0.63 and 0.69 μ and the attenuation coefficients of the heat source with the same wavelengths in an artificial water nebula.

Key: a. m^{-1}
b. μ
c. Cloud

Harris, Sherman and Morse [594] recently published the results of careful laboratory studies of the relation between the radiation intensity scattered by latexes and the angle. A gas laser based on an He-Ne mixture with wavelength 6328 Å and xenon high-pressure arc lamp irradiating a band with width approximately 100 Å, at the center near the wavelength 6328 Å, were used as the radiation sources. The dimension of the latexes varied from 0.088 to 3.49 μ in diameter. An analysis of the measurement results led to authors of [594] to the conclusions that the measurements errors of the radiation scattering indicatrixes of lasers and the xenon lamp coincided in the limit. The coincidence of the indicatrixes is equivalent to the coincidence of the attenuation coefficients.

We note, in conclusion, that the results obtained in articles [592] and [594] must not, of course, be interpreted as proof that there is no difference in the propagation of coherent and noncoherent radiation of the same spectral composition in the scattering media. We can only speak about the approximate equality of the attenuation coefficients for these radiations.

9. The Effect of Measuring Apparatus on the Results of Experimental Studies of the Scattering of Visible and Infrared Waves in the Atmosphere

The theoretical data about the attenuation coefficients for clouds, nebula and mists discussed in this chapter characterize the attenuation of direct monochromatic radiation propagated through the corresponding media. As we already mentioned, strictly speaking, the conditions where it is possible to record only the directattenuated light do not occur in the experiment. Any receiving system, together with the direct attenuation scattered by the medium, records the scattered light, the intensity of which must depend on the angle of vision of the system, the properties of the scattering medium, and the direction of the incident radiation. Thus, the measured attenuatuion coefficient and the measured transparency of the layer must differ from the theoretical ones. The second reason for the difference between the measured values and those forecast by the theory is that, in the experiment, we are not dealing with strictly monochromatic radiation as we are in therory.

Our task is to analyze the effect of the experimental conditions and the measuring apparatus on the corresponding measurement results. This problem is discussed in a similar way in monograph [1]. Below, we give a basic summary of the results obtained by various investigators. It is assumed that the nonmonochromaticity effect of the source on the measurement results can be ignored. This assumption is not essential, since the widely-used monochromatization method for radiation from heat sources makes it possible to single out sufficiently narrow regions of the radiation spectrum, within the limits of which the aerosol attenuation coefficients can be considered to be independent of the wavelength.

1. The Dependence of the Measured Scattering Coefficient on the Photometered Layer of the Atmosphere.

This relation was discovered experimentally for the first time by Sinclair [595], who measured the scattering coefficients of lycopodium particles (the dimensions of the particles were $15 \pm 1\ \mu$) at various distances from the receiver. When the distance varied from 5.5 m to 15 cm, the measured scattering coefficient of a parallel beam of visible light took on values from $2\pi a^2$ to πa^2. Mi theory for this case gives the value $2\pi a^2$.

K. S. Shifrin [467] solved the problem theoretically for large particles with any electrical properties. The case of an opaque sphere was studied theoretically by Brillouin [596]. It is noted in [597], that a similar result was obtained by Moulin and Reynolds in the case of a cylinder. Finally, analogous conclusions were reached when other particles with a nonspherical form

were studied [598]. The reason for the dependence of the measured scattering coefficient on the distance is related to the very peculiar form of the scattering indicatrixes for large particles. Depending on the distance between the particle and the receiver, the latter may receive a larger or smaller part of the energy scattered by the particle. Thus, the measured scattering coefficient turns out to be dependent on the experimental procedure. As K. S. Shifrin [467] has shown, the measured scattering coefficient may be written as follows:

$$\alpha_{meas} = \pi a^2 [2 - \varphi(z)] = 2\pi a^2 \left[1 - \frac{\varphi(z)}{2}\right], \tag{7.55}$$

where $z = \frac{2\pi a}{\lambda} \frac{d}{2l}$, a is the radius of a drop, λ is the wavelength of the scattered light, d is the diameter of the input aperture of the receiver, l is the distance from the drop to the receiver, m is the function tabulated in [467] which takes into account the form of the indicatrix.

E. A. Polyakove [599] verified, experimentally, formula (7.63) for the case of raindrops.

Gumprecht and Sliepcevich [597] used, for the measured coefficient of a localized layer, the expression

$$\alpha_{meas} = \pi a^2 R(z), \tag{7.56}$$

where

$$R(z) = 1 + J_0^2(z) + J_1^2(z); \tag{7.57}$$

$J_0(z)$ and $J_1(z)$ are Bessel functions of the first kind of zero and first orders.

The dependence of the measured scattering coefficients on the aperture of the receiver was detected by V. A. Timofeeva during scattering studies in a milky medium [600, 601].

M. B. Kabanov [602] obtained an expression for the function B (z) in the formula for α_{meas} in the case of large particles

$$\alpha_{meas} = \frac{1}{2} \alpha B(z), \tag{7.58}$$

where the quantity z has the same value as in formula (7.55).

In [602] and [1] the results of the calculations of B (z) are given for various z from 0 to 50. When z varies form 0 to s, the function t runs through values from 2 to 1. Consequently,

the measured scattering coefficient for large particles can differ from the maximum by a factor of 2. In [602], it has also been shown that in the case of small particles, α_{meas} under atmospheric conditions does not depend, for all practical purposes, on the distance, and differs little from α. The results of experimental studies of the relation between the measured scattering coefficient and the parameters of the receiver and the photometered layer of the atmosphere are described in [1]. The measurements were made with artificial nebula. The results gave satisfactory agreement with the theoretical data.

2. Effect of the Scattered Light on the Measured Transparent Atmosphere

If the radiation from the source is concentrated in a certain solid angle, the receiver records not only the radiation propagated from the source along a straight path, but also the radiation scattered by the particle outside the source-receiver line. We will call these parts of the radiation picked up by the receiver respectively the direct and laterally scattered radiation. In this case, the intensity of the illumination E created by this radiation can be written in the form

$$E = E_r + E_D = \frac{I_0}{l^2} e^{-\frac{1}{2}\alpha B(z) l} + E_D, \qquad (7.59)$$

where E_r and E_D are respectively the illumination created on the receiving area of the receiver by the direct and laterally scattered radiation, I_0 is the incident radiation intensity on the scattering layer of thickness l.

Thus, the signal on the receiver, which is usually assumed to be proportional to the transparency of the atmosphere, is determined by the illumination created both by the direct and laterally scattered radiation. In most studies, when the transparency of the atmosphere is measured, the second factor is not taken into account, which can lead, as we well show below, to gross errors.

The first estimates of the role of singly laterally scattered radiation in the atmosphere were obtained by Middleton [603], who calculated the illumination created by the direct E_r and singly laterally scattered E_D radiation, under the following conditions: $a = 2.5\ \mu$, $N = 10^8\ m^{-3}$, $l = 0.2$, 0.5 and 1.0 km, $a = 10\ \mu$, $N = 6.25 \cdot 10^6\ m^{-3}$ and $l = 0.5$ km, $\theta = 0.02$, 0.10, 0.2, and 1.0 rad., $0 \leq \gamma \leq 0.05$ rad. Here, a, N, l, θ and γ are respectively the radius of the particles, their concentration, the distance between the source and receiver, the half-angle of the radiation source cone and the half-angle of the field of vision of the receiver((see Fig. 7.28). The ratio E_D/E_r under the

conditions considered, attained a maximum value of 1.6. The calculated data were confirmed by Middleton experimentally in a nebula in which he obtained the value $E_D/E_r \approx 2$ for a distance of 114 m at $\theta = 0.30$, $\gamma = 0.008$ and a meteorological visibilty range of 125 m.

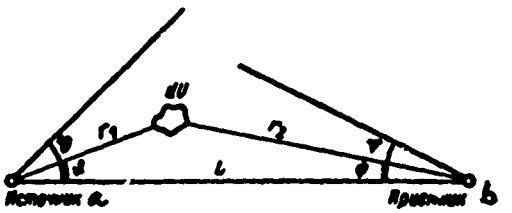

Fig. 7.28. Diagram for the radiation propagated from the source to the receiver.

a. Source
b. Receiver

Stewart and Curcio [604], in order to obtain data about the role of singly laterally scattered radiation in the case of a slightly turbid atmosphere, carried out the experiments for great distances (3.7 and 16.7 km) and a wide range of variation for γ (from 1.5 to 13°) for individual regions of the spectrum in the range 0.36-0.61 μ which were selected by the filters. A treatment of the measurement results made it possible to obtain the following empirical formula for the relation between the actual transparency T and the measured transparency T_ψ:

$$T_\psi = T + 0{,}5(1-T)(1-e^{-2\psi}). \qquad (7.60)$$

Formula (7.60) was obtained for $T > 0.70$, and the coefficient 0.5 is related to the underlying albedo surface.

Extensive studies of the role of singly laterally scattered radiation were carried out by Gibbons and his collaborators [605-607]. For the illumination E_D, he obtained the formula

$$E_D = gI_0 \int_v \frac{F(\varphi) e^{-\alpha(r_1+r_2)\cos\Psi}}{r_1^2 r_2^2}\, dv, \qquad (7.61)$$

where g varies from 0.5 to 1, depending on the character of the underlying surface, v is the scattering volume, F (ϕ) is the

scattering indicatrix, $\phi = \psi + \theta$, and the remaining notation is given in Fig. 7.27. We note that formula (7.61) was obtained earlier by V. M. Meshkov [608], not only for the case of single scattering but for the case of double scattering.

The value of E_D was calculated by Gibbons by integrating numerically formula (7161) for the following parameter values: $\theta = \pi/2$, $\Psi = 8°20'$, 25, 50, 75, and 90°, $\tau = \alpha l = 0.1$, 0.3, 0.9, 1.2, 3.6.

The experimental studies of Gibbons were carried out for great distances, large Ψ and low atmospheric turbidity in the San Francisco Bay area and in the Nevada desert. The distances in the first case varied from 1.18 to 14.37 miles, in the second case, from 0.51 to 13.17 miles. The studies were made for the wavelengths 0.40, 0.50, 0.70, 0.83 and 0.90 μ.

Eldridge and Johnson [609] verified analogous measurements for slanted directions in the atmosphere for $\Psi = 1.5$, 15 and 75° in the visible region, and in the 0.35-2 μ and 0.75-2 μ bands for layers of the atmosphere from 0.5 to 9 km under various meteorological conditions. More detailed data for nebulae and mist were obtained by the authors for an isotropic source and receiver with $\Psi = \pi$ [610]. The empirical formula which was obtained for the transmission function differs from the Buger law, which the authors attribute to the considerable effect of the laterally scattered radiation.

Theoretical and experimental investigations of the effect of scattered radiation on the measured transparency of theatmosphere are given in our work [611-615]. First, we attempted to simplify formula (7.60) in order to be able to calculate E_D for a wide range of conditions in the atmosphere. The essence of this simplification reduces to the following.

We replace, in (7.61), in accordance with the usual rules [616], the variables r and ψ by θ and ψ, and, letting $g = 1$, $F(\phi) = \alpha/4\pi\ f(\phi)$ where $f(\phi)$ is the normalized scattering indicatrix, and, keeping in mind that $\phi = \psi + \theta$, we obtain

$$E_D = \frac{\alpha I_0}{2l} \int_0^{\Psi} d\psi \int_0^{\theta} e^{-kl \frac{\sin\psi + \sin\theta}{\sin(\theta+\psi)}} f(\psi+\theta)\cos\psi\, d\theta. \qquad (7.62)$$

For small ψ or θ, the exponent in (7.62) can be shifted in front of the integral:

$$E_D = \frac{\alpha I_0 e^{-\alpha l}}{2l} \int_0^{\Psi} d\psi \int_0^{\theta} f(\psi+\theta)\cos\psi\, d\theta. \qquad (7.63)$$

It is easily from (7.63), that the double integral under the given experimental conditions does not depend on the distance between the receiver and the source. We introduce the notation

$$D=D(\rho, \Psi, \theta)=\frac{1}{2}\int_0^{\Psi}\int_0^{\theta} f(\psi+\theta)\cos\psi\, d\psi\, d\theta, \tag{7.64}$$

Then

$$E_D=\frac{\alpha I_0 e^{-\alpha l}}{l} D. \tag{7.65}$$

In (7.63), the relation between D and ρ is expressed in terms of the scattering indicatrix $f(\psi,\phi)$.

Formula (7.63), as the estimates which were made have shown, describes the value of E_D with an error which is known to be less than 5% for values $\Psi \leq 0.1$ and a transmission of the atmosphere $T \geq 0.1'$ which occur, in most cases, when the transparency of the atmosphere is measured.

From (7.61), (7.63) and (7.64), a formula for the total illumination on the receiving area of the receiver is easily obtained:

$$E=E_r+E_D=\frac{I_0}{l^2}e^{-\alpha l}[1+\alpha l D(\rho, \Psi, \theta)], \tag{7.66}$$

for which, in turn, we obtain the simple relation

$$\frac{E_D}{E_r}=\tau D, \tag{7.67}$$

where $\tau = \alpha l$ is the optical layer of the medium.

We note that formula (7.63)-(7.66) can be used for any wave band when $\Psi \leq 0.1$, and any homogeneous scattering medium with a known scattering indicatrix.

The methods used and the computational results obtained from calculating the quantity D for various ρ, Ψ and θ are described in detail in [1]. Here we will give only one diagram which illustrates the relation between D and Ψ, for different ρ for the two values $\theta = \pi/2$ and $\pi/6$ (Fig. 7.29).

The numerical values obtained for the quantity D, for various ρ, θ and Ψ, make it possible to estimate quantitatively the role played by singly laterally scattered light under various experimental conditions in the atmosphere. In particular, this data

implies, that for relatively small $\Psi = 0.1$, the quantity D can attain values 0.5-0.7 for large particles, which, for the values of τ often encountered in practice which are equal to several units, is equivalent to a contribution of the laterally scattered light exceeding several times the contribution of the direct attenuated light. Consequently, if this fact is not taken into account in experimental studies of the transparent atmosphere, a higher measured transparency can be obtained, which exceeds several times its true value.

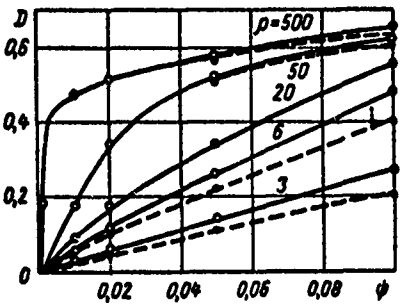

Fig. 7.29. Curves for the function D versus the aperture of the receiver for various ρ and values of the half-angle θ of the radiation source cone: — $\theta = \pi/2$; - - - $\theta = \pi/6$.

Experimental studies of the quantities D in artificial nebulae and in natural nebulae and snowfalls are described, in detail, in monograph [1]. A comparison of the measurement results in artificial nebulae in which the microstructure can be controlled. with the calculated values for the quantity D, has shown satisfactory agreement between the experiment and theory.

In the work of A. P. Ivanov and N. Ya. Khayiullima [616], a detailed experimental study of the effect of the radiation cone angle of the source and the angular aperture of the receiver on the measurement results of the attenuation coefficient was made for various values of the optical layer of the scattering media model. The latter were selected in such a way that their microphysical and optical characteristics (in particular, according to the survival probability of the photon) corresponded to natural media. In [617], the values of $(\alpha_{meas} - \alpha)\alpha^{-1}$ were tabulated for various Ψ, ϑ and τ (in our notation).

Hodkinson and Greenfield [618] calculated the scattering of white light by polydispersed aerosols, taking into account the instrument parameters used for the measurements. The calculations were carried out on the basis of Mi theory for values of the refractive index equal to n = 1.2 (0.2) 2.4, and the Mi parameter in the range $0.1 < \rho < 100$.

The results of the investigations of the quantity E_D, which were described, apply to sufficiently wide radiation beams. At the same time, in the last few years, in conjunction with the use of lasers in communication systems, information transmission, and range-finding and distance-measuring systems, etc., a great need arose, in practice, to investigate the role of the scattered radiation on the measurement results of various magnitudes which characterize the scattering properties of the medium when narrow collimated light beams pass through these. The results of the corresponding studies will be considered in Chapter 9.

Part 2: PROPAGATION OF SPATIALLY BOUNDED LIGHT BEAMS IN THE ATMOSPHERE

8. Characterization of the Radiation from Lasers of Various Types

Introduction

The goal of this chapter is to discuss briefly those characteristics of laser radiation which are significant for the problem of laser radiation propagation in the atmosphere. Some of the main characteristics are, first of all: 1) the spectrum, 2) the energy and power, 3) the coherence, 4) the directionality, 5) the operating conditions, 6) polarized radiation. We do not intend to give here a complete survey of all the work done in this field until the most recent time, in which one type or another of concrete data about the reaction properties of individual lasers was obtained. Primarily we will be interested in the data describing the values of the corresponding parameters which were obtained recently for lasers of various types which are important for the propagatiom of this radiation in the atmosphere.

The overwhelming majority of lasers known at the present time can be divided into four classes: 1) lasers based on ionic crystals, 2) lasers based on glass, 3) gas lasers, 4) semiconductor lasers. Below, we give a description of the fundamental radiation characteristics for the types of lasers which were mentioned, which were obtained mainly by using data published in surveys in the last two to three years [619-643, 701, 831].

1. Lasers Based on Ionic Crystals

It is well known that the first laser was based on a ruby crystal which is a sapphire monocrystal (Al_2O_3) activated by a trivalent chromium ion Cr^{3+}. At the present time, this type of laser is still the most widely used, even though a generation of lasers based on other ionic crystals has been obtained.

Lasers based on ionic crystals are characterized by a high concentration of working particles which are more or less uniformly distributed over the volume of the crystal (10^{17} - 10^{20} cm^{-3}) with a long life of the ionic working levels ($\sim 10^{-3}$ sec). The properties of the working bodies of the lasers under consideration make it possible to obtain great radiation energy under free generation conditions, and giant powers under modulated "goodness"[1] conditions, with a relatively simple solution of the cooling problem of the working elements.

For the base of the working elements in a laser based on crystals, the following are used: Al_2O_3, CaF_2, $CaWO_4$, SrF_2, BaF_2, Sr Cl_2, LaF_3, CeF_3, $SrWO_4$, $CaMoO_4$, $PbMoO_4$, YO_3, Er_2O_3, $Y_3Ga_5O_{12}$, $Gd_3Ga_5O_{12}$, MgF_2, ZnF_2, $Ca(NbO_3)_2$(Table 8.1). Among these, the most widely used are the crystals Al_2O_3, CaF_2, $CaWO_4$ and synthetic garnets.

Depending on the operating conditions, all lasers based on ionic crystals can be classified into three groups: 1) continuous wave, 2) pulsedlasers in free generating conditions, 3) pulsed lasers in modulated "goodness" conditions.

To obtain continuous laser radiation, it is necessary to have a certain number of redundant excited ions per unit volume of the working elements which are formed during continuous pumping. These excess ions are not obtained by far for all working elements of the laser when the known optical pumping sources are used. When the above condition is satisfied, continuous radiation generation becomes possible. The parameters of this radiation (see, for example, Table 8.2) depend on many factors which we will not consider here.

Pulsed radiation of lasers based on ionic crystals takes place in a much simpler manner. The pulse pumping insures generation with considerably larger ionic crystals than contineous generation. At the same time, in pulsed conditions, much greater power is obtained, and in a short time, energy is generated which reaches thousands of joules.

---

[1] Goodness = Q

TABLE 8.1

LIST OF CRYSTALS AND IONS-ACTIVATORS CAUSING LASER RADIATION AT VARIOUS WAVELENGTHS [624, 628]

Кристалл a.	Ион-активатор b	Концентрация иона-активатора, % c	Длина волны излучения ОКГ, Å d
CaF_2	Ho^{3+}		5 512
LaF_3	Pr^{3+}	1	5 985
Y_2O_3	Eu^{3+}	5	6 113
Al_2O_3	Cr^{3+}	0,05	6943, 6 934, 6 929
SrF_2	Sm^{3+}	0,01	6 969
Al_2O_3	Cr^{3+}	0,5	7 009, 7 041, 7 670
CaF_2	Sm^{3+}	0,01	7 083
$CaWO_4$	Nd^{3+}	1	9 145, 10 580, 13 392
$Y_3Al_5O_{12}$	Yb^{3+}		10 296
CaF_2	Nd^{3+}	1	10 460
$CaWO_4$	Pr^{3+}	0,5	10 468
$CaMoO_4$	Nd^{3+}	1,8	10 610
$Y_3Al_5O_{12}$	Nd^{3+}		10 648
CaF_2	Tm^{3+}	0,01	11 160
Er_2O_3	Tm^{3+}		13 340
$Ca(NbO_3)_2$	Er^{3+}		16 100
$CaWO_4$	Er^{3+}	1	16 120
MgF_2	Ni^{3+}	1	16 220
$Y_3Al_5O_{12}$	Er^{3+}		16 602
MgF_2	Co^{3+}	1	17 500, 18 030
$CaWO_4$	Tm^{3+}		19 110
$Y_3Al_5O_{12}$	Tm^{3+}		20 132
$CaWO_4$	Ho^{3+}	0,5	20 460
$Y_3Al_5O_{12}$	Ho^{3+}		20 975
SrF_2	U^{3+}		24 070
CaF_2	Dy^{3+}	0,01	25 588
ZnF_2	Co^{3+}	1	26 113
CaF_2	U^{3+}	0,05	26 130

Key: a. Crystal
b. Ion-activator
c. Ion-activator concentration, %
d. Radiation wavelength of laser, Å

TABLE 8.2

RADIATION CHARACTERISTICS OF THE MOST EFFECTIVE LASERS BASED ON IONIC CRYSTALS WHICH OPERATE IN A CONTINUOUS GENERATION MODE [628]

Рабочее тело [a]	Длина волны излучения, мкм [b]	К. п. д., % [c]	Мощность, вт [d]	Рабочая температура, °К [e]
$Al_2O_3+Cr^{3+}$	0,69	0,1	1	300
$Y_3Al_5O_{12}+Nd^{3+}$	1,06	0,2	200	300
$Y_3Al_5O_{12}+Ho^{3+}$	2,12	5	15	77
CaF_2+Dy^{2+}	2,36	1—1,5	100	77

Key: a. Working element
b. Radiation wavelength, μ
c. Efficiency, %
d. Powers, watt
e. Working temperature, °K

Under modulated "goodness" operating conditions, fantastic powers are obtained. For example, in one industrial sample of a ruby laser, the power 10^9 watt was achieved under modulated "goodness" conditions, when the duration of the pulse was 20 ns, with a divergence of 1 milliradian. Special measures for synchronizing the modes (the so-called coupled mode regime) make it possible to obtain radiation powers on the order of 10^{10}-10^{12} watt, with a duration of the pulse of 10^{-11} - 10^{-13} sec, which can be estimated only with the aid of indirect methods, since the best models of relatively inertia free radiation receivers cannot record pulses of such duration.

We will dwell briefly on the spectral radiation characteristics of lasers based on ionic crystals. Table 8.1 gives the radiation wavelengths which characterixe the center of a narrow spectral interval of the generating laser. If no special measures are taken, the laser radiation is multimodal and occupies a rigid band on the order of several tenths of an Angstrom, where the distribution of the intensity by frequency and time has a characteristically crammed structure. Special measures make it possible to narrow substantially the laser radiation bands up to values on the order of 10^{-3} A. The divergence angle of the radiation from lasers based on ionic crystals without the use of collimating systems depends on the geometric dimensions of the working elements, the radiation wavelength, the material from which the working element is made, and the number of generating

modes. Usually, the divergence angle is several milliradians. The use of special reflectors with selective distribution of the reflecting coefficient, which depends on the incident angle, makes it possible to obtain a divergence which is close to diffraction divergence. The energy distribution in the cross-section of the beam, as a rule, is nonhomogeneous.

The radiation coherence of a laser based on ionic crystals depends on the number of modes. Each mode generates light with a certain degree of coherence. The same applies to the degree of the polarized radiation.

2. A Laser Based on Glass

A specific feature of a laser based on glass, which is activated by trivalent neodyme, ytterbium, holmium, and erbium ions is related to the properties of glass, which can be varied within sufficiently wide limits by changing its chemical properties (Table 8.3). In addition to this, the working elements can be made from glass of various forms and dimensions, beginning with fiberoptics elements, the diameter of which is several microns, with length up to 10 m, and ending with very large bands with 60 mm diameters and length up to 2 m. The most widely used are lasers based on glass with neodyme.

TABLE 8.3

CERTAIN RADIATION CHARACTERISTICS OF LASERS BASED ON GLASS, ACTIVATED BY TRIVALENT NEODYME, YTTERBIUM, HOLMIUM, ERBIUM IONS [629]

Состав стекла а	Ион активатора б	Длина волны излучения, мкм в
Na—La—Si	Nd^{3+}	0,92
Li—Mg—Al—Si	Yb^{3+}	1,015
K—Ba—Si	Nd^{3+}	1,06
K—Ba—Si	Yb^{3+}	1,06
Li—Mg—Al—Si	Ho^{3+}	1,35
La—Ba—Th—B	Nd^{3+}	1,37
Yb—Na—K—Ba—Si	Er^{3+}	1,54
Li—Mg—Al—Si	Er^{3+}	1,55

Key: a. Glass composition
b. Activated ion
c. Radiation wavelength, μ

The most powerful laser is based on glass with neodyme, the energy of which per pulse reaches 5,000 joules when the length of the working rod is 90 cm and the diameter 30 mm. Lasers based on glass with neodyme under modulated "goodness" conditions generate a pulse with a power which reaches several tens of gigawatt lasting for 10-50 ns. The radiation from a laser based on glass is characterized by a more or less uniform distribution over the cross section of the beam. The divergence of the beam has approximately the same values as that in lasers bssed on ionic crystals.

Lasers based on glass have much wider radiation bands than lasers based on ionic crytals. If no special provisions are made, usually lasers based on glass generate a band the width of which is several tens of Angstrom. The considerable narrowing of the radiation spectrum of the laser makes it possible to single out individual radiation lines. At the present time, a generation of lasers based on glass with neodyme was obtained for the spectral region with widths on the order of 10^{-3} Å.

The radiation coherence of lasers based on glass depends to a considerable extent on the number of modes, just as in the case of lasers which are based on ionic crystals.

In lasers based on glass, radiation conditions can be obtained such that the spontaneous radiation which occurs at one end of the bar is completely saturated by the time it reaches the other end (superluminescent conditions). In this case the intensity is uniformly distributed in the radiation spectrum along the contour of the spontaneous emission line, and the radiation itself is not polarized. Its power reaches 10^9 watts at an impulse duration of 70 ns.

3. Gas Lasers

Among all types of lasers, the most widely used lasers are gas lasers. Their basic qualitative difference from other generators is the high radiation monochromacity and the high frequency stability which depends little on external conditions. These properties of gas lasers are responsible for the considerably larger radiation coherence than that found in other lasers. The radiation from gas lasers occupies a very wide and continuously broadening wavelength band. At the present time, this band occupies the spectral region from 2315, 5 Å (Xe II radiation line) to 1 mm. The greatest power in the continuous mode in obtained with gas lasers.

All gas lasers can be divided into the following four classes: 1) lasers based on neutral atoms, 2) lasers based on ions, 3) molecular lasers, and 4) chemical lasers. Depending on the particle

in which the corresponding energy transfer occurs, the radiation line falls into a particle region in the spectrum. The high energy electronic ion transitions occur in the ultraviolet and visible regions, and the electronic transitions in atoms give radiation lines in the visible and nearest infrared region. The vibration-rotation and pure rotation molecular transitions cause the generation of lines which occupy the wide wavelength band from the near infrared region to the microwave region. The radiation wavelength of chemical lasers depends on the energy levels of the particles formed as a result of the chemical reaction between which the corresponding transition occurs.

The most widely used lasers among gas lasers based on neutral atoms are lasers based on mixtures of helium with neon. Among these lasers in turn, the most widely used are generators which irradiate the wavelengths 6328 Å, 1.15 μ, and 3.39 μ. For the most powerful among the atomic lasers emitting at wavelength 6328 Å, a power of 1 watt has been obtained in the continuous mode with a 5-m-long transfer tube. Industrial models of this lasers have a power which is not larger than 100 milliwatt.

Recently, pulsed atomic lasers based on self-limiting transitions were designed with a power on the order of several kilowatts and the duration on the order of several ns. Recently, a laser based on copper vapors was created. It is expected that the efficiency of this generator will reach a value of 30%. Among all types of generators in the continuous mode in the visible region of the spectrum, the greatest radiation power was obtained on ionic lasers (up to 50-100 watts). The most widely used ionic laser is the generator based on ionized argon with a whole series of radiation lines in the 0.48 to 0.52 μ region.

The most widely used molecular lasers are generators based on molecular nitrogen and carbon dioxide. In the first case, the self-limiting electronic-vibration transition is used which generates radiation with wavelengths λ = 3371 Å and duration 20 ns with a maximum attainable power of 0.3-2.5 milliwatts in an impulse with repetition frequency of 300 Hz. The industrial model gives a power of 100 kw, a duration of pulse of 10 ns, repetition frequency from 1 to 100 Hz and a mean maximum power of 100 milliwatts.

A generator based on CO_2 is the most powerful laser among all continuous w a v e lasers in any wave band. Recently, a generator was designed at wavelength 10.6 μ with a power in the continuous mode of several kilowatts. The advantage of CO_2 as the working element for the laser is also that the generation can take place on an entire series of transitions in the spectral interval of order 100 cm^{-1} in the long wave region of the transparent atmosphere window. In addition to this, the long life of

the upper CO_2 level (more than 1 microsecond) enables this generator to operate in the modulated "goodness" mode.

Among the chemical gas lasers, the first laser is the generator in which radiation takes place because of the transition between the metastable and fundamental iodine state. The iodine atoms are obtained during the photodissociation of the CH_3I molecule under the action of ultraviolet radiation. The radiation wavelength of this laser is equal to 1.315 μ. The use of the photodissociation of CF_3I molecules insured a high efficiency value and an energy of 60 joules in a pulse with duration of 100 microseconds. A very promising chemical laser is generally considered to be a generator in which chlorine reacts chemically with hydrogen. Its radiation spectrum lies in the 3 μ region.

We will now consider the spectral characteristics of gas laser radiation. It is known that the width of the spectral radiation region of multimode gas lasers is determined by the Doppler contour. The width of the latter is sufficiently well-known for the radiation from a helium-neon laser with wavelength 6328 Å (1700 MHz). The decreasing Doppler width is inversely proportional to the wavelength. For helium-neon lasers with wavelength 1.15 and 3.39 μ, it is equal to 920 and 310 MHz respectively, for lasers based on carbon dioxide, it is approximately 60 MHz.

The Doppler width for ionic lasers is considerably larger than for atomic and molecular lasers. This is explained by the fact that generation in ionic lasers takes place at high temperatures. For generators based on argon, the width of the Doppler countour is 3500 MHz, and for generators based on krypton and xenon, it is 2500 MHz.

When gas lasers are used, a single mode and single frequency continuous generation with exceptionally high stability of the emitted frequency are more easily obtained than in the case of all other types of lasers. The short-term frequency stability can attain the value 10^{-1} and above. The long-term stability is equal to several units times 10^{-9}, and does not depend for all practical purposes on the external conditions.

A single frequency gas generator which operates in the continuous mode is the best generator among all types of lasers with respect to the value of the three-dimensional and time radiation coherence.

Gas lasers have the highest radiation directivity. The radiation divergence angle of gas lasers depends on the geometric dimensions of the generator, and the radiation wavelength. Without the use of collimating systmes, the angle of vision of industrial laser models is a fraction of a milliradian.

4. Semiconductor Lasers

The exceptionally high concentration of the working elements in semiconductor lasers (on the order of 10^{22} cm^{-1}) makes generation possible using very small volumes for the working elements, which in turn causes high radiation divergence (on the order of 10°).

The most widely used semiconductor laser is the generator based on gallium arsenide which emits a band with a width of several times of Angstrom in the 0.84 μ region. The greatest radiation power was obtained with this laser which was equal in the continuous mode to 3 watts at an efficiency of 15%.

Semiconductor lasers (Table 8.4) can operate both in the continuous and pulse mode. In the later case, the repetition frequency of the pulses can vary within very wide limits.

TABLE 8.4

SEVERAL RADIATION CHARACTERISTICS OF SEMICONDUCTOR LASERS [631]

Material	Radiation wavelength, μ	Pumping method
ZnS	0.32	electronic beam
ZnO	0.38	electronic beam
CdS	0.50	electronic beam, optical
CdS_xSe_{1-x}	0.50-0.69	electronic beam
GaScSe	0.59	electronic beam
$Ga(As_xP_{1-x})$	0.64-0.88	p-n transition
CdSe	0.68	electronic beam
CdTe	0.79	electronic beam
CdS_xSe_{1-x}	0.83	p-n transition
CaAs	0.84	p-n transition, optical, through avalanche sample, electronic beam
InP_xAs_{1-x}	0.89	p-n transition
InP	0.90	p-n transtion

[Table continued on next page.]

[TABLE 8.4 CONTINUED]

Material	Radiation wavenlength, μ	Pumping method
GaSb	1.51	p-n transition, electronic beam
InAs	3.13	p-n transition, electronic beam, optical
Te	3.65	electronic beam
$Hg_xCd_{1-x}Te$	3.76-4.13	optical
PbS	4.27	p-n transition, electronic beam
InSb	5.38	p-n transition, electronic beam, optical
PbTe	6.54	p-n transition, electronic beam
$Pb_xSn_{1-x}Te$	6.54-16.67	optical
PbSe	8.55	p-n transition, electronic beam

5. Variation in the Parameters of the Radiation from Lasers due to Various Factors

Strictly speaking, the radiation parameters of all types of lasers can vary under the influence of various factors. In some cases, the reasons are related to the generating conditions and, in other cases, they are deliberately introduced into the corresponding experiment.

An examples of the first type of factor is the effect of the temperature of the working element of the laser on its radiation spectrum. This effect manifests itself very clearly in the case of a ruby laser. Direct experiments carried out by various investigators have shown that when the temperature of the ruby changes to 13°C, the radiation wavelength varies on the average by 1 Å. This shift does not vary much from model to model. We recall that a displacement of the laser radiation even by a tenth of an Angstrom in the 0.69 μ region can considerably alter its absorption in the atmosphere (see Fig. 3.10). The effect of the temperature on the parameters of the radiation from other lasers is so far not understood sufficiently well.

The temperature at which generation takes place can have an effect on the radiation from the laser not only on rigid bodies, but also in gases and mixtures. Thus, for example, depending on the temperature, the generation from a laser based on CO_2 can occur in various lines.

Together with the temperature changes, the radiation characteristics of the laser can be affected by the concentration of the active mixture, the distribution over the volume, the quality of the resonators, the temperature of the surrrounding medium, the total and partial gas pressures in the case of gas lasers, etc.

In addition to the factors considered above which have an effect on the radiation characteristics of the laser and which are often related to generation conditions which are not controlled, there are cases when investigators deliberately change certain parameters in order to be able to regulate the radiation characteristics of lasers, above all the spectral characteristics of this radiation.

At the present time, a number of methods were developed for changing the spectral radiation characteristics of lasers:

1) the method which singles out individual modes in the radiation from lasers,
2) the parametric generation method,
3) the harmonic generation method,
4) the forced combination scattering method and others.

The simplest method for singling out individual radiation modes of lasers consists of introducing additional mirrors into the laser resonator. When one mirror is introduced, an additional Fabri-Pero interferometer is formed, the refraction coefficients of which depend on the radiation frequency. As a result, the "goodness" of certain modes increases, and undesirable types of vibrations are suppressed. In the process, the energy from the supressed modes can be pumped into the generating modes. The selection of the generating modes increases if two mirrors or a specially selected system of mirrors are introduced into the laser resonator. The rotation of the mirror introduced into the resonator leads to a change in the "goodness" of the corresponding modes, and makes it possible to select in this manner one type or another of modes, or to scan the generating modes over the luminescent contour [643].

At the present time, the radiation from the laser was scanned smoothly experimentally along the luminescent contour [644].

On the basis of the method used to select the individual modes, it was possible to obtain the following radiation data for the ruby laser. The conditions for the single mode generation for a ruby laser with a spectral width of the radiation line less

than 0.001 Å was obtained with a power in a pulse of 5 μ, and wavelength stability ± 0.005 Å without specially controlling the temperature of the working element [645]. The powers 14 and 25 milliwatts were obtained with a width of the radiation line equal to 0.005 Å and 0.008 Å. The single mode generating conditions were obtained also for a laser based on glass with neodyme.

The monochromaticity and the radiation power which were obtained for the ruby laser and the laser based on glass with neodyme made it possible to use the parametric generating, the second harmonic (GBG), and the forced combined scattering (VKR). methods. When these are used, the width of the emitted band can be preserved or can even narrow down under certain conditions, compared to its value in the pulse generator. A combination of the GBG and VKR methods makes it possible to obtain coherent radiation with various wavelengths. In the spectral region 0.4-1.2 μ, using these methods, generation was obtained at more than 40 wavelengths.

The use of the parametric generation methods makes it possible to scan the radiation from lasers in relatively wide regions of the spectrum. At the present time, models of generators in which the frequency can be retuned using the nonlinear KDP [abbreviation unkown] and $LiNbO_3$ crystals have already been designed. The following concrete data was obtained. When the radiation from the second harmonic of the laser based on glass with neodymium passes through the KDP crystal (wavelength 0.53 μ, the power in the pulse is 30-35 milliwatt/cm^2, the duration of the pulse is $2.5 \cdot 10^{-8}$ sec, and the pumping divergence 7'-8') the wavelength was retuned in the region 9571-11775 A. The power of the output signal was equal to 0.5 kilowatt, and the spectral halfwidth was 0.03-0.07 cm^{-1} [644]. The retuned radiation frequency was obtained by using for the radiation excitation the same second harmonic of the laser based on glass with neodymium and the crystal $LiNbO_3$ in the spectral region 0.684-2.335 μ. When the power of the excitation radiation was $5 \cdot 10^{-4}$ watt, the output signal had a power of 50 watt [645]. It is assumed that the radiation frequency can be retuned by this crystal in the 0.59-5 μ region if, during measurements, the temperature of the crystal is also varied.

Finally, we also note the possibility of scanning the radiation frequency from the laser with the aid of the magnetic field in which the generator is placed. The relatively low intensities of the magnetic field can ensure the scanning of the radiation frequency from gas lasers by several tenths of an inverse centimeters. Such frequency shifts can casue a substantial change in the absorption coefficient of the radiation from the laser propagated in the earth's atmosphere.

9. Propagation of Spatially Bounded Optical Radiation Beams In Atmospheric Aerosols

When three-dimensionally bounded light beams are propagated in the aerosol atmosphere, an attenuation of the radiation takes place and a light field scattered by the particles is formed. When the direct and scattered radiation are superimposed, the distribution of the radiation brightness over the cross section of the beam depends in a complex manner on the optical cover of the layer, the geometric dimensions of the beam, the properties of the scattering medium and the polarization state of the incident radiation. This picture can be distorted by instruments which are used in experimental studies.

The goal of this chapter is the discussion of the aforementioned laws which govern the propagation of spatially bounded radiation beams (primarily laser radiation) in various atmospheric aerosols. The principal attention is given to an analysis of the structure of the light field in the direction of small scattering angles (forward scattering) and scattering angles close to 180° (back scattering), since when lasers are used in communications, information transmission, range finding and distance measuring systems, etc., the most important thing is the availability of data about forward and back scattering.

1. Brightness of Radiation Scattered Forward

1. Theoretical Studies. The light field formed through the radiation scattering by aerosol particles is described by the transfer equation, the solution of which entails many mathematical difficulties [646]. For small scattering angles, the brightness of the radiation which is scattered forward can be calculated using the method of small angular approximations for the transfer equation [647 - 649]. However, this method has some important limitations, since it does not take into account the polarizations effects and it is only suitable for beams which are not bounded across the width and for large particles (very elongated scattering indicatrices). The brightness of the radiation which was scattered forward using the method of small angular approximations in various scattering media was calculated in article [650], in which the limits of applicability of A. A. Gershun's formula [651] which describes the brightness of the light scattered forward when only single scattering is taken into account were determined.

In the case of narrow collimated light beams the theoretical determination of the brightness of the radiation scattered forward is a very complex problem. At the present time this problem has only been solved for certain special cases. E. M. Feygel'son [652] obtained an approximate formula for the brightness B of the light scattered under small angles in a projector beam:

$$B = B_0 \frac{f(0)}{4\Gamma_2} e^{-\tau} \varphi(\tau) \theta^2, \tag{9.1}$$

where

$$\varphi(l) = \begin{cases} \left[\tau + \ln\left(\frac{\Gamma_2}{2} + \frac{\Gamma_1}{2} e^{-\tau}\right)\right], & \tau < \tau_0 (z < z_0), \\ \left[\tau + \ln\left(\frac{\Gamma_2}{2} + \frac{\Gamma_1}{2} e^{-\tau_0}\right)\right] + \tau_0 \left(1 - \frac{z_0}{z}\right), & \tau > \tau_0 (z > z_0); \end{cases} \tag{9.2}$$

Γ_1 and Γ_2 are the radiation scattered into the front and rear halfsphere, respectively, the quantity z_0 corresponds to the focus of the projector and is measured along the z axis which coincides with the direction in which the beam is propagated, θ is the beam angle which is related to the radius of the beam by the ratio $\theta = a/z_0$, f(0) is the scattering indicatrix in the forward direction, and τ is the optical layer. As was to be expected, the formula contains parameters which characterize the dimensions of the light beam.

In [653] and [654] more general formulas were obtained for bounded beams. However, their use for corresponding quantitative calculations is more difficult.

M. V. Kabanov [656] derived expressions which can be used to calculate the brightness of light which was scattered once for various geometrical parameters of a narrow beam, the divergence of which is equal to the angle of vision of the receiving system:

$$V = V_0 e^{-\tau} \left[1 + \tau \frac{1}{2} \int_0^{\theta} \int_0^{\Psi} f(m, \rho, \psi + \vartheta)\, d\psi\, d\vartheta\right] = V_0 e^{-\tau} [1 + \tau D], \tag{9.3}$$

where V_0 is the signal value when there is no attenuation in the medium, τ is the optical thickness of the layer, θ and Ψ are the angles of vision of the radiation source and the receiving system, $f(m, \rho, \psi+\vartheta)$ is the normalized scattering indicatrix which depends on the scattering angle $\varphi = \psi + \vartheta$, of the parameter ρ and the complex refractive index of the scattering particles. The quantity D determines the radiation which was scattered once for various parameters Ψ and θ in various scattering media.

If the distance between the radiation source and receiver satisfies the condition $l \gg d/\theta$, where d is the diameter of the receiving objective, formula (9.3) can be used to describe the damping of a narrow collimated beam.

An expression was obtained for the function D in [656] for the case when θ and Ψ are small and equal to one another, and the scattering indicatrix is written in terms of Legendre polynomials

$$D = \frac{1}{2}\left[\Psi\theta + \sum_{n=1}^{\infty} a_n \int_0^{\Psi}\int_0^{\theta} P_n[\cos(\psi+\vartheta)]\, d\psi\, d\vartheta\right] \cong$$
$$\cong \frac{1}{2}\varphi^2 \sum_{n=0}^{\infty} a_n = \frac{1}{2}\varphi^2 A_n, \tag{9.4}$$

where $\varphi = \Psi = \theta$; a_n are the coefficients in the Legendre polynomials which depend on the optical properties of the scattering medium.

It was shown in [656] that when $\rho \geq 5$, (9.4) can be replaced by a simpler expression which is obtained from (9.4) by using the approximate Penndorf formula [657]:

$$D = \frac{\rho^2\varphi^2}{2}\,\frac{K(\rho, m)}{2}, \tag{9.5}$$

where $K(\rho, m)$ is the scattering efficiency factor for the particle.

Expressions (9.4) and (9.5) cannot be applied for large values of ρ, since they were derived without taking into account

the angular dependence of the Legendre polynomials on small φ. In this connection a formula was obtained for D in [656] in which the scattering indicatrix is represented in terms of Bessel functions:

$$D=\frac{1}{2}\int_0^{\varphi}\int_0^{\varphi} f(\psi+\vartheta)\,d\psi\,d\vartheta=\rho\varphi\int_{\rho\varphi}^{2\rho\varphi}\left[2\frac{J_1(z)}{z}\right]^2 dz+ \\ +2[1-J_0^2(\rho\varphi)-J_1^2(\rho\varphi)]-[1-J_0^2(2\rho\varphi)-J_1^2(2\rho\varphi)], \tag{9.6}$$

where J_0 and J_1 are Bessel functions.

We note that when the scattering indicatrix is represented in terms of Bessel functions, it describes the angular distribution of the intensity of the scattered light in the region where the scattering angles φ are several degrees, with an accuracy up to 3% for particles with $\rho \geqslant 60$.

Figure (9.1) gives the results for the quantity D which were calculated using formulas (9.5) and (9.6). Computational results show that in those cases when the angles of vision of the receiving system and the source coincide for narrow collimated radiation beams with a divergence equal to several thousandths of a radian, radiation which was scattered only once forward can be ignored compared to the direct radiation of the beam up to values of the optical layer, and several tenths in nebulae, and even more so in mists. In the case of rain the quantity D is close to unity under the same conditions; therefore, for the value τ = 1 the light which is scattered once in the zone of the beam will have the same brightness as the direct beam.

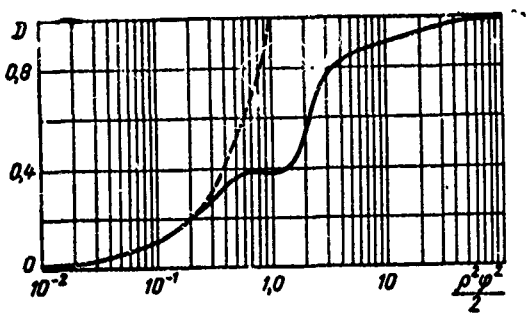

Fig. 9.1. The quantity D vs the parameter ρ obtained on the basis of calculations using formulas (9.5)(dotted curve) and (9.6)(solid curve)

From our point of view a very promising method for solving the radiation transfer problems of spatially bounded light beams in the scattering and absorbing media is the Monte Carlo method. The Monte Carlo method is very effective in the solution of multidimensional radiation transfer problems in media with various optical characteristics when the geometry of the sources and receivers is finite. The relatively slow convergence of the method depends only on the number of statistical tests and the quality of the models. The development of various modifications of the method together with the use of present-day electronic computers made it possible to solve many problems in atmospheric optics. A considerable number of papers were devoted to the theory of the Monte Carlo method as applied to radiation transfer problems (see, for example, [832]). The application of the method to the solution of problems in atmospheric optics was discussed in the work of G. I. Marchuk, and G. A. Mikhaylov [655]. G. A. Mikhaylov and G. M. Krekov perfected certain modifications of the method and developed algorithms and solved a number of problems dealing with the propagation of spatially bounded light beams in various scattering media [658, 659, 783, 833 - 837, 843]. Some of the results obtained will be analyzed below. Here we will discuss briefly the results of studies of radiation which was scattered forward several times which occurs during the propagation of various spatially bounded light beams recorded by a receiver with different area dimensions. The program used for the calculations has the capability to vary the optical properties of the medium and the geometric parameters of the source and receiver within very wide limits. We will restrict outselves to the description of several characteristic cases.

In [837] the angular distribution of the intensity of light which was scattered several times in the plane of the receiver was calculated under the following conditions of the quantitative experiment. The form of the radiating and receiving surfaces was circular. The optical axes of the source and receiver collimators coincide. The radiation intensity of the source is uniformly distributed in a cone with an angle θ equal to 6', 1°, 5°, 10°. The radiation wavelength is equal to 0.45 and 0.7 μ. The radiation is propagated in a water cloud, the indicatrix and the attenuation coefficient of which were obtained in the study of Deirmenjian [517]. The diameters of the source D_1 and the receiver D_2 are equal to, respectively, 4 and 150 mm. The optical layers τ through which the direct beam passes are 3.0, 5.0, 10.0.

Figure 9.2 shows the results of the calculations of the angular distribution of the intensity for radiation scattered

forward several times in the plane of the receiver.

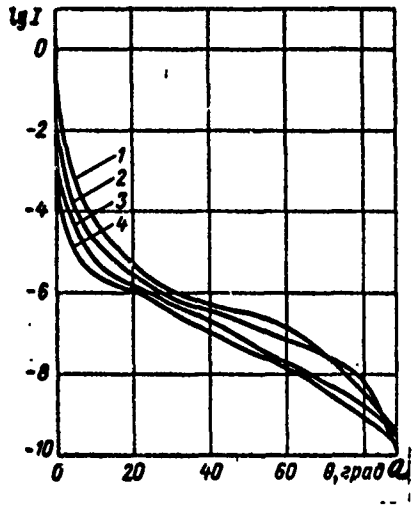

Fig. 9.2. Results of calculations of the angular distribution of the intensity of radiation scattered forward several times (λ = 0.45 μ) in a water cloud with optical layer τ = 5.0 for various divergence angles of the source θ = 6' (curve 1), 1° (curve 2), 5° (curve 3), 10° (curve 4) (the diameters of the source and receiver are equal to 4 and 150 mm, respectively)

Key: a. degrees

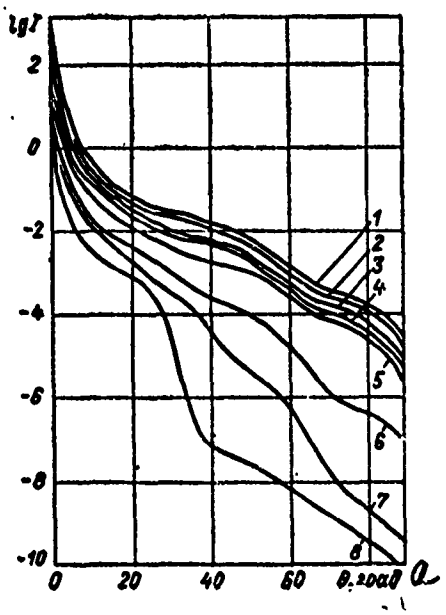

Fig. 9.3. Results of calculations of the angular distribution of the intensity of radiation scattered forward several times (λ = 0.45 μ) in a water cloud with optical layer τ = 4.0 for various diameters of the receiver D(r) = 4.0 m (curve 1), 3.0 m (2), 1.5 m (3), 1.0 m (4), 0.5 m (5), 0.2 m (6), 0.15 m (7) (the diameter and divergence angle of the source are equal to 4 mm and 30', respectively)

Key: a. degrees

For all values of the divergence angle of the source which were studied the intensity of the radiation arriving at the receiving area of the indicator at various angles Ψ varied by 9 - 12 orders of magnitude when Ψ varied from 0° to 90°. We note that to construct diagrams of the type given in Fig. 9.2 data was used for the angles $\Psi = 0, 30', 1^{\circ}, 2^{\circ}, 5^{\circ}, 10^{\circ}, 15^{\circ}, 20^{\circ}, 30^{\circ}, 40^{\circ}, 50^{\circ}, 60^{\circ}, 70^{\circ}, 80^{\circ}, 90^{\circ}$. As was to be expected, the most pronounced angular dependence of the incident radiations on the receiver which is scattered forward occurs with small values of Ψ and θ.

Figure 9.3 gives the computational results for the angular distribution of the intensity for various dimensions of the receiving area of the indicator.

The computational results which were obtained make it possible to analyze quantitatively the dependence of the intensity of the radiation which was scattered forward several times and which is recorded by the receiver for various geometrical parameters of the source and receiver. A comparison of the calculated values with the corresponding results obtained from experimental studies shows that the calculated results are in satisfactory agreement.

2. Experimental Studies. Detailed experimental studies of the brightness of the light scattered forward during the propagation of laser radiation in various media were carried out in our laboratory [660 - 665, 781].

The apparatus which was developed to carry out the studies included the following basic elements: 1) optical quantum generators with working wavelengths 6328 Å (a gas laser in a continuous radiation mode, with beam diameter about 0.4 cm, divergence angle 6') and 6943 Å (a pulsed ruby laser beam diameter 20 - 100 mm, divergence angle 30" - 40"), 2) collimation heat sources, equipped with narrow band interference filters with maximum transmission near the wavelengths 0.63 and 0.69 μ, 3) a receiving system which ensures the photometering of individual regions of the focal image picture of the source and background in the direction of small scattering angles.

The recording of the radiation brightness distribution in the focal plane of the receiving system was carried out photographically or photoelectrically, depending on the manner in which the focal picture was diaphragmed.

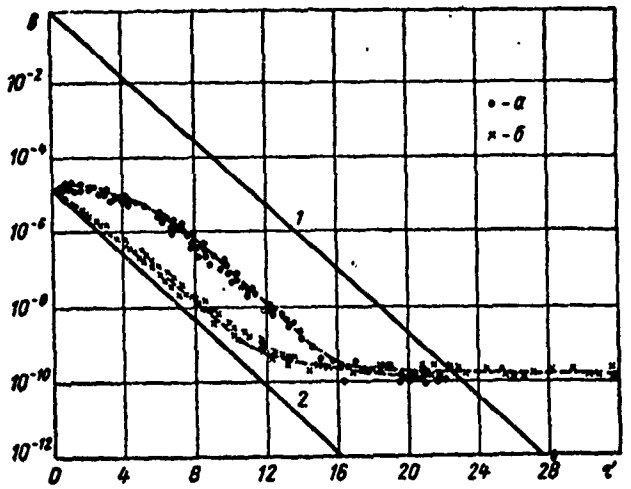

Fig. 9.4. The total brightness of the radiation scattered forward and back vs the optical layer τ in clouds (circles) and mists (crosses)

Curves 1 and 2 characterize the decreasing brightness of direct radiation of the beam and the original background of the source as τ increases according to the Buger law

The measurements were carried out in a chamber with a volume of 30 m^3 in which ligneous fumes were created (the diameter of the particles was 0.8 - 1.0 μ) and artificial water nebula (the mean square diameter of the drops was 8 - 15 μ). The selection of the scattering media was motivated by the desire to obtain data suitable for analyzing the laws which govern the propagation of narrow collimated beams in the earth's atmosphere. The brightness of the direct and scattered radiation were measured with the aid of two metering circuits. In one variant, the radiation source and the receiving system were located on the same line (the direct beam circuit). The length of the beam path was 4 m. In the second variant the light beam from the source was rotated by a plane mirror and sent to the receiving apparatus which was located next to the source (reflected beam circuit). The length of the beam path increased in the process up to 8.3 m, and the angle φ through which the beam was rotated by the mirror could vary from 1°30' to 8°30'.

The simultaneous measurement of the brightness of direct radiation from a laser and a heat source in the scattering medium made it possible to investigate the specific features of the coherent radiation attenuation as compared to noncoherent radiation attenuation.

The measurement results of the brightness of the radiation scattered forward in artificial water clouds and mists obtained using the reflected beam circuit and a gas laser are given in Fig. 9.4. All measurements were processed relative to the original brightness of the source B = 1.

It can be seen from Fig. 9.4 that the background brightness when the optical layer is $\tau = 0$ is not equal to zero. To find the background brightness due only to light scattering, the original background brightness of the source must be subtracted from the total measured background brightness. It can be assumed that the attenuation of the original background of the source is described by the Buger law (line 2). The contribution of the latter to the total background is unimportant for nebulae when $\tau < 4$ and for mists when $\tau < 14$. When the remarks which were made are taken into account, it can be said that the background brightness is equal to the direct radiation brightness when the values of the optical layer are $\tau \simeq 22 - 24$, both for nebula and mists, media in which the dimensions of the scattering particles differ considerably. In the range of optical layers approximately from 2 to 13 the background brightness in nebulae is approximately 1 - 1.5 orders of magnitude greater than in mists. Starting out with some value of the optical layer in nebulae and mists the brightness curves for the background begin to bend. For mists this bend occurs with a smaller value of τ than for nebula. When the values of the optical layers are larger than 20 the background brightness curves practically coincide both for mists and nebulae and do not depend on the value of τ.

The measurement results of background brightness in nebulae and mists which are plotted in Fig. 9.4 were obtained using the reflected beam circuit. This means that during the measurements not only the background due to forward scattering under small angles was recorded but also the background caused by back scattering at small angles during the propagation of the beam from the source to the rotating mirror. We were interested in obtaining the brightness values of both background components. With this aim in mind the rotating mirror was closed and only the background brightness due to back scattering was measured. These measurements have shown that for large τ the background brightness is mainly determined by the radiation which is scattered back.

Figure 9.5 shows the results obtained from measurements of radiation scattered forward in nebula and mists using the direct beam circuit. It can be seen from the figure that in the entire range of values τ considered the background brightness is considerably smaller than the direct radiation brightness.

The relation for the background brightness is described satisfactorily by the calculated data using the formula for single scattering.

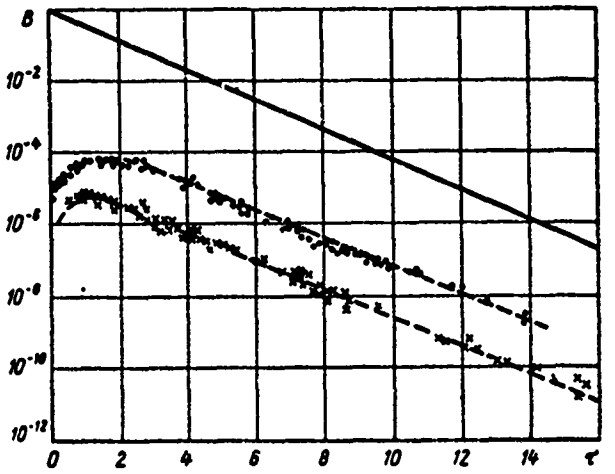

Fig. 9.5. The brightness of radiation scattered forward vs the optical layer in nebulae (dots and mists (crosses)

The dotted curves were constructed on the basis of calculations according to single-scattering theory, the solid line describes direct radiation attenuation in accordance with the Buger law

In addition to the measurements in the chamber with artificial clouds which were considered in our studies, we also investigated the brightness of radiation scattered forward in model media (a slightly turbid milk solution in water, with mean square diameter of the particles 3.5 ± 1.5 μ, and the lycopodium suspension in the mixture of alcohol and water; the radius of the particles was 15 ± 0.5 μ). The width of the beam was characterized by the value of the optical diameter

$$\Delta = \alpha d, \qquad (9.7)$$

where α is the attenuation coefficient, and d is the geometric diameter of the beam. The value of Δ during the measurements was equal to 0.34. The angular aperture of the receiver was

equal to the divergence angle of the radiation from the source.

The measurements results for the slightly turbid milk solution are plotted in Fig. 9.6. The values of the optical layer of the medium are plotted on the abscissa and the brightness values of the direct and scattered light on the ordinate. The brightness of the direct radiation from the laser in the absence of a scattering medium is taken to be equal to one. The curves in the diagram are constructed from the experimental points and the scatter in the brightness values does not exceed 5%. Curve 1 characterizes the change in the brightness of the direct and scattered beam in the zone when the optical diameter of the receiving objective is $\Delta = 0.5$, curve 2 was obtained under the same conditions and describes the variation in the brightness of only the scattered radiation, curve 3, which coincides with curve 2 when $\tau < 15$, was constructed using the results of the calculations for the brightness of singly scattered radiation under measurement conditions in which curve 2 was obtained, curve 4 is analogous to curve 1 but was obtained when the value of the optical diameter of the receiving objective was $\Delta = 9$, curve 5 describes only the variation in the brightness of multiple scattering when the diameter of the receiving objective is $\Delta = 9$.

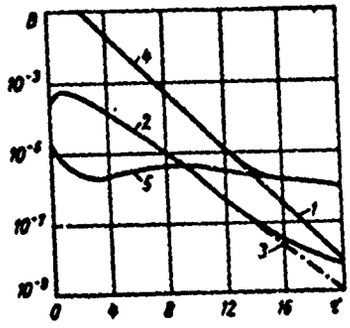

Fig. 9.6. Total brightness of the direct and scattered radiation beam in the zone vs the optical layer of a slightly turbid milk solution

It can be seen from Fig. 9.6 that in the light beam zone which is characterized by the divergence 6' and the cptical diameter $\Delta = 0.34$ when the optical diameter of the receiving objective is 0.50, the brightness of the scattered light is described by the formulas for single scattering [651] up to values of the optical layer equal to $\tau = 15$ and that the absolute value of the brightness is at least one order of

magnitude less than the brightness of the direct radiation attenuated according to the Buger law when the values of τ lie in the interval from 0 to 18. An increase in the optical diameter in the objective of the receiver is equivalent in our experiments to a corresponding increase in its geometrical diameter since the width of the beam and the density of the scattering elements did not change, which in turn was responsible for the more prominent role of multiple scattering in the formation of radiation scattered forward for various optical layers. Thus, for values $\tau > 15$ (the optical diameter of the objective of the receiver is 9.0) the multiple scattering brightness turns out to be larger than the direct radiation brightness. The absolute value of the multiple scattering brightness exceeds the single scattering brightness value when $\tau > 9$, and at the same time it depends little on the value of τ.

To elucidate the dependence of the distribution of the brightness for light scattered several times forward over the cross section of the beam on the diameter of the objective of the receiver, we measured the brightness in different annular zones selected by diaphragms which were mounted in front of the receiver objective. The zone of the beam (zone 1) was screened by a diaphragm as before, which determined the quantity $\Delta = 0.5$, zones 2 - 6 were selected so that each of them characterized the increase in the optical diameter of the objective of the receiver by the amount 1.70. Figure 9.7 gives the measurement results which were obtained. Curves 6 - 10 characterize the variation in the brightness of the radiation scattered several times vs the quantity τ in zones 2 - 6 when the survival probability of the photon is $\lambda = 0.99$, curves 6a - 10a were obtained for a medium with the value $\lambda = 0.92$ for the same zones. Curves 1 - 5 are replotted from Fig. 9.4 using the same numbering. When curves 6 and 6a were obtained it was not possible to eliminate the source background effect in zone 2.

In the studies made with the lycopodium suspension in the alcohol solution with water we obtained results which were qualitatively analogous to the results discussed above. The role played by multiple light scattering in the zone of the beam turned out to be greater than in the case of the slightly turbid milk solution which is caused by the corresponding difference in the elongation of the scattering indicatrix for these media.

To test the accuracy of the Monte Carlo method when the brightness of the radiation which was scattered forward several times was calculated in various scattering media with various

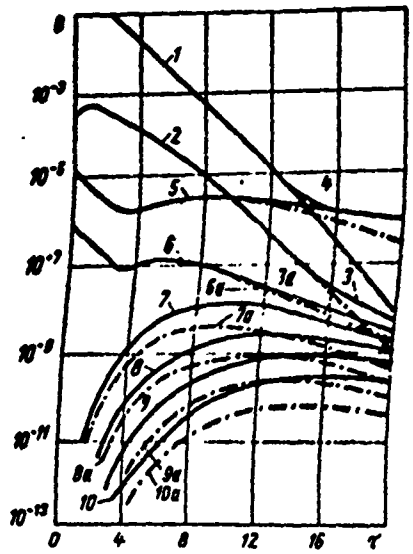

Fig. 9.7. Variation in the brightness of radiation scattered forward several times in various zones of the cross section of the receiver objective for two values of the photon survival probability: $\lambda = 0.99$ (curves 6 - 10) and $\lambda = 0.92$ (curves 6a - 10a)

Curves 1 - 5 are replotted from Fig. 9.4

geometric parameters of the source and receiver the conditions for the measurements which were described were reproduced in [837] and the corresponding calculations were made. Figure 9.8 gives a comparison of the computational results with the experimental values in Fig. 9.7. The calculated values are plotted as dots through which vertical segments pass which characterize the value of the mean square deviation. It can be seen from Fig. 9.8 that the calculated results are in full satisfactory agreement with the experimental values. The discrepancy between the results in the region of small values of τ in curve 2 is due to the effect of the original source background which was not taken into account during the experimental studies.

We were interested in clarifying the limiting values of the optical layers for which, in various scattering media, the dominant role in forward scattering is played by single scattering, which can be calculated rather simply.

The intensity of the radiation which was scattered forward once is written [651] in the form

$$I_{\text{рас}} = I_0 \tau e^{-\tau} \frac{\omega}{4\pi} f(0), \qquad (9.8)$$

Key: a. s

where I_0 is the intensity of the incident radiation on the scattering layer, τ is the optical thickness of the layer, ω is the solid beam angle, $f(0)$ is the value of the scattering indicatrix in the direction of the scattering angle $\theta = 0$ (forward scattering). For small collimation angles we can set $\omega = \pi\alpha^2$ where α is the beam angle. If we use Penndorf's approximating formula [656]

$$\frac{\omega}{4\pi} f(\theta) = \frac{\alpha^2 \rho^2}{4} K(\rho, m), \qquad (9.9)$$

we obtain from (9.8)

$$I_{\text{рас}} = I_0 \tau e^{-\tau} \frac{\alpha^2 \rho^2 K(\rho, m)}{16}, \qquad (9.10)$$

Key: a. s

where $K(\rho, m)$ is the attenuation efficiency factor for a particle with radius a, $\rho = 2\pi a/\lambda$, and λ is the wavelength.

Formula (9.10) can be rewritten in the form

$$I_{\text{рас}} = I_0 \tau e^{-\tau} \eta, \qquad (9.11)$$

Key: a. s

where

$$\eta = \frac{\alpha^2 \rho^2 K(\rho, m)}{16} \qquad (9.12)$$

is a parameter which characterizes the proportion of light scattered by the particle in the forward direction. The values of this parameter can be found using the quantity I_s

which is measured in the experiment.

The limiting values of η which were determined from the experiment enabled us to find the limiting values of the optical layers for which the multiple scattering effect can be ignored when the radiation scattered forward is determined. It turned out that for a beam divergence between the limits $\alpha = 30' - 10''$ the formulas which describe the intensities of the light scattered forward due to only single scattering are valid up to values of the optical layer $\tau < 18$ for particles for which the values of the parameter ρ lie in the range from 1 to 3000. This range of values of the parameter ρ covers practically the dimensions of atmospheric aerosol particles in the visible and infrared regions of the spectrum (mists, clouds, nebulae, drizzle, smoke, dust).

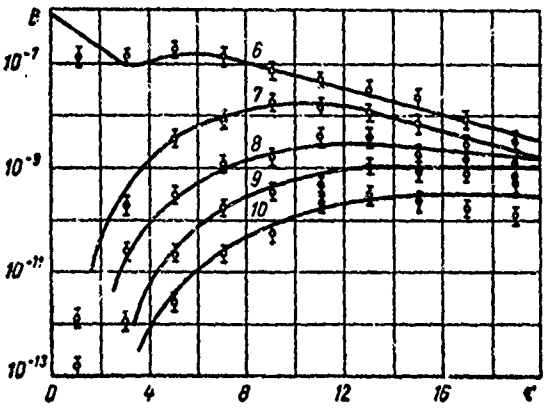

Fig. 9.8. Results of a comparison of experimental values from Fig. 9.7 (curves 6 - 10) with the calculated values obtained using the Monte Carlo method [837]

Experimental studies of the brightness of light scattered forward propagating in various model media with values of the optical layer $\tau < 20$ were carried out in the studies of A. P. Ivanov and A. Ya. Khayrullina [617, 838, 839]. The parameters which characterize the radiation source, the receiver and the scattering medium varied between wide limits (the divergence angle of the source from 7' to 1°44', and the angular aperture of the receiver from 16" to 7°, the optical diameter of the radiating beam from 0 to 0.30, and the optical diameter the radiation receiver from 0 to 0.40). The results which were obtained enabled the authors to estimate quantitatively the systematic measurement error in the attenuation coefficient

of the scattering medium due to the recording by the receiver of the radiation scattered forward. This error is uniquely determined if the optical characteristics of the scattering medium and the geometric parameters of the source and receiver are known.

In conclusion we will consider briefly the results of experimental studies of the brightness of light scattered forward for very large optical layers when the so-called depth conditions occur. A series of light scattering measurements in very turbid media was carried out by V. A. Timofeeva [666 - 668]. According to the results of these measurements, the brightness of the radiation scattered forward varies as the optical layer τ of the medium increases in accordance with the exponential law; however, the attenuation coefficient is smaller than in the case of small optical layers. The brightness of the radiation scattered under various angles for very large τ decreases in accordance with the same exponential law which also applied to the brightness of the light which is scattered forward. The range of values of τ for which the above relation holds is usually called the depth or stationary mode. The radiation brightness in the direction of the angle θ has, in this case, the form

$$B(0) = B_0' \varphi(0)\, e^{-k'(z-z_0)};\quad B_0' = B_0 C_1. \tag{9.13}$$

where B_0 is the initial brightness of the beam in the forward direction, C is a constant which depends on the boundary conditions and the geometric parameters of the light beam, $\varphi(\theta)$ is the angular distribution of the brightness in the depth mode, z is the geometric thickness of the scattering layer, z_0 is the geometric thickness of the scattering layer from which the depth mode begins, k' is the attenuation coefficient which is related to the attenuation coefficient α in the region of small τ by the relation

$$k' = \sqrt{A\alpha}; \tag{9.14}$$

where A is a parameter which depends on the optical properties of the scattering medium which is related to the absorption coefficient α_a by the linear relation

$$A = b\alpha_a \tag{9.15}$$

Key: a. a

The constant b in (9.15) depends on the scattering indicatrix of the medium.

For a constant distance between the source and receiver we can obtain from (9.13) - (9.15) the following formula for the brightness of the radiation scattered forward at depths with the optical layer τ:

$$B(0) = B_0 C e^{-\sqrt{b\alpha_n z}\left(\sqrt{\tau} - \sqrt{\frac{z_0\tau_0}{z}}\right)} = B_0 C' e^{-k\sqrt{\tau}}, \qquad (9.16)$$

$$C' = C e^{-k\sqrt{\frac{z_0\tau_0}{z}}}; \quad k = \sqrt{b\alpha_n z}. \qquad (9.17)$$

Key: a. a

In the case of a pure scattering medium ($\alpha_a = 0$) as can be seen from (9.16) and (9.17) the brightness of the light scattered forward does not depend on the optical layer τ. The presence of absorption in the medium ($\alpha_a \neq 0$) leads to a damping of B(0) with the quantity τ.

The diagram for the angular distribution of the brightness of the scattered light in the presence of the depth mode is a circle. In the case of a pure scattering medium the pole of the diagram lies at the center. When absorption takes place in the medium this pole is shifted back relative to the direction of the propagating light beam and the brightness diagram becomes slightly elongated. As τ increases the form of the diagram remains unchanged and is characterized by the quantity

$$R = \frac{B(0)}{B(\theta)} = 1 + \mu\frac{\alpha_n}{\alpha_p}. \qquad (9.18)$$

Key: a. a
b. s

where μ is a parameter which depends on the scattering indicatrix of the medium.

G. V. Rozenberg obtained a formula which is analogous to (9.18) on the basis of theoretical consideration [669].

A large series of measurements of the brightness of the scattered radiation in the presence of the depth mode in various model media was carried out by A. B. Ivanov and his collaborators [670 - 677]. The geometric parameters of the light beam were varied during the measurements. For small diameters of the light beam the depth mode occurred with values of the optical layer $\tau > 500$. On the basis of an analysis of the experimental data the following empirical formula was obtained which describes the illumination of the medium at great depths under a parallel light beam:

$$E = E_0 e^{-(\tau-\tau_0)\sqrt{\frac{a_n a}{a_n a}}}\left(1-e^{-p\frac{S}{\tau}}\right), \qquad (9.19)$$

Key: a. a
b. s

where τ_0 is the optical layer with which the depth mode begins, q is a parameter which depends on the scattering indicatrix, $S = k^2Q$ is the optical area of the beam cross section, k is the attenuation coefficient, Q is the geometrical cross section of the beam, p is a parameter which depends on the absorption and scattering coefficient and the scattering indicatrix.

Formula (9.19) can be rewritten in the form

$$B = B_0'\left(1-e^{-p'\frac{d}{\tau}}\right), \qquad (9.20)$$

where d is the diameter of the beam, τ is the optical layer, p' is a parameter which depends on the optical characteristics of the medium.

In [670 - 677] is was discovered that the brightness of the scattered light in the depth regime is proportional to the divergence angle of the narrow collimated beam.

2. Attenuation of Direction Radintion in Scattering Media. Limits of Applicability of the Buger Law

Direct monochromatic radiation of a collimated beam propagating in a scattering medium without natural radiation in it is attenuated according to the Buger law, if the particles of the medium scatter the radiation independently. Usually the direct radiation carries one type or another of useful information. Therefore, from the standpoint of practical applications it is very important to know what the limiting conditions are during which the direct radiation can be isolated from the radiation scattered forward from the background. Clearly this can be done in those cases when the brightness of the direct radiation is greater than the brightness of the background. If the brightness of the background is greater than the brightness of the direct radiation, when the useful information carried by the beam is extracted, insurmountable difficulties can arise which are related to the fact that the radiation scattered forward is formed, in the final analysis, by the beam itself. In this case to select the direct radiation signal from the background of the scattered radiation, it is necessary that the brightness of the signal be greater than the brightness of the light which is scattered forward. It is easy to see why the most convenient conditions when the useful signal is measured are those conditions when the angular aperture of the receiver and the divergence angle of the source are equal. In this case the receiving system will intercept the entire beam and the minimum radiation from the scattered background, since for large values of the input objective with the same useful signal, the background noise signal will be larger (see para. 1).

In the case when the useful signal is considerably larger than the signal from the light scattered forward, we can say that the Buger law can be applied to describe the measured attenuation of a narrow collimated beam which is propagated in the scattering medium and completely intercepted by the receiving system. Thus, an investigation of the limits of applicability of the Buger law to the description of the measured attenuation in the medium will enable us to answer the question about the range of action of a particular system in which narrow collimated light beams are used to transfer the useful information through various scattering media.

A detailed investigation of the limits of applicability of the Buger law for various concrete measurements circuits in various scattering media was carried out by us in our laboratory in the studies quoted in the preceding section, in which together

with the measurements of the brightness of the radiation scattered forward the brightness of the direct beam was determined. Here we will summarize some of the results of these investigations from the standpoint of the limits of applicability of the Buger law. We emphasize again that we are dealing with the limits of applicability of the Buger law to the description of the attenuated light beam which is measured in the experiment and which is propagated through the scattering medium. It is clear that these limits must depend not only on the optical properties of the scattering medium but also on the geometric parameters of the beam and the receiving system. We will consider the case when the divergence angle of the beam and the angular aperture of the receiver are equal to one another.

Figure 9.9 gives the measurement results for the brightness B of a laser beam which depends on the optical layer of a milk solution diluted with water. A gas laser was used in the measurements with divergence 6' and beam diameter d = 0.4 cm. Each curve in the diagram refers to a certain value of the optical beam diameter $\Delta = \alpha d$. Δ was varied in the interval from 0.09 to 12.0 by increasing the density of the scattering elements. All measurement results are reduced to unit brightness of the beam incident to the scattering layer.

The criterion for the applicability of the Buger law to the description of the measured brightness of the beam with the quantity τ is the rectilinear relation between lgB and τ. It can be seen from Fig. 9.9, in which the quantity B is plotted in logarithmic coordinates that the rectilinear sections of the curves depend to a considerable extent on the optical diameter of the beam. The limiting values of τ change very abruptly when the Δ are small ($\Delta < 0.74$). When Δ increases the limiting values τ decrease more slowly and when $\Delta > 1.48$ they are practically independent of Δ and are approximately equal to $\tau = 12$.

The relation obtained for the limits of applicability of the Buger law which described the variation in the measured brightness of the beam with the value τ of the optical diameter of the beam can be used to explain the different role played by multiple light scattering in the zone of the beam for various Δ. As Δ increases due to a change in the particle concentration when the geometric diameter of the beam is constant or when the latter increases when the concentration of the scattering elements is constant, the role of multiple scattering in the formation of the light scattered in the zone of the beam becomes more important in comparison with radiation scattered once. For sufficiently large Δ "saturation" of the contribution of multiple scattering

occurs. For small Δ the single scattering contributes more to the field which is scattered forward. This is due to a shift in the limits of applicability of the Buger law which is used to describe the measured damping of the beam in the direction of large values of τ.

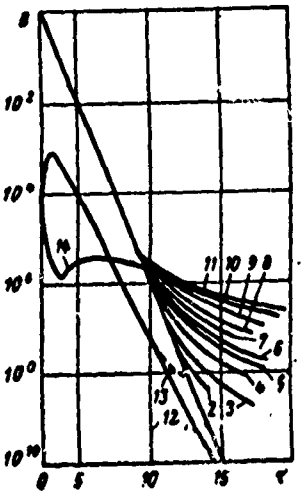

Fig. 9.9. The limits of appliability of the Buger law to the description of the measured attenuation of a narrow collimated light beam in the scattering medium vs the optical diameter Δ of the beam: 1) Δ = 0.09, 2) 0.34, 3) 0.74, 4) 1.11, 5) 1.48, 6) 2.22, 7) 3.96, 8) 3.56, 9) 7.12, 10) 9.0, 11) 12.0

Analogous changes in the limits of applicability of the Buger law arise, as paragraph 1 implies, when the optical diameter of the objective of the receiving collimater is increased and the optical diameter of the light beam remains constant.

The measurement results from the model medium plotted in Fig. 9 allows us to draw a number of conclusions about the applicability of the Buger law to the description of the attenuation of narrow collimated light beams in various atmospheric aerosols. The optical diameters of these beams in the optically most dense aerosols, clouds and nebulae at a meteorological visibility range S_M = 50 m and geometrical diameter of the beam d = 0.4 cm in the visible region of the spectrum do not exceed the minimum values of Δ obtained from

the studies which are plotted in Fig. 9.9. In fact, the attenuation coefficient in the case under consideration (see Chap. 7) is approximately equal to $8 \cdot 10^{-4} cm^{-1}$; therefore, when d = 0.4 cm, $\Delta = 0.0003$. Clouds and nebulae on one hand and on the other hand the weak solution of milk in distilled water, do not differ much in their microphysical and optical characteristics. Therefore, the results which are plotted in Fig. 9.9 can be used to analyze approximately the limits of applicability of the Buger law to the description of the damping of a collimated beam in clouds and nebulae. Keeping in mind the fact that in a dense cloud or nebula (S_M = 50 m) the quantity Δ is considerably smaller than its minimum value in Fig. 9.6 when d = 0.4 cm, we can say with assurance that the limits of applicability of the Buger law lie in this case beyond the limiting value $\tau = 25$. This statement agrees fully with the experimental data [660] which we obtained during measurements in artificial water nebulae. It can be expected that the aforementioned limit will also hold when the geometric diameter of the beam is equal to 100 cm, since in this case $\Delta = 0.08$.

The optical diameters of beams propagated through mists, precipitation, dry aerosols, have, as a rule, smaller values than those in clouds and nebulae. Therefore, the Buger law can describe the measured attenuation of collimated light beams when the divergence and diameter of the beam do not exceed 6' and 100 cm and the angular aperture of the receiver is equal to the beam divergence in all atmospheric aerosols when the value of the optical layer τ is 25 or greater in the visible region of the spectrum. We note that the most sensitive radiation receivers in the visible region record the radiation which passes through a medium layer with $\tau \cong 30 \div 35$, if the density of the energy on the layer is equal to 10^{-3} w. The result which was obtained can also be extended to the infrared region of the spectrum which differs from the visible region by the relatively smaller values of the parameter ρ and the large (illegible).

3. Brightness of the Radiation which is Scattered Back

A knowledge of the brightness of the radiation scattered back is very important for the solution of many applied problems, for example, when narrow collimated light beams are used for range and distance finding purposes in the scattering media in order to determine the aerosol transparency component of these media and to find the albedo of various surfaces and in the solution of a number of other problems. In this section we will briefly discuss the results of the theoretical and experimental studies of back scattering in the atmosphere

which were obtained recently.

1. Theoretical Studies. The calculation of the albedo of clouds at various zenith distances of the sun by solving numerically the transfer equation was carried out by E. M. Feygel'son [652]. On the basis of the fact that the albedo of the clouds depends little on the zenith distance of the sun, the author of [652] concludes that the radiation scattered back depends little on the scattering angle. The dependence of the albedo of clouds on their optical layer τ turns out to be more important, and the growth of the albedo with τ slows down when the optical layers are large and approach "saturation." Thus, the value of the brightness of the radiation scattered back is determined by some finite scattering layer. The optical thickness of this effective layer decreases, as L. M. Romanova has shown, in the presence of absorption in the medium. The albedo of clouds was calculated for various zenith distances of the sun in the infrared region in the 1.9 - 4.3 μ range in the work of Bortki [679].

Articles [680 - 682] contain the calculated data for the intensity of the radiation scattered back which are needed in order to determine the aerosol component of the transparent atmosphere. The amount of light scattered back by an aerosol layer turns out to be proportional to the degree of atmospheric turbidity. The calculations were carried out for various models of mists and nebulae. K. S. Shifrin and I. L. Zel'manovich [683] calculated in detail the quantities (illegible).

Some of the data obtained was discussed by us in paragraph 5 in which we present the results of studies dealing with the propagation of light pulses in scattering and absorbing media.

2. Experimental Studies. Experimental studies of the brightness of light scattered back for various scattering media irradiated by narrow collimating beams were carried out in our laboratory [660, 686]. These studies were necessitated by the paucity of both the corresponding theoretical and experimental data about back scattering by atmospheric aerosols.

Optical quantum generators were used for the measurements at wavelengths 0.63 μ (helium-neon laser, continuous operating mode), 0.69 μ (pulsed ruby laser) and 1.06 μ (pulsed laser based on glass with neodymium). The measurements at wavelengths 0.63 and 0.69 μ were made in artifical nebulae and mists and at wavelength 1.06 μ under natural conditions in the presence of mists and snowfall.

The results of the measurements of the brightness of the radiation from a gas laser scattered at an angle of 171°31' (λ = 0.63 μ, beam diameter 1 cm, divergence 6') in artificial nebulae are plotted in Fig. 9.10 for various optical layers (crosses). The measured values of the total brightness of radiation scattered forward and back (circles) are also plotted in the same figure which were obtained using the circuits: source--rotary mirror--receiver (the rotary angle of the beam was 8°30'). When the brightness of the radiation scattered at an angle of 171°30' was measured, the rotary mirror was closed.

If the original background of the source is eliminated from the measurement results, we can see that when the optical layer increases from 0 to 1 the brightness of the light which is scattered back increases and reaches a maximum and then first decreases relatively fast and later slowly as τ increases. When $\tau > 8$ it remains practically constant and reaches a value which is equal to the brightness of the direct beam when $\tau \cong 23$.

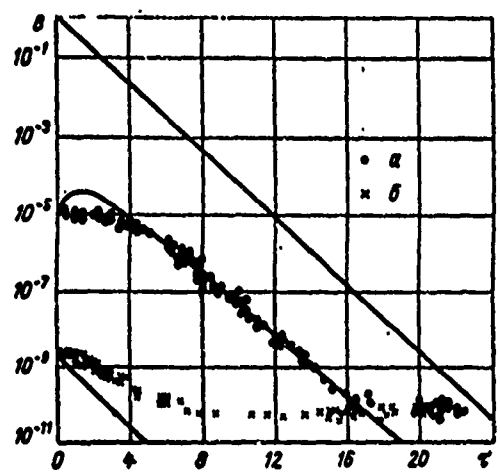

Fig. 9.10. Total brightness of the radiation scattered forward and back vs the optical layer of clouds (circles) and the brightness of radiation scattered back (crosses)

Straight lines characterize the decrease in the brightness of the direct radiation beam and the initial radiation background of the source in accordance with the Buger law

The measurements of the brightness of the radiation from a gas laser scattered by ligneous smoke at an angle of 171°30' have shown that its values coincide with the values obtained in clouds when $\tau > 20$. For smaller values of τ the brightness of the light scattered back by the clouds is smaller than that scattered by mists.

Figure 9.11 gives the measurement results for the brightness of laser radiation with wavelength 0.63 μ scattered at an angle of 172° by clouds and mists. The measurements were carried out without using a rotary mirror with a beam of diameter 0.4 cm with a divergence of 6'. The optical axes of the receiver and source intersected at an angle of 8°. The values of the optical layer τ which were plotted in the figure refer to the scattering layer from the source to the receiver. The brightness values are scaled down to the initial brightness of the direct beam. Each point in the diagram is obtained by averaging the results obtained from 5 - 10 measurements.

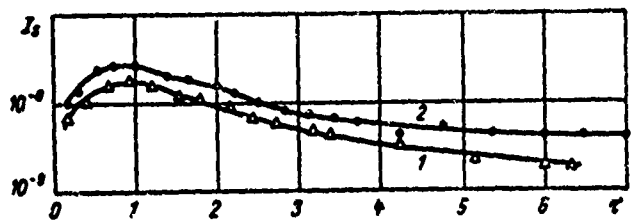

Fig. 9.11. Variation in the brightness of laser radiation scattered at an angle of 172°, λ = 0.62 μ by nebulae (1) and ligneous smoke (2)

It can be seen from Fig. 9.11 that the absolute values of the brightness of the light scattered at an angle of 172° in nebulae and mists in the optical layer interval considered are on the order of magnitude of $\sim 10^{-8} - 10^{-9}$ of the initial brightness of the direct beam.

The measurements of the backward scattering in mists and snowfall were made using a pulsed laser based on glass with neodymium (λ = 1.06 μ) and made it possible to obtain certain preliminary estimates for the backward scattering values. In the presence of mists characterized by the meteorological visibility range S_M = 3 - 7 km, the brightness of the back.

scattering is on the order of magnitude of 10^{-10} of the initial brightness of the direct beam. The occurrence of snowfall does not practically change the brightness of the back scattering of radiation from lasers with wavelenths 1.06 μ.

4. Polarization Characteristics of the Scattered Radiation

The polarized state of the radiation scattered at various angles is very important in the solution of many applied problems connected with the transmission of information with the aid of a narrow radiation beam. In fact, if the scattering layer of the medium is irradiated by linear polarized (illegible)

The theoretical discussion of the problem of the polarized state of the scattered radiation based on solving the general transfer equation is an extremely complex problem. The solution of the transfer equation without taking into account the polarized characteristics of the incident and scattering field, as we already have noted, has so far not yet been obtained for narrow collimated beams. In this respect the information about the polarized state of the scattered radiation which is needed to solve many problems is obtained from the experiment. However, even the experimental investigations mainly deal with the study of the polarized characteristics of the scattered radiation in an elementary volume [506, 507, 688] or in. wide beams and large optical layers of scattering media. [672, 689 - 691].

New possibilities of studying experimentally the polarized characteristics of the scattered field during the propagation of narrow collimated light beams in the scattering media are offered by using for the radiation sources optical quantum generators with linear polarized radiation. The problems with the highest priority are the study of the polarized state of the radiation scattered forward and back at small angles in various scattering media. An attempt to carry out a study of this type was made in our laboratory [692].

Measurements of the polarized characteristics of the scattered radiation were carried out for the angles 1°30' (forward direction) and 172° (back). The quantities measured were the intensity of the light I_1 with the vector $\vec{E}$ in the scattering plane and the light intensity I_2 with the vector $\vec{E}$ perpendicular to the scattering plane. The ratio $\Delta = I_1/I_2$ characterizes the radiation depolarization. The values of the quantity Δ make it possible to determine the polarization degree of the scattered light

$$\rho = \frac{\cdot - 1}{\cdot + 1}. \qquad (9.21)$$

(Illegible)

The quantities I_1 and I_2 are reduced to the original intensity of the direct beam radiation which falls on the scattering layer. It can be seen from the figures that the relation between the polarization degree of the radiation scatterd forward and the optical layer τ in the range of values of τ considered can be approximated by the straight line

$$p(\tau) = p_0 - k\tau, \tag{9.22}$$

where p_0 and k are empirical parameters, the values of which depend on the properties of the scattering medium, which vary little when the divergence angle of the source varies between the limits 40" to 6'.

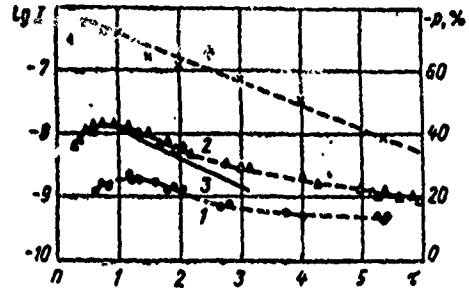

Fig. 9.12. The dependence on the optical layer of the nebula: 1) of the intensity of the light scattered forward with the vector $\vec{E}$ in the scattering plane, 2) the intensity of the light scattered back with the vector $\vec{E}$ in the plane perpendicular to the scattering plane, 3) the intensity of the radiation scattered back calculated in accordance with single-scattering theory, 4) polarization degrees of the radiation scattered back.

(Illegible)

Extrapolating the linear relation (9.22) to the value zero of τ gives a value p which is smaller than that in the source. (The polarization degree of the radiation from the source according to the measurements which were made was greater than

0.99). This means that in the range of small τ the relation between p and τ cannot be linear.

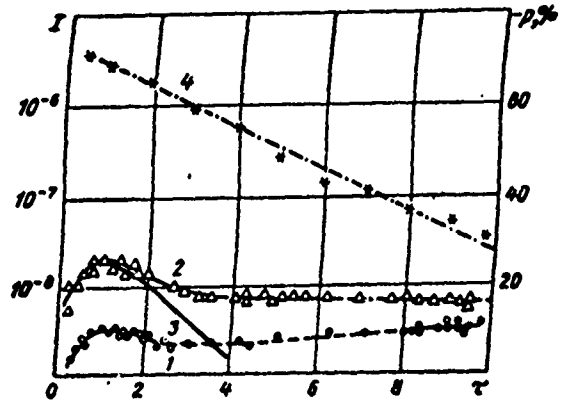

Fig. 9.13. The dependence on the optical layer of ligneous smoke of: 1) the intensity of the light scattered back with the vector $\vec{E}$ in the scattering plane, 2) the intensity of the light scattered back with the vector $\vec{E}$ in the plane perpendicular to the scattering plane, 3) the intensity of the light scattered back calculated according to single scattering theory, 4) the degree of polarization of the radiation scattered back

Figure 9.14 gives the results of measurements of the intensities I_1 and I_2 of the radiation scattered forward in nebulae and mists under the angle $1^{\circ}30'$ for various optical layers. As was to be expected the value of the sum $I_1 + I_2$ during the measurements in the nebula within the range of measurement errors did not differ from the value I_1, which indicates that the radiation scattered forward is not depolarized. The value of I_1, as can be seen from the figure, is larger than I_2 by 2.5 orders of magnitude. Thus, radiation depolarization practically does not occur during forward scattering under small angles (illegible).

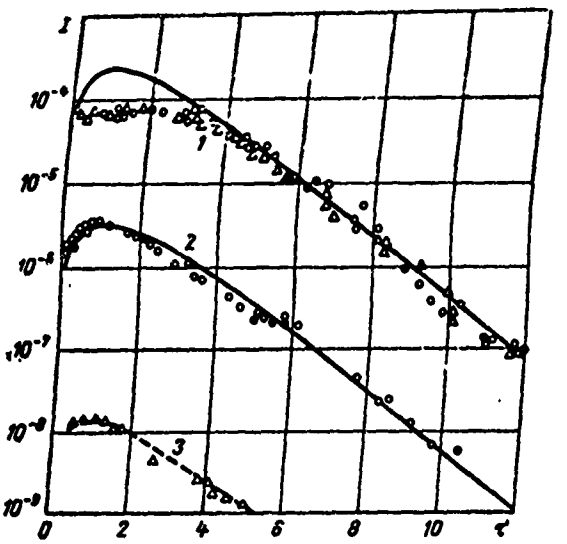

Fig. 9.14. The total intensity $I_1 + I_2$ (triangles) and the intensity I_1 (circles) of the radiation scattered forward in nebulae vs the optical layer (curve 1) and the intensities I_1 (curve 2), I_2 (curve 3) and vs τ in ligneous smoke

Solid and dotted curves are calculated using the formula from single scattering theory

These describe satisfactorily the measurement results in the range of values of the optical layer $\tau \leqslant 12$.

5. Propagation Of A Directed Radiation Pulse In The Scattering And Absorbing Medium

The design and practical use of pulsed lasers with pulses of small duration in range finding systems, distance measuring systems and other devices designed to operate in the atmosphere requires that the laws which govern the non-stationary scattering of light in media with various survival probabilities of the photon be studied. The last quantity can vary considerably in the atmosphere depending on the wavelength at which the pulse is generated.

One of the most important problems in the nonstationary scattering of the radiation is the study of the space-time

variation of the pulse shape during propagation at various optical depths of the absorbing and scattering medium. First it is necessary to know the change in the shape of an infinitely short pulse since any pulse can be represented in the form of a set of pulses of infinitely short duration.

Detailed calculations of the deformation of an instantaneous pulse propagated in various scattering media were carried out in article [836] using the Monte Carlo method. We will discuss some of the results which were obtained.

The calculation of the distribution of photons recorded by the receiver with diameter D_2 = 15 cm over the paths when a water cloud δ was irradiated by a pulse from a source with diameter D_1 = 8 mm with divergence angle θ = 30' was carried out for the radiation wavelengths 0.45 and 0.7 μ. The wavelengths were selected on the basis of the available data for the scattering coefficients and indicatrix of the water clouds [517]. The measure of the pulse diffusion adopted was the dimensionless run of the photons $t = t' c\sigma$, where t' is the actual time of the run, $t' = l/c$, l is the path of the run, c is the velocity of light, $\sigma = 0.016525\ m^{-1}$ is the attenuation coefficient. The parameter t is interpreted as the optical layer through which the photon passes along the path from the source to the receiver. The calculations were carried out for values of the optical layer equal to τ = 1.0, 2.0, 5.0, 10.0. When the relation between the intensity of the radiation which was scattered forward several times and the angle at which this radiation was incident to the receiver were constructed, the parameter t was varied with step 0.05 for τ = 1.0, 2.0, 5.0 and with step 0.1 for τ = 10. For example, for τ = 5.0 the parameter t took on the values t = 5.0, 5.05, 5.1, etc. We note that the parameter step Δt = 0.05 correspond approximately for the value $\sigma = 0.016525\ m^{-1}$ to a time which is equal to 10 nsec. The values of the arrival angles of the photons at the receiving area of the radiation detector which were selected were equal to 0°, 0.5°, 1°, 2°, 5°, 10°, 15°, 20° (10°) 90°.

The calculated results were plotted as graphs in the form of a family of curves which reconstruct the complete picture of the angular and time distribution of the photon flux for given values of the parameters of the source and receiver, the optical layer and the radiation wavelength. The calculated values which were obtained for τ = 5.0, λ = 0.7 μ are illustrated in Fig. 9.15. The angles at which the photon arrives to the area of the receiver is plotted on the abscissa (the angle is measured from the normal to the area) and on the ordinate the radiation intensity is plotted on a logarithmic

scale. Curve 1 characterizes the angular distribution of the photon flux which passes through paths which are equivalent to values of τ in the interval from 5.0 to 5.05. In other words this curve determines the proportion of photons which arrived at the receiving area of the indicator with a time lag not exceeding 10 nsec. Curves 2, 3 and 4 refer to photons with time lags from 10 to 20, from 20 to 30 and from 30 to 40 nsec.

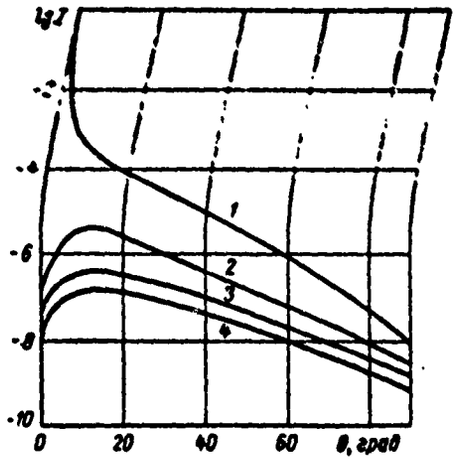

Fig. 9.15. Results of calculations of the angular distribution of the photon flux in the area of the receiver with diameter 150 mm during the propagation of a light beam with 8 mm diameter and divergence angle 30', wavelength 0.7 μ in a water cloud with the optical layer $\tau = 5.0$.

Curves 1 - 4 were constructed for values of the parameter t which differed successively by the amounts $\Delta t = 0.05 \approx 10$ nsec

Figure 9.16 shows some of the results obtained from the calculations of the angular distribution of photon fluxes when the scattering medium studied is a mist with an ionic distribution of the particles by dimension (the parameter $\beta = 4$) when $\tau = 2.0$. The data for the scattering indicatrix when the value of the refractive index is $n = 1.50$ were taken from article [572]. The attenuation coefficient was assumed to be equal to $\sigma = 0.00010555\ m^{-1}$. The angular and time characteristics of the photon distribution with various scattering multiplicity were also studied in [843] for cases when the optical layer of the water cloud between the source and receiver takes on the

scale. Curve 1 characterizes the angular distribution of the photon flux which passes through paths which are equivalent to values of τ in the interval from 5.0 to 5.05. In other words this curve determines the proportion of photons which arrived at the receiving area of the indicator with a time lag not exceeding 10 nsec. Curves 2, 3 and 4 refer to photons with time lags from 10 to 20, from 20 to 30 and from 30 to 40 nsec.

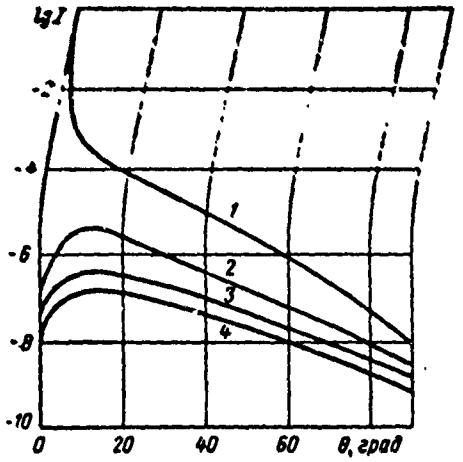

Fig. 9.15. Results of calculations of the angular distribution of the photon flux in the area of the receiver with diameter 150 mm during the propagation of a light beam with 8 mm diameter and divergence angle 30', wavelength 0.7 μ in a water cloud with the optical layer $\tau = 5.0$.

Curves 1 - 4 were constructed for values of the parameter t which differed successively by the amounts $\Delta t = 0.05 \approx 10$ nsec

Figure 9.16 shows some of the results obtained from the calculations of the angular distribution of photon fluxes when the scattering medium studied is a mist with an ionic distribution of the particles by dimension (the parameter $\beta = 4$) when $\tau = 2.0$. The data for the scattering indicatrix when the value of the refractive index is $n = 1.50$ were taken from article [572]. The attenuation coefficient was assumed to be equal to $\sigma = 0.00010555\ m^{-1}$. The angular and time characteristics of the photon distribution with various scattering multiplicity were also studied in [843] for cases when the optical layer of the water cloud between the source and receiver takes on the

values $\tau = 1.0$, 3.0, 5.0 and 10.0. The indicatrix and the scattering coefficients were taken from article [517]. The calculations were made for values of the source and receiver diameters equal to 4 and 150 mm, and the divergence angle of the source equal to 30'.

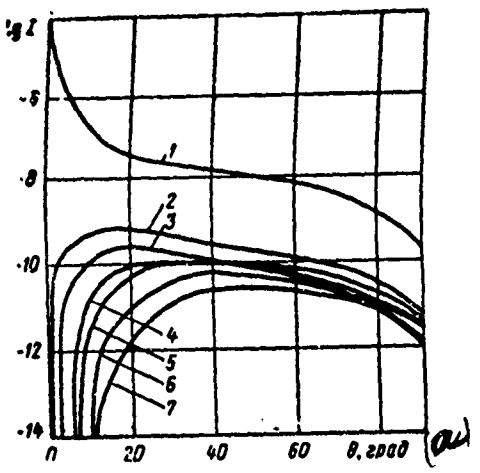

Key: a. degrees

Fig. 9.16. Results of calculations of the angular distribution of the photon flux in the plane of the receiver with diameter 150 mm during the propagation of a light beam with 8 mm diameter and divergence angle 30' in mist with $\tau = 2.0$ when the value of the refractive index of the particles is $n = 1.5$

Curves 1 - 7 differ from one another successively in the value of the parameter t by the amount 0.05 or, approximately, by 1.56 msec

The curves showing the relation between the radiation intensity and the time caused by photons with various scattering multiplicities for the values $\tau = 1.0$ and 10.0 and wavelength $\lambda = 0.7$ μ are plotted in Figs. 9.17 and 9.18. It can be seen clearly from the figures that the roles of the various scattering multiplicities in the deformation of the instantaneous light pulse are redistributed when the optical layer varies from 1.0 to 10.0.

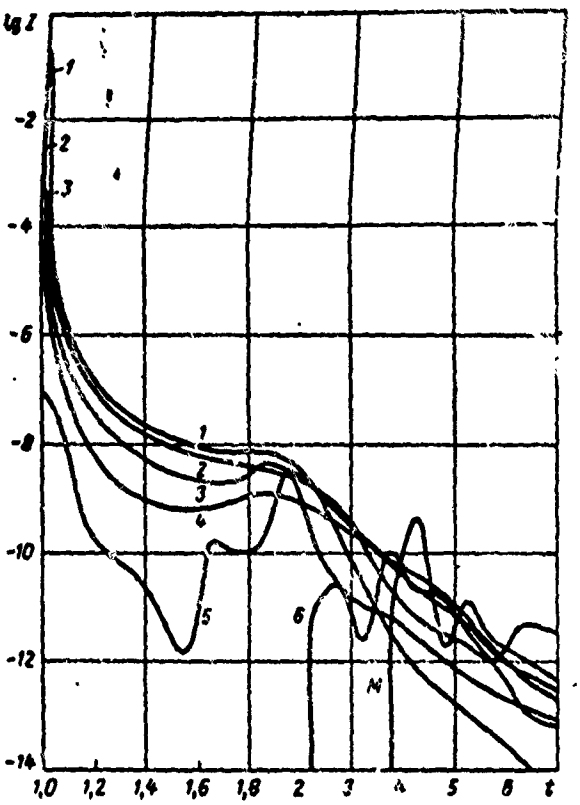

Fig. 9.17. Results of calculations for the radiation intensity time curve caused by photons with different scattering multiplicities for the wavelength 0.7 μ and the value $\tau = 1.0$ in a water cloud

The diameters of the source and receiver are equal to 4 and 150 mm. Curves 1, 2, ..., 6 correspond to 1, 2, ..., 6 scattering multiplicities, curve M to all scattering multiplicities greater than 6

Figure 9.19 shows some of the results of calculations of the back scattering δ of a radiation pulse of a narrow light beam propagated in a cloudy medium.

By solving approximately the nonstationary transfer equation for an unbounded beam, L. M. Romanova [693 - 695] investigated the distribution of photons over the runs in the reflected and arriving light when an infinitely short radiation

pulse was scattered isotropically.

The calculations have shown that the signal which is reflected from the scattering medium is formed when the latter is irradiated by a δ pulse, the most important role is played by the bounded layer of the medium which is adjacent to the radiation source.

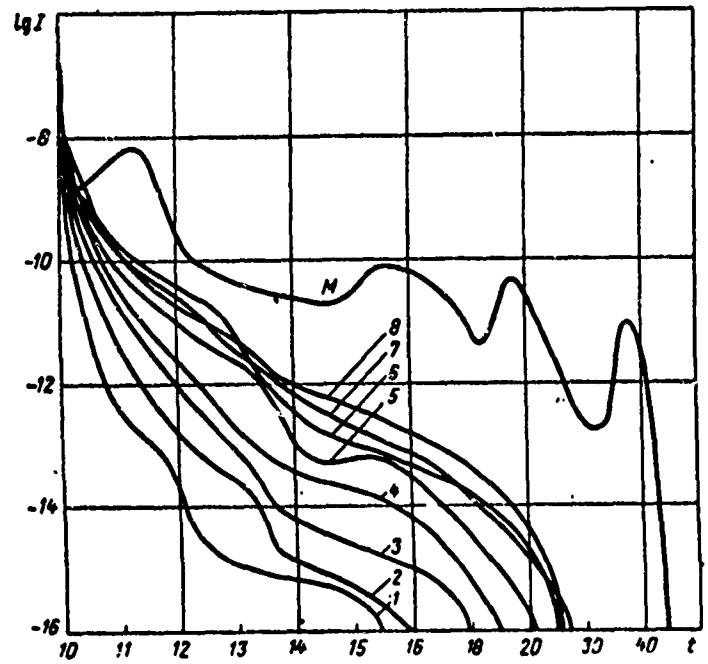

Fig. 9.18. Calculation results for the radiation intensity time curve caused by photons with various scattering multiplicities for the wavelength 0.7 μ and the value τ = 10.0 in a water cloud

The diameters of the source and receiver are equal to 4 and 150 mm. Curves 1, 2, ..., 8 correspond to 1, 2, ..., 8 scattering multiplicities, curve M to all multiplicities greater than 8

In article [842] the nonstationary transfer equation was formulated and solved approximately for the single and double scattering of a narrow collimated beam. In the calculations a spherical scattering indicatrix was used. The solutions of the equation are valid for media in which the photon survival

probability is less than 0.8 (the absorption coefficient of the medium is one-fourth of the scattering coefficient). Calculations have shown that the distortion of the rectangular pulse when it passes through the medium layer is mainly caused by double scattering and depends, to a considerable extent, on the ratio of the duration of the incident pulse on the layer to the aperture of the receiver. The shape of the front of the reflected pulse is determined both by the single and double scattered radiation.

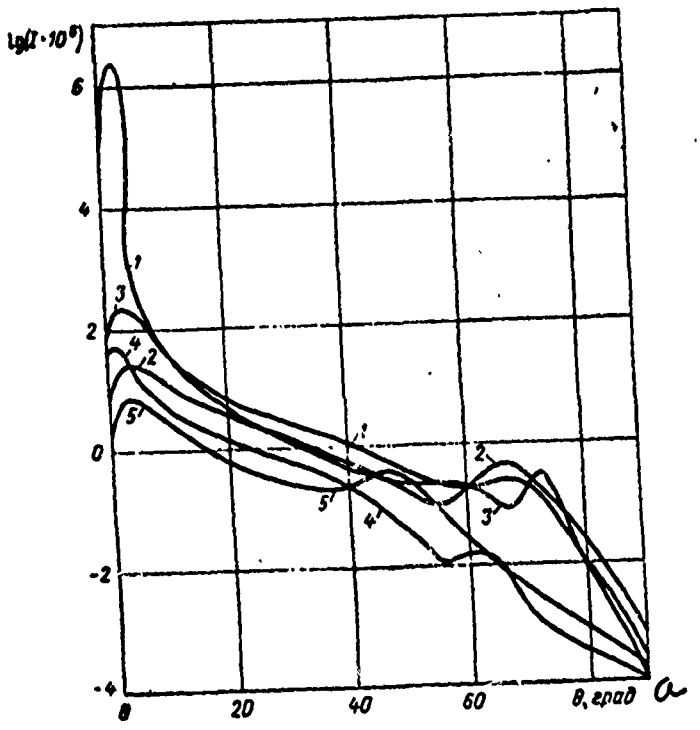

Fig. 9.19. Results of calculations of back scattering б of a radiation pulse from a cloudy medium

Curve 1--the source and receiver are combined. Curves 2, 3, 4, 5--the receiver is at various distances from the source

Key: a. degrees

The reflection of a short pulse from an infinite layer of the medium with a scattering indicatrix which is sharply elongated forward (which is more characteristic of the conditions in the atmosphere than in the previous case) is discussed in the studies of A. B. Ivanov and I. A. Katsev [840, 841]. The scattering indicatrix is given in the form of the ratio of the radiation flux scattered forward by an elementary volume to the sum of the fluxes scattered forward and backward. The results of the calculations have shown that the larger the survival probabilities of the photon and the more the scattering indicatrix is elongated forward, the larger the duration of the reflected pulse. At the same time the duration of the reflected pulse is inversely proportional to the attenuation index of the medium.

Experimental studies dealing with the propagation of pulses of small duration in various scattering media are still in the stage of obtaining the first results.

An attempt is made in article [852] to find a relation between the transparent atmosphere and the parameters of the pulse signal reflected from it. During measurements in natural nebulae it was discovered that the duration and lag of the pulse reflected in the medium depend on the value of the attenuation coefficient α. As α increases from 0.001 to 0.01 m^{-1}, the duration of the reflected pulse varies from 2 - 3 to 0.5 msec.

The deformation of the radiation pulse of a semiconductor laser based on gallium arsenide was studied experimentally in the author's laboratory (wavelength 0.84 μ) during reflection from artificial water clouds and mists [852]. The duration of the original pulse on the 0.5 level by amplitude was equal to 8 nsec. The attenuation coefficients of the medium varied from 0.02 to 1.0 m^{-1}. The receiver and source of the radiation were located in such a way that their optical axes intersected inside the sphere investigated at an angle of 1° at a distance of 7 m from the front boundary.

Some results obtained from the studies of the pulse deformation reflected from clouds with various densities are plotted in Fig. 9.20. The vertical lines in the diagram are spaced 10 nsec from one another. The pulse from the source is shifted to the right by 50 nsec from its true position and its amplitude is reduced 10^5 times.

It can be seen from the figure that when the attenuation coefficient decreases or, equivalently, when the optical density of the medium decreases, the duration of the forward

front of the reflected pulse increases and its curvature decreases.

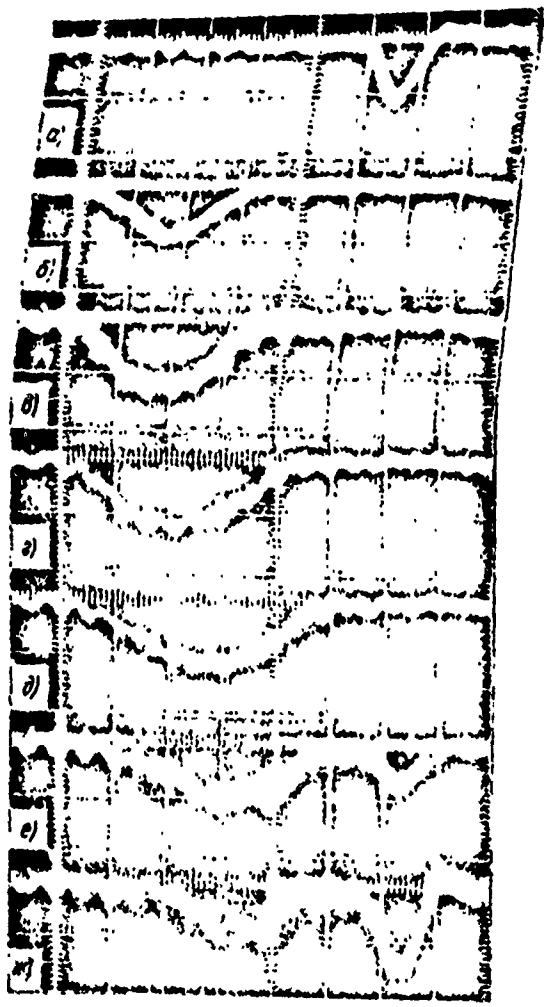

Fig. 9.20. Oscillograms of radiation pulses reflected from cloud layers with various values of the attenuation coefficients: a) radiation pulse from the source, b) $\alpha = 1.5\ m^{-1}$, c) $\alpha = 0.84\ m^{-1}$, d) $\alpha = 0.43\ m^{-1}$, e) $\alpha = 0.25\ m^{-1}$, f) $\alpha = 0.13\ m^{-1}$, g) α 0.08 m^{-1}

At the same time the duration of the rear front of the reflected pulse also first increases and then begins to decrease.

The latter is caused by the effect of the rear boundary of the scattering medium. The sharp pulse in the right lower part of the oscillogram is caused by the reflection of the radiation from the rear wall of the chamber in which the measurements were made.

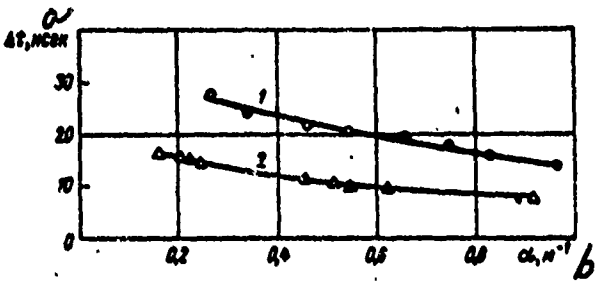

Fig. 9.21. The duration of the pulses reflected from nebulae and mists vs the attenuation coefficients

Key: a. nsec
b. m^{-1}

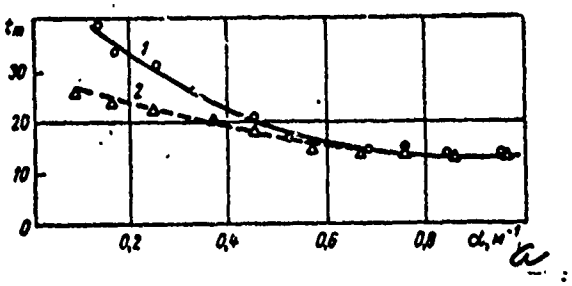

Fig. 9.22. The lag in the pulses reflected from nebulae and mists vs the attenuation coefficients

Key: a. m^{-1}

Figure 9.21 gives the relation between the duration of the pulses reflected from nebula (top curve) and mists (bottom curve) and the value of the attenuation coefficient. As seen from the diagram in both cases the duration of the reflected pulses decreases as the attenuation coefficient increases and

tends to the duration of the pulse from the source. This is related to the fact that the reflected signal is primarily formed in layers in the immediate vicinity of the source. The length of these layers decreases as the density of the medium increases. Equal durations of the pulses reflected from nebulae and mists for the same values of α are apparently brought on by the corresponding difference in the scattering indicatrices of these media.

The pulse delays t_m of pulses reflected by nebula 1 and mists 2 vs the values of the attenuation coefficient are plotted in Fig. 9.22. We note that by a pulse delay we mean the time interval between the time when the pulse was dispatched and the maximum value of the signal which was received. It can be seen from the figure that for nebulae the quantity t_m decreases faster when α increases than in the case of mists. For values $\alpha > 0.5\ m^{-1}$ the difference in the values t_m for nebulae and mists vanishes for all practical purposes. The following qualitative explanation for the different relation between t_m and small α in nebulae and mists can be given. When the optical densities of the medium are small, the principal role in the formation of the reflected signal is played by small scattering multiplicities when the difference in the scattering indicatrices of the media has an important effect on the formation of this signal. The pulse reflected in nebulae is formed from more distant layers than in the case of mists.

In conclusion we note that the results of the experimental studies of the deformation of a pulse reflected from nebulae which were described were also obtained computationally, using the Monte Carlo method [835]. The calculated and experimental data were in satisfactory agreement, which again confirms the effectiveness of the Monte Carlo method when it is used to investigate the laws which govern the propagation of spatially bounded light beams in scattering and absorbing media.

10. Nonlinear Effects Which Accompany the Propagation of Powerful Light Radiation in the Atmosphere

During the propagation in the atmosphere of optical radiation of giant power which is attained during the operation of individual pulsed lasers in the modulated "goodness" mode in the great energy of many lasers in the free generation pulses and during operation in the continuous mode there arises a series

of nonlinear effects which accompany the propagation of this radiation in the atmosphere.

The presence of the effect mentioned above is first of all responsible for the inapplicability of the Buger law to the description of the damped radiation due both to molecular absorption by gaseous components in the atmosphere and due to the scattering by aerosol particles.

When the power and energy of the optical radiation are large, the other laws which govern the propagation of optical waves described in the preceding chapters of the monograph are also inapplicable.

In this chapter we will discuss some multiphoton effects which do not require that interference phenomena be taken into account (multiphoton ionization, dissociation, leading to a breakdown in the pure air layer), the spectroscopic saturation effect which causes the partial brightness of the absorbing dark layer, the self-focusing effect of the beam caused by the nonlinear relation for the refractive index of the medium irradiated by a powerful radiation flux, and the vaporization effects of aerosol particles under the action of pulse and continuous radiation sources of great power and energy.

1. Probability of Multiphoton Processes

A relatively large number of papers are devoted to the theoretical investigation of multiphoton processes. The reader can find an analysis of these papers and a detailed bibliography in the surveys [857-860]. In [857] papers are discussed in which the usual variant from perturbation theory is applied to the description of multiphoton processes induced by the corresponding interaction of the radiation field with the substance. The processes which are discussed in greatest detail in [857] are two photon processes, in particular light resonance scattering by atoms.

To describe multiphoton processes, the formalism of scattering theory was used in article [858]. The probabilities of these processes were calculated with the aid of the diagram technique used in perturbation theory.

Multiphoton transitions in the optical wavelength band are discussed in survey [859]. The work dealing with multiphoton ionization in inertial gases is analyzed in detail.

In article [860] breakdown in gases, the multiquantum photo effect and a number of allied problems are discussed.

In this chapter we discuss the problem of multiphoton processes during the propagation of powerful optical radiation following a procedure developed by S. D. Tvorogov and L. I. Nesmelova [696]. During the discussion we only refer to those articles which have a direct bearing on the material discussed.

We will first consider the problem of calculating the probability of a transition of some quantum system from some fixed state into another state.

We denote by H the Hamiltonian of the system. Then the evolution of the wavefunction ψ of the system is described by the Schrodinger equation

$$i\hbar \frac{\partial \psi}{\partial t} = H\psi. \tag{10.1}$$

The formal solution of (10.1) can be written in the form

$$\psi(t) = S(t)\psi(0), \tag{10.2}$$

where $\psi(0)$ is the initial value of the wavefunction, and S(t) is a unitary operator describing the time evolution of the system. (10.1) and (10.2) imply

$$i\hbar \frac{\partial S}{\partial t} = HS, \quad S(0) = 1. \tag{10.3}$$

The relations (10.3) define completely the mathematical problem of computing the operator S.

We will consider some operator M with the eigenfunctions φ_n. If our system is in a state which is described by some φ_n, the quantity which corresponds to the operator M takes on some fixed value M_n.

We will now select for the initial condition ψ some function φ_n. Because φ_n is orthonormal, the function $\psi(t)$ can be

written as follows

$$\psi(t) = \sum C_m(t)\,\varphi_m. \tag{10.4}$$

According to the general rule of quantum mechanics, the quantity $|C_m(t)|^2$ defines the probability that the system under investigation will be in the state described by the function φ_m at the instant t.

Substituting (10.4) in (10.2) and selecting the initial conditions so that $\psi(0) = \varphi_n$,

$$\sum_{m'} C_{m'}(t)\,\varphi_{m'} = S(t)\,\varphi_n. \tag{10.5}$$

Multiplying both sides of (10.5) on the left by φ_m^* and integrating the functions φ with respect to the variables ξ, and using the relation $\int \varphi_m^* \varphi_{m'}\, d\xi = \delta_{mm'}$, we obtain $C_m = \langle \varphi_m | S(t) | \varphi_n \rangle$. Here the symbol $\langle\ \rangle$ denotes the scalar product which is defined as usual:

$$\langle f | S | g \rangle = \int f^*(\xi)\, Sg(\xi)\, d\xi.$$

We will denote by W_{mn} the probability that our system will make a transition from state φ_n into state φ_m in time t. The definition of C_m implies that

$$W_{mn} = |\langle \varphi_m | S(t)\,\varphi_n \rangle|^2. \tag{10.6}$$

We will now apply the result (10.6) to the analysis of a system consisting of a molecule (atom) and the electromagnetic field. The total Hamiltonian of the system is in this case

$$H = H_0 + H_R + H_{0R}, \tag{10.7}$$

where H_0 is the Hamiltonian of the molecule, H_R is the Hamiltonian of the radiation field, and H_{0R} is the Hamiltonian of the interacting field and the molecule.

We will denote by $\varkappa_n(x)$ and $\psi_{n_k}(\xi)$ the eigenfunctions of H_0 and H_R. The function $\varkappa_n(x)$ is a function of the molecular variables x and describes a certain state of the molecule. The function $\psi_{n_k}(\xi)$ defines the state of the field in which the number of photons is n_k, and is a function of the field variables. Below we will consider a monochromatic field.

We let $M = H_0 + H_R$. Then, because H_0 and H_R can be commuted, $\varphi_n = \varkappa_n(x)\,\psi_{n_k}(\xi)$ since these operators operate on different variables. The functions which were written down describe the situation when the molecule is in state $\varkappa_n$ and the field contains n_k photons. We will assume that the molecule made a transition to some state $\varkappa_m$ and that this transition led to the absorption of N photons. Then in the final state of the system the plus molecule in the field will be determined by the function $\varphi_m = \varkappa_m \psi_{n_k - N}$. According to relation (10.6) the probability of the transition can be calculated from the formula

$$W = |\langle \varkappa_m \psi_{n_k - N} | S | \varkappa_n \psi_n \rangle|^2. \qquad (10.8)$$

The operator S can be found from (10.2) after substitution of (10.7) in (10.3). The operator H_0 is the usual operator for a molecule or atom which takes into account all interactions between the atomic or molecular particles. The other two operators in (10.7) have in longwave approximation the form

$$H_R = \hbar\omega a^* a,$$
$$H_{0R} = \beta P (a + a^*) + \alpha (a + a^*)^2,$$

where

$$\beta = -(e/m)(2\pi\hbar/\omega)^{1/2}, \quad \alpha = e^2\pi\hbar/\eta\omega c;$$

h is the Planck constant, c is the velocity of light, ω is the frequency of the field, a and a* are the birth and death process operators for the photons, P is the projection of the vector $m\vec{v}$ in the photon polarization direction, m, e, $\vec{v}$ are the mass, charge and velocity operator for the particles. We also note that the eigenfunctions H_R are the eigenfunctions of a harmonic oscillator.

Formula (10.8) enables us to calculate the probability of N-photon absorption in time t. Usually the matrix elements are integrals of fast oscillating functions. Therefore, for the probability of the transition F per unit time we can write the relation

$$F = \lim_{t\to\infty} \frac{d}{dt} |\langle \varkappa_m \psi_{n_k - N} | S | \varkappa_n \psi_{n_k} \rangle|^2. \tag{10.9}$$

The energy spectrum of the operator H_0 consists of discrete levels and a continuous path. The wavefunctions which corresponds to the energy values of the continuous spectrum describe the dissociated or ionized state of an atom or a molecule. If these functions are substituted in (10.9) instead of x_m, we obtain the probability of N-photon dissociation or ionization.

2. Calculations of the Transition Probability by Successive Approximations

After substitution of (10.7) in (10.3) we obtain an equation for calculating the operator S:

$$i\hbar \frac{\partial S}{\partial t} = (H_0 + H_R + H_{0R}) S. \tag{10.10}$$

We will now pass on to representation of the interaction. We set $S = g(t) \exp[(t/i\hbar)(H_0 + H_R)]$. Then (10.10) implies that

$$i\hbar \frac{\partial g}{\partial t} = H'_{0R}(t) g(t), \quad g(0) = 1, \tag{10.11}$$

and $H'_{0R}(t) = \exp[-(t/i\hbar)(H_0+H_R)]\, H_{0R} \exp[(t/i\hbar)(H_0+H_R)]$.
We let $g(t) = \sum_{n=0}^{\infty} g_n(t)$ and using the usual iterative procedure we obtain the recurrence equations $i\hbar(\partial g_n/\partial t) = H'_{0R} g_{n-1}(t)$, $g_0 = 1$. After we solve successively these equations we can calculate F.

The final result for F has the form [696]:

$$F = \sum_{n=n'}^{\infty} F_n \sum_{k=k'}^{2n-1} n_k^k \beta^{2(2n-k)} \alpha^{2(k-n)} \times \times \left(C_k^{\frac{k+N}{2}}\right)^2 \cdot |\{P_{2n-k}, I_{k-n}\}|^2. \qquad (10.12)$$

In the above C_j^j, is the binomial coefficient, $n' = (N+1)/2$, if N is odd, and $n' = N/2$ when N is even, $k' = N$ for $n \leqslant N$ and $k' = n$ for $n > N$. The prime in the second sum denotes that when we sum over k we must keep the terms for which $(k + N)/2$ is an integer

$$F_n = \frac{2\pi}{\hbar^2} \times \times \left\{ \frac{\delta(E_A/\hbar - E_B/\hbar - n\omega)}{(E_B - E_{A_1} + \hbar\omega)^2 (E_B - E_{A_2} + 2\hbar\omega)^2 \ldots (E_B - E_{A_{n-1}} + (n-1)\hbar\omega)^2} + \right.$$
$$+ \frac{\delta[E_A/\hbar - E_{A_1}/\hbar - (n-1)\omega]}{(E_{A_1} - E_B - \hbar\omega)^2 (E_{A_1} - E_{A_2} + \hbar\omega)^2 \ldots (E_{A_1} - E_{A_{n-1}} + (n-2)\hbar\omega)^2} + \ldots$$
$$\left. \ldots + \frac{\delta(E_A/\hbar - E_{A_{n-1}}/\hbar - \omega)}{(E_{A_{n-1}} - E_B - (n-1)\hbar\omega)^2 (E_{A_{n-1}} - E_{A_1} - (n-2)\hbar\omega)^2 \ldots (E_{A_{n-1}} - E_{A_{n-2}} - \omega)^2} \right\},$$

where E_B and E_A are respectively the energy in the initial and final state of the system and E_c are the eigenvalues of the operator H_0.

The expression defined by the symbol $\{P_{2n-k}, I_{k-n}\}$, is constructed as follows. We write the matrix element $\langle \varphi_{A_n} | N(PI) | \varphi_B \rangle$, where φ_{A_1} are the eigenfunctions of the

H_0, and N(PI) is the sum of all permutations of (2n - k) operators P and k - n unit operators I. The intermediate subscripts are written in the sequence A_n, A_{n-1}, A_{n-2}, ..., B and then the summation extends over these subscripts

In the expression for F_n the summation extends over all subscripts A_1, A_2, ..., A_l, ...

The subscript n in (10.12) numbers the various orders from perturbation theory (according to the operator H_{OR}). If only the first term is taken into account in the operator H_{OR}, then we sum over n with n' = N.

Further, as the corresponding estimates imply, when F is analyzed, both terms in the interaction operator H_{OR} must be taken into account. We note that the multiphoton processes were calculated on the basis of only the first term in the interaction operator in [697, 861]. In article [698] processes are analyzed in which several photons with different frequencies participate. These processes are also called multiphoton processes. However the authors of [698] consider only cases which must be called single photon in the sense of formula (10.8) (N = 1). Of course, when such situations are discussed it suffices to take into account only the first term in the operator H_{OR}, a proposition which was stated by the authors of the article under consideration in the form of a special theorem.

In the case of a transition into the continuous spectrum (multiphoton dissociation and ionization processes) relation (10.12) must be integrated with respect to the energy of the finite state after it has been multiplied by the density for these states. The presence of δ-functions in this state reduces the integration to replacing the δ-functions by $\hbar\rho$, where ρ is the density of the states mentioned above:

$$\rho = (m/\hbar^2)(2\pi)^{-3} k\, d\Omega;$$

dΩ is an element of the solid angle, $k = \hbar^{-1}\sqrt{E/m}$, $E = E_{A_l} + (n - l)\hbar\omega - E'$, E', is the dissociation or ionization energy and the indices n and l are defined in accordance with the procedure used to construct the quantity F_n.

3. Estimates of the Probability of Multiphoton Photoionization and Photodissociation

The probabilities for a multiphoton process can only be calculated if the matrix elements of the dipole moment and the energy levels of the molecule or atom are known. Using the data available in the literature about the energy spectrum and the matrix elements of dipole transitions, the ionization probabilities were calculated for a hydrogen atom during two-, three- and four-photon absorption. The values of F obtained for various wavelengths are given in Table 10.1.

In the case of atmospheric gas molecules, when the processes considered are analyzed, we are dealing with electronic molecular weights. In this case the calculation of the matrix elements and the energy levels is an exceptionally complex problem. The corresponding data is available at the present time only for the simplest atoms and molecules. The situation is analogous when the wavefunction of a multiatom dissociated molecule is analyzed, which must be known in order to calculate the matrix elements of the dipole moment in (10.12).

Because of the facts which were mentioned, below we give only estimates for several quantities which characterize multiphoton processes. It is assumed in these estimates that the matrix elements of the dipole moment are quantities on the order of magnitude of 10^{-18} CGSE units.

TABLE 10.1

VALUES OF F FOR VARIOUS λ

N = 2		N = 3		N = 4	
λ, мкм a	F, сек⁻¹ b	λ, мкм	F, сек⁻¹	λ, мкм	F, сек⁻¹
0,135	$7\cdot10^{-30}n_k^2$	0,258	$10^{-50}n_k^3$	0,344	$2\cdot10^{-72}n_k^4$
0,128	$2\cdot10^{-29}n_k^2$	0,253	$10^{-50}n_k^3$	0,335	$10^{-72}n_k^4$
0,124	$9\cdot10^{-29}n_k^2$	0,248	$10^{-50}n_k^3$	0,326	$6\cdot10^{-72}n_k^4$
0,122	$2\cdot10^{-28}n_k^2$	0,243	$2\cdot10^{-48}n_k^3$	0,317	$6\cdot10^{-73}n_k^4$
0,118	$3\cdot10^{-29}n_k^2$	0,238	$10^{-51}n_k^3$	0,310	$5\cdot10^{-73}n_k^4$
0,113	$2\cdot10^{-30}n_k^2$	0,234	$10^{-51}n_k^3$	0,302	$5\cdot10^{-73}n_k^4$

[1] Примечание: n_k — число фотонов в единице объема ($см^{-3}$); N — число поглощенных фотонов.

Key: a. λ, μ
b. F, sec^{-1}

(continued next page)

Key, Table 10.1 (cont'd)

1. Note: n_k is the number of photons per unit volume (cm^{-3}), N is the number of absorbed photons

The characteristics of an N-photon process are estimated regardless of which process actually occurs (photoionization, photodissociation, change in the electronic or vibration rotation state).

Table 10.2 gives the values which were calculated under the conditions mentioned for various terms of the sum in (10.12), for N from 1 to 12.

Table 10.3 gives the probabilities for multiphoton processes (N = 1(1) 12) for various n_k. The table gives the quantity b in the expression $F = 10^b$ for various a in the expression $n_k = 10^a$.

When we know the probabilities of the corresponding transitions, we can estimate the absorption coefficient τ of a multiphoton process. τ and F are related by [71]

$$\tau[cm^{-1}] = \frac{F(I)\,n_0}{Ic}, \qquad (10.13)$$

Key: a. cm^{-1}

where n_0 is the number of absorbing molecules per unit volume, I is the radiation intensity, where in the case of a plane wave

$$I = c\hbar\omega_k n_k. \qquad (10.14)$$

The differential relation for determining the radiation absorbed now has the form

$$dI = -\tau(I)\,I\,dx, \qquad (10.15)$$

where x is the distance covered by the light beam in the medium.

TABLE 10.2
VALUES OF DIFFERENT TERMS IN THE SUM (10.12)

N	E, сек⁻¹ а					
	1	2	3	4	5	6
1.	$10^{-9,33}n_k$					
2	$10^{-32,49}n_k^2$					
3	$10^{-58,6}n_k^3$	$10^{-94,9}n_k^4$				
4	$10^{-74,9}n_k^4$	$10^{-116,2}n_k^5$				
5	$10^{-95,4}n_k^5$	$11^{-136,7}n_k^6$	$10^{-178,2}n_k^8$			
6	$10^{-117,7}n_k^6$	$10^{-158,7}n_k^7$	$10^{-199,9}n_k^{10}$			
7	$10^{-123,9}n_k^7$	$10^{-179,5}n_k^8$	$10^{-220,6}n_k^{11}$			
8	$10^{-160,5}n_k^8$	$10^{-201,2}n_k^{10}$	$10^{-242,6}n_k^{12}$	$10^{-284,1}n_k^{14}$		
9	$10^{-181,2}n_k^9$	$10^{-222,0}n_k^{11}$	$10^{-263,5}n_k^{13}$	$10^{-304,9}n_k^{15}$	$10^{-346,3}n_k^{17}$	
10	$10^{-203,2}n_k^{10}$	$10^{-244,0}n_k^{12}$	$10^{-285,3}n_k^{14}$	$10^{-326,5}n_k^{16}$	$10^{-367,9}n_k^{18}$	
11	$10^{-224,1}n_k^{11}$	$10^{-265}n_k^{13}$	$10^{-306,1}n_k^{15}$	$10^{-347,4}n_k^{17}$	$10^{-388,8}n_k^{19}$	$10^{-430,2}n_k^{21}$
12	$10^{-246,2}n_k^{12}$	$10^{-287}n_k^{14}$	$10^{-327,8}n_k^{16}$	$10^{-369,1}n_k^{18}$	$10^{-412,3}n_k^{20}$	$10^{-451,3}n_k^{22}$

Key: a. E, sec^{-1}

TABLE 10.3
THE VALUES OF a AND b IN THE EXPRESSIONS $n_k = 10^a$, $F = 10^b$

N	a						
	18	19	20	21	22	20,5	21,5
1	8,2	9,2	10,2	11,2	12,2	10,7	11,7
2	3,6	5,6	7,6	9,6	11,6	8,6	10,6
3	1,4	4,4	7,4	11,1	16,0	9,5	13,6
4	−2,9	1,1	5,1	9,8	15,8	7,3	12,8
5	−5,4	−0,1	4,6	11,1	19,8	7,5	15,3
6	−9,7	−3,7	2,3	10,3	20,1	5,8	15,0
7	−12,1	−5,1	1,9	10,9	23,7	6,0	17,2
8	−16,5	−8,5	−0,5	10,1	23,9	4,0	17,0
9	−19,3	−10,3	−1,3	10,9	27,7	3,9	19,2
10	−23,2	−13,2	−3,2	10,8	28,1	2,5	19,2
11	−26,1	−15,2	−4,1	11,5	31,8	2,0	21,3
12	−30,2	−18,2	−6,2	10,7	32,7	0,3	21,7

In the case of a homogeneous medium we obtain from (10.15) and (10.13)

$$x = -\frac{c}{n_0}\int \frac{dI}{F(I)}. \qquad (10.16)$$

The integral in (10.16) can always be evaluated since in our case F is according to (10.12) and (10.14) a polynomial in I. However, to write down explicit expressions we must know the corresponding coefficients. After the integral is evaluated we can find I(x) by solving the equation which is obtained. In general form the entire problem can be described for any N.

For the single photon process from (10.16) follows the well-known exponentially decreasing intensity. For a two-photon process we have

$$T = \frac{I_0 x \gamma_2 n_0}{c+1},$$

where $T = I/I_0$, I_0 is the radiation intensity incident on the medium layer, γ_2 is the coefficient in front of I^2 in the expression for F for the case of a two-photon process. For a three-photon process we have the equation

$$x = \Gamma_1 I^{-2} + \Gamma_2 \ln I + \Gamma_3 \operatorname{arctg} \Gamma_4 I + \text{const},$$

where Γ_j are constants.

The last equation no longer allows us to write the expression for T in explicit form. For $N > 3$ equation (10.16) has even a more complex form.

An analysis of the data in Tables 10.2 and 10.3 shows that for certain N and n_k in the sum (10.12) we can restrict ourselves only to several terms. Then $F(I) = \gamma_j I^{b_j}$, and for the ratio I/I_0 we have the formula

$$\frac{I}{I_0} = \frac{1}{\sqrt[b_j]{\frac{I_0^{b_j-1}x}{\sigma}+1}}, \qquad (10.17)$$

$$\sigma = \frac{c}{n_0 k (b_j - 1) (\hbar\omega_{kc})^{b_j - 1}}. \qquad (10.18)$$

When the I_0 are sufficiently large we can ignore the 1 in (10.17) and write the equation

$$x = \sigma \left(\frac{I/I_0}{I_0}\right)^{b_j - 1}; \qquad (10.19)$$

which enables us to calculate the distance x which corresponds to a particular value of the transparency $T = I/I_0$ (Table 10.4).

We note that as the estimates have shown, the results of such calculations do not depend much on the selected value of T. The number zero in the table denotes that the required absorption takes place at the very beginning when the radiation is propagated in the medium (the phenomenon can have the character of an explosion), the ∞ symbol shows that the corresponding distance is greater than 10^7 cm.

TABLE 10.4

THE VALUES OF THE DISTANCES PASSED BY THE BEAM FOR VARIOUS N, n_k, $n_0 = 2.4 \cdot 10^{19}$ AND T = 0.1

N	n_k, cm^{-3} a				
	10^{17}	10^{18}	$10^{18,5}$	10^{19}	10^{20}
2	$3 \cdot 10^4$	$3 \cdot 10^3$	$3 \cdot 10^{2,5}$	$3 \cdot 10^2$	$3 \cdot 10^1$
3	$2 \cdot 10^6$	$2 \cdot 10^5$	$2 \cdot 10^4$	2	$2 \cdot 10^{-4}$
4	∞	$3 \cdot 10^7$	$2 \cdot 10^{6,5}$	$2 \cdot 10^1$	$2 \cdot 10^{-4}$
5	∞	$5 \cdot 10^6$	$5 \cdot 10^4$	$8 \cdot 10$	0
6	∞	$7 \cdot 10^7$	$4 \cdot 10^{4,5}$	4	0
7	∞	∞	$2 \cdot 10^5$	$2 \cdot 10^{-1}$	0
8	∞	∞	$3 \cdot 10^{5,5}$	3	0
9	∞	∞	10^7	2	0
10	∞	∞	$8 \cdot 10^{7,5}$	$8 \cdot 10^{-1}$	0
11	∞	∞	∞	$8 \cdot 10^{-2}$	0
12	∞	∞	∞	$9 \cdot 10^{-2}$	0

Key: a. n_k, cm^{-3}

Using the quantity F we can determine the time needed for the decay of a particular proportion of molecules or atoms. The corresponding expression follows from the well-known decay relation:

$$n = n_0 e^{-Ft}, \tag{10.20}$$

where n and n_0 are the number of molecules (atoms) "preserved" at the instant t and when t = 0. If we define the time for the partial decay τ^0 as the interval in which the ratio n/n_0 attains a certain value, then

$$\tau^0 = \frac{\ln n_0/n}{F}. \tag{10.21}$$

Table 10.5 gives the values of τ^0 for $n/n_0 = 0.1$ and various N and n_k. The ∞ symbol denotes in this table that τ^0 is greater than 10^4 sec.

The process considered can occur during molecular or atomic decay of the medium in the focus of some lens. The relation between the photon density n_{k_t} in the focus of the lens and in the incident beam n_k can be determined from the correspondence principle. If R is the radius of the lens and f is its focal distance, then

$$n_{k_t} = n_k \frac{R^2 \omega_k^2}{8 f^2 c^2}. \tag{10.22}$$

The order of the N-photon process is easily estimated from the relation

$$N = \left[\frac{E_1 - E_2}{\omega_k}\right],$$

where the symbol [ ] denotes the integer part of the number, E_1 is the ionization or dissociation energy, E_2 is the energy of the lower (as a rule fundamental) state.

TABLE 10.5

VALUES OF τ^0 IN SECONDS FOR VARIOUS N and n_k WHEN $n/n_0 = 1$

N	n_k		
	10^{18}	10^{19}	10^{20}
2	$10^{-3,3}$	$10^{-5,3}$	$10^{-7,3}$
3	10^{-1}	10^{-4}	10^{-7}
4	$10^{0,3}$	$10^{0,7}$	$10^{-4,7}$
5	∞	$10^{0,8}$	$10^{-4,3}$
6	∞	$10^{1,1}$	$10^{-1,9}$
7	∞	∞	$10^{-1,5}$
8	∞	∞	$10^{0,9}$
9	∞	∞	$10^{1,7}$
10	∞	∞	$10^{2,6}$
11	∞	∞	$10^{4,5}$
12	∞	∞	$10^{6,6}$

TABLE 10.6

DISSOCIATION ENERGY E_D OF THE MOLECULES O_2, N_2, CO_2, H_2O, THE IONIZATION ENERGY E_I OF THE ATOMS N, O, C, H AND THE ORDERS OF THE MULTIPHOTON PROCESSES FOR THE RADIATION FROM LASERS BASED ON GLASS WITH NEODYMIUM $\lambda = 1.06\ \mu$ (N_1) AND A RUBY LASER $\lambda = 0.69\ \mu$ (N_2)

a Молекула	O_2	N_2	CO_2	H_2O	b Атом	N	O	C	H
E_D, ev	5,08	9,76	2,8	5,1	E_I, ev	14,5	13,6	11,27	13,6
N_1	5	9	3	5	N_1	13	12	10	12
N_2	3	6	2	3	N_2	9	8	7	8

Key: a. Molecule
b. Atom

Table 10.6 gives the values of the dissociation energy for molecules of the main atmospheric gases and the ionization energy of their atoms.

4. Spectroscopic Saturation Effect

The spectroscopic saturation effect in the case of elastic molecular collisions was studied in sufficient detail, for example in [699, 700]. We will analyze completely the quantum variant of this effect in which it is possible to study non-elastic molecular collisions in a single-photon light absorption process. The saturation problem in multiphoton processes is described in article [862].

The Hamiltonian for the problem under consideration can be written in the form

$$H = H_1 + H_2 + H_c(t) + H_R + H_{1R}, \qquad (10.23)$$

where H_1, H_2 and H_R are the Hamiltonians of the first and second molecules and of the radiation field. The operator $H_c(t)$ takes into account the interaction between the two molecules (collision) which depends on time, and H_{1R} the interaction between the field and the first (light absorbing) molecule. The second molecule does not absorb the radiation (at least during single photon interaction) but only deforms the state of the first molecule.

Since in this problem we are dealing with connected states the initial condition must be formulated for some instant of time t = 0 which is considered to coincide with the time when some collision begins. The solution to problem (10.23) must further be sought for an instant of time $t \gg \tau$, where τ is some critical (correlation) time which depends on the nature of the interaction $H_c(t)$. With certain known approximation τ can be interpreted as the mean lead time with which one molecule leads another or the collision time of the molecules.

Arguments which are almost exactly the same as those made in paragraph 1 enable us to obtain the results:

$$P_{BA} = |\langle \psi_{n_{k-1}}(\tau)\, \varphi_m(\tau) | S | \psi_{n_k}(0)\, \varphi_n(0) \rangle|^2. \qquad (10.24)$$

Here P_{BA} is the probability that the system will make a transition from state A into state B in the time τ, and the state is defined as some state of the field in which the number of photons is equal to n_k and the n-state of the interacting molecules, the state B is the m-state of the molecules and the state of the field in which the number of photons is n_{k-1}. The following notation is used in expression (10.24): ψ_{n_k} are the eigenfunctions of the operator H_R, $\varphi_n(0)$ are the eigenfunctions of the operator $H_1 + H_2$, $\varphi_n(t) = S_c(t)\varphi_n(0)$. The operators S and S_c satisfy the equations

$$i\hbar \frac{\partial S}{\partial t} = HS, \tag{10.25}$$

$$i\hbar \frac{\partial S_c}{\partial t} = (H_1 + H_2 + H_c(t))\, S_c. \tag{10.26}$$

The functions $\psi_{n_{k-1}}(\tau) = S_R \psi_{n_{k-1}}$ and $S_R = \exp\left(\frac{t}{i\hbar} H_R\right)$. Hence, in (10.24) $\psi_{n_{k-1}}(\tau)$ can be replaced by $\psi_{n_{k-1}}(0)$.

Further, expression (10.24) must be summed over m to take into account all possible transitions which accompany the absorption of a single photon from a fixed state into any other state. After this operation

$$\sum_{(B)} P_{BA} = \langle P_n(0) \,|\, F \,|\, \varphi_n(0) \rangle, \tag{10.27}$$

$$F = \int \bar{\psi}_{n_k}(p)\, U^{-1}(p, q)\, \psi_{n_{k-1}}(p)\, \psi_{n_{k-1}}(p') \times \times U(p', q)\, \psi_{n_k}(p')\, dp\, dp', \tag{10.28}$$

where P are the variables of the field function, and q are the variables of the molecular functions. The operator $U = SS'^{-1}$, $S' = S_c S_R$. Since the operator U is unitary, it follows that F is a Hermitian operator.

Further (10.27) must be averaged over the initial molecular states. According to the general rule averaging a quantity of the type considered leads to the relation

$$P = S_p \rho_0 F. \tag{10.29}$$

Here P denotes the sum $\sum_{(A)} P_{BA}$, ρ_0 which is averaged over the initial molecular states and ρ is the Boltzman density matrix for the Hamiltonian $H_1 \overset{0}{+} H_2$.

We note that the result (10.29) can be obtained if we start out with the expression for the density matrix ρ which satisfies the equation

$$i\hbar \frac{\partial \rho}{\partial t} = H\rho - \rho H \tag{10.30}$$

with the Hamiltonian of the system (10.23) and the initial conditions

$$\rho^{(0)}_{nn_k, nn_k} = 1, \quad \rho^{(0)}_{mm_k, nn_k} = 0. \tag{10.31}$$

Then the expression (10.24) for the probability of a transition $A \to B$ is written as a diagonal element $\rho_{mn_{k-1}, mn_{k-1}}$ in the density matrix, and after summing over the finite state and averaging over the initial states of the system $H_1 + H_2$ we arrive at expression (10.29).

The expression for P must be averaged over the collisions. Technically this is done using the procedure described in article [71].

Equation (10.25) is further solved according to perturbation theory for the interaction operator H_{1R}. The integrals (10.28) are evaluated using the rules for the birth & death process operators for photons. A method for computing the sums (10.29) which is based on group theory is given in [71, 56]. Because of laboriousness we omit all intermediate calculations and give the finite expression for the function which we write immediately

$$\omega = \frac{P}{n_k c \tau}, \qquad (10.32)$$

which is interpreted as the absorption coefficient for a single absorbing molecule:

$$\omega = 2\gamma \sum_{\substack{a, b \\ \alpha, \beta}} \frac{\rho_{aa}^{(0)}}{2a+1} \times \times \frac{|\langle a\alpha | \mu | b\beta \rangle|^2 (\sigma_{ba}^{(r)})^2}{(\omega_k - \omega_{ba} + \sigma_{ba}^{(i)})^2 + (\sigma_{ba}^{(r)})^2 + 2\eta\tau n_k (\sigma_{ba}^{(2)}) |\langle a\alpha | \mu | b\beta \rangle|^2}. \qquad (10.33)$$

The following notation is used in (10.33): $\gamma = 2\pi\omega_k/\hbar c$, $\eta = 2\pi\omega_k \hbar^{-1}$, $\sigma_{ba}^{(r)}$ is the halfwidth, $\sigma_{ba}^{(i)}$ is the shift and ω_{ba} is the center of the spectral line, $\rho_{aa}^{(0)}$ are the diagonal elements of the Boltzman density matrix for the operator H_1, H_1, $\langle a\alpha | \mu | b\beta \rangle$ are the matrix elements of the dipole moment written as singular eigenfunctions of the operator H_1, and c is the velocity of light. We further note that when (10.33) is calculated only terms which contain the frequency differences are taken into account.

The term in the numerator which depends on n_k formally denotes the saturation effect. The calculation which was described emphasizes an idea which is known: the saturation effect results from the fact that the density matrix of the molecule in the presence of a strong field is different from the Boltzman matrix.

5. Light Absorption When The Saturation Effect Is Taken Into Account

Using relation (10.33), we can write the following expressions for the absorption coefficient of light at frequency ν:

$$k(\nu, I) = \sum_j \frac{a_j}{b_j(\nu) + c_j(\nu) I}. \qquad (10.34)$$

Here the summation is carried out over all lines which contributes to the light absorption at a given frequency, $a_j = S_j\gamma_j/\pi$, $b_j = (\nu - \nu_j)^2 + \gamma_j^2$, $c_j = \tau\gamma_j |\mu_j|^{-2}c^{-2}$, S_j, γ_j, ν_j and μ_j are the intensities, halfwidths, center and square of the matrix element of the dipole moment of line j, and I is the radiation intensity. We note that ν_j and γ_j are measured in inverse centimeters.

The relation which describes the variation in the intensity of the radiation in the medium has the form

$$dI = -k(I)\,I\,d\omega, \qquad (10.35)$$

where ω is the settled layer of the absorbing gas. The initial condition for (10.35) is the usual condition: $K = I_0$ when $\omega = 0$.

In essence equation (10.35) follows from the definition (10.32) of the quantity ω as the ratio of the amount of energy absorbed to the incident radiation intensity.

For a homogeneous medium equation (10.35) can be integrated exactly. However, the process involves laborious numerical calculations. Therefore (10.35) is solved more simply by successive approximations, taking advantage of the small c_jK. To achieve this equation (10.35) must be written in the form $dI/I = -k(I)\,d\omega$, and for the zero approximation we must take $I^{(0)} = I_0 \cdot \exp(-k_0\omega)$, where $k_0 = \Sigma a_j/b_j$. After several computations we obtain [703]:

$$T = T_0 \prod_j \left(\frac{1 + I_0\varkappa_j}{1 + I_0\varkappa_j T_0}\right)^{\frac{a_j}{b_j k_0}} \qquad (10.36)$$

In the above $T = I/I_0$, $T = I/I_0$, $T_0 = \exp(-k_0\omega)$, $\varkappa_j = c_j/b_j$.

The expressions for a_j and b_j imply that k_0 should be interpreted as the attenuation coefficient, which is calculated without taking into account the dependence of the molecular density matrix on the magnitude of the field. Then T_0 is the transparency which is defined as usual for a given radiation frequency. (10.36) implies that for $I_0\varkappa_j \ll 1$, $T = T_0$.

Relation (10.36) enables us to estimate the saturation effect on the transparent layer of the absorbing medium. If

$$I_0 \varkappa_j T_0 \gg 1, \quad \overset{a}{\text{то}} \quad T = 1. \tag{10.37}$$

Key: a. then

The quantity τ can be estimated on the basis of the following considerations. The collision time can be considered as the transition time of the colliding molecules from one rectilinear section of their trajectory to another. Using the corresponding results given for the solution of this problem in [704], we can write:

$$\tau = \tau_0 P^{-1/2} T^{-1/6}. \tag{10.38}$$

In (10.38) T is the absolute temperature, P is the pressure, and τ_0 is a quantity which is almost constant. If P is expressed in atm then the value of τ_0 has the order of magnitude 10^{11}. Keeping in mind the last remark we can estimate, using (10.37), the intensity at which the saturation effect becomes manifest. Along the lines used for the estimates in paragraph 3, we further let $\alpha_j = 0.1$ cm^{-1} and $T_0 = 0.1$, and we obtain for I_0 a value of the order of magnitude 10^{14} erg/cm^2/sec.

6. Self-Focusing Of A Laser Beam

The propagation of powerful laser radiation in the medium can lead to a change in the value of the refractive index in the beam channel. The difference between the values of the refractive index of the medium in the beam channel and outside the channel can be such that the divergence of the beam is eliminated. This phenomenon has been called the self-focusing of the laser beam. This phenomenon has already been studied in a relatively large number of papers [705 - 719, 844 and others].

It turns out that when the divergence of the beam is φ, in order to eliminate it, the refractive index must be changed in the beam channel compared to its value outside the channel by an amount Δn which is approximately equal to φ^2.

If the first linear term in the expansion for the polarization vector over the field in the medium is proportional to the third power of the electrical field intensity E, the refractive coefficient of such medium can be represented in the form

$$n = n_0 + n_2 E^2, \tag{10.39}$$

where n_0 is the usual refractive index, and n_2 is a coefficient which characterizes the nonlinear properties of the medium. Formula (10.39) is written on the assumption that the successive nonlinear terms of the expansion are small in comparison with the first two terms.

The nonlinear dependence of the refractive coefficient of the medium on the electrical field intensity is caused mainly by the Kerr effect and by electrostriction. In addition to this when absorption takes place in the medium, the corresponding nonlinear effect can be caused by the thermal expansion of the gas due to its heating by the absorbed wave energy.

It is known that the Kerr effect is related to the orientation of the dipole molecular moments in the direction of the strong electrical field which causes the practically inertia-free occurrence of the anisotropic properties of the refractive medium. The electrostriction effect boils down to the fact that in the region where the radiation is active, additional volumetric pressure

$$P = \frac{1}{8\pi} \rho \frac{\partial \varepsilon}{\partial \rho} E^2 \tag{10.40}$$

and the force

$$F = \operatorname{grad} P, \tag{10.41}$$

arrive, where ρ is the density and ε is the dielectric permeability of the medium. By solving the electrodynamic equations and the linearized perturbation equations for the dielectric permeability, it is possible to obtain expression for the threshold self-focusing power P_{thr}, caused by the Kerr and electrostriction effects. The value of the self-focusing power can be estimated approximately from the simple formula

$$P_{\text{a thr}} \approx \frac{\lambda c}{n_2}, \qquad (10.42)$$

Key: a. thr

where λ is the radiation wavelength, and c is the velocity of light.

Thus, the threshold self-focusing power can be smaller, the smaller the wavelength and the greater the nonlinear properties of the medium. Certain liquids have the lowest self-focusing thresholds, on the order of several tens of kilowatt. The threshold powers for gases are tens and hundred thousandths of kilowatts. This means that the self-focusing conditions will manifest themselves during the propagation of laser radiation in the atmosphere. We recall that the radiation from a number of lasers exceeds considerably by power in the pulse the threshold self-focusing power values in gases which were mentioned above.

The unit measurements which were made in the atmosphere confirmed the presence of self-focusing laser beams and have shown that together with the focusing of the beam as a whole, fine threads are formed within the beam. It should be noted that self-focusing theory forecasts the decomposition of light beams into individual components when the radiation power exceeds considerably P_{thr}. However, in the experiment fine threads are observed at powers which do not exceed P_{thr}. For the time being it is difficult to interpret unequivocally qualitatively the origin of these threads. One possible mechanism can be connected with the fluctuations in the value of the refractive index of air caused by turbulent movements in the atmosphere. Apparently these fluctuations can enhance the occurrence of the self-focusing effect at powers which are lower than the threshold power for a homogeneous medium.

So far the self-focusing phenomenon of a laser beam in the atmosphere has not yet been studied in detail.

7. The Action Of The Powerful Radiation Field On Atmospheric Aerosol Particles

The irradiation of atmospheric aerosol particles by powerful directed radiation is accompanied by a number of effects which

lead to a change in the conditions under which the radiation is propagated in the medium. Among these effects, of greatest practical interest is the vaporization of particles due to the energy absorbed by these from the field. A change in the dimensions of the particles causes a corresponding change in the three-dimensional polydispersed attenuation coefficients. Thus, the transparency of the scattering medium layer becomes dependent on the incident radiation intensity.

The slow vaporization of particles in the thermal field has been studied in sufficient detail. The most complete survey of the corresponding theoretical and experimental studies is given in the monograph of N. A. Fuks [720]. The results obtained in these studies can not be used to estimate the particle vaporization in a powerful radiation field. Studies of this phenomenon were undertaken only recently. Below we present some of the results which were obtained.

The vaporization of solid and liquid spherical particles in the radiation field in an unbounded gas medium was discussed by Williams [721]. Using the Knudsen kinetic equation, the author of [721] finds the rate at which the particles are vaporized. However, the vaporization coefficient in the Knudsen equation remains undetermined. Only preliminary estimates are given for it.

K. S. Shifrin and Zh. K. Zolotova [722] studied the vaporization kinetics of a drop under the action of solar radiation. Making the assumption that the vaporization has a stationary character, they obtained a simple analytical expression which describes the variation in the radius of the drop as a function of time:

$$\left.\begin{aligned} r &= r_0 e^{-\eta t}, \quad \frac{8\pi\varkappa}{\lambda} r \ll 1, \\ r &= r_0 - \eta' t, \quad \frac{8\pi\varkappa}{\lambda} r \gg 1, \end{aligned}\right\} \tag{10.43}$$

where r_0 and r are the radius of the drops before and after the radiation effect, t is time, η and η' are parameters, $\varkappa$ is the absorption index for the particle substance and λ is the wavelength.

It can be seen from (10.43) that for the given wavelength the radius of large drops changes, under the action of solar radiation, linearly with time, and for small drops exponentially.

Theoretical studies of the vaporization of atmospheric aerosol particles under the action of powerful radiation were carried out recently in the author's laboratory [723 - 725]. Below we give a brief discussion of the main results obtained in these studies.

1. General Equations. The heat and mass transfer processes when the general equations are derived are based on the mathematical Enscod-Chapman theory for nonhomogeneous gases [726]. The final equations which were obtained for the distribution of the partial pressure of water vapor and temperature in the particle in a spherical coordinate system have the form

$$\frac{\partial p}{\partial t}-\frac{p}{T^1}\frac{\partial T^1}{\partial t}=D\left(\frac{2}{\rho}\frac{\partial p}{\partial \rho}+\frac{\partial^2 p}{\partial \rho^2}\right)\frac{P}{P-p}+$$
$$+D\frac{P}{(P-p)^2}\left(\frac{\partial p}{\partial \rho}\right)^2, \qquad (10.44)$$

$$\frac{\partial T^1}{\partial t}=\frac{\lambda^1 R_n}{C_p}\frac{a}{\mu^a P-(\mu^w-\mu^a)p}\frac{T^1}{b}\left(\frac{\partial^2 T^1}{\partial \rho^2}+\frac{2}{\rho}\frac{\partial T^1}{\partial \rho}\right)+$$
$$+D\frac{T^1}{P-p}\left(\frac{\partial^2 p}{\partial \rho^2}+\frac{2\partial p}{\rho\,\partial \rho}\right)+$$
$$+D\mu^w P\frac{aT^1}{(P-p)^2\left[\mu^w P-(\mu^w-\mu^a)p\right]}\frac{\dot{p}}{b}\left(\frac{\partial p}{\partial \rho}\right)^2, \qquad (10.45)$$

Key: a. a
b. w

where p is the partial pressure of the water vapor, P is the total pressure in the medium, T^1 is the temperature of the medium, D is the diffusion coefficient of water vapor in air, ρ is the polar radius of the particle, λ^1 is the thermal conductivity of the medium, C_p is the heat capacity of the medium at constant pressure, R_n is the universal gas constant, μ^a is the molecular weight of air, μ^w is the molecular weight of water vapor.

The temperature field in the particle is described by the nonhomogeneous thermal conductivity equation

$$\frac{\partial T^1}{\partial t}=\varkappa^1\left(\frac{\partial^2 T^1}{\partial \rho^2}+\frac{2}{\rho}\frac{\partial T^1}{\partial \rho}\right)+I, \qquad (10.46)$$

where T^i is the temperature in the particle, $\varkappa^i$ is the thermal conductivity of the particle substance, I is the source function

$$I = \frac{3\mathcal{J}w(t)K_a(r, \lambda, m)}{4C_L\gamma_L r^3}. \qquad (10.47)$$

In the last formula $\mathcal{J}$ — is the thermal equivalent of water, w is the power of the radiation flux, C_L and γ_L are the thermal capacity and the density of the particle substance, K_a is the optical absorption coefficient of the particle.

Equations (10.44) - (10.46) define the vaporization kinetics of one particle in the radiation field. The boundary conditions for these equations have the form

The initial conditions:

$$t=0;\ p(\rho, 0)=p_\infty;\ T^i(\rho, 0)=T^i(\rho, 0)=T_\infty, \qquad (10.48)$$

The boundary conditions:

$$\rho=r,\ T^i(r, t)=T^i(r, t)=T_0(r, t),\ \rho(r, t)=p_0(T_0),$$
$$Lj_m^0+j_Q^0=\lambda^i\left(\frac{\partial T^i}{\partial\rho}\right)_{\rho=r}, \qquad (10.49)$$
$$\rho\to\infty,\ T^i\to T_\infty,\ p\to p_\infty,$$

where T_0 is the temperature on the surface of the particle, j_m and j_Q are the mass of the vapor and heat flows.

The initial conditions are formulated assuming thermodynamic equilibrium for the particle and the surrounding medium before the action of the radiation. The function $\rho_0(T_0)$ in (10.49) characterizes the dependence of the elasticity of the saturated vapor on the temperature on the surface of the particle. For particles with radius $r>1$ μ this function has the form

$$p_0(T_0)=p_r e^{L\mu^{\tilde{n}}/RnT_r}e^{-L\mu^{\tilde{n}}/RnT_0}, \qquad (10.50)$$

Key: a. v

where L is the specific evaporation heat. For particles with $r \leqslant 1$ μ the corresponding corrections must be introduced in (10.50). The analysis proposed which is used when equations (10.44) - (10.46) are derived makes it possible to determine the limits of their applicability. The equations obtained can be applied to describe the mass and heat transfer process in the water drop system in the air when $p = p_{cr} < P$, $T^1 = T_{boil}$, $v = v_{vs}$, where T_{boil} is the boiling temperature of water, v is the velocity of the mass flow, and v_{vs} is the velocity of sound.

In cases when the quantities, p, T^1, and v attain values which exceed p_{cr}, T_{boil} and v_{vs}, the vapor and heat flow masses can be described by the approximate states if we assume that

$$j_m = \frac{\mu^{II} p}{R_n T^1} \overset{a}{v}_{\overset{b}{ss}}, \tag{10.51}$$

$$j_Q = C_p \gamma_g T^1 \overset{a}{v}_{\overset{b}{ss}}, \tag{10.52}$$

Key: a. v
b. vs

where γ_g is the density of the vapor gas mixture.

The boundary conditions in this case have the form

$$L \frac{\mu^{II} p_0}{R_n T_0} \overset{a}{v}_{\overset{b}{ss}} + C_p^{II} \frac{\mu^{II} p_0}{R_n} \overset{a}{v}_{\overset{b}{ss}} = \lambda^1 \left(\frac{\partial T^1}{\partial \rho} \right)_{\rho = r}, \tag{10.53}$$

Key: a. v
b. vs

and the vaporization kinetics of the drop are described by the equation

$$\frac{dr}{dt} = -\frac{1}{\gamma_L} \frac{\mu^{II} p_0}{R_n T_0} \overset{a}{v}_{\overset{b}{ss}}. \tag{10.54}$$

Key: a. v
b. vs

Equations (10.44), (10.45) can be solved only numerically. In this respect the corresponding algorithms and programs written in the Algol 60 language were developed for the computations.

2. Quasistationary Fields. In the case of quasistationary temperature fields and partial pressure of water vapor, when these are only determined by the surface temperature of the particle, we obtain from equations (10.44) and (10.45) expressions for the partial pressure p and the temperature T^1 in the form

$$p = P - \frac{(P-p_0)\frac{T^l}{T_0}\frac{r}{\rho}}{(P-p_\infty)\frac{T^l}{T_\infty}\left(\frac{r}{\rho}-1\right)}, \tag{10.55}$$

$$T^l = \frac{r}{\rho}(T_0 - T_\infty) + \frac{C_p D}{\lambda^l R_n} \times$$
$$\times \left[\mu^{\text{II}} P \ln\frac{P-p}{P-p_\infty} - (\mu^{\text{a}} - \mu^{\text{II}})(p-p_\infty)\right] +$$
$$+ \frac{r}{\rho}\frac{C_p D}{\lambda^l R_n}\left[\mu^{\text{II}} P \ln\frac{P-p_\infty}{P-p_0} - (\mu^{\text{b}} - \mu^{\text{II}})(p_\infty - p_0)\right] + T_\infty. \tag{10.56}$$

Key: a. v
b. a

From these equations we can obtain asymptotic expressions for p which do not contain T^1 and an expression for T^1 which does not contain p when $(\rho - r) \ll 1$ (the points near the surface of the particle). Because of the unwieldiness of the formulas which were obtained we shall not give these here.

When the vaporization rate of the drop is calculated, the temperature which depends both on the fields in the particle and the temperature distribution in the volume must be known. To determine the temperature in the drop a boundary value problem which is known in mathematical physics as the third boundary value problem for a parabolic equation must be solved. The solution of this problem enabled us to obtain the following transcendental equation for determining the temperature T_0 on the surface of the drop:

$$T_0+\frac{2r}{\varkappa^{i2}}\sum_{n=1}^{\infty}\frac{(-1)^n\pi n}{\pi^3n^3(1+n^2\pi^2)}\left\{I_r+\frac{2\varkappa^{i2}}{r^2}\times\right.$$

$$\left.\times\theta[1-(-1)^n]\right\}(1-e^{-\left(\frac{\varkappa^i n\pi}{r}\right)^2 t})+\frac{2}{r}\sum_{n=1}^{\infty}\frac{(-1)^n}{1+n^2\pi^2}\times \qquad (10.57)$$

$$\times\left\{T_\infty r-\theta\frac{(-1)^n[n^2\pi^2+2]-2}{n^2\pi^2}\right\}e^{\left(\frac{\varkappa^i n\pi}{r}\right)^2 t}+\frac{0}{r}=0,.$$

where

$$\theta=\frac{\lambda'}{\lambda^i}T_0r-\frac{D\mu^{(a)}p_r}{\lambda^iR_n}\ln(P-p_0)\left(C_g+\frac{L}{T_0}\right)+$$

$$+\frac{C_pD_r}{\lambda^iR_n}(\mu^{(b)}-\mu^{(a)})p_0-\frac{\lambda'T_\infty}{\lambda^i}r+\frac{D\mu^{(a)}p_r}{\lambda^iR_n}\times \qquad (10.58)$$

$$\times\ln(P-p_\infty)\left(C_p+\frac{L}{T_\infty}\right)-\frac{C_pD}{\lambda^iR_n}(\mu^{(b)}-\mu^{(a)}).$$

Key: a. v
b. a

If the solution of equation (10.57) for T_0 is known, then calculating the rate at which the drop vaporizes is not particularly difficult and can be carried out using the formulas

$$\frac{dr}{dt}=-\frac{1}{\gamma_L}j^0_m, \qquad (10.59)$$

$$j^0_m=\frac{\mu^{(b)}Dp}{rR_n}\left[\frac{1}{T_\infty}\ln(P-p_\infty)-\frac{1}{T_0}\ln(P-p_0)\right]. \qquad (10.60)$$

3. Stationary vaporization of the drop during continuous irradiation. When a radiation flow which is constant in time acts continuously on a drop, we can assume that the heat flows absorbed by the drop which are carried away from it together with the vaporizing steam are equal. This fact enables us to write the balance equation as

$$4\pi\lambda'(T_0-T_\infty)+4\pi rL(T)D[c_n(T_0)-c_{n\infty}]=$$
$$=\pi r^2\omega K_n(r), \qquad (10.61)$$

Key: a. v

where c_v is the concentration of water vapor in the medium.

Equation (10.61) enables us to determine the temperature on the surface of the drop.

Figure 10.1 gives the results when equation (10.61) is solved graphically.

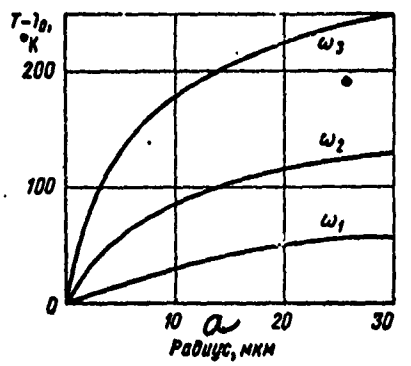

Fig. 10.1. Results of calculations of temperature variations in drops of different dimensions during continuous irradiation by a radiation flux $\omega_1 = 10^2$ w/cm^2, $\omega_2 = 10^3$ w/cm^2, $\omega_3 = 10^4$ w/cm^2, $T_0 = 273^\circ$K, $\lambda = 10.6$ μ

Key: a. radius, μ

The rate at which the drop evaporates can be estimated by integrating the kinetic equation for stationary vaporization

$$r\frac{dr}{dt}=-\frac{D}{\gamma_L}[c_n(T)-c_{n\infty}]. \qquad (10.62)$$

Approximate graphical integration of the last equation using tabular values of c_v (T) for the same parameter values as in Fig. 10.1 enabled us to obtain curves for the radius of

the drop as a function of time (Fig. 10.2). These curves are approximated satisfactorily by the equation

$$r(t)=\begin{cases} r_0-0{,}494\omega^{1{,}103}t, & pr \gg 1, \\ r_0 e^{-0{,}494\omega^{1{,}103}t}, & pr \ll 1, \end{cases} \qquad (10.63)$$

where: $p=8\pi\varkappa/\lambda$; $q=\exp[-0{,}2(|m|-1)]$;

and m is the complex refractive index of water.

4. Vaporization of a drop under the action of single radiation pulses. If a single pulse acts on the drop with a duration for which the energy absorption process by the drop can be considered to be adiabatic, then the temperature of the drop after the action of the pulse can be determined from the formula

$$T_{\text{п}}^{\text{в}} = T_\infty + \frac{1{,}8\cdot 10^3 K_{\text{п}}^{\text{в}}(r_0)\,E}{r_0}, \qquad (10.64)$$

Key: a. п
b. в

where E is the energy of the pulse in joules per square centimeter and r_0 is the initial radius of the drop in microns

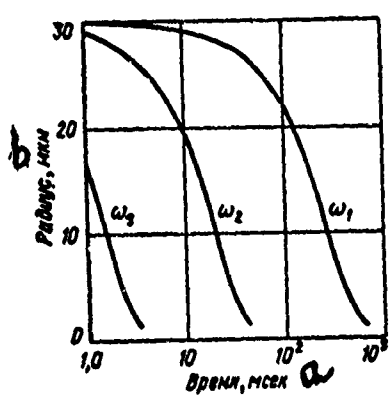

Key: a. time, msec
b. radius, μ

Fig. 10.2. Results of calculations of variation in the radius of the drops as a function of time when it is continuously irradiated by a flux with wavelengths 10.6 μ and power $\omega_1 = 10^2$ w/cm^2, $\omega_2 = 10^3$ w/cm^2, $\omega_3 = 10^4$ w/cm^2. Initial radius of drop $r_0 = 30$ μ

Estimates show that when $T_n \leqslant 400^\circ K$ due to a single pulse the vaporization of the drop slightly changes its radius.

Values $T_n \geqslant T_{cr} = 647^\circ K$ for a liquid phase are meaningless so they need not be considered. Thus, the effect exerted by the action of a single pulse on the drops which are of interest are those for which the temperature T_n lies in the range

$$400^\circ K \leqslant T_n < T_{cr}. \qquad (10.65)$$

Key: a. n
b. cr

The current temperature of the drop, assuming that it is uniformly distributed over the volume, can be found from the simple relation

$$C_L m\, dT = L\, dm, \qquad (10.66)$$

from which we can easily obtain an expression for the temperature of the drop as a function of its radius:

$$T = T_n + \beta \ln \frac{r}{r_0}, \qquad (10.67)$$

Key: a. n

where

$$\beta = \frac{6L(T_n)\gamma_L(T_\infty)}{C_L[L(T_n)\rho_L - L(T_\infty)]}. \qquad (10.68)$$

Key: a. n

From (10.67) we obtain an expression for the final radius of the drop, after the action on it of a single pulse

$$r_f = r_0 e^{-(T_n - T_\infty)/\beta}. \qquad (10.69)$$

Key: a. f
b. n

Figure 10.3 shows the results of calculations for the final radius of a drop irradiated by a single radiation pulse with wavelength 10.6 μ. We note that in the general case the relation between the final radius of the particle and the initial radius is not linear since the difference $T_n - T_\infty$ and the value of β depend on r_0.

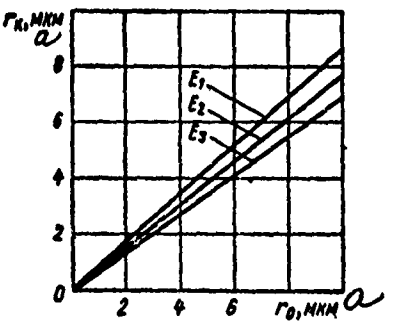

Fig. 10.3. Results of calculations of the final radius of a drop as a function of its initial radius for energy values in the pulse $E_1 = 2.00 \cdot 10^3$ joule/cm^2, $E_2 = 2.66 \cdot 10^3$ joule/cm^2, $E_3 = 2.93 \cdot 10^3$ joule/cm^2

Key: a. μ

Formula (10.69) implies that the final radius of the drop can only be equal to zero when $T_n = T_{cr} = 647^\circ$K, when $\beta = 0$, since $L(T_{cr}) = 0$.

The formulas which were considered are valid when the duration of the pulse is less than the time in which the dimension and temperature of the drop can change to any noticeable extent. Estimates have shown that this time must be on the order of magnitude of 10^{-4} sec.

In the case when $T_n > T_{cr}$ we should expect the drop to burst, during which the water vapor under high pressure hits the air and forms a compression wave. This wave, as the estimates show, equalizes the vapor pressure in the medium surrounding the drop at a distance from the drop approximately equal to 10 r_0, and the byproducts of the burst also impart their energy to the air. It turns out that the time in which the above-mentioned phenomenon takes place can be expressed by

the simple formula

$$t = \frac{r_0}{U_x} \frac{10^3}{3} [ce\kappa], \qquad (10.70)$$

Key: a. sec

where U_x is the propagation velocity of the compression wave. For water drops with a radius of 10 μ the scattering time is a quantity on the order of magnitude of 10^{-6} sec.

5. The action of radiation on a polydispersed aerosol. To determine the radiation action on a polydispersed aerosol we must know how the distribution function by dimension for the particles changes due to this action. As a first approximation we can assume that the radiation acts on each polydispersed aerosol particle independently. This assumption is justified by the fact that the humidity content in aerosol particles per unit volume is considerably less than the humidity content of the air in which the particle is found.

Taking into consideration the assumption which was made, we can easily obtain an expression for the distribution function by dimension for the particles f(r,t) which also includes a variable for time. In the case of continuous irradiation of a polydispersed aerosol with an initial distribution function by dimension for the particles which can be described by the gamma distribution [see formula (5.4)] we obtain the following expression for f(r,t):

$$f(r, t) = \begin{cases} \frac{1}{\Gamma(\mu+1)} \mu^{\mu+1} \frac{1}{\bar{r}_0} \left(\frac{r+S}{\bar{r}_0}\right)^{\mu} e^{-\mu\left(\frac{r+S}{\bar{r}_0}\right)}, & (10.71) \\ \frac{e^{pS}}{\Gamma(\mu+1)} \mu^{\mu+1} \frac{1}{\bar{r}_0} \left(\frac{re^{pS}}{\bar{r}_0}\right) e^{-\mu\left(\frac{re^{pS}}{\bar{r}_0}\right)}, & (10.72) \\ pr \ll 1, \end{cases}$$

where μ is a parameter which characterizes the halfwidth of the distribution, $S = 0.494\, q\omega^{1.102}t$, and $\bar{r}_0$ is the most probable radius of the particle.

Substituting formulas (10.71), (10.72) in (7.3) we can calculate the three-dimensional attenuation coefficient.

In the case of large particles where the function $K(\rho, m) = 2$, we obtain a sufficiently simple expression for the three-dimensional attenuation coefficient when $\mu = 2$:

$$\alpha(\omega, t) = 2\pi N_0 (S^2 + 3\bar{r}_0 S + 3\bar{r}_0^2) e^{-2S/\bar{r}_0}, \qquad (10.73)$$

where N_0 is the number of particles per unit volume.

For small and "soft" particles

$$\alpha(\omega, t) = \frac{\pi N_0}{\Gamma(\mu+1)} \mu^{\mu+1} \times \\ \times \left[\frac{32\pi (n-1)(\operatorname{tg}\beta) r^{-3} \Gamma(\mu+4)}{3\lambda \mu^{\mu+1}} e^{-3pS} + \right. \\ \left. + \frac{8\pi^2 (1-\operatorname{tg}^2\beta) \bar{r}_0^4 \Gamma(\mu+5)}{\lambda^2 \mu^{\mu+5}} e^{-4pS} \right], \qquad (10.74)$$

where $\operatorname{tg}\beta = \frac{\varkappa}{n-1}$; and n is the refractive index of water.

During the action of a radiation pulse on a polydispersed aerosol, the distribution function of the particles by dimension, when the relation between the final and initial radius of the particle can be considered to be linear, becomes skewed, changing the most probable value of the radius of the particle. In this case the three-dimensional coefficient must be calculated from the usual formulas, and only for the value of the most probable radius we must take the quantity $\bar{r}_0 k$, where k is a parameter which depends on the energy of the pulse and the optical cross section of the particle.

The approximate vaporization theory of spherical particles under the action of powerful continuous quasilinear and optical pulse radiation is the first attempt to describe quantitatively a very complex phenomenon. The degree of confidence in the theory, as usual, can be determined during the corresponding experimental studies, the first results for which were obtained in articles [727, 728]. However, the number of sources used during measurements in these studies was too small to enable us to make definite conclusions about the agreement of theoretical and experimental values.

We also note that the vaporization of drops is by far not the only effect which accompanies the propagation of powerful

optical radiation in a polydispersed water aerosol. When light pulses with great power and of small duration act on a water aerosol, the aerosol particles begin to move in a direction which is determined by their nonuniform heating. As a result of such directed movement, the particles may coagulate.

When the power of the incident radiation on the aerosol is great, it may become necessary to take into account the effect of light pressure which can be calculated without great difficulty. The nonstationary vaporization of water aerosol particles apparently must lead to the formation of conditions under which the radiation in the beam channel is defocused and assumes an abnormal refractive direction.

The investigation of the effects described and their effect on the vaporization of particles are future tasks. Now we can only say that from the standpoint of energy losses in powerful optical radiation the vaporization effect in the water aerosol is the dominant effect if we do not take into account the losses in the directed radiation flux due to particle scattering.

11. The Propagation of Bounded Light Beams in the Turbulent Atmosphere

A light wave propagating in the real atmosphere undergoes in addition to energy losses caused by radiation absorption and scattering phenomena fluctuations in amplitude and phase due to the random space-time distribution of the refractive index of air. The latter is caused by turbulent movements in the atmosphere which entail random changes in the temperature and in the refractive index related to it. Estimates have shown that variations in air temperature by $1^{\circ}C$ cause a change in the refractive index by an amount which is on the order of magnitude 10^{-6} [729]. The amplitude of the fluctuations which occur in the temperature at a given point attains values equal to tenths of a degree and the fluctuation period varies from milliseconds to seconds. The amplitude of the temperature pulses along horizontal paths in the atmosphere can reach several degrees for points situated from one another at distances on the order of magnitude $10^2 - 10^3$ m [730].

The effect of space-time fluctuations in the refractive index of the atmosphere on the characteristics of unbounded plane and spherical waves has been studied in sufficient detail both theoretically and experimentally. In the well-known monographs of V. I. Tatarskiy [463, 731] the theory and results of experimental studies are discussed systematically.

However, the theoretical and experimental results which were obtained for unbounded beams generally cannot be used directly to estimate quantitatively the corresponding parameters of bounded beams. This fact makes it necessary that new theoretical and experimental studies be carried out which are important and valuable in an applied sense in connection with the possibility of using bounded laser beams in communication, information transmission, range and distance finding systems, and other devices designed for operation in the atmosphere.

In this chapter we discuss the main results obtained in studies of the effect of the turbulent atmosphere on the parameters of spatially bounded light beams under various propagation conditions.

1. General Considerations

As a result of turbulent movements in the atmosphere, nonhomogeneities are formed which extend over hundreds of meters and above (macrononhomogeneities) up to dimensions l_0 on the order of magnitude

$$l_0 \sim \sqrt[4]{\nu^3/\varepsilon}, \tag{11.1}$$

The quantity l_0 is called the internal turbulence scale, ν the kinematic viscosity, ε the thermal energy dissipation rate of the nonhomogeneity. The dimension l_0 near the surface of the earth has the order of magnitude of 1 mm.

The field of the refractive index n of a medium with random nonhomogeneities is usually characterized by the structural function [463]

$$D_n(r) = \overline{[n(r_1+r) - n(r_1)]^2}, \tag{11.2}$$

where r is the distance between the points.

The structural function for the temperature field is introduced analogously

$$D_T(r) = \overline{[T(r_1+r) - T(r_1)]^2}. \tag{11.3}$$

The form of the functions $D_n(r)$ and $D_T(r)$ for the inertial interval [731] assuming locally isotropic and homogeneous turbulence was obtained by A. M. Obukhov [732]. The corresponding laws were named the two-third Kolmogorov-Obokhov equation:

$$D_n(r) = C_n^2 r^{2/3}, \tag{11.4}$$

$$D_T(r) = C_T^2 r^{2/3}, \tag{11.5}$$

where $l_0 < r < L_0$, L_0 and L_0 is the external turbulence scale.

The magnitudes C_n and C_T are called the structural constants of the refractive index and the air temperature fluctuations and are related to one another for the wavelengths 0.5 μ by the relation

$$C_n\,[\underset{a}{см^{-1/3}}] = \frac{79{,}2\cdot 10^{-6} P\,[\underset{b}{мб}]}{T^2\,[°K]}\, C_T\,[\underset{c}{град}\cdot \underset{a}{см^{-1/3}}]. \tag{11.6}$$

Key: a. cm
b. mb
c. deg

The values of C_n in the layer of the atmosphere near the surface of the earth lie in the range 10^{-7} to 10^{-9} $cm^{-1/3}$ [741]. Methods for determining the structural constants of the refractive index are based on the use of data for the mean values of the characteristics of meteorological fields [733, 846] and data about temperature fluctuations [847]. In the last few years optical methods have been developed for determining C_n [848 - 850].

The mean square fluctuation of the logarithm of the intensity of an unbounded plane monochromatic wave propagated in a turbulent atmosphere is defined by the relation

$$\sigma^2 = 2{,}24 k^{7/6} \int_0^L C_n^2 (L-x)^{5/6}\, dx, \tag{11.7}$$

where k is the wave number, L is the distance covered by the wave in the atmosphere.

In the case of a homogeneous atmosphere from the standpoint of turbulent conditions, C_n^2 does not vary over the entire

path L and we obtain from (11.7)

$$\sigma_0^2 = 1{,}23 C_n^2 k^{7/6} L^{11/6}. \qquad (11.8)$$

The quantity C_n does depend on the altitude of the atmospheric layer:

$$C_n^2(z) = C_n^2(z_0)\left(\frac{z}{z_0}\right)^{-\alpha}, \qquad (11.9)$$

where z_0 is a fixed altitude ($z > z_0$), the index $\alpha = 2/3$ in the presence of dynamic turbulence in the atmosphere and $\alpha = 4/3$ in the case of free convection [463].

The formulas for the variance for the fluctuation in the logarithm of the intensity describe correctly the case of so-called weak fluctuations defined by the condition $\sigma \ll 1$. V. I. Tatarskiy [851], when he solved the wave equation using the approximation from geometric optics, obtained a formula for the mean square fluctuations in the logarithm of the amplitude σ_x^2 for the case of strong fluctuations:

$$\sigma_x^2 = 1 - [1 + 6\sigma_0^2]^{-1/6},$$

which agrees well with the experimental data in [751], even though in the experiment the conditions under which geometric optics are applicable were not satisfied.

The mean square fluctuations in the angle of arrival for an infinite plane wave in the focal plane of the objective are expressed by the relation [463]

$$\sigma_\varphi^2 = 2{,}8 b^{-1/3} \sec\theta \int_{z_0}^{\infty} C_n^2(z)\, dz, \qquad (11.10)$$

where θ is the zenith distance of the source, z_0 is the altitude at which the receiving objective is located, and b is the diameter of the objective.

The measurements which were carried out by L. R. Tsvang [734] from airplanes have shown that formula (11.9) with $\alpha = 4/3$ is valid up to altitudes at which cumulus clouds are formed. Taking infinity for this altitude, we can obtain immediately from (11.10) and (11.9) a simple expression for σ_ψ^2 [735]:

$$\sigma_\psi^2 = 2{,}8b^{-1/3}\sec\theta\, z_0 3C_n^2(z_0). \tag{11.11}$$

The quantity σ_ψ^2 is related to the frequency spectrum of the fluctuations of the angles of arrival by the relation

$$\sigma_\psi^2 = \int \omega_\psi(f)\,df. \tag{11.12}$$

In article [736] a formula was derived for the frequency spectrum of the fluctuations in the angles of arrival for the case of a homogeneous turbulent atmosphere:

$$\omega_\psi(f) = 0{,}045\sigma_\psi^2 \sin^2\left(\frac{\pi b f}{v_1}\right)\left(\frac{b}{v_1}\right)^{-5/3} f^{-8/3}, \tag{11.13}$$

where f is the frequency, v_1 is the wind velocity component which is perpendicular to the direction in which the wave propagates for a congealed turbulence model.

2. Theoretical Studies of the Fluctuations in the Parameters of Bounded Beams Propagating in the Atmosphere

A. I. Kon and V. I. Tatarskiy [737] derived an expression which can be used to calculate fluctuations in the phase and the effective expansion of a bounded beam propagating in a turbulent atmosphere.

The problem was solved approximately using the Rytov-Obukhov method of smooth perturbations. In the expression for the logarithm of a small perturbation in the field ψ which represents the solution of the wave equation and is expressed in terms of the characteristics of the incident and perturbing fields as follows:

$$\psi_1 = \psi - \psi_0 = \ln\frac{A}{A_0} + i(s - s_0) \tag{11.14}$$

(A, A_0 and s, s_0 are, respectively, the amplitude and phase of the perturbed and incident fields) the value of the unperturbed field is substituted, the amplitude of which is distributed over the cross section of the beam in accordance with the law

$$A_0 = A_0' \exp\left(-\frac{y^2+z^2}{a^2}\right), \qquad (11.15)$$

where A_0' is the amplitude of the incident wave on the beam axis, a are the dimensions of the beam, y and z are coordinates in the plane of the beam cross section which is propagated in the direction of the x-axis. Next, the expression is written for the structural fluctuation function of the phase D_s which contains the quantity $s_1 = \mathrm{Im}\,\psi_1$. Next, the integrals in the expression D_s are evaluated approximately using the conditions

$$g = 2L/ka^2 \ll 1 \quad (\text{или } a^2 \gg \lambda L), \qquad (11.16)$$

$$a^4 \gg \lambda^3 L^3 l_0^2. \qquad (11.17)$$

Key: a. or

If only the fluctuations in the propagating direction are determined, the values of D_s are used for $|\vec{\rho}| \ll l_0$, where $\vec{\rho} = \vec{\rho}_1 - \vec{\rho}_2$, $\vec{\rho}_1$ and $\vec{\rho}_2$ are the radius-vectors of points in the plane x = L. For D_s in the geometric optics approximation ($\sqrt{\lambda L} \ll l_0$), a formula is obtained which differs from the corresponding expression in the case of an infinite plane wave by small corrections. When the expression for D_s is found when $\sqrt{\lambda L} \gg l_0$ (an important case in practice) the parameter θ is introduced:

$$\theta^2 = 2L^2\varkappa_m^2/k^2a^2, \qquad (11.18)$$

where $\varkappa_m$ is the wavenumber which characterizes the internal turbulence scale. The parameter θ characterizes the ratio of the width of the diaphragmed beam to the geometric width of the beam.

In the asymptotic case $\theta \gg 1$ the following expression is obtained for the structural function D_s

$$D_s(\rho, R) = 0{,}46k^2aC_n^2k_m^{-2/3}\rho^2 \ln 2\theta^2 \times \\ \times \left[2{}_1F_1\left(\frac{1}{6}, 1, \frac{2R^2}{a^2}\right) - {}_1F_1\left(\frac{1}{6}, 2, \frac{2R^2}{a^2}\right)\right], \qquad (11.19)$$

where ${}_1F_1$ is a singular hypergeometric function, R is the numerical value of the vector $\vec{R} = \frac{1}{2}(\vec{\rho}_1 + \vec{\rho}_2)$ (the vectors $\vec{\rho}$ and $\vec{R}$ are assumed to be parallel, and the line which connects the observation points $\vec{\rho}_1$ and $\vec{\rho}_2$ passes through the center of the beam). Formula (11.19) differs considerably from the corresponding expression for D_s in the case of an infinite wave.

Using (11.19), the authors of [737] found an approximate expression for the effective mean square fluctuation of the angle of arrival

$$\sigma^2_{\varphi\,\text{эфф}} \overset{a}{\cong} 0{,}1C_n^2kal_0^{5/3}\ln 2\theta^2, \qquad (11.20)$$

Key: a. eff

which implies that for large θ (large L) $\sigma^2_{\Downarrow\text{eff}}$ increases much more slowly as the distance increases (it becomes proportional to lnL, not to L, as in the case of an infinite wave). This is explained by the fact that in the case of a bounded beam the scattered waves are ejected from the beam when L is large and no longer contributes to the fluctuation. When θ = 10 (beam width 50 cm, l_0 = 1 mm, L = 5 km, λ = 0.5 μ) $\sigma^2_{\Downarrow}$ differs by a factor of 4 from the value calculated from formula (11.10) for an infinite wave. It should be noted that by $\sigma^2_{\Downarrow\text{eff}}$ we mean the value of $\sigma^2_{\Downarrow}$ which is obtained by averaging over the cross section of the beam when the distribution of the amplitude (11.15) is taken into account.

In [737] a formula was also obtained which can be used to determine the linear expansion of the beam as a function of the distance covered by it in the turbulent medium. The random expansion of the beam on the path L is equal to

$$R = \int_0^L \Delta\varphi(x)\,dx. \qquad (11.21)$$

Assuming that the linear correlation coefficient for $\Delta\varphi(x)$ is close to one [738] and using (11.20) the authors of [737] obtained for R_{eff} the formula

$$R_{eff} \approx \sqrt{\langle R^2\rangle} \cdot \text{const}\, C_n l_0^{1/3} (ka\ln\Omega)^{1/3} L, \qquad (11.22)$$

which shows that for large L ($\Omega \gg 1$) R_{eff} is proportional to L, not $L^{3/2}$, as in the case $\Omega \ll 1$.

Calculations of the amplitudes of the fluctuations in a specially bounded beam have shown that the corresponding expression for σ^2 differs from the expression (11.7) in the case of an unbounded wave by small corrections on the order of magnitude g^2.

Formula (11.15) which describes the distribution law for the amplitude of the wave over the cross section of the beam does not always correspond to the conditions of the experiment; however, the authors of [737] emphasize that the basic qualitative conclusions obtained in the article remain valid even if the functions A_0 (y, z) are expressed differently.

Z. I. Feyzulin and Yu. A. Kravtsov [739] considered the problem of the expansion of a spatially bounded beam, propagating in a turbulent atmosphere. In the study they took into account both the beam spreading and its defractive expansion and oscillation of the entire beam about the propagation direction. The total expansion of the beam is written in the form

$$\langle\overline{\rho^2}\rangle = \overline{\Delta\rho^2} + \overline{\rho_c^2}, \qquad (11.23)$$

where

$$\langle\overline{\rho^2}\rangle = \frac{\int_S \rho^2 \overline{I_0(\vec{\rho})}\,d\vec{\rho}}{\int_S I_0(\vec{\rho})\,d\vec{\rho}}; \qquad (11.24)$$

$$\overline{\rho_c^2} = \frac{\int\limits_S \int \overline{(\vec{\rho}_1, \vec{\rho}_2)}\, I_s(\vec{\rho}_1)\, I_s(\vec{\rho}_2)\, d\vec{\rho}_1\, d\vec{\rho}_2}{\left(\int\limits_S I_s(\vec{\rho})\, d\vec{\rho}\right)^2} \qquad (11.25)$$

The term $\overline{\rho}_c^2$ characterizes the oscillation of the entire beam about the propagation direction, $\overline{\Delta\rho^2}$ defines the expansion of the beam relative to the disturbed position of its center. In [739] expressions are derived for the mean intensity of the field $I_s(\rho)$ at the point with radius-vector ρ and the correlation function of the intensity $\overline{I_s(\vec{\rho}_1)\, I_s(\vec{\rho}_2)}$ in the plane S which is perpendicular to the direction in which the beam is propagated. The propagating wave is considered to be constant. The method of smooth perturbations is used in computing the statistical characteristics which enter the unknown expressions [463].

We give one of the terms in the expression for $\overline{\langle\rho^2\rangle}$, which was obtained in [739], which characterizes the expansion of the beam due to the scatter of the fluctuations in the refractive index of air in the case of isotropic turbulence:

$$\frac{L^2}{2k^2}\Delta D_\psi(\theta) = 2{,}19 C_n^2 l_0^{-1/3} L^3, \qquad (11.26)$$

where D_ψ is the structural function of the complex phase.

The expression for f' simplifies considerably in the case of a gaussian distribution of the field in the cross section of the beam:

$$\overline{\langle\rho^2\rangle} = a^2 + \frac{L^2}{k^2 a^2} + 2{,}19 C_n^2 l_0^{-1/3} L^3. \qquad (11.27)$$

The last formula does not imply that the width of the beam increases more slowly as the distance increases when L is large, a result obtained in article [737]. The authors of [739] attribute the different results to the fact that in their work and in article [737] different measures were adopted for the width of the beam.

Next, two specific cases when the "center of gravity" of the beam oscillates are analyzed in [739]: the case of large scale nonhomogeneities, when the dimensions of the beam are much smaller than the dimensions of the nonhomogeneities, and

the case of small scale nonhomogeneities (the dimensions of the nonhomogeneities are much smaller than the width of the beam). It is shown that in the first case the beam does not expand, but the entire beam is shifted about the propagation direction. The second case cannot be analyzed easily quantitatively. Qualitative considerations imply that the displacement of the "center of mass" of the beam must be insignificant in this case.

The total expansion of the beam was determined in [739] for the following values of the parameters: $a = 35.7$ cm, $l_0 = 0.1$ cm, $\lambda = 0.5$ μ, $C_n = 0.02 \cdot 10^{-6}$ $cm^{-1/3}$, and the distances $L_1 = 15$ km, $L_2 = 145$ km, which turned out to be equal, respectively, to about 91 cm and 25.5 m.

We will briefly characterize the results which were obtained in other theoretical studies. An analysis of the quantitative data from the theory for fluctuations in the parameters of a laser beam propagated in a turbulent atmosphere as applied to the operation of laser systems was carried out in the survey article of Davis [744]. In the work of Fried and Seidman [745] an estimate is given for the variance of the logarithm of the amplitude for a laser beam propagating along a horizontal path in the atmosphere.

Hufnagll and Stanley [750] developed a statistical transfer theory for optical images in the atmosphere. In [750] a formula was derived for the optical transfer function which characterizes the transfer coefficients of three-dimensional frequencies in the atmosphere:

$$M(\lambda R f) = e^{-\frac{1}{2} k^2 \langle [S(p)]^2 \rangle},$$

where $f = p/\lambda R$ is the three-dimensional frequency, p are the linear dimensions of the observed object, R is the focal distance of the receiver lens

$$\langle S^2 \rangle = 2{,}91 p^{5/3} \int_0^z C_n^2(z')\, dz'.$$

The angular brackets show sufficiently large averaging over time.

Fried [742, 743] studied theoretically the effect of the turbulent state in the atmosphere on the optical resolution determined by the optical transfer function during long and short photographic exposures and also the limiting resolution of images obtained from photographs taken from top to bottom throughout the atmosphere.

Several quantitative estimates for the effect of atmospheric turbulence on the parameters of spatially bounded light beams were also obtained in articles [740, 746 - 749, 752] and others. In article [747] the limiting dimensions of the radiation source and receiver were determined for which a disturbance in the spatial coherence of a light beam caused by atmospheric turbulence does not yet occur. The authors of article [749] estimated the limiting dimensions of the diameter of the cross section of the light beam beyond which the turbulent movements in the atmosphere sharply decrease the spatial coherence of the beam. In [740] an expression was obtained for the normalized variance of the intensity fluctuations by averaging over the aperture which is called the aperture averaging factor. The dependence of the flicker intensity of the source on its angular dimensions is investigated in article [752].

3. Experimental Studies of the Fluctuations of Parameters in Spatially Bounded Beams Propagating in the Turbulent Atmosphere

1. Fluctuations In Intensity. The fluctuations in the intensity of a spatially bounded laser beam propagating in a turbulent atmosphere depend on the meteorological conditions, the optical length of the beam path, the diameter of the aperture of the source and receiver, the receiver time constant, the measurement time (exposure), the radiation wavelength, and beam focusing.

The following quantities are adopted as a quantitative measure of the fluctuations in the intensity I of a beam in the theory:

$$\sigma^2 = \overline{(\ln I - \overline{\ln I})^2}, \tag{11.28}$$

or [759]

$$M^2 = \overline{I^2(t)/\overline{I(t)}^2},$$
$$\overline{I(t)} = \lim_{T\to\infty} \frac{1}{2T} \int_{-T}^{T} I(t)\,dt; \tag{11.29}$$

$$\overline{I^2(t)} = \lim_{T\to\infty} \frac{1}{2T} \int_{-T}^{T} [I(t) - \overline{I(t)}]^2 dt, \qquad (11.30)$$

and the standard deviation from the mean of the measured signal is

$$\sigma_n = \sqrt{M^2}. \qquad (11.31)$$

The quantities measured in the experiment are

$$\bar{I} = \frac{1}{N} \sum_{i=1}^{N} I_i, \qquad (11.32)$$

$$\overline{I^2} = \frac{1}{N} \sum_{i=1}^{N} I_i^2, \qquad (11.33)$$

$$\sigma_k^2 = \frac{\overline{I^2} - \bar{I}^2}{\bar{I}^2}. \qquad (11.34)$$

When the fluctuations in the intensity I are distributed according to the lognormal law, σ_k^2 and σ^2 are related by

$$\sigma^2 = \ln(1 + \sigma_k^2). \qquad (11.35)$$

A general idea about the character and amplitude of the fluctuations in the intensity of the signal can be obtained from Figs. 11.1 and 11.2 which give the recorded signals obtained in articles [751] and [766].

Figs. 11.3 - 11.5 give the values of σ vs the distance between the source and receiver, the divergence angle of the laser beam, and the aperture diameter of the receiver [755]. In all diagrams the curves pass through points which correspond to the mean arithmetic value of σ, and the vertical line segments indicate the range of values of σ in individual measurements, due both to measurement errors and to changes in the

$$\overline{I^2(t)} = \lim_{T\to\infty} \frac{1}{2T} \int_{-T}^{T} |I(t) - \overline{I(t)}|^2 dt, \qquad (11.30)$$

and the standard deviation from the mean of the measured signal is

$$\sigma_n = \sqrt{\overline{M^2}}. \qquad (11.31)$$

The quantities measured in the experiment are

$$\bar{I} = \frac{1}{N} \sum_{i=1}^{N} I_i, \qquad (11.32)$$

$$\overline{I^2} = \frac{1}{N} \sum_{i=1}^{N} I_i^2, \qquad (11.33)$$

$$\sigma_k^2 = \frac{\overline{I^2} - \bar{I}^2}{\bar{I}^2}. \qquad (11.34)$$

When the fluctuations in the intensity I are distributed according to the lognormal law, σ_k^2 and σ^2 are related by

$$\sigma^2 = \ln(1 + \sigma_k^2). \qquad (11.35)$$

A general idea about the character and amplitude of the fluctuations in the intensity of the signal can be obtained from Figs. 11.1 and 11.2 which give the recorded signals obtained in articles [751] and [766].

Figs. 11.3 - 11.5 give the values of σ vs the distance between the source and receiver, the divergence angle of the laser beam, and the aperture diameter of the receiver [755]. In all diagrams the curves pass through points which correspond to the mean arithmetic value of σ, and the vertical line segments indicate the range of values of σ in individual measurements, due both to measurement errors and to changes in the

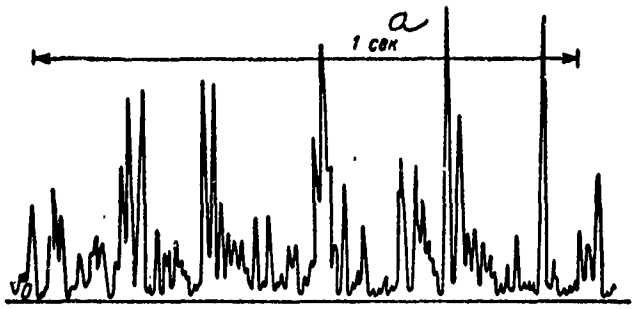

Fig. 11.1. Example of recorded fluctuation in signal propagated in the atmosphere according to the data in article [751]

Key: a. sec

meteorological conditions during which the measurements were made. All curves were obtained using a laser based on a helium and neon mixture with wavelength $\lambda = 6328$ Å which operated in a continuous mode. The measurements were made at night.

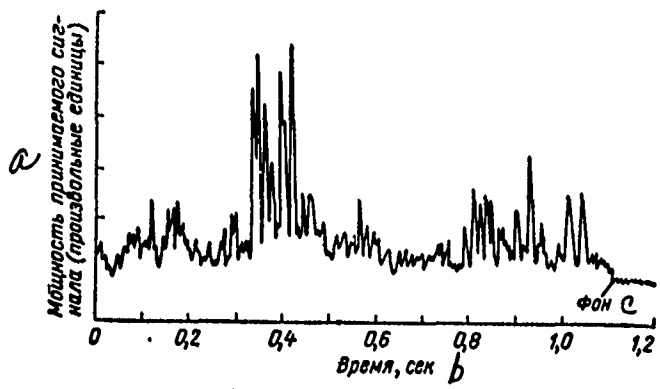

Fig. 11.2. Example of the values of the signal propagated in the atmosphere as a function of time according to the data in article [766]

Key: a. power of the signal received (arbitrary units)
b. time, sec
c. background

Curve 11.3 was constructed on the basis of measurements made on paths 0.1, 0.25 and 1.2 km long. At the end of each path a plane rotary mirror was placed. Thus the light beam covered during the measurements distances of 0.2, 0.5 and 2.4 km. The diameter of the beam at the output of the collimating system was equal to 14.4 cm, the beam divergence was 10" for the distances L = 0.2, 0.5 km, and 17" for a distance of 2.4 km. The diameter of the receiver aperture was equal to 4 mm for L = 0.2, 0.5 km and 14 mm for L = 2.4 km. It can be seen from the diagram that in the range of values for the distance investigated, the quantity σ varied approximately by a factor of 1.5. Since distances between 0.5 and 2.4 km are not available, no definite answer can be given to the problem of the saturation in the relation between σ and L. We note that in article [751] a more pronounced dependence of σ on L was discovered than that plotted in Fig. 11.3. In the work of Buck [766] saturation in the quantity σ was detected at a distance of 0.55 km.

When the dependence of the quantity σ on the angular beam divergence was measured, the latter varied from 10" to 90" when the diameter of the beam at the output from the collimated system was equal to 12.5 cm, the measurement distance was 500 m, and the diameter of the input aperture of the receiver was 1.6 mm. It can be seen from the curve in Fig. 11.4 that as the expansion angle α of the beam increases from 10" to 50" the value of σ decreases, and as α increases further σ also increases.

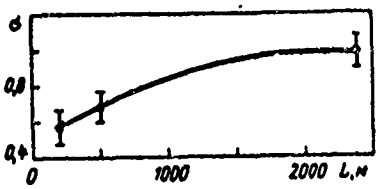

Fig. 11.3. σ vs the distance L between the source and receiver according to the data in [755]

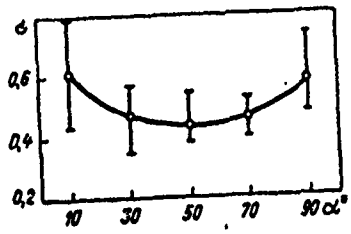

Fig. 11.4. σ vs the laser radiation divergence angle according to the data in [755]

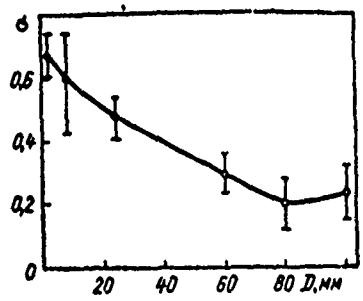

Fig. 11.5. σ vs the aperture diameter of the receiver according to the data in [755]

When the dependence of σ on the aperture diameter of the receiving system D was measured (see Fig. 11.5), the latter was equal to 0.2, 0.8, 2.4, 6.0, 8.0 and 10.0 cm, the distance was L = 0.5 km, the beam diameter at the output from the collimating system was 12.5 cm and the angular expansion was 70". As D increased from 0.2 to 8.0 cm the value of σ decreased approximately by a factor of 3 when D = 10 cm, the measured value turned out to be slightly larger than when D = 8 cm.

A detailed study of the relation between the fluctuations in the intensity of the radiation from a gas laser with wavelength 0.63 μ (the beam diameter at the 0.7 level was equal to 3.5 mm) and the diameter of the receiving aperture using a measurement path 8 km long was carried out by Fried [768].

The results of the measurements have shown that the variance σ^2 decreases as the diameter of the receiving aperture increases from 0.1 to 10 cm. A further increase in the diameter up to 1 m had practically no effect on changes in the values of σ^2. For all values of the diameter of the receiving aperture it was discovered that the intensity obeyed a lognormal distribution. The variance of the fluctuations in intensity which were calculated by Fried [854] on the basis of formulas in the existing theory [731] for various values of the receiving aperture contradicted the values obtained in his own experiment when the receiving apertures were large. In this respect a hypothesis is proposed in [768] that two independent effects must exist which determine the value of the variance of the fluctuations in the intensity of a beam which is propagated in a turbulent atmosphere. One effect is such that the intensity is normally distributed and the other such that it is lognormally distributed when the apertures are large. However, the dominant role is played by the second effect. We note that a discrepancy between the theory of weak fluctuations and the experiment has also been discovered when the values of the receiving apertures were large during experimental studies carried out in the author's laboratory [754]. The measurements were made with a receiving aperture 70 cm wide. The diameter of the light beam at the output and its divergence were equal to 25 cm and 30', respectively. The value of the variance of the fluctuations in these measurements turned out to be larger than that forecast by the theory, and the intensity was lognormally distributed. In addition, within the limits of measurement errors, no dependence was discovered between the value of the variance between the fluctuations and the radiation wavelength.

In article [766] in measurements with a large receiving aperture diameter when the entire beam was intercepted by the receiving system, a value smaller than 0.02 was obtained for σ, for which the signal could be considered practically stable and independent of time. This fact indicated that the fluctuations in the signal caused by the corresponding changes in the molecular absorption and aerosol scattering during the measurements were small.

The authors of articles [767] and [755] investigated the distribution of the intensity of beams from lasers with wavelengths 6328 Å propagating in the atmosphere over various distances. In the first article the measurements were made at distances of 4.5 and 14.5 km with a beam with 0.35 cm diameter when it entered the atmosphere. In [755] a beam with an initial diameter of 1.4 cm was used at distances of 0.2, 0.5, 2.4 and 7.0 km. In [767] 68, in [755] 28 intensity distributions were

developed out of which 51 and 23, respectively, turned out to be lognormal.

Chu [855] studied the fluctuations in the intensity of radiation from three lasers with different wavelengths: 0.63, 3.51 and 10.6 μ. The measurements were carried out over a path 2.6 km long with values of the receiving aperture equal to 5, 12.5 and 15 cm, respectively, for the three wavelengths mentioned above. The fluctuation spectrum of the intensity was investigated with the aid of a spectral analyzer. Up to frequencies 100 Hz the signal decreases exponentially with the frequency. When the frequencies are large, the signal does not decrease as rapidly, which is possibly due to the effect of noise from the ground. The dependence of the fluctuations in intensity on the emitted wavelengths was not as fast as $\lambda^{-1/2}$ which is obtained theoretically from a congealed turbulence model. This result cannot be explained by the different values of the receiving apertures during measurements with different wavelengths.

In Hohn's work [769] the frequency spectra of fluctuations in the intensity of a laser beam (λ = 6328 Å) were studied with an initial diameter of 0.35 cm for distances of 4.5 and 14.5 km. It turned out that the normalized spectrum of the fluctuations in light intensity U(f), where f is the frequency, does not depend much on the diameter of the receiving aperture which was varied in the experiments from 0.5 to 8.0 cm. In [769] data were also obtained for the characteristic frequency of the fluctuations or the frequency which corresponds to the maximum in the curve U(f). The relation for this frequency which was obtained as a function of the distance and the mean wind velocity component which is perpendicular to the direction in which the light is propagated, differed from that forecast by the theory and also from the relation obtained from the empirical formula developed by V. I. Tatrskiy [463]. This relation agreed satisfactorily with the corresponding experimental values obtained by Ryznar [761].

Figure 11.6 shows the spectra U(f) for various values of the diameter of the receiving aperture obtained in one series of measurements in [769]. The values of the frequency f_m which correspond to the maximum of the curve U(f) were varied from measurement to measurement in an interval approximately from 40 to 140 Hz. The distribution halfwidth was varied between the limits from 4 to 18. By the distribution halfwidth we mean the quantity

$$\gamma_{1/2} = f_2/f_1, \qquad (11.36)$$

where f_2 and f_1 are frequencies which satisfy the condition

$$U(f_2) = U(f_1) = \frac{1}{2} U(f_m). \qquad (11.37)$$

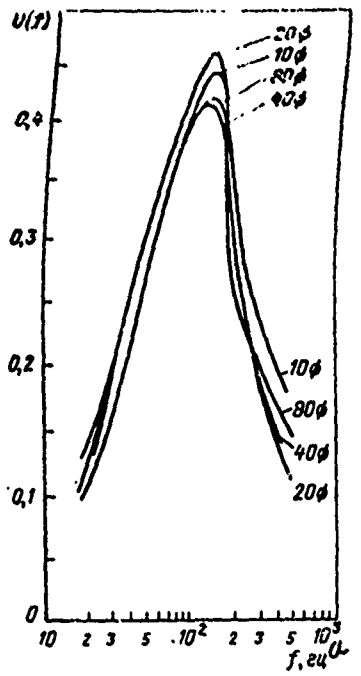

Fig. 11.6. Spectra of the function U(f) for various values of the receiving aperture according to the data from one series of measurements in article [769]

Key: a. Hz

A study of the three-dimensional structure of pulse radiation from lasers propagating in a turbulent atmosphere was carried out in the author's laboratory [770]. The measurements were carried out with a ruby laser (wavelength 0.69 μ) which operated in the free generation mode (the duration of the individual pulses was on the order of magnitude of 0.5 msec, with power of several hundreds of watts, and beam divergence 6'). The structure of the radiation from the laser was studied at distances from the source equal to

0.25, 1.2, 3.5 and 10 km. The corresponding pictures of the structures were photographed from screens mounted at the distances mentioned above. The use of neutral filters made it possible to obtain photographs with normal blackness. The photometering of cross sections of the images which were obtained was carried out in such a way that not less than 10 intensity measurements were made in the region where the theoretical value of the correlation radius was approximately equal to $\sqrt{\lambda L}$ [731]. In each frame 2 - 6 profiles were photmetered vertically and 1 profile across the frame. The photometered profiles were processed on an electronic computer, with the aid of which the correlation functions for the fluctuations in the intensity, the variance and the mean intensity value were calculated.

TABLE 11.1

VALUES OF THE CORRELATION RADIUS ρ DETERMINED EXPERIMENTALLY AND THEORETICALLY

a Расстояние L, км	Экспериментальные значения ρ, см b			c Расчетное значение ρ, см	d Число фотометрических разрезов
	e минимальное	f максимальное	g среднее		
0,25	4,7	17	9,1	1,3	37
1,2	4	12,8	10	2,9	23
3,5	3	14	9,5	4,9	15
10,0	—	—	8,1	8,3	52

Key:
a. distance, L, km
b. experimental values of ρ, cm
c. calculated value of ρ, cm
d. number of photometric profiles
e. minimum
f. maximum
g. mean

Table 11.1 gives the values of the correlation radius which was determined by processing the experimental data and from calculations using the formula $\rho = \sqrt{\lambda L}$.

An analysis of the experimental data obtained from the standpoint of the distribution for the intensity has shown that for the distances 0.25, 1.2 and 3.5 km these do not deviate from the normal distribution of the natural logarithm of the intensity. In this case, using formula (11.35) we can determine the value of σ^2 from the experimental data. When the measurements were carried out at a distance of 10 km. it was discovered that the intensity does not obey a lognormal distribution.

In the case when the intensity has a lognormal distribution the relation between σ^2 and the distance and the divergence angle of a laser beam were determined. It turned out that the value of σ^2 increases up to a distance of L = 3.5 km and then drops slowly. The curve for σ^2 as a function of the beam divergence φ has a minimum which occurs for a value of φ which is approximately 50". We note that for the value of φ we have here taken the value of the beam divergence which is determined from the dimensions of the radiation spot and the distance during measurements on paths of short length.

Experimental data for fluctuations in the intensity of narrow light beams were also obtained in articles [753, 758, 760, 762 - 765, 892]. The relation between the intensity of the fluctuations, their frequency spectrum for the radiation from a gas laser (λ = 0.63 μ) and the diameter of the receiving aperture which varied from 3.5 to 50 cm was investigated in article [758]. Fluctuations in the polarized radiation from the same laser due to the fluctuations in intensity were investigated in [765] at a distance of 5 miles in the layer of the atmosphere near the earth's surface. Additional detailed studies must be made to explain the nature of the fluctuations in the polarized radiation which were discovered in order to be able to separate with sufficient accuracy the fluctuations measured into components caused by atmospheric aerosols and turbulent nonhomogeneities in the atmosphere.

Fluctuations in the intensity of a projector beam in the layer of the atmosphere near the earth's surface at distances from 1 to 30 km were investigated in article [892]. The distribution of the logarithm of the fluctuations in intensity turned out to be approximately normal. In [892] the frequency spectrum of the fluctuations in intensity and the degree of modulation of the radiation by the atmosphere was also investigated for various diameters of the receiving aperture, the values of which varied from 13 to 4 cm. By the degree of modulation we mean the ratio of the mean amplitude of the signal to its mean value. It turned out that the degree of modulation is inversely proportional to the diameter of the receiving aperture. For small values of the latter, saturation was discovered in the relation investigated.

2. Changes in the Beam Diameter With the Distance. Turbulent movements in the atmosphere cause expansion of the beam diameter in addition to the expansion caused by geometric and diffractive expansion. So far this problem has not been studied adequately.

In articles [757, 766, 770] some data were obtained which can be used to estimate the possible expansion in beams emitted from lasers under various conditions in the atmosphere. During measurements which were made at a distance of 15 and 145 km, the beam divergence increased by 8" and 13", respectively [757]. In article [766] on the basis of the results obtained from measurements of the diameter D of the beam at various distances up to 145 kilometers with an initial diameter of 10 cm at night under conditions when the atmosphere was slightly turbid, the following empirical formula was obtained for D:

$$D = \alpha L^{\beta}, \qquad (11.38)$$

where $\alpha = 4.5 \cdot 10^{-6}$ and $\beta = 1.2$, where D was measured in centimeters and L in meters. It is noted in [766] that under mist conditions and during the day the diameter of the beam can increase several times compared to its value which is obtained from formula (11.38).

The relation between the diameter of a focused beam and the initial value of the diameter was also investigated in [766]. During propagation in a vacuum these quantities are inversely proportional. Measurements in a turbulent atmosphere has shown that the diameter of the focused beam decreases as a function of the aperture diameter of the source only up to a value of the latter which is equal to 11 cm. As the initial diameter of the beam increases further, focusing no longer improves. Figure 11.7 shows the above relation which was obtained from the experiment (top curve, the length of vertical segments which characterize the scatter in the experimental data). The bottom curve in this diagram refers to the case when a focused beam is propagated in a vacuum. The slight rise in the top curve when the diameters of the source aperture are larger than 11 cm is explained in [766] by an aberration of the optical system.

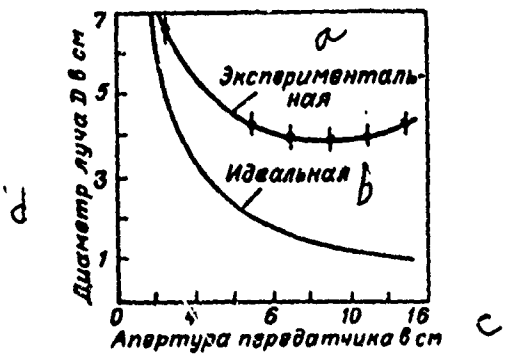

Fig. 11.7. The diameter of a focused beam vs its initial diameter according to the data in article [766]

Key: a. experimental curve
b. ideal curve
c. aperture of source in cm
d. beam diameter D in cm

Various linear dimensions of the spot for the radiation from a pulsed ruby crystal laser were observed in article [770] during measurements at the same distance. Thus, at a distance of 10 km the linear dimensions of the beam cross section fluctuated approximately from 0.7 to 2 m in pulses which followed one another every 45 sec.

3. Fluctuations in the Arrival Angle of a Spatially Bounded Beam. The fluctuations in the arrival angle of the radiation with the aid of which the image is formed in the focal plane of the objective cause the image to shift and spread. Shifted images occur in those cases when the dimensions of the nonhomogeneities caused by the turbulent movements in the atmosphere are larger than the diameter of the objective. Small scale nonhomogeneities displace individual elements of the beam and cause "spreading" of the image.

Experimental studies of the fluctuations in the angle of arrival of beams from a gas laser propagated in the layer of the atmosphere near the earth's surface were carried out in the author's laboratory [756]. The measurements were made at a distance of 1.2 km with a gas laser based on a mixture of helium with neon (wavelength 6328 Å), operating in a continuous generating axial vibration mode, with a heat source the luminescent body of which was bounded by appropriate diaphragms. The initial diameter of the beam d_0 and its

divergence φ were equal to 2.5 mm and 110".

When a telescope was used in which the diameter of the objective was d = 19, 27 and 38 mm, the beam divergence angle was close to the diffraction angle and equal to 20" = 70". The diameter of the receiver objective was equal to 2.4, 4.8, 8.0 and 10.0 cm. The images of the sources were recorded on highly sensitive moving film. The time in which the random fluctuations in the position of the image occurred was 20 - 30 sec. Altogether 96 values of the arrival angle were obtained.

The measure adopted for the vibrations in the source was the quantity

$$\sigma_{\varphi}=\sqrt{\frac{\sum_i \Delta_i^2}{n}} \tag{11.39}$$

where Δ_i is the deviation in the angle of arrival measured every 0.2 sec, n is the number of measurements Δ_i, and the summation extends over all deviations for a given realization.

The variance of the fluctuations in the angle of arrival was calculated from the formula

$$\sigma_{\varphi}^2=\frac{\sum_i x_i^2 n_i}{n}, \tag{11.40}$$

where x_i is the deviation of the image trace from the mean value. For each value of the beam diameter at the input aperture the mean value of σ_{φ}^2 was determined as the arithmetic mean over all realizations. The error in σ_{φ}^2 varied approximately in the 10 - 20% range.

The distribution functions for the fluctuations in the angles of arrival were determined. It turned out that 62 out of 64 distributions were normal with values of σ_{φ}^2 from 0. 8 to 10.8 squared angular seconds.

The relation between the quantity σ_φ^2 for a non-collimated beam and the diameter of the receiver objective D_{rec} in centimeters has the form

$$\sigma_\varphi^2 \sim (D_{rec})^{-1/3}. \qquad (11.41)$$

Key: a. rec

The numerical values of σ_φ^2 for each D_{rec} which vary between limits depend on the meteorological conditions during which the measurements are made.

As the initial diameter of the beam increases from 2.5 to 27 mm the variance of the arrival angle increases sharply which is apparently connected to the transition from a spherical wave to a plane wave. A further increase in the beam diameter leads to a slight decrease in the variance of the fluctuations of the angles of arrival.

During the propagation of laser beams in the atmosphere, in addition to the high frequency fluctuations in the angles of arrival, a slow shift of the beams is observed.

In the work of Buck [766] a deviation of a beam emitted from a laser $\lambda = 6328$ Å was observed which reached a value of 4 m at a distance of 10 km in 30 min.

4. Studies of the Coherence of Laser Radiation Propagated in a Turbulent Atmosphere. A distortion in the phase front of the wave and a redistribution of the intensity in the beam cross section caused by turbulent motions in the atmosphere lead to a deterioration in the space and time coherence of laser radiation. The latter has a considerable effect on the efficiency of communication systems constructed on the basis of optical heterodyne oscillators.

A quantitative measure of the radiation coherence is the coherence function, whose normalized value coincides with the optical transfer function which characterizes the resolution capacity of optical receivers which are used to record the images of objects in the atmosphere [750, 856]. The measurement of the coherence function can provide a solution for the converse problem, i.e., finding the turbulence parameters of the atmosphere on the basis of these measurements. Thus, a study of the coherence function of the radiation propagated

in the atmosphere is important from an applied standpoint.

When the coherence of the radiation propagated in the atmosphere is studied experimentally, the interference picture which arises when the fields of the beam which passed through the layer of the atmosphere are superimposed is analyzed together with the reference beam. In work on interferometry with a large base [771-773] interference bands of finite width are recorded by means of photographs. It is shown in this work that it is possible to observe interference bands with large visibility. V. I. Vaytsel and S. S. Khmelevets [774] developed an interference method which makes it possible to determine the characteristics of atmospheric turbulence from measurements of the coherence of optical radiation. Data for the coefficient C_n were obtained on the basis of this method. The same authors investigated the effect of atmospheric turbulence on the resolution capacity of interference receivers [775] and also on the spectrum of the signal from the photomultiplier in the optical heterodyne oscillator [776]. Studies of the spatial coherence of laser radiation and the effect of atmospheric turbulence on it were carried out by V. V. Pokasov and S. S. Khmelevepsov [777, 778]. The measurements were made in the layer of the atmosphere near the earth's surface on paths 100 and 200 m long. Two methods were used, the foundations for which were developed in articles [863, 856, 864 and 750]. The results obtained from studies of the dependence of the coherence function on the temperature gradient were in satisfactory agreement with the theory. The dependence of the coherence function on the distance between the points in the cross section of the beam did not agree with that forecast by the theory, which the authors considered to be a limitation of the approximation from geometrical optics used in the theory.

Values of the structural constant C_n of the refractive index were obtained on the basis of experimental data for the coherence function in article [777]. The values of C_n were determined simultaneously from meteo-element measurements at the altitudes 20 cm and 2.0 m. A comparison of the values of C_n obtained by the two methods has shown that the values agree satisfactorily for values of the temperature gradient $\Delta T \leqslant 0{,}6°C$ (an exception to this is the case $\Delta T = 0$, in which according to the meteodata $C_n = 0$, and according to the second method $C_n = 0.008 \cdot 10^{-6} cm^{-1/3}$). When $\Delta T > 0{,}6°C$, the values of C_n which were determined from measurements of the coherence function and from the meteodata differ by a greater amount the

larger the value of ΔT. Thus, when $\Delta T = 1.0^{\circ}C$, the difference is 100%, and when $\Delta T = 2.2^{\circ}C$ it is 200%. In all cases when the value of C_n was determined from the meteoelement measurements, it turned out to be smaller than that obtained from measurements of the coherence function. This means that when $\Delta T > 0{,}6^{\circ}C$, the spatial coherence of the radiation decreases much faster than the theory implies. It should be noted that during all measurements the wind velocity did not exceed 0.2 - 0.3 m/sec.

SUPPLEMENT 1

1. ARDC MODEL OF THE ATMOSPHERE FOR ALTITUDES FROM 0 to 30 km [3]

a Высота, км	b Температура, °K	c Давление, мб	d Плотность, г·см⁻³	e Число молекул в единице объема, см⁻³	f Высота однородной атмосферы, км
0	288,16	$1{,}01325 \cdot 10^{3}$	$1{,}2250 \cdot 10^{-3}$	$2{,}5476 \cdot 10^{19}$	8,4344
1	281,66	$8{,}9876 \cdot 10^{2}$	1,1117	2,3118	8,2468
2	275,16	7,9501	1,0066	2,0933	8,0591
3	268,67	7,0121	$9{,}0926 \cdot 10^{-4}$	1,8909	7,8713
4	262,18	6,1660	8,1935	1,7039	7,6835
5	255,69	5,4048	7,3643	1,5315	7,4957
6	249,20	4,7217	6,6011	1,3728	7,3077
7	242,71	4,11[illegible]	5,9002	1,2270	7,1198
8	236,23	3,5651	5,2578	1,0934	6,9317
9	229,74	3,0800	4,6706	$9{,}7130 \cdot 10^{18}$	6,7436
10	223,26	2,6500	4,1351	8,5993	6,5554
11	216,78	2,2700	3,6480	7,5864	6,3672
12	216,66	1,9399	3,1194	6,4870	6,3656
13	216,66	1,6579	2,6659	5,5441	6,3676
14	216,66	1,4170	2,2785	4,7385	6,3696
15	216,66	1,2112	1,9475	4,0501	6,3716
16	216,66	1,0353	1,6647	3,4619	6,3736
17	216,66	$8{,}8496 \cdot 10$	1,4230	2,9593	6,3756
18	216,66	7,5652	1,2165	2,5298	6,3776
19	216,66	6,4674	1,0399	2,1627	6,3796
20	216,66	5,5293	$8{,}8909 \cdot 10^{-5}$	1,8490	6,3816
21	216,66	4,7274	7,6015	1,5808	6,3836
22	216,66	4,0420	6,4995	1,3[illegible]	6,3856
23	216,66	3,4562	5,5575	1,1[illegible]	6,3876
24	216,66	2,9554	4,7522	$9{,}882[illegible] \cdot 10^{17}$	6,3896
25	216,66	2,5273	4,0639	8,4513	6,3916
26	219,34	2,1632	3,4359	7,1453	6,4728
28	225,29	1,5949	2,4663	5,1290	6,6525
30	231,24	1,1855	1,7861	3,7144	6,8323

Key:
a. altitude, km
b. temperature, $^{\circ}K$
c. pressure, mb
d. density, $g.cm^{-3}$
e. number of molecules per unit volume, cm^{-3}
f. altitude of homogeneous atmosphere, km

larger the value of ΔT. Thus, when $\Delta T = 1.0^{\circ}C$, the difference is 100%, and when $\Delta T = 2.2^{\circ}C$ it is 200%. In all cases when the value of C_n was determined from the meteoelement measurements, it turned out to be smaller than that obtained from measurements of the coherence function. This means that when $\Delta T > 0{,}6^{\circ}C$, the spatial coherence of the radiation decreases much faster than the theory implies. It should be noted that during all measurements the wind velocity did not exceed 0.2 - 0.3 m/sec.

SUPPLEMENT 1

1. ARDC MODEL OF THE ATMOSPHERE FOR ALTITUDES FROM 0 to 30 km [3]

a Высота, км	b Температура, °K	c Давление, мб	d Плотность, г·см⁻³	e Число молекул в единице объема, см⁻³	f Высота однородной атмосферы, км
0	288,16	$1{,}01325 \cdot 10^{3}$	$1{,}2250 \cdot 10^{-3}$	$2{,}5476 \cdot 10^{19}$	8,4344
1	281,66	$8{,}9876 \cdot 10^{2}$	1,1117	2,3118	8,2468
2	275,16	7,9501	1,0066	2,0933	8,0591
3	268,67	7,0121	$9{,}0926 \cdot 10^{-4}$	1,8909	7,8713
4	262,18	6,1660	8,1935	1,7039	7,6835
5	255,69	5,4048	7,3643	1,5315	7,4957
6	249,20	4,7217	6,6011	1,3728	7,3077
7	242,71	4,11[illegible]	5,9002	1,2270	7,1198
8	236,23	3,5651	5,2578	1,0934	6,9317
9	229,74	3,0800	4,6706	$9{,}7130 \cdot 10^{18}$	6,7436
10	223,26	2,6500	4,1351	8,5993	6,5554
11	216,78	2,2700	3,6480	7,5864	6,3672
12	216,66	1,9399	3,1194	6,4870	6,3656
13	216,66	1,6579	2,6659	5,5441	6,3676
14	216,66	1,4170	2,2785	4,7385	6,3696
15	216,66	1,2112	1,9475	4,0501	6,3716
16	216,66	1,0353	1,6647	3,4619	6,3736
17	216,66	8,8496·10	1,4230	2,9593	6,3756
18	216,66	7,5652	1,2165	2,5298	6,3776
19	216,66	6,4674	1,0399	2,1627	6,3796
20	216,66	5,5293	$8{,}8909 \cdot 10^{-5}$	1,8490	6,3816
21	216,66	4,7274	7,6015	1,5808	6,3836
22	216,66	4,0420	6,4995	1,3[illegible]	6,3856
23	216,66	3,4562	5,5575	1,1[illegible]	6,3876
24	216,66	2,9554	4,7522	$9{,}882[illegible] \cdot 10^{17}$	6,3896
25	216,66	2,5273	4,0639	8,4513	6,3916
26	219,34	2,1632	3,4359	7,1453	6,4728
28	225,29	1,5949	2,4663	5,1290	6,6525
30	231,24	1,1855	1,7861	3,7144	6,8323

Key: a. altitude, km
b. temperature, $^{\circ}K$
c. pressure, mb
d. density, $g.cm^{-3}$
e. number of molecules per unit volume, cm^{-3}
f. altitude of homogeneous atmosphere, km

2. ALTITUDE OF ISOBAR SURFACES IN THE LAYER FROM 25 to 100 KM, GEOPOTENTIAL KILOMETERS [3]

Summer

a Уровни в атмосфере, мб	Широта b								
	0°	10°	20°	30°	40°	50°	60°	70°	80°
20	26,5	26,5	26,6	26,9	27,1	27,3	27,4	27,5	27,6
16	27,9	28,0	28,1	28,4	28,6	28,8	28,9	29,0	29,1

Key: a. levels in atmosphere, mb
b. latitude

Continued

a Уровни в атмосфере, мб	Широта b								
	0°	10°	20°	30°	40°	50°	60°	70°	80°
12	29,8	29,9	30,0	30,3	30,6	30,8	30,9	31,0	31,1
10	31,1	31,1	31,2	31,6	31,8	32,1	32,2	32,3	32,4
8	32,6	32,6	32,8	33,1	33,4	33,7	33,8	33,9	34,0
6	34,6	34,6	34,8	35,2	35,5	35,7	35,9	36,0	36,1
4	37,5	37,5	37,8	38,2	38,5	38,8	38,9	39,0	39,1
3	39,7	39,7	40,0	40,4	40,7	41,0	41,1	41,2	41,2
2,5	41,1	41,1	41,4	41,8	42,2	42,5	42,5	42,6	42,6
2,0	42,8	42,9	43,2	43,6	44,0	44,2	44,3	44,4	44,3
1,6	44,6	44,6	44,9	45,4	45,8	46,1	46,1	46,1	46,0
1,2	47,0	47,0	47,3	47,7	48,2	48,5	48,5	48,5	48,4
1,0	48,4	48,5	48,8	49,2	49,7	50,1	50,1	50,0	49,9
0,8	50,3	50,3	50,6	51,1	51,6	52,0	52,0	51,9	51,8
0,6	52,7	52,7	53,0	53,4	54,0	54,4	54,5	54,4	54,2
0,4	—	56,0	56,2	56,6	57,2	57,7	57,8	57,8	57,6
0,3	—	—	58,4	58,8	59,4	60,0	60,1	60,1	59,9
0,2	—	—	—	61,8	62,3	63,0	63,2	—	—
0,15	—	—	—	63,9	64,4	65,1	65,4	—	—
0,10	—	—	—	66,7	67,1	67,8	68,2	—	—
0,08	—	—	—	68,3	68,6	69,3	70,0	—	—
0,04	—	—	—	72,7	73,0	73,6	74,0	—	—
0,02	—	—	—	77,0	77,1	77,6	78,0	—	—
0,01	—	—	—	81,1	81,1	81,4	81,8	—	—
0,004	—	—	—	86,6	86,4	86,5	86,7	—	—
0,002	—	—	—	90,9	90,6	90,6	90,5	—	—
0,001	—	—	—	95,4	95,1	94,9	94,7	—	—
0,0005	—	—	—	100,2	99,8	99,5	99,2	—	—

Key: a. levels in atmosphere, mb
b. latitude

Winter

a Уровни в атмосфере, мб	b Широта								
	0°	10°	20°	30°	40°	50°	60°	70°	80°
20	26,1	26,1	26,2	26,2	26,2	26,1	25,7	25,2	25,0
16	27,5	27,5	27,6	27,6	27,6	27,5	27,1	26,6	26,3
12	29,4	29,4	29,5	29,5	29,4	29,3	28,8	28,3	28,0
10	30,6	30,6	30,7	30,6	30,6	30,4	30,0	29,4	29,0
8	32,1	32,1	32,2	32,1	32,0	31,8	31,3	30,7	30,3
6	34,1	34,0	34,1	34,0	33,9	33,7	33,1	32,4	32,0
4	37,0	37,0	37,0	36,8	36,6	36,3	35,7	34,9	34,5
3	39,1	39,0	39,0	38,9	38,7	38,2	37,6	36,7	36,2
2,5	40,4	40,4	40,4	40,2	40,0	39,5	38,8	37,9	37,6
2,0	42,1	42,1	42,1	41,9	41,6	41,1	40,3	39,3	38,8

Key: a. levels in atmosphere, mb
b. latitude

Continued

a Уровни в атмосфере, мб	Широта b								
	0°	10°	20°	30°	40°	50°	60°	70°	80°
1,6	43,9	43,8	43,8	43,6	43,2	42,6	41,8	40,8	40,3
1,2	46,2	46,1	46,1	45,8	45,4	44,7	43,8	42,8	42,2
1,0	47,6	47,6	47,5	47,2	46,8	46,1	45,1	44,0	43,5
0,8	49,5	49,4	49,3	49,0	48,5	47,7	46,7	45,6	45,0
0,6	51,8	51,8	51,6	51,3	50,7	49,8	48,7	47,6	47,0
0,4	55,2	55,1	55,0	54,5	53,9	52,9	51,7	50,4	49,7
0,3	—	57,4	57,2	56,8	56,1	55,1	53,8	52,5	51,8
0,2	—	60,5	60,4	60,0	59,3	58,3	56,9	55,5	54,8
0,15	—	—	—	62,1	61,4	60,4	59,1	—	—
0,10	—	—	—	65,0	64,4	63,6	62,2	—	—
0,08	—	—	—	66,5	66,0	65,2	63,9	—	—
0,04	—	—	—	71,1	70,6	70,0	68,9	—	—
0,02	—	—	—	75,4	75,0	74,4	73,5	—	—
0,01	—	—	—	79,6	79,2	78,6	77,8	—	—
0,004	—	—	—	85,0	84,7	84,3	83,7	—	—
0,002	—	—	—	89,3	89,1	88,9	88,4	—	—
0,001	—	—	—	93,7	93,7	93,6	93,3	—	—
0,0005	—	—	—	98,4	98,6	98,6	98,3	—	—

Key: a. levels in atmosphere, mb
b. latitude

3. THE TEMPERATURE IN THE LAYER OF THE ATMOSPHERE FROM 25 to 100 km, °K [3]

Summer

a Уровни в атмосфере, мб	b Широта 0°	10°	20°	30°	40°	50°	60°	70°	80°
20	220	220	222	224	226	230	233	235	236
16	223	223	225	227	229	232	234	236	237
12	227	227	229	231	233	236	237	239	239
10	230	230	232	234	237	239	240	242	242
8	234	234	237	239	242	244	244	245	244
6	240	240	243	246	249	251	250	250	248
4	251	251	254	257	261	261	259	257	254
3	260	260	263	266	269	267	264	261	257
2,5	265	265	267	270	273	271	267	264	260
2,0	271	271	272	274	277	276	273	268	265
1,6	274	274	276	277	281	282	279	274	271
1,2	278	278	279	279	285	290	289	284	279
1,0	279	279	280	279	285	293	293	289	283
0,8	280	280	280	278	283	291	294	292	288

Key: a. levels in atmosphere, mb
b. latitude

Continued

a Уровни в атмосфере, мб	b Широта 0°	10°	20°	30°	40°	50°	60°	70°	80°
0,6	280	279	277	274	277	285	290	291	290
0,4	—	274	270	265	265	272	276	278	280
0,3	—	—	262	259	254	261	267	269	270
0,2	—	—	—	248	244	247	254	—	—
0,15	—	—	—	242	237	238	245	—	—
0,10	—	—	—	233	227	226	232	—	—
0,08	—	—	—	228	222	220	226	—	—
0,04	—	—	—	214	208	205	203	—	—
0,02	—	—	—	202	197	189	186	—	—
0,01	—	—	—	200	194	186	180	—	—
0,004	—	—	—	208	202	194	185	—	—
0,002	—	—	—	218	212	204	195	—	—
0,001	—	—	—	229	226	217	210	—	—
0,0005	—	—	—	241	243	238	234	—	—

Key: a. levels in atmosphere, mb
b. latitude

Winter

a Уровни в атмосфере, мб	Широта b								
	0°	10°	20°	30°	40°	50°	60°	70°	80°
20	214	213	213	214	214	214	209	204	201
16	218	217	216	216	214	214	208	203	200
12	222	221	220	218	216	213	208	203	199
10	226	225	223	220	217	213	208	203	199
8	230	229	228	224	220	214	209	203	199
6	237	236	234	230	225	218	212	206	202
4	246	245	243	239	234	226	219	212	208
3	253	253	251	247	240	232	224	217	213
2,5	257	257	256	252	245	236	228	220	217
2,0	263	262	260	256	249	241	233	225	221
1,6	268	267	264	260	253	244	236	229	225
1,2	274	273	269	265	257	248	238	232	229
1,0	277	276	272	267	260	250	239	233	231
0,8	279	279	274	270	262	252	241	235	232
0,6	281	280	277	273	265	255	245	237	234
0,4	276	276	275	274	268	259	250	243	239
0,3	—	270	269	269	267	262	255	247	244
0,2	—	257	256	257	259	263	259	254	251
0,15	—	—	—	249	253	261	262	—	—
0,10	—	—	—	236	243	254	262	—	—
0,08	—	—	—	232	237	247	258	—	—
0,04	—	—	—	218	220	224	229	—	—
0,02	—	—	—	207	209	211	216	—	—
0,01	—	—	—	200	204	207	214	—	—

Key: a. levels in atmosphere, mb
b. latitude

Continued

a Уровни в атмосфере, мб	Широта b								
	0°	10°	20°	30°	40°	50°	60°	70°	80°
0,004	—	—	—	205	210	218	224	—	—
0,002	—	—	—	214	220	228	236	—	—
0,001	—	—	—	224	233	239	244	—	—
0,0005	—	—	—	236	245	250	250	—	—

Key: a. levels in atmosphere, mb
b. latitude

SUPPLEMENT 2

VALUES OF THE ABSORPTION COEFFICIENT α, THE REFRACTIVE INDEX x AND THE REFRACTIVE INDEX n OF PURE WATER, ACCORDING TO THE DATA OF THE AUTHOR AND HIS COLLABORATORS FOR VARIOUS WAVELENGTHS IN THE INTERVAL 0.55 - 25.3 μ

№ п/п	ν, см⁻¹	λ, μ	α, см⁻¹	x	n
1	395	25,31	1130	0,229	1,700
2	405	24,65	1190	0,234	1,702
3	415	24,09	1230	0,236	1,709
4	425	23,52	1210	0,227	1,738
5	435	22,98	1300	0,238	1,784
6	445	22,47	1790	0,320	1,833
7	455	21,97	2300	0,402	1,802
8	465	21,50	2590	0,444	1,763
9	475	21,05	2800	0,470	1,722
10	485	20,61	3010	0,495	1,695
11	495	20,21	3180	0,511	1,665
12	505	19,80	3370	0,531	1,637
13	515	19,41	3480	0,537	1,601
14	525	19,04	3540	0,537	1,575
15	535	18,69	3710	0,552	1,544
16	545	18,34	3780	0,552	1,516
17	555	18,01	3870	0,553	1,496
18	565	17,69	3980	0,560	1,459
19	575	17,39	4070	0,563	1,421
20	585	17,09	4100	0,557	1,394
21	595	16,80	4110	0,550	1,367
22	605	16,52	4150	0,546	1,329
23	615	16,26	4150	0,536	1,324

Key: a. serial number
b. cm^{-1}

Continued

a № п/п	b ν, см⁻¹	λ, μ	b α, см⁻¹	x	n
24	625	16,00	4130	0,526	1,292
25	635	15,74	4020	0,504	1,280
26	645	15,50	3990	0,492	1,248
27	655	15,26	3970	0,483	1,242
28	665	15,03	3960	0,474	1,222
29	675	14,81	3850	0,454	1,192
30	685	14,59	3680	0,427	1,177
31	695	14,38	3520	0,403	1,175
32	705	14,18	3380	0,382	1,194
33	715	13,98	3520	0,392	1,192
34	725	13,79	3600	0,396	1,166
35	735	13,61	3510	0,380	1,147
36	745	13,42	3350	0,358	1,126
37	755	13,24	3220	0,339	1,115
38	765	13,07	3100	0,323	1,107
39	775	12,91	2940	0,302	1,102
40	785	12,73	2750	0,279	1,097
41	795	12,57	2620	0,262	1,096
42	805	12,42	2470	0,245	1,095
43	815	12,26	2360	0,230	1,096
44	825	12,12	2270	0,219	1,100
45	835	11,97	2170	0,207	1,102
46	845	11,83	2020	0,190	1,103
47	855	11,69	1960	0,182	1,107
48	865	11,56	1930	0,177	1,113
49	875	11,42	1690	0,154	1,110
50	885	11,29	1520	0,137	1,112
51	896	11,16	880	0,122	1,118
52	946	10,57	800	0,067	1,144
53	996	10,04	580	0,047	1,105
54	1047	9,55	550	0,042	1,180
55	1098	9,11	530	0,038	1,203
56	1148	8,71	530	0,037	1,228
57	1198	8,35	540	0,036	1,250
58	1249	8,01	540	0,034	1,262
59	1300	7,69	560	0,034	1,277
60	1350	7,41	560	0,033	1,292
61	1401	7,14	560	0,032	1,303
62	1451	6,89	600	0,033	1,316
63	1502	6,66	610	0,032	1,301
64	1553	6,44	720	0,037	1,297
65	1595	6,27	1130	0,056	1,379
66	1611	6,21	1140	0,056	1,401
67	1626	6,15	2180	0,107	1,371
68	1641	6,09	2940	0,143	1,342
69	1656	6,03	2760	0,133	1,275
70	1671	5,98	2390	0,114	1,239

Key: a. serial number
b. cm^{-1}

Continued

№ п/п	ν, см⁻¹	λ, μ	α, см⁻¹	x	n
71	1686	5,93	1730	$0,815 \cdot 10^{-1}$	1,224
72	1701	5,87	1090	$0,511 \cdot 10^{-1}$	1,202
73	1716	5,83	550	$0,211 \cdot 10^{-1}$	1,208
74	1731	5,77	445	$0,205 \cdot 10^{-1}$	1,222
75	1746	5,72	467	$0,213 \cdot 10^{-1}$	1,231
76	1761	5,67	650	$0,294 \cdot 10^{-1}$	1,261
77	1797	5,57	271	$0,125 \cdot 10^{-1}$	1,275
78	1848	5,41	232	$0,105 \cdot 10^{-1}$	1,287
79	1898	5,27	232	$0,103 \cdot 10^{-1}$	1,309
80	1949	5,13	249	$0,107 \cdot 10^{-1}$	1,312
81	1999	5,00	309	$0,123 \cdot 10^{-1}$	1,317
82	2046	4,89	362	$0,136 \cdot 10^{-1}$	1,321
83	2096	4,77	386	$0,142 \cdot 10^{-1}$	1,323
84	2146	4,66	386	$0,138 \cdot 10^{-1}$	1,327
85	2196	4,55	348	$0,122 \cdot 10^{-1}$	1,329
86	2246	4,45	296	$0,100 \cdot 10^{-1}$	1,329
87	2296	4,36	252	$0,083 \cdot 10^{-1}$	1,329
88	2396	4,17	181	$0,559 \cdot 10^{-2}$	1,335
89	2446	4,09	160	$0,521 \cdot 10^{-2}$	1,338
90	2496	4,01	134	$0,428 \cdot 10^{-2}$	1,343
91	2546	3,93	127	$0,397 \cdot 10^{-2}$	1,347
92	2596	3,85	116	$0,359 \cdot 10^{-2}$	1,357
93	2646	3,78	122	$0,369 \cdot 10^{-2}$	1,364
94	2696	3,71	134	$0,398 \cdot 10^{-2}$	1,370
95	2746	3,64	166	$0,484 \cdot 10^{-2}$	1,376
96	2796	3,58	218	$0,621 \cdot 10^{-2}$	1,394
97	2846	3,51	290	$0,813 \cdot 10^{-2}$	1,398
98	2896	3,45	418	$0,115 \cdot 10^{-1}$	1,416
99	2946	3,39	630	$0,170 \cdot 10^{-1}$	1,478
100	2996	3,34	900	$0,240 \cdot 10^{-1}$	1,458
101	3006	3,33	313	$0,828 \cdot 10^{-2}$	1,460
102	3021	3,31	417	$0,111 \cdot 10^{-1}$	1,468
103	3036	3,29	680	$0,179 \cdot 10^{-1}$	1,467
104	3051	3,28	1300	$0,338 \cdot 10^{-1}$	1,458
105	3066	3,26	990	$0,257 \cdot 10^{-1}$	1,452
106	3081	3,25	1010	$0,261 \cdot 10^{-1}$	1,463
107	3096	3,23	1180	$0,303 \cdot 10^{-1}$	1,465
108	3111	3,71	1410	$0\ 361 \cdot 10^{-1}$	1,478
109	3126	3,20	1740	$0,443 \cdot 10^{-1}$	1,489
110	3141	3,18	2100	$0,532 \cdot 10^{-1}$	1,492
111	3156	3,17	3060	$0,637 \cdot 10^{-1}$	1,495
112	3171	3,15	3070	$0,772 \cdot 10^{-1}$	1,504
113	3186	3,16	3690	$0,923 \cdot 10^{-1}$	1,509
114	3201	3,12	4420	0,110	1,513
115	3216	3,11	5320	0,132	1,514
116	3231	3,10	6660	0,164	1,515
117	3246	3,08	7610	0,187	1,489

Key: a. serial number
b. cm^{-1}

Continued

№ п/п	ν, см⁻¹	λ, μ	α, см⁻¹	x	n
118	3261	3,07	6910	0,171	1,467
119	3276	3,05	7930	0,193	1,494
120	3291	3,03	9250	0,224	1,469
121	3306	3,02	9950	0,240	1,451
122	3321	3,01	10390	0,249	1,430
123	3336	2,99	10830	0,259	1,414
124	3351	2,98	11120	0,264	1,396
125	3366	2,97	11280	0,266	1,374
126	3381	2,96	11350	0,267	1,353
127	3396	2,94	11660	0,273	1,337
128	3411	2,93	11750	0,274	1,314
129	3426	2,92	11880	0,276	1,288
130	3441	2,91	12230	0,283	1,260
131	3456	2,89	11670	0,269	1,232
132	3471	2,88	11080	0,254	1,210
133	3486	2,87	10770	0,237	1,190
134	3501	2,86	9940	0,226	1,175
135	3516	2,84	9310	0,210	1,147
136	3531	2,83	8610	0,194	1,131
137	3546	2,82	7530	0,169	1,110
138	3561	2,81	5940	0,133	1,094
139	3576	2,79	4890	0,109	1,088
140	3591	2,78	4480	$0,994 \cdot 10^{-1}$	1,100
141	3606	2,77	3600	$0,794 \cdot 10^{-1}$	1,108
142	3621	2,76	2950	$0,648 \cdot 10^{-1}$	1,112
143	3636	2,75	2360	$0,517 \cdot 10^{-1}$	1,133
144	3651	2,74	1780	$0,384 \cdot 10^{-1}$	1,138
145	3666	2,73	1050	$0,227 \cdot 10^{-1}$	1,141
146	3696	2,71	730	$0,157 \cdot 10^{-1}$	1,181
147	3746	2,67	247	$0,526 \cdot 10^{-2}$	1,221
148	3796	2,63	183	$0,386 \cdot 10^{-2}$	1,234
)	3846	2,60	146	$0,304 \cdot 10^{-2}$	1,245
50	3896	2,57	128	$0,263 \cdot 10^{-2}$	1,255
51	3946	2,53	119	$0,240 \cdot 10^{-2}$	1,261
152	3996	2,50	103	$0,206 \cdot 10^{-2}$	1,264
153	4046	2,47	88,9	$0,175 \cdot 10^{-2}$	1
154	4096	2,44	63,8	$0,124 \cdot 10^{-2}$	1,269
155	4146	2,41	56,3	$0,108 \cdot 10^{-2}$	
156	4196	2,38	48,6	$0,921 \cdot 10^{-3}$	
157	4246	2,36	40,4	$0,757 \cdot 10^{-3}$	1,274
158	4296	2,33	34,0	$0,631 \cdot 10^{-3}$	
159	4346	2,30	29,9	$0,548 \cdot 10^{-3}$	
160	4396	2,27	27,2	$0,492 \cdot 10^{-3}$	1,286
161	4446	2,25	25,3	$0,453 \cdot 10^{-3}$	
162	4496	2,22	24,5	$0,424 \cdot 10^{-3}$	1,289
163	4546	2,19	24,9	$0,436 \cdot 10^{-3}$	
164	4596	2,18	25,9	$0,449 \cdot 10^{-3}$	1,294

Key: a. serial number
b. cm^{-1}

Continued

a, № п/п	ν, $см^{-1}$	λ, μ	α, $см^{-1}$	κ	n
165	4646	2.15	27,5	$0,471 \cdot 10^{-3}$	
166	4696	2.13	29,6	$0,502 \cdot 10^{-3}$	1,297
167	4746	2.11	32,7	$0,548 \cdot 10^{-3}$	
168	4780	2,09	37,0	$0,616 \cdot 10^{-3}$	1,300
169	4830	2,07	40,6	$0,669 \cdot 10^{-3}$	
170	4878	2,05	45,5	$0,743 \cdot 10^{-3}$	1,304
171	4938	2,03	48,3	$0,778 \cdot 10^{-3}$	
172	4987	2,01	55,8	$0,891 \cdot 10^{-3}$	1,304
173	5040	1,98	70,3	$0,111 \cdot 10^{-2}$	
174	5105	1,96	85,2	$0,133 \cdot 10^{-2}$	1,306
175	5165	1,94	106	$0,163 \cdot 10^{-2}$	
176	5208	1,92	123	$0,187 \cdot 10^{-2}$	1,305
177	5277	1,89	119	$0,179 \cdot 10^{-2}$	
178	5333	1,88	68,4	$0,102 \cdot 10^{-2}$	1,303
179	5376	1,86	25,0	$0,371 \cdot 10^{-3}$	
180	5449	1,84	15,5	$0,227 \cdot 10^{-3}$	1,309
181	5602	1,78	13,6	$0,193 \cdot 10^{-3}$	
182	5635	1,77	12,6	$0,177 \cdot 10^{-3}$	
183	5710	1,75	12,4	$0,173 \cdot 10^{-3}$	1,310
184	5880	1,70	9,71	$0,131 \cdot 10^{-3}$	
185	6030	1,66	9,71	$0,128 \cdot 10^{-3}$	1,311
186	6200	1,61	9,71	$0,125 \cdot 10^{-3}$	
187	6370	1,57	10,7	$0,133 \cdot 10^{-3}$	1,312
188	6470	1,55	14,6	$0,179 \cdot 10^{-3}$	
189	6570	1,52	17,6	$0,213 \cdot 10^{-3}$	1,313
190	6660	1,50	21,8	$0,253 \cdot 10^{-3}$	
191	6770	1,48	28,5	$0,335 \cdot 10^{-3}$	1,313
192	6690	1,43	30;9	$0,352 \cdot 10^{-3}$	1,314
193	7100	1,41	24,0	$0,269 \cdot 10^{-3}$	
194	7210	1,39	14,5	$0,160 \cdot 10^{-3}$	1,314
195	7275	1,37	6,91	$0,756 \cdot 10^{-4}$	
196	7420	1,35	3,33	$0,347 \cdot 10^{-4}$	1,315
197	7540	1,33	2,21	$0,233 \cdot 10^{-4}$	
198	7670	1,30	1,62	$0,169 \cdot 10^{-4}$	1,315
199	7800	1,28	1,33	$0,136 \cdot 10^{-4}$	
200	7920	1,26	1,33	$0,133 \cdot 10^{-4}$	1,316
201	8060	1,24	1,38	$0,136 \cdot 10^{-4}$	
202	8186	1,22	1,44	$0,141 \cdot 10^{-4}$	1,316
203	8320	1,20	1,49	$0,143 \cdot 10^{-4}$	
204	8460	1,18	1,48	$0,139 \cdot 10^{-4}$	1,317
205	8600	1,16	1,41	$0,131 \cdot 10^{-4}$	
206	8760	1,14	1,13	$0,102 \cdot 10^{-4}$	1,317
207	8900	1,12	0,423	$0,378 \cdot 10^{-5}$	
208	9040	1,11	0,242	$0,212 \cdot 10^{-5}$	1,318
209	9190	1,09	0,190	$0,176 \cdot 10^{-5}$	
210	9350	1,07	0,161	$0,137 \cdot 10^{-5}$	1,319
211	9500	1,05	0,187	$0,156 \cdot 10^{-5}$	

Key: a. serial number
b. cm^{-1}

Continued

a № п/п	b ν, см⁻¹	λ, μ	b α, см⁻¹	κ	n
212	9660	1,04	0,243	$0,199 \cdot 10^{-5}$	1,320
213	9800	1,02	0,321	$0,260 \cdot 10^{-5}$	
214	9950	1,01	0,402	$0,322 \cdot 10^{-5}$	1,321
215	10100	0,99	0,508	$0,401 \cdot 10^{-5}$	
216	10200	0,98	0,522	$0,408 \cdot 10^{-5}$	0,323
217	10350	0,97	0,456	$0,352 \cdot 10^{-5}$	
218	10450	0,96	0,363	$0,277 \cdot 10^{-5}$	1,325
219	10650	0,94	0,221	$0,165 \cdot 10^{-5}$	
220	10800	0,93	0,171	$0,126 \cdot 10^{-5}$	1,326
221	10900	0,92	0,121	$0,88 \cdot 10^{-6}$	
222	11000	0,91	$0,853 \cdot 10^{-1}$	$0,62 \cdot 10^{-6}$	1,327
223	11200	0,89	$0,749 \cdot 10^{-1}$	$0,53 \cdot 10^{-6}$	
224	11300	0,88	$0,673 \cdot 10^{-1}$	$0,47 \cdot 10^{-6}$	1,329
225	11450	0,87	$0,606 \cdot 10^{-1}$	$0,42 \cdot 10^{-6}$	
226	11600	0,86	$0,563 \cdot 10^{-1}$	$0,39 \cdot 10^{-6}$	1,330
227	11700	0,85	$0,533 \cdot 10^{-1}$	$0,36 \cdot 10^{-6}$	
228	11820	0,85	$0,510 \cdot 10^{-1}$	$0,34 \cdot 10^{-6}$	1,331
229	11950	0,84	$0,466 \cdot 10^{-1}$	$0,31 \cdot 10^{-6}$	
230	12100	0,83	$0,386 \cdot 10^{-1}$	$0,25 \cdot 10^{-6}$	1,331
231	12150	0 82	$0,306 \cdot 10^{-1}$	$0,20 \cdot 10^{-6}$	
232	12300	0,82	$0,250 \cdot 10^{-1}$	$0,16 \cdot 10^{-6}$	
233	12400	0,81	$0,248 \cdot 10^{-1}$	$0,16 \cdot 10^{-6}$	
234	12550	0,80	$0,241 \cdot 10^{-1}$	$0,15 \cdot 10^{-6}$	1,333
235	12650	0,79	$0,263 \cdot 10^{-1}$	$0,17 \cdot 10^{-6}$	
236	12800	0,78	$0,287 \cdot 10^{-1}$	$0,18 \cdot 10^{-6}$	
237	12900	0,78	$0,300 \cdot 10^{-1}$	$0,19 \cdot 10^{-6}$	
238	13000	0,77	$0,312 \cdot 10^{-1}$	$0,19 \cdot 10^{-6}$	1,333
239	13150	0,76	$0,318 \cdot 10^{-1}$	$0,19 \cdot 10^{-6}$	
240	13300	0,75	$0,319 \cdot 10^{-1}$	$0,19 \cdot 10^{-6}$	
241	13450	0,74	$0,312 \cdot 10^{-1}$	$0,18 \cdot 10^{-6}$	1,333
242	13550	0,74	$0,295 \cdot 10^{-1}$	$0,17 \cdot 10^{-6}$	
243	13650	0,73	$0,226 \cdot 10^{-1}$	$0,13 \cdot 10^{-6}$	
244	13800	0,72	$0,159 \cdot 10^{-1}$	$0,92 \cdot 10^{-7}$	
245	13850	0,72	$0,131 \cdot 10^{-1}$	$0,75 \cdot 10^{-7}$	
246	14000	0,71	$0,100 \cdot 10^{-1}$	$0,57 \cdot 10^{-7}$	1,333
247	14100	0,71	$0,86 \cdot 10^{-2}$	$0,49 \cdot 10^{-7}$	
248	14300	0,70	$0,73 \cdot 10^{-2}$	$0,47 \cdot 10^{-7}$	
249	14300	0,70	$0,68 \cdot 10^{-2}$	$0,38 \cdot 10^{-7}$	
250	14500	0,70	$0,62 \cdot 10^{-2}$	$0,34 \cdot 10^{-7}$	1,333
251	14600	0,68	$0,60 \cdot 10^{-2}$	$0,33 \cdot 10^{-7}$	
252	14750	0,68	$0,68 \cdot 10^{-2}$	$0,37 \cdot 10^{-7}$	1,332
253	14900	0,67	$0,59 \cdot 10^{-2}$	$0,32 \cdot 10^{-7}$	
254	14950	0,67	$0,56 \cdot 10^{-2}$	$0,30 \cdot 10^{-7}$	1,332
255	15100	0,662	$0,57 \cdot 10^{-2}$	$0,30 \cdot 10^{-7}$	
256	15200	0,644	$0,55 \cdot 10^{-2}$	$0,29 \cdot 10^{-7}$	
257	15300	0,653	$0,55 \cdot 10^{-2}$	$0,29 \cdot 10^{-7}$	
258	15400	0,649	$0,52 \cdot 10^{-2}$	$0,27 \cdot 10^{-7}$	

Key: a. serial number
b. cm^{-1}

Continued

a № п/п	b ν, см⁻¹	λ, μ	b α, см⁻¹	κ	n
259	15500	0,645	$0,54 \cdot 10^{-2}$	$0,28 \cdot 10^{-7}$	
260	15600	0,641	$0,52 \cdot 10^{-2}$	$0,27 \cdot 10^{-7}$	1,3318
261	15700	0,636	$0,52 \cdot 10^{-2}$	$0,26 \cdot 10^{-7}$	
262	15800	0,632	$0,49 \cdot 10^{-2}$	$0,25 \cdot 10^{-7}$	
263	15850	0,630	$0,50 \cdot 10^{-2}$	$0,25 \cdot 10^{-7}$	1,3314
264	16000	0,625	$0,48 \cdot 10^{-2}$	$0,24 \cdot 10^{-7}$	
265	16050	0,623	$0,51 \cdot 10^{-2}$	$0,25 \cdot 10^{-7}$	
266	16200	0,617	$0,51 \cdot 10^{-2}$	$0,25 \cdot 10^{-7}$	
267	16250	0,615	$0,50 \cdot 10^{-2}$	$0,25 \cdot 10^{-7}$	1,3314
268	16350	0,611	$0,50 \cdot 10^{-2}$	$0,24 \cdot 10^{-7}$	
269	16450	0,607	$0,49 \cdot 10^{-2}$	$0,24 \cdot 10^{-7}$	
270	16500	0,606	$0,45 \cdot 10^{-2}$	$0,22 \cdot 10^{-7}$	1,3314
271	16700	0,598	$0,43 \cdot 10^{-2}$	$0,21 \cdot 10^{-7}$	
272	16900	0,591	$0,39 \cdot 10^{-2}$	$0,18 \cdot 10^{-7}$	
273	17050	0,586	$0,37 \cdot 10^{-2}$	$0,17 \cdot 10^{-7}$	
274	17200	0,581	$0,36 \cdot 10^{-2}$	$0,17 \cdot 10^{-7}$	
275	17400	0,574	$0,39 \cdot 10^{-2}$	$0,18 \cdot 10^{-7}$	1,3314
276	17550	0,569	$0,39 \cdot 10^{-2}$	$0,18 \cdot 10^{-7}$	
277	17650	0,566	$0,39 \cdot 10^{-2}$	$0,18 \cdot 10^{-7}$	
278	17900	0,558	$0,36 \cdot 10^{-2}$	$0,16 \cdot 10^{-7}$	
279	18100	0,552	$0,39 \cdot 10^{-2}$	$0,17 \cdot 10^{-7}$	
280	18300	0,546	$0,41 \cdot 10^{-2}$	$0,18 \cdot 10^{-7}$	1,3314

Key: a. serial number
b. cm^{-1}

Bibliography

1. Zuev, V. E., Prozrachnost' atmosfery dlya vidimykh i infrakrafnykh luchey, "Transparent Atmosphere for Visible and Infrared Beams," Sovetskoe Radio (Soviet Radio), 1966.

2. Kondrat'ev, K. Ya., Aktinometriya, "Actinometry," Gidrometoizdat (State Scientific and Technical Hydrometeorological Publishing House), 1965.

3. Gudi, R. M., Atmosfernaya Radiatsiya, "Radiation in the Atmosphere, Part 1, Theoretical Foundations," "Mir" Publishing House, 1966.

4. Fligli',R., Buzinger Dzh., Vvedenie v fiziku atmosfery, "Introduction to the Physics of the Atmosphere," "Mir" Publishing House, 1965.

5. Tverskoy, P. N., Kurs Meteorologii, "A Course in Meteorology," Gidrometoizdat (State Scientific and Technical Hydrometeorological Publishing House), 1962.

6. Gutnik, M., Appl. Optics, 1962, Vol. 1, No. 5, p. 670.

7. Malkevich, M. S., Samsonov, Yu. B., Koprova, L. I., UFN (Progress of Physical Sciences), Vol. 80, No. 1, p. 93.

8. Houghton, J. T., in the collection, Les problems meteorologiques de la strotosphere et de la mesosphere, "Meteorological Problems in the Stratosphere and the Mesosphere," Presses universitaires de France 108, boulevard sant-Germain, Paris, 1966.

9. Komarov, V. S., Izevstiya A. N. SSSR, Seriya Fizika atmosfery i okeana, "Reports of the USSR Academy of Science, Physics of the Atmosphere and the Ocean," Vol. IV, No. 11, 1968, p. 1160. Studies of the Scientific Research Institute of Aeroclimatology, 1968, Ed. 47.

10. Howard, J. N. and Garing, J. S., Infrared Phys., 1962, Vol. 2, No. 3, p. 155.

11. Komarov, V. S., Marchenko, A. S., Trudy nauchno-issledovatel' skogo instituta aeroklimatologii "Studies of the Scientific Research Institute for Aeroclimatology," 1969.

12. Komarov, V. S., Meteorologiya i Gidrologiya, (Meteorology and Hydrology), No. 1, 1969.

13. Komarov, V. S., Trudy Nauchno-issledovatel'skogo instituta aeroklimatologii, (Studies of the Scientific Research Institute for Aeroclimatology), Issue 47, 1968, Issue 58, 1969.

14. Carion, H. R., Appl. Optics, 1965, Vol. 4, No. 9, p. 1089.

15. Bazhenov, V. A., Ivanova, R. N., Miroshnikov, M. M., Izvestiya SSSR, Seriya fizika atmosfery i okeana, (Reports of the USSR Academy of Science, Physics of the Atmosphere and the Ocean), Vol. 2, No. 3, 1966, p. 248.

16. Rozenberg, G. V., Sumerki, "Twilight," Fizmatgiz, 1963.

17. Fedynskiy, A. V., Perov, S. P., Chizhov, A. F., Izvestiya AN SSSR, Ser. Fizika atmosfery i okeana, (Reports of the USSR Academy of Science, Physics of the Atmosphere and the Ocean), Vol. 3, No. 5, 1967, p. 557.

18. "Atmosfernyi ozon," (Ozone in the Atmosphere), edited by A. Kh. Khrgian, Moscow State University Publications, 1961.

19. Khrgian, A. Kh., Kuznetsov, G. I., Kondrat'eva, A. N., Issledovanie atmosfernogo ozona, "Study of Ozone in the Atmosphere," Izd. AN SSSR, (USSR Academy of Science Publications), 1965.

20. Khvostikov, I. V., Fizika Ozonosfery i ionosfery, "Physics of the Ozonosphere and Ionosphere," Izd'vo AN SSR, (USSR Academy of Science Publications), 1963.

21. Gushchin, G. P., Ozon i aerosinopticheskie usloviya v atmosfere, "Ozone and Aerosynoptic Conditions in the Atmosphere," Gidrometeoizdat, (State Scientific and Technical Hydrometeorological Publishing House), 1964.

22. Dutsch, H. U., Archiv. Meteorol. Geophys., (Archives for Meteorology and Geophysics), Series A, Vol. 11, 1959.

23. Yakovleva, A. V., Kudryavtseva, L. A., Britaev, A. S., et al., in the collection Iskusstbennye sputniki zemli (Artificial Earth Satellities), Issue 14, USSR Academy of Science Publications, 1962, p. 57.

24. Haldane, J. B. C., Nature, 1936, Vol. 137, No. 3466.

25. Callendar, G. S., Quart. Journ. Roy. Met. Soc., 1938, Vol. 64, No. 275; 1940, Vol. 66, No. 287.

26. Glucauf, E., Nature, 1944, Vol. 153, No. 3890, p. 620.

27. Bluch, K., Geophys., 1948, Vol. 3, p. 63.

28. Revelle, R. and Suess, H. E., Tellus, 1957, Vol. 9, No. 1.

29. Slocum, G., Monthly Weather Rev., 1955, Vol. 83, No. 10.

30. Fonselius, S., Koroleff, F., Warme, K. E., Tellus, 1956, Vol. 8, No. 2.

31. Bray, J. R., Tellus, 1959, Vol. 11, No. 2.

32. Bishof, W., Tellus, 1960, Vol. 12, No. 2.

33. Lyutsarev, S. V., Trudy Instituta Okeanologii (Studies of the Institute for Oceanology at the USSR Academy of Science), Vol. 47, 1961, p. 199.

34. Bruavich, S. V., Lyutsarev, S. V., DAN SSSR (Reports of the USSR Academy of Science), Vol. 136, No. 2, 1961, p. 405.

35. Suess, H. E., Science, 1958, Vol. 122, p. 415.

36. Arnold, J. R., Andersen, E. C., Tellus, 1957, Vol. 9, No. 1.

37. Keeling, C. D., Tellus, 1960, Vol. 12, No. 2.

38. Takanashi, T., Journ. Geoph. Res., 1961, Vol. 60, No. 2.

39. Tomislav, P., Meteorol. Zpravy (Meteorological News), Vol. VIII, No. 5, 1955.

40. Misra, R. K., Ind. Journ. Meteor. and Geoph., 1950, No. 1

41. Voytikova, T. D., Trudy Glavnoy geofizicheskoy observatorii (Studies of the Central Geophysical Observatory), Issue 118, 1961, p. 82.

42. Seeley, J. S. and Houghton, J. T., Infrared Physics, 1961, Vol. 1, No. 2, p. 116.

43. Migeotte, M., Neven, L., and Swenson, J., Met. Soc. Sci., Liege (spec. issue), 1956.

44. Bouman, R. L., Shaw, J. Appl. Optics, 1963, Vol. 2, No. 2, p. 176.

45. Shaw, J. H. Astrophys. Journ., 1958, Vol. 128, p. 428.

46. Funk, U., Rank, D. H., Wiggins, T. A., Journ. Optic. Soc. Amer., 1964, Vol. 54, No. 4, p. 472.

47. Gudi, R. M., Fizika stratosfery, "Physics of the Stratosphere," Gidrometeoizdat (State Scientific and Technical Hydrometeorological Publishing House), 1958.

48. Birkeland, J. W. and Shaw, J. H., Journ. Optic. Soc. Amer., 1959, Vol. 49, No. 6, p. 637.

49. McMath, R. R., Pierce, A. K., Mohler, O. C., Goldberg, L., and Donovan, R. A., Phys. Rev., 1950, Vol. 78, p. 65.

50. Gertsberg, G., Spekpry i stroenie dvukhatomnykh molekul "Spectra and Structure of Two-Atom Molecules," Foreign Literature Publications, 1949.

51. El'yashevich, M. A., Atomnaya i molekulyarnaya spektroskopiya "Atomic and Molecular Spectroscopy," Fizmatgiz (State Physics-Mathematic Publications), 1962.

52. Erlandsson, J., Arkiv fur Fysik (Archives for Physics), 1956, Vol. 10, p. 65.

53. Gordi, V., Smit, V., Tramborulo, R., Radiospektroskopiya "Radiospectroscopy," Gostekhizdat (State Technical Publications), 1955.

54. Kondrat'ev, V. N., Struktura atomov i molekul,"Structure of Atoms and Molecules," Fizmatgiz (State Physics-Mathematics Publications), 1959.

55. Lorents, H. A., Proc. Amst., Acad. Soc., 1906, Vol. 8, p. 591.

56. Anderson, P. W., Phys. Rev., 1959, Vol. 76, p. 647, 1950, Vol. 80, p. 511.

57. Benedict, W. S., Kaplan, L. D., Journ. Chem. Phys., 1959, Vol. 30, p. 388.

58. Benedict, W. S., Kaplan, L. D., Journ. Quant. Spectrosc. Rad. Transfer, 1964, Vol. 4, No. 3, p. 453.

59. Galkina, L. I., Zuev, V. E., Izvestiya vuzov SSSR, seriya fizika (News of USSR Higher Institutions of Learning, Physics Series), No. 4, 1962, p. 69.

60. Plyler, E. K., Gailar, N. M. and Wiggins, T. A., Journ. Res. Nat. Bur. Stand., 1952, Vol. 48, p. 221.

61. Madden, R. F., Journ. Chem. Phys., 1961, Vol. 35, p. 2083.

62. Drayson, S. R., Appl. Optics, 1966, Vol. 5, No. 3, p. 385.

63. Goldberg, L. B., in the collection "The earth as a planet," ed. Kuiper, G. P., Chicago Univ. Press, 1954, p. 434.

64. Dufay, J. Ann. d'astrophys, (J. for Astrophysics), Vol. 5, 1942.

65. Dianov-Klokov, V. I., Optika i spektroskopiya, "Optics and Spectroscopy," Vol. 16, 1964, p. 409.

66. Rank, D. H., Pierre, A. G. St., and Wiggins, T. A., Journ. Molecul. Spectr., 1965, Vol. 18, No. 4, p. 418.

67. Breen, R. G., "The shift and shape of spectral lines," Pergamon Press, Oxford-London-New York-Paris, 1961.

68. Traving, G., Uber die Theorie der Druckverbreiterung von specktrallinien, "The theory of Pressure Broadening in Spectral Lines," Karlsruhe, Braun, 1960.

69. Sobel'man, I. I., USN (Progress of Physical Sciences), Vol. 54, Issue 4, No. 4, 1954, p. 551.

70. Chen, S. Y., Takeo, M., Rev. Mod. Phys., 1957, Vol. 29, p. 20.

71. Tsao, C. J., and Curnutte, B., Journ. Quant. Spectr. Rad. Transf., 1962, Vol. 2, No. 1, p. 41.

72. Rautian, S. G., Sobel'man, I. I., USN (Progress of Physical Sciences), Vol. 90, No. 2, 1966, p. 209.

73. Plass, G. N. and Fivel, D. I., Astrophys. Journ., 1953, Vol. 117, p. 225.

74. Surtees, W. J., Journ. Optic. Soc. Amer., 1965, Vol. 55, No. 7, p. 893.

75. Fried, B. D., and Conte, S. D., "The Plasma Dispersion Function," Academic Press, New York, 1961.

76. Young, C., Journ. Quant. Spectr. Rad. Tr., 1965, Vol. 5, No. 3, p. 549.

77. Shved, G. M., Tsaritsyna, I. V., in the collection Problemy fiziki atmosfery (Problems of Atmospheric Physics), No. 1, Leningrad State University Publications, 1963, p. 71.

78. Winters, B. H., Silverman, S., and Benedict, W. S., Journ. Wuant. Spectr. Rad. Transfer, 1964, vol. 4, p. 527.

79. Kyle, T. G., Murcray, D. G., Murcray, F. H., and Williams, W. J. Journ. Opt. Soc. Amer., 1966, Vol. 56, No. 11, p. 1421.

80. Burch, D. E., Patty, R. R., and Gryvnak, D. A., Journ. Optic. Soc. Amer., 1965, Vol. 55, No. 5, p. 606.

81. Burch, D. E. and Gryvnak, D. A., Journ. Quant. Spectr. Rad. Transf., 1966, Vol. 6, No. 3, p. 229.

82. Ladenburg, R., Reiche, F., Ann. d. Phys., 1913, Vol. 42, p. 181.

83. Elsasser, W. M., Harvard Met. Studies, 1942, No. 6.

84. Kondrat'ev, K. Ya., Perenos dlinnovolnovogo izlucheniya v atmosfere, "Long wave radiation transfer in the atmosphere," Gostekhizdat (State Technical Publications), 1950.

85. Zuev, V. E., Tvorogov, S. D., Izvestiya vuzov SSSR, seriya fizika (News of USSR Higher Institutions of Learning, Physics Series), No. 1, 1965, p. 185.

86. Zuev, V. E., Tvorogov, S. D., Izvestiya vuzov SSSR, seriya fizika (News of USSR Higher Institutions of Learning, Physics Series), No. 2, 1965, p. 170.

87. Matossi, F., Mayer, R., Rauscher, E., Phys. Rev., 1949, Vol. 76, No. 6 p. 1049.

88. Zuev, V. E., Tvorogov, S. D., Izvestiya vuzov SSSR, seriya fizika (News of USSR Higher Institutions of Learning, Physics Series), No. 4, 1966, p. 26.

89. Elsasser, W. M., "Heat transfer by infrared radiation in the atmosphere," Harvard, 1942.

90. Kondrat'ev, K. Ya., Luchistyy teploobmen v atmosfere, "Radiant Heat Exchange in the Atmosphere," Gidrometeoizeat (State Scientific and Technical Hycrometeorological Publishing House), 1956.

91. Goody, R. M., Quart. Journ. Roy. Met. Soc., 1952, Vol. 78, p. 336.

92. Plass, G. N., Journ. Opt. Soc. Amer., 1958, Vol. 48, No. 10, p. 690.

93. Godson, W. L., Journ. Opt. Soc. Am., 1955, Vol. 12, No. 3; Proc. Toronto Meteorol. Conf., Toronto, 1953, 1954.

94. Kaplan, L., Proc. Toronto Meteor. Conf., Toronto, 1953, Vol. 43.

95. Soshnikov, V. N., Optika i spektroskopiya, "Optics and Spectroscopy," Vol. 10, No. 4, 1961, p. 448.

96. Wyatt, P. J., Stull, V. R., Plass, G. N., Journ. Optic Soc. Amer., 1962, Vol. 52, No. 11, p. 1209.

97. Soshnikov, V. N., Optika i spektroskopiya, "Optics and Spectroscopy," Vol. 12, No. 1, 1962, p. 123.

98. Plass, G. N., Advances Molecul. Spectrosc., Vol. 3, Oxford-London-New York-Paris, Pergamon Press, 1962, p. 1326.

99. Godson, W. L. Archiv. fur Meteorol., Geophys. und Bioklim., (Archives for Meteorology, Geophysics and Bioclimatology), Vol. 12, No. 1, p. 1, 1962.

100. Godson, W. L. Archiv. fur Meteorol. Geophys. und Bioklim. (Archives for Meteorology, Geophysics and Bioclimatology), Voo. 13, No. 2, p. 196, 1963.

101. Gershun, A. A., Ocherk po istorii fotometrii. Izbrannye trudy po fotometrii i svetot ekhnike, "A Survey of the History of Photometry, Selected work in Photometry and Light Technology," Fizmatgiz (State Physics-Mathematics Publications), 1958.

102. Strong, F. S., Annal. Chem., 1952, Vol. 24, p. 338.

103. Vavilov, S. I., Mikrostruktrua sveta, "Microstructure of Light," Izd-vo AN SSSR, (USSR Academy of Science Publication), 1950.

104. Houghton, J. T., Quart. Jour. Roy. Met. Soc., 1963, Vol. 89, No. 381, p. 332.

105. Angstrom K., Oversing of K. Vetensk Akad. Forh., 1889, Vol. 46, p. 546; 1890, Vol. 47, p. 331; Phys. Rev., 1892, Vol. 1, p. 597; Ann. d. Phys., 1901, Vol. 6, p. 163; Arkiv f. Mathem. astronom. och. Fysik, 1907, Vol. 4, No. 30.

106. Schaefer, C., Ann. d. Physik, (Annals of Physics), Vol. 16, 1905, p.93.

107. Evan von Bahr., Ann. d. Phys. (Annals of Physics), Vol. 29, 1909, p. 780; 1910, Vol. 33, p. 585; Phys. Zeit., (J. for Physics), Vol. 12, 1911, p. 1167; Verh deutsche Phys. ges. (Proceedings of the German Physics Soc), Vol. 15, 1913, p. 673.

108. Rank, D. H., Guenther, A. H., Shearer, J. H. and Wiggins, T. A., Journ. Opt. Soc. Am., 1957, Vol. 47, p. 144.

109. Plyler, E. K. and Blaine, L. K., Journ. Res. Nat. Bur. Stand., 1959, Vol. 62, No. 1.

110. Rank, D. H., Eastman, D. P., Bertley, W. B., Skorinko, G., and Wiggins, T. A., Journ. Opt. Soc. Am., 1960, Vol. 50, No. 8, p. 821.

111. Nielsen, J. R., Throhnton, V., Dalle, E. B., Rev. Modern Phys., 1944, Vol. 16, p. 307.

112. Howard, J. N., Burch, D. E., and Williams, D., Journ. Optic. Soc. Amer., 1956, Vol. 46, p. 186, 237, 242, 334, 452.

113. Zuev, V. E., Elyashberg, N. E., Safronov, G. I., Izvestiya Vuzov SSSR, seriya fizika(News of USSR Higher Institutions of Learning, Physics Series), No. 5, 1960, p. 77.

114. Zuev, V. E., Koshelev, B. P., Izvestiya Vuzov SSSR, seriya fizika (News of USSR Higher Institutions of Learning, Physics Series), No. 6, 1961, p. 172.

115. Kozlov, V. P., Fedorova, E. O., Optika i spektroskopiya (Optics and Spectroscopy), Vol. 10, No. 5, 1961.

116. Dmitrievskiy, O. D., Neporent, B. S., Nikitn, V. A., UFN (Progress of Physical Sciences), Vol. 64, 1958, p. 447.

117. Raytian, S. G., UFN (Progress of Physical Sciences), Vol. 66, 1958, p. 475.

118. Petrash, G. G., Optika i spectrokskopiya (Optics and Spectroscopy), Vol. 6, No. 6, 1959, p. 792; Vol. 8, 1960, No. 1, p. 122; 1960, Vol. 9, No. 3, p. 423.

119. Petrash, G. G., Rautian, S. G., Inzhenerno-fizicheskiy zhurnal (J. for Engineering & Physics), Vol. 1, 1958, p. 61, p. 80.

120. Dmitrievskiy, O. D., Nikitin, V. A., Zhurnal Optiko-Mekhanicheskaya Promyshlennost' (J. for Industrial Optics and Mechanics), No. 4, 1957, p. 9. Optika i spektroskopiya (Optics and Spectroscopy), Vol. 8, 1960, p. 120.

121. Nikitin, V. A., Optika i spektroskopiya (Optics & Spectroscopy), Vol. 4, 1958, p. 523.

122. Kyle, T. G. and Green, J. O., Jour. Opt. Soc. Am., 1965, Vol. 55, No. 7, p. 895.

123. Rank. D. H. and Wiggins, T. A., Journ. Quant. Spectr. Rad. Tr., 1963, Vol. 3, No. 4, p. 377.

124. Dennison, D., Rev. Mod. Phys., 1931, Vol. 3, p. 280.

125. Bonner, L., J. Phys. Rev., 1934, Vol. 46, p. 458.

126. Escart, C., Phys. Rev., 1959, Vol. 47, p. 552.

127. Khachkuruzov, G. A., Trudy Gosudarstvennogo instituta prikladnoy khimii (Studies of the State Institute for Applied Chemistry), Vol. 42, 1959, p. 51.

128. Wang, S. E., Phys. Rev., 1929, Vol. 34, p. 243.

129. Ray, B. S., Zeit. fur Phys., (J. for Physics), Vol. 78, 1932, p. 74.

130. Hainer, R. M., Cross, P. C., King, G. W., Journ. Chem. Phys., 1943, Vol. 11, p. 27.

131. Hainer, R. M., Cross, P. C., King, G. W., Journ. Chem. Phys., 1949, Vol. 17, p. 826.

132. Wilson, E. B. and Howard, B., Journ. Chem. Phys., 1936, Vol. 4, p. 260.

133. Wilson, E. B., Journ. Chem. Phys., 1937, Vol. 5, p. 617.

134. El'yashevich, M. A., Trudy gosudarstvennogo opticheskogo instituta (Studies of the State Optical Institute), Vol. 4, 1939, Issue 106.

135. Shaffer, W. H. and Nielsen, H. H., Phys. Rev., 1939, Vol. 56, p. 188.

136. Majumdar, D., Proc. Phys. Soc., 1954, Vol. 67, p. 351; 1958, Vol. 72, p. 635.

137. Majumdar, D., Gosh, A. K., Spectrochem. Acta., 1962, Vol. 18, p. 615.

138. Benedict, W., Gailar, N., Plyler, E. K., Jour. Chem. Phys., 1956, Vol. 24, p. 1139.

139. Zuev, V. E., Ippolitov, I. I., Makushkin, Yu. S., Orolov, A. A., Fomin, V. V., DAN SSSR (Reports of the USSR Academy of Science), Vol. 179, No. 1, 1968, p. 51.

140. Zuev, V. E., Ippolipov, I. I., Makushkin, Yu. S., Orlov, A. A., Fomin, V. V., Optika i spektrosckopiya (Optics & Spectroscopy), Vol. 25, No. 1, 1968.

141. Zuev, V. E., Ippolipov, I. I., Makushkin, Yu. S., Fomin, V. V., Doklad na XIV general 'noy assamblee MGGS (Report read at the XIV General Session of the International Union of Geodesy and Geophysics, Switzerland), Sept., 1967.

142. Makushkin, Yu. S., Izvestiya vuzov SSSR, seriya fizika (News of USSR Higher Institutions of Learning, Physics Series), No. 6, 1966, p. 70.

143. Makushkin, Yu. S., Izvestiya vuzov SSSR, seriya fizika (News of USSR Higher Institutions of Learning, Physics Series), No. 2, 1967, p. 79.

144. Makushkin, Yu. S., Izvestiya vuzov SSSR, seriya fizika (News of USSR Higher Institutions of Learning, Physics Series), No. 3, 1967, p. 153.

145. Makushkin, Yu. S., in the collection Trudy Mezhvuzovskogo Soveshchaniya po spektral'noy prozrachnosti atmosfery (Reports of the Inter-University Confern. on the Spectral Transparency of the Atmosphere) (June 1965), Publications of the Tomsk State University, 1968.

146. Makushkin, Yu. S., Optika i spektroskopiya (Optics & Spectroscopy), Vol. 25, No. 1.

147. Ippolitov, I. I., Makushkin, Yu. S., Optika i Spektrosckopiya (Optics & Spectroscopy), Vol. 24, No. 4, 1968, p. 530.

148. Nielsen, H. H., Rev. Mod. Phys., 1951, Vol. 23, p. 90.

149. Goldsmith, M., Amat, G., Nielsen, H. H., Journ. Chem. Phys., 1956, Vol. 24, p. 1178.

150. Podolsky, B., Phys. Rev., 1928, Vol. 32, p. 812.

151. Goldsmith, M., Amat, G., Nielsen, H. H., Journ. Chem. Phys., 1957, Vol. 27, p. 838.

152. Amat, G., Nielsen, H. H., Journ. Chem. Phys., 1957, Vol. 27, p. 845.

153. Amat, G., Nielsen, H. H., Journ. Chem. Phys., 1962, Vol. 36, p. 1859.

154. Blokhintsev, D. I., Osnovy kvantovoy mekhaniki, "Foundations of Quantum Mechanics," Vysshaya skhola (Higher Institutions of Learning Publications), 1963.

155. Sleator, W. W. Astrophys. Journ., 1918, Vol. 48, p. 125.

156. Sleator, W. W. and Phelps, E. R., Astroph. Journ., 1925, Vol. 62, p. 28.

157. Plyler, E. K., Sleator, W. W., Phys. Rev., 1931, Vol. 37, p. 1493.

158. Plyler, E. K., Phys. Rev., 1932, Vol. 39, p. 77.

159. Mecke, R., Zeit. fur Phys. (J. for Physics), Vol. 81, 1933, p. 313.

160. Boumann, W. and Mecke, R., Zeit fur Phys. (J. for Physics), Vol. 81, 1933, p. 445.

161. Freudenberg, K. and Mecke, R., Zeit. fur Phys. (J. for Physics), Vol. 81, 1933, p. 465.

162. Nielsen, H. H., Phys. Rev., 1941, Vol. 59, p. 565; 1942, Vol. 62, p. 422.

163. Nelson, R. C., Benedict, W. S., Phys. Rev., 1948, Vol. 74, p. 703.

164. Benedict, W. S., Plyler, E. K., Journ. Res. Nat. Bur. Stand., 1951, Vol. 46, p. 246.

165. Benedict, W. S., Bull. Amer. Phys. Soc., 1948, Vol. 23, p. 54; Phys. Rev., 1948, Vol. 74, p. 1246.

166. Benedict, W. S., Claassen, H. H., and Shaw, J. H., Journ. Res. Nat. Bur. Stand., 1952, Vol. 49, p. 91.

167. Dalby, F. W. and Nielsen, H. H., Journ. Chem. Phys., 1956, Vol. 25, p. 934.

168. Benedict, W. S., Bass, A. M., Plyler, E. K., Journ. Res. Nat. Bur. Stand., 1954, Vol. 52, p. 64.

169. Barnes, R. B., Benedict, W. S., Phys. Rev., 1935, Vol. 47, p. 918.

170. Randall, H. M., Dennison, D. M., Ginsberg, N., and Weber, L. R., Phys. Rev., 1937, Vol. 52, p. 160.

171. Dennison, D. M., Rev. Modern Phys., 1940, Vol. 12, p. 174.

172. Yaroslavskiy, N. G., Stanevich, A. E., Optika i spektroskopiya (Optics & Spectroscopy), Vol. 5, 1958, p. 384, Vol. 7, 1959, p. 626.

173. Furashov, N. I., Optika i spektroskopiya (Optics & Spectroscopy), Vol. 20, No. 3, 1966, p. 427.

174. Minnaret, M., Mulders, G. F., and Houtgast, J., Photometric Atlas of the Solar Spectrum λ3612 to λ8771, Amsterdam, 1940.

175. Babcock, H. D. and Moore, C. E., The solar spectrum, λ6600 to λ13495, Washington, Carnegie Institute of Washington Publ. 579, 1947.

176. Mohler, O. C., Pierce, A. K., McMath, R. R., and Goldberg, L., Atlas of the Solar Spectrum from 0.84 to 2.55 microns, Univ. of Mich. Press., Ann Arbor, Mich., 1950.

177. Mohler, O. C. and Benedict, W. S., Phys. Rev., 1948, Vol. 74, p. 702.

178. Mohler, O. C., Tables of Solar Spectrum Wave Length 1.20 - 2.55 microns., Univ. of Mich. Press., Ann Arbor, Mich., 1955.

179. Shaw, J. H., Chapman, R. M., Howard, J. N., and Oxholm, M. L., Astrophys. Journ., 1951, Vol. 113, p. 268.

180. Shaw, J. H., Oxholm, M. L., and Claassen, H. H., Astrophys. Journ., 1952, Vol. 116, p. 354.

181. Migeotte, M., Neven, L., and Swenson, J., The Solar spectrum from 2.8 to 23.7 microns., Univ. of Liege, Final report, Part I, 1956, Part II, 1957.

182. Migeotte, M., Neven, L., Swenson, J., Benedict, W. S., The Solar spectrum from 2.8 to 23.7 microns, Part II, Institute d'Astrophysique de l'Universit'de Liege, (Institute of Astrophysics at Liege Univ), 1957.

183. Delbouille, L., Roland, G., Atlas Photometrique du spectre solair de λ 7498 a 12016 (Atlas of the Solar Spectrum from λ7498 to λ12016), Liege, 1963.

184. Farmer, C. B. and Key, P. J., Appl. Opt. 1965, Vol. 4, No. 9, p. 1051.

185. Curcio, I. A., Drummeter, L. F., and Knestrick, G. L., Appl. Optics, 1964, Vol. 3, No. 12, p. 1401.

186. Moore, C. E., Minnaert, M. G. J., and Houtgast, J., Tables of Spectral lines of the Atmosphere from λ2935 to λ 8700 Å., Washington Govt. print. off., 1966.

187. Oppenheim, U. P., and Goldman, A., Atlas and wavenumber tables of water vapor absorption at 1200°K in the 1.9 and 2.7 μ regions, Scientific report No. 1 AFEOAR 63-111, Haifa, Is., 1964.

188. Schwendenman, R. H. and Laurie V. W., Tables of line strengths for rotational transmissions of asymmetric rotor molecules, Pergamon Press, New York, 1958.

189. Calfee, R. F., Journ. Quant. Spectr. Rad. Transfer, 1966, Vol. 6, No. 3, p. 221.

190. Ippolipov, I. I., Izvestiya vuzov SSSR (News of the USSR Higher Institutions of Learning, Physics Series, No. 7, 1967, p. 1945.

191. Cross, P. C., Hainer, R. M., and King G. W., Journ. Chem. Phys., 1944, Vol. 12, p. 210.

192. Ippolitov, I. I., Optika i spektroskopiya (Optics and spectroscopy), Vol. 27, No. 3, 1969, p. 458.

193. Khachkuruzov, G. A., Trudy Gosudarstvennogo instuta prikladnoy khimii (Studies of the State Institute for Applied Chemistry), Vol. 46, 1960, p. 66.

194. Papousek, D., Pliva, J., Collect. Czech. Chem. Comm. (Czech. J. for Chem.), Vol. 29, 1964, p. 1973.

195. Vasilevskiy, K. P., Neporent, B. S., Optika i spektroskopiya (Optics & Spectroscopy), Vol. 7, 1959, p. 572.

196. Vasilevskiy, K. P., Neporent, B. S., Optika i spektroskopiya (Optics & Spectroscopy), Vol. 4, 1958, p. 474.

197. Vasilevskiy, K. P., Optika i spektroskopiya (Optics & Spectroscopy), Vol. 11, 1961, p. 207.

198. Sanderson, R. B. and Ginsburg, N., Journ. Quant. Spectr. Rad. Tr., 1963, Vol. 3, No. 4, p. 435.

199. Saidy, F., Quart. Journ. Roy. Met. Soc., 1961, Vol. 87, No. 384, p. 578.

200. Bolle, H. J., Journ. Optic. Soc. Amer., 1966, Vol. 56, No. 4, p. 560.

201. Goldman, A. and Oppenheim, U. P., Appl. Optics, 1966, Vol. 5, No. 6, p. 1073.

202. Jaffe, J. H. and Benedict, W. S., Journ. Quant. Spectr. Rad. Transf., 1963, Vol. 3, No. 1, p. 87.

203. Hirshfeld, M. A., Jaffe, J. H. and Ross, G., Journ. Quant. Spectr. Rad. Transf., 1966, Vol. 6, No. 3, p. 311.

204. Landau, L. D., Lifshits, E. M., Teoriva polya "Theory of the Field," Fizmatgiz (State Physics-Mathematics Publ.) 1962.

205. Davydov, A. S., Kvantovaya makhanika, "Quantum Mechanics," Fizmatgiz (Physics-Mathematics Publ.), 1963.

206. Zuev, V. E., in the collection Trudy Mezhvuzovskogo soveshchaniya po spektral'noy prozrachnosti atmosfery [Studies of the Inter-university Scientific Conference on the Spectral Transparency of the Atmosphere], (June 1965, Tomsk), Tomsk State Univ. Publ., 1965.

207. Gradshteyn, I. S. and Ryzhik, I. M., Tables of integrals, sums, series, and products, Fizmatgiz, Phys. Math. Publ., 1962.

208. Becker, G. E. and Autler, S. H., Phys. Rev., 1946, Vol. 70, p. 300.

209. Cowling, T. G., Phil. Mag., 1950, Vol. 41, p. 109.

210. Benedict, W. S., Journ. Opt. Soc., Am., 1957, Vol. 47, p. 1056.

211. Kondrat'ev, K. Ya., Timofeev, Yu. M., Izvestiya AN SSSR, seriya fizika atmosfery i okeana (Reports of the USSR Academy of Science, Series Physics of the Atmosphere and the Ocean), Vol. 2, No. 3, 1966, p. 272.

212. Plass, G. N., Stull, V. R., Theoretical study of high temperature emissivities and atmospheric transmission, Contract, Bedford, 1960.

213. Howard, J. N., Burch, D. E., Williams, D., Near infrared transmission through Synthetic atmosphere, Contract, Ohio Univ., 1955.

214. Stull, V. R., Wyatt, P. J. and Plass, G. N., The infrared absorption of water vapor, Report SSD-TDR-62-127, Vol II, Space Systems Div., Air Force Systems Comm., Los Angeles, California, 1962.

215. Stull, V. R., Wyatt, R. J. and Plass, G. N., The infrared absorption of carbon dioxide, Report SSD-TDR-62-127, Vol. III, Space Systems Div., Air Force Systems Comm., Los Angeles, California, 1962.

216. Burch, D. E. Gryvnak, D., Singlton, E. B., France, W. L. and Williams, D. W., Infrared absorption by CO_2 water vapor and minor atmospheric constituents, AFCRL-62-698, AFCRL, Bedford, Mass., July, 1962.

217. Wyatt, P. J., Stull, V. R. and Plass, G. N., Appl. Optics, 1964, Vol. 3, No. 2, p. 229.

218. Oppenheim, U. P. and Ben-Aryeh, Y., Journ. Quant. Spectrosc. Rad. Trans., 1964, Vol. 4, No. 4, p. 559.

219. Zuev, V. E., Nesmelova, L. I., Sapozhnikova, V. A., Tvorogov, S. D., in the collection Aktinometriya i optika atmosfery, Trudy V Mezhvedomstvennogo soveshchaniya po aktinometrii i optike atmosfery (Atmospheric Actinometry & Optics), "Studies of the Fifth Interdepartmental Committee on actinometry and optics in the atmosphere," edited by G. V. Rozenberg, Nauka Publishers, 1964.

220. Zuev, V. E., in the collection Yubeleynyy sbornik trudov Tomskogo universitata po fizike, "Anniversary collection of articles of Tomsk Univ. in physics," Tomsk Univ. Publ., 1970.

221. Burch, D. E. and Williams, D. W., Appl. Optics, 1963, Vol. 2, No. 6.

222. Larmor, L. and Passman, S., Proc. IRIS, 1956, Vol. 1, No. 1, p. 1; 1956, Vol. 1, No. 2, p. 15.

223. Langer, R. M., Proc. IRIS, pt. 2, July, 1958.

224. Roach, W. T., Quart. Journ. Roy. Met. Soc., 1961, Vol. 87, No. 373, p. 346.

225. Zuev, V. E., Izvestiya vuzov SSSR, seriya Fizika (News of USSR Higher Institutions of Learning, Physics Series), 1961, No. 3, 6, 1962; No. 1, 3, 6 in the collection Rasseyanie i polyarizatsiya sveta v zemnoy atmosfere, "Light Scattering and polarization in the earth's atmosphere," Publ. of the Kazakh Academy of Science, 1962.

226. Burch, D. E., Singleton, E. B., Williams, D., Appl. Optics, 1962, Vol. 1, No. 3, p. 359.

227. Palmer, C. H., Journ. Optic. Soc. Amer., 1960, Vol. 50, p. 1232.

228. Izatt, J., Ph.D. Dissertation, Johns Hopkins Univ., 1960.

229. Goody, R. M. and Wormell, T. W., Proc. Roy. Soc., A, 1951, Vol. 209, p. 178.

230. Cross, P. S. and Daniels, F., Journ. Chem. Phys., 1934, Vol. 2, p. 6.

231. Edwards, D. K., Journ. Opt. Soc. Amer., 1960, Vol. 50, p. 617.

232. Stauffer, F. R. and Walsh, T. E., Journ. Opt. Soc., Am., 1966, Vol. 56, No. 3, p. 401-406.

233. Palmer, C. H., Journ. Opt. Soc., Amer., 1957, Vol. 47, p. 1024, 1028, 1054; 1959, Vol. 49, p. 1139; 1960, Vol. 50, p. 1232.

234. Burch, D. E. and Reisman, E., Journ. Opt. Soc. Am., 1966, Vol. 56, No. 4, p. 556.

235. Goldstein, R., Journ. Quant. Spectr. Rad. Transfer, 1964, Vol. 4, No. 2, p. 343.

236. Ludwig, C. B., Ferriso, C. C. and Abeyta, C. N., Journ. Quant. Spectr. Rad. Transf., 1964, Vol. 5, No. 2, p. 281.

237. Gray, L. D. and Penner, S. S., Journ. Quant. Spectr. Rad. Transf., 1965, Vol. 5, No. 4, p. 611.

238. Ferriso, C. C., Ludwig, C. B. and Thomson, A., Journ. Opt. Soc. Amer., 1965, Vol. 55, No. 5, p. 617.

239. Ferriso, C. C. and Ludwig, C. B., Journ. Opt. Soc., Am., 1966, Vol. 56, No. 4, p. 560.

240. Goldman, A. and Oppenheim, U. P., Journ. Opt. Soc., Amer., 1965, Vol. 55, No. 7, p. 794.

241. Edwards, D. K., Flornes, B. J., Glassen, L. K. and Sun, W., Appl. Optics, 1965, Vol. 4, No. 6, p. 715.

242. Ferriso, C. C. and Ludwig, C. B., Journ. Quant. Spectrosc. Rad. Transf., 1964, Vol. 4, p. 215.

243. Ferriso, C. C. and Ludwig, C. B., Journ. Chem. Phys., 1964, Vol. 41, p. 1668.

244. Moller, F., Beit. Geophys. (Contributions to Geophysics), Vol. 58, 1942, p. 27.

245. Gebbie, H. A., Harding, W. R., Hilsum, C., Pryce, A. W. and Roberts, Proc. Roy. Soc., 1951, Vol. 206, No. 1084, p. 87.

246. Taylor, J. Yattes, H. W., Journ. Opt. Soc., Am., 1957, Vol. 47, No. 3, p. 223.

247. Adel, A., Astrophys. Journ., 1939, Vol. 89, p. 1.

248. Anthony, R., Phys. Rev., 1952, Vol. 85, p. 674.

249. Feygel'son, E. M., Izvestiya ANSSSR, seriya geofizicheskaya (News of the USSR Academy of Science, Geophysics series), No. 4, 1951, p. 92.

250. Roach, W. T. and Goody, R. M., Quart, Journ. Roy. Met. Soc., 1958, Vol. 84, p. 319.

251. Volz, F., Ann. d. Meteorol., 1957, Vol. 8, p. 34.

252. Bignell, K., Saiedy, F. and Sheppard, P. A., Journ. Optic. Soc., Amer., 1963, Vol. 53, No. 4, p. 466.

253. Kondrat'ev, K. Ya., Badinov, I. Ya., Ashcheulov, S. V., Andreev, S. D., Izvestiya ANSSSR, seriya Fizika atmosfery i okeana (Reports of the USSR Academy of Science, Physics of the Atmosphere and Ocean Series), Vol. 1, No. 4, 1965, p. 363.

254. Kaplan, L. D., in the collection Les problem' meteorologiques de la Stratosphere et de la mesosphere, "Meteorological problems in the stratosphere and mesosphere," Presses universitaires de France (French Univ. press), Boulevard Saint-Germain, Paris, 1966, p. 307.

256. Yamomoto, G., Sasamory, T., Sci. Reports, Tohoku Univ., Series 5, Geophys., 1958, Vol. 10, No. 2, p. 37, 1961, Vol. 13, p. 1.

257. Gordon, H. R. and McCubbin, T. K., Jr., Journ. Molecul. Spectrosc., 1965, Vol. 18, No. 1, p. 73.

258. Kaplan, L. D., Eggers, D. F., Journ. Chem. Phys., 1950, Vol. 25, p. 876.

259. Nielsen, A. H., Yao, Y. T., Phys. Rev., 1945, Vol. 68, p. 173.

260. Benedict, W. S., Herman, R. C., Silverman, S., Journ. Chem. Phys., 1951, Vol. 19, No. 10, p. 1325.

261. Courtoy, C. P., Canad. Journ. Phys., 1957, Vol. 35, p. 608.

262. Gray, L. D. and Selvidge, J. E., Journ. Quant. Spectrosc. Rad. Transf., 1965, Vol. 5, No. 2, p. 291.

263. Calfee, R. F. and Benedict, W. S., Appl. Optic., 1966, Vol. 5, No. 10, p. 1695, Carbon dioxide Spectral Line positions and intensities calculated for 2.05 and 2.7 microns region, Natl. Bur. of Standards, Washington, D. C., 1966.

264. Williams, D., Appl. Optics, 1966, Vol. 5, No. 10, p. 1696.

265. Gordon, H. R. and McCubbin, T. K., Jr., Journ. of Molec. Spectrosc., 1966, Vol. 19, No. 2, p. 137.

266. Vasilevskiy, K. P., Kazbanov, V. A., Derviz, T. E., Optika i spektroskopiya (Optics and Spectroscopy), Vol. 23, No. 6, 1967, p. 888.

267. Boese, R. W., Miller, J. H. and Inn, E. C. J., Journ. Quant. Spectr. Rad. Transf., 1966, Vol. 6, No. 6, p. 717.

268. Gorchakova, I. A., Malkevich. M. S., Izvestiya AN SSSR seriya fizika atmosfery i okeana (Reports of the USSR Academy of Science, Physics of the Atmosphere and Ocean Series), Vol. 2, No. 6, 1966, p. 585.

269. Stull, V. R., Wyatt, P. J. and Plass, G. N. Appl. Opt., 1964, Vol. 3, No. 2. p. 243.

270. Megill, L. R. and Jamnick, P. M., Journ. Optic. Soc., Amer., 1961, Vol. 51, No. 11, p. 1294.

271. Gray, L. D., Journ. Opt. Soc., Amer., 1966, Vol. 56, No. 4, p. 555.

272. Gray, L. D. and McClatchey, R. A., Journ. Opt. Soc., Amer., 1965, Vol. 55, No. 11, p. 1567.

273. Burch, D. E., Gryvnak, D. A. and Williams, D., Appl. Opt., 1962, Vol. 1, No. 6, p. 759.

259. Nielsen, A. H., Yao, Y. T., Phys. Rev., 1945, Vol. 68, p. 173.

260. Benedict, W. S., Herman, R. C., Silverman, S., Journ. Chem. Phys., 1951, Vol. 19, No. 10, p. 1325.

261. Courtoy, C. P., Canad. Journ. Phys., 1957, Vol. 35, p. 608.

262. Gray, L. D. and Selvidge, J. E., Journ. Quant. Spectrosc. Rad. Transf., 1965, Vol. 5, No. 2, p. 291.

263. Calfee, R. F. and Benedict, W. S., Appl. Optic., 1966, Vol. 5, No. 10, p. 1695, Carbon dioxide Spectral Line positions and intensities calculated for 2.05 and 2.7 microns region, Natl. Bur. of Standards, Washington, D. C., 1966.

264. Williams, D., Appl. Optics, 1966, Vol. 5, No. 10, p. 1696.

265. Gordon, H. R. and McCubbin, T. K., Jr., Journ. of Molec. Spectrosc., 1966, Vol. 19, No. 2, p. 137.

266. Vasilevskiy, K. P., Kazbanov, V. A., Derviz, T. E., Optika i spektroskopiya (Optics and Spectroscopy), Vol. 23, No. 6, 1967, p. 888.

267. Boese, R. W., Miller, J. H. and Inn, E. C. J., Journ. Quant. Spectr. Rad. Transf., 1966, Vol. 6, No. 6, p. 717.

268. Gorchakova, I. A., Malkevich, M. S., Izvestiya AN SSSR seriya fizika atmosfery i okeana (Reports of the USSR Academy of Science, Physics of the Atmosphere and Ocean Series), Vol. 2, No. 6, 1966, p. 585.

269. Stull, V. R., Wyatt, P. J. and Plass, G. N. Appl. Opt., 1964, Vol. 3, No. 2. p. 243.

270. Megill, L. R. and Jamnick, P. M., Journ. Optic. Soc., Amer., 1961, Vol. 51, No. 11, p. 1294.

271. Gray, L. D., Journ. Opt. Soc., Amer., 1966, Vol. 56, No. 4, p. 555.

272. Gray, L. D. and McClatchey, R. A., Journ. Opt. Soc., Amer., 1965, Vol. 55, No. 11, p. 1567.

273. Burch, D. E., Gryvnak, D. A. and Williams, D., Appl. Opt., 1962, Vol. 1, No. 6, p. 759.

274. Edwards, D. K. and Menard, W. A., Appl. Opt., 1964, Vol. 3, No. 7, p. 847.

275. Edwards, D. K. and Sun, W. Appl. Opt., 1964, Vol. 3, No. 12, p. 1501.

276. Varanasi, P. and Lauer, J. L., Journ. Quant. Spectr. Rad. Transf., 1966, Vol. 6, No. 1, p. 127.

277. Clough, S. A. and Kneizis, F. X., Journ. Chem. Phys., 1966, Vol. 44, No. 5, p. 1855.

278. Clough, S. A., Kneizys, F. X., Ozone Absorption in the 9.0 micron region, AFCRL-62-862, Report, Air Force Cambridge Res. Labs., 1965.

279. White, J. U., Alpert, N. L., Debell, A. G. and Chapman, R. M., Journ. Opt. Soc. Amer, 1957, Vol. 47, No. 5, p. 358.

280. Walshaw, C. D., An experimental investigation of the 9.6 mkm band of ozone, Thesis Cambridge Univ., 1954.

281. Nexsen, W. E., Jr., Sci. Report, No. 1, Contr. AF19(604)-1003 with the Ohio State Univ. AFCRL-TN-56-265, 1965.

282. McCaa, D. J. and Shaw, J. H., Appl. Optics, 1963, Vol. 2, p. 581.

283. Trajmar, S., Paper presented at symposium on molecular structure and spectroscopy, Columbus, Ohio, 1963.

284. Trajmar, S., McCaa, D. J., Journ. Molec. Spectrosc., 1964, Vol. 14, No. 3, p. 244.

285. Gora, E. K., Journ. Molec. Spectrosc., 1959, Vol. 3, p. 78.

286. Gebbie, H. A., Stone, N. W. B., Topping, G., Gora, E. K., Clough, S. A. and Kneizys, F. X., Journ. of Molecul. Spectrosc., 1966, Vol. 19, No. 1, p. 7.

287. Walshaw, C. D., Quart. Journ. Roy. Met. Soc., 1957, Vol. 83, No. 357, p. 315.

288. Altshuller, T. L., Infrared transmission of clear atmosphere, Document 61SD 199, Gen. Elec. Co., Philadelphia, Pa., Dec., 1961.

305. Hathaway, C. E., Hoover, G. M. and Williams, D., Journ. Opt. Soc. Amer., 1966, Vol. 56, No. 4, p. 555.

306. Edwards, D. K., Appl. Optics, 1965, Vol. 4, No. 10, p. 1352.

307. Benedict, W. S., Herman, R., Moore, G. E. and Silverman, S., Astrophys. Journ., 1962, Vol. 135, No. 1, p. 277.

308. Shaw, J. H., France, W. L., Intensities and widths of single lines of the 4.7 microns CO fundamental scientific rep. 4 on Project 587, Ohio State Univ., 1956.

309. Dowling, J. M. and Hall, R. T., Journ. Molec. Spectrosc., 1966, Vol. 19, No. 1, p. 108.

310. Weinberg, J. M., Fishburne, E. S. and Rao, K. N., Journ. of Molec. Spectrosc., 1965, Vol. 18, No. 4, p. 428.

311. Gryvnak, D. A. and Shaw, J. H., Journ. Opt. Soc. Amer., 1962, Vol. 52, No. 5, p. 539.

312. Hathaway, C. E., Hoover, G. M. Tubbs, L. D. and Williams, D., Journ. Optic. Soc. Amer., 1966, Vol. 56, No. 10, p. 1422.

313. Abu-Romia, M. M. and Tien, C. L., Journ. Quant. Spectrosc. Rad. Transf., 1966, Vol. 6, No. 2, p. 143.

314. Shaw, J. H. and Houghton, J. T., Appl. Optics, 1964, Vol. 3, No. 6, p. 773.

315. Hoover, G. M., Hathaway, C. E. and Williams, D., Appl. Optics, 1967, Vol. 6, No. 3, p. 481.

316. Gray, L. D. and McClatchey, R. A., Appl. Optics, 1965, Vol. 4, p. 1624.

317. Penner, S. S. and Varanasi, P., Journ. Quant. Spectr. Rad. Transf., 1966, Vol. 6, No. 2, p. 181.

318. Sakai, H. and Stauffer, F. R., Journ. Opt. Soc. Amer., 1964, Vol. 54, p. 759.

319. Sakai, H., Journ. Opt. Soc. Amer., 1966, Vol. 56, No. 1, p. 127.

320. Plass, G. N., Journ. Opt. Soc. Amer., 1965, Vol. 55, No. 1, p. 104.

321. Şakai, H., Journ. Opt. Soc. Amer., 1966, Vol. 56, No. 4, p. 556.

322. Plass, G. N., Journ. Opt. Soc. Amer., 1964, Vol. 55, No. 5, p. 593.

323. Plass, G. N., Appl. Optics, 1965, Vol. 4, p. 69.

324. Balandin, N. I., Kuznetsova, E. S., Podkladenko, M. V., Prikladnaya spektroskopiya (Applied Spectroscopy), Vol. 1, No. 1, 1964, p. 66.

325. Podkladenko, N. V., Trudy mezhvuzovskogo nauchnogo soveshchaniya po spektral'noy prozrachnosti atmosfery v vidimoy i infrakrasnoy oblastyakh spektra, "Studies of the inter-university scientific conference on the spectral transparency of the atmosphere in the visible and infrared regions of the spectrum," Tomsk State Univ. Publ., 1968, p. 106.

326. Curcio, J. A. and Buttrey D. V. E., Appl. Optics, 1966, Vol. 5, No. 2, p. 231.

327. Zuev, V. E., Izvestiya vuzov SSSR, seriya Fizika (News of USSR Higher Institutions of Learning, Physics Series), No. 3, 1967, p. 138.

328. Zuev, V. E., Izvestiya vuzov SSSR, seriya Fizika (News of USSR Higher Institutions of Learning, Physics Series), No. 10, 1967, p. 53.

329. Zuev, V. E., Pokasov, V. V., Pkhalagov, Yu. A., Sosnin, A. V., Khmelevtsov, S. S., Izvestiya AN SSSR, seriya Fizika atmosfery i okeana (Reports of the USSR Academy of Science, Physics of the Atmosphere and Ocean Series), Vol. 4, No. 1, 1968, p. 63.

330. Antipov, B. A., Zuev, V. E., Sapozhnikova, V. A., Izvestiya vuzov SSSR, seriya Fizika (News of USSR Higher Institutions of Learning, Physics Series), No. 7, 1967, p. 142.

331. Antipov, B. A., Zuev, V. E., Sapozhnikova, V. A., Izvestiya vuzov SSSR, seriya Fizika (News of USSR Higher Institutions of Learning, Physics Series), No. 6, 1967, p. 158.

332. Edwards, B. N. and Burch, D. E., Journ. Opt. Soc. Amer., 1965, Vol. 55, No. 2, p. 174.

333. Chu, T. S. and Hogg, D. C., The Bell System Technical Journ., 1966, Vol. 45, No. 2, p. 301.

334. Long, R., Lewis, T. H., In the collection "Lasers and Applications," Columbus, Ohio, USA, 1963, p. 209.

335. McCubbin, T. K., Jr. and Darone, R., Journ. Opt. Soc. Amer., 1966, Vol. 56, No. 4, p. 555.

336. Long, R. K. and McCoy, J. H., Journ. Opt. Soc. Amer., 1967, Vol. 57, No. 4, p. 570.

337. Howe, J. A. and McFarlane, R. A., Journ. Molec. Spectrosc., 1966, Vol. 19, No. 2, p. 224.

338. Calfee, R. F. and Gates, D. M., Appl. Optics, 1966, Vol. 5, No. 2, p. 287.

339. Zuev, V. E., Tvorogov, S. D., Izvestiya vuzov SSSR (News of USSR Higher Institutions of Learning, Physics Series), No. 6, 1965, p. 84.

340. Plass, G. N., Appl. Optics, 1963, Vol. 2, No. 5, p. 515.

341. Plass, G. N., Transmittance Tables for Slant Path in the Stratosphere, SSD-TDR-62-127, Vol. V, Space Systems Div., Air Force Systems Comm., Los Angeles, Cal. (22 May 1963).

342. Plass, G. N., Appl. Optics, 1964, Vol. 3, No. 4, p. 479.

343. Makushkin, Yu. S., Prikladnaya spektroskopiya (Applied Spectroscopy), Vol. 8, No. 6, 1968, p. 1068.

344. Kondratyev, K. Y., Badinov, I. J., Gaevskaya, G. N., Nicolsky, G. A., Shved, G. M., In the collection "Les problems meteorologiques de la Stratosphere et de la mesosphere, "Meteorological problems in the atmosphere and mesosphere," Presses universitaires de France 108 (French Univ. Press), Boulevard Saint-Germain, Paris, 1966, p. 271.

345. Murcray, D. G., Murcray, F. H. and Williams, W. J., Journ. Opt. Soc. Amer., 1965, Vol. 55, No. 10, p. 1239.

346. Murcray, D. G., Murcray, F. H., Williams, W. J., Leslie, F. E., Journ. Geophys. Rec., 1960, Vol. 65, p. 11; Journ. Optic. Soc. Amer., 1961, Vol. 51, No. 2, p. 186.

347. Murcray, D. G., Murcray, F. H., Williams, W. J., Journ. Geophys. Res., 1962, Vol. 67, No. 2, p. 759.

348. Neporent, B. S., Kifeleva, M. S., Optika i spektroskopiya (Optics and Spectroscopy), Vol. 16, No. 5, 1964, p. 803.

349. Yates, D. M., Journ. Optic. Soc. Amer., 1960, Vol. 50, No. 12, p. 1299.

350. Yates, D. M. and Harrop, W. J., Appl. Optics, 1963, Vol. 2, No. 9, p. 887.

351. Houghton, J. T., Seeley, J. S., Quart. Journ. Roy. Met. Soc., 1960, Vol. 86, No. 369, p. 358.

352. Houghton, J. T., Hughes, N. D. P., Moss, T. S. and Seeley, J. S., Phil. Trans. Roy. Soc., 1962, Vol. 254, No. 1043, p. 47.

353. Houghton, J. T., Quart. Journ. Roy. Meteor. Soc., 1963, Vol. 89, No. 381, p. 319.

354. Cumming, C., Stratospheric composition from infrared solar spectra thesis, International Symposium on Radiation Processes, Leningrad, 1964.

355. Stauffer, F., Strong, J. Appl. Optics, 1962, Vol. 1, No. 2, p. 129.

356. Brown, A. H., Roberts, V., Journ. Sci. Instrum., 1953, Vol. 30, No. 1, p. 5.

357. Jones, F. H., Roberts, V., Proc. Roy. Soc. A, 1956, Vol. 236, No. 1205, p. 171.

358. Levin, L. M., Issledovaniya po fizike grubodispersnykh aerozoley, "Studies in the Physics of Large Dispersed Aerosols," USSR Academy of Science Publ., 1961.

359. Borovikov, A. M., et al., In the collection Fizika oblakov (Physics of Clouds), Edited by A. Kh. Khrgian, Gidrometeoizdat (State Scientific and Technical Hydrometeorological Publishing House), 1961.

360. Khuan-Mey-Yuan', Izvestiya AN SSSR, seriya geofizicheskaya (Reports of the USSR Academy of Science, Geophysics Series), No. 2, 1963, p. 362.

361. Meyson, B. Dzh., Fizika oblakov "Physics of Clouds," Gidrometeoiezdat (State Scientific and Technical Hydrometeorological Publishing House), 1961.

362. Rittberger, W., Archiv. fur Meteorol., Geophys. und Bioklim., Ser. A, (Archives for Meteorology, Geophysics and Bioclimatology, Series A), Vol. 11, No. 3, 1959, p. 333.

363. Best, A. C., Quart. Journ. Roy. Met. Soc., 1951, Vol. 77, p. 418.

364. Khrgian, A. Kh., Mazin, I. P., Trudy tsentral'noy aerologicheskoy observatorii, "Studies of the Central Aerological Observatory," 7th ed., 1952, p. 56.

365. Borovikov, A. M., Trudy tsentral'noy aerologicheskoy observatorii, "Studies of the Central Aerological Observatory," 1948, No. 3, p. 3.

366. Levin, L. M., DAN SSSR (Reports of the USSR Academy of Science), Vol. 9, No. 6, 1954, p. 1045.

367. Kolmogorov, A. N., DAN SSSR (Reports of the USSR Academy of Science), Vol. 31, No. 2, 1941.

368. Levin, L. M., Izvestiya AN SSSR, seriya geofizicheskaya (Reports of the USSR Academy of Science, Geophysics Series), No. 10, 1958, p. 1211.

369. Shifrin, K. S., Trudy Glavnoy geofizicheskoy observatorii "Studies of the Central Geophysical Observatory," No. 46, 1955, p. 5.

370. Fuks, N. A., Mekhanika aerozoley, "Mechanics of Aerosols," Izd-vo AN SSSR (USSR Academy of Science Publications," 1955.

371. D'yachenko, P. V., Trudy Glavnoy geofizicheskoy observatorii, "Studies of the Central Geophysical Observatory," No. 101, 1959, p. 3.

372. Khrgian, A. Kh., Mazin, I. P., Trudy Tsentral'noy aerologicheskoy observatorii, "Studies of the Central Aerological Observatory," No. 17, 1956, p. 36.

373. Dergach, A. L., Trudy Arkticheskogo i Antarkticheskogo nauchno-issledovatel'skogo instituta, "Studies of the Arctic and Antarctic Scientific-Research Institute," Vol. 228, 1959, p. 55.

374. Nikandrov, V. Ya., Trudy Arkticheskogo i Antarkticheskogo Nauchno-issledovatel'skogo instituta, "Studies of the Arctic and Antarctic Scientific-Research Institute," Vol. 228, 1959, p. 146.

375. Dolgin, I. M., Trudy Arkticheskogo i Antarkticheskogo Nauchno-issledovatel'skogo Instituta, "Studies of the Arctic and Antarctic Scientific-Research Institute," Vol. 239, 1962, p. 5.

376. Voskresenskiy, A. I., Trudy Arkticheskogo i Antarkticheskogo Nauchno-issledovatel'skogo Instituta, "Studies of the Arctic and Antarctic Scientific-Research Institute," Vol. 239, 1962, p. 64.

377. Voskresenskiy, A. I., Dergach, A. L., In the collection Issledovanie oblakov, osadkov i grozovogo elektrichestva, "A Study of Clouds, Precipitation, and Thunderstorm Electricity," USSR Academy of Science Publ., 1961, p. 101.

378. Kazach, V. I., Izvestiya AN SSSR, seriya geofizicheskaya (Reports of the USSR Academy of Science, Geophysics Series), No. 5, 1963, p. 805.

379. Arnulf, A., Bricard, T., Cure E., Veret, C., Journ. Opt. Soc. Amer., 1957, Vol. 47, No. 6, p. 491.

380. Wiener, F. M., Ball, J. H., Gosgos, C. M., Journ. Geophys. Res., 1961, Vol. 66, No. 11, p. 3974.

381. Eldridge, R. G., Journ. Meteorol., 1961, Vol. 18, No. 5, p. 671.

382. May, K. R., Quart. Journ. Roy. Met. Soc., 1961, Vol. 87, No. 374, p. 535.

383. Okita, T., Journ. Meteor. Soc. Japan., 1962, Vol. 40, No. 1, p. 39.

384. Eldridge, R. G., Journ. Atm. Sci., 1966, Vol. 23, No. 5, p. 605.

385. Mazin, I. P., Skosyreva, V. D., Trudy Tsentral'noy aerologicheskoy observatorii, "Studies of the Central Aerological Observatory," No. 36, 1961, p. 43.

386. Nikandrova, G. T., Trudy Glavnoy geofizicheskoy observatorii, "Studies of the Central Geophysical Observatory," No. 126, 1962, p. 70.

387. Selezneva, E. S., Meteorologiya i gidrologiya, "Meteorology and Hydrology," No. 2, 1948.

388. Pedersen, K. Todsen, M., Geophys. publ., 1960, Vol. 21, No. 7.

389. Minervin, V. E., Trudy Tsentral'noy aerologicheskoy observatorii, "Studies of the Central Aerological Observatory," No. 36, 1961, p. 62.

390. Schumacher, P., Journ. Aircraft, 1964, Vol. 1, No. 1.

391. Minervin, V. E., In the collection Issledovanie oblakov, osadakov i grozovogo elektrichesta, "Study of Clouds, Precipitation and Thunderstorm Electricity," USSR Academy of Science Publ., 1961, p. 91.

392. Borovikov, A. M., Mazin, I. P., Nevzorov, A. N., Trudy Tsentral'noy aerologicheskoy observatori, "Studies of the Central Aerological Observatory," No. 36, 1961.

393. Borovikov, A. M., Mazin, I. P., Nevzrov, A. N., Izvestiya AN SSSR, seriya Fizika atmosfery i okeana (Reports of the USSR Academy of Science, Physics of the Atmosphere and Ocean Series), Vol. 1, No. 3, 1965, p. 291.

394. Okita, T., Tellus, 1961, Vol. 13, No. 4, p. 509.

395. Petenchuk, O. P., Drozdova, V. M., Trudy Glavnoy geofizicheskoy observatorii, "Studies of the Central Geophysical Observatory," No. 185, 1966, p. 117.

396. Junge, C. E., Advance in Geophys., 1958, Vol. 4, p. 1.

397. Makhon'ko, K. P., Izvestiya AN SSSR, seriya geofizicheskaya (Reports of the USSR Academy of Science, Geophysics Series), No. 1, 1963, p. 183.

398. Twomey, S. and Severynse, G. T., Journ. Atm. S., 1964, Vol. 21, No. 5, p. 558.

399. Fedorov, M. M., DAN SSSR (Reports of the USSR Academy of Science), Vol. 118, No. 4, 1958, p. 691.

400. Makhon'ko, K. P., Izvestiya AN SSSR, seriya geofizicheskaya (Reports of the USSR Academy of Science, Geophysics Series), No. 8, 1959, p. 1235.

401. Spurny, K. and Pich, J., Studies Geophys. & Geolog., 1961, Vol. 5, No. 11, p. 85.

402. Hatch, T., Choate, S., J. Frankl. Inst., 1929, Vol. 207.

403. Voegtlin, C., Hodge, H., Pharmacology & Toxicology of Uranium Compounds, New York, 1949.

404. Podzimek, J., Studies Geophys. & Geolog., 1959, Vol. 3, No. 4.

405. Podzimek, J. and Cernoch, I., Geophys., Pure & Appl., 1961, Vol. 50, No. 3, p. 96.

406. Junge, C. E., Journ. Meteorol., 1955, Vol. 12, p. 13.

407. Laktionov, A. G., Izvestiya AN SSSR, seriya geofizicheskaya (Reports of the USSR Academy of Science, Geophysics Series), No. 3, 1958, p. 419.

408. Laktionov, A. G., Izvestiya AN SSSR, seriya geofizicheskaya (Reports of the USSR Academy of Science, Geophysics Series), No. 4, 1960, p. 566.

409. Plass, G. N., Appl. Optics, 1966, Vol. 5, No. 1, p. 149.

410. Okita, T., Journ. Meteorol. Soc. Japan., 1957, Vol. 35, No. 2.

411. Junge, C. E., Chagnon, C. W. and Manson, J. E., Science, 1961, Vol. 133, No. 3463, p. 1478.

412. Junge, C. E., Manson, J. E., Journ. Geophys. Res., 1961, Vol. 66, No. 7, p. 2163.

413. Friedlander, C. K., Journ. Meteorol., 1960, Vol. 17, No. 3, p. 373; ;961, Vol. 18, No. 6, p. 753.

414. Idlif, G. N., Izvestiya astrofizicheskogo instituta AN Kaz SSR, (Reports of the Kazakh SSR Astrophysical Institute), Vol. 4, Nos. 5-6, 1957, p. 3.

415. Goetz, A., Priening, O., Kallai, T., Geophys., Pure & Appl., 1961, Vol. 50, No. 3, p. 67, 79.

416. Khrgian, A. Kh., Fizika atmosfery, "Physics of the Atmosphere," Gostekhizdat (State Technical Publ.), 1953.

417. Laktionov, A. G., Izvestiya AN SSSR, seriya gofizicheskaya (Reports of the USSR Academy of Science, Geophysics Series), No. 9, 1960, p. 1397.

418. Gayvoronskiy, I. I., Trudy Tsentral'noy aerologicheskoy observatorii, "Studies of the Central Aerological Observatory," No. 4, 1949, p. 46.

419. Penndorf, R., Journ. Meteorol., 1954, Vol. 11, No. 3, p. 245.

420. Selezneva, E. S., Yudin, M. I., Trudy Glavnoy geofizicheskoy observatorii, "Studies of the Central Geophysical Observatory," No. 105, 1960, p. 37.

421. Selezneva, E. S., In the collection Issledovaniea oblakov, osadkov i grozovogo elektrichestva, "Study of Clouds, Precipitation and Thunderstorm Electricity," Izd-vo AN SSSR (USSR Academy of Science Publ.), 1961, p. 96. Trudy Glavnoy geofizicheskoy observatorii, "Studies of the Central Geophysical Observatory," No. 134, 1962, p. 3.

422. Dergach, A. L., Trudy Glavnoy Geofizicheskoy observatorii, "Studies of the Central Geophysical Observatory," No. 105, 1960, p. 30.

423. Junge, C. E., Chagnon, C. W., Manson, J. E., Journ. Meteorol., 1961, Vol. 18, No. 1, p. 81.

424. Chagnon, C. W., Junge, C. E., Journ. Meteorol., 1961, Vol. 18, No. 6, p. 746.

425. Manson, J. E., Junge, C. E., Chagnon, C. W., Chem. reactions lower and upper atmosphere, New York-London, Interscience, 1962, p. 139.

426. Junge, C. E., Journ. Meteorol., 1961, Vol. 18, No. 4.

427. Durbin, W. S., Geophys., Pure & Appl., 1959, Vol. 42, No. 1, p. 11.

428. Durbin, W. S., White, G. D., Tellus, 1961, Vol. 13, No. 2, p. 260.

429. Singleton, F., Durbin, W. G., Quart. Journ. Roy. Meteor. Soc., 1961, Vol. 88, No. 377, p. 315.

430. Wright, F. W., Hodge, P. W., Nature, 1962, Vol. 195, No. 4838, p. 269.

431. Laktionov, A. G., Trudy vsesoyouznogo nauchnogo meteorologicheskogo soveshchaniya"Reports read at the All Union Scientific Meteorological Conference," Gidrometeoizdat (State Scientific and Technical Hydrometeorological Publ. House), Vol. 6, 1963, p. 60.

432. Georgievskiy, Yu. S., Driving, A. Ya., et al., Prozhektornyy luch v atmosfere, "The Projector Beam in the Atmosphere," Ed. by Prof. G. V. Rozenberg, USSR Academy of Science Publ., 1960.

433. Rossler, F., Vassy, E., C. R. Acad. Sci., 1962, Vol. 254, No. 11, p. 2041.

434. Mikirov, A. E., DAN SSSR (Reports of the USSR Academy of Science), Vol. 142, No. 3, 1962, p. 587.

435. Gushchin, G. P., Trudy Glavnoy Geofizicheskoy observatorii, "Studies of the Central Geophysical Observatory," No, 125, 1962, p. 54.

436. Rabinovich, Yu. I., Trudy Glavnoy geofizicheskoy observatorii, "Studies of the Central Geophysical Observatory," Issue 125, 1962, p. 54.

437. Collis, R. T. H. and Ligda, M. G H., Journ. Atmosph. Sc., 1966, Vol. 23, No. 2, p. 255.

438. Fiocco, G. and Grams, G., Journ. Atmosph. Sci., 1964, Vol. 21, No. 3, p. 323.

439. Deirmendjian D., Journ. Geoph. Res., 1965, Vol. 70, No. 3.

440. Newkirk, G., Kroening, J. L., Journ. Atmosph. Sc., 1965, Vol. 22, No. 5, p. 567.

441. Elterman, L. and Campbell, A. B., Journ. Atm. Sc., 1964, Vol. 21, No. 4, p. 457.

442. Elterman, L., Journ. Opt. Soc. Amer., 1965, Vol. 55, No. 11, p. 1583.

443. Elterman, L., Appl. Optics, 1966, Vol. 5, No. 11, p. 1769.

444. Elterman, L., An Atlas of Aerosol Attenuation and Extinction Profiles for the Troposphere and Stratosphere, Environmental Research Papers, No. 241, AFCRL, Mass., 1966.

445. Kondrat'ev, K. Ya., Nikol'skiy, G. A., Esipova, E. N., Izvestiya AN SSSR, seriya Fizika atmosfery i okeana (Reports of the USSR Academy of Science, Physics of the Atmosphere and the Ocean Series), Vol. 2, No. 4, 1966.

446. Newkirk, G., Jr., and Eddy, J. A., Journ. Atmosph. Sc., 1964, Vol. 21, No. 1, p. 35.

447. Elterman, L., Atmospheric Attenuation Model, 1964, in the Ultraviolet, Visible and Infrared Regions for Altitudes to 50 km., Environmental Research Papers, No. 46, AFCRL, Mass., 1964.

448. Elterman, L., Appl. Optics, 1964, Vol. 3, No. 6, p. 745.

449. Kelkar, V. N., Indian Journ. Meteor. and Geophys., 1962, Vol. 13, No. 2, p. 173.

450. Mason, B. J. and Andrews, Quart. Journ. Roy. Met. Soc., 1960, Vol. 86, p. 346.

451. Polyakova, E. A., Shifrin, K. S., Trudy Glavnoy Geofizicheskoy observatorii, "Studies of the Central Geophysical Observatory," No. 42, 1953, p. 84.

452. Polyakova, E. A., Trudy Glavnoy Geofizicheskoy observatorii, "Studies of the Central Geophysical Observatory," No. 68, 1957, p. 92.

453. Polyakova, E. A., Trudy Glavnoy Geofizicheskoy observatorii, "Studies of the Central Geophysical Observatory," No. 100, 1960, p. 45.

454. Marshall, T. S., Palmer, W. Journ. Meteor., 1948, Vol. 5, No. 4, p. 165.

455. Zel'manovich, I. L., Trudy Glavnoy Geofizicheskoy observatorii, "Studies of the Central Geophysical Observatory," No. 100, 1960, p. 58.

456. Tvorogov, S. D., Izvestiya vuzov SSSR, seriya Fizika (News of USSR Higher Institutions of Learning, Physics Series), No. 3, 1965, p. 147.

457. Green, H. S., Wolf, E., Proc. Phys. Soc., 1953, Vol. 66A, p. 1129.

458. Wolf, E., Proc. Phys. Soc., 1959, Vol. 74, p. 269.

459. Roman, P., Acta Phys. Hung., (Hungarian Journ. of Phys.), Vol. 4, 1957, p. 209.

460. Tvorogov, S. D., Izvestiya SSSR, Seriya Fizika (News of USSR Higher Institutions of Learning), No. 3, 1965, p. 175.

461. Van de Huest, H. C., Light Scattering by Small particles, New York-London, 1957. Russian translation edited by V. V. Sobolev, Foreign Literature Publ., 1961.

462. Schiff, L. J., Phys. Rev., 1956, Vol. 103, p. 443.

463. Tatarskiy, V. I., Teoriya fluktuatskionnykh yavleniy pri rasprostranenii voln v turbulentnoy atmosfere, "The Theory of Fluctuation Phenomena during propagation of waves in a turbulent atmosphere," USSR Academy of Science Publ., 1959.

464. Born, M., Wolf, E., Principles of Optics, New York, 1959.

465. Sokolov, V. V., Tvorogov, S. D., Zhurnal Prikladnoy spektroskopii (J. of Applied Spectroscopy), Vol. 8, No. 3, 1968, p. 493.

466. Landau, L. D., Lifshits, E. M., Elektrodinamika sploshnvkh sred, "Electrodynamics of continuous media," Gostekhizdat (State Technical Publications), 1957.

467. Shifrin, K. S., Rasseyanie sveta v mutnoy srede, "Light Scattering in a Turbid Medium," Gostekhizdat (State Technical Publications), 1951.

468. Tvorogov, S. D., Izvestiya Vuzov SSSR, seriya fizika (News of USSR Higher Institutions of Learning, Physics Series), No. 1, 1961, p. 87.

469. Shifrin, K. S., Trudy glavnoy geofizicheskoy observatorii "Studies of the Central Geophysical Observatory," No. 26, 1951, p. 83.

470. Johnson, J. C. and Terrell, J. R., Journ. Opt. Soc. Amer., 1955, Vol. 45, No. 6, p. 451.

471. Penndorf, R. B., Journ. Opt. Soc. Amer., 1956, Vol. 46, p. 1001; 1957, Vol. 47, p. 603, Journ. Meteor., 1956, Vol. 13, p. 219; Journ. Phys. Chem., 1958, Vol. 62, p. 1537.

472. Deirmendjian, D., Clasen, R. and Viezee, W., Journ. Opt. Soc. Amer., 1961, Vol. 51, No. 6, p. 620.

473. Stephens, J. J. and Gerhardt, J. R., Journ. Meteor., 1961, Vol. 18, No. 6, p. 818.

474. Herman, B. M., Quart, Journ. Roy. Met. Soc., 1962, Vol. 88, No. 376, p. 143.

475. Penndorf, R., Research in Aerosol Scattering in the Infrared, Sci. Rep. 5., Tech. Rep. RAD-TR-61-32, U.S. Dept. of Commerce, Off. of Techn. Serv., 1961.

476. Irvine, W. M., Bull. Astronom. Inst., Netherlands, 1964, Vol. 17, No. 4, p. 266.

477. Irwine, W. M., Journ. Opt. Soc. Amer., 1965, Vol. 55, No. 1, p. 16.

478. Orchard, S. E., Journ. Opt. Soc. Amer., 1965, Vol. 55, No. 9, p. 1190.

479. Plass, G. N., Appl. Optics, 1966, Vol. 5, No. 2, p. 279.

480. Kattawar, G. W. and Plass, G. N., Appl. Optics, 1967, Vol. 6, No. 8, p. 1377.

481. Shifrian, K. S., Zel'manovich, I. L., Tablitsy po svetorasseyaniyu, uglovye funktsii, "Light Scattering Tables, Vol. 1, Angular Functions," Gidromteoizdat (State Scientific and Technical Hydrometeorological Publ. House), 1966.

482. Fhifrian, K. S., Zel'manovich, I. L., Tablitsy po svetorasseyaniyu, Tablitsy matrits rasseyaniya i sostavlyayushchikh rasseyannogo polya, "Light Scattering Tables, Vol. 2, Tables of Scattering Matrices and Components of the scattered field," Gidrometeoizdat (State Scientific and Technical Hydrometeorological Publishing House), 1968.

483. Shifrin, K. S., Zel'manovich, I. L., Tablitsy po svetorasseyaniyu, Koeffitsienty oslableniya, rasseyaniya i luchevogo davleniya, "Light Scattering Tables, Vol. 3 Attenuation, Scattering, and Beam Pressure Coefficients," Gidrometeoizdat (State Scientific and Technical Hydrometeorological Publ. House), 1968.

484. Shifrin, K. S., Izvestiya AN SSSR, seriya geofizicheskaya, (Reports of the USSR Academy of Science, Geophysics Series), No. 2, 1952, p. 15.

485. Kerker, M., Kratohvil, J. P. and Matijevic, E., Journ. Opt. Soc. Amer., 1962, Vol. 52, No. 5, p. 551.

486. Fenn, R. W. and Oser, H., Appl. Optics, 1965, Vol. 4, No. 11, p. 1504.

487. Kerker, M., Kauffman, L. H. and Farone, W. A., Journ. Opt. Soc. Amer., 1966, Vol. 56, No. 8, p. 1053.

488. Plass, G. N., Appl. Optics, 1965, Vol. 4, No. 12, p. 1616.

489. Deirmenjian, D., Quart. Journ. Roy. Met. Soc., 1960, Vol. 86, p. 371.

490. Penndorf, R., Journ. Opt. Soc. Amer., 1962, Vol. 52, No. 4, p. 402.

491. Clark, G. C., Journ. Opt. Soc. Amer., 1957, Vol. 47, No. 1.

492. Volz, F., Ber. Dent. Wetterd., 1954. Vol. 2, No. 13.

493. Penndorf, R., Journ. Opt. Soc. Amer., 1957, Vol. 47, No. 2, p. 176.

494. Foldy, L., Phys. Rev., 1945, Vol. 67, p. 107.

495. Lax, M., Rev. Mod. Phys., 1951, Vol. 23, p. 287; Phys. Rev., 1952, Vol. 85, p. 621.

496. Waterman, P. C., Truell, R., Journ. Math. Phys., 1961, Vol. 2, p. 512.

497. Twersky, V., Journ. Math. Phys., 1962, Vol. 3, p. 700.

498. Gnedin, Yu. N., Dolginov, A. Z., ZhETF (Journ. of Experimental and Theoretical Physics), Vol. 45, 1963, p. 1136.

499. Gnedin, Yu. N., Dolginov, A. Z., Astronomicheskiy zhurnal (Astronomical Journ.), Vol. 43, 1966, p. 800.

500. Porovoy, A. G., Izvestiya vuzov SSSR, seriya Fizika (News of USSR Higher Institutions of Learning, Physics Series), No. 2, 1966, p. 175.

501. Porovoy, A. G., Izvestiya vuzov SSSR, seriya Fizika (News of USSR Higher Institutions of Learning, Physics Series), No. 6, 1966, p. 50.

502. Porovoy, A. G., Izvestiya vuzov SSSR, seriya Fizika (News of USSR Higher Institutions of Learning, Physics Series), No. 4, 1967, p. 97.

503. Porovoy, A. G., Izvestiya vuzov SSSR, seriya Fizika (News of USSR Higher Institutions of Learning, Physics Series), No. 5, 1967, p. 7.

504. Rozenberg, G. V., Uspekhi fizicheskikh nauk, "Achievements of Physical Sciences," Vol. 56, No. 1, 1955, p. 77.

505. Malkova, Z. S., Izvestiya AN SSSR, seriya fizika atmosfery i okeana (Reports of the USSR Academy of Science, Physics of the Atmosphere and the Ocean Series), Vol. 1, No. 1, 1965, pp. 109-113.

506. Gorchakov, G. I., Rozenberg, G. V., Izvestiya AN SSSR, seriya Fizika atmosfery i okeana (Reports of the USSR Academy of Science, Physics of the Atmosphere and the Ocean Series), Vol. 1, No. 12, 1965, p. 1279.

507. Gorchakov, G. I., Izvestiya AN SSSR, seriya fizika atmosfery i okeana (Reports of the USSR Academy of Science, Physics of the Atmosphere and the Ocean Series), Vol. 2, No. 6, 1966, p. 595.

508. Levin, L. M., In the collection Issledovanie po eksperimental'noy i teoreticheskoy fizike, "Studies in Experimental and Theoretical Physics," dedicated to the memory of Academician G. S. Lansberg, USSR Academy of Science Publ., 1959, p. 121.

509. Shifrin, K. S., Raskin, V. S., Optika i spektroskopiya (Optics and Spectroscopy), Vol. 11, No. 2, 1961, p. 268.

510. Tvorogov, S. D., Izvestiya vuzov SSSR, seriya fizika (News of USSR Higher Institutions of Learning, Physics Series), No. 1, 1961, p. 87.

511. Tvorogov, S. D., Izvestiya vuzov SSSR, seriya fizika (News of USSR Higher Institutions of Learning, Physics Series), No. 4, 1962, p. 175.

512. Tvorogov, S. D., Izvestiya vuzov SSSR, seriya fizika (News of USSR Higher Institutions of Learning, Physics Series), No. 3, 1962, p. 174.

513. Zuev, V. E., Kabanov, M. V., Koshelev, B. P., Tvorogov, S. D., Khmelevtsov, S. S., In the collection Aktinometriya i optika atmosfery (Trudy V Mezhvedomstvennogo soveshchaniya po aktinometrii i optike atmosfery), "Actinometry and optics of the atmosphere (Studies of the V Interdepartmental Conference on Actinometry and Optics of the Atmosphere)," edited by G. V. Rozenberg, Nauka Publ., 1964.

514. Zuev, V. E., Kabanov, M. V., Koshelev, B. T., Tvorogov, S. D., Khmelevtsov, S. S., Izvestiya vuzov SSSR, seriya Fizika (News of the USSR Higher Institutions of Learning, Physics Series), No. 3, 1964, p. 92.

515. Zuev, V. E., Kabanov, M. V., Koshelev, B. T., Tvorogov, S. D., Khmelevtsov, S. S., Izvestiya vuzov SSSR, seriya Fizika (News of the USSR Higher Institutions of Learning, Physics Series), No. 3, 1965, p. 147.

516. Zuev, V. E., Tvorogov, S. D., Izvestiya vuzov SSSR, seriya Fizika (News of the USSR Higher Institutions of Learning, Physics Series), No. 2, 1966, p. 143.

517. Diermenjian, D., Appl. Opt., 1964, Vol. 3, No. 2, p. 187.

518. Centeno, M., Journ. Opt. Soc. Amer., 1941, Vol. 31, p. 244.

519. Sonchik, V. K., Lotasov, V. P., Chernyavskaya, N. A., In the collection Trudy mezhvuzovskogo soveshchaniya po spektral'noy prozrachnosti atmosfery v vidimoy i infrakrasnoy oblasti, "Studies of the Inter-University Conference on the Spectral Transparency of the Atmosphere in the Visible and Infrared Regions," (June, 1965), Tomsk State Univ. Publ., 1968.

520. Zuev, V. E., Lopasov, V. P., Sonchik, V. K., Izvestiya AN SSSR, seriya Fizika atmosfery i okeana (Reports of the USSR Academy of Science, Physics of the Atmosphere and the Ocean Series), Vol. 3, No. 1967, p. 60.

521. Zuev, V. E., Sonchik, V. K., Izvestiya AN SSSR, seriya Fizika atmosfery i okeana (Reports of the USSR Academy Of Science, Physics of the Atmosphere and Ocean Series), Vol. 5, No. 7, 1969, p. 745.

522. Rubens, H., Ladenburg, E., Verh. D. Ges., 1909, Vol. 11, No. 16.

523. Kislovskiy, L. F., Optika i spektroskopiya (Optics and Spectroscopy), Vol. 7, No. 3, 1959, p. 311.

524. Kondrat'ev, K. Ya., Burgova, N. P., Gaynulin, I. F., Togunova, G. F., In the collection Problemy fiziki atmosfery, "Problems in the Physics of the Atmosphere," Leningrad State Univ. Publ., No. 2, 1963.

525. Zuev, V. E., Sokolov, V. V., Tvorogov, S. D., Doklad na Vsesoyuznon mezhvedomstevnnom soveshchanii to rasseyaniyu sveta v atmosfere, "Report read at the All Union Inter-Departmental Conference on Light Scattering in the Atmosphere," Chernovtsy, 1967.

526. Zuev, V. E., Kabanov, M. V., Koshelev, B. P., Tvorogov, S. D., Khmelevtsov, S. S., Izvestiya vuzov SSSR, seriya Fizika (News of USSR Higher Institutions of Learning, Physics Series), No. 2, 1964, p. 90.

527. Zuev, V. E., Koshelev, B. P., Tvorogov, S. D., Khmelevtsov, S. S., Izvestiya SSSR, seriya Fizika (News of USSR Higher Institutions of Learning, Physics Series), No. 3, 1966, p. 121.

528. Zuev, V. E., Koshelev, B. P., Tvorogov, S. D., Khmelevtsov, S. S., Izvestiya AN SSSR, seriya Fizika atmosfery i okeana (Reports of the USSR Academy of Science, Physics of the Atmosphere and the Ocean Series), No. 5, 1955, p. 509.

529. Koshelev, B. T., Izvestiya vuzov SSSR, seriya Fizika (News of USSR Higher Institutions of Learning, Physics Series), No. 3, 1966, p. 126.

530. Arnulf, A., Bricard, J., Beit. Phys. Atmosph. (Contributions to the Physics of the Atmosphere), Vol. 33, Nos. 1/2, 1960, p. 9.

531. Kurnick, S. W. Zitter, R. N., Williams, D. W., Journ. Opt. Soc. Amer., 1960, Vol. 50, p. 578.

532. Gates, D. M. and Shaw, C. D., Journ. Opt. Soc. Amer., 1960, Vol. 50, p. 876.

533. Bocharov, E. I., Izvestiya AN SSSR, Seriya geofizicheskaya (Reports of the USSR Academy of Science, Geophysics Series), No. 5, 1958, p. 678.

534. Zabrodskiy, G. M., Morachevskiy, V. G., Trudy Arkticheskogo i Antarkticheskogo instituta, voprosy fiziki oblakov i tumanov, "Studies of the Arctic and Antarctic Institute, Problems in the Physics of Clouds and Nebulae," Vol. 228, No. 1, 1959, p. 68.

535. Zabrodskiy, G. M., Morachevskiy, V. G., Trudy Arkticheskogo i Antarkticheskogo instituta, voprosy fiziki oblakov i tumanov, "Studies of the Arctic and Antarctic Institute, Problems in the Physics of Clouds and Nebulae," Vol. 239, No. 2, p. 48; Trudy vsesoyuznogo nauchnogo meteorologicheskogo soveshchaniya, "Studies of the All-Union Scientific Meteorological Conference," Vol. 6, 1963, p. 102.

536. Trappenberg, R., Arch. Meteor., Geoph. Biokl. A, 12, 1960, No. 1. p. 125.

537. McCubbin, T. K., Journ. Opt. Soc. Amer., 1952, Vol. 42; p. 876.

538. Rozenberg, G. V., Izvestiya AN SSSR, seriya Fizika atmosfery i okeana (Reports of the USSR Academy of Science, Physics of the Atmosphere and the Ocean Series), Vol. 3, No. 9, 1967, p. 936.

539. Sharonov, V. V., Izmerenie i raschet vidimosti dalekikh predmetov, "Measurement and Calculation of the Visibility of Distant Objects," Gostekhizdat (State Technical Publ.), 1947.

540. Shifrin, K. S., Raskin, V. S., Trudy Glavnoy geofizcheskoy observatorii, "Studies of the Central Geophysical Observatory," No. 100, 1960, p. 3.

541. Shifrin, K. S., Raskin, V. S., In the collection Aktinometriya i atmosfernaya optika, "Actinometry and Atmospheric Optics," Gidrometeoizdat (State Scientific and Technical Hydrometeorological Publ. House), 1961, p. 178.

542. Shifrin, K. S., Raskin, V. S., Trudy glavnoy geofizicheskoy observatorii, "Studies of the Central Geophysical Observatory," No. 109, 1961, pp. 155, 161.

543. Zuev, V. E., Sokolov, V. V., Trovorogov, S. D., Izvestiya vuzov SSSR, seriya Fizika (News of USSR Higher Institutions of Learning, Physics Series), No. 3, 1966, p. 7.

544. Zuev, V. E., Sokolov, V. V., Trovorogov, S. D., Izvestiya vuzov SSSR, seriya Fizika (News of USSR Higher Institutions of Learning, Physics Series), No. 1, 1969, p. 107.

545. Popov, O. I., Optika i spektroskopiya (Optics and Spectroscopy), Vol. 3, No. 5, 1957, p. 504.

546. Curcio, J., Journ. Opt. Soc. Amer., 1961, Vol. 51, No. 5, p. 548.

547. Knestrick, G. L., Cosden, T. H. and Curcio, J. A., Journ. Opt. Soc. Amer., 1962, Vol. 52, No. 9, p. 1010.

548. Passman, S. and Larmore, L., Proc. IRIS, 1956, Vol. 1, No. 2, p. 15.

549. Junge, C., Gerlands Beit. Geoph. (Contributions to Geography), Vol. 46, 1935, p. 108.

550. Wright, H. L., Quart, Journ. Roy. Met. Soc., 1940, Vol. 66, p. 66.

551. Boilean, A. R., Scripps Inst. of Oceanography, Univ. of Calif., Feb., 1959, p. 1.

552. Buma, T., J. Bull. Amer. Meteor. Soc., 1960, Vol. 41, p. 357.

553. Middleton, W. E. K., Vision through the atmosphere, The Univ. of Toronto Press, Toronto, 1952, ch. 3, p. 24.

554. Georgievskiy, Yu. S., Izvestiya AN SSSR, seriya Fizika atmosfery i okeana (Reports of the USSR Academy of Science, Physics of the Atmosphere and the Ocean Series), Vol. 2, No. 5, 1966, p. 494.

555. Shifrin, K. S., Minin, I. N., Trudy Glavnoy geofizicheskoy observatorii, "Studies of the Central Geophysical Observatory," No. 68, 1957, p. 5.

556. Faraponova, G. P., Trudy Tsentral'noy aerologicheskoy observatorii, "Studies of the Central Aerological Observatory," No. 23, 1957, p. 23; No. 32, 1959, p. 3.

557. Handbook of Geophysics and Space Environments AFCRL, Office of Aerospace Research U.S. Air Force, 1965.

558. Rabinovich, Yu. I., In the collection Aktinometriya i atmosfernaya optika, "Actinometry and Atmospheric Optics," Gidrometeoizdat (State Scientific and Technical Hydrometeorological Publ. House), 1961, p. 146; reprinted in Trudy Glavnoy Geofizicheskoy observatorii, "Studies of the Central Geophysical Observatory," No. 118, 1961, p. 18.

559. Rabinovich, Yu. I., Guseva, L. N., Trudy Glavnoy Geofizicheskoy observatorii, "Studies of the Central Geophysical Observatory," No. 118, 1961, p. 69.

560. Atmosfernyy Ozon, "Ozone in the Atmosphere," ed. by G. P. Gushchina, Material from the III Interdepartmental Conference on Atmospheric ozone held on 21-23 May 1963, Gidrometeoizdat (State Scientific and Technical Hydrometeorological Publ. House), 1965.

561. Gushchin, G. P., In the collection Aktinometriya i atmosfernaya optika, "Actinometry and Atmospheric Optics," Gidrometeoizdat (State Scientific and Technical Hydrometeorological Publ. House), 1961, p. 218.

562. Gushchin, T. P., Issledovanie atmosfernogo ozona, "Study of Ozone in the Atmosphere," Gidrometeoizdat (State Scientific and Technical Hydrometeorological Publ. House), 1963.

563. Penndorf, R., Journ. Meteor., 1954, Vol. 11, No. 3.

564. Packer, D. and Lock, C., Journ. Opt. Soc. Amer., 1951, Vol. 41, No. 7.

565. Toropova, T. P., Izvestiya astrofizicheskogo instituta AN Kaz.SSR (Reports of the Astrophysical Institute of the Kazakh Academy of Science), Vol. 10, 1960, p. 71.

566. Zuev, V. E., Kabanov, M. V., Pkhalagov, Yu. A., Izvestiya AN SSSR, seriya Fizika atmosfery i okeana (Reports of the USSR Academy of Science, Physics of the Atmosphere and the Ocean Series), Vol. 4, No. 7, 1968, p. 778.

567. Driving, A. Ya., Smirnova, A. I., Izvestiya AN SSSR, seriya geofizicheskaya (Reports of the USSR Academy of Science, Geophysics Series), No. 3, 1958, p. 337.

568. Schmolinsky, F., Meteor. Zeit. (Meteorological Journal), Vol. 61, 1944, No. 6.

569. Foitzik, L. and Zskhaeck, H., Zeit fur Meteorol. (Meteorological Journal), Vol. 7, No. 1, 1953, p. 1.

570. Polyakova, E. A., Tret'yakov, V. V., Trudy Glavnoy geofizicheskoy observatorii, "Studies of the Central Geophysical Observatory," No. 100, 1960, p. 53.

571. Jefferson, G. J., Meteor. Mag., 1961, Vol. 90, No. 1067, p. 163.

572. Shifrin, K. S., Chayanova, E. A., Trudy Glavnoy geofizicheskoy observatorii, "Studies of the Central Geophysical Observatory," No. 170, 1965, p. 93.

573. Shifrin, K. S., Perel'man, A. Ya., Punina, V. A., Trudy Glavnoy geofizicheskoy observatorii, "Studies of the Central Geophysical Observatory," No. 183, 1966, p. 18.

574. Barteneva, O. D., Izvestiya AN SSSR, seriya geofizicheskaya (Reports of the USSR Academy of Science, Geophysics Series), No. 12, 1960, p. 1852.

575. Belov, V. S., Izmerenie osnovnykh opticheskikh kharakteristik prizemnogo sloya vozdukha, "Measurement of fundamental optical characterics of air in the layer near the earth's surface," Gidrometeoizdat (State Scientific and Technical Hydrometeorological Publ. House), 1956.

576. Hulbert, E. O., Journ. Opt. Soc. Amer., 1941, Vol. 31.

577. Bullrich, K., Meteor. Zeit. (Meteorological Journal), Vol. 61, 1944, p. 270.

578. Bullrich, K. and Moller, F., Optik (Optics), Vol. 2, 1947.

579. Reger, E. and Siedentopf, Optik (Optics), Vol. 1, 1946, p. 15.

580. Barteneva, O. D., Bashilov, G. Ya., Izvestiya AN SSSR, seriya geofizicheskaya (Reports of the USSR Academy of Science, Geophysics Series), No. 4, 1961, p. 613.

581. Toropova, T. P., Izvestiya Astrofizicheskogo institua AN Kaz.SSR (Reports of the Astrophysical Institute of Kazakh Academy of Science), Vol. 9, 1959, p. 108.

582. Boyko, P. N., Lifshits, G. Sh., Toropova, T. P., Izvestiya astrofizicheskogo instituta AN Kaz.SSR, (Reports of the Astrophysical Institute of the Kazakh Academy of Science), Vol. 8, 1959, p. 98.

583. Pyaskovskaya-Fesenkova, E. V., Issledovaniya rasseyaniya sveta v zemnoy atmosfere, "Studies of Light Scattering in the Earth's Atmosphere," Publications of the USSR Academy of Science, 1957.

584. Kastrov, V. G., Trudy Tsentral'noy aerologicheskoy observatorii, "Studies of the Central Aerological Observatory," No. 32, 1959, p. 84.

585. Lyubovtseva, Yu. S., Rozenberg, G. V., Izvestiya AN SSSR, seriya Fizika atmosfery i okeana (Reports of the USSR Academy of Science Physics of the Atmosphere and the Ocean Series), Vol. 2, No. 3, 1966, p. 248.

586. Belov, V. F., Trudy tsentral'noy aerologicheskoy observatorii, "Studies of the Central Aerological Observatory," No. 23, 1957, p. 63. Trudy Vsesoyuznogo nauchnogogo meteorologicheskogo soveshchaniya, "Studies of the All-Union Scientific Meteorological Confern.," Vol. 6, 1963, p. 52.

587. Chayanov, B. A., Trudy Tsentral'noy aerologicheskoy observatorii, "Studies of the Central Aerological Observatory," No. 32, 1959, p. 17.

588. Kompaniets, A. I., Izvestiya AN SSSR, seriya Fizika atmosfery i okeana (Reports of the USSR Academy of Science, Physics of the Atmosphere and Ocean Series), Vol. 1, No. 3, 1965, p. 335.

589. Bullrich, K., Adv. In Geophys., 1964, Vol. 10, p. 101.

590. Kabanov, N. V., In the collection Trudy mezhvuzovskogo soveshchaniya po spektral'noy prozrachnosti atmosfery v vidimoy i infrakrasnoy oblasti, "Studies of the Inter-University Confern. on the Spectral Transparency of the Atmosphere in the Visible and Infrared Regions," June 1965, Tomsk State Univ. Publ., 1968.

591. Carrier, L. W. and Nugent, L. J., Appl. Optics, 1965, Vol. 4, No. 11, p. 1457.

592. Bukatyy, V. I., Kabanov, M. V., Koshelev, B. P., Smirnov, B. A., Savel'ev, B. A., Khmelevtsov, S. S., Izvestiya Vuzov SSSR, seriya Fizika (News of USSR Higher Institutions of Learning, Physics Series), No. 8, 1967, p. 139.

593. Woodward, D. H., Appl. Optics, 1963, Vol. 2, No. 11, p. 1205.

594. Harris, F. S., Jr., Sherman, G. C. and Morse, E. L., ieee Transactions on Antennas and Propagation, 1967, Vol. AP-15, No. 1, p. 141.

595. Sinclair, D., Journ. Opt. Soc. Amer., 1947, Vol. 37, p. 475.

596. Brillouin, L., Journ. Appl. Phys., 1949, Vol. 20, No. 11, p. 1110.

597. Gumprecht, R. O. and Sliepcevich, C. M., Journ. Phys. Chem., 1953, Vol. 57, p. 90.

598. King, R., U-Tay-Tszun', Rasseyanie i difraktsiya elektromagnitnykh voln, "Scattering and Diffraction of Electromagnetic Waves," Foreign Literature Publications, 1962.

599. Polyakova, E. A., Trudy Glavnoy Geofizicheskoy observatorii, "Studies of the Central Geophysical Observatory," No. 68, 1957, p. 88.

600. Timofeeva, V. A., Trudy Morskogo Gidrofizicheskogo instituta, "Studies of the Marine Hydrophysical Institute," Vol. 3, 1953, p. 35.

601. Timofeeva, V. A., Koveshnikova, L. A., Izvestiya AN SSSR, seriya Fizika atmosfery i okeana (Reports of the USSR Academy of Science, Physics of the Atmosphere and the Ocean Series), Vol. 2, No. 3, 1966, p. 320.

602. Kabanov, V. M., In the collection Aktinometriya i optika atmosfery (Trudy V Mezhvedomstvennogo soveshchaniya po aktinometrii i optike atmosfery), "Actinometry and Optics of the Atmosphere (Studies of the V Interdepartmental Confern. on Actinometry and Atmospheric Optics)," ed. by G. V. Rozenberg, Nauka Publ., 1964.

603. Middleton, W. E. K., Journ. Opt. Soc. Amer., 1949, Vol. 39, No. 7.

604. Stewart, H. S. and Curcio, J. A., Journ. Opt. Soc. Amer., 1952, Vol. 42, p. 801.

605. Gibbons, M. G., Journ. Opt. Soc. Amer., 1958, Vol. 48, p. 550; 1959, Vol. 49, p. 702.

606. Gibbons, M. G., Nichols, J. R., Laughridge, F. I. and Rudkin, Journ. Opt. Soc. Amer., 1961, Vol. 51, p. 633.

607. Gibbons, M. G., Laughridge, F. I., Nichols, J. R. and Krause, N. A., Journ. Opt. Soc. Amer., 1962, Vol. 52, p. 38.

608. Meshkov, V. V., Osnovy Svetotekhniki, "Foundations of Light Technology," No. 1, Gosenergoizdat (State Power Engineering Publications), 1957.

609. Eldridge, R. G. and Johnson, J. C., Journ. Opt. Soc. Amer., 1958, Vol. 48, p. 463.

610. Eldridge, R. G. and Johnson, J. C., Journ. Opt. Soc. Amer., 1962, Vol. 52, p. 787.

611. Zuev, V. E., Kabanov, M. V., Borovoy, A. G., Izvestiya Vuzov SSSR, seriya Fizika (News of USSR Higher Institutions of Learning, Physics Series), No. 6, 1963, p. 162.

612. Zuev, V. E., Kabanov, M. V., Izvestiya vuzov SSSR, seriya Fizika (News of USSR Higher Institutions of Learning, Physics Series), No. 1, 1964, p. 168.

613. Zuev, V. E., Kabanov, M. V., Savel'ev, B. A., Izvestiya Vuzov SSSR, seriya Fizika (News of USSR Higher Institutions of Learning, Physics Series), No. 5, 1964, p. 80.

614. Zuev, V. E., Kabanov, M. V., In the collection Aktrinometriya i optika Atmosfery (Trudy V Mezhvedomstevnnogo soveshchaniya po aktinometrii i optike atmosfery), "Actinometry and Optics of the Atmosphere (Studies of the V Interdepartmental Confern. on Actinometry and Optics of the Atmosphere)," ed. G. V. Rozenberg, Nauka Publ., 1964.

615. Zuev, V. E., Kabanov, M. V., Izvestiya Vuzov SSSR, seriya Fizika (News of USSR Higher Institutions of Learning, Physics Series), No. 6, 1965, p. 175.

616. Smirnov, V. I., Kurs vysshey matematiki, "A Course in Higher Mathematics," Vol. 2, Gostekhizdat (State Technical Publications), 1948.

617. Ivanov, A. P., Khayrullina, A. Ya., Izvestiya AN SSSR, seriya Fizika atmosfery i okeana (Reports of the USSR Academy of Science, Physics of the Atmosphere and Ocean Series) Vol. 2, No. 7, 1966, p. 721.

618. Hodkinson, J. R. and Greenfield, J. R., Appl. Optics, 1965, Vol. 4, No. 11, p. 1463.

619. Prokhorov, A. N., Uspekhi fizcheskikh nauk, "Progress in Physical Sciences," Vol. 85, 1965, p. 599.

620. Basov, N. G., Uspekhi fizcheskikh nauk, "Progress in Physical Sciences," Vol. 85, 1965, p. 585.

621. Akhmanov, S. A., Khokhlov, R. V., Uspekhi fizicheskikh nauk, "Progress in Physical Sciences," Vol. 88, No. 3, 1966, p. 439.

622. Meyman, Elektronika (Electronics), Vol. 38, No. 8, 1965, p. 55.

623. Taunf, Ch., Uspekhi fizicheskikh nauk, "Progress in Physical Sciences," Vol. 88, No. 3, 1966, p. 461.

624. Kalimskiy, A. A., Osiko, V. V., Izvestiya AN SSSR, seriya neorganicheskie materialy (Reports of the USSR Academy of Science, Inorganic Materials Series), Vol. 1, No. 12, 1965, p. 2049.

625. Kit and Presli, TIIER (Abbreviation unknown), Vol. 54, No. 10, 1966, p. 7.

626. Bridges, W. B. and Chester, A. N., Appl. Optics, 1965, Vol. 4, No. 5, p. 573.

627. Johnson, Elektronika (Electronics), Vol. 39, No. 8, 1966, p. 3.

628. Kiss, Z. J. and Pressley, R. J., Appl. Optics, 1966, Vol. 5, No. 10, p. 1474.

629. Snitzer, E., Appl. Optics, 1966, Vol. 5, No. 10, p. 1487.

630. Bloom, A. L., Appl. Optics, 1966, Vol. 5, No. 10, p. 1500.

631. Nathan, M. I., Appl. Optics, 1966, Vol. 5, No. 10, p. 1514.

632. Khokhlov, R. V., Uspekhi fizicheskikh nauk (Progress of Physical Sciences), Vol. 87, 1965, p. 17.

633. Pimental, G. C., Scientific Amer., 1966, Vol. 214, No. 4, p. 32.

634. Opticheskie kvantovye generatory. Noveyshie issledovaniya i primeneniya opticheskoy kvantovoy elektroniki, "Optical Quantum Generators. Latest Studies and Applications of Optical Quantum Electronics," Collection of articles ed. by F. V. Bunkin, Mir Publ., 1966.

635. Labuda, E. F., Gordon, E., Miller, R. C., IEEE, Journ. Quant. Electron., 1965, Vol. 1, No. 6, p. 273.

636. Polanyi, I. C., Appl. Optics, 1965, suppl. No. 2, p. 109.

637. Paananen, R. A., IEEE, Spectrum., 1966, Vol. 3, No. 6, p. 88.

638. Bogoroditskiy, N. P., Pikhtin, A. N., Yas'kov, D. A., Izvestiya leningradskogo elektrotekhnicheskogo instituta (Reports of the Leningrad Electrotechnical Institute), Issue 57, No. 21, p. 3.

639. Patel, C. K. N., Chim. Phys. & Phys., Chim. Biocl., 1967, Vol. 64, No. 1, p. 82.

640. Walter, W. T., Solimene, N., Piltch, M., Gould, G., IEEE, Journ. Quant. Electron., 1966, Vol. 2, No. 9, p. 474.

641. Johnson, A. R. I., Laser Focus, 1966, Vol. 2, No. 17, p. 19.

642. Survey of Laser Products Microwaves, 1966, Vol. 5, No. 10, p. 56, 58, 62.

643. Manger, H., Zeitschrift fur angewandtl. Phys. (Journ. for Applied Phys.), Vol. 18, No. 4, p. 275.

644. Akhmanov, S. A., Kovrigin, A. I., Kolesov, V. A., Piskarskas, A. S., Fadeev, V. V., Pis'ma v Zh ETF (Letters to the Journ. of Experimental and Theoretical Phys.), Vol. 3, No. 9, 1966, p. 372.

644a. Danileyko, M. V., Kravchenko, V. I., Odulov, S. G., Pogorelyy, O. N., Soskin, M. S., Ukrainskiy fizcheskiy zhurnal (Ukranian Journ. of Phys.), Vol. 12, No. 4, 1967, p. 669.

645. Muller, R. C., Nordland, W. A., Appl. Phys. Letters, 1967, Vol. 10, No. 2, p. 53.

646. Sobolev, V. V., Perenos luchistoy energii v atmosferakh zvezd i planet, "Transfer of Beam Energy in Atmospheres, Stars, and Planets," Gostekhizdat (State Technical Publ.), 1956.

647. Wang, M. C., Guth, E., Phys. Rev., 1951, Vol. 84, No. 6, p. 1092.

648. Romanova, L. M., Optika i spektroskopiya (Optics and Spectroscopy), Vol. 13, No. 3, 1962, p. 429.

649. Romanova, L. M., Optika i spektroskopiya (Optics and Spectroscopy), Vol. 13, No. 6, p. 819.

650. Kabanov, M. V., Savel'ev, B. A., Izvestiya AN SSSR, seriya Fizika atmosfery i okeana (Reports of the USSR Academy of Science, Physics of the Atmosphere and Ocean Series), Vol. 3, No. 6, 1967, p. 658.

651. Gershun, A. A., Izbrannye trudy po fotometrii i svetotekhnike, "Selected Studies in Photometry and Light Technology," Fizmatgiz (Physics-Mathematics Publ.), 1958.

652. Feygel'son, E. M., Radiatsionnye protsessy v sloisto-obraznykh oblakakh, "Radiation Processes in Stratus Clouds," Nauka Publ, 1964.

653. Dolin, L. S., Izvestiya vuzov SSSR, seriya Radiofizika (News of USSR Higher Institutions of Learning, Radiophysics Series), Vol. 9, No. 1, 1966, p. 61.

654. Kolesov, A. K., Vestnik LGU, seriya matematika, mekhanika astronomiya, "Herald of Leningrad State University, Mathematics, Mechanics, Astronomy Series," Vol. 1, 1966, p. 160.

655. Marchuk, G. I., Mikhaylov, G. A., Izvestiya AN SSSR, seriya Fizika atmosfery i okeana (Reports of the USSR Academy of Science, Physics of the Atmosphere and Ocean Series), Vol. 3, 1967, p. 258.

656. Kabanov, M. V., Izvestiya Vuzov SSSR, seriya Fizika (News of USSR Higher Institutions of Learning, Physics Series), No. 8, 1967, p. 26.

657. Penndorf, R. B., Journ. Opt. Soc. Amer., 1962, Vol. 52, No. 7, p. 797.

658. Krekov, G. M., Mikhaylov, G. A., Kargin, B. A., Izvestiya Vuzov SSSR, seriya Fizika (News of the USSR Higher Institutions of Learning, Physics Series), No. 4, 1968, p. 110.

659. Krekov, G. M., Mikhaylov, G. A., Kargin, B. A., Izvestiya Vuzov SSSR, Seriya Fizika (News of USSR Higher Institutions of Learning, Physics Series), No. 5, 1968, p. 54.

660. Zuev, V. E., Kabanov, M. V., Savel'ev, B. A., DAN SSSR, (Reports of USSR Acad. of Science), No. 2, Vol. 175, 1967, p. 327.

661. Zuev, V. E., Kabanov, M. V., Savel'ev, B. A., Izvestiya AN SSSR, seriya Fizika atmosfery i okeana (Reports of the USSR Academy of Science, Physics of the Atmosphere and the Ocean Series), Vol. 3, No. 7, 1967, p. 724.

662. Kabanov, M. V., Savel'ev, B. A., Izvestiya AN SSSR, seriya Fizika atmosfery i okeana (Reports of the USSR Academy of Science, Physics of the Atmosphere and the Ocean Series), Vol. 4, No. 9, 1968, p. 960.

663. Kabanov, M. V., Sevel'ev, B. A., Fadeev, V. Ya., Izvestiya Vuzov SSSR, seriya Fizika (Reports of the USSR Higher Institutions of Learning, Physics Series), No. 7, 1967, p. 140.

664. Savel'ev, B. A., Izvestiya Vuzov SSSR, seriya Fizika (Reports of USSR Higher Institutions of Learning, Physics Series), No. 12, 1967, p. 135.

665. Savel'ev, B. A., Izvestiya Vuzov SSSR, seriya Fizika (Reports of USSR Higher Institutions of Learning, Physics Series), No. 12, 1967, p. 136.

666. Timofeeva, V. A., Trudy morskogo gidrofizicheskogo instituta "Studies of the Marine Hydrophysical Institute," No. 3, 1953, p. 35.

667. Timofeeva, V. A., DAN SSSR (Reports of the USSR Academy of Science), Vol. 113, 1957, p. 556.

668. Timofeeva, V. A., Izvestiya AN SSSR, seriya geofizicheskaya (Reports of USSR Academy of Science, Geophysics Series), No. 2, 1957, p. 265.

669. Rozenberg, G. V., DAN SSSR (Reports of the USSR Academy of Science), Vol. 145, No. 4, 1962, p. 775.

670. Ivanov, A. P., Makarevich, S. A., Izvestiya AN SSSR, seriya geofizicheskaya (Reports of the USSR Academy of Science, Geophysics Series), No. 11, 1963, p. 1754.

671. Ivanov, A. P., Sherbaf, I. D., DAN BSSR (Reports of the Bielorussian Academy of Science), Vol. 7, No. 10, 1963, p. 673.

672. Ivanov, A. P., Sherbaf, I. D., In the collection Aktrinometriya i optika atmosfery, "Actinometry and Optics of the Atmosphere," Nauka Publ., 1964.

673. Ivanov, A. P., Il'ich, G. K., DAN BSSR (Reports of the Bielorussian Academy of Science), Vol. 9, No. 5, 1965, p. 301.

674. Ivanov, A. P., Sherbaf, I. D., Optika i spektroskopiya (Optics and Spectroscopy), Vol. 18, No. 14, 1965, p. 698.

675. Ivanov, A. P., Il'ich, G. K., DAN BSSR (Reports of the Bielorussian Academy of Science), Vol. 9, No. 7, 1965, p. 428.

676. Ivanov, A. P., Sherbaf, I. D., Izvestiya AN SSSR, seriya Fizika atmosfery i okeana (Reports of the USSR Academy of Science, Physics of the Atmosphere and the Ocean Series), Vol. 2, No. 3, 1966, p. 312.

677. Ivanov, A. P., Sherbaf, I. D., Zhurnal Prikladnoy spektroskopii (Journ. of Applied Spectroscopy), Vol. 5, No. 2, 1966, p. 195.

678. Romanova, L. M., Optika i spektrosckopiya (Optics and Spectroscopy), Vol. 14, No. 2, 1963, p. 262.

679. Bartky, C. E., Appl. Optics, 1965, Vol. 4, No. 7, p. 847.

680. Twomey, S. and Howell, H. B., Appl. Optics, 1965, Vol. 4, No. 4, p. 501.

681. Fenn, R. W., Appl. Optics, 1966, Vol. 5, No. 2, p. 293.

682. Gavrilov, V. A., Vidimost' v atmosfere, "Visibility in the Atmosphere," Gidrometeoizdat (State Scientific and Technical Hydrometeorological Publ. House), 1965.

683. Shifrin, K. S., Zel'manovich, I. L., Trudy Glavnoy geofizicheskoy observatorii, "Studies of the Central Geophysical Observatory," No. 170, 1965, p. 61.

684. Kozlov, V. P., Fedorova, E. O., Optiko-mekhanicheskaya promyshlennost', "Optical and Mechanical Industry," No. 3, Issue 1, p. 1.

685. Munick, R. J., Journ. Opt. Soc. Amer., 1965, Vol. 55, No. 7, p. 893.

686. Donchenko, V. A., Kabanov, M. V., Savel'ev, B. A., Samokhvalov, I. V., Izvestiya Vuzov SSSR, seriya Fizika (News of USSR Higher Institutions of Learning, Physics Series), No. 1, 1968, p. 158.

687. Gilbert, G. D. and Pernika, J. C., Appl. Optics, 1967, Vol. 6, No. 4, p. 741.

688. Eiden, R., Appl. Optics, 1966, Vol. 5, No. 4, p. 569.

689. Timofeeva, V. A., Izvestiya AN SSSR, seriya geofizcheskaya (Reports of the USSR Academy of Science, Geophysics Series), No. 5, 1961, p. 766.

690. Timofeeva, V. A., DAN SSSR, (Reports of the USSR Academy of Science), Vol. 147, No. 3, 1962, p. 604.

691. Timofeeva, V. A., Vostroknutov, A. A., Koveshnikova, L. A., Izvestiya AN SSSR, seriya Fizika atmosfery i okeana (Reports of the USSR Academy of Science, Physics of the Atmosphere and the Ocean Series), Vol. 2, No. 12, 1966, p. 1259.

692. Kabanov, M. V., Savel'ev, B. A., Samokhvalov, I. V., Izvestiya AN SSSR, seriya Fizika atmosfery i okeana (Reports of the USSR Academy of Science, Physics of the Atmosphere and the Ocean Series), Vol. 4, No. 10, 1958.

693. Romanov, L. M., Izvestiya AN SSSR, seriya Fizika atmosfery i okeana (Reports of the USSR Academy of Science, Physics of the Atmosphere and the Ocean Series), Vol. 1, No. 6, 1965, p. 599.

694. Romanova, L. M., Izvestiya AN SSSR, seriya Fizika atmosfery i okeana (Reports of the USSR Academy of Science, Physics of the Atmosphere and Ocean Series), Vol. 1, No. 10, 1965, p. 1022.

695. Romanova, L. M., Izvestiya AN SSSR, seriya Fizika atmosfery i okeana (Reports of the USSR Academy of Science, Physics of the Atmosphere and Ocean Series), Vol. 2, No. 8, 1966, p. 844.

696. Nesmelova, L. I., Tvorogov, S. D., Izvestiya Vuzov SSSR, seriya Fizika (News of USSR Higher Institutions of Learning, Physics Series), No. 5, 1967, p. 141.

697. Bebb, H. B., Gold, A., Phys. Rev., 1966, Vol. 143, No. 1, p. 1.

698. Cohan, N. V. and Hameka, H. F., Phys. Rev., 1966, Vol. 151, No. 4, p. 1076.

699. Tauns, Ch., Shavelov, A., Radiospektroskopiya (Radiospectroscopy), Foreign Literature Publications, 1959.

700. Karplus, R. Schwinger, J., Phys. Rev., 1949, Vol. 73, No. 9, p. 1020.

701. Akhmanov, S. A., Khokhlov, R. V., UFN (Progress of Physical Sciences), Vol. 95, No. 1, 1968, p. 231.

702. Zuev, V. E., In the collection Yubileynyy sbornik trudov Tomskogo gosudarstvennogo universiteta po fizike, "Anniversary Collection of Articles in Physics Published by the Tomsk State University," Tomsk State Univ. Publ., 1970.

703. Nesmelova, L. I., Tvorogov, S. V., In the collection Trudy Mezhvuzovskogo soveshchaniya po spektral'noy prozrachnosti atmosfery v vidimoy i infrakrasnoy oblasti, "Studies of the Inter-University Confern. on the Spectral Transparency of the Atmosphere in the Visible and Infrared Regions," Tomsk State Univ. Publ., 1968.

704. Landau, L. D., Lifshits, E. M., Mekhanika, "Mechanics," Fizmatgiz (Phys.-Math. Publ.), 1966..

705. Askar'yan, G. A., Zh.ETF Pif'ma (Journ. of Experimental and Theoretical Phys., Letters), Vol. 4, No. 10, 1966, p. 400.

706. Rayzer, Yu. P., Zh. ETF, pis'ma. (Journ. of Experimental and Theoretical Phys., Letters), Vol. 4, No. 1, 1966, p. 3.

707. Rayzer, Yu. P., Zh. ETF, pis'ma. (Journ. of Experimental and Theoretical Phys., Letters), Vol. 4, No. 4, 1966, p. 124.

708. Rayzer, Yu. P., Zh. ETF, pis'ma. (Journ. of Experimental and Theoretical Phys., Letters), Vol. 4, No. 8, 1966, p. 286.

709. Yankauskas, Z. K., Izvestiya Vuzov SSSR, seriya radiofizika (News of the USSR Higher Institutions of Learning, Radiophysics Series), Vol. 9, No. 2, 1966, p. 412.

710. Litvak, A. G., Izvestiya Vuzov SSSR, seriya radiofizika (News of USSR Higher Institutions of Learning, Radiophysics Series), Vol. 9, No. 3, 1966, p. 629.

711. Shen, I. R., Journ. Opt. Soc. Amer., 1966, Vol. 56, No. 10, p. 1425.

712. Chiao, R. Y., Garmire, E., Townes, C. H., Phys. Rev. Letters, 1964, Vol. 13, p. 479; erratum, Phys. Rev. Lett., 1965, Vol. 14, p. 1056.

713. Akhmanov, S. A., Sukhorukov, A. P., Khokhlov, R. V., Zh ETF (Journ. of Experimental and Theoretical Phys.), Vol. 50, No. 6, 1966, p. 1537.

714. Barkhudarova, G. M., Voronov, G. S., Gorbunkov, V. M., Delone, N. B., Zh ETF (Journ. of Experimental and Theoretical Phys.), Vol. 49, No. 2, 1965, p. 386.

715. Wang, C. C., Phys. Rev. Letters, 1966, Vol. 16, p. 344.

716. Akhmanov, S. A., Khokhlov, R. V., Problemy nelineynoy optiki, "Problems of Nonlinear Optics," USSR Academy of Science Publications, 1964.

717. Akhmanov, S. A., Sukhorukov, A. P., Khokhlov, R. V., UFN (Progress of Physical Sciences), Vol. 93, No. 1, 1967, p. 19.

718. Zel'dovich, Ya. B., Rayzer, Yu. P., Zh ETF, pis'ma. (Journ. of Experimental and Theoretical Phys., Letters), Vol. 3, No. 3, 1966, p. 137.

719. Akhmanov, S. A., Krindach, D. P., Sukhorukov, A. P., Khokhlov, R. V., Zh ETF, pis'ma. (Journ. of Experimental and Theoretical Physics, Letters), Vol. 6, No. 2, 1967, p. 509.

720. Fuks, N. A., Isparenie i rost kapel' v gazoobraznoy srede, "Vaporization and Increase in Drops in a Gaseous Medium," USSR Academy of Science Publ., 1958.

721. Williams, T. A., Journ. Heat & Mass. Transf., 1965, Vol. 8, p. 575.

722. Shifrin, K. S., Zolotova, Zh. K., Izvestiya AN SSSR, seriya Fizika atmosfery i okeana (Reports of the USSR Academy of Science, Physics of the Atmosphere and Ocean Series), Vol. 2, No. 12, 1966, p. 1311.

723. Kuzikovskiy, A. V., Khmelevtsov, S. S., Izvestiya, AN SSSR, seriya Fizika atmosfery i okeana (Reports of the USSR Academy of Science, Physics of the Atmosphere and Ocean Series), Vol. 4, No. 3, 1968, p. 363.

724. Kuzikovskiy, A. V., Izvestiya Vuzov SSSR, seriya Fizika (News of USSR Higher Institutions of Learning), No. 5, 1970, p. 95.

725. Kuzikovskiy, A. V., Khmelevtsov, S. S., Trudy IX Vsesoyuznoy konferetsii po rasprostraneniyu radiovoln, "Studies of the IX National Conference on the Propagation of Radiowaves," Kharkov, 1969.

726. Chapman, S., Cauling, T., Matemat cheskaya teoriya neodnorodnykh gazov, "Mathematical Theory of Nonhomogeneous Gases," Foreign Literature Publications, 1960.

727. Bukatyi, V. I., Pogodaev, V. A., Izvestiya Vuzov SSSR, seriya Fizika (News of USSR Higher Institutions of Learning, Physics Series), No. 1, 1970, p. 141.

728. Dukatyi, V. I., Khmelevtsov, S. S., Izvestiya Vuzov SSSR, seriya Fizika (News of the USSR Higher Institutions of Learning, Physics Series), No. 1, 1968, p. 91.

729. Khodara, Trudy IIEP (Studies of [abbreviation unknown]), Vol. 54, No. 3, p. 836.

730. Zaytsev, V. A., Ledokhovich, A. A., Trudy Glavnoy geofizicheskoy observatorii, "Studies of the Central Geophysical Observatory," Vol. 156, 1964, p. 118.

731. Tatarskiy, V. I., Rasprostranenie voln v turbulentnoy atmosfere, "Propagation of Waves in the Turbulent Atmosphere," Nauka Publ., 1967.

732. Obukhov, A. N., Izvestiya AN SSSR, seriya geofizicheskaya (Reports of the USSR Academy of Science, Geophysics Series), Vol. 13, 1949, p. 58.

733. Bovsheverov, V. M., Gurvich, A. S., Kalistratova, M. A., Izvestiya Vuzov SSSR, seriya Radiofizika (News of USSR Higher Institutions of Learning), Vol. 4, No. 5, 1961, p. 886.

734. Tsvang, L. R., Izvestiya AN SSSR, seriya geofizcheskaya (Reports of the USSR Academy of Science, Geophysics Series), No. 10, 1963, p. 1594.

735. Kalistratova, M. A., Izvestiya Vuzov SSSR, seriya Radiofizika (News of USSR Higher Institutions of Learning, Radiophysics Series), Vol. 9, No. 1, 1966, p. 50.

736. Golitsyn, G. S., Gurvich, A. S., Tatarskiy, V. I., Akusticheskiy zhurnal (Journ. of Acoustics), Vol. 6, No. 6, 1960, p. 187.

737. Kon, A. I., Tatarfkiy, V. I., Izvestiya Vuzov SSSR, seriya Radiofizika (News of USSR Higher Institutions of Learning, Radiophysics Series), Vol. 8, No. 5, 1965, p. 870.

738. Chernov, L. A., Rasprostranenie voln v srede so sluchaynymi neodnorodnostyami, "Propagation of Waves in a Medium with Random Nonhomogeneities," USSR Academy of Science Publications, 1958.

739. Feyzulin, Z. I., Kravtsov, Yu. A., Izvestiya Vuzov SSSR, seriya radiofizika (News of USSR Higher Institutions of Learning, Radiophysics Series), Vol. 10, No. 1, 1967, p. 68.

740. Fried, D. L., Jour. Opt. Soc. Amer., 1967, Vol. 57, No. 2, p. 169.

741. Davis, J. I., Appl. Optics, 1966, Vol. 5, No. 1, p. 139.

742. Fried, D. L., Journ. Opt. Soc. Amer. 1966, Vol. 56, No. 10, p. 1372.

743. Fried, D. L., Journ. Opt. Soc. Amer., 1966, Vol. 56, No. 10, p. 1380.

744. Fried, D. L. and Schmeltzer, R. A., Applied Optics, 1967, Vol. 6, No. 10, p. 1729.

745. Fried, D. L. and Seidman, Journ. Opt. Soc. Amer., 1967, Vol. 57, No. 2, p. 181.

746. Munick, R. J., Journ. Opt. Soc. Amer., 1965, Vol. 55, No. 5, p. 594.

747. Straub, H. W., Appl. Optics, 1965, Vol. 4, No. 7, p. 875.

748. Shah, B. R., Journ. Opt. Soc. Amer., 1966, Vol. 56, No. 4, p. 559.

749. Consortini, A., Ronchi, L., Scheggi, A. M., and Toraldo di Francia, G., Radio Sci. Journ. Res., 1966, Vol. 1, p. 523.

750. Hufnagell, R. E. and Stanley, N. R., Journ. Opt. Soc. Amer., 1964, Vol. 54, p. 52.

751. Gracheva, M. E., Gurvich, A. S., Izvestiya Vuzov SSSR, Seriya Radiofizika (News of USSR Higher Institutions of Learning, Radiophysics Series), Vol. 8, No. 4, 1965, p. 717.

752. Kon, A. I., Tatarskiy, V. I., Izvestiya Vuzov SSSR, seriya Radiofizika (News of USSR Higher Institutions of Learning, Radiophysics Series), Vol. 7, No. 2, 1964, p. 306.

753. Gurvich, A. S., Kon, A. I., Izvestiya Vuzov SSSR, seriya Radiofizika (News of USSR Higher Institutions of Learning, Radiophysics Series), Vol. 7, No. 4, 1964, p. 790.

754. Kabanov, M. V., Pershin, A. A., Pkhalagov, Yu. A., Izvestiya Vuzov SSSR, Seriya Fizika (News of USSR Higher Institutions of Learning, Physics Series), No. 9, 1968, p. 121.

755. Khmelevtsov, S. S., Tsvyk, R. Sh., Izvestiya Vuzov SSSR, seriya Radiofizika (News of USSR Higher Institutions of Learning, Radiophysics Series), No. 1, 1970.

756. Borisov, B. D., Sazanovich, V. N., Khmelevtsov, S. S., Izvestiya Vuzov SSSR, seriya Fizika (News of USSR Higher Institutions of Learning, Physics Series), No. 1, 1969.

757. Hinchman, W. R., Buck, A. L., Proc. IEEE, 1964, Vol. 52, p. 305.

758. Mevers, G. E., Fried, D. L. and Keister, M. P., Journ. Opt. Soc. Amer., 1965, Vol. 55, No. 11, p. 1575.

759. Edwards, B. N. and Steen, R. R., Appl. Optics, 1965, Vol. 4, No. 3, p. 311.

760. Collings, S. A. and Mouroe, M., Journ. Opt. Soc. Amer., 1966, Vol. 56, No. 4, p. 560.

761. Ryznar, E., Appl. Optics, 1965, Vol. 4, p. 1416.

762. Subramanian, M. and Collinson, J. A., Bell System Techn. Journ., 1967, Vol. 46, No. 3.

763. Subramanian, M. and Collinson, J. A., Bell System Techn. Journ., 1965, Vol. 44, p. 543.

764. Goldstein, B. S., Miles, P. A. and Chabot, A., Proc. IEEE, 1965, Vol. 53, p. 1172.

765. Fried, D. L. and Mevers, G. E., Journ. Opt. Soc. Amer., 1965, Vol. 55, p. 740.

766. Buck, A. L., Appl. Optics, 1967, Vol. 6, No. 4, p. 703.

767. Hohn, D. H., Appl. Optics, 1966, Vol. 5, No. 9, p. 1427.

768. Fried, D. L., Mevers, G. E. and Keister, M. P., Journ. Opt. Soc. Amer., 1967, Vol. 57, No. 6. p. 787.

769. Hohn, D. H., Appl. Optics, 1966, Vol. 5, No. 9, p. 1433.

770. S"edin, V. Ya, Khmelevtsov, S. S., Izvestiya Vuzov SSSR, Seriya Radiofizika (News of USSR Higher Institutions of Learning, Radiophysics Series), No. 1, 1970.

771. Herrick, R. B., Mayer-Arrendt, J. R., Appl. Optics, 1966, Vol. 5, No. 6, p. 981.

772. Marocuma, T., Nefflen, K. F., Lawrence, T. R., Klucher, T. M., Journ. Opt. Soc. Amer., 1963, Vol. 53, No. 3.

773. McNish, A. G., Science, 1964, Vol. 146, p. 117.

774. Vaytsel', V. I., Khmelevtsov, S. S., Tezisy doklada na I konferentsii po perenosu informatsii lazernym izlucheniem, "Reports read at the I Conference on Information Transmission by Laser Beams," Kiev State Univ. Publ., 1968.

775. Vaytsel', V. I., Khmelevtsov, S. S., Tezisy doklada na I konferentsii po perenosy informatsii lazernym izlucheniem, "Reports read at the I Conference on Information Transmission by Laser Beams," Kiev State Univ. Publ., 1968.

776. Vaytsel', V. I., Khmelevpsov, S. S., Izvestiya Vuzov SSSR, seriya Fizika (News of USSR Higher Institutions of Learning, Physics Series), No. 6, 1968, p. 87.

777. Pokasov, V. V., Khmelevtsov, S. S., Izvestiya Vuzov SSSR, seriya Fizika (News of USSR Higher Institutions of Learning, No. 5, 1968, p. 82.

778. Poksav, V. V., Khmelevtsov, S. S., Optika i spektroskopiya (Optics and Spectroscopy), Vol. 25, No. 6, 1968, p. 945.

779. Zuev, V. E., Ippolitov, I. I., Makushkin, Yu. S., Trudy Mezhdunarodnogo simpoziuma po radiatsionnym protsessam v atmosfere, "Studies of the International Symposium on Radiation Processes in the Atmosphere," Bergen, Norway, August, 1968.

780. Zuev, V. E., Marchuk, G. I., Galin, V. Ya., Ippolitov, I. I., Makushkin, Yu. S., Tvorogov, S. D., Fomin, V. V., Trudy Mezhdunarodnogo simpoziuma po radiatsionnym protsessam v atmosfere, "Studies of the International Symposium on Radiation Processes in the Atmosphere," Bergen, Norway, August, 1968.

781. Zuev, V. E., Kabanov, M. V., Savel'ev, B. A., Samokhvalov, I. V., Sokolov, V. V., Tvorogov, S. D., Trudy Mezhdunarodnogo simpoziuma po radiatsionnym protsessam v atmosfere, "Studies of the International Symposium on Radiation Processes in the Atmosphere," Bergen, Norway, August, 1968.

782. Antipov, B. A., Zuev, V. E., Sapozhnikova, V. A., Sosnin, A. V., Khmelevtsov, S. S., Trudy Mezhdunarodnogo simpoziuma po radiatsionnym protsessam v atmosfere, "Studies of the International Symposium on Radiation Processes in the Atmosphere," Bergen, Norway, August, 1968.

783. Krekov, G. M., Mikhaylov, G. A., Trudy Mezhdunarodnogo simpoziuma po radiatsionnym protsessam v atmosfere, "Studies of the International Symposium on Radiation Processes in the Atmosphere," Bergen, Norway, August, 1968.

784. Kostkowski, H. J. and Bass, A. M., Journ. Opt. Soc. Amer., 1956, Vol. 46, p. 1060.

785. Seshadri, K. S. and Jones, R. N., Spectrochemica Acta., 1963, Vol. 19, p. 1013.

786. Bastin, J. Q., Grear, A. E., Jons, G. O., Smith, H. J. T., Wright, P. J., Proc. of the Roy. Soc., 1964, Vol. 278, No. 1375, p. 543.

787. Ryadov, V. Ya., Furashov, N. I., Izvestiya vuzov SSSR, seriya Radiofizika (News of USSR Higher Institutions of Learning, Radiophysics Series), Vol. 9, No. 5, 1966, p. 1075.

788. Dryagin, Yu. A., Kislyakov, A. G., Kukin, L. M., Naumov, A. I., Fedoseev, L. I., Izvestiya Vuzov SSSR, seriya Radiofizika (News of USSR Higher Institutions of Learning, Radiophysics Series), Vol. 9, No. 5, 1966, p. 1078.

789. Ryadov, V. Ya., Furashov, N. I., Optika i Spektroskopiya (Optics and Spectroscopy), Vol. 24, No. 2, 1968, p. 178.

790. Zuev, V. E., Nesmelova, L. I., Tvorogov, S. D., In the collection Trudy Mezhvuzovskogo soveshchaniya po spektral' noy prozrachnosti atmosfery v vidimoy i infrakrasnoy oblasti, "Studies of the Inter-University Conference on the Spectral Transparency of the Atmosphere in the Visible and Infrared Regions," Tomsk, June, 1965, Tomsk State Univ. Publ., 1968.

791. Golubitskiy, B. M., Moskalenko, N. I., Izvestiya AN SSSR, seriya Fizika atmosfery i okeana (Reports of the USSR Academy of Science, Physics of the Atmosphere and the Ocean Series), Vol. 4, No. 1, 1968, p. 85.

792. Golubitskiy, P. M., Miurmyants, S. O., Moskalenko, N. I., Doklad na VII vsesoyuznom soveshchanii po aktinometrii i atmosfernoy optike 27 - 31 Maya 1968 g., "Report Read at the VII National Conference on Actinometry and Atmospheric Optics on 27 - 31 May 1968, Leningrad."

793. Moskalenko, N. I., Izvestiya AN SSSR, seriya Fizika atmosfery i okeana (Reports of the USSR Academy of Science, Physics of the Atmosphere and Ocean Series), Vol. 4, No. 7, 1968, p. 777. Doklad na VII Vsesoyuznom soveshchanii po aktinometrii i atmosfernoy optike 27 - 31 Maya 1968, g, "Report Read at the VII National Conference on Actinometry and Atmospheric Optics on 27 - 31 May, 1968, Leningrad."

794. Kiseleva, M. S., Optika i spektroskopiya (Optics and Spectroscopy), Vol. 24, No. 3, 1968, p. 401.

795. Rossetti, C. and Barchewitz, P., Comptes Rendus Acad. Sc. (Academy of Science, Accounts Rendered), Paris, Series B, 1966 Vol. 262, p.1966.

796. Rossetti, C., Bourbonneux, F., Farreng, R. and Barchewitz, P., Comptes Rendus Acad. Sc. (Academy of Science, Accounts Rendered), Paris, Series B, Vol. 262, 1966, p. 1684.

797. Farreng, R., Rossetti, C., Bourbonneux, F. and Barchewitz, P., Comptes Rendus Acad. Sc. (Academy of Science, Accounts Rendered), Paris, Series B, 1966, Vol. 263, p. 241.

798. Herzberg, G., Kolebatel'nye 1 vrashchatel'nye spektry mnogoatomnykh molekul, "Vibration and Oscillation Spectra of Multi-atom Molecules," Foreign Literature Publ., 1949.

799. Babcock, H. D., Herzberg, L., Astrophys. Journ., 1948, Vol. 108, p. 167.

800. Adiks, T. G., Dianov-Klokov, V. I., Izvestiya AN SSSR, seriya Fizika atmosfery i okeana (Reports of the USSR Academy of Science, Physics of the Atmosphere and Ocean Series), Vol. 4, No. 10, 1968, p. 1052.

801. Schlapp, R., Phys. Rev., 1937, Vol. 51, No. 5.

802. Wark, D. Q., Mercer, D. H., Appl. Optics, 1965, Vol. 4, No. 7.

803. Malkevich, M. S., Trudy Glavnoy Geofizicheskoy observatori, "Studies of the Central Geophysical Observatory," No. 166, 1964, p. 282.

804. Saiedy, F., Killeary, D. T., Morgan, W. A., Appl. Optics, 1965, Vol. 4, No. 4.

805. Moeller, G. and Rigden, J. D., Appl. Phys. Letters, 1966, Vol. 8, p. 69.

806. Zuev, V. E., Sosnin, A. V., Khmelevtsov, S. S., Izvestiya AN SSSR, seriya Fizika atmosfery i okeana (Reports of the USSR Academy of Science, Physics of the Atmosphere and Ocean Series), Vol. 5, No. 2, 1969, p. 201.

807. Kondratyev, K. J., Andreev, S. D., Badinov, I. J., Grishechkin, V. S., and Popova, L. V., Appl. Optics, 1965, Vol. 4, No. 9, p. 1069.

808. Neporent, B. S., Kiseleva, M. S., Makogomenko, A. G., Shlyakhov, V. I., Appl. Optics, 1967, Vol. 6, No. 11, p. 1845.

809. Kiseleva, M. S., Reshetnikova, I. N., Fedorova, E. O., Doklad na VII Vsesoyuznom soveshchanii po aktinometrii i atmosfernoy optike 27 - 31 Maya 1968, g, "Report Read at the VII National Conference on Actinometry and Atmospheric Optics on 27 - 31 May 1968, Leningrad."

810. Ivlev, L. S., Bursakova, N. S., Surikov, O. N., In the collection Problemy fiziki atmosfery, "Problems of Atmospheric Physics," No. 6, 1968, Leningrad State Univ. Publ.

811. Fenn, R. Beitr. Physik d Atmosph. (Contributions to Physics of the Atmosphere), Vol. 37, 1964, p. 69.

812. Bullrich, K. Eiden, R., Jaenicke, R., Novak, W., Mainz., Final technical report, Contract DA-91-591-EUC-3458, 1966.

813. Ivlev, L. S., Surikov, O. N., In the collection Problemy fiziki atmosfery, "Problems of the Physics of the Atmosphere," No. 6, 1968, Leningrad State Univ. Publ.

814. Tanaka, M., Special Contributions, Geophysical Institute, Kyoto Univ., 1966, No. 6, p. 47.

815. Toba, Y., Special Contributions, Geophysical Institute, Kyoto Univ., 1966, No. 6, p. 59.

816. Toba, Y. and Tanaka, M., Special Contributions, Geophysical Institute, Kyoto Univ., 1965, No. 5, p. 81.

817. Toba, Y., Tanaka, M., Journ. Meteor. Soc. Japan, 1963, Ser. II, Vol. 41, No. 3, p. 135.

818. Toba, Y., Tellus., 1965, Vol. 27, No. 1, p. 131; No. 3, p. 366.

819. Toba, Y., Tellus, 1966, Vol. 28, No. 1, p. 132.

820. Ivanov, A. I., Livshits, G. Sh., Pavlov, V. E., Tashenov, B. T., Teysel', Ya. A., Rasseyanie sveta v atmosfere, "Light Scattering in the Atmosphere," Nauka Publ. Kazakh, SSR, 1968.

821. Ivlev, L. S., Yanchenko, E. L., Doklad na Vsesoyuznom soveshchanii po rasseyaniyu sveta v atmosfere, "Report Read at National Conference on Light Scattering in the Atmosphere," Alma-Ata, November, 1969.

822. Nikolaeva-Tereshkova, V. V., Rozenberg, G. V., Izvestiya AN SSSR, seriya Fizika atmosfery i okeana (Reports of the USSR Academy of Science, Physics of the Atmosphere and the Ocean Series), Vol. 1, No. 4, 1965, p. 386.

823. Feoktistov, K. P., Rozenberg, G. V., Sandomirskiy, A. B., Sergeevich, V. N., Sonechkin, D. M., In the collection Trudy Vsesoyuznoy konferentsii po fizike kosmicheskogo prostranstva, "Studies of the National Conference on Space Physics," Nauka Publ. 1965.

824. Bunakova, A. M., Ivlev, L. S., In the collection Problemy fiziki atmosfery, "Problems of Atmospheric Physics," No. 5, Leningrad State Univ. Publ., 1967.

825. Toropova, T. P., In the Collection Trudy Astrofizicheskogo instituta AN Kaz. SSR, Voprosy astrofiziki i atmosfernoy optiki, "Studies of the Astrophysical Institute of the Kazakh Academy of Science. Problems in Astrophysics and Atmospheric Optics," Vol. 8, Nauka Publ., Kazakh SSR, 1967.

826. Toropova, T. P., Obasheva, S. O., In the Collection Trudy Astrofizicheskogo instituta AN Kaz. SSR, Voprosy astrofiziki i atmosfernoy optiki, "Studies of the Astrophysical Institute of the Kazakh Academy of Science. Problems in Astrophysics and Atmospheric Optics," Vol. 8, Nauka Publ., Kazakh SSSR, 1967.

827. Livshitz, G. Sh., Rasseyanie sveta v atmosfere ch 1, Trudy astrofizicheskogo instituta AN Kaz. SSR, "Light Scattering in the Atmosphere, Part 1, Studies of the Astrophysical Institute of the Kazakh Academy of Science," Vol. 6, 1965.

828. Barteneva, O. D., Davgyallo, E. N., Polyakova, E. A., Eksperimental'nye issledovaniya opticheskikh svoystv prizemnogo sloya atmosfery. Trudy Glavnoy geofizicheskoy observatorii, "Experimental Studies of Optical Properties in the Layer of the Atmosphere near the Earth's Surface. Studies of the Central Geophysical Observatory," Issue 220, Gidrometeoizdat (State and Technical Hydrometeorological Pulb. House), 1967.

829. Shifrin, K. S., Chayanova, E. A., Izvestiya AN SSSR, seriya Fizika atmosfery i okeana (Reports of the USSR Academy of Science, Physics of the Atmosphere and Ocean Series), Vol. 3, 1967, p. 274.

830. Pavlov, V. E., Astronomicheskiy zhurnal (Astronomical Journ.), Vol. 41, No. 1, p. 122, No. 3, p. 546, 1964.

831. Tychinskiy, V. P., UFN (Progress of Physical Sciences), Vol. 91, No. 3, 1967, p. 389.

832. Metod Monte-Carlo v probleme perenosa izlucheniy (The Monte-Carlo Method in Radiation Transfer) Collection of articles ed. by Associate Member of the USSR Academy of Science, G. I. Marchuk, Atomizdat (Atom Publications), 1967.

833. Krekov, G. M., Mikhaylov, G. A., Kargin, B. A., Izvestiya vuzov SSSR, seriya Fizika (News of USSR Higher Institutions of Learning, Physics Series), No. 9, 1968, p. 99.

834. Krekov, G. M., Mikhaylov, G. A., Izvestiya vuzov SSSR, seriya Fizika (News of USSR Higher Institutions of Learning), No. 10, 1968, p. 145.

835. Krekov, G. M., Krekova, M. M., Samokhvalov, I. V., Izvestiya Vuzov SSSR, seriya Fizika (News of USSR Higher Institutions of Learning, Physics Series), No. 5, 1969.

836. Krekov, G. M., Izevestiya Vuzov SSSR, seriya Fizika (News of USSR Higher Institutions of Learning, Physics Series), No. 6, 1969, p. 74.

837. Krekov, G. M., Trudy IX Vsesoyuznoy konferentsii po rasprostraneniyu radiovoln, "National Conference on the Propagation of Radiowaves," Kharkov, 1969.

838. Ivanov, A. P., Khayrullina, A. Ya., Izvestiya AN SSSR, seriya Fizika atmosfery i okeana (Reports of the USSR Academy of Science, Physics of the Atmosphere and Ocean Series), Vol. 3, No. 5, 1967, p. 537.

839. Khayrullina, A. Ya., Ivanov, A. P., Zhurnal Prikladnoy spektroskopii (Journ. of Applied Spectroscopy), Vol. 7, No. 2, 1967, p. 255.

840. Ivanov, A. P., Katsev, I. L., Izvestiya AN SSSR, seriya fizika atmosfery i okeana (Reports of the USSR Academy of Science, Physics of the Atmosphere and Ocean Series), Vol. 3, No. 7, 1967, p. 714.

841. Katsev, I. L., Ivanov, A. P., Zhurnal Prikladnoy Spektroskopii (Journ. of Applied Spectroscopy), Vol. 7, No. 5, 1967, p. 714.

842. Belyantsev, A. N., Dolin, L. S., Savel'ev, V. A., Izvestiya Vuzov SSSR, Seriya Radiofizika (News of USSR Higher Institutions of Learning, Radiophysics Series), No. 10, No. 4, 1967, p. 489.

843. Krekov, G. M., Izvestiya vuzov SSSR, seriya Fizika (News of USSR Higher Institutions of Learning, Physics Series), No. 7, 1969, p. 7.

844. Armand, S. A., Radiotekhnika i elektronika (Radiotechnology and Electronics), Vol. 14, No. 4, 1969, p. 587.

845. Saiedy, F., Jacobonritz, H., Wark, D. Q., Journ. Atm. Sci., 1967, Vol. 21, No. 1.

846. Monin, A. S., Obukhov, A. N., Trudy geofizicheskogo instituta, "Studies of the Geophysical Institute," No. 24, 1954, p. 151.

847. Tsvang, L. R., Izvestiya AN SSSR, seriya geofizicheskaya (Reports of the USSR Academy of Science, Geophysics Series), No. 8, 1960, p. 1252.

848. Gurvich, A. C., Meleshkin, B. N., Izvestiya AN SSSR, seriya Fizika atmosfery i okeana (Reports of the USSR Academy of Science, Physics of the Atmosphere and the Ocean Series), Vol. 2, No. 7, 1966, p. 688.

849. Rogers, C. B., Journ. Opt. Soc. Amer., 1965, Vol. 55, No. 9, p. 1151.

850. Ward, R. C. and Berry G. V., Appl. Optics, 1967, Vol. 6, No. 6, p. 1136.

851. Tatarskiy, V. I., Izvestiya vuzov SSSR, seriya Radiofizika (News of USSR Higher Institutions of Learning, Radiophysics Series), Vol. 10, No. 1, 1967, p. 48.

852. Richard, T., Brown, Jr., 12th Conference Radar Meteorology, Norman, Okla., 1966.

853. Kabanov, N. V., Samokhvalov, I. V., Izvestiya vuzov SSSR, seriya Fizika (News of USSR Higher Institutions of Learning, Physics Series), No. 3, 1969, p. 80.

854. Fried, D. L., Journ. Opt. Soc. Amer., 1967, Vol. 57, No. 2, p. 169.

855. Chu, T. S., Appl. Optics, 1967, Vol. 6, No. 1, p. 163.

856. Beran, M. J., Journ. Optic. Soc. Amer., 1966, Vol. 56, No. 11, p. 1475.

857. Bonch-Bruavich, A. M., Khodovoy, V. A., UFN (Progress of Physical Sciences), Vol. 85, No. 1, 1965, p. 3.

858. Wallace, R., Molec. Phys., 1966, Vol. 11, p. 457.

859. Lukaszewski, M., Postepy fiz. (Progress of Physics), Vol. 18, 1967, p. 287.

860. Rayzer, Yu. P., UFN (Progress of Physical Sciences), Vol. 87, No. 1, 1965.

861. Morton, V. M., Proc. Phys. Soc., 1967, Vol. 92, p. 301.

862. Pierre, N., Pierre, V. C. R., Acad. Sci., 1966, Vol. AB 262, B 1337.

863. Beran, M., Parrent, J., Theory of Partial Coherence., Englewood Cliff, N. Y., 1964.

864. Taylor, L., Journ. Opt. Soc. Amer., 1967, Vol. 57, No. 3, p. 304.

865. Atmosfernyy Ozon, "Ozone in the Atmosphere," ed. G. P. Gushchin, Gidrometeoizdat (State Scientific and Technical Hydrometeorological Publ. House), 1966.

866. Vasilevskiy, K. P., Kazbanov, V. A., Boldyrev, V. A., Doklad na VII vsesoyuznom soveshchanii po aktinometrii i atmosfernoy optike 27 - 31 Maya 1968, "Report Read at the VII National Conference on Actinometry and Atmospheric Optics on 27 - 31 May 1968," Leningrad.

867. Golubitskiy, B. N., Moskalenko, N. I., Izvestiya AN SSSR, seriya Fizika atmosfery i okeana (Reports of the USSR Academy of Science, Physics of the Atmosphere and the Ocean Series), Vol. 4, No. 1, 1968, p. 90.

868. Golubitskiy, B. N., Moskalenko, N. I., Izvestiya AN SSSR seriya Fizika atmosfery i okeana (Reports of the USSR Academy of Science, Physics of the Atmosphere and the Ocean Series), Vol. 4, No. 3, 1968, p. 346.

869. Moskalenko, N. I., Golubitskiy, B. M., Mirumyants, S. O., Doklad na VII vsesoyuznom soveshchanii po aktinometrii i atmosfernoy optike 27 - 31 Maya 1968, "Report Read at the VII National Conference on Actinometry and Atmospheric Optics on 27 - 31 May 1968," Leningrad.

870. Golubitskiy, B. M., Moskalenko, N. I., Izvestiya AN SSSR, seriya Fizika atmosfery i okeana (Reports of the USSR Academy of Science, Physics of the Atmosphere and the Ocean Series), Vol. 4, No. 3, 1968, p. 360.

871. Farmer, C. B., Houghton, J. T., Nature, 1966, Vol. 209, No. 5030.

872. Golubitskiy, B. N., Mirumyants, S. O., Tantashev, N. V., Filippov, V. L., Artem'eva, L. N., Doklad na VII vsesoyuznom soveshchanii po aktinometrii i atmosfernoy optike 27 - 31 Maya 1968, "Report Read at the VII National Conference on Actinometry and Atmospheric Optics on 27 - 31 May 1968," Leningrad.

873. Filippov, V. L., Mirumyants, S. O., Izvestiya AN SSSR, seriya Fizika atmosfery i okeana (Reports of the USSR Academy of Science, Physics of the Atmosphere and the Ocean Series), Vol. 5, No. 6, 1969, p. 638.

874. Ashcheulov, S. V., Kondrat'ev, K. Ya., Styro, D. P., In the collection Problemy fiziki atmosfery, "Problems in Atmospheric Physics," No. 5, Leningrad State Univ. Publ., 1967.

875. Bolle, H. J., Memoires de la Societe Royale des Sciences de Liege (Memoires of the Royal Scientific Society of Liege), Vol. 26, 1964.

876. Davis, P. A and Viezee, W., Journ. Geophys. Res., 1964, Vol. 69, No. 18.

877. Kiseleva, M. S., Milinina, I. N., Fedorova, E. O., Doklad na VII vsesoyuznom soveshchanii po aktinometrii i atmosfernoy optike 27 - 31 Maya 1968, "Report Read at VII National Conference on Actinometry and Atmospheric Optics on 27 - 31 May 1968," Leningrad.

878. Wacker, P. F. and Pratto, M. R., Microwave Spectral Tables, Vol. II, Line Strengths of Asymmetric Rotors NBS Monograph, 70, Natl. Bur. of Standards, Wash., D. C., 1964.

879. Gates, D. M., Calfee, R. F. and Hansen, W., Appl. Optics, 1963, Vol. 2, No. 11, p. 1117.

880. Gates, D. M., Calfee, R. F., Hansen, D. W. and Benedict, W. S., Line parameters and computed Spectra for water vapor bands at 2.7, NBS Monograph, 71, Natl. Bur. of Standards, 1964.

881. Benedict, W. S., Calfee, R. F., Line Parameters for the 1.9 and 6.3 micron water vapor bands ESSA professional paper 2, U.S. Dept. of Commerce, Wash., D. C., 1967.

882. Pokrovskiy, A. G., In the collection Problemy fiziki atmosfery, "Problems of Atmospheric Physics," No. 5, 1967, Leningrad State Univ. Publ.

883. Timofeev, Yu. M., In the collection "Problemy fiziki atmosfery, "Problems in atmospheric physics," Leningrad State Univ. Publ., No. 5, 1967.

884. Kondrat'ev, K. Ya., Timofeev, Yu. M., Doklad na VII vsesoyuznom soveshchanii po aktinometrii i atmosfernoy optike 27 - 31 Maya 1968, "Report Read at the VII National Conference on Actinometry and Atmospheric Optics on 27 - 31 May 1968," Leningrad.

885. Ben Aryek, Y., Journ. Quant. Spectr. Rad. Transfer., 1967, Vol. 7, No. 1, p. 211.

886. Sakai, H., Line Strengths and widths in the ν_2 water band.

887. Pongtongcharoen, P., Intensities in Heated Water Vapor in the region 4 - 5 μ, M.S. thesis, Catholic Univ., Wash., D. C., 1965.

888. Kirienko, G. A., Toropova, T. P., Kharitonova, G. A., Ibragimov, N. M., Doklad na VII vsesoyuznom soveshchanii po aktonometrii i atmosfernoy optike 27 - 31 Maya 1968, "Report read at the VII National Conference on Actinometry and Atmospheric Optics on 27 - 31 May 1968," Leningrad.

889. Gal'tsev, A. P., Osipov, V. M., Doklad na VII vsesoyuznom soveshchanii po aktinometrii i atmosfernoy optike 27 - 31 Maya 1968, "Report Read at the VII National Conference on Actinometry and Atmospheric Optics on 27 - 31 May 1968," Leningrad.

890. Gal'tsev, A. P., In the collection Problemy Fizika atmosfery, "Problems of Atmospheric Physics," No. 5, 1967, Leningrad State Univ. Publ.

891. Kozhevnikov, N. I., Sarchev, A. P., Sitnik, G. F., Khlystov, A. I., Doklad na VII vsesoyuznom soveshchanii po aktinometrii i atmosfernoy optike 27 - 31 Maya 1968, "Report read at the VII National Conference on Actinometry and Atmospheric Optics on 27 -31 May 1968," Leningrad.

892. Siedentopf, H., Mayer, U., Optik (Optics), Vol. 22, No. 9, 1965, p. 626.

893. Zuev, V. E., Sosnin, A. V., Khmelevtsov, S. S., Doklad na VII vsesoyuznom soveshchanii po aktionmetrii i atmosfernoy optike 27 - 31 Maya 1968, "Report read at the VII National Conference on Actinometry and Atmospheric Optics on 27 - 31 May 1968," Leningrad.

894. Junge, H., Khimicheskiy sostav i radiaktivnost' atmosfery "Chemical Composition and Radioactivity of the Atmosphere," Mir Publ., 1965.

895. Rozenberg, G. V., UFN (Progress of Physical Sciences), Vol. 95, No. 1, 1968, p. 157.

896. Shedlovsky, J. P., Blifford, I. H., Jr., Doklad na XIV general'noy assamblee MGGS, "Report read at the XIV General Session of the International Union of Geodesy and Geophysics," Geneva, Sept. 1967.

897. Gorchakov, G. I., Rozenberg, G. V., Izvestiya AN SSSR, seriya Fizika atmosfery i okeana (Reports of the USSR Academy of Science, Physics of the Atmosphere and Ocean Series), Vol. 3, No. 6, 1967, p. 611.

898. Rozenberg, G. V., Gorchakov, G. I., Izvestiya AN SSSR, seriya Fizika atmosfery i okeana (Reports of the USSR Academy of Science, Physics of the Atmosphere and Ocean Series), Vol. 3, No. 7, 1967, p. 699.

899. Georgievskiy, Yu. G., Doklad na Vsesoyuznom meshvedomstvennom soveshchanii po rasseyaniyu sveta v atmosfere, "Report Read at the National Interdepartmental Conference on Light Propagation in the Atmosphere," Chernovtsy, June 1967.

900. Selazneva, E. S., Atmosfernye aerozoli, "Atmospheric Aerosols," Gidrometeoizdat (State Scientific and Technical Hydrometeorological Publishing House), 1966.

901. Sandomirskiy, A. B., Al'tovskaya, N. P., Trifonova, G. I., Izvestiya AN SSSR, seriya Geofizicheskaya (Reports of the USSR Academy of Science, Geophysics Series), No. 7, 1964, p. 121.

902. Pyldmaa, V. K., Rozenberg, G. V., Izvestiya AN SSSR, seriya Fizika atmosfery i okeana (Reports of the USSR Academy of Science, Physics of the Atmosphere and Ocean Series), Vol. 2, No. 8, 1966, p. 820.

903. Koprov, L. I., Doklad na Vsesoyuznom mezhvedomstvennom soveshchanii po rasseyaniyu sveta v atmosfere, "Report Read at National Interdepartmental Conference on Light Scattering in the Atmosphere," Chernovtsy, June 1967.

904. Rozenber, G. V., Sandomirskiy, A. B., Pyldmaa, V. K., In the collection "Serebristye oblaka." Trudy Mezhdunarodnogo simpoziuma , "'Silver Clouds.' Papers read at the International Symposium in Tallin," 1966, VINITI (All-Union Institute of Scientific and Technical Information for Science and Technology) at the Council of Ministers and the USSR Academy of Science, 1967, p. 94.

905. Rozenberg, G. V., Sandomirskiy, A. B., Izvestiya AN SSSR, seriya Fizika atmosfery i okeana (Reports of the USSR Academy of Science, Physics of the Atmosphere and the Ocean Series), Vol. 3, No. 2, 1967, p. 151.

906. Rozenberg, G. V., Lyubovtseva, Yu. S., Izvestiya AN SSSR, seriya Fizika atmosfery i okeana (Reports of the USSR Academy of Science, Physics of the Atmosphere and Ocean Series), Vol. 3, 1967, No. 2, p. 172.

907. Zuev, V. E., Ippolitov, I. I., Makushkin, Yu. S., Doklad na VII vsesoyuznom soveshchanii po aktinometrii i atmosfernoy optike 27 - 31 Maya 1968, "Report read at VII National Conference on Actinometry and Atmospheric Optics on 27 -31 May 1968," Leningrad.

908. Zuev, V. E., Kabanov, M. V. and Savelev, B. A., Appl. Optics, 1969, Vol. 8, No. 1.

909. Zuev, V. E., Doklad na VII vsesoyuznom soveshchanii po aktinometrii i atmosfernoy optike 27 - 31 Maya 1968, "Report read at VII National Conference on Actinometry and Atmospheric Optics on 27 - 31 May 1968," Leningrad.

910. Zuev, V. E., Doklad na VII vsesoyuznom soveshchanii po aktinometrii i atmosfernoy optike 27 - 31 Maya 1968, "Report read at VII National Conference on Actinometry and Atmospheric Optics on 27 - 31 May 1968," Leningrad.

Table of Contents

Foreword 1

PART 1

ABSORPTION OF VISIBLE AND INFRARED WAVES IN THE EARTH'S ATMOSPHERE 4

1. The Earth's Atmosphere as an Absorbing Medium 4
   1. Composition of the Atmosphere. Variations in pressure and Temperature. 4
   2. Distribution of Water Vapor in the Atmosphere 7
   3. Distribution of Ozone in the Atmosphere 28
   4. Distribution of CO_2, O_2, CH_4, N_2O and CO in the Atmosphere 31

2. Origin and General Characterization of Absorption Spectra of Atmospheric Gases 33
   1. Energy and Spectra of Molecules 33
   2. Rotation Energy and Rotation Spectra of Molecules 35
   3. Vibration Energy and Vibration-Rotation Spectra of Molecules 47
   4. Electronic Energy and Electronic Spectra of Molecules 57
   5. Form of a Spectral Line 57
   6. Intensity of a Spectral Line 66
   7. General Characterization of Absorption Spectra of Atmospheric Gases 68

3. Absorption of Visible and Infrared Waves in a Homogeneous Atmosphere 90
   1. Fundamental Definitions 90
   2. Absorption of Individual Lines 94
   3. Absorption by Groups of Overlapping Lines 100
   4. Limits of Applicability of the Buger-Beer Law 111
   5. Fine Structure of the Vibration-Rotation and Pure Rotation Spectrum of Water Vapor 116
   6. Absorption Function in Narrow Regions of the Vibration-Rotation and Pure Rotation Spectrum of Water Vapor 140
   7. Fine Structure of Absorption Spectrum of Carbon Dioxide 154
   8. Absorption Functions in Various Regions of the CO_2 Spectrum 159

Table of Contents (Cont'd)

9. Structure and Absorption Functions in the Ozone Spectrum 162
10. Fine Structure and Absorption Functions of the Oxygen Spectrum 164
11. Fine Structure and Absorption Functions of Spectra of Small Admixtures in the Atmosphere 165
12. Absorption in Overlapping Lines and Bands 170
13. Radiation Absorptions by Selective Sources 172
14. Laser Radiation Absorption in the Atmosphere 174

4. Absorption of Visible and Infrared Waves in the Non-homogeneous Atmosphere 196

1. Spectral Transmission (Absorption) Transmission (Absorption Function) 196
2. Direct Calculation of Spectral Transmission and Transmission Functions 197
3. Approximate Calculation of the Absorption Function H 200
4. Approximate Methods for Taking Into Account the Temperature when the Function H is Calculated 206
5. Approximate Determination of the Spectral Transmission of the Non-homogeneous Atmosphere 208
6. Calculation of the Absorption Function Taking Into Account the Curvature of the Earth 209
7. Experimental Study of Absorption Functions H 214
8. Laser Radiation Absorption in the Non-homogeneous Atmosphere 220

PART 2

SCATTERING OF VISIBLE AND INFRARED WAVES IN THE EARTH'S ATMOSPHERE 223

5. The Earth's Atmosphere as a Scattering Medium 223

1. Clouds and Nebulae 224
2. Mists 237
3. Precipitation 250

6. Scattering of Visible and Infrared Waves by a Single Particle 252

1. Representation of Polarized Light 252
2. Scattering of a Plane Monochromatic Wave 255
3. Scattering, Absorption and Attenuation Coefficients 257

Table of Contents (Cont'd)

4. The Scalar Approximation in the Scattering Light Problem 261
5. Scattering of the Nonhomogeneous Field 265
6. Laws which Govern the Scattering of Visible and Infrared Waves by a Single Spherical Particle 271
7. Light Scattering by Non-spherical Particles 294

7. Scattering of Visible and Infrared Waves in the Atmosphere 295

1. Molecular Scattering of Visible and Infrared Waves 296
2. Wave Scattering by a System of Particles 298
3. Studies of the Scattering Matrix 302
4. Energy Characteristics in the Scattering of Visible and Infrared Waves by Clouds and Nebulae 304
5. Energy Characteristics of the Scattering of Visible and Infrared Waves by Mists 323
6. Energy Characteristics of the Scattering of Visible and Infrared Waves by Precipitation 338
7. Scattering Indicatrices of Polydispersed Aerosols 339
8. Laser Radiation Scattering in the Atmosphere 343
9. The Effect of Measuring Apparatus on the Results of Experimental Studies of the Scattering of Visible and Infrared Waves in the Atmosphere 346

PART 3

PROPAGATION OF SPATIALLY BOUNDED LIGHT BEAMS IN THE ATMOSPHERE 353

8. Characterization of the Radiation from Lasers of Various Types 353

Introduction 353
1. Lasers Based on Ionic Crystals 354
2. A Laser Based on Glass 357
3. Gas Lasers 358
4. Semiconductor Lasers 361
5. Variation in the Parameters of the Radiation from Lasers due to Various Factors 362

9. Propagation of Spatially Bounded Optical Radiation Beams in Atmospheric Aerosols 365

1. Brightness of Radiation Scattered Forward 365
2. Attenuation of Direct Radiation in Scattering Media. Limits of Applicability of the Buger Law 383

Table of Contents (Cont'd)

3. Brightness of the Radiation which is Scattered Back 386
4. Polarization Characteristics of the Scattered Radiation 390
5. Propagation of a Directed Radiation Pulse in the Scattering and Absorbing Medium 393

10. Nonlinear Effects which Accompany the Propagation of Powerful Light Radiation in the Atmosphere 403

1. Probability of Multiphoton Processes 404
2. Calculations of the Transition Probability by Successive Approximations 408
3. Estimates of the Probability of Multiphoton Photoionization and Photodissociation 411
4. Spectroscopic Saturation Effect 418
5. Light Absorption When the Saturation Effect is Taken into Account 421
6. Self-focusing of a Laser Beam 423
7. The Action of the Powerful Radiation Field on Atmospheric Aerosol Particles 425

11. The Propagation of Bounded Light Beams in the Turbulent Atmosphere 438

1. General Considerations 439
2. Theoretical Studies of the Fluctuations in the Parameters of Bounded Beams Propagating in the Atmosphere 442
3. Experimental Studies of the Fluctuations of Parameters in Spatially Bounded Beams Propagating in the Turbulent Atmosphere 448

Supplement 1 463
Supplement 2 468
Bibliography 475